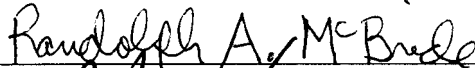
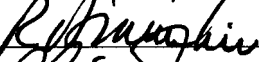
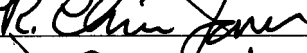
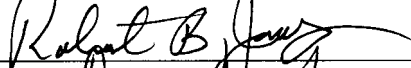
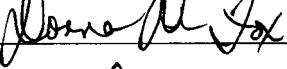
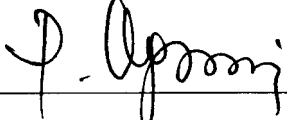


STRATIGRAPHIC ARCHITECTURE, MORPHODYNAMICS, AND EVOLUTION OF
BREACHES ALONG CEDAR ISLAND, VA: A LOW-PROFILE, WASHOVER-
DOMINATED, TRANSGRESSIVE BARRIER ISLAND

by

J. Thomas Hanley
A Dissertation
Submitted to the
Graduate Faculty
of
George Mason University
in Partial Fulfillment of
The Requirements for the Degree
of
Doctor of Philosophy
Environmental Science and Policy

Committee:

	Dr. Randolph A. McBride, Dissertation Director
	Dr. Richard J. Diecchio, Committee Member
	Dr. R. Christopher Jones, Committee Member
	Dr. Julia A. Nord, Committee Member
	Dr. Albert P. Torzilli, Graduate Program Director
	Dr. Robert B. Jonas, Department Chairperson
	Dr. Donna Fox, Associate Dean, Student Affairs & Special Programs, College of Science
	Dr. Peggy Agouris, Dean, College of Science
Date: <u>Dec. 9, 2015</u>	Fall Semester 2015 George Mason University Fairfax, VA

Stratigraphic Architecture, Morphodynamics, and Evolution of Breaches along Cedar
Island, VA: A Low-profile, Washover-dominated, Transgressive Barrier Island

A Dissertation submitted in partial fulfillment of the requirements for the degree of
Doctor of Philosophy at George Mason University

by

J. Thomas Hanley
Master of Science
Syracuse University, 1976
Bachelor of Science
Virginia Polytechnic Institute and State University, 1973

Director: Randolph A. McBride, Professor
Department of Environmental Science and Policy

Fall Semester 2015
George Mason University
Fairfax, VA



This work is licensed under a [creative commons attribution-noncommercial 3.0 unported license](https://creativecommons.org/licenses/by-nc/3.0/).

DEDICATION

This is dedicated to the memory of my loving parents, Col. James F. Hanley and Mrs. Florence C. Hanley.

ACKNOWLEDGEMENTS

I would like to thank first and foremost my committee members, Dr. Randolph A. McBride, advisor and committee chairman, Dr. Richard J. Diecchio, Dr. R. Christopher Jones, and Dr. Julia A. Nord for their support and thoughtful words of advice during this research. Their help has been invaluable and I am very grateful for the time they have spent answering my questions along the way.

I would like to thank my children, Cathryn Comer and James Hanley, for their love and support throughout this process. Wade Ballou and Christopher Seminack have been especially helpful and supportive during the completion of my dissertation. Their guidance and patience was invaluable.

Sean Fate and the other personnel at VIMS – Eastern Shore Laboratory were instrumental in making the field work a success. There were numerous people that helped with the field work at various times and their help is greatly appreciated.

I am also very grateful to all the people who've helped in one way or another during my research. Jim Zackrison and Sal Salerno were especially helpful with various aspects of the lab work.

I would not have been able to complete this project without the love and guidance of my Lord, Jesus Christ.

TABLE OF CONTENTS

	Page
List of Tables	vii
List of Figures	viii
Abstract	xiv
Introduction.....	1
Statement of Purpose.....	1
Area of Investigation.....	4
Goals and Scientific Objectives	10
Research Questions and Multiple Working Hypotheses.....	11
Significance of Research.....	13
Regional Setting.....	14
Location of study area.....	14
Barrier island morphology and physical processes along the Delmarva	23
Quaternary Geology of the Delmarva Peninsula.....	30
Concepts and Previous Studies	42
Barrier islands	42
Washover processes and deposits	45
Definition of breach vs. tidal inlet.....	49
Barrier island breaches	49
Tidal inlets and tidal deltas.....	50
Modern tidal inlet stratigraphy.....	54
Ancient tidal inlet and breach deposits	60
Methods and Datasets	69
Field Methods.....	69
Laboratory Methods	86
Grain-size Analysis	88
Results.....	95

Cedar Island ephemeral inlet sedimentology	106
Surface sediment distribution	106
Primary facies and surfaces	111
Interpretation of depositional environments	122
Vertical grain-size trends	127
Sorting vs. skewness	180
Cedar Island ephemeral inlet stratigraphy	184
Correlation of strike geologic cross sections	186
Correlation of dip geologic cross-sections	195
Tidal Prism Calculations	203
Discussion	206
Compare and contrast ephemeral Cedar Island Inlet with other tidal inlets	208
Spikes in water-flow velocity	211
Eight-stage model depositional model of an ephemeral tidal inlet	211
Conclusions	228
Future research	231
Appendix	233
Appendix A – Vibracore and pulse auger description sheets	233
Appendix B – Vibracore photographs	267
Appendix C – Plots of grain-size trends	306
References	366
Supplemental Material A – Grain-size data sheets	375
Supplemental Material B – GRADISTAT output sheets	376

LIST OF TABLES

Table	Page
Table 1: Temporal relationships of the strata in the eastern Virginia part of the Central Delmarva Peninsula (after Mixon, 1985; after Hobbs,2003).....	32
Table 2:Subfacies of washover deposits and their characteristics and location (from Sedgwick & Davis, 2003).	47
Table 3: Sedimentary characteristics of washover deposits (after Heward, 1981; Schwartz, 1975).	48
Table 4: Parameters used to distinguish tidal-inlet deposits from fluvial deposits in sedimentary rocks (after Kanen, 1969).	55
Table 5: Tidal-channel environments and their corresponding units (after Kumar & Sanders, 1974).....	56
Table 6: Sedimentary characteristics of tidal-inlet deposits (after Heward, 1981).....	59
Table 7: Data on the grain-size samples collected from each field location.	70
Table 8: Historical openings and closings of Cedar Island breach over the past 60 years (from Moyer, 2007).	96
Table 9: Summary of characteristics of facies found in the Cedar Island Inlet sediments.	117
Table 10: Tidal prism calculations for Cedar Island Inlet.	204
Table 11: Upward trends in grain-size for depositional environments, Cedar Island Inlet.	208

LIST OF FIGURES

Figure	Page
Figure 1: Aerial photograph of Cedar Island Breach, March 20, 1994 showing the southernmost part of Cedar Island, Wachapreague Inlet, and Parramore Island immediately south of Cedar Island Inlet (after Moyer, 2007).	2
Figure 2: Cedar Island location map (Google Earth, 2015).	5
Figure 3: Low-oblique aerial photographs of Cedar Island, Virginia, looking north-northwest, taken August 31, 2011 by Randolph A. McBride.	6
Figure 4: Aerial photograph showing Cedar Island, Cedar Island Inlet, and other locations. Historical imagery from October 2006 (Google Earth, 2015).	7
Figure 5: Cedar Island ephemeral tidal-inlet zone, looking southwest, after it closed in early 2007. Taken August 31, 2011 by Randolph A. McBride.	9
Figure 6: Area of Cedar Island Inlet looking south. Parramore Island is in the distance with Wachapreague Inlet in between. Taken April 23, 2010.	10
Figure 7: Location map of the Eastern Shore of Virginia (after Chase-Dunn, 2015).	15
Figure 8: Middle Atlantic barrier island coastlines, showing sequences of barriers (from Fisher, 1982).	16
Figure 9: Map of the Delmarva Peninsula and New Jersey showing the locations of the elements of coastal compartments (from Oertel & Kraft, 1994).	18
Figure 10: Location of the six geomorphic elements in the Delmarva Coastal Compartment (from Oertel et al., 2009).	19
Figure 11: Location of the Chesapeake Bight – “Arc of Erosion” (after Krantz, 2015). .	21
Figure 12: Evolution of Assateague Island (from Goettle, 1981).	22
Figure 13: Map of Holocene-Pleistocene unconformity showing the position of present-day drainage and tidal inlets in relation to Pleistocene drainage around Cedar Island, Virginia. Depths are in meters below mean sea level. (from Morton & Donaldson, 1973).	26
Figure 14: General geography of the Chesapeake Bay region during the late Pliocene. This is displayed over the outline of the modern geography of the Chesapeake Bay. The approximate location of barrier islands is shown by a dashed line. Coastal plain sediments are shown in light gray and deltaic sediments are shown in dark gray. (from Hobbs, 2003)	35
Figure 15: Geographic setting at the time of maximum transgression prior the end of the Pliocene. (from Hobbs, 2003)	35
Figure 16: General geographic setting showing the emergence of the coastal plain in gray during a relative highstand at the end of the Pliocene. (from Hobbs, 2003)	36

Figure 17: General geographic setting a late Pliocene lowstand. The coastal plain is shown in gray with the major rivers crossing it. The location of the river channels is highly speculative. (from Hobbs, 2003)	36
Figure 18: The first indication of the proto-Chesapeake Bay resulting from the growth of the Accomack Spit (Accomack Member of the Omar Formation) in light gray and contemporaneous deposits, in dark gray, east of the pre-existing landforms. (from Hobbs, 2003)	37
Figure 19: General geography of the Chesapeake Bay region showing the merging of the Susquehanna and Potomac river systems to form the Exmore Channel that crossed south of the Accomack Spit during oxygen isotope Stage 12 or 14. (from Hobbs, 2003)	37
Figure 20: General geography of the Chesapeake Bay region during oxygen isotope Stage 10 showing the Belle Haven Channel that connected the Susquehanna-Potomac system with the Rappahannock during Stage 11. This resulted from the blockage of the Exmore Channel by the Accomack Spit extending during Stage 11. (from Hobbs, 2003)	38
Figure 21: Initial growth of the Nassawadox Spit during Stage 9(?). (from Hobbs, 2003)	38
Figure 22: During Stage 8 or 6, the Eastville Channel formed. (from Hobbs, 2003)	39
Figure 23: General geography of the Delmarva Peninsula during Stage 7 and/or Stage 5 with sea-level 4 – 6 m above present sea-level. (from Hobbs, 2003)	39
Figure 24: General geography of the Delmarva Peninsula during Stage 4 -2 lowstand. (from Hobbs, 2003)	40
Figure 25: General geography of the Delmarva Peninsula as it exists today. “C” marks the approximate location of the Chesapeake Channel and “TS” marks the approximate location of the Trimble Shoals Channel. (from Hobbs, 2003)	40
Figure 26: Sketch map of mixed-energy barrier island (from Davis, 1994)	43
Figure 27: General sketch of the barrier island complex showing the major sedimentary environments (from Davis, 1994)	44
Figure 28: Generalized cross-section of washover deposits; A – subaqueous deposition showing foreset laminae; B – supratidal deposition showing only horizontal stratification (from Sedgewick & Davis, 2003)	46
Figure 29: Generalized sketch of a tidal-inlet system (from Davis, 1994)	52
Figure 30: Generalized ebb-tidal delta model (from Davis, 1994)	53
Figure 31: Generalized flood-tidal delta model (from Davis, 1994)	54
Figure 32: Vertical sequence of a modern tidal inlet, Fire Island Inlet, USA. (from Donselaar & Nio, 1982)	58
Figure 33: Hand auger for sediment sampling (from US Air Force, 2015)	71
Figure 34: Map showing location of hand-auger samples	72
Figure 35: Map showing location of trenches	74
Figure 36: Trench T4.	75
Figure 37: Surface-sediment sampling.	76
Figure 38: Map showing location of surface-sediment samples	77
Figure 39: Map showing location of push core.	78
Figure 40: Push core.	79
Figure 41: Push core during excavation	80

Figure 42: Map showing location of vibracores.	81
Figure 43: Portable vibracore rig used to core unconsolidated sediment.	83
Figure 44: Map showing location of pulse augers.	85
Figure 45: Pulse auger equipment.....	86
Figure 46: Gilson AutoSiever.	90
Figure 47: GRADISTAT printout using data from vibracore C1, sample 006.	92
Figure 48: Vertical grain-size trends plotting the statistical moments (mean, sorting, and skewness) for vibracore, C1.....	94
Figure 49: Aerial photographs of ephemeral tidal inlets along the southern portion of Cedar Island, Virginia, showing three active tidal inlets over the past 60 years: (A) October 14, 1957 (Byrne, et al., 1975); (B) March 19, 1994 (Google Earth, 2015a); (C) October 29, 2006 (Google Earth, 2015a).....	99
Figure 50: Location map of the southern portion of Cedar Island showing geomorphic features (Google Earth, 2015b).....	100
Figure 51: Low-oblique aerial photographs of Cedar Island, Virginia. (A) The low-profile, washover-dominated barrier island, with the view to the north-northwest. The arrow points to the final channel position of the last Cedar Island tidal inlet (open from 1998 to 2007), which opened to the north, migrated south in the direction of net longshore sediment transport, and then closed. In the background is Metompkin Inlet and farther northward, Metompkin Island, Virginia. For scale, see the shrimp trawler marooned on the foreshore after losing power during winter and tropical storm Nor'Ida in November 2009. Also, the abandoned beach house is located in the surf zone, left behind as the barrier-island shoreline rapidly migrates landward. (B) The low-profile, washover-dominated barrier island, with the view to the southwest into Burtons Bay. The double-headed arrow indicates the orientation of the final channel position of the last Cedar Island tidal inlet. Along the backbarrier shoreline, relict flood-tidal deltas exist that are overlain by or grade into coalescing washover fans, flats, and terraces. Taken August 31, 2011 by Randolph A. McBride.	102
Figure 52: Cedar Island location map showing primary geomorphic features (Google Earth, 2015b).....	105
Figure 53: Map showing the distribution of mean grain size for all surface samples, divided into fine-grained samples (> 2.0 phi) and medium-grained samples (< 2.0 phi).	107
Figure 54: Map showing the distribution of sorting for all surface samples.	109
Figure 55: Map showing the distribution of skewness for all surface samples.	111
Figure 56: Vibracore 16 showing Facies 1 and Facies 6	118
Figure 57: Vibracore C11 showing Facies 1, Facies 2, and Facies 15.	119
Figure 58: Vibracore C1 showing Facies 4, Faices 5, Facies 10, and Facies 12.	120
Figure 59: Vibracore C10 (bottom 372 cm) showing Facies 11 and Facies 15.....	121
Figure 60: Vibracore C16 showing two depositional environments, beach-washover-aeolian (BWA) and tidal inlet.	123
Figure 61: Vibracore C1 showing three depositional environments, beach-washover-aeolian (BWA), flood-tidal delta, and estuary.	124

Figure 62: Vibracore C10 (bottom 372 cm) showing the estuary depositional environment.	125
Figure 63: Photograph of Vibracore C1 with depositional environments delineated (BWA – beach-washover-aeolian, OFTD –older flood-tidal delta).	128
Figure 64: Grain-size graph for Vibracore C1 (OFTD – older flood-tidal delta, FTD – flood-tidal delta, BWA – beach-washover-aeolian). Skewness is dimensionless.	129
Figure 65: Photograph of Vibracore C2 with depositional environments delineated (BWA – beach-washover-aeolian, FTD – flood-tidal delta, OTI – older tidal inlet).	131
Figure 66: Grain-size graph for Vibracore C2 (BWA – beach-washover-aeolian, FTD – flood-tidal delta, OTI – older tidal inlet). Skewness is dimensionless.	132
Figure 67: Photograph of Vibracore C3 with depositional environments delineated (BWA – beach-washover-aeolian).	134
Figure 68: Grain-size graph for Vibracore C3 (BWA – beach-washover-aeolian. FTD – flood-tidal delta). Skewness is dimensionless.	135
Figure 69: Photograph of Vibracore 4 with depositional environments delineated (BWA – beach-washover-aeolian, FTD – flood-tidal delta).	136
Figure 70: Grain-size graph for Vibracore C4 (BWA – beach-washover-aeolian, FTD – flood-tidal delta). Skewness is dimensionless.	137
Figure 71: Photograph of Vibracore C5 with depositional environments delineated (BWA – beach-washover-aeolian, FTD – flood-tidal delta).	138
Figure 72: Grain-size graph for Vibracore C5 (BWA – beach-washover-aeolian, FTD – flood-tidal delta). Skewness is dimensionless.	139
Figure 73: Photograph of Vibracore C6 with depositional environments delineated (BWA – beach-washover-aeolian, TI- tidal inlet).	141
Figure 74: Grain-size graph for Vibracore C6 (BWA – beach-washover-aeolian, TI- tidal inlet). Skewness is dimensionless.	142
Figure 75: Photograph of Vibracore C7 with depositional environments delineated (BWA – beach-washover-aeolian, TI – tidal inlet).	143
Figure 76: Grain-size graph for Vibracore C7 (BWA – beach-washover-aeolian, TI – tidal inlet). Skewness is dimensionless.	144
Figure 77: Photograph of Vibracore C8 with depositional environments delineated (BWA – beach-washover-aeolian, FTD – flood-tidal delta).	146
Figure 78: Grain-size graph for Vibracore C8 (BWA – beach-washover-aeolian, FTD – flood-tidal delta). Skewness is dimensionless.	147
Figure 79: Photograph of Vibracore C9 with depositional environments delineated (BWA – beach-washover-aeolian).	148
Figure 80: Grain-size graph for Vibracore C9 (BWA – beach-washover-aeolian, FTD – flood-tidal delta). Skewness is dimensionless.	149
Figure 81: Photograph of the upper part of Vibracore C10 with depositional environments delineated (FTD – flood-tidal delta).	150
Figure 82: Photograph of lower part of Vibracore C10 with depositional environments delineated.	151
Figure 83: Grain-size graph for Vibracore C10 (BWA – beach-washover-aeolian). Skewness is dimensionless.	152

Figure 84: Photograph of Vibracore C11 with depositional environments delineated (BWA – beach-washover-aeolian, TI - tidal inlet, E - estuary).	153
Figure 85: Grain-size graph for Vibracore C11 (BWA – beach-washover-aeolian, TI – tidal inlet). Skewness is dimensionless.	154
Figure 86: Photograph of Vibracore C12 with depositional environments delineated (BWA – beach-washover-aeolian, TI – tidal inlet, E - estuary).	156
Figure 87: Grain-size graph for Vibracore C12 (BWA – beach-washover-aeolian, TI – tidal inlet). Skewness is dimensionless.	157
Figure 88: Photograph of Vibracore C13 with depositional environments delineated (BWA – beach-washover-aeolian, TI – tidal inlet).	159
Figure 89: Grain-size graph for Vibracore C13 (BWA – beach-washover-aeolian, TI – tidal inlet). Skewness is dimensionless.	160
Figure 90: Photograph of Vibracore C14 with depositional environments delineated (E - estuary).	161
Figure 91: Grain-size graph for Vibracore C14 (BWA – beach-washover-aeolian). Skewness is dimensionless.	162
Figure 92: Photograph of Vibracore C15 with depositional environments delineated (BWA – beach-washover-aeolian).	163
Figure 93: Grain-size graph for Vibracore C15 (BWA – beach-washover-aeolian, TI – tidal inlet). Skewness is dimensionless.	164
Figure 94: Photograph of Vibracore C16 with depositional environments delineated (BWA – beach-washover- aeolian).	166
Figure 95: Grain-size graph for Vibracore C16 (BWA – beach-washover-aeolian, TI – tidal inlet). Skewness is dimensionless.	167
Figure 96: Photograph of Vibracore C17 with depositional environments delineated (BWA – beach-washover-aeolian, TI – tidal inlet).	169
Figure 97: Grain-size graph for Vibracore C17 (BWA – beach-washover-aeolian, TI – tidal inlet). Skewness is dimensionless.	170
Figure 98: Photograph of Vibracore C18 with depositional environments delineated (BWA – beach-washover-aeolian).	172
Figure 99: Grain-size graph for Vibracore C18 (BWA – beach-washover-aeolian, TI – tidal inlet). Skewness is dimensionless.	173
Figure 100: Location map of cores with beach-washover-aeolian depositional environment showing the upward trends of grain-sizes.	175
Figure 101: Location map of cores with tidal -inlet depositional environment showing the upward trends of grain-sizes.	177
Figure 102: Location map of cores with flood-tidal delta depositional environment showing the upward trends of grain-sizes.	179
Figure 103: Sorting versus skewness. (A) Sediment samples from elevations above +50 cm (n = 69). (B) Sediment samples from elevations between +50 and –50 cm (n = 364). (C) Sediment samples from elevations below –50 cm (n = 471). (D) All sediment sample data combined (n = 904).	184
Figure 104: Location map of all ten cross sections.	185

Figure 105: Location map for strike geologic cross sections A – A', A – B', and A – C'.	187
.....	
Figure 106: Strike geologic cross sections A – A' (A), A – B' (B), and A – C' (C).....	190
Figure 107: Location map for strike geologic cross sections D – D' and E – D'	192
Figure 108: Strike geologic cross sections D - D' (A) and E - D' (B).	194
Figure 109: Location map for dip geologic cross sections H – H', F – F', G – G', D' – G', and D' – C.....	197
Figure 110: Dip geologic cross sections H – H' (A), F – F' (B), G – G' (C), D' – G' (D) and D' – C (E).....	202
Figure 111: Stage 1 - Island Breach.....	214
Figure 112: Stage 2 - Breach evolving to wave-dominated tidal inlet.	215
Figure 113: Aerial photograph of Cedar Island Inlet at Stage 2, taken March 19,1994 (Google Earth, 2015b).	216
Figure 114: Stage 3 - Flood-tidal delta forms.....	217
Figure 115: NASA photograph of Cedar Island Inlet in 1957 showing formation of a flood-tidal delta (Byrne et al. 1975).....	218
Figure 116: Stage 4 - Inlet migration.....	219
Figure 117: Stage 5 - Inlet channel rotates.	220
Figure 118: Aerial photograph of Cedar Island Inlet taken on September 22, 2005 showing the tidal-inlet channel counterclockwise rotation, Stage 5 (Google Earth, 2015b).	221
.....	
Figure 119: Stage 6 - Loses tidal prism.	222
Figure 120: Aerial photograph of Cedar Island Inlet taken on October 26, 2006 in Stage 6 (Google Earth, 2015b).	223
Figure 121: Stage 7 – After the inlet closes, shoreline advances along inlet breach zone.	224
.....	
Figure 122: Long-term (1852 – 2007) and short-term (2007 – 2010) linear regression rates (LRR) of shoreline change of Cedar Island. Cell 4 is located in area of Cedar Island Inlet. The long-term rate is in blue and the short-term rate is in red (Richardson, 2012).	225
.....	
Figure 123: Stage 8 – Closes – Stasis.	226
Figure 124: Oblique aerial photograph showing the Cedar Island Inlet in Stage 8 (Randolph A. McBride, 2011).	227

ABSTRACT

STRATIGRAPHIC ARCHITECTURE, MORPHODYNAMICS, AND EVOLUTION OF BREACHES ALONG CEDAR ISLAND, VA: A LOW-PROFILE, WASHOVER-DOMINATED, TRANSGRESSIVE BARRIER ISLAND

J. Thomas Hanley, Ph.D.

George Mason University, 2015

Dissertation Director: Dr. Randolph A. McBride

Island breaching has occurred at least three times (1956, 1993, and 1998) over the past 60 years in the same place along southern Cedar Island, Virginia. Each time, the breach captured enough tidal prism to remain open, become a tidal inlet, migrated laterally to the south in the direction of net longshore sediment transport, and closed in four to nine years. Twenty-five sediment cores have been analyzed to determine the horizontal and vertical trends within the inlet throat, flood-tidal delta, and washover deposits within the repeatedly breached area. When open, the latest tidal inlet (1998–2007) had a maximum depth of 4.5 m to 2.6 m and ranged in width from 250 m to 54 m. The latest tidal inlet initially captured approximately 18% of the available tidal prism from Wachapreague Inlet, Virginia. Fifteen primary facies were identified that consist mostly of sand, shell, and mud layers. They represent four depositional environments: beach-washover-aeolian, tidal inlet, flood-tidal delta, and estuarine. The sand facies were

deposited in the beach–washover–aeolian, tidal-inlet, and flood-tidal delta environments; the shell facies were deposited in the beach–washover–aeolian environment and at the base of the tidal-inlet environment (channel floor); and the mud facies were deposited only in the estuarine environment. The gross sedimentology (shell, sand, silt, and clay) of the tidal-inlet fill sediments typically showed a fining-upward succession with a coarse shell lag at the channel base and grading upward to fine sand. However, the vertical grain-size trends of some sediment cores coarsened upward based on the sand, silt, and clay fractions.

The evolution of Cedar Island Inlet was studied to determine the life stages of an ephemeral tidal inlet. From this study, eight stages were identified showing how an ephemeral tidal inlet evolves during the time from which it is breached to when it closes. The inlet begins as a shore-normal breach. If it captures enough of the existing tidal prism to remain open, it will evolve into a tidal inlet. The inlet migrates in the direction of net longshore sediment transport, which is southerly in this area. During lateral migration, the inlet begins to rotate counterclockwise with a resulting shore-oblique channel orientation to the adjacent shoreline of 47 degrees in the case of Cedar Island Inlet. Finally, the inlet loses hydraulic efficiency causing the tidal prism to decrease and the inlet closes. An eight-stage model is presented that synthesizes the morphodynamic evolution of Cedar Island Inlet from opening to closing.

INTRODUCTION

Statement of Purpose

The formation, migration, and infilling of barrier breaches influences the sediment budget and dynamic behavior of barrier island systems (Greenwood and Keay, 1979; Boothroyd, 1985; Davis, 1994). Breaches are temporary features along barrier-island coastlines where overwash processes from storms often occur. These breaches allow water and sediment to be exchanged between the ocean and the estuary. When the breach captures all or part of the tidal prism for a year or more, it becomes classified as a tidal inlet (Seminack and McBride, 2015). Tidal prism is the volume of water that moves in or out of a tidal inlet during one tidal cycle (e.g., from mean high tide to mean low tide), excluding freshwater input. The southernmost part of Cedar Island (Figure 1) has experienced breaches in the past and evidence exists that it continues to experience overwash processes and minor breaching. Three times over the past 60 years, a breach has opened through the same area of southern Cedar Island, captured part of the tidal prism from Wachapreague Inlet to the south between Cedar and Parramore Islands, and evolved into a tidal inlet. Each time, Cedar Island Inlet migrated south, in the direction of net longshore sediment transport, experienced decreased hydraulic efficiency, lost tidal prism back to Wachapreague Inlet, and subsequently closed.



Figure 1: Aerial photograph of Cedar Island Breach, March 20, 1994 showing the southernmost part of Cedar Island, Wachapreague Inlet, and Parramore Island immediately south of Cedar Island Inlet (after Moyer, 2007).

Tidal inlets have been studied extensively (Pierce, 1970; Byrne et al., 1974; Hayes, 1980; Boothroyd, 1985; Davis, 1994; McBride, 1999; Seminack and McBride, 2015) but breaches and ephemeral tidal inlets have been much less studied. Schwartz (1975) studied washover deposits on the Outer Banks of North Carolina and Leatherman (1976) studied the overwash processes and aeolian transport on Assateague Island, Virginia and Maryland. These important studies defined the stratigraphy and mechanics of overwash deposition. Tidal inlets and washover deposits are both formed by the same

process: a storm surge that occurs during northeasters or tropical systems (hurricanes). If the storm is intense enough, a breach will occur and it may be open temporarily for several weeks to months before closing as a result of longshore sediment transport. A breach can become a tidal inlet when it captures and retains enough tidal prism to remain open for years or longer (Seminack and McBride, 2015). A tidal inlet may become permanent if it captures the entire tidal prism from any other tidal inlets that are close to it.

Tidal inlets are the primary channels that separate barrier islands in the barrier-island system. The dominant factors that affect tidal-inlet morphology were studied by Fitzgerald and Fitzgerald (1977); Nummedal and Fisher (1978); Hayes, (1979, 1980); Davis and Hayes, 1984; Hayes (1994); and Hayes and Fitzgerald (2013). Features of tidal inlets include the tidal channel and ebb- and flood-tidal deltas. The morphology of the tidal deltas was studied by Boothroyd (1985) and Davis (1994). Kanes (1969) differentiated between sediments deposited by a tidal inlet in a barrier-island system and those deposited by a fluvial system. Kumar and Sanders (1974) defined the sedimentary sequences of a migrating tidal inlet in their study of Fire Island Inlet, which has been open for at least 115 years. Moslow and Heron (1978) studied relict inlets from the Holocene section of the Core Banks of North Carolina and found a distinct sedimentary sequence that consisted of three types of deposits: channel floor, channel, and inlet margin.

Greenwood and Keay (1979) studied a breach, North Inlet, which was open for six years in the barrier-island system in Kouchibouguac Bay, New Brunswick, Canada.

They noted that barrier-island systems are influenced by the formation, migration, and closing of barrier breaches.

Breach and ephemeral tidal inlet studies have focused on the surface morphology of these features. However, this study will explore the stratigraphy of an ephemeral, wave-dominated tidal inlet, and present a depositional model that includes eight-stages showing the evolution of a wave-dominated ephemeral tidal inlet based on Cedar Island Inlet.

Area of Investigation

Cedar Island is a mixed-energy, washover-dominated, transgressive barrier island located along the open-ocean shoreline of the Delmarva Peninsula in Virginia (Figure 2). It is bounded by Metompkin Inlet and Metompkin Island to the north (Figure 3) and Wachapreague Inlet and Parramore Island to the south (Figure 1). Cedar Island is 10.5 km long and averages 242 m in width (Google Earth, 2015). To the west, the southern one-third of the island is backed by open bay (Burton's Bay) and the northern two-thirds is backed by an extensive tidal salt marsh (Gaunt, 1991) (Figure 3). The southern portion of Cedar Island is a spit, which is dominated by washover processes. The spit extends south for 3.9 km to Wachapreague Inlet at its southern tip (Figure 4). North of the spit the island's dune height increases and the tidal marshes to the west of the dunes increase the island's width (Google Earth, 2015).



Figure 2: Cedar Island location map (Google Earth, 2015).



Figure 3: Low-oblique aerial photographs of Cedar Island, Virginia, looking north-northwest, taken August 31, 2011 by Randolph A. McBride.



Figure 4: Aerial photograph showing Cedar Island, Cedar Island Inlet, and other locations. Historical imagery from October 2006 (Google Earth, 2015).

Cedar Island was stable during large portions of the 20th century. After 1962, it began to narrow at an increased rate because of island breaches on southern Metompkin Island. Sediment trapped in Metompkin Bay due to breaches led to interruption of longshore sediment transport to Cedar Island (Gaunt, 1991). Cedar and pine forests on Cedar Island have been nearly eliminated by barrier-island retreat and, as a result, remnants of estuarine salt marsh are exposed along the foreshore and are currently eroding (Richardson, 2012).

Three times in the past 60 years, the spit at the southern end of Cedar Island has been breached and an ephemeral tidal inlet has formed. The tidal-inlet area extends 1.3 km south of Great Gut Cove (Figure 3). Each time, the ephemeral tidal inlet formed, migrated south in the direction of net longshore sediment transport, rotated, and closed (Moyer, 2007). Figure 5 shows the area of the last ephemeral tidal inlet after it closed in early 2007. The southern tidal-inlet area is low in profile and washover-dominated with ripple marks, pools, and abundant shells. Figure 6 provides a view of the area on April 23, 2010 showing the featureless area of Cedar Island Inlet.

This dissertation will use geomorphic analysis to study the former Cedar Island Inlet and its evolution from a barrier-island breach to a tidal inlet to an ephemeral tidal inlet. It will include facies and depositional environment identification and stratigraphic correlation. This study will investigate the geologic framework of former Cedar Island Inlets by collecting sediment cores. The regional setting will be detailed, including the coastal geomorphology, processes operating along the Delmarva Peninsula, and the geologic history of the area. A review of the important concepts and previous studies pertinent to this study will be presented including barrier islands, washover processes, breaches, tidal inlets, tidal-inlet stratigraphy, and ancient tidal-inlet deposits. Finally, the results and discussion will be presented and conclusions drawn.



Figure 5: Cedar Island ephemeral tidal-inlet zone, looking southwest, after it closed in early 2007. Taken August 31, 2011 by Randolph A. McBride.



Figure 6: Area of Cedar Island Inlet looking south. Parramore Island is in the distance with Wachapreague Inlet in between. Taken April 23, 2010.

Goals and Scientific Objectives

The overall goal of this study is to understand the impact of barrier island breaching and subsequent tidal-inlet formation on the morphodynamics, sedimentology, and stratigraphic architecture of low-profile, washover-dominated, transgressive barrier islands.

Specific scientific objectives of this study are:

- to determine if the deposits of the ephemeral tidal inlet can be differentiated from the other depositional environments on southern Cedar Island;

- to determine if the three periods of inlet opening and closing over the past 60 years can be distinguished from each other based on geomorphology, sedimentology, and stratigraphy;
- to compare the deposits from Cedar Island Inlet to ancient tidal-inlet deposits to find comparisons; and
- to develop a depositional model that synthesizes the evolution of an ephemeral wave-dominated tidal inlet.

Research Questions and Multiple Working Hypotheses

Examination of historical aerial photography of the Cedar Island breach zone led to a number of scientific questions:

- How does island breaching occur at Cedar Island Inlet?
- What is the stratigraphic architecture of a barrier-island breach that opens, becomes a tidal inlet, migrates laterally in the direction of net longshore-sediment transport, and closes?
- Does the Cedar Island Inlet reflect a wave-dominated, mixed energy, or a tide-dominated inlet morphology?
- What are the evolutionary stages of development for an ephemeral tidal inlet as expressed by Cedar Island Inlet?
- Once the breach is established, what are the primary hydrodynamic processes associated with barrier-island breaches and ephemeral tidal inlets?

- Does Cedar Island exhibit cyclic or episodic barrier-island breaching?
- Can barrier-island breaches be identified in the ancient stratigraphic record?

The multiple working hypotheses for this study are based on delineating the stratigraphic signature of a laterally migrating, ephemeral tidal inlet using the tools of geomorphology, stratigraphy, and sedimentology. Four working hypotheses were developed to guide the current research.

1. Barrier-island breaches, which stay open to become tidal inlets, migrate, rotate, lose hydraulic efficiency, and close, have stratigraphic signatures that are similar or identical to documented tidal-inlet stratigraphy, both in modern and ancient deposits.
2. Barrier-island breaches, which stay open to become tidal inlets, migrate, rotate, lose hydraulic efficiency, and close, have stratigraphic signatures that are distinctly dissimilar to documented tidal-inlet stratigraphy, both in modern and ancient deposits.
3. The tidal prism captured by a wave-dominated tidal inlet stays the same as the tidal entrance evolves from a breach to a tidal inlet.
4. The tidal prism captured by a wave-dominated tidal inlet changes as the tidal entrance evolves from a breach to a tidal inlet.

Significance of Research

Understanding the morphodynamics, sedimentology, stratigraphy, and evolution of breaches along southern Cedar Island will yield a depositional model that will help identify similar deposits in other ancient and modern breach locations. This depositional model will document the different stages of inlet development, thus clarifying the processes and resulting deposits involved as a breach opens, evolves into a tidal inlet, and closes.

REGIONAL SETTING

Location of study area

The Delmarva Peninsula is located in the Coastal Plain geologic province in the mid-Atlantic region (Mixon, 1985) and is part of the states of Delaware, Maryland, and Virginia. It is bounded by the Atlantic Ocean to the east, Chesapeake Bay to the west, Delaware Bay to the north and the mouth of Chesapeake Bay to the south (Figure 7). The Delmarva Peninsula is a spit that has enlarged southward beginning in the Pliocene growing initially from sediments supplied by the Delaware Bay and the Susquehanna River Basin with sediments from the other large regional rivers (Potomac, Rappahannock, and James) contributing during the Quaternary (Hobbs, 2003). Therefore, the Delmarva Peninsula consists mostly of unconsolidated sediments, which have been derived from erosion of the Piedmont, Blue Ridge, and Valley and Ridge geologic provinces, which lie to the west (Hobbs, 2003).



Figure 7: Location map of the Eastern Shore of Virginia (after Chase-Dunn, 2015).

Fisher (1967, 1982) recognized four distinct coastal units along the Delmarva Peninsula as shown in Figure 8: “(1) an updrift spit or cusped foreland; (2) a slightly convex seaward headland; (3) a slightly concave-convex barrier island unit; and (4) one or more strongly concave units of barrier islands.”

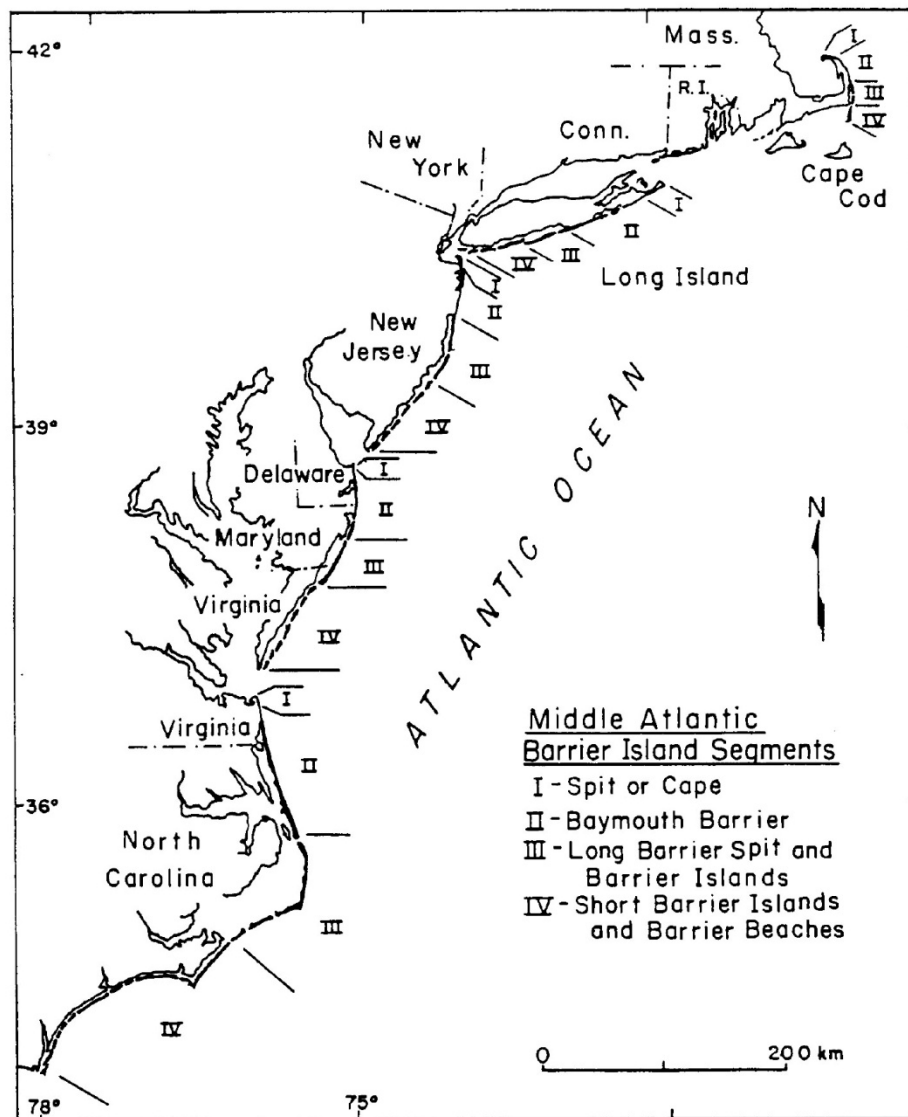


Figure 8: Middle Atlantic barrier island coastlines, showing sequences of barriers (from Fisher, 1982).

In 1994, Oertel & Kraft defined the Delmarva Coastal Compartment (Figure 9) as primarily Holocene in age and, like Fisher (1967, 1982), consisting of four coastal components, which they identify as : (1) cusped spit element, (2) eroding headland element, (3) “wave-dominated” spit and barriers, and (4) “tide-dominated” barrier islands. Cape Henlopen is the cusped spit element that is fed by northward longshore sediment transport, which is transporting sediment from the headlands element. South of the eroding headland element is Fenwick Island, a barrier spit, and 13 barrier islands (Oertel & Kraft, 1994). Oertel et al. (2008) detailed six geomorphic elements in the Delmarva Coastal Compartment (Figure10). From north to south, they are:

Element 1 – Cape Henlopen, which forms a left-hand spit complex;

Element 2 – Eroding headlands along the axis of the Delmarva interfluvium;

Element 3 – A right-hand spit that occurs between the Bethany Beach headlands and Ocean City, MD;

Element 4 – Assateague Island, which is a wave-dominated barrier island;

Element 5 – Mixed energy, tide-dominated barrier islands of antecedent origin that occur between Assateague Island and the mouth of the Chesapeake Bay; and

Element 6 – Fisherman Island, which is an emergent barrier island at the southern end of the Compartment.

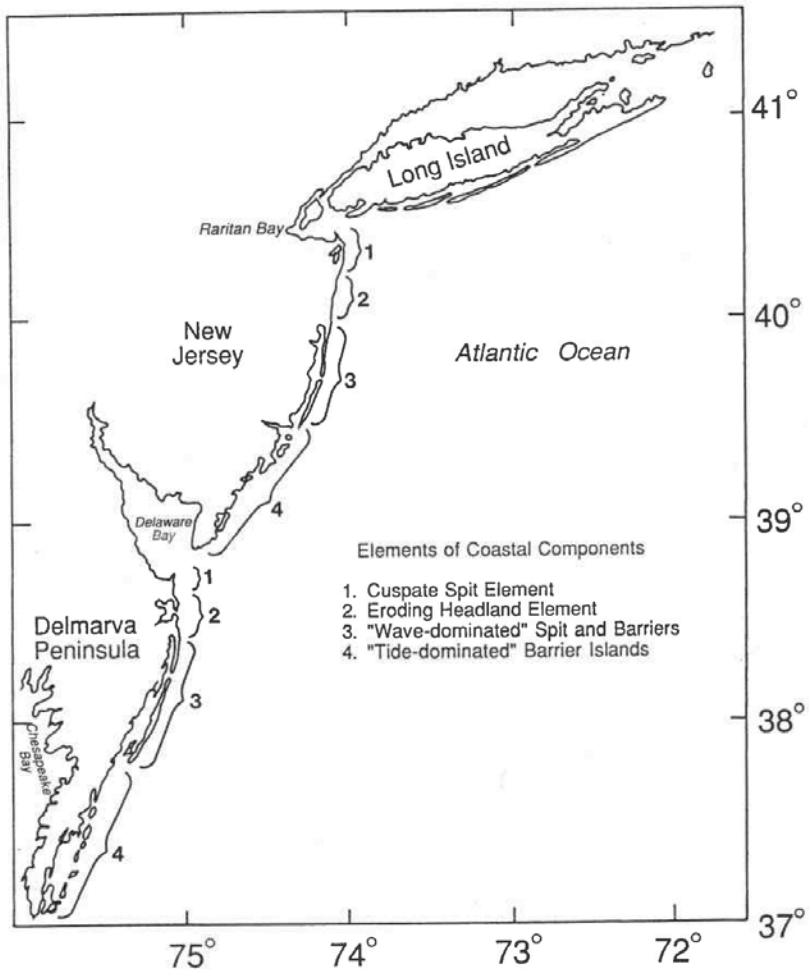


Figure 9: Map of the Delmarva Peninsula and New Jersey showing the locations of the elements of coastal compartments (from Oertel & Kraft, 1994).

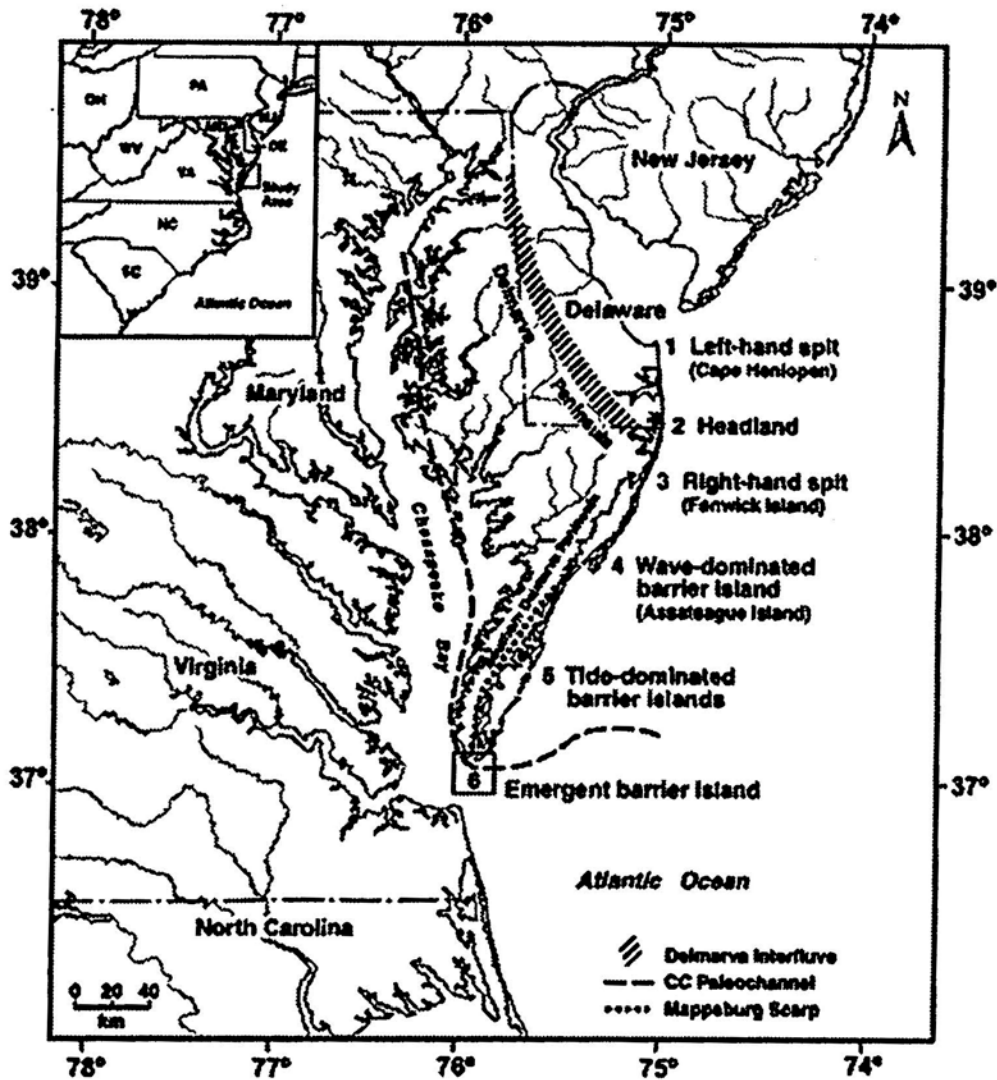


Figure 10: Location of the six geomorphic elements in the Delmarva Coastal Compartment (from Oertel et al., 2009).

Cedar Island lies within the Chincoteague Bight (also known as Chesapeake Bight), which is the exposed, open embayment between the southern end of Assateague Island and the northern end of Parramore Island (Leatherman et al., 1982; Demarest & Leatherman, 1985). Two intermediate sized capes, Cape Assateague to the north and Cape Parramore to the south, anchor the Bight. The linear distance between the two capes

has reduced by about 10 km from approximately 45 km around 1850 to approximately 35 km in 2007 because of the continued growth of Assateague Island to the south. Demarest & Leatherman (1985) describe the Chincoteague Bight as an “Arc of Erosion” (Figure 11), which extends from Wallops Island, south of Assateague Island, to the north end of Parramore Island and includes Wallops, Assawoman, Metompkin, and Cedar Islands. The curved shoreline continues to the northeast of Wallops Island and eventually crosses Assateague Island about 20 km north of Wallops. According to Goettle (1981), Assateague Island evolved during the Holocene by spit accretion. The Chincoteague Barrier (Figure 12, Stage I) transgressed landward as sea level rose. Assateague Island elongated towards the south by spit accretion as it eroded the Chincoteague Barrier (Figure 12, Stage II). During Stage III, another spit grew, which became what is now Piney Island, when inlet broke through the spit. Assateague Island continued to extend southwestward by additional spits forming. The tips of these spits were destroyed as the straight portion of Assateague migrated landward because of rising sea levels. The latest spit, Fishing Point, first formed between 1859 and 1887 and elongated rapidly until the 1920s. Accretion continued to the southwest on Fishing Point after that at a reduced rate (Goettle, 1981).

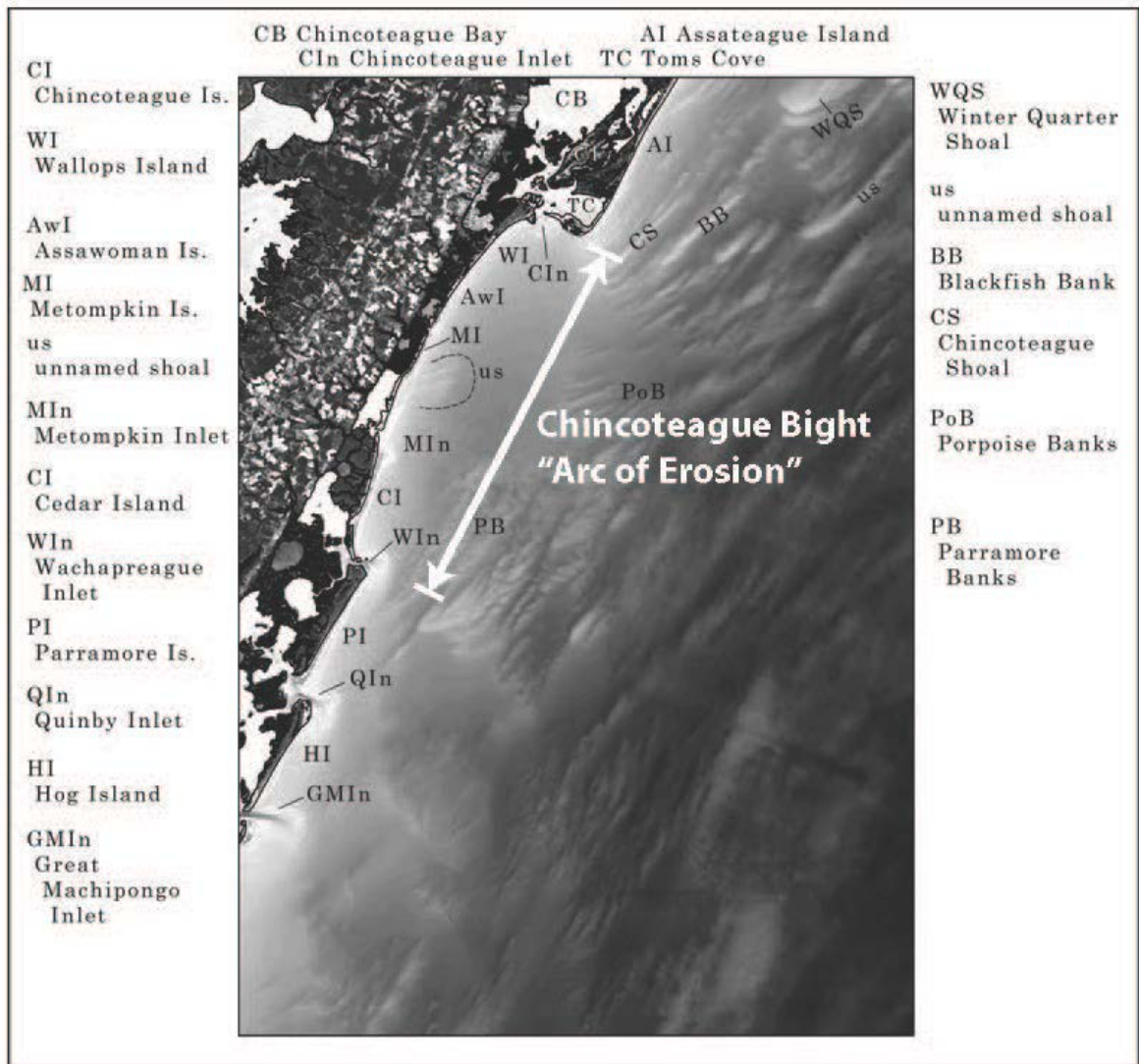


Figure 11: Location of the Chesapeake Bight – “Arc of Erosion” (after Krantz, 2015).

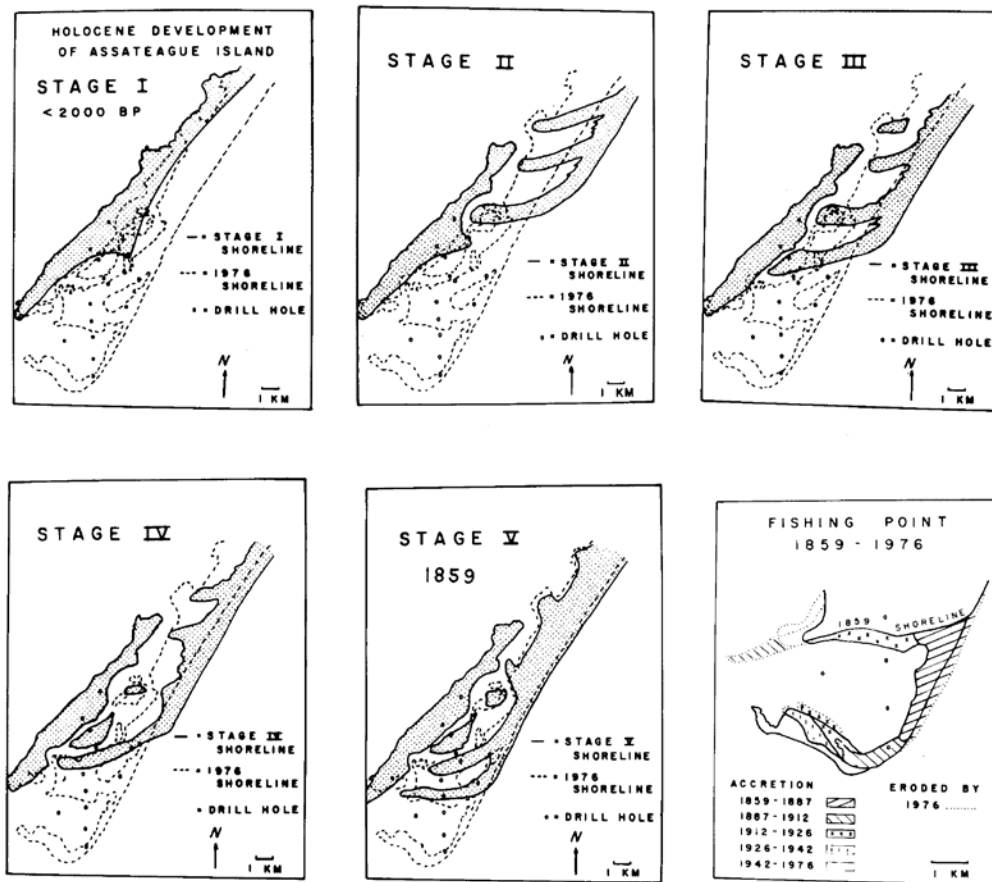


Figure 12: Evolution of Assateague Island (from Goettle, 1981).

The mid-Atlantic shoreline has a typical, dual-shoreline configuration (coast and estuary) that was formed by Holocene transgression with leading and trailing shores. The subaerial leading transgressive edge is now located along the inner mainland shore of barrier lagoons, while the trailing edge is located at the outer coast where it is formed of headlands, barrier islands, and spits. The configuration of the shoreline is controlled by the complexity of the flooded antecedent shore. The shorelines of Assawoman, Metompkin, and Cedar Islands have receded at a rate of four – five m/yr (Oertel et al., 2008).

Cedar Island formed in late Holocene as the Holocene transgression continued, which drove the coastline landward. Cedar Island and the other islands (Metompkin, Assawoman, and Wallops Islands) formed more recently than most of the more southerly islands on the Virginia Coast, which have undergone a longer history of landward migration (Oertel et al., 2008). Many of these southerly island systems are hypothesized to have formed in the middle Holocene, between 5,000 and 7,000 years ago (Oertel & Kraft, 1994).

Relative sea-level rise ranges from 3.41 mm/yr at Lewes, Delaware to 5.52 mm/yr at Wachapreague, Virginia to 6.02 mm/yr at the Chesapeake Bay Bridge Tunnel (NOAA, 2015b).

Barrier island morphology and physical processes along the Delmarva

Most of the morphologic features along the Delmarva coast remain in a relatively natural state. The variation of these features can be attributed primarily to the natural characteristics of a marine transgression (Oertel & Kraft, 1994). From Cape Henlopen to Ocean City Inlet, the coast is oriented N-S. From Ocean City Inlet to Cape Charles, the orientation is NE-SW. The barrier islands along the southern Delmarva Peninsula are mixed-energy, tide-dominated and have well-developed tidal inlets with deep inlet throats and large ebb-tidal deltas that extend one to seven km into the Atlantic. The barrier lagoons are shallow basins with a veneer of muddy-sand flats and deep tidal channels that form dendritic drainage patterns, which converge towards tidal inlets. Cross-island washover processes intermittently inject coarse-grained deposits into the lagoon where they mix with fine-grained lagoonal deposits (Oertel & Kraft, 1994).

Cedar Island is a low-profile, washover-dominated, transgressive barrier island that is migrating rapidly landward. It is 10.5 km long and lies at a slight angle to the mainland coast. The relief of the low dune fields behind the beach ranges from 1.8 to 2.5 m. Metompkin Inlet, at the north end, is flood-tide dominated and is in the process of closing (Rice et al., 1976).

Wachapreague Inlet, at the south end of Cedar Island, is an offset coastal inlet (Hayes et al., 1970; DeAlteris & Byrne, 1975). It is 1.5 km long, 445 m wide, and approximately 21 m deep (Richardson, 2012). It is dominated by ebb-flow with a scarcity of flood-tidal deposits and an extensive and well-studied ebb-tidal delta. Dawson Shoals, part of the ebb-tidal delta, are ephemeral and are related to sediment circulation within the inlet. The southern flank of Wachapreague Inlet, on the north end of Parramore Island, is kept at a steep slope and is subject to some erosion. The northern flank slopes more gently into the inlet due to the influence of sediment from the north (Richardson, 2012). Boone & Byrne (1981) suggest that ebb flow is directed to the northeast along the north flank whereas flood flow follows a more southerly path through the inlet.

Wachapreague Inlet has migrated south by 1 m/yr from 1852 to 1973 in response to the southerly littoral drift and has rotated counterclockwise from a southeast orientation to an easterly orientation (DeAlteris & Byrne, 1975). The migration has resulted in the north flank of Parramore Island losing material while the southern end of Cedar Island has gained sand forming a sand spit, which extends from the barrier island (DeAlteris & Byrne, 1973). The net drift from north of the inlet was estimated to be no more than 450,000 m³/yr (Byrne et al., 1973).

Sediments within Wachapreague Inlet reflect the environment in which they are deposited. The sediments in the deep inlet throat consist of a veneer of very coarse sediments (shell debris, cobbles, and gravels) overlying a stiff, cohesive sandy clay substrate (DeAlteris & Byrne, 1973). Surrounding the inlet throat, the sediments are well-sorted, medium-to-fine sand. In the areas both inside and outside the immediate vicinity of the inlet throat the sediments consist of very fine silty beds (DeAlteris & Byrne, 1973).

Morton & Donaldson (1973) collected sediment cores from Wachapreague Lagoon that indicated that the Holocene sediments in the lagoon were underlain by Pleistocene-aged barrier and offshore marine deposits. These sediments are reworked from the barrier islands. They then migrate through the inlets and become trapped in the lagoon. Deposition of sediments in the lagoon was influenced by the underlying Pleistocene surface. Wachapreague Inlet has remained relatively stable and lies within the antecedent drainage of the Pleistocene (Figure13) (Morton & Donaldson, 1973).

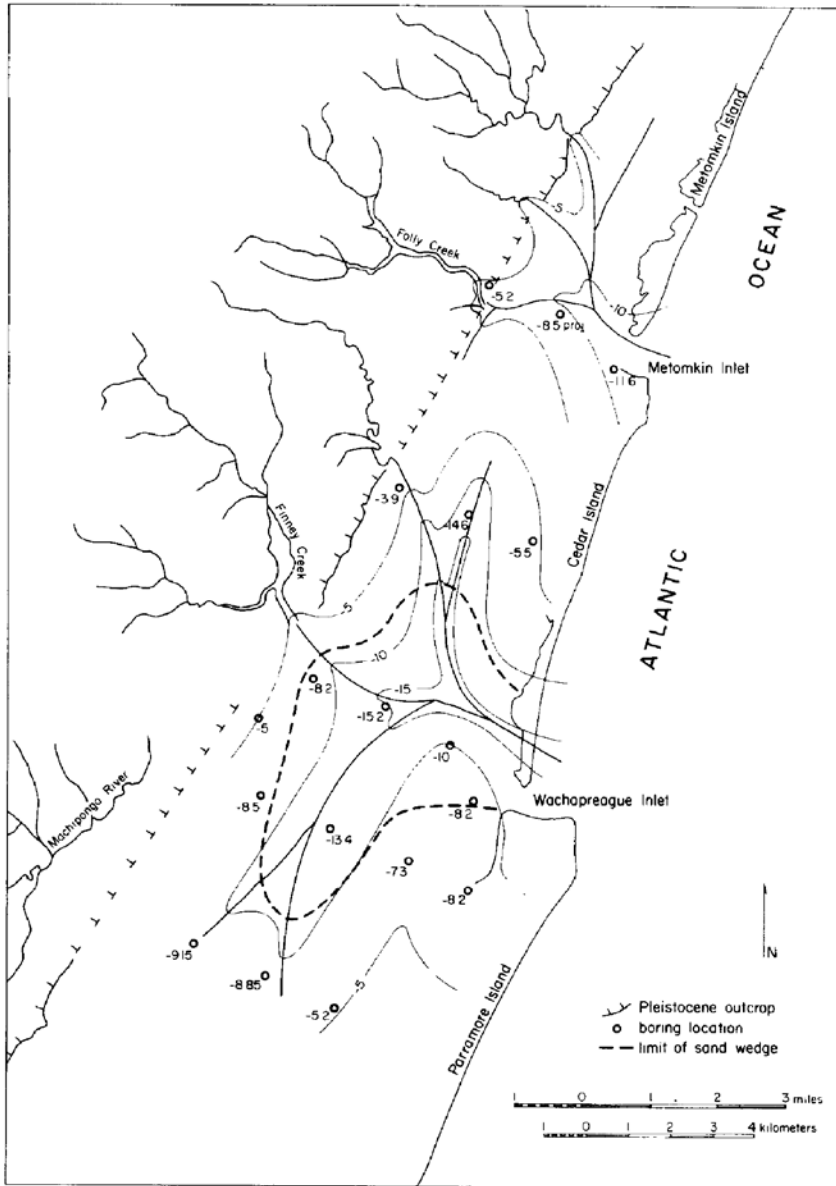


Figure 13: Map of Holocene-Pleistocene unconformity showing the position of present-day drainage and tidal inlets in relation to Pleistocene drainage around Cedar Island, Virginia. Depths are in meters below mean sea level. (from Morton & Donaldson, 1973).

The Mid-Atlantic coast has been indirectly affected as sea level and sedimentation rise and fall with glacial advances and retreats during four major periods of glaciation.

Regionally, the relative sea-level rise is high along the Mid-Atlantic coast at a rate of 3 -4

mm/yr, where tidal ranges are high and coastal subsidence is occurring (Hapke et al., 2010). The Mid-Atlantic shore is undergoing both long-term and short-term net rates of change of -0.6 m/yr and -0.3 m/yr, respectively (Hapke et al, 2010). The results of their study show that 67 percent of the Mid-Atlantic is undergoing long-term shoreline change and 42 percent is undergoing short-term shoreline change (Hapke et al., 2010).

Historically, the Virginia portion of the Delmarva Peninsula has been eroding more rapidly, at a rate of up to 10 m/yr, than the rest of the Mid-Atlantic coastline, at a rate of approximately 1.5 m/yr, even though this part of the Delmarva Peninsula is relatively undeveloped (Nebel et al., 2013).

The group of barrier islands that includes Cedar Island belongs to have been experiencing parallel beach retreat in historical times (Leatherman et al., 1982). This area has been starved of sediment since Fishing Point formed at the southern tip of Assateague Island. Fishing Point acts as a sediment trap for barrier islands south of it (Leatherman et al, 1982).

Cedar Island has experienced a long-term shoreline retreat of -5.5 m/yr for the period 1852 – 2007 and a short-term shoreline retreat of -15.4 m/yr for the period 2007 – 2010 (Richardson, 2013).

The coast along the U.S. Atlantic has unequal semi-diurnal tides. The tide level along the Virginia portion of the Delmarva Peninsula is classified as low mesotidal with an average spring tidal range of 1.4 m (Byrne et al., 1974). Tidal ranges of the estuaries behind the barrier islands are nearly equivalent to the ocean tides and lag behind them by approximately 15 minutes (Oertel & Kraft, 1994). The tidal prism that flows through

Wachapreague Inlet was determined to be $6.09 \times 10^7 \text{ m}^3$ in 2011 and has increased from $2.33 \times 10^7 \text{ m}^3$ in 1852 (Richardson, 2012).

During the summer, the waves along the Delmarva Peninsula are generally from the southeast and during the winter, they are generally from the northeast with a mean annual wave height of 0.55 m (Nebel et al., 2013). Winds are moderate at about 4.5 m/s and do not play an important role in eroding the barrier beaches. Summer conditions are conducive to beach progradation on the upper shoreface, except during storms (Oertel & Kraft, 1994).

Net longshore sediment transport moves an estimated $115,000 \text{ m}^3$ to $460,000 \text{ m}^3$ of sand per year to the south with an estimated $300,000 \text{ m}^3$ deposited at Fishing Point spit on the southern end of Assateague Island (Oertel & Kraft, 1994).

Two distinct weather systems produce storms that affect the Delmarva Peninsula: tropical cyclones (tropical storms and hurricanes) and extratropical cyclones (northeasters). Hurricanes are cyclonic, tropical systems that move into the area from the south during the summer and early fall.

Northeasters are low-pressure, anti-cyclonic storms that occur during the fall, winter, and spring. They generally move along the coast and produce strong, south-flowing longshore currents that can move large quantities of sediment. Northeasters are more frequent and larger in magnitude than hurricanes and, therefore, cause more damage to the shorelines of the Virginia barrier islands (Davis & Fox, 1974; Davis et al., 1993; Zhang et al., 2002). Also, northeasters can linger off the coast for a while allowing the build-up of a substantial storm surge, especially if it lingers for several tidal cycles. The

worst storm of the 20th century along the Delmarva Peninsula was the Ash Wednesday storm in March, 1962. It lingered through five high tides over three days leading to a storm surge that caused 2 m of water to cover parts of the town of Chincoteague, Virginia. Winds were as high as 110 km/hr and waves as high as 12 m were experienced along the Delmarva coastline (NOAA, 2014).

Although not as devastating as the Ash Wednesday storm of 1962, the worst storms of the 21st century along the Delmarva have been Hurricane Isabel (September 18, 2003), Tropical Storm Ernesto (September 1, 2006), Hurricane Irene (August 27, 2011), and Hurricane Sandy (October 28 – 30, 2012) (NOAA, 2015d).

Byrnes & Gingerich (1987) studied the effects of Hurricane Gloria (September 27, 1985) on Metompkin Island, Virginia, which lies just north of Cedar Island. Ten profiles were established along the shoreline of Metompkin Island. They measured the change in profile to determine the magnitude of cross-island sediment transport from May to October, 1985. They found that the northern beach segments migrated landward at -18.53 m/yr while the southern beach segment migrated more slowly at -4.15 m/yr (Byrnes& Gingerich, 1985).

On Cedar Island, tropical cyclone frequency and shoreline migration rates appear to be linked. In a study by Nebel et al. (2013), an increase in tropical cyclone frequency affected the Atlantic coast of the Delmarva beginning in 1980 was correlated with the increase in the rate of shoreline retreat on Cedar Island between 1980 and 2006. The Cedar Island ocean shoreline underwent a retreat rate of -5.5 m/yr from 1852 until 2007, which increased to -15.4 m/yr from 2007 until 2010 (Richardson, 2012).

Quaternary Geology of the Delmarva Peninsula

The Delmarva Peninsula formed during the Pleistocene responding to coastal processes and major cycles of sea-level rise and fall. During Pleistocene periods of high sea-level, the Delmarva Peninsula lengthened and formed a major barrier spit. Ancient, now-filled channels that underlie the Chesapeake Bay and cross beneath the Delmarva Peninsula developed during the Quaternary and, possibly, very late Tertiary lowstands of sea level. As the Delmarva Peninsula lengthened, the more northerly channel systems were diverted progressively southward. The Virginia portion of the Delmarva Peninsula formed by sea-level highstands that were followed by subsequent lowstands, which modified the steep flanks of the previous highstands to resemble wave-cut scarps found on the western shore of the Chesapeake Bay (Hobbs, 2004). Mixon (1985) identified nine scarps and shorelines in this portion of the Delmarva Peninsula.

In the southern Delmarva Peninsula, the oldest Pleistocene formation is the Omar Formation, which unconformably overlies the Yorktown Formation of Pliocene age (Table 1). In the northern and central Delmarva Peninsula, the Omar Formation represents a single transgressive-regressive cycle (Owens & Denny, 1979), has the characteristics of barrier and/or nearshore shelf deposits and consists of sandy, silty, and gravelly deposits ranging about 6 to 27 m in thickness (Mixon, 1985). Further, Mixon (1985) found that the Accomack Member of the Omar Formation (up to 24 m thick) consists of sand, gravel, silt, clay, and peat and represents an interglacial highstand that occurred before the Sangamonian interglacial period when sea level was 12 to 14 m

above present. Grott & Jordan (1999) found evidence in Delaware that the Omar Formation was deposited during at least three interglacial (5e, 9, and 11) and two cold oxygen-isotope stages. Within the Omar Formation lies evidence of the Exmore paleochannel that represents regressive stages and are probably cold oxygen-isotope stages 12 and 10 (Toscano & York, 1992). The Omar is bounded upward by an unconformity related to the Eastville paleochannel, which occurs at oxygen-isotope stage 6. Stratigraphically overlying the Omar Formation is the Joynes Neck Formation, which consists mainly of loose, fine to coarse, yellowish-gray quartz sand interspersed with beds or stringers of pebbly sand or sandy gravel. In the type locality, the Joynes Neck Formation is 9 m thick. Disconformably overlying the Joynes Neck Formation is the Wachapreague Formation, which consists of two distinct lithic units. In the type section, the lower unit consists of clayey and silty, fine to very fine gray sand and clay-silt and is approximately 6 m thick. The upper lithic unit is 5.2 m thick and consists of medium to very coarse gravely sand. The pebbles are typically 1 in or more in their largest dimension and are mainly black chert and quartz (Mixon, 1985).

Table 1: Temporal relationships of the strata in the eastern Virginia part of the Central Delmarva Peninsula (after Mixon, 1985; after Hobbs,2003).

Geologic Period	Stratigraphic Name
Holocene	
Pleistocene	Wachapreague Formation
	Joynes Neck Sand
	Omar Formation (Accomack Member)
Pliocene	

The Quaternary geology of the Delmarva Peninsula begins in the late Pliocene when the general geography of the Chesapeake Bay region is dominated by deltas of the ancestral James, Potomac, Susquehanna, and Delaware Rivers, tidal-flat deposits related to the York and Rappahannock River systems, and a series of barrier islands that protected the Virginia coastline from higher energy marine conditions (Figure14) (Hobbs, 2003). A marine transgression occurred then that resulted in deposition of shallow marine and deltaic sediments (Figure15) (Hobbs, 2003). By the end of the Pliocene, the general geography of the Delmarva Peninsula emerges in Figure16 when the major river systems are established during a relative sea-level highstand and the core of the Delmarva was

formed by the reworking of the deltaic sediments associated with the ancestral Susquehanna and Delaware Rivers (Hobbs, 2003). During a late Pliocene sea-level lowstand (Figure 17), the major river systems cross the wide coastal plain (Hobbs, 2003). Figure 18 shows the growth of the Accomack member of the Omar Formation, which is thought to have formed as the Accomack Spit (a barrier spit) during the middle to late Pleistocene (oxygen isotope Stage 13 or 11) (Hobbs, 2003). The western shore of the proto-Chesapeake Bay north of the Rappahannock River was sheltered from oceanic processes while the shoreline to the south remained open to oceanic processes (Hobbs, 2003). The regression that occurred during oxygen isotope Stage 14 or 12, made the Susquehanna River and the Potomac River merge and flow south of the Accomack Spit to the ocean through the Exmore Channel, instead of flowing across the coastal plain (Figure 19) (Hobbs, 2003). Subsequently, the Exmore Channel was filled in during a Stage 11 or 9 transgression and the barrier spit was extended that resulted in the Susquehanna-Potomac River systems combining with the Rappahannock River and flow through the Belle Haven Channel (Figure 20) (Hobbs, 2003). The initial growth of the Nassawadox Spit occurred during the Stage 7 or 9 highstand (Figure 21) (Hobbs, 2003). The following transgression, which occurred during Stage 6 or 8, the major river systems would be forced to move south around the southern end of the Nassawadox Spit to flow through the newly formed Eastville Channel before flowing across the coastal plain (Figure 22) (Hobbs, 2003). During Stage 7 and/or 5, with sea level 4 to 6 m above present level, the Delmarva Peninsula lengthened to near its present length and sediments of the Wachapreague Formation and others, were deposited and widened the peninsula (Figure

23) (Hobbs, 2003). Between Stages 4 and 2 lowstand, the major channels joined together into the Cape Charles Channel in the late Pleistocene (Figure 24) (Hobbs, 2003). The most recent rise in sea-level, which began about 18,000 years ago resulted in the Delmarva Peninsula's current geographic position (Hobbs, 2003). The Cape Charles Channel has moved south and west by about 10 km because of sediment that has been deposited at the mouth of the Chesapeake Bay in a continuation of the processes that created the Delmarva Peninsula (Figure 25) (Hobbs, 2003).

In recent literature, information on crustal displacement of mantle material due to continental ice-sheet growth creating a forebulge, sometimes with as much as tens of meters of uplift, has led to a re-evaluation of the causes of relative sea-level rise along the US East Coast (Scott et al., 2010). It is speculated that "large portions of the eastern U.S. will subside several tens of meters more due to forebulge relaxation" (Scott et al., 2010, p. 175). OSL (optically stimulated luminescence) dating provided a re-interpretation of late Pleistocene stratigraphy in the Virginia coastal plain with the region being strongly influenced by glacioisostatic effects. This leads to a new understanding of the relative sea-level during the deposition of the Wachapreague Formation, which indicates that sea level was lower during this time than originally thought (Scott et al., 2010).

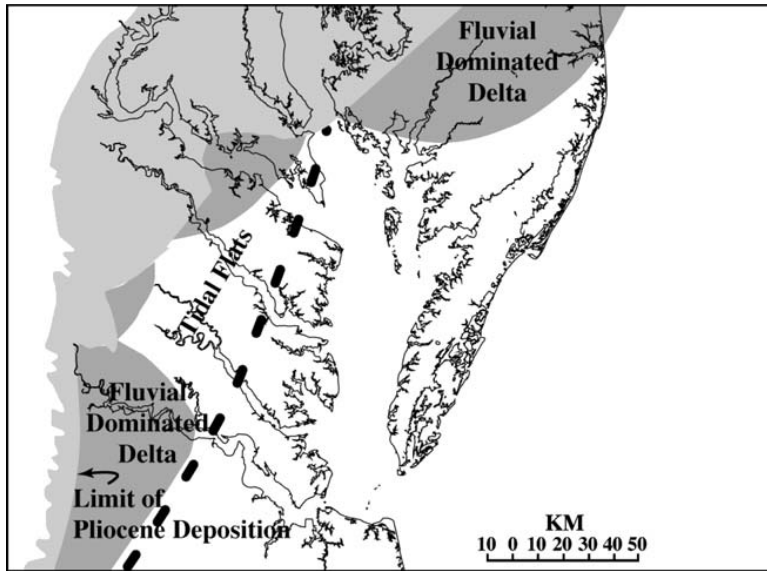


Figure 14: General geography of the Chesapeake Bay region during the late Pliocene. This is displayed over the outline of the modern geography of the Chesapeake Bay. The approximate location of barrier islands is shown by a dashed line. Coastal plain sediments are shown in light gray and deltaic sediments are shown in dark gray. (from Hobbs, 2003)

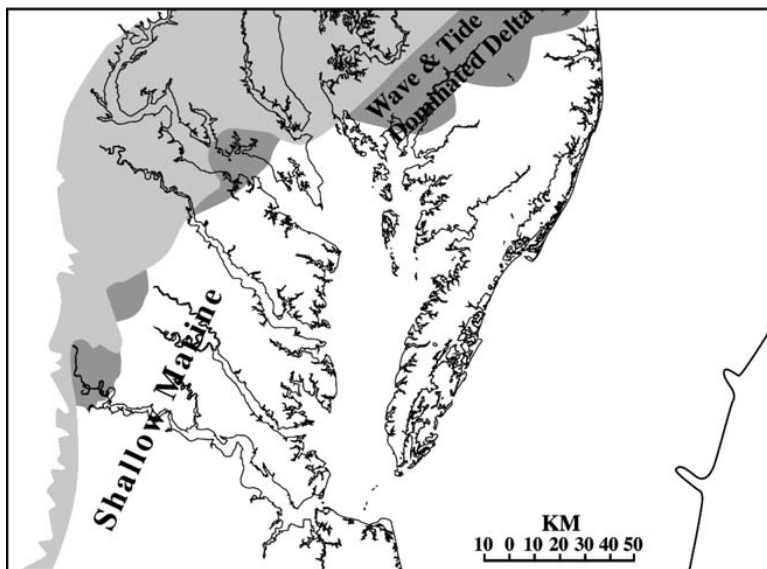


Figure 15: Geographic setting at the time of maximum transgression prior the end of the Pliocene. (from Hobbs, 2003)

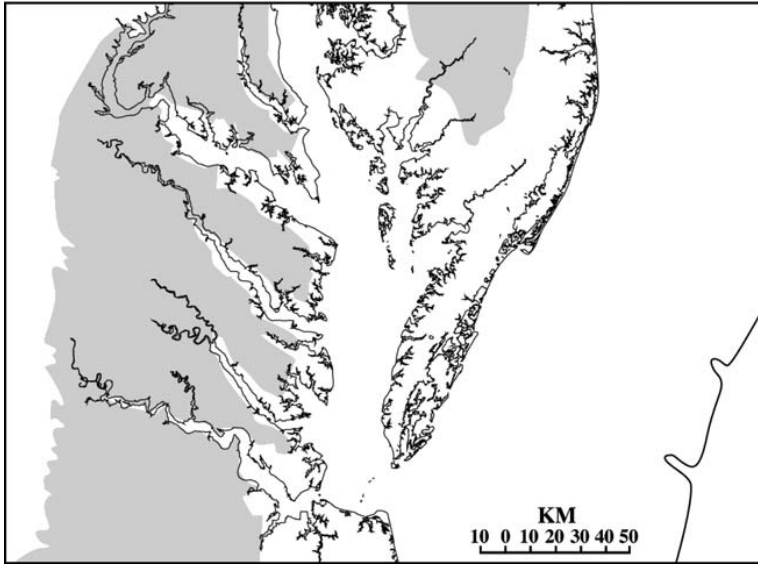


Figure 16: General geographic setting showing the emergence of the coastal plain in gray during a relative highstand at the end of the Pliocene. (from Hobbs, 2003)

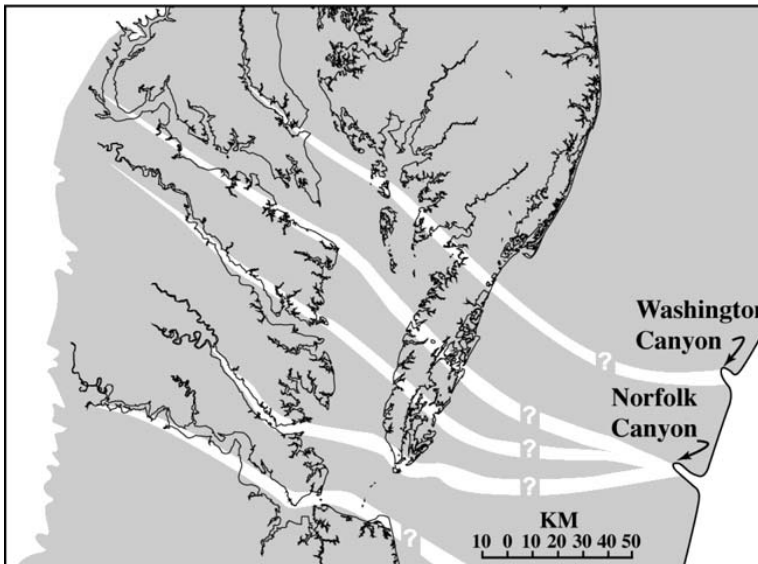


Figure 17: General geographic setting a late Pliocene lowstand. The coastal plain is shown in gray with the major rivers crossing it. The location of the river channels is highly speculative. (from Hobbs, 2003)

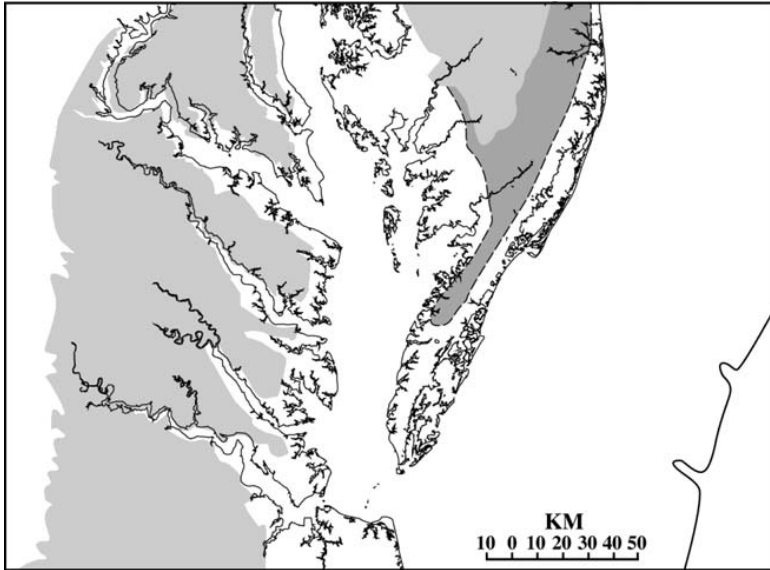


Figure 18: The first indication of the proto-Chesapeake Bay resulting from the growth of the Accomack Spit (Accomack Member of the Omar Formation) in light gray and contemporaneous deposits, in dark gray, east of the pre-existing landforms. (from Hobbs, 2003)

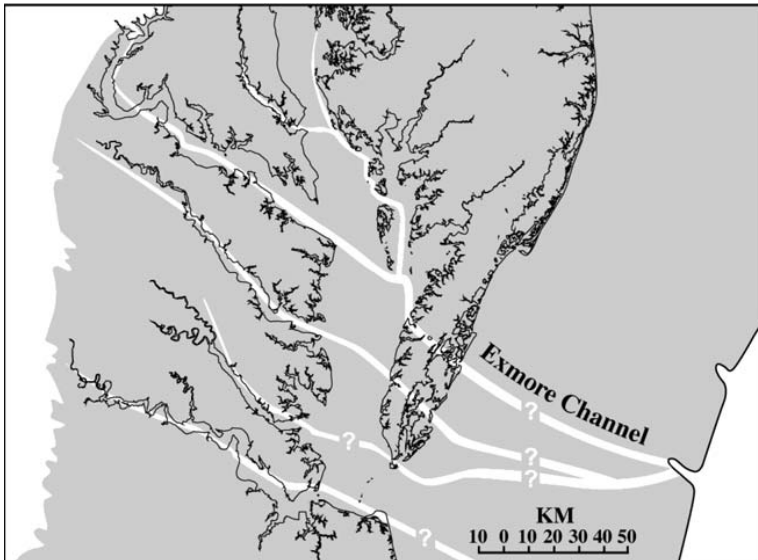


Figure 19: General geography of the Chesapeake Bay region showing the merging of the Susquehanna and Potomac river systems to form the Exmore Channel that crossed south of the Accomack Spit during oxygen isotope Stage 12 or 14. (from Hobbs, 2003)

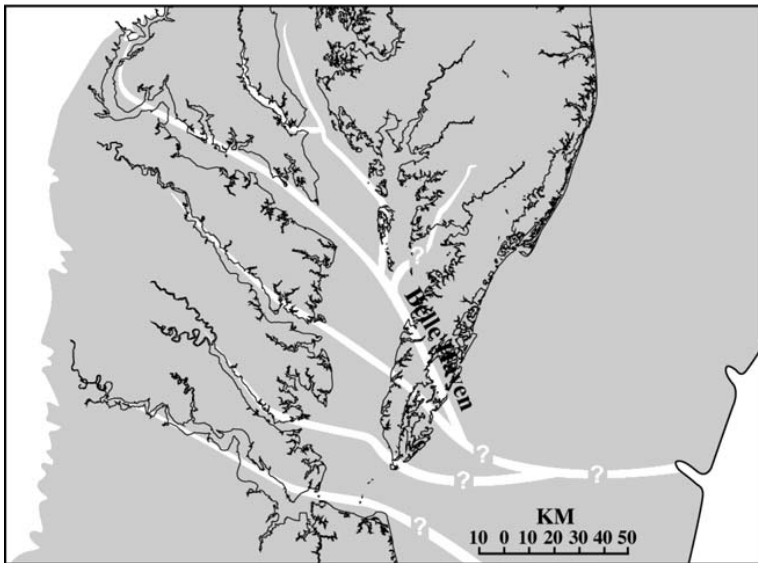


Figure 20: General geography of the Chesapeake Bay region during oxygen isotope Stage 10 showing the Belle Haven Channel that connected the Susquehanna-Potomac system with the Rappahannock during Stage 11. This resulted from the blockage of the Exmore Channel by the Accomack Spit extending during Stage 11. (from Hobbs, 2003)

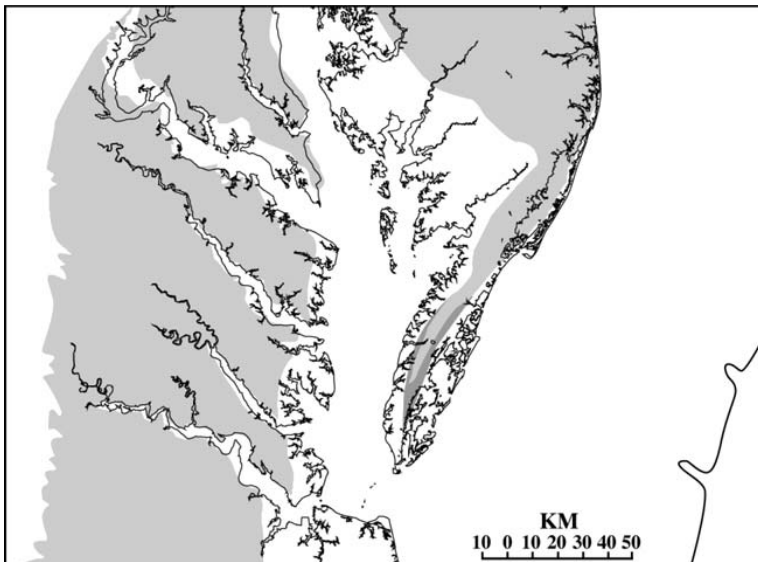


Figure 21: Initial growth of the Nassawadox Spit during Stage 9(?). (from Hobbs, 2003)

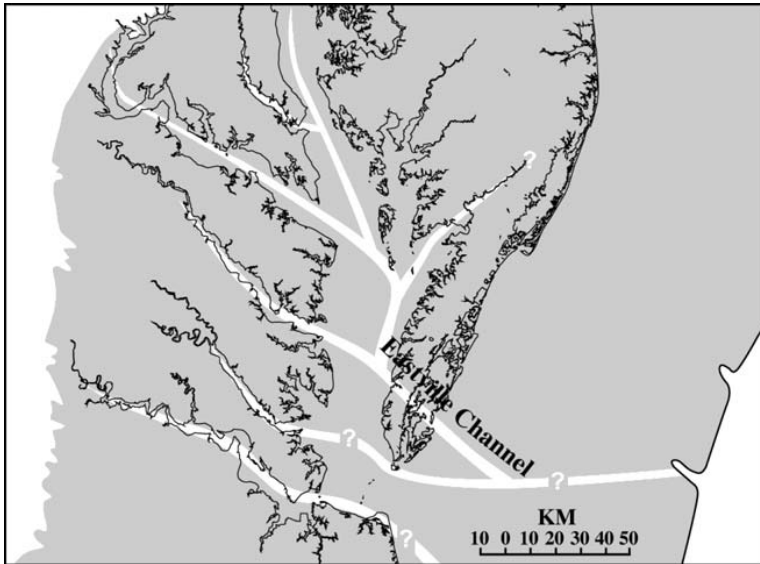


Figure 22: During Stage 8 or 6, the Eastville Channel formed. (from Hobbs, 2003)

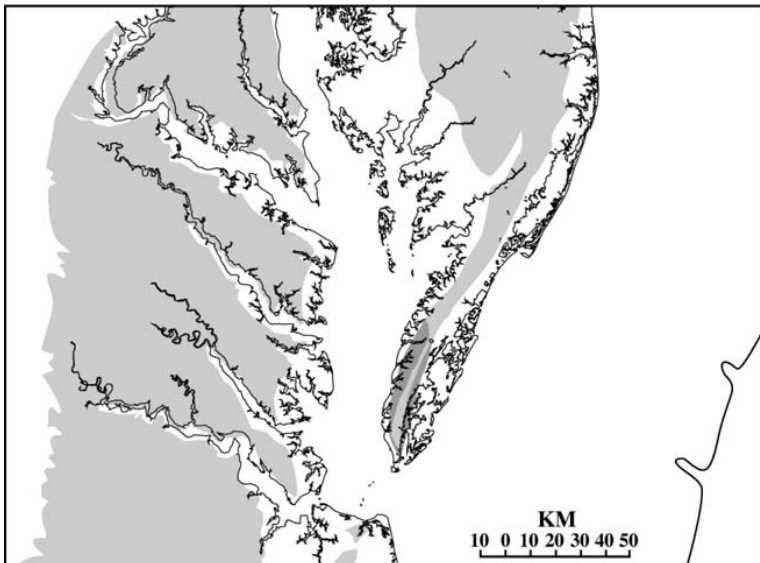


Figure 23: General geography of the Delmarva Peninsula during Stage 7 and/or Stage 5 with sea-level 4 – 6 m above present sea-level. (from Hobbs, 2003)

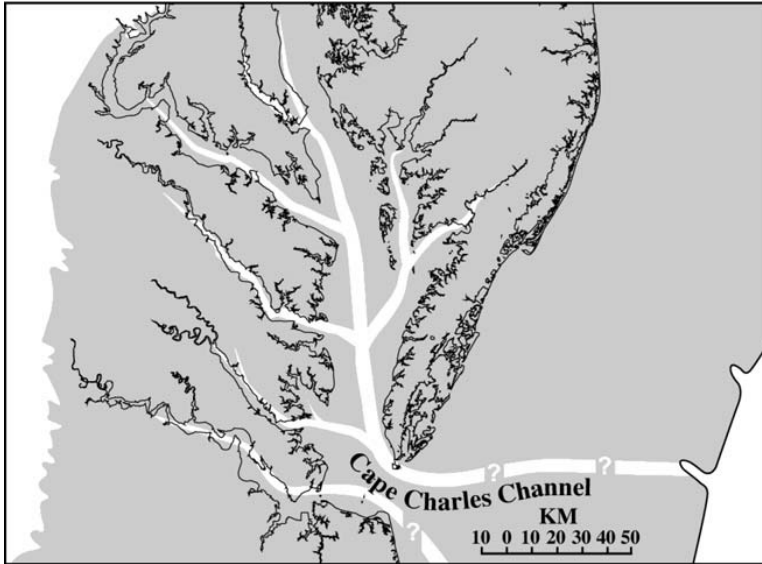


Figure 24: General geography of the Delmarva Peninsula during Stage 4 -2 lowstand. (from Hobbs, 2003)

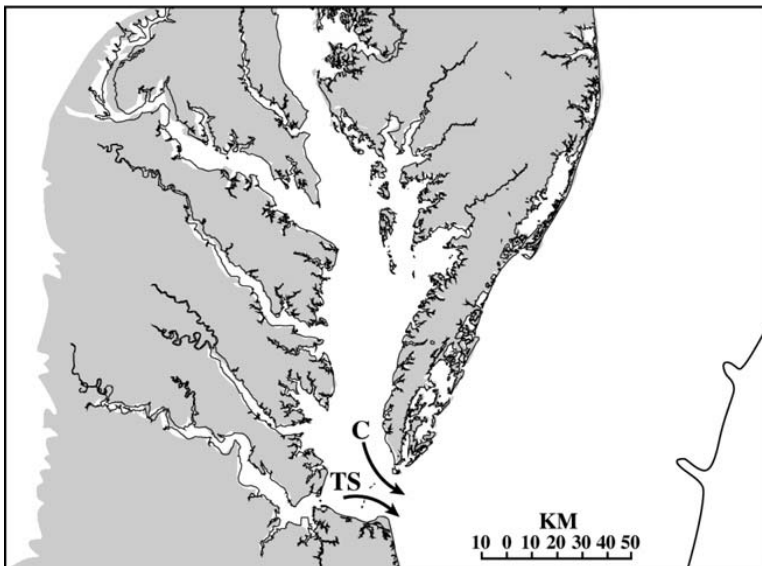


Figure 25: General geography of the Delmarva Peninsula as it exists today. "C" marks the approximate location of the Chesapeake Channel and "TS" marks the approximate location of the Trimble Shoals Channel. (from Hobbs, 2003)

The Piedmont, Blue Ridge, and Valley and Ridge geologic provinces from New York to Virginia were drained by rivers that passed through ancient, now-filled channels to be emptied into the Atlantic Ocean (Hobbs, 2003). These channels are referred to as the Exmore, Belle Haven, Eastville, and Cape Charles from oldest to youngest (Hobbs, 2003). They step in that order from north to south and cross under the present location of the Delmarva Peninsula (Hobbs, 2003). The Delmarva Peninsula formed during the Quaternary with the more northerly channel systems being diverted progressively southward as the major barrier spit lengthened (Hobbs, 2003).

CONCEPTS AND PREVIOUS STUDIES

Barrier islands

Barrier islands are elongate, shore-parallel islands that are composed predominately of unconsolidated sediments. They protect land masses that are adjacent to them and are separated by wetland environments (Davis, 1994). The mid-Atlantic coast is a broad, gently sloping coastal plain on a trailing edge continental margin. It is a favorable setting for barrier island formation especially during periods of sea-level rise, which is occurring during the current Holocene transgression (Nummedal, 1983).

The morphology of barrier islands depends on the influences of wave and tidal processes, climate, sediment supply, and geologic framework (Riggs et al., 1995). Thus, barrier islands along coasts that are dominated by wave processes are long and narrow with a few active inlets, whereas along coasts that have significant tidal influences they tend to be short and stubby and be separated by more permanent tidal inlets. Mixed-energy coasts lie in between these two and exhibit a relatively large tidal prism that results in the formation of a substantial ebb-tidal delta (Figure 26) (Davis, 1994).

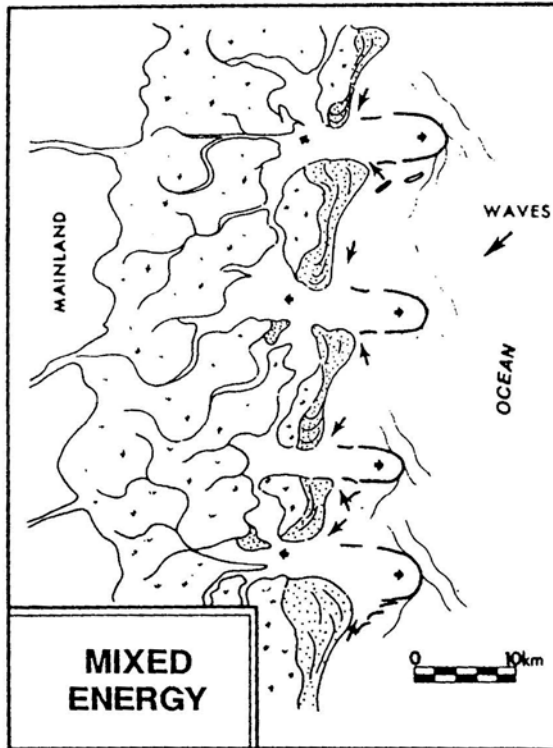


Figure 26: Sketch map of mixed-energy barrier island (from Davis, 1994).

All barrier-island systems consist of six major sedimentary environments: mainland, backbarrier lagoon/tidal marsh, barrier island, barrier-island platform, inlet and inlet shoals, and shoreface (Figure 27) (Oertel, 1985; Davis, 1994). The barrier island environment is subdivided into three sedimentary environments: dunes, washover fans, and beach (backshore and foreshore) (Davis, 1994). The beach, which consists of the area from the base of the dunes to mean low tide line, is dominated by hydrodynamic processes including wave action, rip currents, tidal currents, and storm-induced flow (Davis, 1994; Swift, 1975). The mainland is separated from the barrier island by the backbarrier lagoon/tidal marsh, which consists of intertidal and subtidal environments

(Davis, 1994). The inlet and inlet shoals are important sediment sinks in the barrier island system. The inlet system consists of three sedimentary environments: flood-tidal delta, inlet channel fill, and ebb-tidal delta (Davis, 1994).

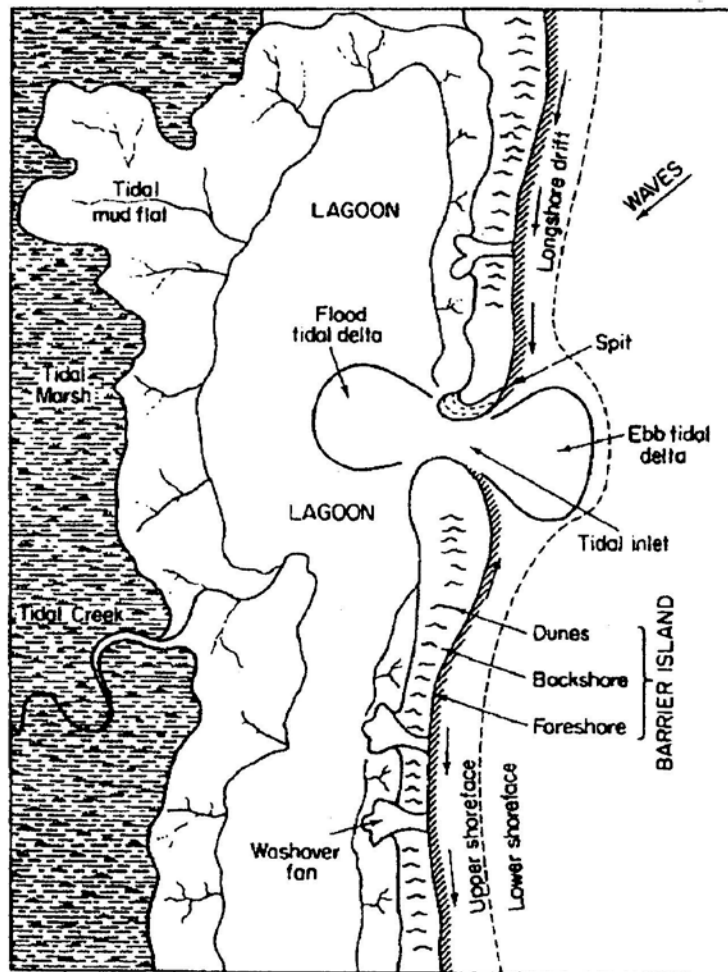


Figure 27: General sketch of the barrier island complex showing the major sedimentary environments (from Davis, 1994).

Washover processes and deposits

Washover deposits are common features along barrier-island coastlines where hurricanes and northeasters occur. Washover deposits are the result of storm surge cascading across the barrier island. These deposits usually consist only of sediment deposited on the barrier island (Leatherman, 1976). If the storm surge is strong enough to carry sediment across the island to the estuary, sediment can also be deposited subaqueously to form a washover delta. If the storm surge breaches the dunes on the foreshore, a constricted channel is formed. After passing through the dunes, the washover deposits on the bayside of the dunes then spread out and form a washover fan (Dickinson et al., 1972).

Washover sediments typically are deposited on a scoured surface (Andrews, 1970). A thin, basal layer of shells forms the initial deposit during the storm (Dickinson et al., 1972). Overlying this layer are “horizontally bedded, alternating layers of quartz sand, shell fragments, and heavy minerals that reflect changing hydraulic competence and tidal variations during the storm surge” (Kochel & Dolan, 1986, p. 902). On their distal ends, the washover deposits “interfinger with beach, dune, barrier flat, tidal flat, and in some cases lagoonal beds” (Dickinson et al., 1972, p. 202). Whether or not these deposits are preserved in the stratigraphic record is dependent on bioturbation, thickness, storm frequency, and sea-level change. Normal-grade sand deposits are the most common subfacies that are preserved followed by bioturbated muddy sands and the undifferentiated muddy sediments (Sedgewick & Davis, 2003). Figure 28 displays the generalized stratigraphy of washover deposits.

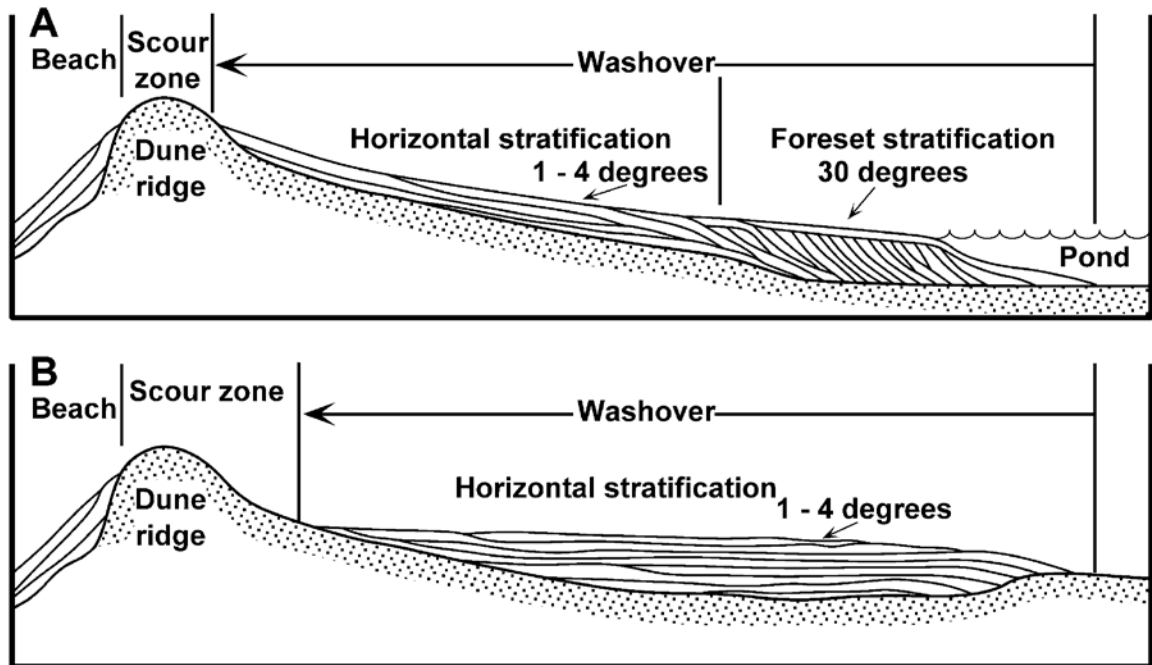


Figure 28: Generalized cross-section of washover deposits; A – subaqueous deposition showing foreset laminae; B – supratidal deposition showing only horizontal stratification (from Sedgwick & Davis, 2003).

Washover deposits may have graded bedding, reverse grading, or no grading. In general, washover deposits have abundant shells, are relatively free of mud, and consist of quartz sand with heavy minerals. Table 2 summarizes the five subfacies that were delineated by texture, composition, and bioturbation as identified in Sedgwick & Davis (2003).

Table 2: Subfacies of washover deposits and their characteristics and location (from Sedgwick & Davis, 2003).

Subfacies	Characteristics	Location	Problems
Stratified sand	Unit contacts visible	Proximal to mid-fan, most common in proximal	May show aeolian influence
	Planar or landward-dipping sand Laminae of shell debris and heavy minerals throughout Variable composition, enriched shell and heavy minerals if source material permits May have basal lag of shell or heavy minerals Low mud content	Generally supratidal	If land direction not known, may resemble shoreface
Normal-graded sand	Unit contacts visible	Channel throat, proximal, and mid-fan	Might be bioturbated laminated sand subfacies
	Coarse basal lag from scour Bioturbated or unstratified upper unit Variable composition, shell material abundant where source material permits Mud content increasing at unit top	Supra- to subtidal	
Reverse-graded sand	Unit contacts visible Coarsening-upward units from flow sorting or reworking Variable composition, heavy mineral-enriched base where source material permits	Proximal fan	May show aeolian influence
Bioturbated muddy sand	Unit contacts visible	Distal fan	Difficult to interpret as washover without additional information
	Mottled non-stratified sand Moderate shell and heavy-mineral content, non-stratified	Inter- to subtidal	
Undifferentiated washover sediments (?)	Unit contacts not visible	Distal fan	Difficult to interpret as washover without additional information
	Mottled or peaty sediment Moderate shell or heavy-mineral content, non-stratified	Inter- to subtidal	

The sedimentary characteristics of washover deposits are summarized in Table 3.

Table 3: Sedimentary characteristics of washover deposits (after Heward, 1981; Schwartz, 1975).

WASHOVER DEPOSITS

Composition: locally derived detritus from shoreface, beach, and foreshore that consists of sand, carbonate particles, heavy minerals and typically mud-free.

Sedimentary structures: gently landward dipping parallel lamination predominant, landward oriented tabular and trough cross-stratification; inverse and normally graded laminae; faunal bioturbation and plant rootlet disturbance.

Fauna: mixed marine and lagoonal.

Geometry: elongate or semicircular, tabular to prism shaped, typically interbedded with lagoonal deposits

Paleocurrents: parallel lamination and cross-stratification oriented landward dominantly perpendicular to shoreline trend.

Preservation potential: transgressive shorelines – high because of relatively low position in transgressive sequence; regressive shorelines – high but may undergo subaerial modification, generally poorly developed except during the early stages of regressions.

Definition of breach vs. tidal inlet

The terms breach and tidal inlet have been used interchangeably. A breach is a coastal geomorphic feature that forms in response to the impact of a storm. In general, it remains open from several weeks to months before closing as a result of longshore sediment transport. A breach can become a tidal inlet when it captures enough tidal prism to remain open for years or longer (Seminack & McBride, 2015). An ephemeral tidal inlet remains open for several years before it closes due to longshore sediment transport but subsequently reopens repeatedly.

Barrier island breaches

Tidal inlets and washover deposits are both formed by the same process, a storm surge that occurs during a storm. The storm surge causes water to flow across the barrier island, which moves water and sediment from the ocean side to the estuary side. As the surge loses velocity, the entrained sediment is deposited on the barrier. If the surge is strong and large enough, it will carry the sediment into the waters of the estuary and form a subaqueous washover delta. Tidal inlets, which start as breaches in the barrier island, are usually formed by one of two mechanisms: landward-directed surge or seaward-directed surge. During landward-directed surge, the beach ridge is overtopped where the barrier island is narrow and extensive tidal flats are not present. Higher water velocities must occur, which result in more sediment being transported to the waters of the estuary. Thus erosion occurs across the barrier island resulting in a breach. During seaward-directed surge, the water in the estuary increases during the storm. As the storm passes, the wind direction changes and the level of the water on the ocean side of the island

recedes. This causes the water in the estuary to rush back across the island, thus creating a breach. If the breach is large enough, it may become a tidal inlet for a few hours to years. It may become a permanent tidal inlet. A breach remaining open and becoming a tidal inlet is dependent upon the breach capturing enough tidal prism where water is able to pass through the channel with enough velocity during each tidal cycle to keep sediment from closing the breach (Pierce, 1970; Andrews, 1970).

Whether a tidal inlet or washover fan occurs depends on several factors that are present at the time of the storm. “These factors include topography of the barrier, the lagoon floor, and the near-shore sea bottom; the sea-state conditions; the type of storm generating the surge; and the direction, either from the lagoon or the sea, from which the surge comes.” (Pierce, 1970, p. 230)

Tidal deltas form after barrier breaching leads to inlet development. As tidal currents ebb and flow through the inlet, they carry sediment that comes from longshore transport and the erosion of the actual channel. When the velocity of the current flow slackens, the sediment load deposits on the ocean side in the form of ebb-tidal deltas and on the estuary side as flood-tidal deltas (Hennessey & Zarillo, 1987).

Tidal inlets and tidal deltas

The primary channels that separate barrier islands in the barrier-island system are tidal inlets. Inlets allow water and sediment to travel between the ocean and the backbarrier lagoon. The dominant factors that affect tidal-inlet morphology are tidal range, tidal prism, significant wave height, and the storage and geometry of the backbarrier lagoon (Fitzgerald & Fitzgerald, 1977; Nummedal & Fischer, 1978). Tidal

inlets are an important sediment sink in the barrier-island system. Interactions between sediment and wave and tidal processes result in a wide variety of inlets in a given stretch of barrier-island coasts (Davis, 1994).

Tidal inlets play an integral part in barrier-island systems but overall that part depends on their size and distribution. In general, tidal inlets consist of two or three primary elements: flood-tidal delta, inlet channel, and ebb-tidal delta (Figure 29) (Davis, 1994). Tidal processes dominate inlets. Waves are important in ebb-tidal deltas, have an indirect role in the inlet channels, and play a minor to insignificant role on the flood-tidal deltas (Davis, 1994).

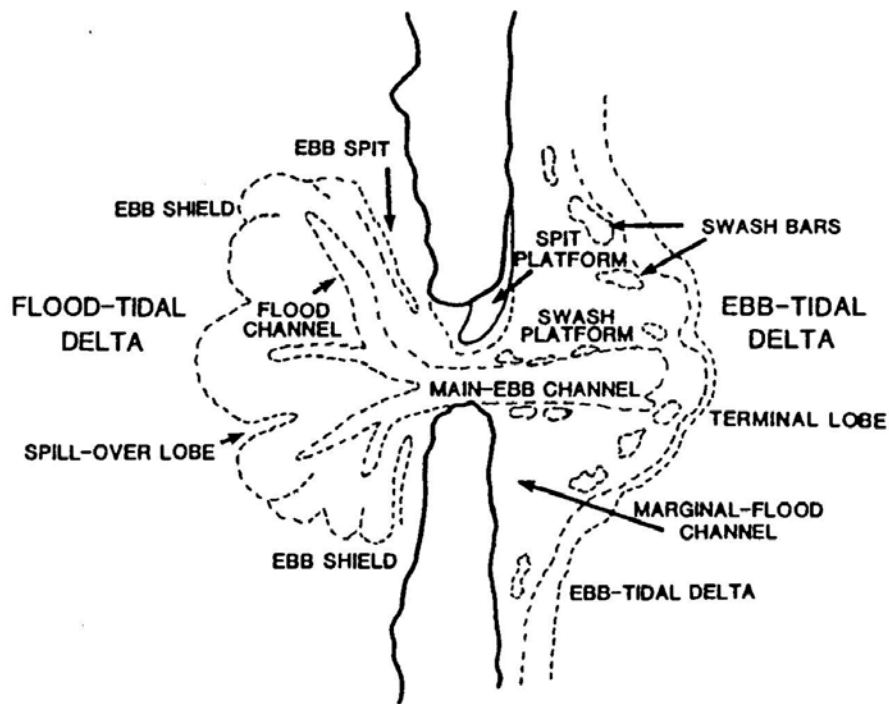


Figure 29: Generalized sketch of a tidal-inlet system (from Davis, 1994).

Hayes (1979, 1980) and Boothroyd (1985) studied tidal inlets, specifically the morphology of ebb- and flood-tidal deltas. Ebb-tidal deltas are the sediment accumulations on the seaward side of a tidal inlet as a result of tidal currents, waves, and wave-generated longshore currents. Ebb-tidal deltas typically have channel-margin linear bars, swash bars, lateral flood channels, a main ebb channel, and a terminal lobe (Figure 30) (Davis, 1994). The inlet channel provides a means for tides and sediment to move in and out of the backbarrier lagoon and does not tend to accumulate much sediment within it (Davis, 1994). Increasing wave influence, especially wave-generated longshore currents, increase the instability of the tidal channel and migration can occur in the

direction of the dominant littoral drift (Davis, 1994). Over time, continued wave dominance can cause the inlet to close (Davis, 1994). Flood-tidal deltas are the sediment accumulations on the landward side of the tidal inlet and are typically unaffected by waves (Davis, 1994). They represent one of the largest accumulations of sand-sized sediment in the barrier-island system (Davis, 1994). Hayes (1975, 1980) proposed a model for the general morphology of a flood-tidal delta that resembles a horseshoe crab (Figure 31). As the tide rises and floods through the main inlet channel, sediment is transported landward and is transported up the flood ramp (Davis, 1994). When the tide ebbs, the currents flow around the sand body and rework the margins of the sediment deposited by the flood tide (Davis, 1994).

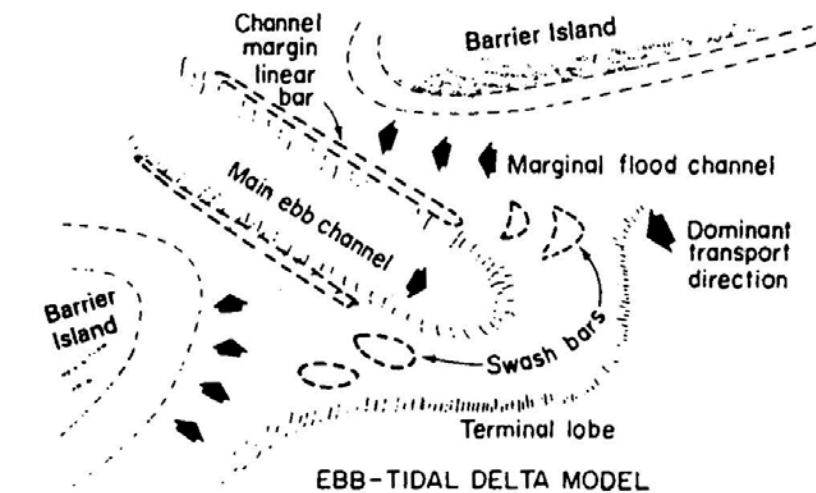


Figure 30: Generalized ebb-tidal delta model (from Davis, 1994).

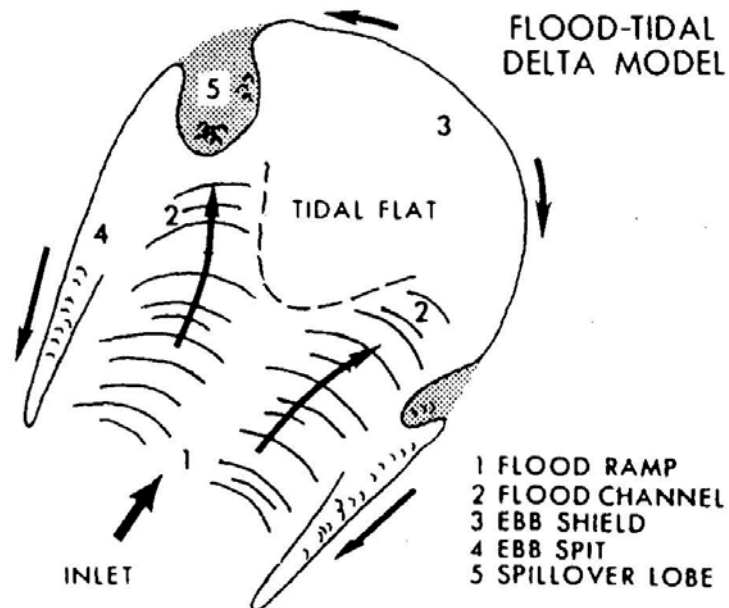


Figure 31: Generalized flood-tidal delta model (from Davis, 1994).

Modern tidal inlet stratigraphy

Deposits of tidal inlets, tidal channels in tidal flats, estuarine channels, and rivers have been confused with each other in the past thus causing misinterpretation of the depositional environment for some formations of sedimentary rocks. Hoyt and Henry (1965) were the first to identify tidal inlet sedimentation as a significant finding in the recognition of ancient barrier islands using their observations of the Georgia barrier islands to create their model. They focused on the importance of inlet migration in the identification process. Kanen (1969) compared coastal depositional environments with fluvial depositional environments and identified four parameters that are important in differentiating between alluvial and barrier-island facies complexes: “configuration of basal contact, grain size, nature of enclosing and associated sediments, and type and

nature of cross-bedding.” (Kanes, 1969, p. 261). Table 4 shows the differences that Kanes (1969) found between these two depositional environments

Table 4: Parameters used to distinguish tidal-inlet deposits from fluvial deposits in sedimentary rocks (after Kanes, 1969).

Parameter	Tidal inlet deposits	Fluvial deposits
Grain size	Fining upwards	Coarsening upwards
Basal contact	Basal lag deposits commonly composed of shells or cobbles	Coarse grained sand deposits
Cross-bedding	Two directional dipping cross-bedding	One directional dipping cross-bedding
Enclosing sediments	Similar to those that cap barrier-island facies	Grade upward into backswamp, marsh, natural levees, or shallow-lake and bay sediments.
Faunal assemblages	Marine and brackish water fauna	Lack of marine and brackish water fauna; abundance of wood and terrestrial plant debris

Kumar & Sanders (1974) defined the sedimentary sequence for a migrating tidal inlet in their classic study of the Fire Island Inlet, located east of New York City. This inlet migrated WSW for 115 years at a rate of 64 m/yr. Their inlet sequence consisted of five units that they placed in two separate environments. Table 5 identifies these relationships. They defined each of these units in terms of their individual sedimentary structures and textures. The channel-floor environment forms the bottom of the channel and is the lowest unit in the inlet sequence. It consists of a layer of lag gravel that contains mostly large shells and pebbles. The existence of this lag-gravel layer is important in identifying tidal inlets in ancient sedimentary environments, especially if a distinctive shell layer exists (Kumar & Sanders, 1974).

Table 5: Tidal-channel environments and their corresponding units (after Kumar & Sanders, 1974).

Tidal-channel environment	Tidal-inlet sequence unit
Inlet Channel	Channel floor
	Deep channel
	Shallow channel
Spit	Spit-platform
	Subaerial spit

The bedforms in the deep channel consist of large sand waves that form asymmetrically with the steeper face perpendicular to the ebb flow. This results in sedimentary structures that are cross-laminated with large-scale cross-laminated units followed by small-scale cross-laminated units, which culminates in an arrangement of trough-shaped cross-laminae. The sediments in the deep-channel environment on Fire Island consist of mostly medium to coarse sand and include pebbles and large shells. Evidence of microfauna is missing probably due to the constant movement of the bottom and the rapid water flow at ebb and flood peaks making the environment virtually impossible for foraminifera to exist there. Shells fragments were typically a mixture of open-ocean and bay species and the pebbles were mainly quartzite rock fragments and large pieces of mollusk shells (Kumar & Sanders, 1974).

The shallow-channel unit is a thin layer and the characteristic feature of this unit is the absence of structures that are typically built by the migration of large sand waves. No differences between the textures of the shallow- and deep-channel units exists, the size fractions are about the same, and microfauna are absent in the shallow-channel

sediments as in the deep-channel sediments. The sedimentary structures within this unit consist of plane beds that are overlain by cross-laminae (Kumar & Sanders, 1974).

The spit environment in the tidal-inlet sequence consists of the spit-platform and the subaerial-spit units. The spit-platform unit is always under water but at low tide it is only barely covered by water. The spit-platform is similar in structure to a typical delta with topset, foreset, and bottomset components. The medium to coarse sand in this unit generally fines upward from the bottomset to the foreset beds but then coarsens again in the topset beds. The most prominent sedimentary structures within this unit are the foreset beds (Kumar & Sanders, 1974).

The subaerial-spit unit is at the top of the inlet sequence. The sediments range from coarse to medium sands and are mainly composed of quartz. Small bays, created by washover, may form on the top of this unit. Muds will settle out of suspension in these small water bodies and their bottoms may become populated by lagoonal mollusks, such as oysters and thus become bioturbated. In the geologic record, these bay sediments appear as lenses of muddy sediments with mollusk fossils within well-sorted clean sands (Kumar & Sanders, 1974).

All of these units are summarized in Figure 32. Kumar & Sanders (1974) conclude that tidal-inlet sequences should be a common occurrence in the geologic record, since they occur under approximately 20 to 40% of all modern barrier islands.

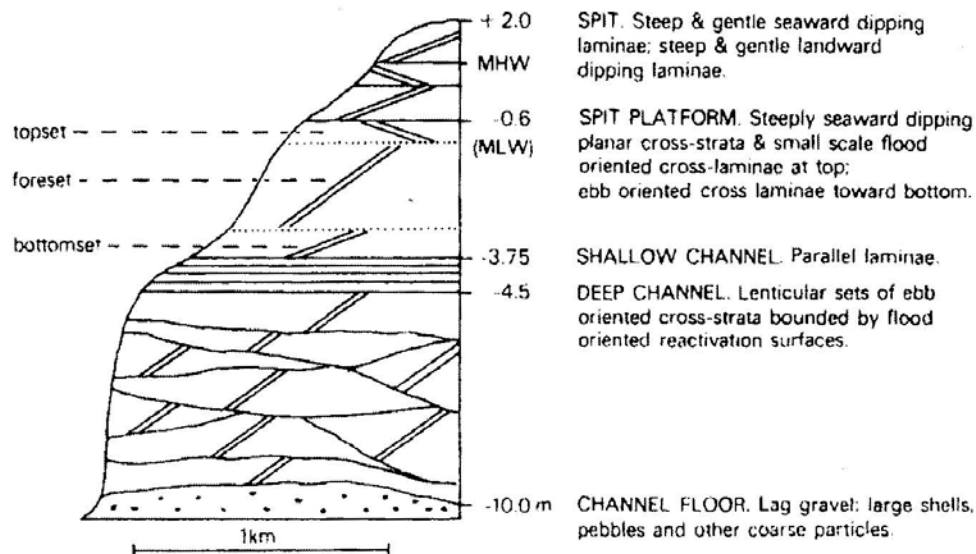


Figure 32: Vertical sequence of a modern tidal inlet, Fire Island Inlet, USA. (from Donselaar & Nio, 1982).

Moslow & Heron (1978) studied relict inlets from the Holocene section of the Core Banks in North Carolina. They concluded that each inlet-fill body had a distinct stratigraphic sequence that consisted of three depositional facies, starting from the bottom: an inlet floor that contains a coarse shell and gravel lag; a channel that contains medium to coarse sand and some shell fragments; and an inlet margin that contains clean, very fine- to medium-grained sand (Moslow & Heron, 1979).

The sedimentary characteristics of tidal-inlet deposits are summarized in Table 6.

Table 6: Sedimentary characteristics of tidal-inlet deposits (after Heward, 1981).

TIDAL-INLET DEPOSITS (barrier islands and distributary channel mouths of wave-dominated deltas)

Ephemeral inlets open for a few hours to few years, other inlets of greater permanency.

Composition: sand, silt, clay, glauconite; shelly conglomeratic lag at base, fines upward (but strongly dependent on local sediment sources); mud clasts and drapes may occur throughout the sequence.

Sedimentary structures: tabular and trough cross-stratification, reactivation surfaces, parallel and cross-lamination, scale of cross-stratification generally decreases upwards; faunal bioturbation.

Fauna: mixed marine and lagoonal, frequently contain shells reworked from adjacent and underlying deposits.

Geometry: relatively stable inlets mostly oriented perpendicular to shoreline trend, whilst migrating inlets commonly are oblique; erosively overlie shoreface, beach, backbarrier, lagoon or older deposits.

Paleocurrents: ebb-dominated (seaward), more rarely flood-dominated (landward) or bipolar oriented cross-stratification; paleocurrents for relatively stable inlets oriented perpendicular to shoreline trend, for migrating inlets obliquely; recurved spit cross-stratification, if preserved at top of inlet sequence, with widely variable orientation.

Preservation potential: transgressive shorelines – high because of low position in transgressive sequence; regressive shorelines – high but inlets generally common.

Ancient tidal inlet and breach deposits

Tidal inlets have a good potential to be preserved in the stratigraphic record because of their nature to incise deeply (several tens of meters in some cases) and their tendency to migrate laterally along the shoreline in the direction of longshore sediment transport (Uhlir et al., 1988). Tidal inlets have been identified as being preserved in the stratigraphic record in numerous articles. The following is a sampling of those papers.

One of the earliest known tidal-inlet deposits is in the Lower Cambrian Hardeberga Formation, which lies unconformably on the Proterozoic basement in Scania, southern Sweden (Hamberg, 1991). It is 120 m thick. The Hardeberga Formation represents a tidal-channel environment that occurred behind a coastal-barrier system. The Tobisvik Member within the Hardeberga Formation is a 7 to 8 m thick sandstone body that was laid down on an erosional surface. It is medium- to very coarse-grained with high inclined beds that are 20 cm to 80 cm thick, cross-bedded, and dipping at 15° to 23° to the east. These beds were interpreted as being deposited in a migrating tidal inlet. Bipolar paleocurrent patterns occur, which are interpreted as being caused by the tidal currents within the inlet channel (Hamberg, 1991).

The lower Paleozoic Peninsula Formation, located in South Africa on the Cape Peninsula, is a 750 m quartz arenite complex that overlies fine-grained, back-barrier, tidal-flat deposits, which make up the Graffwater Formation. The Peninsula Formation is made up of five distinct sandstone facies, which are distinguished by different sets of sedimentary structures. The fourth of these facies (Facies 4) is made up of large-scale channel deposits that are thought to be the result of lateral migration of tidal inlets. This

facies has a maximum thickness of 40 m. The base of Facies 4 lies on an eroded surface and is a coarse sand with pebbles and cross-stratification. The base is overlain by 15 cm to 80 cm sets of cross-stratification that tends to fine upward in some places. Though not widespread, reactivation surfaces and herringbone reversals are found. Skolithos and arthropod tracks are found but are rare. In one location, an inlet sequence exists, which is dominated by ebb-flow structures and upward fining and is overlain by planar beds that dip at a low angle. This is interpreted as a spit-beachface deposit that overlies an infilled inlet. Facies 4 compares closely to the inlet sequence of Kumar & Sanders (1974) as discussed in Hobday & Tankard (1978).

The upper Silurian – lower Devonian Keyser Limestone in the central Appalachian Valley and Ridge consists of sediments that were deposited in a complex of lagoonal, barrier, and shallow offshore environments, which represent a regional transgression (Barwis & Makurath, 1978). The Keyser Limestone is underlain by the tidal-flat deposits of the Tonoloway Limestone. The Clifton Forge Sandstone Member of the Keyser Limestone is in the upper Silurian part of the Keyser Limestone. It consists of a 21-m sequence of well-rounded, medium- to fine-grained, well-sorted quartz arenites, which generally fine upward. The basal unit of the Clifton Forge Sandstone Member is 1.5 m thick and consists of thin-bedded, medium- to coarse-grained, calcareous sandstone with broken and abraded crinoid fragments and abundant brachiopod valves. This is interpreted as being a channel lag, which was deposited as the barrier island transgressed over the landward tidal-flats that make up the Tonoloway Limestone. The basal unit is overlain by a 4.1 m layer of cross-bedded, medium-grained sandstone. The bottom of this

sandstone is consistent with channel-bottom scour since it undulates and lies disconformably over the basal unit. Cross bedding is bipolar that is representative of reversing tidal currents. The resulting herringbone cross bedding preserves the channel-bottom megaripples, which are indicative of deep-channel tidal-inlet deposits (Kumar & Sanders, 1974). The contact between the deep-channel, tidal-inlet deposits, and the overlying sandstone, which represents the shallow-channel, tidal-inlet deposits, is gradational. This sandstone is 1.8 m in thickness and consists of well-sorted, fine sands that are identical to the underlying sands. Cross bedding in this sandstone is also bipolar, but the sets of cross bedding are thinner than in the deep-channel deposits. The bedding in the deep-channel and shallow-channel deposits is lenticular (Barwis & Makurath, 1978).

The Devonian Bokkeveld Group of South Africa is a 1,500 to 3,000 m thick sequence of sediments that represent a deltaic origin. It consists of shallow-marine faunas that are similar to those found on wave-dominated deltas. Tidal-inlet and tidal-channel deposits dominate among the delta-front sands. These are found as lenticular beds that range from 30 cm to 8 m in thickness. They are comprised of very well sorted, fine- to medium-grained quartz arenites. These beds are separated by erosion surfaces that are littered with quartz pebble and mud clast lag deposits. “These mutually truncating channels display varying degrees of en echelon and stacked geometries.” (Tankard & Barwis, 1982, p. 965). Both grain size and bedding thickness decrease upward, though when considering the whole sequence, a tendency exists for both grain size and bedding thickness to increase upward. Current reversals are indicated by herringbone and

reactivation surfaces, which are common. Skolithos tubes, which extend down from the bedding surface, are found in many of the thin-bedded sandstones. Tidal-channel and tidal-inlet deposits are typically underlain by distributary-mouth-bar deposits, which results in a sequence of composition that grades upward from graywacke to lithic arenite, and finally to quartz arenite. The origin of these deposits is tidal-channel reworking of delta-front and delta-plain sediments (Tankard & Barwis, 1982).

Upper Carboniferous orthoquartzites that are found within the Pocahontas Basin in southern West Virginia have been interpreted as being deposited in barrier-island and backbarrier environments. These differ from orthoquartzites found in Alabama with which they are correlative but the typical barrier-island sedimentary structures are missing. The major orthoquartzite sandstone bodies found in the Pocahontas Basin are subdivided into three facies: Facies 1 that represents a migrating tidal-inlet environment, Facies 2 that represents an ebb-tidal delta environment, and Facies 3 that represents a backbarrier environment that has meandering tidal channels and washover deposits. The vast majority of the orthoquartzite complex consists of Facies 1. Facies 1 is a medium-grained, locally conglomeratic sandstone with both trough and planar cross-stratification. The conglomeratic interbeds occur near the base of the facies or immediately above scour surfaces and consist of quartz pebbles, mudclasts, and plant debris. The conglomerates are followed, in sequence, by cross-stratified sandstone layers that become thinner upward in the vertical section. Where it is possible to determine the channel trend, the beds dip in an oblique direction to that trend that indicates accretion at the margin of the channel and, therefore, migration of the channel. Herringbone cross-stratification does

not occur but successive sets of foresets are observed to diverge by as much as 120° .

Reactivation surfaces are commonly found within this facies. Siltstone interbeds are more abundant towards the tops of these sequences, which can have a siltstone or mudstone layer up to one meter thick at the top. These siltstones have ripple cross-lamination, lenticular bedding, and are locally bioturbated. Complete vertical sequences are preserved in less than 30% of Facies 1 because they appear to be truncated at the top, but sequences are superimposed on each other in multiples of from two to five with only the top sequence lacking evidence of erosion at the top (Hobday & Horne, 1977).

Two sandstone oil reservoirs have been described in the Mississippian Aux Vases Formation, Rural Hill Field, Illinois by Weimer et al. (1981). They have been interpreted as being shoreline sands that were deposited linearly and parallel to the depositional trend and tidal-channel sands, which are generally perpendicular to the depositional trend and occur in elongate and confined areas. These two sandstones have different textures, cementation, and sedimentary structures that are distinctive. The shoreline sandstones are horizontal to nearly horizontally laminated and fine-grained. The tidal-channel sandstones are cross-bedded and very fine-grained. The shoreline sandstones are less porous (15%) than the tidal-channel sandstones (21%). This is because the grain size in the shoreline sandstones has been increased by authigenic silica overgrowths while the tidal-channel sandstones do not exhibit this kind of cementation. They do exhibit similarities. Both are clean, well-sorted, mature orthoquartzites that contain less than one percent clay. Cross bedding in the tidal-channel sandstones is truncated at the top of the sequence and tangential at the bottom. Herringbone cross-beds occur in the core

indicating opposing dominant flood- and ebb-tidal currents. In the lower Aux Vases Formation, the shoreline and tidal-channel sandstones interfinger, which indicates that the two depositional environments were contemporaneous. In the upper Aux Vases Formation, the tidal-channel sandstones are also confined in elongate belts but are separated laterally by tidal flat and marsh deposits. This stratigraphic sequence indicates that the Aux Vases Formation represents a regression. The Aux Vases Formation is overlain by the Renault oolitic limestones, which indicate that a transgression followed the deposition of the Aux Vases Formation (Weimer et al., 1981). Interestingly, no mention in the text nor indication in the core photographs included in the article identify that the tidal-channel sandstones have channel lag deposits or exhibit scouring at the base.

The upper Jurassic Sundance Formation is located in north-central Wyoming in the Bighorn Basin. This formation is overlain by the non-marine sediments of the Morrison Formation. The uppermost 20 m of the Sundance Formation contains a coquina facies and a sandstone facies. Both of these facies are thought to have been laid down by laterally accreting, tidal-inlets. The coquina facies contains lateral-accretion surfaces and large-scale trough cross bedding. The cross bedding occurs towards the top of the unit. The axes of these troughs are roughly perpendicular to the dip of the lateral-accretion surfaces, which implies that in addition to shore-parallel inlet movement, shore-normal transport of the coquina material occurred near the base of the tidal-inlet channels. “The comparison of maximum-dip azimuths of the large-scale cross-stratification with the coquina facies versus that of the large-scale cross-lamination in the sandstone facies

implies that different processes controlled the transport and deposition of the two facies. The large-scale cross-stratification in the coquina facies dips predominately E and W, while the large-scale cross-lamination in the sandstone facies implies generally NW-SE transport directions. The E-W modes of the coquina measurements may indeed be the result of lateral accretion of tidal inlets along an E-W trending shoreline. According to Uhlier et al. (1988), the NW-SE oriented sandstone trough cross-lamination may be the record of large-scale bedforms moving seaward and landward with the ebbing and flowing tides. Horizontal lamination is common in the upper part of the sandstone facies. This probably means that this part of the sandstone facies was formed in the shallow waters of the spit platforms of the tidal inlets (Kumar & Sanders, 1974). In some places these laminations are underlain by a thin coquina facies, which consists of relatively whole shells. This probably represents lag deposits in tidal creeks that meander within the sand flats behind barrier islands. The coquina facies is entirely absent in the southernmost part of the Bighorn Basin, which suggests that that this part of the Sundance shoreline did not have tidal inlets. The upper part of the Sundance Formation fines upward. The sandstone facies of the Sundance Formation is conformably overlain by the terrestrial sediments of the Morrison Formation in the Bighorn Basin, which is evidence that the sandstone facies represents tidal-inlet deposition rather than an offshore sand body as has been concluded by other authors (Uhlir et al., 1988).

The Eocene Pano Formation is located in the southern Pyrenees, Spain and consists of mostly calcareous sediments (Donselaar & Nio, 1982). The lower part of the Pano Formation represents the remains of barrier islands that have been inundated by a

relative rise in sea level and consists mainly of vertically stacked, tidal-inlet fill deposits. This part of the formation can be up to 30 m thick. Three phases of barrier-island formation have been recognized and are thought to represent three time periods when the relative sea level increase has been in equilibrium with the sediment supply entering the coastal area. Each of these subsequent barrier-island phases is stratigraphically higher on the coastal plain than the previous one. The lower part of the Pano Formation consists of medium-bedded to thick-bedded calcarenites that consist of five separate tidal-inlet sequences each bounded by an erosion surface. These sediments are well sorted and mostly fine sands. The base of each sequence consists of coarse-grained lag deposits that consist of clay pebbles, gravel, benthic foraminifera, and coarse to very coarse sands. The sediments fine upward with the top identified by finer sands and/or overlying marls. Between the third and fourth tidal-inlet sequences is a sequence that has been identified as a washover-scour deposit, which probably represents erosion that occurred during a severe storm. The vertical stacking of the tidal-inlet sequences is caused by lateral migration of the tidal inlet. Bipolar cross-bed sets are found in these tidal-inlet sequences with dip directions that are oriented NW-SE along the tidal-channel axis, which is normal to the NE-SW oriented coastline. The middle and upper parts of the Pano Formation consist of mixed tidal-inlet, lagoon, and washover types of deposits with some of the tidal-inlet deposits but are probably lagoonal tidal channels because their upper parts are filled with burrows (Donselaar & Nio, 1982).

The modern delta of the Niger River has barrier islands at its distal end (Oomkens, 1974). This coastal barrier complex consists of 20 barrier islands that are each

separated by a tidal inlet. Coring into the deltaic sediments has identified tidal-channel sands that were deposited during the late Quaternary and that most of the sand has been preserved in the form of tidal-inlet deposits. The tidal inlets that formed between the late Quaternary barrier islands migrated along the shoreline in the direction of longshore sediment transport. The basal unit in a tidal channel-fill sequence from the late Quaternary lies on an erosional surface and consists of a very coarse-grained lag deposit that contains clay pebbles and organic debris. Above the lag deposit, clastic material is found that exhibits trough cross bedding, which makes up most of the tidal-channel fill. This clastic interval fines upward and has an upward increase in clay content and the number of burrows within it. A concentration of thin, clay beds near the top of the sequence is interpreted to be caused by seasonal variations. The channel-fill sequence can be overlain by marine silts or clays if the tidal channel is outside of the coastline, by clastic material that is free of clay, horizontally bedded or is cross-bedded if the tidal channel is proximal to the coastline, and intertidal sediments with high clay content and bioturbated if the tidal channel is completely without contact with waves. Sediment in the Niger delta tidal channels is sourced from both river sediments longshore currents, which explains the occurrence of so much clay within these sequences (Oomkens, 1974).

METHODS AND DATASETS

Field Methods

Field samples were collected from April 24, 2009 through March 12, 2011 from 41 different locations, including 18 vibracores, eight pulse augers, one push core, five trenches, and nine hand augers. Table 7 shows the sample type, field sample identification number, abbreviated sample identification number, latitude, longitude, and length/depth of each sample in the order in that they were collected. Abbreviated sample identification numbers are in a format that are easier to read and are used throughout this dissertation to identify each sample. Additionally, 33 surface samples were collected by Kristin Ewer on April 23, 2010.

Table 7: Data on the grain-size samples collected from each field location.

Date	Sample Type	Sample number	ID	Latitude	Longitude	Length
4/29/09	Hand auger	AUGER09-01	A1	37° 36' 41.46" N	75° 36' 56.46" W	1.52 m
	Hand auger	A-0902	A2	37° 36' 42.84" N	75° 36' 56.22" W	1.22 m
	Hand auger	A-0903	A3	37° 36' 44.16" N	75° 36' 56.34" W	0.61 m
	Hand auger	A-0904	A4	37° 36' 44.88" N	75° 36' 56.34" W	1.22 m
	Hand auger	A-0905	A5	37° 36' 45.96" N	75° 36' 56.40" W	1.22 m
	Hand auger	A-0906	A6	37° 36' 47.58" N	75° 36' 56.34" W	1.22 m
	Hand auger	A-0907	A7	37° 36' 54.06" N	75° 36' 56.88" W	1.22 m
	Hand auger	A-0908	A8	37° 36' 51.28" N	75° 36' 56.58" W	1.22 m
	Hand auger	A-0909	A9	37° 36' 49.44" N	75° 36' 56.34" W	1.22 m
4/23/10	Trench	T-1	T1	37° 36' 39.33" N	75° 37' 15.242" W	0.35 m
	Trench	T-2	T2	37° 36' 40.14" N	75° 37' 11.93" W	0.34 m
	Trench	T-3	T3	37° 36' 42.44" N	75° 37' 6.27" W	0.42 m
	Trench	T-4	T4	37° 36' 44.82" N	75° 36' 59.15" W	0.44 m
	Trench	T-5	T5	37° 36' 46.44" N	75° 36' 53.53" W	0.54 m
6/17/10	Push core	PC1-100617	PC1	37° 36' 39.33" N	75° 37' 15.242" W	0.80 m
9/17/10	Vibracore	CIB100917-C1	C1	37° 36' 21.45" N	75° 37' 21.29" W	5.58 m
	Vibracore	CIB100917-C2	C2	37° 36' 29.05" N	75° 37' 15.92" W	5.15 m
9/18/10	Vibracore	CIB100918-C3	C3	37° 36' 35.31" N	75° 37' 28.25" W	4.41 m
	Vibracore	CIB100918-C4	C4	37° 36' 42.21" N	75° 37' 27.45" W	3.59 m
	Vibracore	CIB100918-C5	C5	37° 36' 45.48" N	75° 37' 19.55" W	5.37 m
	Vibracore	CIB100918-C6	C6	37° 36' 48.46" N	75° 37' 13.07" W	0.30 m
10/8/10	Vibracore	CIB101008-C7	C7	37° 36' 41.59" N	75° 37' 9.47" W	1.30 m
	Vibracore	CIB101008-C8	C8	37° 36' 37.96" N	75° 37' 19.59" W	4.17 m
	Vibracore	CIB101008-C9	C9	37° 36' 57.01" N	75° 37' 2.64" W	2.16 m
	Vibracore	CIB101008-C10	C10	37° 36' 58.53" N	75° 37' 22.59" W	7.69 m
10/9/10	Vibracore	CIB101009-C11	C11	37° 36' 39.75" N	75° 37' 2.56" W	2.74 m
	Vibracore	CIB101009-C12	C12	37° 36' 44.91" N	75° 36' 57.21" W	2.54 m
	Vibracore	CIB101009-C13	C13	37° 36' 48.68" N	75° 36' 55.60" W	1.73 m
	Vibracore	CIB101009-C14	C14	37° 36' 39.40" N	75° 36' 54.46" W	2.87 m
	Pulse auger	CIB101009-PA1	PA1	37° 36' 40.59" N	75° 37' 5.15" W	4.00 m
	Pulse auger	CIB101009-PA2	PA2	37° 36' 45.22" N	75° 36' 57.15" W	3.62 m
	Pulse auger	CIB101009-PA3	PA3	37° 36' 44.86" N	75° 36' 53.07" W	3.45 m
	Pulse auger	CIB101009-PA4	PA4	37° 36' 47.62" N	75° 36' 52.95" W	3.45 m
10/10/10	Pulse auger	CIB101010-PA5	PA5	37° 36' 47.80" N	75° 36' 56.49" W	3.00 m
	Pulse auger	CIB101010-PA6	PA6	37° 36' 50.64" N	75° 36' 56.52" W	3.60 m
	Pulse auger	CIB101010-PA7	PA7	37° 36' 50.24" N	75° 36' 52.72" W	3.25 m
	Pulse auger	CIB101010-PA8	PA8	37° 36' 55.92" N	75° 36' 54.09" W	3.00 m
3/12/11	Vibracore	CIB110312-C15	C15	37° 37' 6.75" N	75° 36' 48.64" W	1.50 m
	Vibracore	CIB110312-C16	C16	37° 36' 57.5" N	75° 36' 52.40" W	3.01 m
	Vibracore	CIB110312-C17	C17	37° 36' 51.36" N	75° 37' 2.69" W	1.58 m
	Vibracore	CIB110312-C18	C18	37° 36' 43.68" N	75° 36' 58.29" W	2.31 m

Nine auger samples were collected on April 24, 2009 using an open-bail hand auger (Figure 33) across the last known location of the inlet throat of Cedar Island Inlet. The auger bail was filled four times at each of eight sampling locations (Figure 34). In the ninth auger location, the bail encountered refusal after being filled only two times. The sediment from retrieval of each auger-bail constitutes a separate grain-size sample.



Figure 33: Hand auger for sediment sampling (from US Air Force, 2015) .

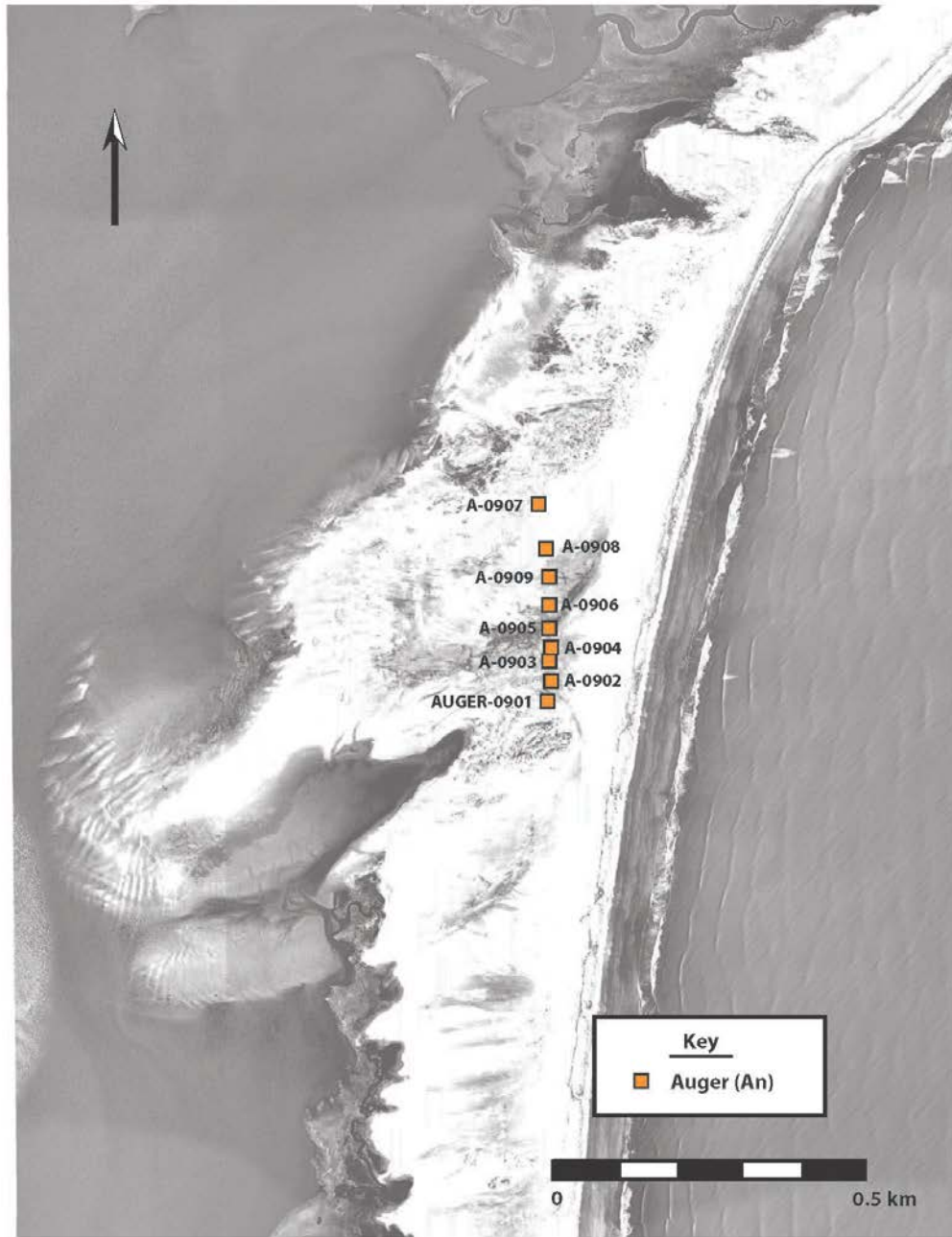


Figure 34: Map showing location of hand-auger samples.

Five trenches were dug on April 25, 2010 approximately along the middle of the last location of the inlet throat of Cedar Island Inlet (Figure 35). They were dug with shovels until the water table was reached. Trenches were dug at approximately right-

angles to each other (i.e., strike and dip directions) at each trench location. Each of the two faces in the trench was cleaned using a trowel (Fig 36). The first trench (T1) was dug at the landward end of the inlet throat. Each subsequent trench was dug at a location that was in a more seaward direction. Sediment samples were taken at 2 cm intervals from the top to the bottom of each trench on one face.

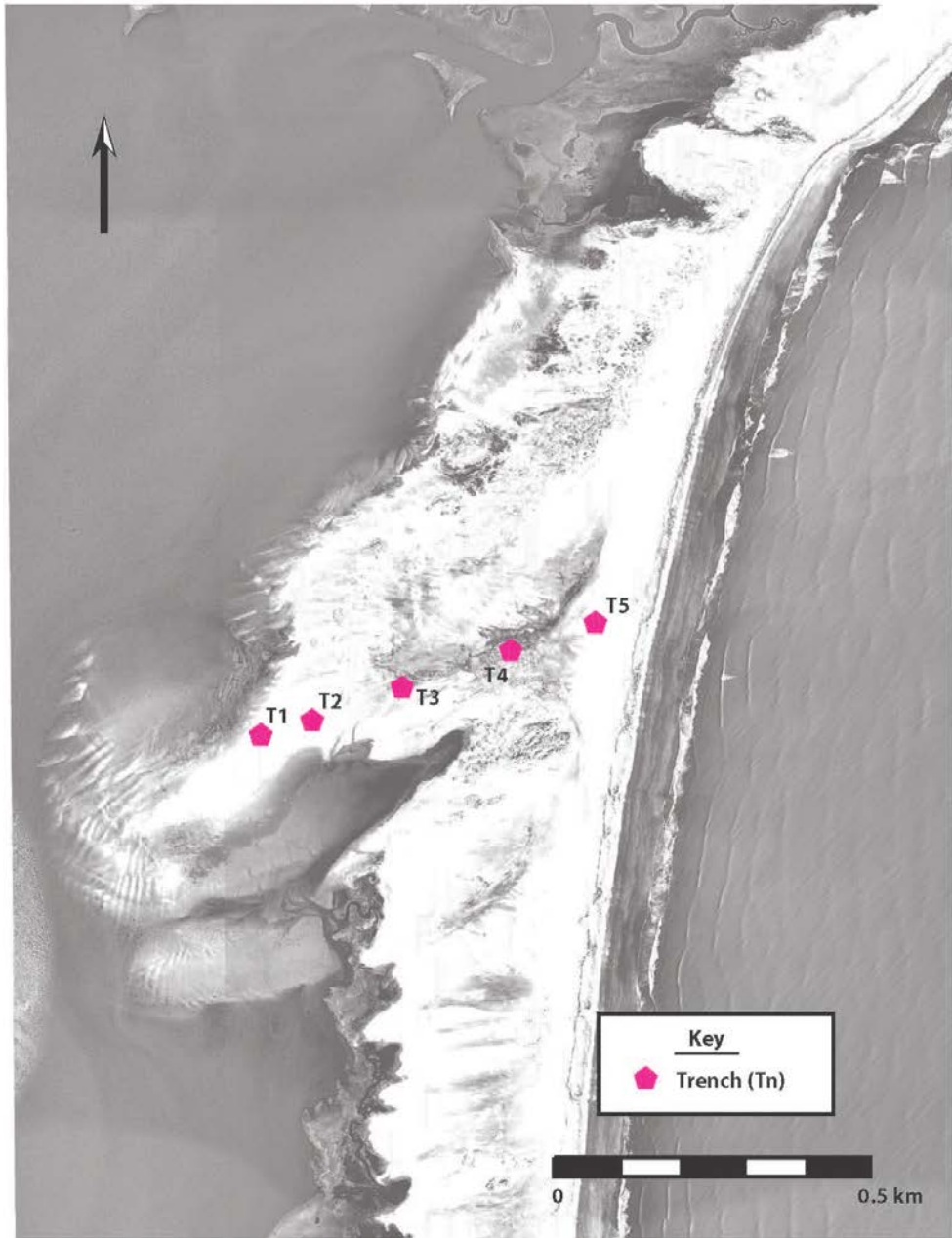


Figure 35: Map showing location of trenches.



Figure 36: Trench T4.

Surface-sediment samples were collected by Kristin Ewer on April 23, 2010 (Figure 37). Samples were collected from the surface of each of 33 locations with 23 taken along the approximate middle of the last location of the inlet throat and 10 taken in three transects at right angles to the last location of the inlet throat (Figure 38). Exact locations were measured using an all-in-one laser surveying technology.



Figure 37: Surface-sediment sampling.

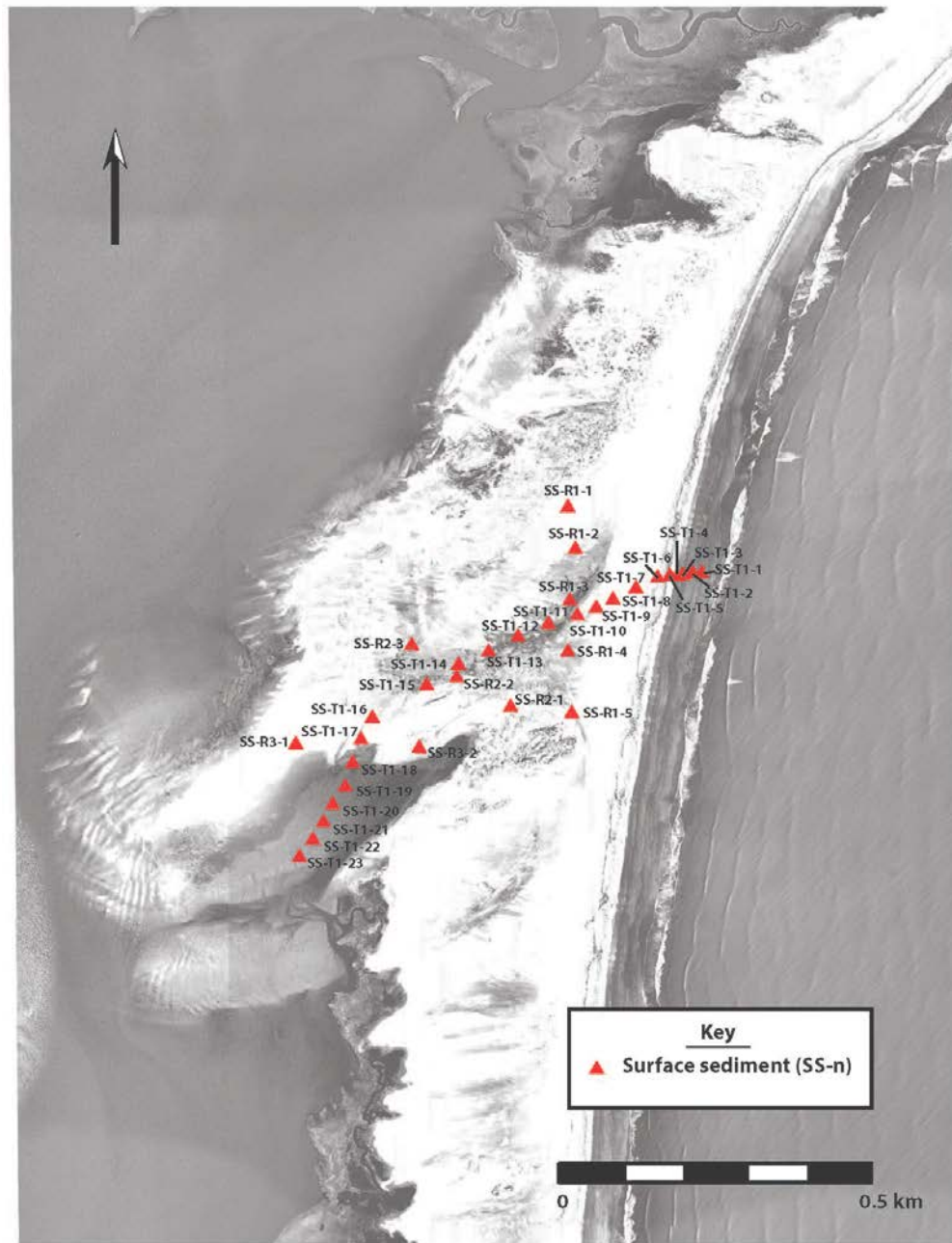


Figure 38: Map showing location of surface-sediment samples.

One push core was collected on June 17, 2010 in the middle of the last known location of the inlet throat (Figure 39). The core was collected using a 7.5 cm aluminum irrigation pipe that was pushed into the sediment (Figure 40). The pipe was sealed on top

with a plastic core cap. The core was then dug out and retrieved (Figure 41). The bottom was sealed with a plastic core cap after retrieval. The core was 0.95 m in length.



Figure 39: Map showing location of push core.



Figure 40: Push core.



Figure 41: Push core during excavation.

Between September 2010 and March 2011, 18 vibracores were collected in the Cedar Island breach zone to investigate the sedimentologic and stratigraphic signatures of the inlet deposits (Figure 42). Aerial photographs from the last breach were used to determine the approximate core locations. The final location was decided in the field and depended on the existing conditions (e.g., tides).

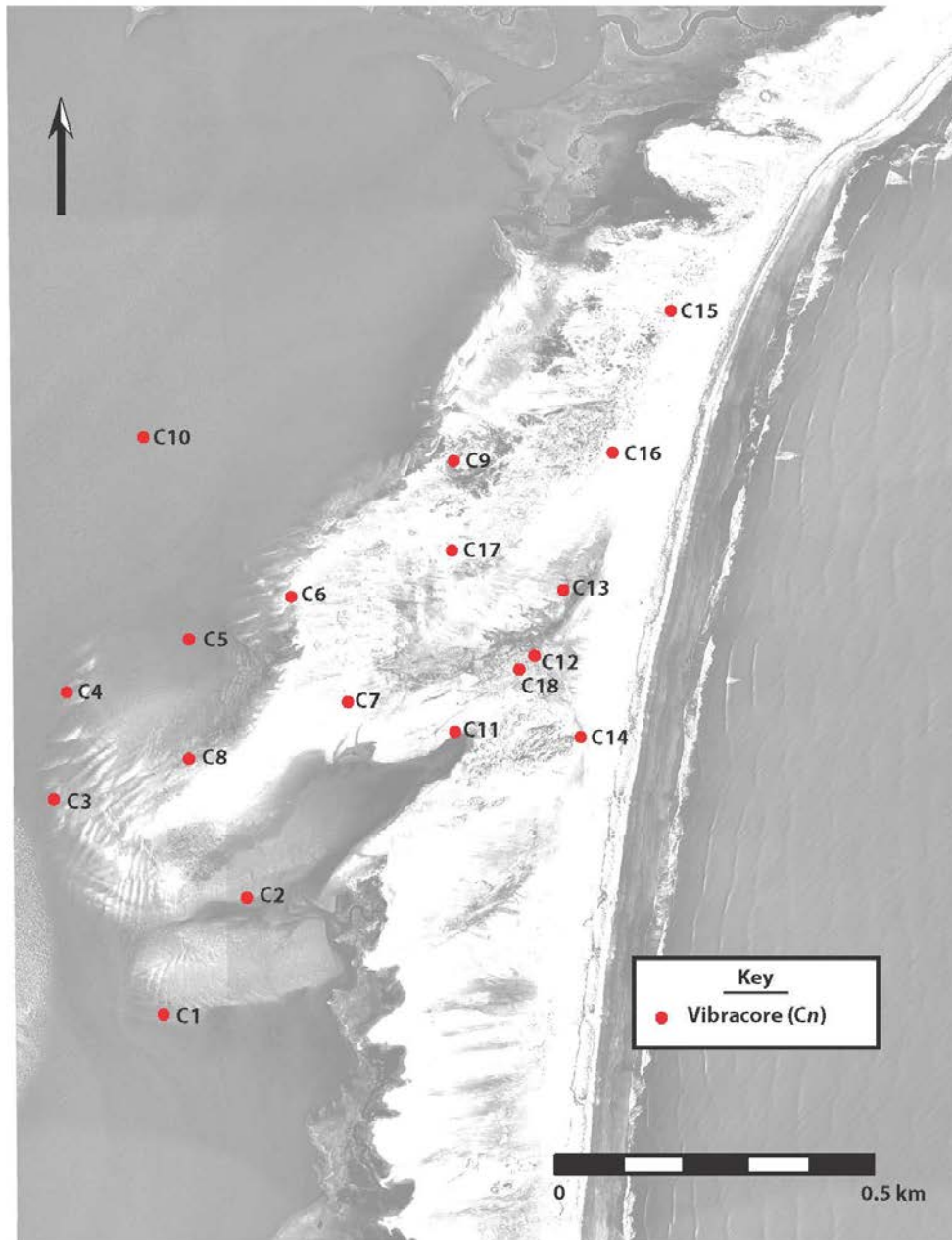


Figure 42: Map showing location of vibracores.

Vibracoring is the standard practice of collecting continuous, unconsolidated sediment cores in water-saturated sediments (Lanesky et al., 1979). Vibracoring relies

upon the principle of liquefaction to displace fine-grained sediments such as sand, silt, and clay, which allows the core tube to pass through the sediments (Smith, 1984).

The vibracore used in this study consisted of an Oztec 5-horsepower concrete vibrator, a fabricated vibrator head assembly, 7.5 cm aluminum, irrigation pipe as the sediment core tubes, an aluminum tripod, and several come-alongs used to retrieve the tubes after coring (Stone, 2006) (see Figure 43). The vibracore parts, tools, and personnel were transported to Cedar Island by one of several different boats from Virginia Institute of Marine Science- Eastern Shore Laboratory located in Wachapreague, Virginia.



Figure 43: Portable vibracore rig used to core unconsolidated sediment.

The vibracore tripod was set up over the coring location and the vibrator head assembly was attached to the core tube. The vibrator was engaged and the core tube was advanced into the sediments until either the core tube met refusal or the length of the core tube had fully penetrated the sediment. If the tube was longer than where the vibrator head assembly was attached, then the vibrator was stopped, the vibrator head assembly was moved up the core tube and re-attached. The vibrator was engaged again until either of the previous two situations occurred. Prior to winching the core out of the ground, the

top of the tube was filled with water. Then a core cap was screwed into place to create a vacuum and to prevent losing sediment from the bottom during core retrieval with a come-along. Just before the core tube was pulled completely out of the hole, a plastic core cap was prepared. This cap was placed over the bottom of the core tube just as it left the hole. This cap was taped in place. The end cap was unscrewed from the top of the core and replaced with a plastic core cap. The core sample was cut into 1 m sections and each new end was covered with plastic core cap. Then the core samples were transported to the laboratory at George Mason University for further processing prior to grain-size analysis.

On October 8 and 9, 2010, eight pulse-auger sediment core samples were collected from the Cedar Island breach zone (Figure 44). These samples were collected using an Edelman hand auger and an Eijkelkamp bailer boring system (Seminack, 2011) (Figure 45). Sediment samples were collected roughly at 10-cm intervals until either the auger met refusal or a mud layer was reached. The sediment samples were placed in plastic, zip-lock bags and transported to the laboratory at George Mason University.

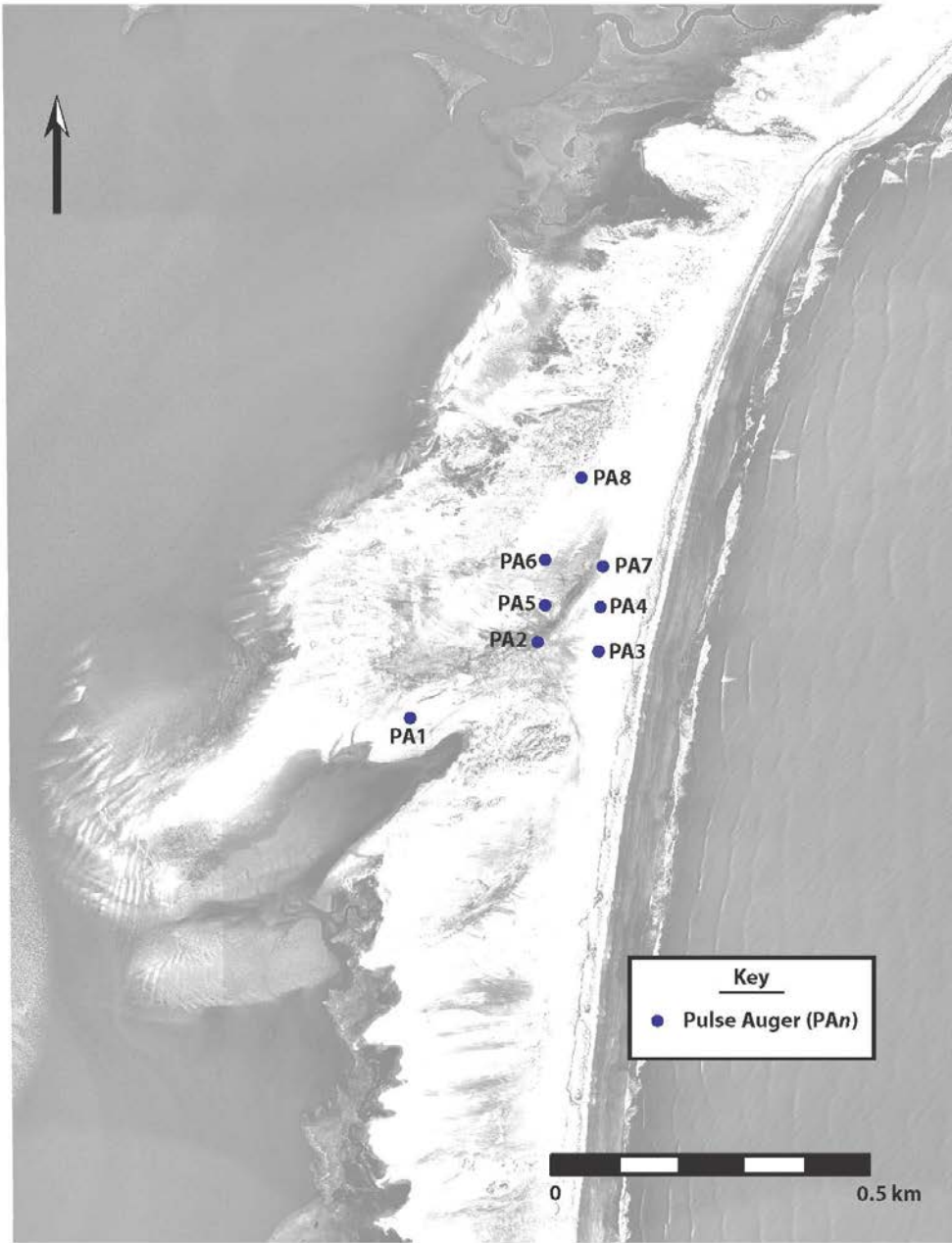


Figure 44: Map showing location of pulse augers.



Figure 45: Pulse auger equipment.

Laboratory Methods

All of the vibracores were stored at the laboratory at George Mason University at room temperature until they were processed. Two cuts were made lengthwise down each side of each 1 m core section using a SKIL circular saw with a metal-cutting blade. The cuts were made off-center so that the core could be opened into 1/3 and 2/3 pieces using piano wire and spatulas (Stone, 2006). The smaller side was used for sub-sampling and the larger side was used for core description and photographs. After opening, the larger side was trimmed and cleaned with a spatula to smooth out any roughness in the surface. Then this side was described for stratigraphic and sedimentary features plus other pertinent information and a description of each of the primary facies using sheets

modified from Boyles et al. (1986). These log forms can be found in Appendix A. All vibracores were photographed using a Nikon D40 digital camera. All core photographs are included in Appendix B. The larger side of each core section was sealed in plastic and stored in the laboratory at George Mason University for future work.

The smaller side of each vibracore section was sampled at 4-cm intervals using a stainless-steel spoon taking care to leave the sediment next to the aluminum tube alone to avoid longitudinal contamination. Each sample was divided into two sub-samples, one to be used for grain-size analysis and the other to be used for future micropaleontological analysis. Each sub-sample was placed into a labeled zip-lock bag. The remaining sediment was thrown out and the aluminum tube was recycled.

Each vibracore was described using a vibracore description sheet (Appendix A). These sheets allow for general information to be recorded on the vibracores such as core ID, date collected, elevation, compaction, latitude and longitude, core length, total length (incorporating compaction amount), and a brief description of the location where the vibracores was collected. Additional information on sedimentary texture and structure, % sand, physical characteristics, and stratification type can be recorded. Additional information was recorded for each vibracore along its length for photography, grain-size samples, and microfossil samples. Space for description and remarks is located on the right-side of the vibracore description sheet, which was used to make facies descriptions. If the vibracores was more than four meters long, an additional vibracore description sheet was added.

Grain-size Analysis

The grain-size samples were air-dried by placing each on a piece of newspaper for at least 12 hours. After that time, each sample was placed on another piece of newspaper and allowed to air-dry for at least an additional 12 hours. The dried samples were then placed back into the original zip-lock bag that had been turned inside-out and allowed to air-dry. Most of the sand samples did not exhibit any clumping, but sand samples with clumps were disaggregated using a mortar and pestle.

Samples that were not mud were analyzed for the amount of different grain sizes using a Gilson AutoSiever (Figure 46). Approximately one tablespoon of a representative portion of the sample was collected from the sample bag and placed in a plastic container for which the tare weight had been measured and recorded using an Ohaus chemical balance. The gross weight was measured and recorded to determine if there was at least 10 g of the sample in the container. If not, more of the sample was added and the final gross weight was measured and recorded. Each sample was over 10 g. Each of the sieves had its tare weight measured and recorded before each sample was sieved. For sand samples, the sieves ranged from 0 phi to 4 phi in 1/4 phi intervals with a fines collector to measure the amount finer than 4 phi. For sand and silt samples, the sieves ranged from 0 phi to 5 phi in 1/4 phi intervals with a fines collector to measure the amount finer than 5 phi. The sieves were ordered into three stacks and the sample was placed in the top of the first stack with the lowest phi values. The finer portion of the sample from the first run would end up in the fines collector at the bottom. This portion of the sample would be placed in the top of the second stack of sieves. This procedure was followed for the final

stack of sieves. Each of the sieves was weighed after sieving and the gross weight was recorded. The portion of the sample that ended up in the fines collector after the third sieving, was emptied into a separate container for which the tare weight had been measured and recorded. The container was weighed to measure the gross weight of the portion of the sample, which was finer than the last sieve. The sample weights were calculated by the following formula: $\text{sample weight} = \text{gross weight} - \text{tare weight}$. All weights were measured in grams.



Figure 46: Gilson AutoSiever.

The Gilson AutoSiever allows the user to enter the maximum amplitude of vibrations and three separate time intervals: 1) a ramp-up time to maximum vibration amplitude, 2) the time for which maximum vibration amplitude is applied to the sample, and 3) a ramp-down time to zero vibration amplitude. The maximum vibration amplitude that was used throughout this study was 33 vibrations with a ramp-up time of 1 minute, a

maximum vibration amplitude time of 2 minutes, and a ramp-down time of 1 minute. The Gilson AutoSiever allows the user to save the maximum amplitude and time interval for storage of this program and its re-use. This same program was used throughout this project. For each grain-size sample, data were recorded on a data sheet. All data sheets for each grain-size analysis are compiled in Appendix C.

The statistics for each sample were calculated using the program GRADISTAT (Blott & Pye, 2001). Four parameters are used in quantifying grain-size distributions: 1) the mean (a measure of central tendency); 2) sorting (a measure of the spread of the distribution around the mean or standard deviation); 3) skewness (a measure of the symmetrical nature of the distribution); and 4) kurtosis (a measure of the concentration of grain sizes relative to the mean). Figure 50 shows output from a typical GRADISTAT statistical calculation. GRADISTAT calculates the mean, mode(s), sorting, skewness, kurtosis, and a set of cumulative percentile values: D_{10} , D_{50} (median), D_{90} , D_{90}/D_{10} , $D_{90} - D_{10}$, D_{75}/D_{25} , and $D_{75} - D_{25}$. GRADISTAT also classifies the sample type (in Figure 47, Unimodal, Well sorted), the sediment name (in Figure 50, Well Sorted Fine Sand), and the textural group (in Figure 47, Sand). In addition, the grain-size distribution and the percentages of each sediment type are displayed. GRADISTAT output for each of the analyses can be found in Appendix D.

SAMPLE STATISTICS						
SAMPLE IDENTITY: C1-006			ANALYST & DATE: ,			
SAMPLE TYPE: Unimodal, Well Sorted			TEXTURAL GROUP: Sand			
SEDIMENT NAME: Well Sorted Fine Sand						
	μm	ϕ	GRAIN SIZE DISTRIBUTION			
MODE 1:	196.0	2.356	GRAVEL: 0.0%		COARSE SAND: 1.2%	
MODE 2:			SAND: 99.2%		MEDIUM SAND: 4.4%	
MODE 3:			MUD: 0.8%		FINE SAND: 78.2%	
D ₁₀ :	114.2	2.084			V FINE SAND: 15.4%	
MEDIAN or D ₅₀ :	166.7	2.584	V COARSE GRAVEL: 0.0%		V COARSE SILT: 0.8%	
D ₉₀ :	235.9	3.130	COARSE GRAVEL: 0.0%		COARSE SILT: 0.0%	
(D ₉₀ / D ₁₀):	2.066	1.502	MEDIUM GRAVEL: 0.0%		MEDIUM SILT: 0.0%	
(D ₉₀ - D ₁₀):	121.7	1.047	FINE GRAVEL: 0.0%		FINE SILT: 0.0%	
(D ₇₅ / D ₂₅):	1.494	1.251	V FINE GRAVEL: 0.0%		V FINE SILT: 0.0%	
(D ₇₅ - D ₂₅):	66.70	0.579	V COARSE SAND: 0.0%		CLAY: 0.0%	
	METHOD OF MOMENTS			FOLK & WARD METHOD		
	Arithmetic	Geometric	Logarithmic	Geometric	Logarithmic	Description
	μm	μm	ϕ	μm	ϕ	
MEAN (\bar{x}):	171.9	158.0	2.584	165.5	2.595	Fine Sand
SORTING (σ):	64.19	1.721	0.496	1.316	0.396	Well Sorted
SKEWNESS (sk):	4.014	-6.242	-1.097	-0.028	0.028	Symmetrical
KURTOSIS (k):	42.49	59.67	9.556	0.908	0.908	Mesokurtic

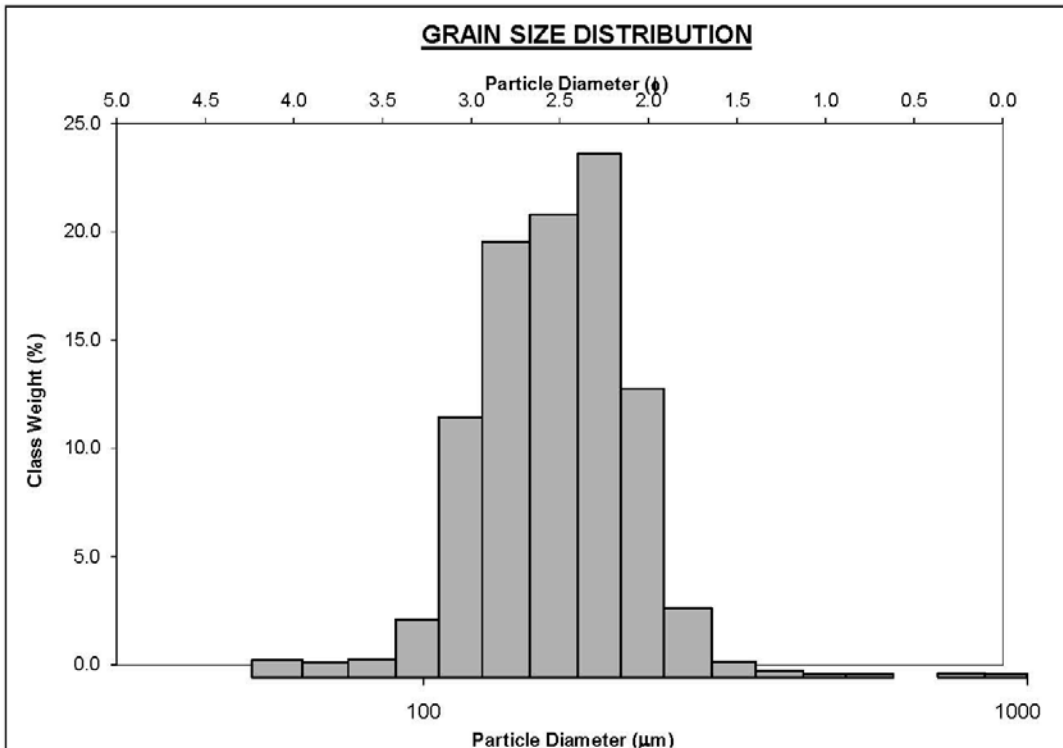


Figure 47: GRADISTAT printout using data from vibracore C1, sample 006.

Statistical calculations typically assume that the population being described is best fitted to a normal or Gaussian distribution with an arithmetic scale. This is seldom used by sedimentologists because the coarse sediments are emphasized at the expense of the finer particles (Blott & Pye, 2001). Geometric scales provide "equal emphasis on small differences in fine particles and larger differences in coarse particles" (Blott & Pye, 2001, pg. 1238). Thus, sedimentologists commonly use a base 2 logarithmic scale called the Udden-Wentworth grade scale. Krumbein (1938) proposed transforming the data to create a phi (ϕ) distribution (a type of log-normal distribution) using the formula: $\phi = -\log_2 d$, where d is the grain diameter in mm. This allows for equal emphasis on small differences in fine-grained sediment and large differences in coarse-grained sediments (Blott & Pye, 2001). The ϕ distribution is typically used by sedimentologists and will be used in this study.

Folk and Ward (1957) provided the most widely used formulae for calculating the first four moments of the ϕ distribution:

$$\text{Mean: } M_Z = \frac{\phi_{16} + \phi_{50} + \phi_{84}}{3}$$

$$\text{Standard deviation: } \sigma_I = \frac{\phi_{84} - \phi_{16}}{4} + \frac{\phi_{95} - \phi_5}{6.6}$$

$$\text{Skewness: } Sk_I = \frac{\phi_{16} + \phi_{84} - 2\phi_{50}}{2(\phi_{84} - \phi_{16})} + \frac{\phi_5 + \phi_{95} - 2\phi_{50}}{2(\phi_{95} - \phi_5)}$$

$$\text{Kurtosis: } K_G = \frac{\phi_{95} - \phi_5}{2.44(\phi_{75} - \phi_{25})}$$

These statistics are used in this study and they are displayed on the GRADISTAT output (Figure 47) under the title indicating the "Folk & Ward Method" in the column titled "Logarithmic ϕ ".

The first three moments of the grain-size distribution for each of the cores, pulse augers, trenches, and augers were plotted using Microsoft Excel. The data were displayed relative to the sample depth (see Figure 48). This was used to identify vertical grain-size trends in the sediment cores. These graphs can be found in Appendix E.

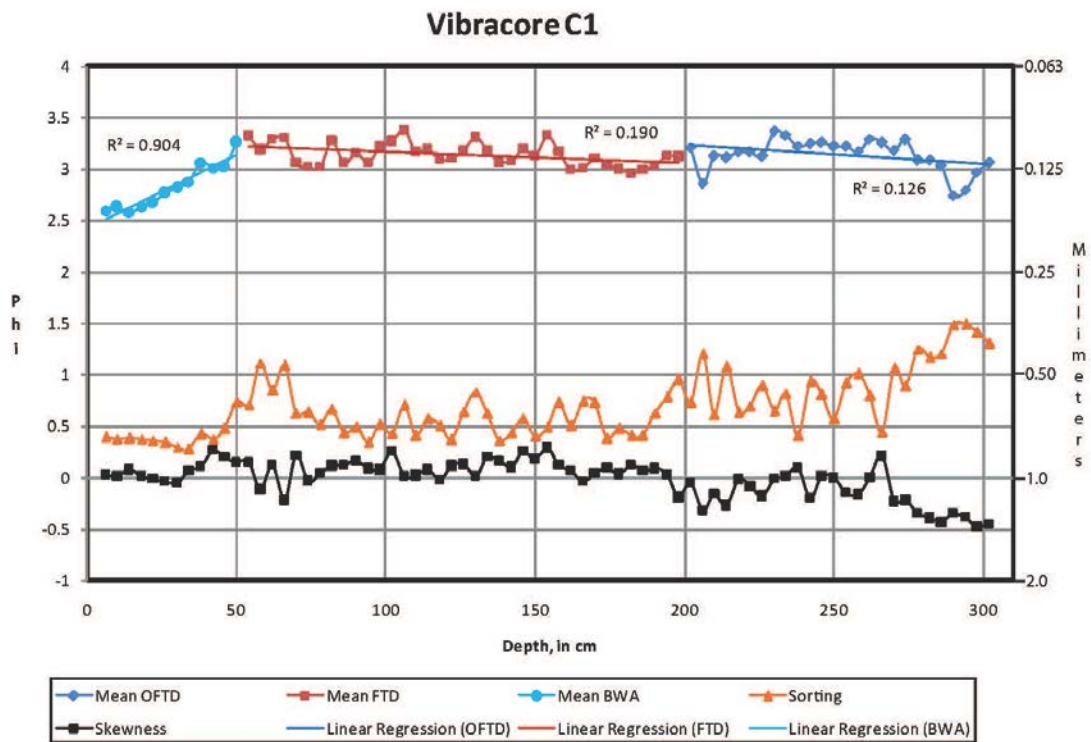


Figure 48: Vertical grain-size trends plotting the statistical moments (mean, sorting, and skewness) for vibracore, C1.

RESULTS

The breaching of southern Cedar Island has occurred at least three times over the past 60 years (Table 8). After each opening, the breach captured enough tidal prism to become a tidal inlet, migrated south in the direction of net longshore sediment transport, and then closed. Each time, the ephemeral tidal inlet remained open for four to nine years. Each time, the ephemeral tidal inlet eventually closed again because it could not capture enough tidal prism from the larger tide-dominated Wachapreague Inlet approximately 4 km to the south, which has a deep inlet throat (~21 m) and is naturally stabilized within the Pleistocene antecedent drainage system (Morton and Donaldson, 1973). The aerial photographs in Figure 49 show each ephemeral tidal inlet when it was open. These display a typical wave-dominated inlet morphology—a well-developed flood-tidal delta, a moderately defined inlet throat, and a small to nonexistent ebb-tidal delta. As found on Figure 50, specific geomorphic features that characterize the former ephemeral tidal-inlet zone include a topographic low indicating the last channel position and relict flood-tidal deltas along the backbarrier shoreline that are overlain by or grade into coalescing washover fans, flats, and terraces. The fine sand of the ephemeral tidal-inlet area contains scattered shell fragments that are smaller than those found seaward of the berm. The northern and southern edges of the last known ephemeral tidal-inlet position are higher in elevation and form dune terraces that are anchored by vegetation

and large shell armoring that is concentrated by wind deflation. The shells increase in size and completeness from the tidal-inlet center to its edges.

Table 8: Historical openings and closings of Cedar Island breach over the past 60 years (from Moyer, 2007).

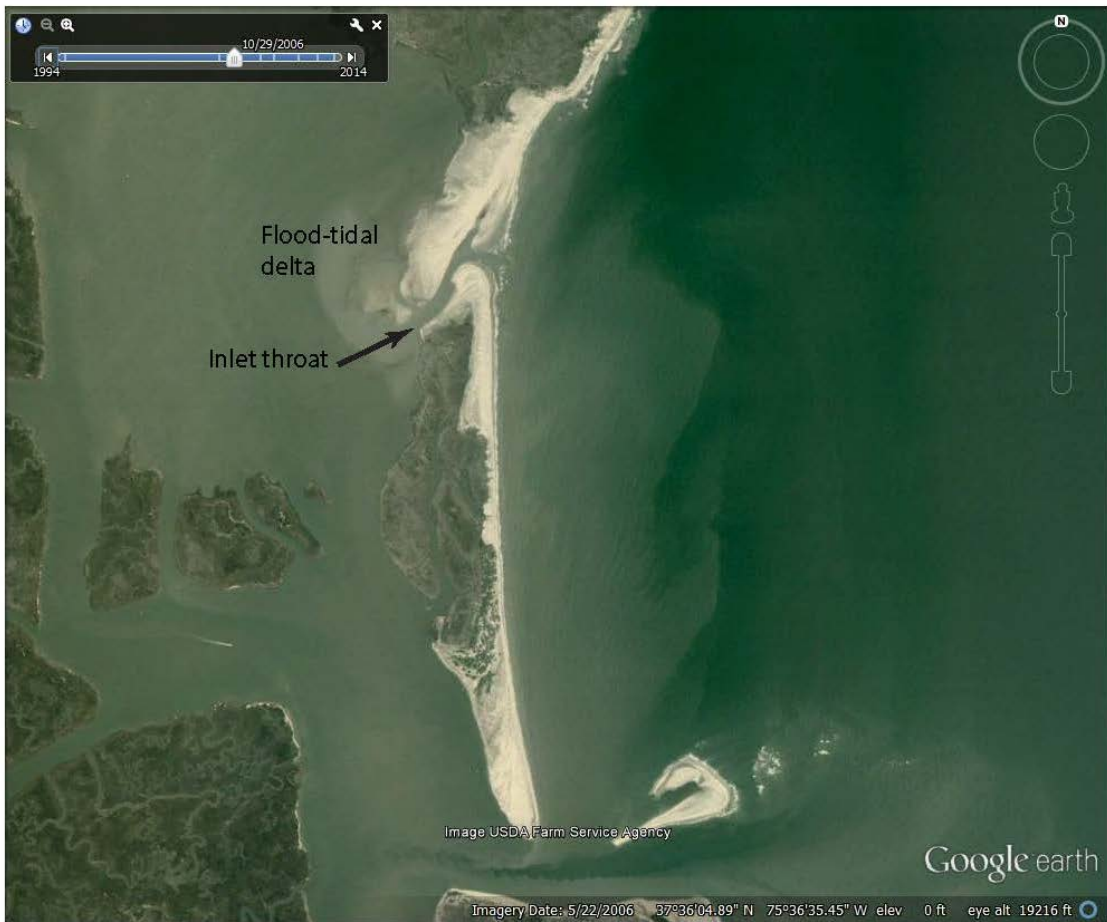
TIME	STATUS	LIKELY CAUSE
January 1956	Open	January 8-12 Northeaster
March 1962	Closed	March 6-8, "Ash Wednesday Storm"
March 1993	Open	March 12-15 Northeaster
July 1997	Closed	July 24-25 TS Danny
Jan/Feb 1998	Open	Jan 27-28 and/or Feb. 3-5 Northeasters
Dec 2006 or Jan 2007? (confirm closed April 28, 2007)	Closed	Healing by normal coastal processes?



A



B



C

Figure 49: Aerial photographs of ephemeral tidal inlets along the southern portion of Cedar Island, Virginia, showing three active tidal inlets over the past 60 years: (A) October 14, 1957 (Byrne, et al., 1975); (B) March 19, 1994 (Google Earth, 2015a); (C) October 29, 2006 (Google Earth, 2015a).



Figure 50: Location map of the southern portion of Cedar Island showing geomorphic features (Google Earth, 2015b).

Figure 51A is a photograph of the location of the Cedar Island Inlet that shows the low-profile, washover-dominated barrier island, with the view to the north-northwest. Figure 51B shows the location of the Cedar Island Inlet with the view to the southwest into Burtons Bay. Along the backbarrier shoreline, relict flood-tidal deltas exist that are overlain by or grade into coalescing washover fans, flats, and terraces.



A



B

Figure 51: Low-oblique aerial photographs of Cedar Island, Virginia. (A) The low-profile, washover-dominated barrier island, with the view to the north-northwest. The arrow points to the final channel position of the last Cedar Island tidal inlet (open from 1998 to 2007), which opened to the north, migrated south in the direction of net longshore sediment transport, and then closed. In the background is Metompkin Inlet and farther northward, Metompkin Island, Virginia. For scale, see the shrimp trawler marooned on the foreshore after losing power during winter and tropical storm Nor'Ida in November 2009. Also, the abandoned beach house is located in the surf zone, left behind as the barrier-island shoreline rapidly migrates landward. (B) The low-profile, washover-dominated barrier island, with the view to the southwest into Burtons Bay. The double-headed arrow indicates the orientation of the final channel position of the last Cedar Island tidal inlet. Along the backbarrier shoreline, relict flood-tidal deltas exist that are overlain by or grade into coalescing washover fans, flats, and terraces. Taken August 31, 2011 by Randolph A. McBride.

The last ephemeral tidal inlet is estimated to have been 419 m wide in 1998, shortly after it opened, and 54 m wide in 2005, just over a year before it closed (Moyer, 2007). Over the nine years that the ephemeral tidal inlet was open, the inlet channel migrated approximately 333 m southwest in the direction of net longshore sediment transport and rotated counter-clockwise 47° to face the predominant wave direction from

the northeast, and then rotated slightly clockwise before closing. The lateral migration rate was approximately 35.5 m/yr. Moyer (2007) found that the ephemeral tidal inlet captured approximately 12% of the available tidal prism from Wachapreague Inlet, then steadily lost its tidal prism and closed by Jan 2007.

Greenwood & Keay (1979) studied a similar barrier breach called North Inlet located in Kouchibouguac Bay, Southern Gulf of St. Lawrence, Canada. North Inlet was open for six years from 1971 to 1977. They classified it as flood-dominated and found that the tidal prism of the ephemeral inlet was $1.19 \times 10^6 \text{ m}^3$ in 1973 and captured approximately 8% of the available tidal prism from a nearby tidal inlet to the south, Little Gully. After the initial opening, the inlet was approximately 100 m wide. The inlet began migrating in 1972. Between 1972 and 1974, the inlet migrated 60 m to the south at a rate of 30 m/yr in the direction of net longshore sediment transport, after which it stabilized and rotated clockwise. The rotation of the main inlet channel through the flood-tidal delta was caused by the channel gradually being filled and a subsidiary channel getting more of the tidal flow. Thus, the tidal flow moved in a channel that was oriented in a northwest-southeast direction instead of west-east. At the same time, littoral drift caused lateral progradation of the updrift inlet shoreline and diverted inlet flow to the south. Closure of the tidal inlet was associated with the gradual expansion of the flood-tidal delta, restriction of the tidal channel, and rotation of the channel from normal to subparallel to the shoreline. (Greenwood & Keay, 1979).

The southern end of Cedar Island is a thin extension of the main part of the island (Figure 52). It is bounded on the south by Wachapreague Inlet, which has been relatively

stable in location since the post-glacial sea level rise with some southward migration (Rice et al., 1976; DeAlteris & Byrne, 1975; Richardson, 2012). Wachapreague Inlet has a large ebb-tidal delta that is mostly submerged, except for Dawson Shoals, which is subaerial and exists on the northern side of the ebb-tidal delta. Wachapreague Inlet does not have a well-developed flood-tidal delta. The flood tide flows mostly into Burtons Bay to the northwest of the inlet through several channels in the estuary and back-barrier salt marshes. In addition, a reduced amount of the flood tide flows into Bradford Bay to the west and Swash Bay to the southwest through smaller channels (Figure 52). Five channels flow into Burton Bays from Wachapreague Inlet, which are bounded by subaerial marshes.

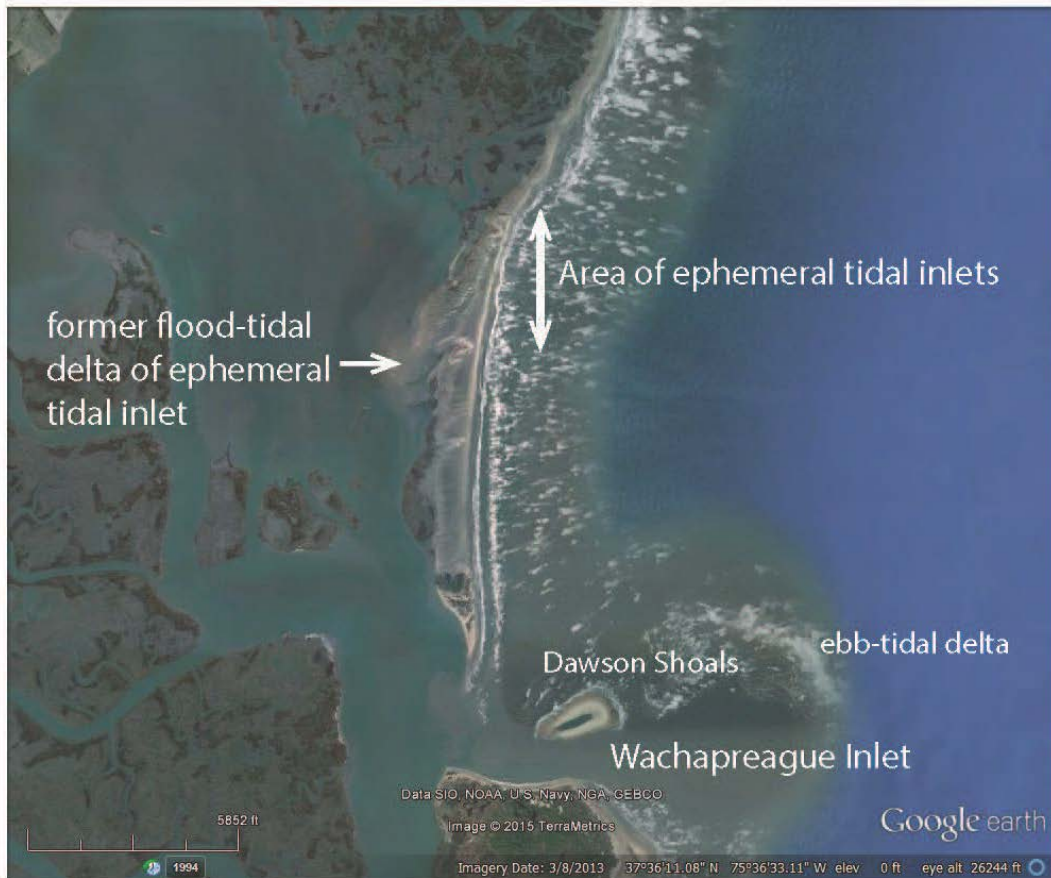


Figure 52: Cedar Island location map showing primary geomorphic features (Google Earth, 2015b).

From south to north, barrier fringe marshes are found along the backside of Cedar Island, north of the southern tip and extend 2.6 km to the north. North of the barrier fringe salt marshes is the subaqueous remnants of the southernmost extent of the flood-tidal delta from the last ephemeral tidal inlet. The next 0.8 km of Cedar Island is the zone of the three ephemeral tidal inlets and, therefore, the barrier island is thin with no marsh behind it (open bay-backed barrier island). Just to the north of this, Cedar Island is backed by extensive salt marshes and tidal creeks (saltmarsh-backed barrier island),

which fill the area between the beach and the mainland until the next tidal inlet to the north, Metompkin Inlet (see Figure 52).

Cedar Island ephemeral inlet sedimentology

Surface sediment distribution

Mean

The data for the surface sediment samples were combined with the data from the surface samples of the vibracores, push core, trenches, and pulse augers to determine the distribution of statistical parameters and groups of statistical parameters for analytical purposes. The total number of data points is 64. Figure 53 shows the distribution of mean grain-size divided into two classes, finer-grained ($> 2.0 \phi$) and medium grained-sand ($< 2.0 \phi$). The mean grain-size for the surface sediments range from 1.643 to 2.905 ϕ . The map shows that the surface samples are predominately fine-grained (83%) with those that are medium-grained are second (17%). Fine grain sizes are typically found in the inlet throat and flood-tidal delta areas, while medium grain sizes are predominately found along the beach and into the surf zone. This indicates that the surface sediments in the inlet throat and flood-tidal delta areas were affected by overwash and aeolian processes that deposited finer grained sediments. The surface sediments along the beach and the surf zone experienced winnowing, and possibly some deflation, as a result of wave and wind action that transport the finer-grained sediments away from the beach, the coarser grained sediments are left behind.

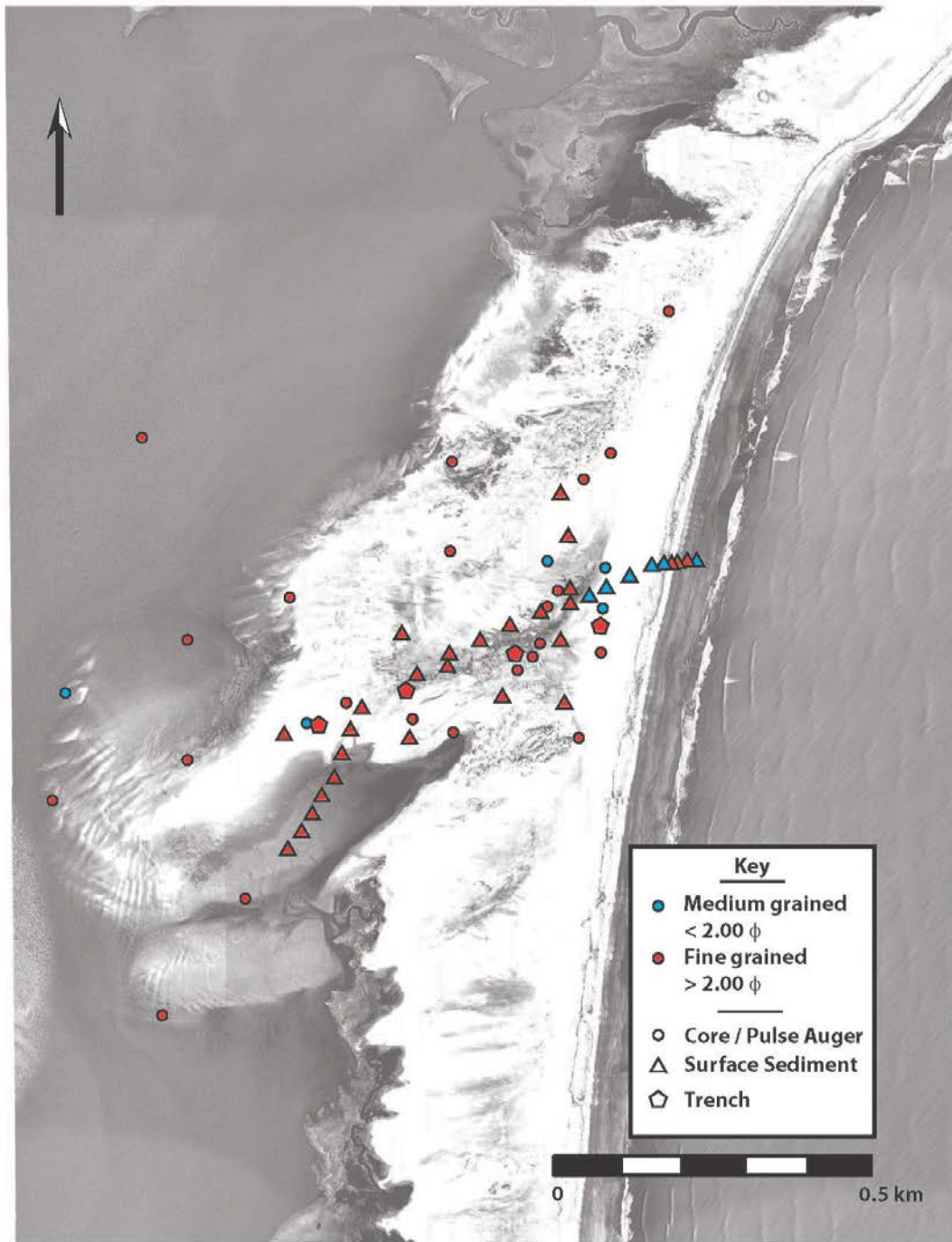


Figure 53: Map showing the distribution of mean grain size for all surface samples, divided into fine-grained samples ($> 2.0 \phi$) and medium-grained samples ($< 2.0 \phi$).

Standard Deviation

Figure 54 shows the distribution of sorting or standard deviation as defined by Folk (1980). The map shows that 53% (34) of the samples are well-sorted and are distributed throughout the area, while 38% (24) of the samples are moderately well-sorted and 9% (6) are moderately sorted. The moderately sorted samples are found mostly near the beach and along the flood-tidal delta area. These samples show slightly less sorting than the other samples because of their proximity to the active nearshore. They experience mixing with sediments from longshore transport and those at the distal end of the flood-tidal delta area where the locations are not as exposed to aeolian processes which reduces the sorting process.

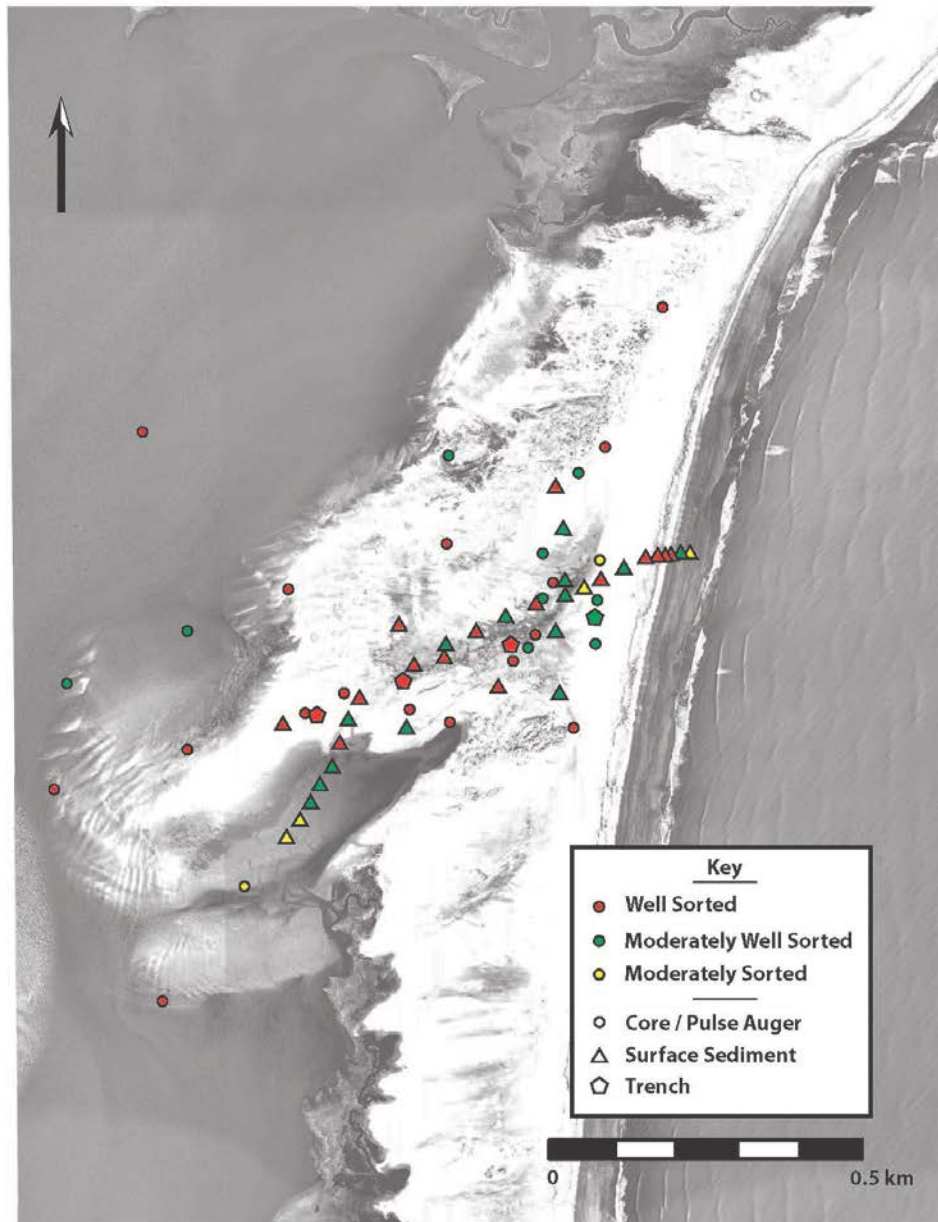


Figure 54: Map showing the distribution of sorting for all surface samples.

Figure 55 shows the distribution of skewness as defined by Folk (1980). The map shows that 64% (41) of the samples have distributions that are nearly symmetrical. They are distributed evenly throughout the area and are indicative of a normal distribution of

grain sizes. Finely skewed samples (positive) are located mostly along the last position of the tidal inlet channel and make up 20% (13) of the samples, reflecting the predominance of fine grains in these areas and may indicate winnowing of the sediments by aeolian processes. Coarsely skewed samples (negative), which make up 16% (10) of the samples, are located in the surf zone, the beach, and along the distal end of the inlet channel through the flood-tidal delta, which is indicative of the predominance of coarse grains and may reflect the processes of longshore-sediment transport, in the case of the surf zone and beach, and the wave action from the estuary affecting the surface sediments in area of the former flood-tidal delta by moving the fine-grained sediments into the estuary waters.

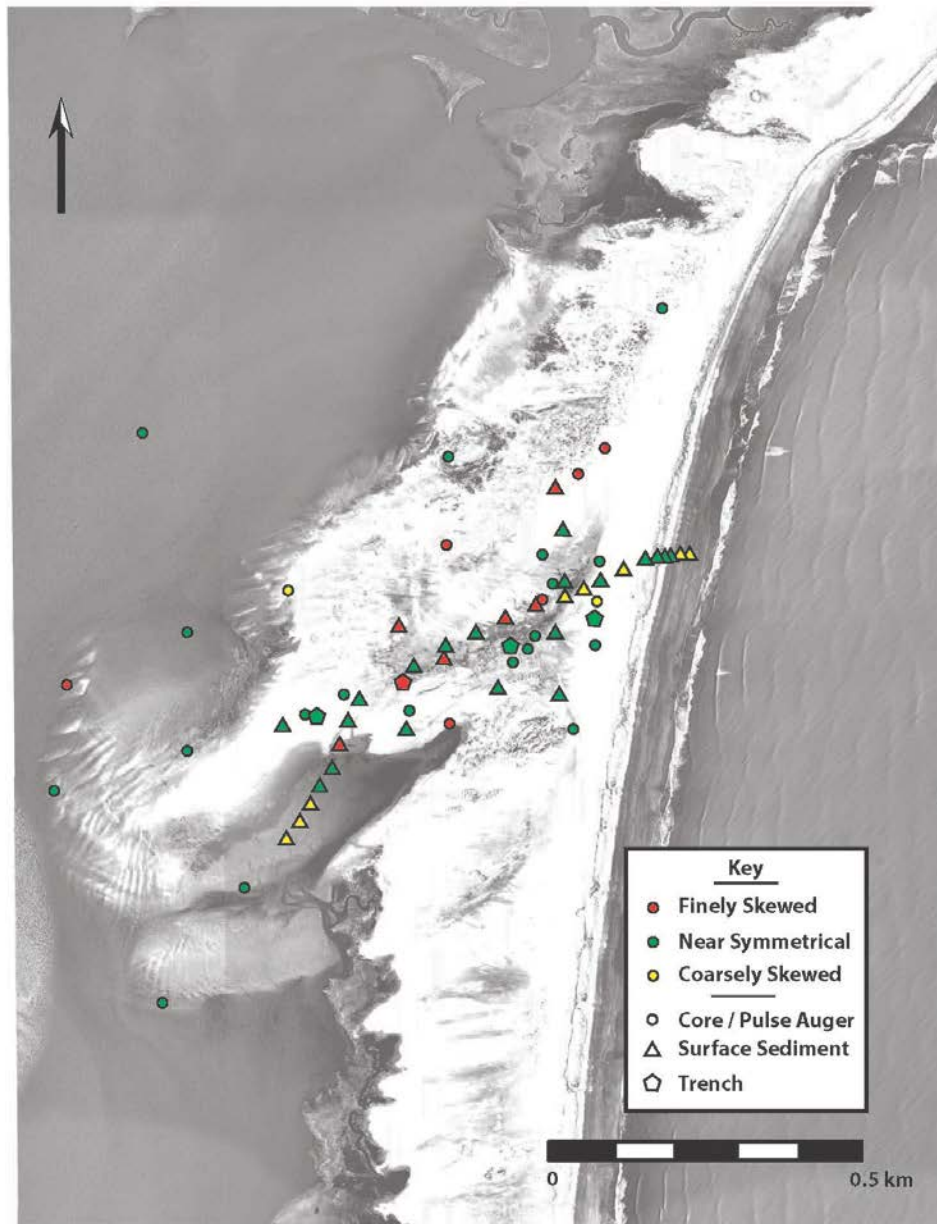


Figure 55: Map showing the distribution of skewness for all surface samples.

Primary facies and surfaces

Fifteen primary facies consisting mostly of sand, shell, and mud units were identified from the 25 sediment cores collected in the former Cedar Island tidal-inlet

zone. Facies were delineated based on texture, color, physical sedimentary structures, and biogenic sedimentary structures. Table 9 contains the relevant characteristics of these facies. The five sand facies are tan to light gray, very fine to medium sand. The one shell facies consists of disarticulated shell fragments with larger fragments up to 8 cm in a tan, fine to medium sand matrix. The nine mud facies are characterized by light gray to dark gray mud with disarticulated shells and shell fragments scattered throughout and some articulated *in situ* shells. Most of the mud facies have horizontal laminations and bioturbation. Some contain very fine to fine sand.

A detailed description of each facies is found below:

Facies 1: Tan, very fine to medium sand (73 observations) (Figures 56 and 57)

This facies is dominated by massive, tan, well-sorted to moderately well-sorted, fine to medium sand with occasional horizontal laminations and cross bedding with a complete lack of biogenic sedimentary structures. Minor amounts of mica occur and occasional scattered, disarticulated shell fragments are found, some large in size (up to 8 cm). Grain size ranges from 1.31 to 3.15 phi with a unit thickness ranging from 3 to 185 cm. This facies tends to coarsen upward mostly but shows no grain-size trends in some units.

Facies 2: Tan to light gray, very fine to medium sand (17 observations) (Figure 57)

This facies consists of tan to light gray, well-sorted to moderately well-sorted, symmetrical to coarsely skewed, very fine to medium sand with some mica present and is generally massive with some minor horizontal laminations and a complete lack of

biogenic sedimentary structures. Occasional small, scattered, disarticulated shell fragments with a few medium-gray mud inclusions. Grain size ranges from 1.32 to 3.20phi and this facies ranges from 7 to 260 cm thick. This facies tends to coarsen upward.

Facies 3: Light gray to tan, fine to medium sand (3 observations)

This unit is characterized by massive, light gray to tan, well-sorted to moderately sorted, fine to medium sand with some small to large scattered, disarticulated shell fragments (up to 3 cm) and a complete lack of biogenic sedimentary structures. Grain size ranges from 1.61 to 2.48phi and thickness ranges from 15 to 135 cm. This facies shows no vertical grain-size trend.

Facies 4: Light gray, very fine to medium sand (8 observations) (Figure 58)

This facies consists of massive, light gray, moderately well-sorted, symmetrical to coarsely skewed, very fine to medium sand and a complete lack of biogenic sedimentary structures. Some mica is present and occasional scattered, disarticulated shell fragments. Grain size ranges from 1.80 to 3.06phi and this facies ranges from 20 to 240 cm thickness. This facies tends to coarsen upward.

Facies 5: Light gray, very fine to medium sand with dark-gray laminations (11 observations) (Figure 58)

This facies is characterized by light gray, very well-sorted to poorly sorted, very fine to medium sand with dark gray horizontal laminations and some minor bioturbation with occasional small disarticulated shell fragments. Mica is present throughout. Grain

size ranges from 1.98 to 3.38 phi and this facies ranges from 12 to 299 cm in thickness.

This facies tends to coarsen upward.

Facies 6: Shell layer (19 observations) (Figure 56)

This unit is dominated by a shell layer in a tan, well-sorted to moderately sorted, coarsely to very coarsely skewed, medium to fine sand matrix, which contains small to medium scattered, disarticulated shell fragments with larger fragments up to 8 cm and a complete lack of biogenic sedimentary structures. Also contains disarticulated large oyster and bivalve fragments up to 10 cm. Some gastropod shells were also present.

Grain size in this unit ranges from 1.28 to 2.70 phi and thickness ranges from 3 to 43 cm.

This facies tends to coarsen upward mostly but also tends to fine upward in some units.

Facies 7: Light gray, clayey, silty, very fine to fine sand (4 observations)

This unit consists of light gray, clayey, silty, well-sorted, symmetrical to finely skewed, very fine to fine sand with mica throughout. Horizontal laminations and some bioturbation are present. Grain size ranges from 2.54 to 3.95 phi, and thickness ranges from 16 to 125 cm. This facies tends to coarsen upward.

Facies 8: Light gray, laminated muddy, very fine to fine sand (1 observation)

This facies is characterized by light gray, laminated muddy very fine to fine sand. Some bioturbation present only in the lower part of this facies. Some shell fragments at the base with mica present. Grain size ranges from 2.11 to 3.08 phi and is 32 cm thick. This facies tends to fine upward.

Facies 9: Light to medium gray sandy silty clay (1 observation)

This unit features light to medium gray, poorly sorted, very coarsely to coarsely skewed, sandy silty clay with bioturbation decreasing upward. Some scattered, disarticulated shell fragments are present and mica is present throughout. This facies tends to fine upward.

Facies 10: Light gray mud (3 observations) (Figure 58)

This unit is characterized by light gray, horizontally laminated mud with mica throughout and dominated by bioturbation. Small, scattered, disarticulated shell fragments are found but rare.

Facies 11: Medium-dark gray mud (4 observations) (Figure 59)

This unit is characterized by medium-dark gray massive mud with some sand with horizontal laminations present and some lenticular bedding. Mica is abundant to not present. Occasional scattered, disarticulated shell fragments with some complete articulated gastropod shells that have been transported. Bioturbation ranges from high to not present with some burrows (1 to 1.5 cm) and some large burrows (7 to 10 cm).

Facies 12: Medium gray mud (8 observations) (Figure 58)

This unit is dominated by medium gray mud with abundant mica and some sand. Bioturbation ranges from high to not present. Articulated razor clams shells are infrequent but found *in situ* with both halves present). Shell fragments are found scattered throughout. Some horizontal laminations are present.

Facies 13: Medium to dark gray laminated sandy mud (1 observation)

This facies is characterized by medium to dark gray laminated sandy mud. Some bioturbation is present. Mica present throughout.

Facies 14: Dark gray silty clay (1 observation)

This unit consists of dark gray silty clay with horizontal laminations. Subtle bioturbation throughout with some gastropod and disarticulated mollusk shell fragments.

Facies 15: Dark gray mud (7 observations) (see Figures 57 and 59)

This unit features dark gray massive sandy mud. Mica is abundant to not present. Occasional shell fragments with some bioturbation.

These descriptions are summarized in Table 9.

Table 9: Summary of characteristics of facies found in the Cedar Island Inlet sediments.

Facies No.	Sediment Type	Description	No. obs.	Grain size, in phi	Thickness, in cm
1	Sand	Massive, tan, well-sorted to moderately well-sorted, occasional horizontal laminations	73	1.31 – 3.15	3 - 185
2	Sand	Generally massive, tan to light gray, well-sorted to moderately well-sorted, some minor horizontal laminations	17	1.32 – 3.20	7 – 260
3	Sand	Massive, light gray to tan, well-sorted to moderately well-sorted	3	1.61 – 2.48	15 – 135
4	Sand	Massive, light gray, moderately well-sorted	8	1.80 – 3.06	20 – 240
5	Sand	Light gray, very well-sorted, dark gray horizontal laminations	11	1.98 – 3.38	12 – 299
6	Shell layer	Tan, well-sorted to moderately sorted sand matrix	19	1.28 – 2.70	3 – 43
7	Clayey silty sand	Light gray, well-sorted, horizontal laminations	4	2.54 – 3.95	16 – 125
8	Muddy sand	Light gray	1	2.11 – 3.08	32
9	Silty clay	Light to medium gray, poorly sorted,	1	-	43
10	Mud	Light gray, horizontally laminated	3	-	21 – 104
11	Mud	Massive, medium-dark gray, some horizontal laminations, some flaser bedding	4	-	12 - 406
12	Mud	Medium gray	8	-	16 - 437
13	Sandy mud	Medium to dark gray	1	-	48
14	Silty clay	Dark gray	1	-	59
15	Mud	Massive, dark gray	7	-	4 - 157

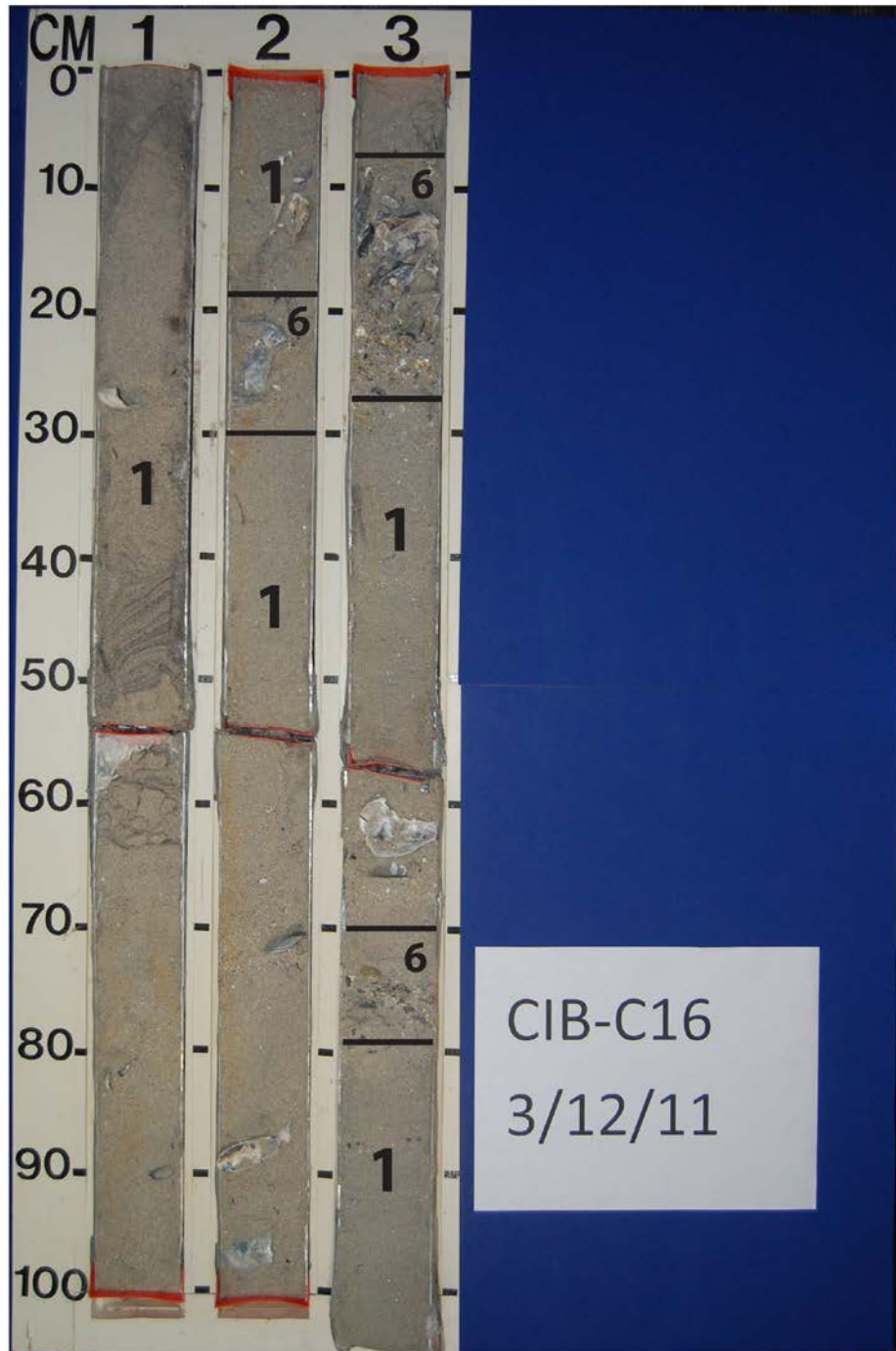


Figure 56: Vibracore 16 showing Facies 1 and Facies 6

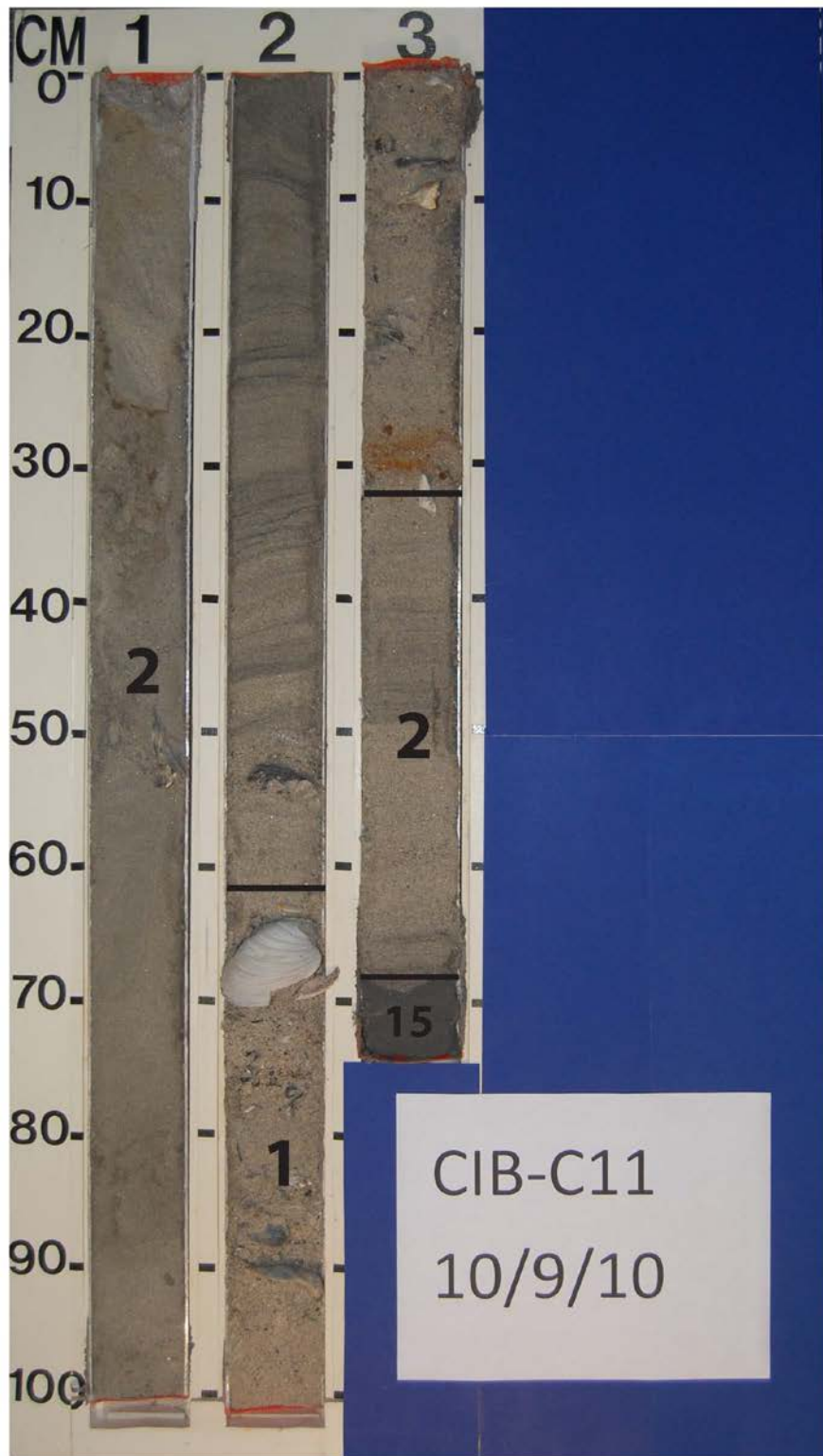


Figure 57: Vibracore C11 showing Facies 1, Facies 2, and Facies 15.

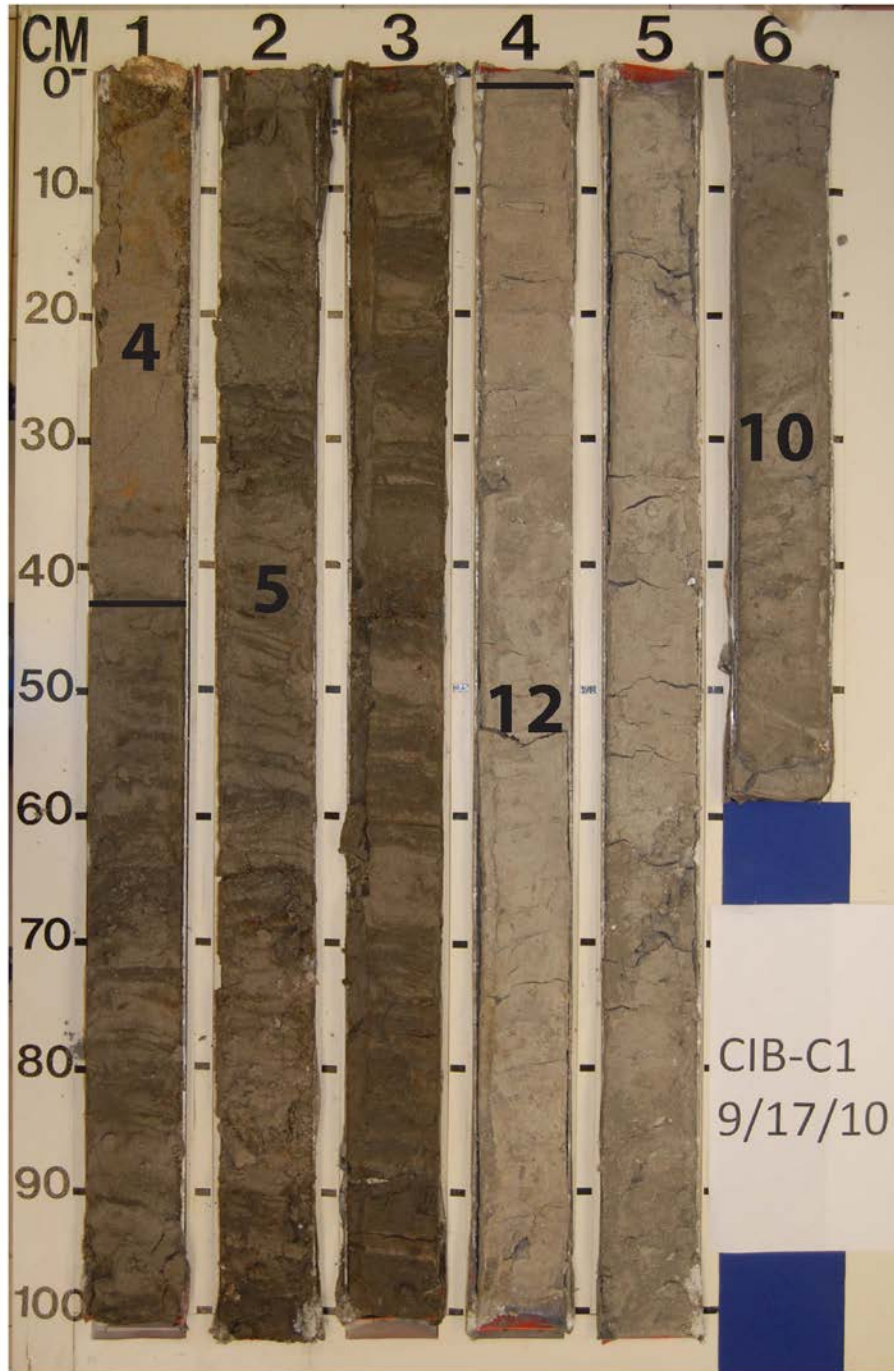


Figure 58: Vibracore C1 showing Facies 4, Faices 5, Facies 10, and Facies 12.



Figure 59: Vibracore C10 (bottom 372 cm) showing Facies 11 and Facies 15.

Interpretation of depositional environments

Four depositional environments were identified from the 15 sediment facies:

Beach–washover–aeolian: Tan to light-gray, very fine to medium sand with some large shell fragments and minor shell layers (Figure 61).

Tidal-inlet: Mostly tan with some light- to medium-gray, fine to medium sand (that tends to be negatively skewed and either fines upward or coarsens upward), interspersed with shell layers or shell fragments and shell lag at the base, massive bedding with minor medium-gray laminations (Figure 60).

Flood-tidal delta: Light- to medium-gray with some tan, fine to medium sand and silty sand, horizontal laminations, some small to medium shell fragments, and some bioturbation (Figure 61).

Estuary: Light- to dark-gray mud with bioturbation and horizontal laminations (Figure 62).

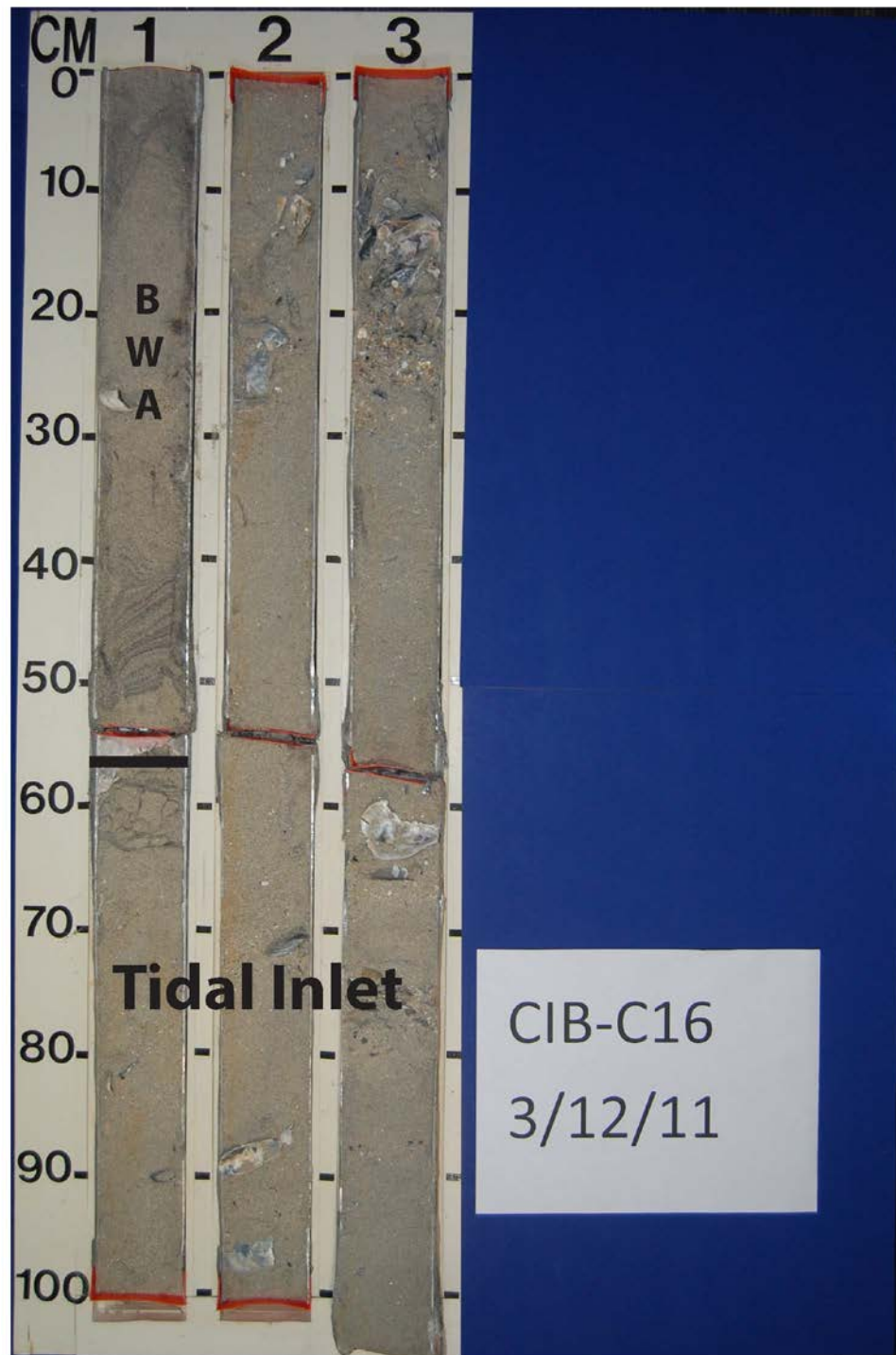


Figure 60: Vibracore C16 showing two depositional environments, beach-washover-aeolian (BWA) and tidal inlet.

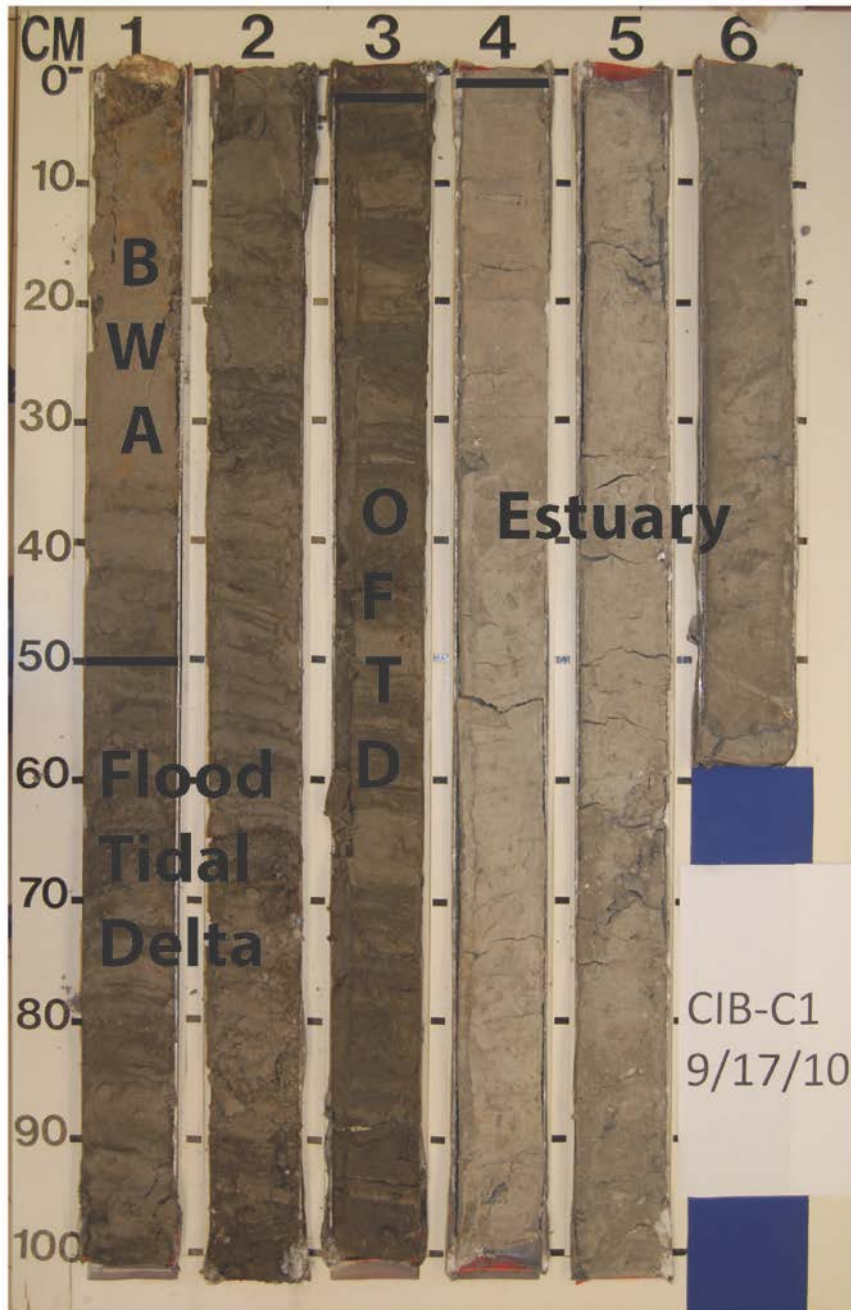


Figure 61: Vibracore C1 showing three depositional environments, beach-washover-aeolian (BWA), flood-tidal delta, and estuary.

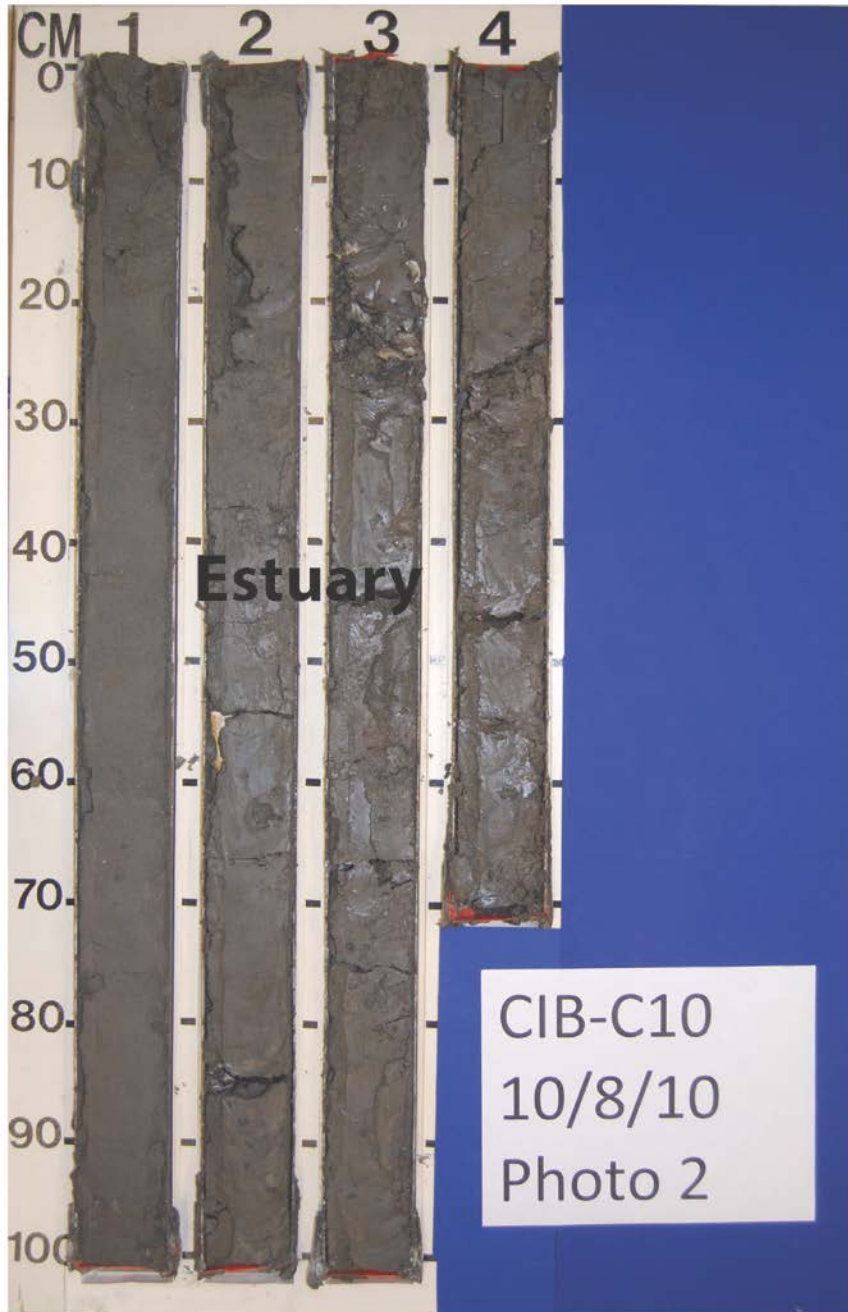


Figure 62: Vibracore C10 (bottom 372 cm) showing the estuary depositional environment.

Facies 7 (clayey, silty sand) through Facies 15 (mud) were designated as belonging to the estuary depositional environment. Facies 6, shell layer, was put into the tidal inlet depositional environment. The sand facies (Facies 1 -6) were interpreted on the basis of sediment type, geographic location, and stratigraphic horizon and were placed in either the beach-washover-aeolian, flood-tidal delta, or tidal inlet depositional environments.

A paralic sequence includes a range of sedimentary environments that are deposited at or near sea level and therefore, neither marine nor continental but in the transitional area between the two. The main environments that create paralic deposits are shore systems, deltas, and estuaries. The sedimentary sequence in the study area exhibits a typical paralic sequence from the Delmarva Peninsula of estuarine deposits overlain by a barrier lithosome (Belknap and Kraft, 1985; Kraft et al., 1987). The ephemeral tidal inlets scoured into underlying estuarine deposits and formed a channel diastem between the underlying estuarine deposits and the tidal-inlet deposits. A channel diastem is defined as “a local surface of erosion resulting from the lateral migration of a channel floor” (Nummedal & Swift, 1987, p. 246). The flood-tidal delta deposits formed a sharp contact with the underlying estuarine deposits. The beach-washover-aeolian deposits overlying all of the study area formed a gradational contact with all of the underlying sediments.

Vertical grain-size trends

Vertical grain-size plots for each of the 18 vibracores showing mean grain size, sorting, and skewness with depositional environments indicated are presented below. The plots are paired with a whole core photograph with depositional environments delineated.

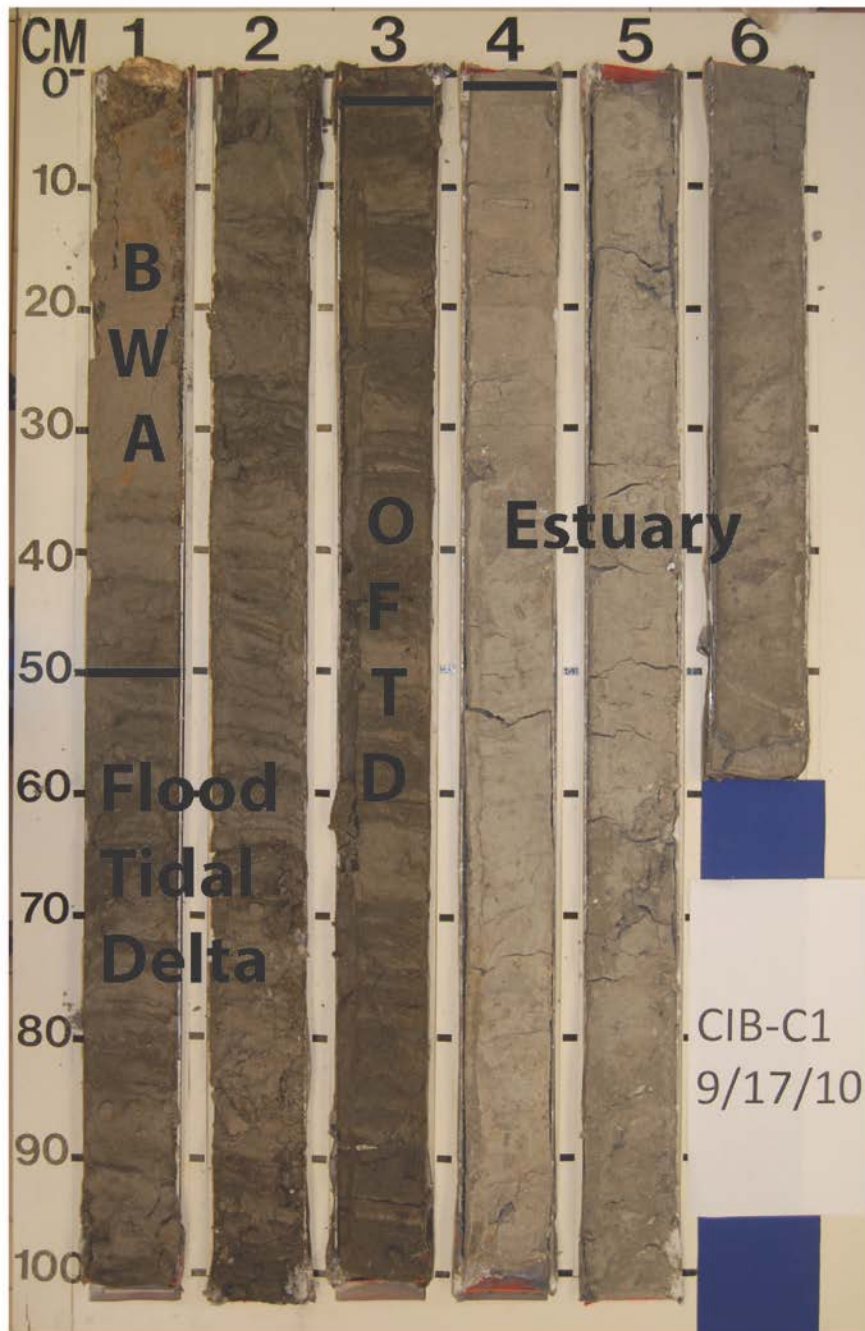


Figure 63: Photograph of Vibracore C1 with depositional environments delineated (BWA – beach-washover-aeolian, OFTD –older flood-tidal delta).

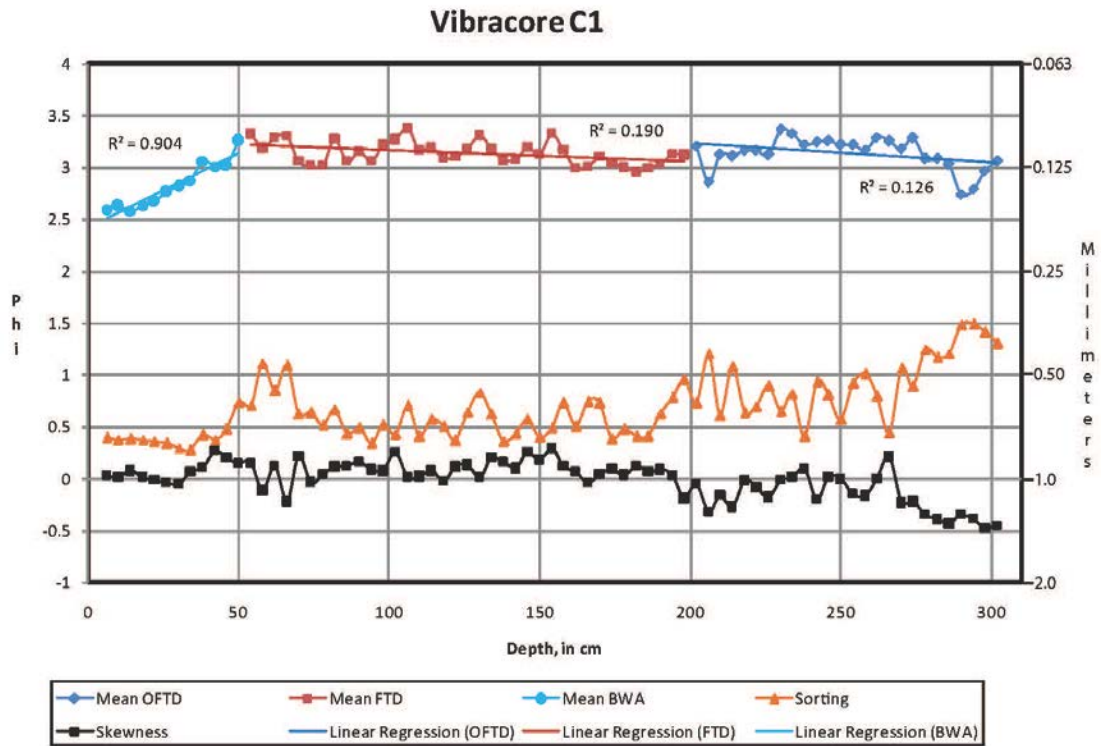


Figure 64: Grain-size graph for Vibracore C1 (OFTD – older flood-tidal delta, FTD – flood-tidal delta, BWA – beach-washover-aeolian). Skewness is dimensionless.

Figure 63 shows the depositional environments present in Vibracore C1. The grain-size data for C1 (Figure 64) show an overall trend of becoming better sorted upward and trending from negative to positive skewness upward. The older flood-tidal delta deposits show a slight fining upward trend in mean grain sizes, are poorly sorted above the estuary deposits, and tend to become better sorted upward, and trend from negative to positive skewness. The flood-tidal-delta deposits show a slight fining upward trend in mean grain sizes, become slightly less sorted upward, and generally show

positive skewness. The beach-washover-aeolian deposits coarsen upward, become better sorted upward and show less positive skewness upward.

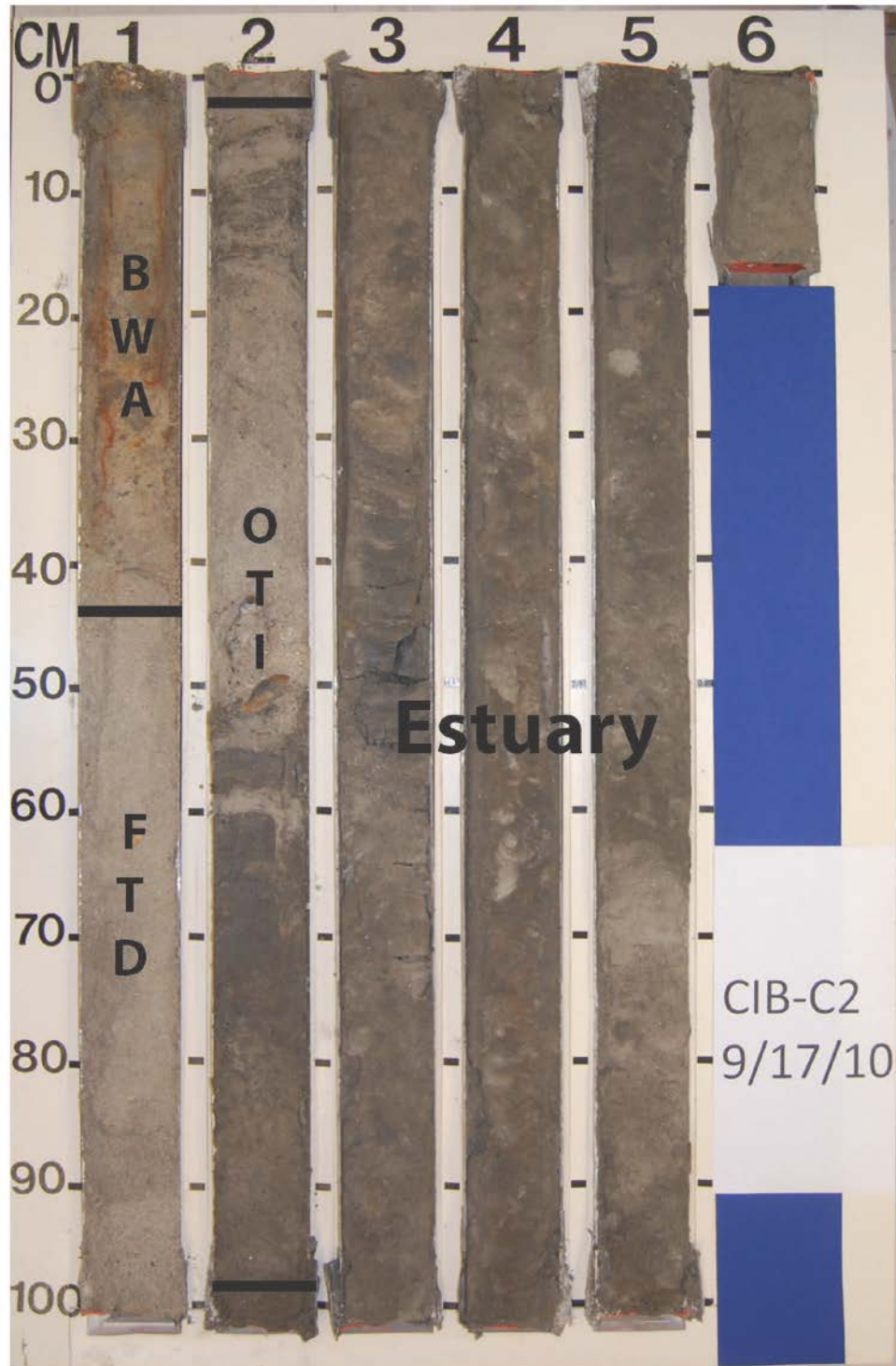


Figure 65: Photograph of Vibracore C2 with depositional environments delineated (BWA – beach-washover-aeolian, FTD – flood-tidal delta, OTI – older tidal inlet).

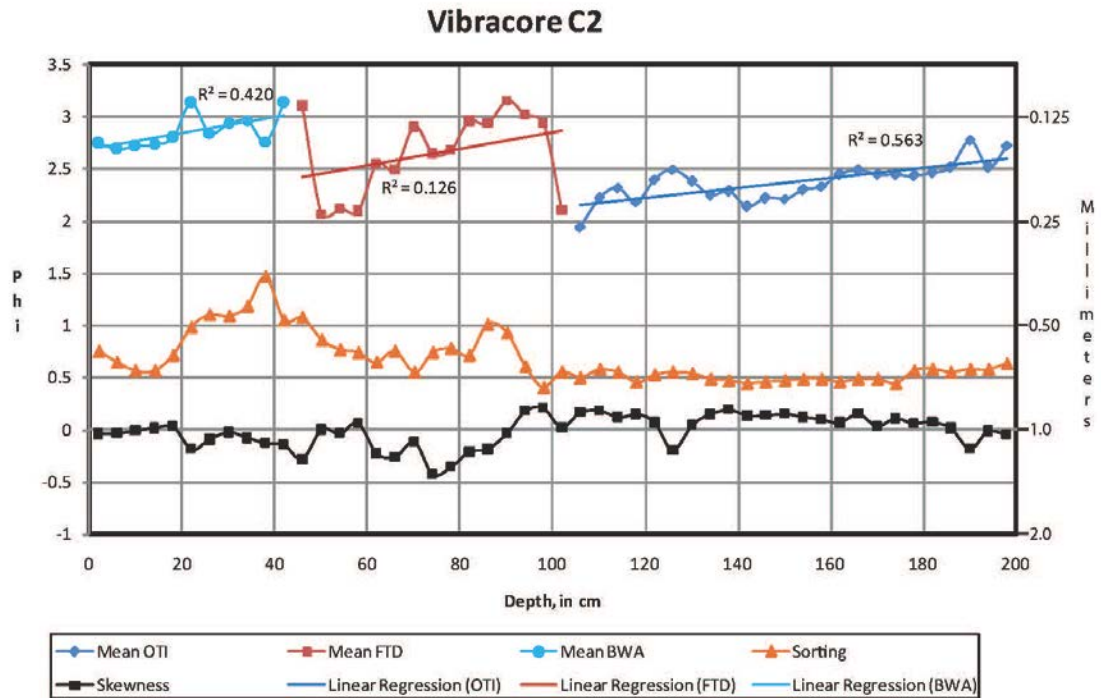


Figure 66: Grain-size graph for Vibracore C2 (BWA – beach-washover-aeolian, FTD – flood-tidal delta, OTI – older tidal inlet). Skewness is dimensionless.

Figure 65 shows the depositional environments present in Vibracore C2. The grain-size data for C2 (Figure 66) show an overall trend of becoming less sorted upward, and negatively skewed upward. The older tidal-inlet deposits coarsen upward, indicate little change in sorting upward, and trend from nearly symmetrical to positive skewness upward. The flood-tidal delta deposits coarsen upward, tend to become better sorted upward, and trend from positive to negative skewness. The beach-washover-aeolian

deposits coarsen upward, become less sorted upward, and little change in skewness. All of the depositional environments show a coarsening upward trend in Vibracore C2.

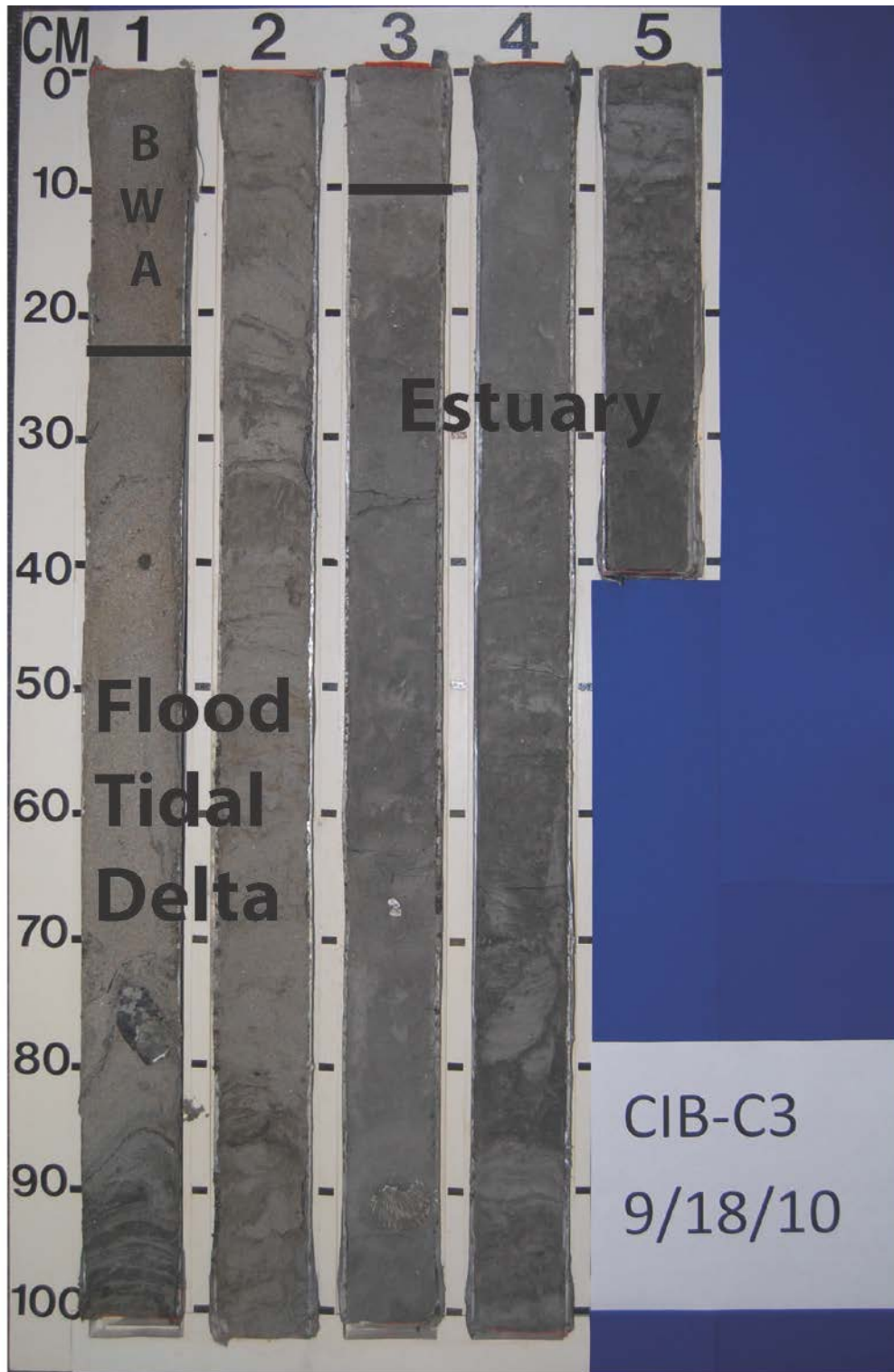


Figure 67: Photograph of Vibracore C3 with depositional environments delineated (BWA – beach-washover-aeolian).

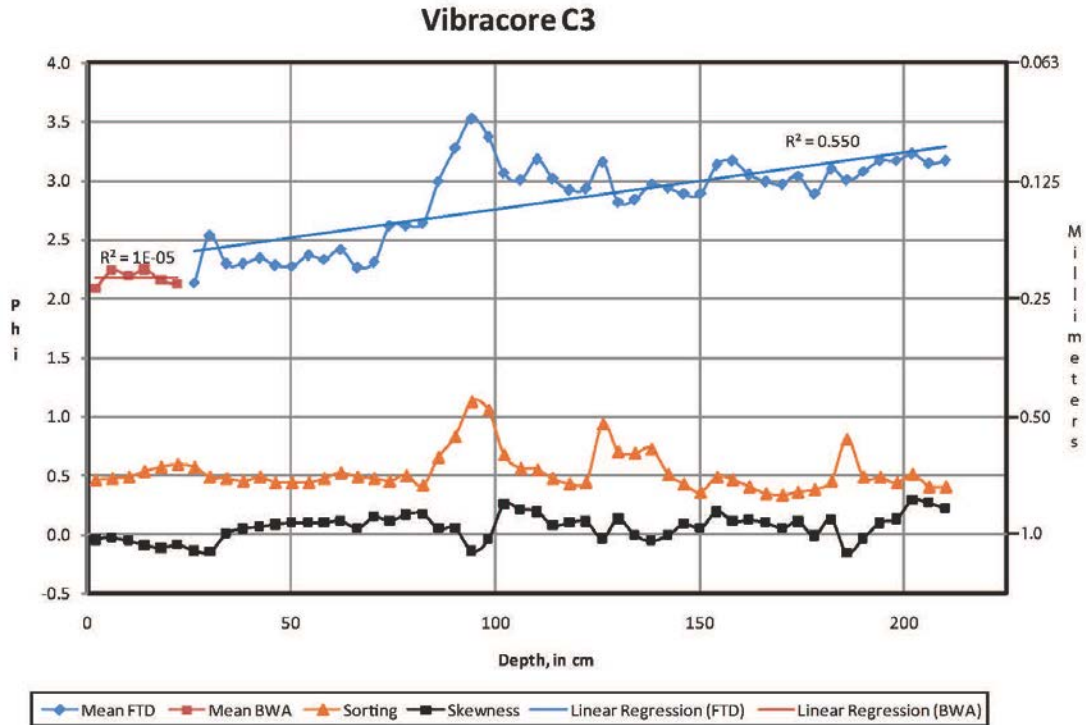


Figure 68: Grain-size graph for Vibracore C3 (BWA – beach-washover-aeolian. FTD – flood-tidal delta). Skewness is dimensionless.

Figure 67 shows the depositional environments present in Vibracore C3. The grain-size data for C3 (Figure 68) show an overall trend of coarsening upward, no trend in sorting, and trending from positive to negative skewness. The flood-tidal delta deposits coarsen upward, show no overall trend in sorting, and little change in skewness. The beach-washover-aeolian deposits show no upward trend in grain size, tend to become better sorted, and trend from negative skewness to nearly symmetrical.

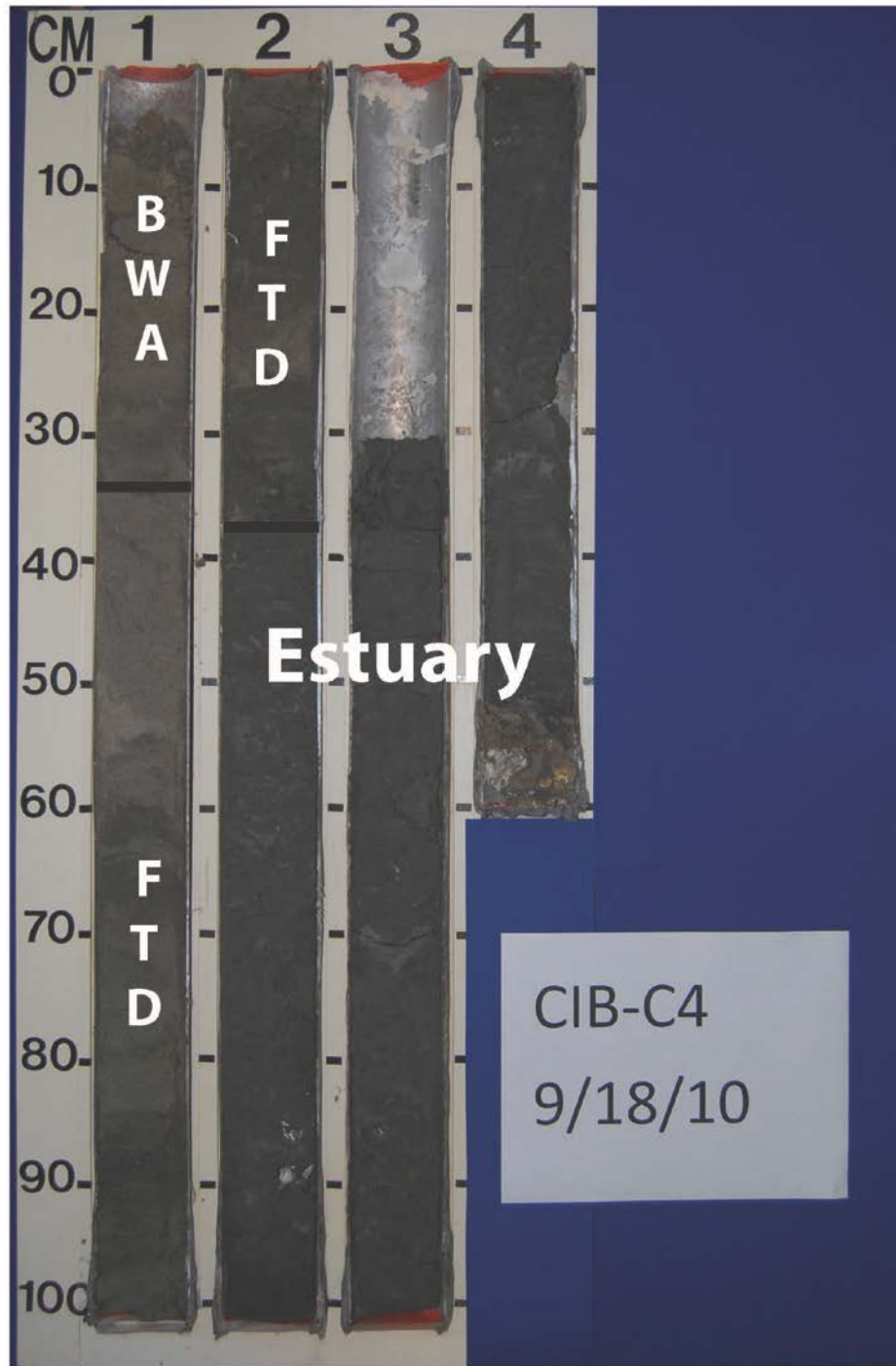


Figure 69: Photograph of Vibracore 4 with depositional environments delineated (BWA – beach-washover-aeolian, FTD – flood-tidal delta).

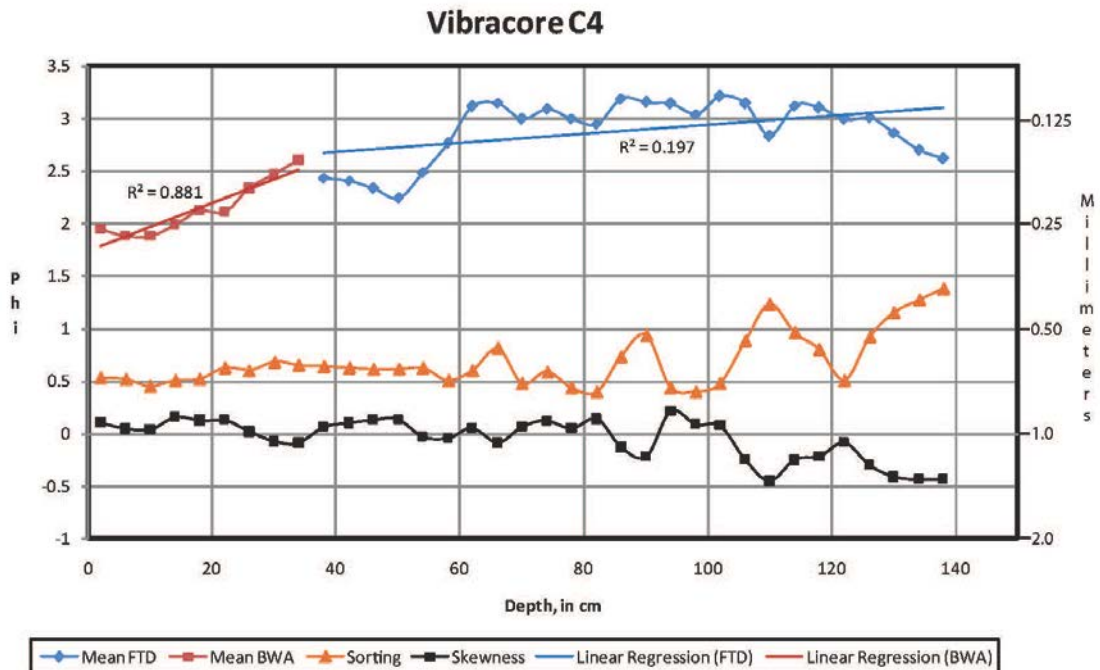


Figure 70: Grain-size graph for Vibracore C4 (BWA – beach-washover-aeolian, FTD – flood-tidal delta). Skewness is dimensionless.

Figure 69 shows the depositional environments present in Vibracore C4. The grain-size data for C4 (Figure 70) show an overall trend of coarsening upward, becoming better sorted upward, and trend from negative to positive skewness upward. The flood-tidal delta deposits coarsen upward, become better sorted, and trend from negative skewness to nearly symmetrical. The beach-washover-aeolian deposits coarsen upwards, become slightly better sorted, and tend from nearly symmetrical to positive skewness.

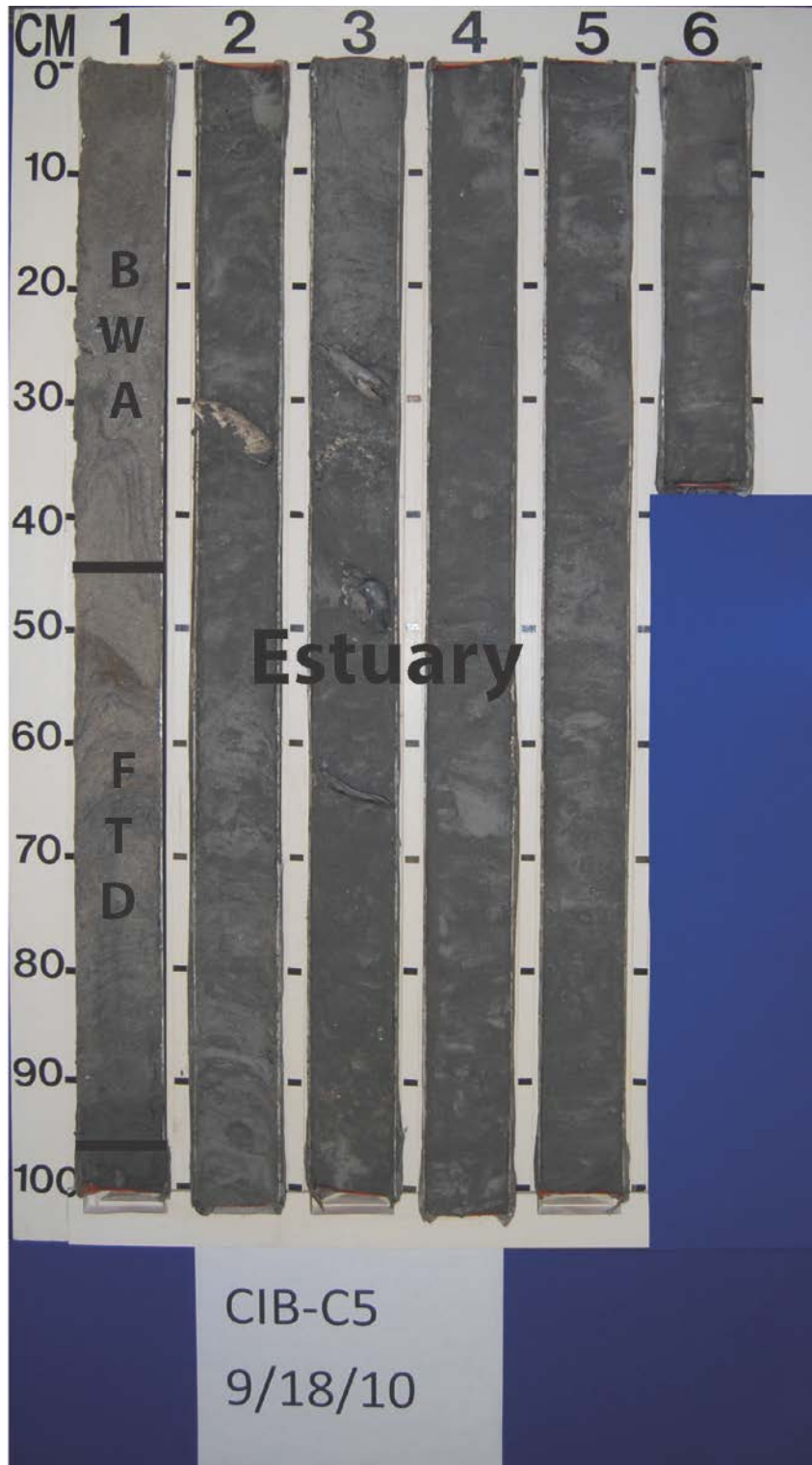


Figure 71: Photograph of Vibracore C5 with depositional environments delineated (BWA – beach-washover-aeolian, FTD – flood-tidal delta).

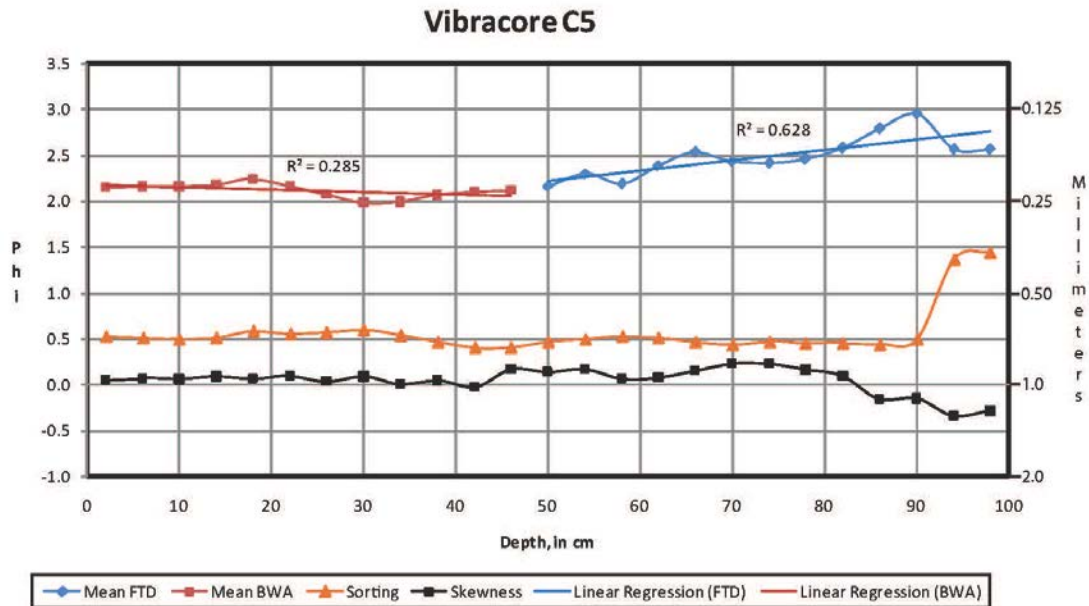


Figure 72: Grain-size graph for Vibracore C5 (BWA – beach-washover-aeolian, FTD – flood-tidal delta). Skewness is dimensionless.

Figure 71 shows the depositional environments present in Vibracore C5. The grain-size data for C5 (Figure 72) show an overall trend of slightly coarsening upward, showing no trend in sorting above the bottommost sediments, and trend from negative to positive skewness upward. The flood-tidal delta deposits coarsen upward, are poorly sorted just above the estuary deposits and become better sorted upward, and trend from negative to positive skewness. The beach-washover-aeolian deposits slightly fine upward

slightly, are either moderately well sorted or well sorted with no trend upward, and trend from positive skewness to nearly symmetrical upward.

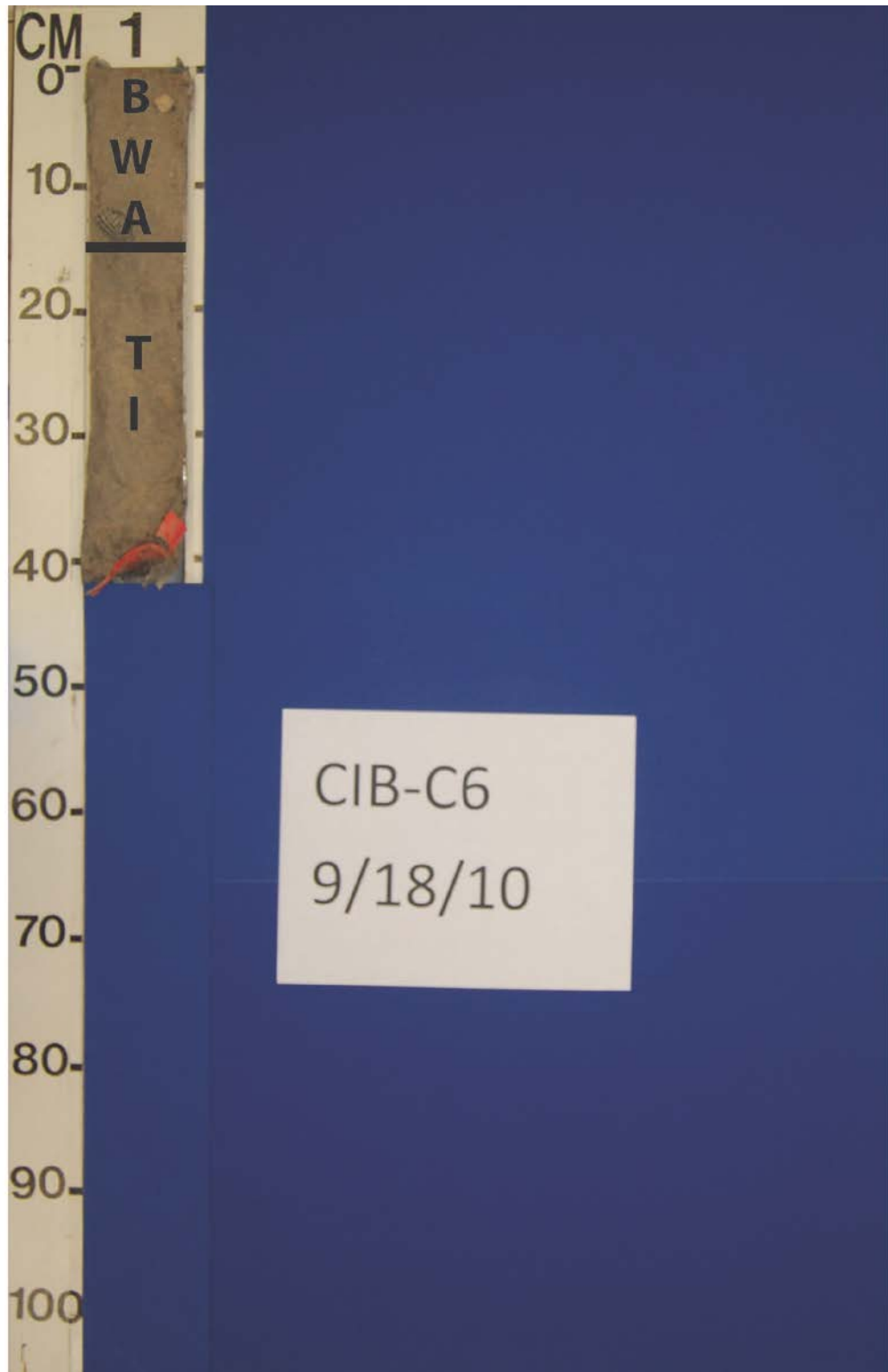


Figure 73: Photograph of Vibracore C6 with depositional environments delineated (BWA – beach-washover-aeolian, TI- tidal inlet).

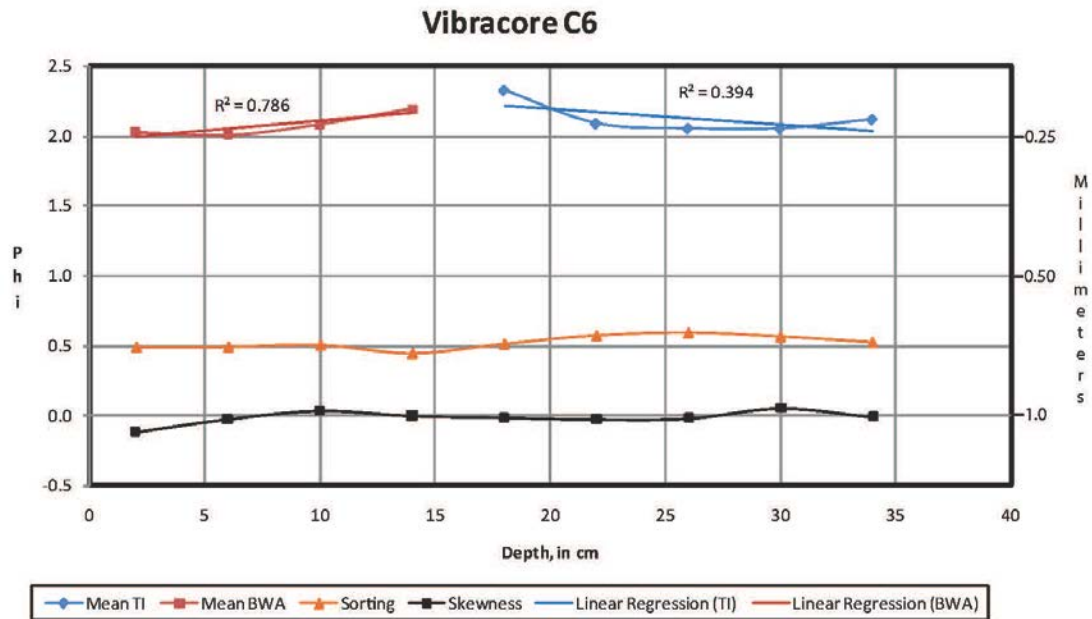


Figure 74: Grain-size graph for Vibracore C6 (BWA – beach-washover-aeolian, TI- tidal inlet). Skewness is dimensionless.

Figure 73 shows the depositional environments present in Vibracore C6. The graph of grain-size data for C6 (Figure 74) shows no overall trend in mean grain size, sorting, or skewness. The tidal-inlet deposits fine upward slightly, become slightly better sorted upward, and are nearly symmetrical (no trend in skewness). The beach-washover-aeolian deposits coarsen upward slightly, are moderately well sorted and well sorted with no upward trend, and are mostly nearly symmetrical.

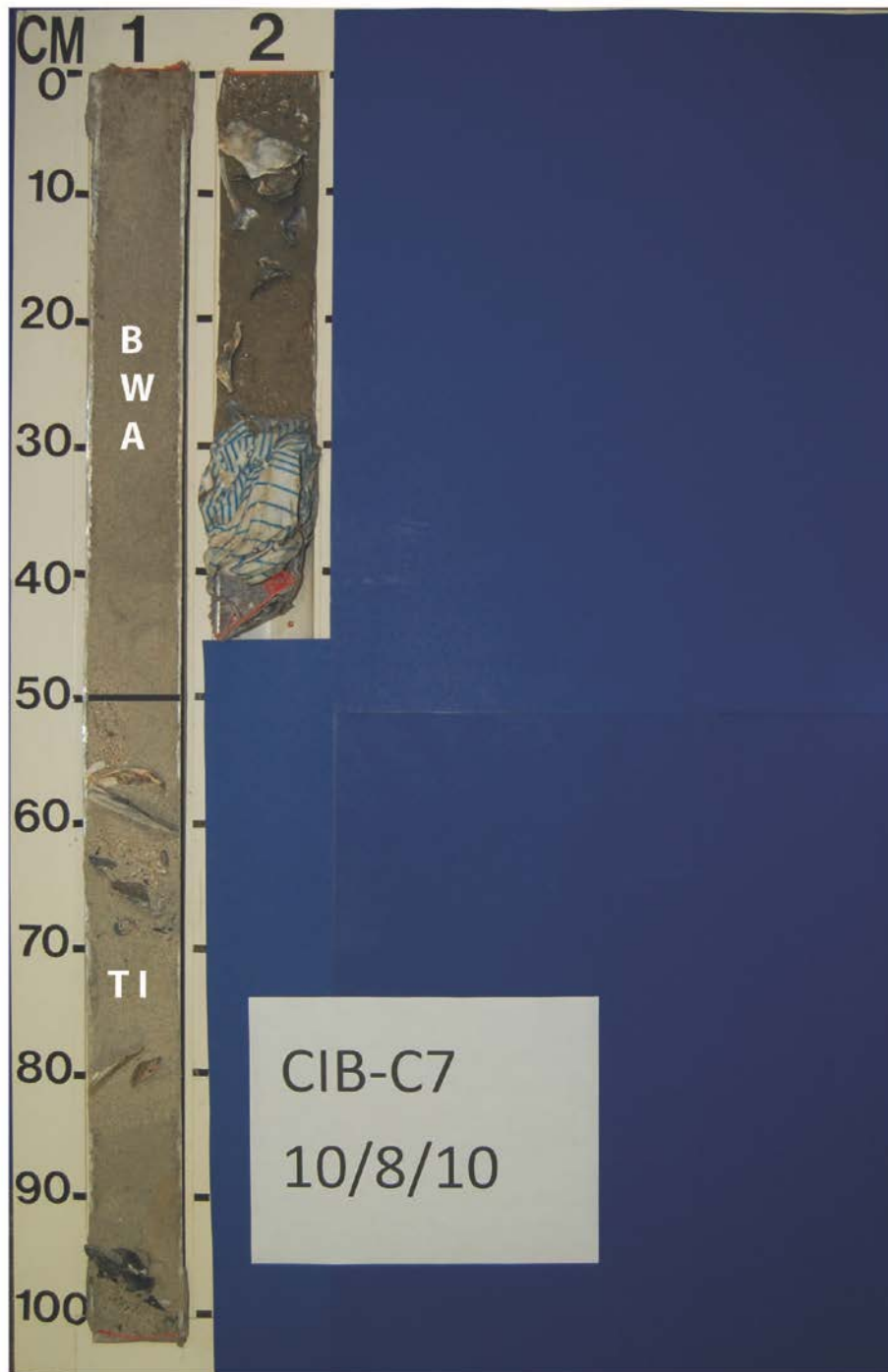
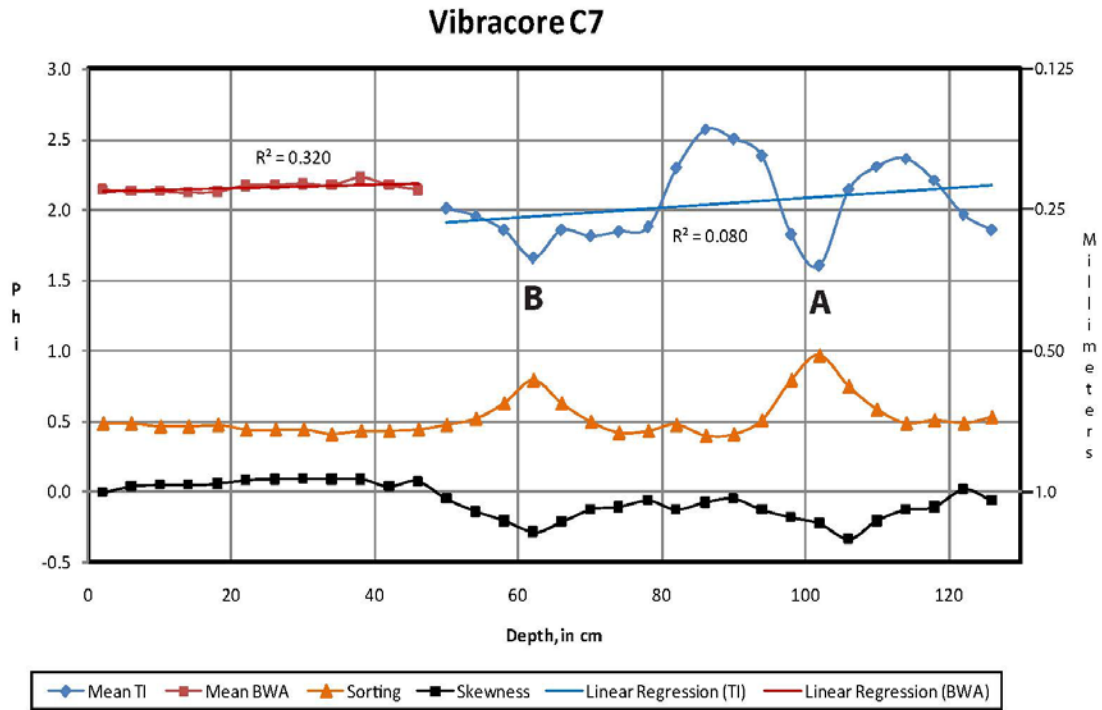


Figure 75: Photograph of Vibracore C7 with depositional environments delineated (BWA – beach-washover-aeolian, TI – tidal inlet).



A = Spike in water flow velocity

Figure 76: Grain-size graph for Vibracore C7 (BWA – beach-washover-aeolian, TI – tidal inlet). Skewness is dimensionless.

Figure 75 shows the depositional environments present in Vibracore C7. The grain-size data for C7 (Figure 76) show an overall trend of becoming slightly better sorted upward, and trend from negative skewness to nearly symmetrical upward. The tidal-inlet deposits fine upwards, show a slight upward trend in better sorting, and an upward trend from nearly symmetrical to negative skewness. Two spikes are present that represent an increase in water-flow velocity as reflected in the tidal-inlet deposits, A and B (Figure 76). Spike A, at a depth of 102 cm, and spike B, at a depth of 62 cm, coarsen then fine upward, becomes less well sorted then better sorted upward, and trend from

nearly symmetrical to negatively skewness then nearly symmetrical upward. The beach-washover-aeolian deposits slightly coarsen upward, become less sorted upward, and are nearly symmetrical showing no trend in skewness upward.

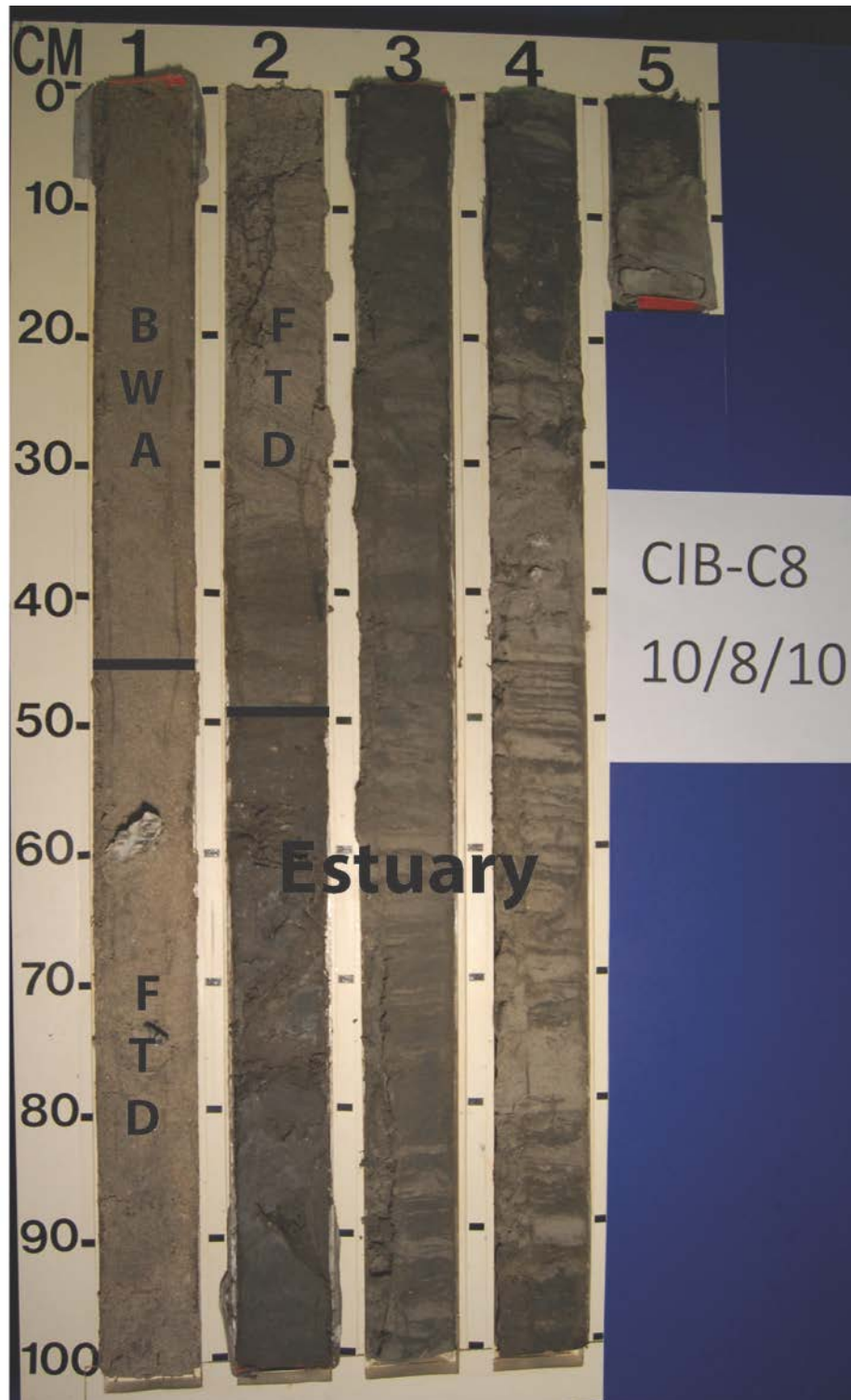


Figure 77: Photograph of Vibracore C8 with depositional environments delineated (BWA – beach-washover-aeolian, FTD – flood-tidal delta).

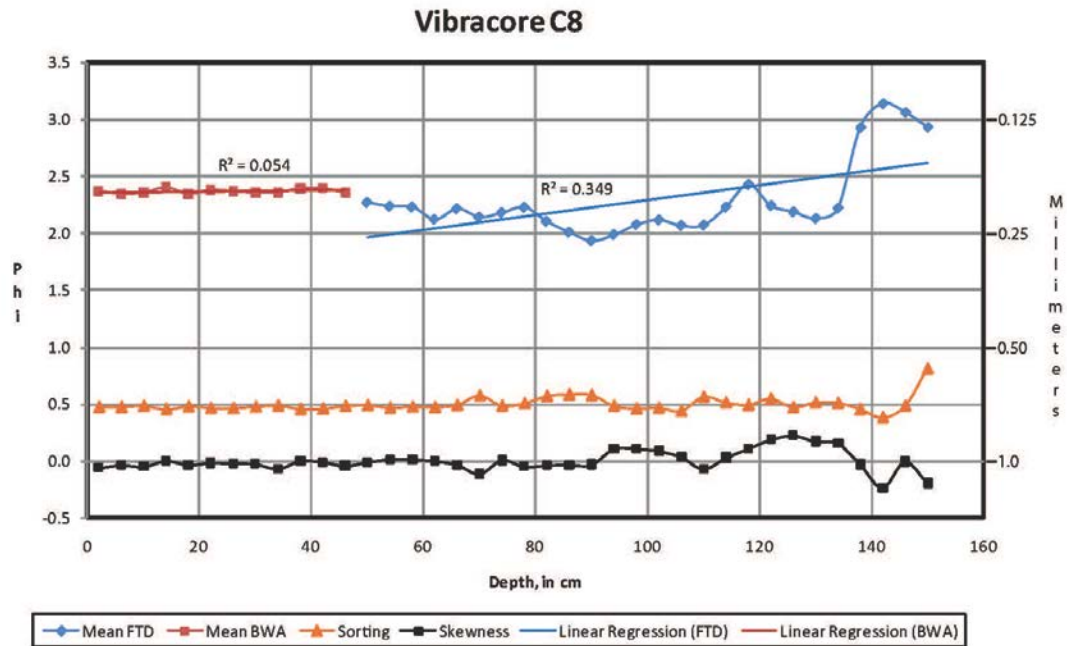


Figure 78: Grain-size graph for Vibracore C8 (BWA – beach-washover-aeolian, FTD – flood-tidal delta). Skewness is dimensionless.

Figure 77 shows the depositional environments present in Vibracore C8. The grain-size data for C8 (Figure 78) show no overall upward trend in sorting, and a trend from positive skewness to nearly symmetrical. The flood-tidal delta deposits fine upward, are moderately sorted above the estuary deposits then become slightly better sorted upward, and show little change in skewness upward. The beach-washover-aeolian deposits are fine sand with no upward trends in mean grain size, sorting, or skewness.

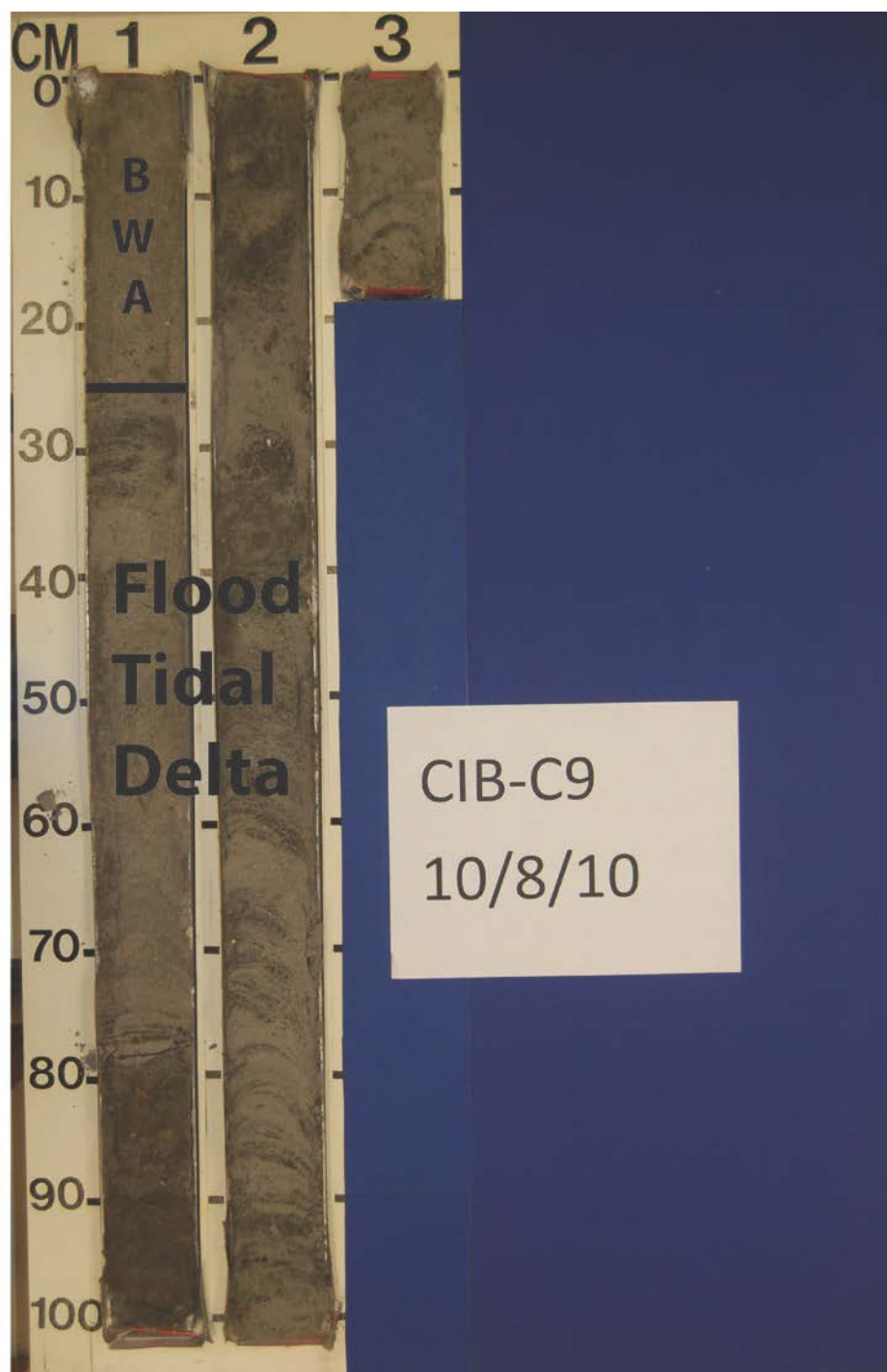


Figure 79: Photograph of Vibracore C9 with depositional environments delineated (BWA – beach-washover-aeolian).

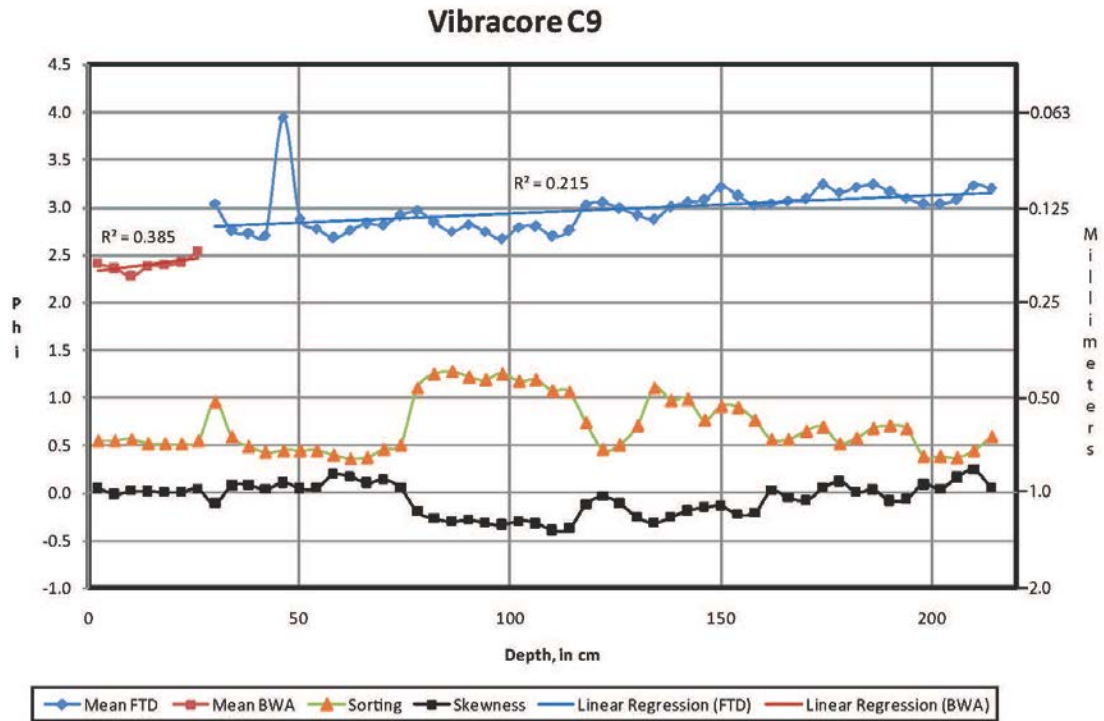


Figure 80: Grain-size graph for Vibracore C9 (BWA – beach-washover-aeolian, FTD – flood-tidal delta). Skewness is dimensionless.

Figure 79 shows the depositional environments present in Vibracore C9. The grain-size data for C9 (Figure 80) show an overall upward trend of coarsening upward, becoming less sorted upward, and going from positive to negative to positive skewness upward. The flood-tidal delta deposits coarsen upward slightly, trend from moderately well sorted to poorly sorted then become better sorted upward, and trend from positive to negative skewness for most of the deposits then show positive skewness upward. The beach-washover-aeolian deposits coarsen upward, are moderately well sorted, and nearly symmetrical.

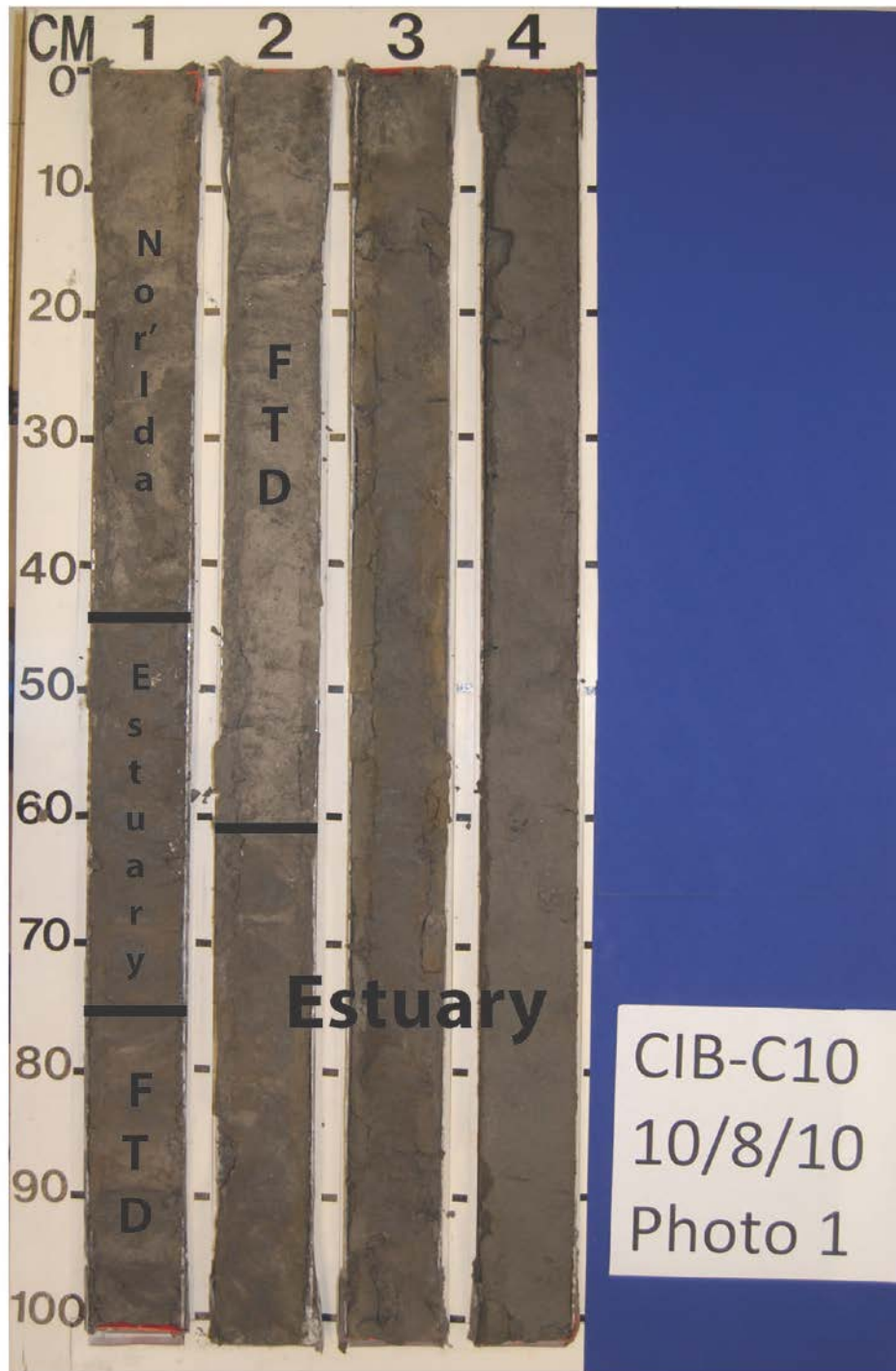


Figure 81: Photograph of the upper part of Vibracore C10 with depositional environments delineated (FTD – flood-tidal delta).

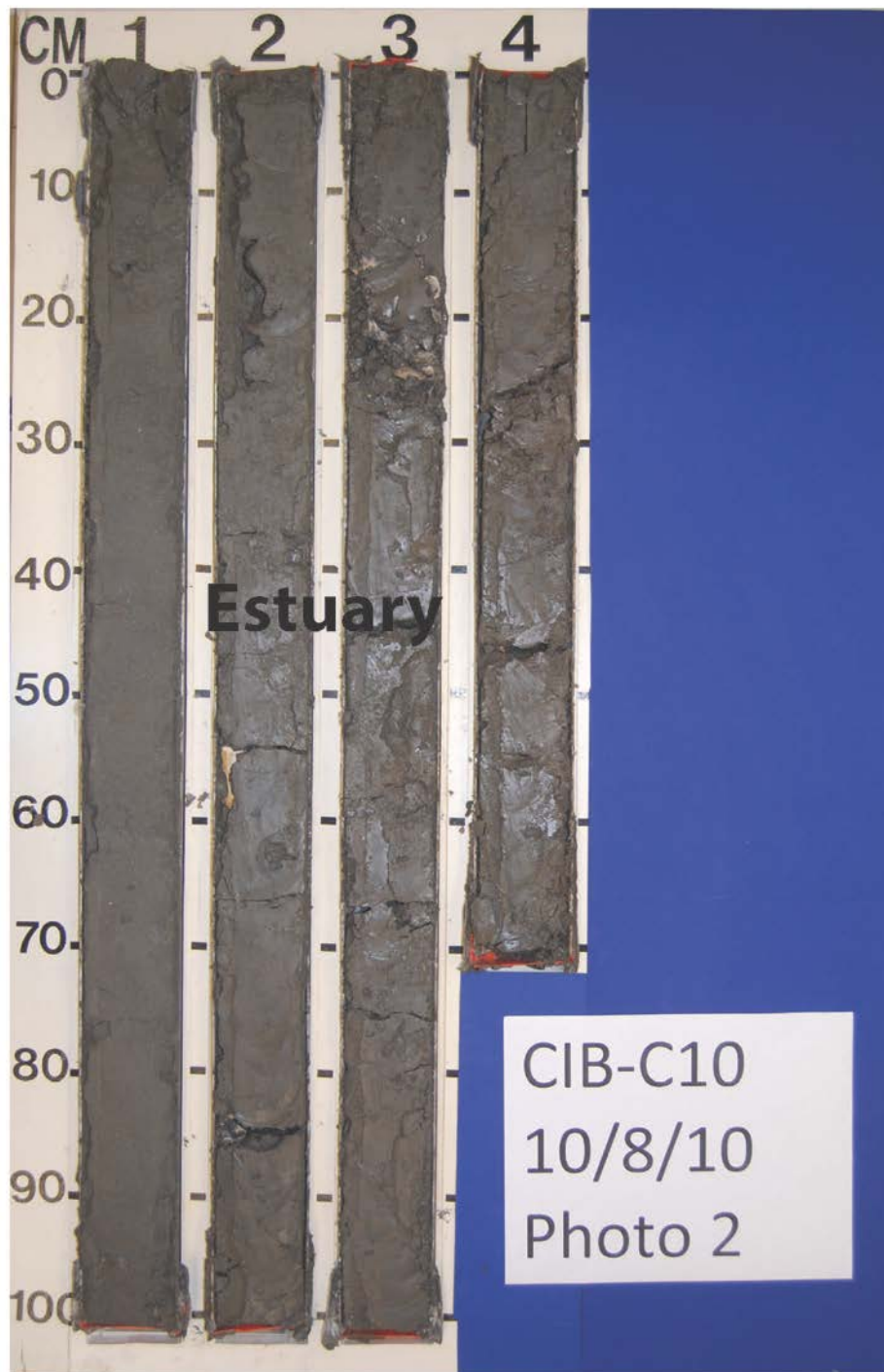


Figure 82: Photograph of lower part of Vibracore C10 with depositional environments delineated.

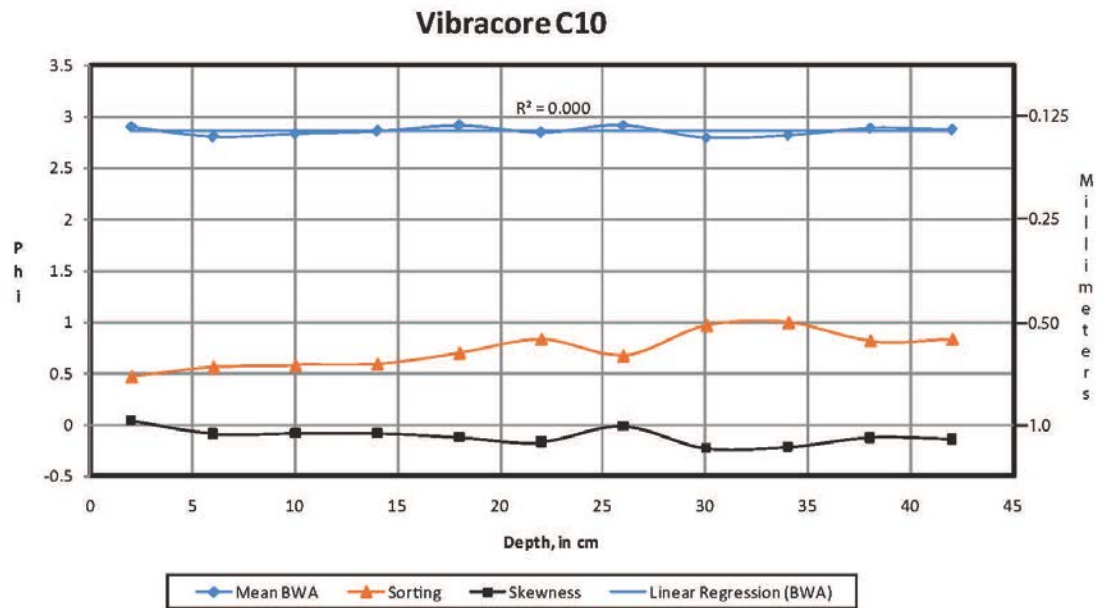


Figure 83: Grain-size graph for Vibracore C10 (BWA – beach-washover-aeolian). Skewness is dimensionless.

Figure 81 and 82 shows the depositional environments present in Vibracore C10. The Nor’ Ida washover deposits (Figure 83) are fine grained, show a trend of becoming better sorted upward, and trend from negative skewness to nearly symmetrical upward.

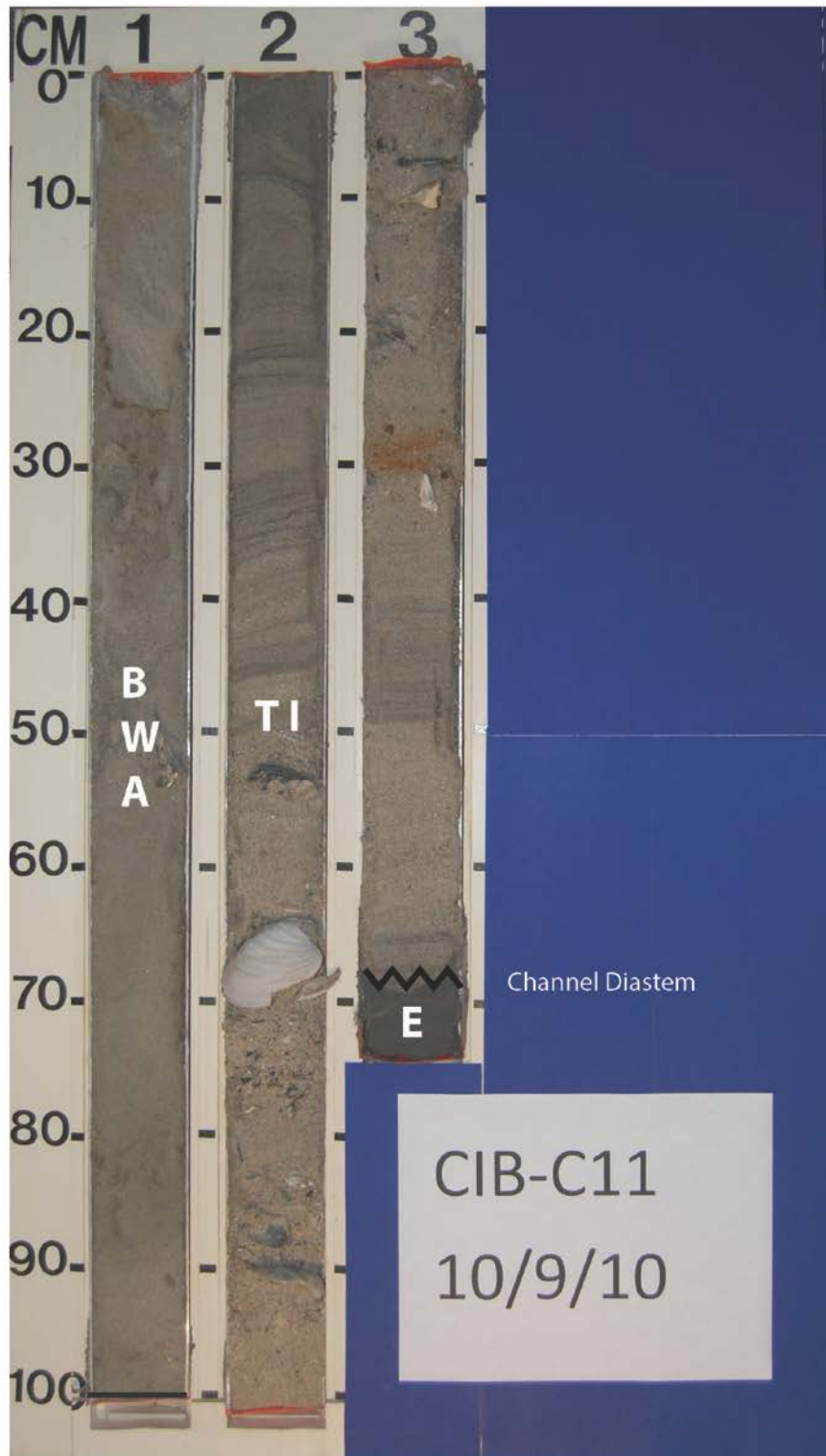
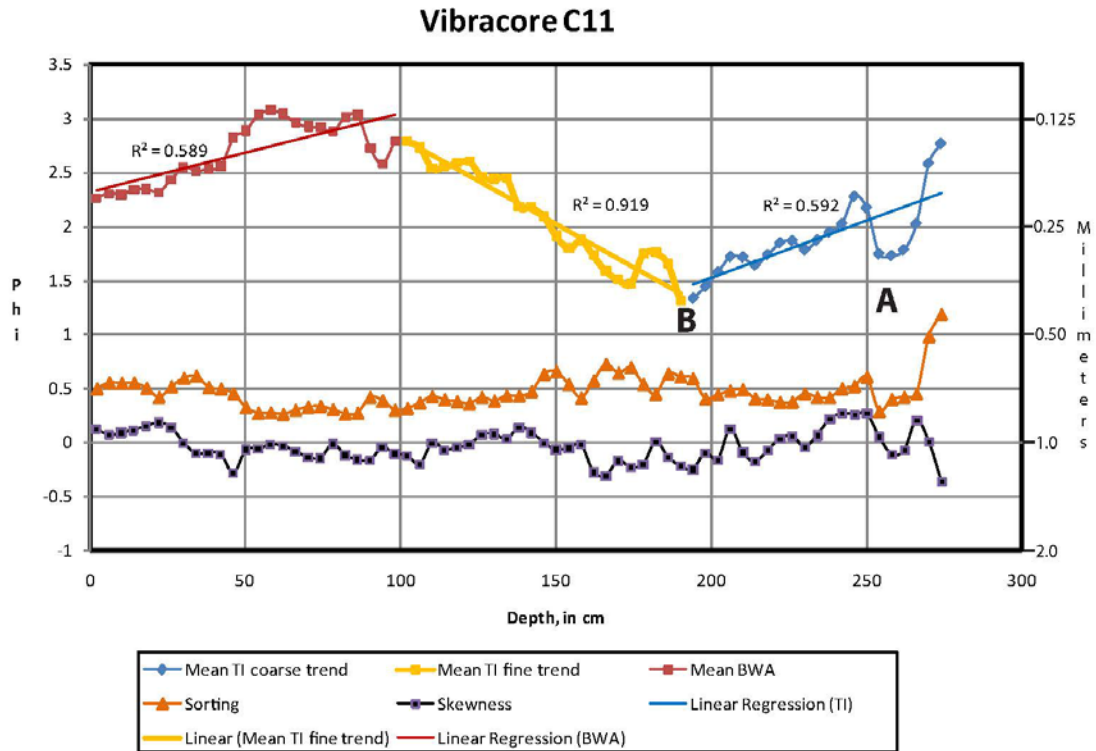


Figure 84: Photograph of Vibracore C11 with depositional environments delineated (BWA – beach-washover-aolian, TI - tidal inlet, E - estuary).



A = Spike in water flow velocity

Figure 85: Grain-size graph for Vibracore C11 (BWA – beach-washover-aeolian, TI - tidal inlet). Skewness is dimensionless.

Figure 84 shows the depositional environments present in Vibracore C11. The grain-size data for C11 (Figure 85) show an overall trend of becoming slightly better sorted upward and fluctuate from positive to negative to positive skewness upward. The tidal-inlet deposits are fine grained, poorly sorted, and negatively skewed just above the estuary deposits. They coarsen upward and then fine upward. The deposits become slightly better sorted upward and trend from positive to negative to positive skewness upward. Two spikes exist that represent an increase in water-flow velocity in the tidal-

inlet deposits, A and B (see Figure 85). Spike A, at a depth of 258 cm, and spike B, at a depth of 190 cm, coarsen upward then fine upward with no attendant correlation with sorting or skewness. The beach-washover-aeolian deposits coarsen upward, become less sorted upward, and trend from negative to positive skewness upward.

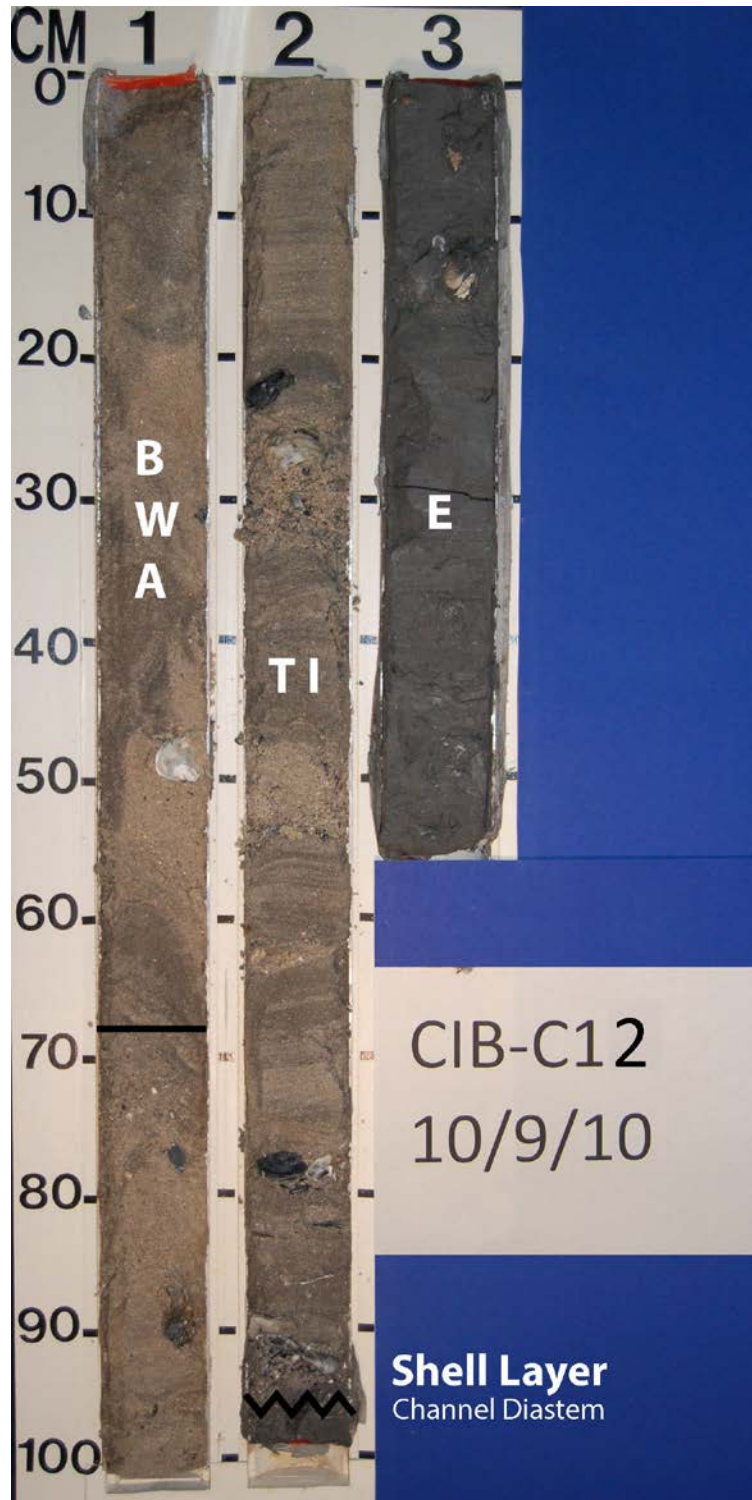
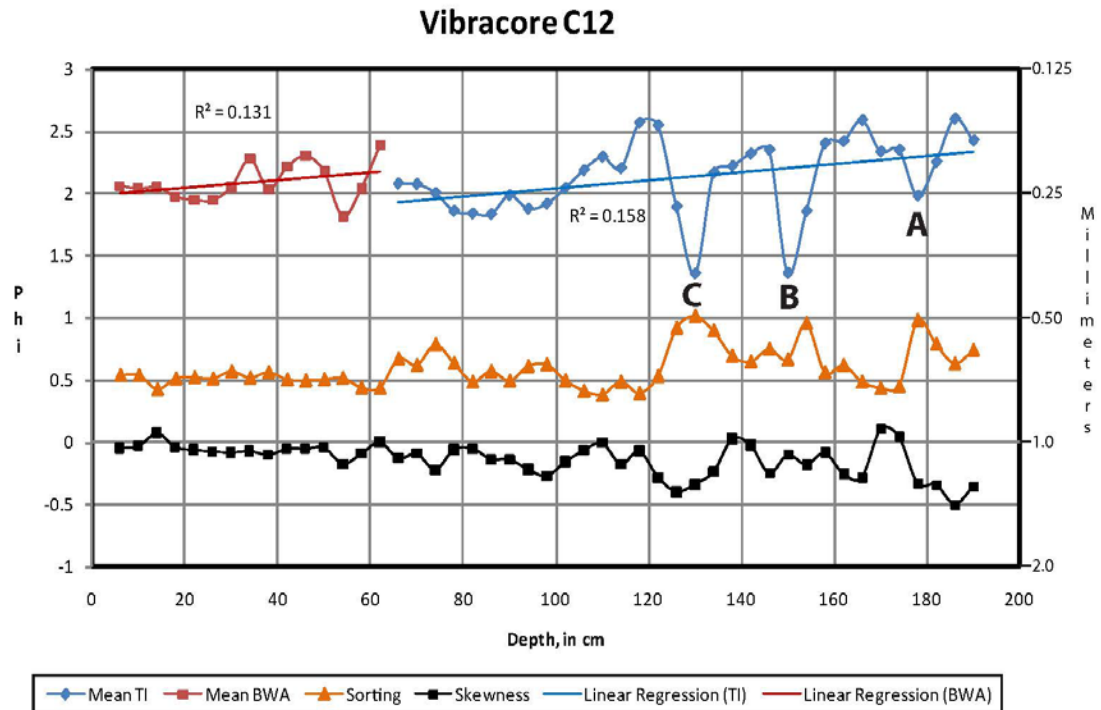


Figure 86: Photograph of Vibracore C12 with depositional environments delineated (BWA – beach-washover-aeolian, TI – tidal inlet, E - estuary).



A = Spike in water flow velocity

Figure 87: Grain-size graph for Vibracore C12 (BWA – beach-washover-aeolian, TI - tidal inlet). Skewness is dimensionless.

Figure 86 shows the depositional environments present in Vibracore C12. The grain-size data for C12 (Figure 87) show become better sorted upward, and dominated by negative skewness. The tidal-inlet deposits coarsen upward, become better sorted upward, and show negative skewness. Three spikes exist that represent an increase in water-flow velocity in the tidal-inlet deposits, A, B, and C (see Figure 87). Spike A, at a depth of 178 cm, spike B, at a depth of 150 cm, and spike C, at a depth of 130 cm, coarsen upward then fine upward and become poorly sorted and then better sorted. The

beach-washover-aeolian deposits coarsen upward, show no sorting trend upward, and are near symmetrical regarding skewness.

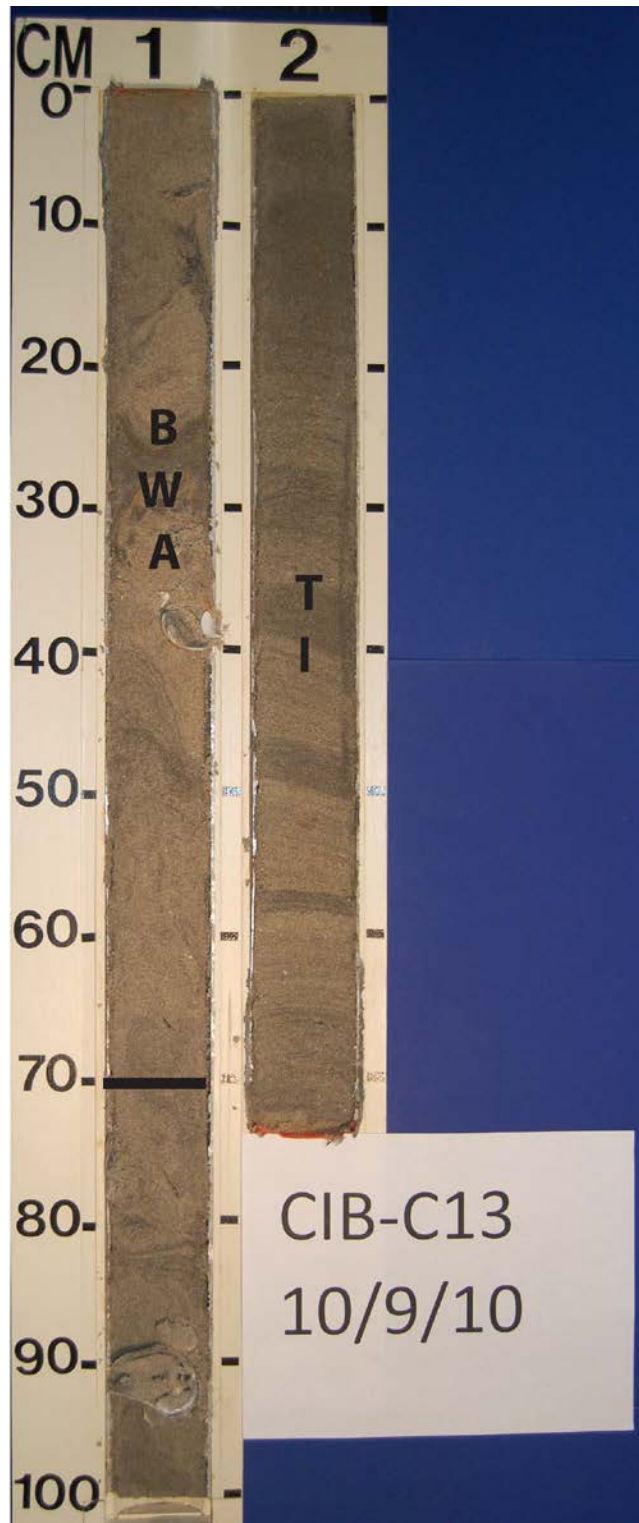


Figure 88: Photograph of Vibracore C13 with depositional environments delineated (BWA – beach-washover-aeolian, TI – tidal inlet).

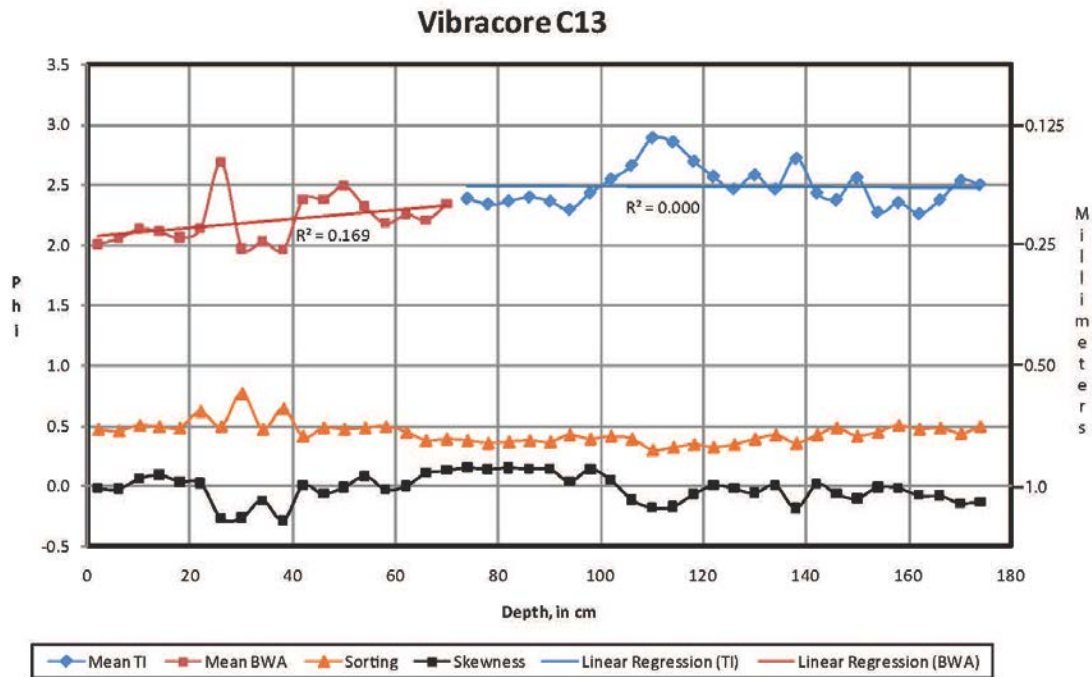


Figure 89: Grain-size graph for Vibracore C13 (BWA – beach-washover-aeolian, TI – tidal inlet). Skewness is dimensionless.

Figure 88 shows the depositional environments present in Vibracore C13. The grain-size data for C13 (Figure 89) show an overall trend coarsening upward, become slightly less sorted upward, and show no trend in skewness upward. The tidal-inlet deposits fine upward, then at a depth of 110 cm begin to coarsen upward, no trend in sorting, and show a strong trend from negative to positive skewness upward. The beach-washover-aeolian deposits coarsen upward, are slightly less sorted upward, and trend from positive to negative to positive skewness upward.

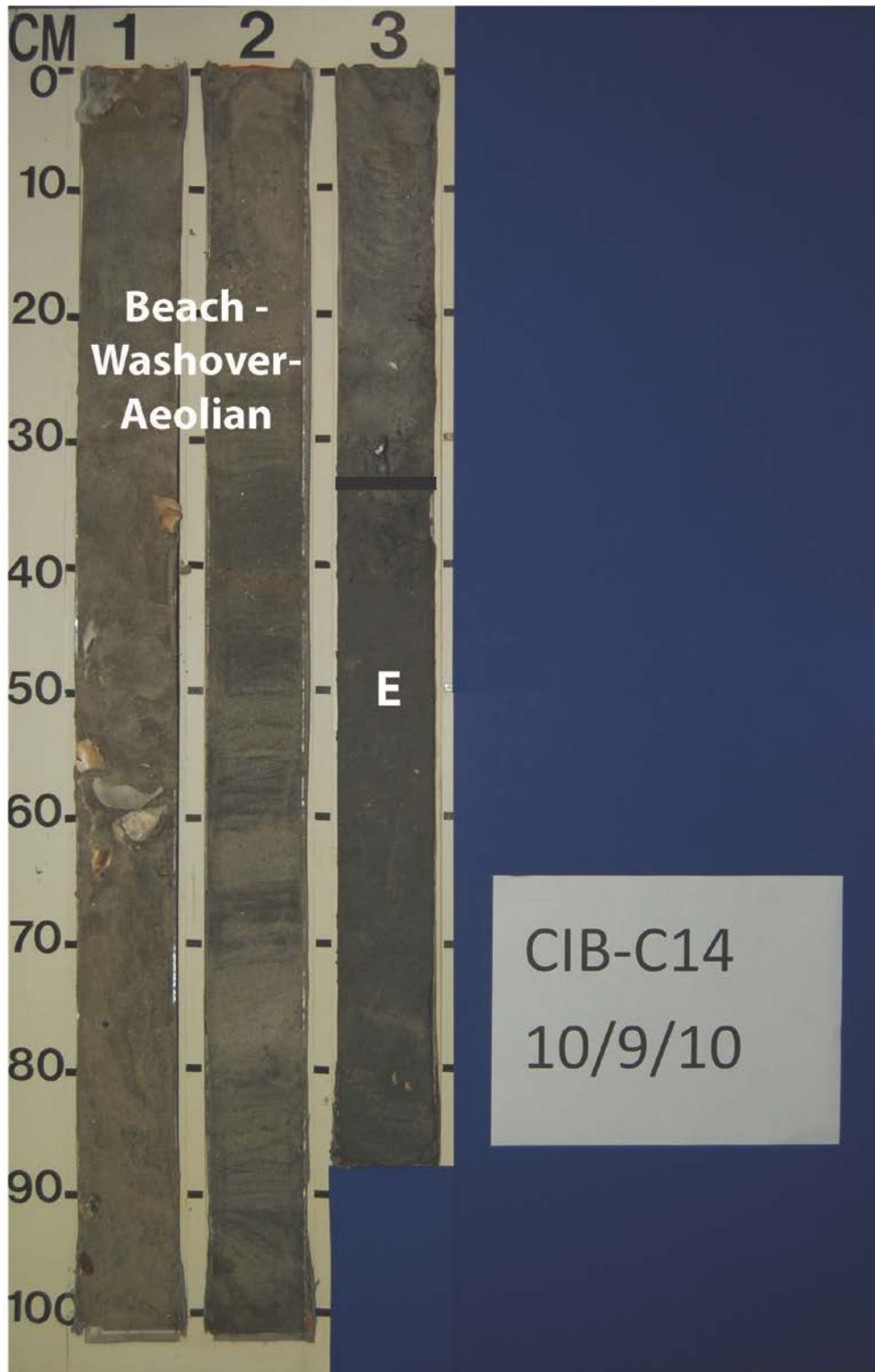


Figure 90: Photograph of Vibracore C14 with depositional environments delineated (E - estuary).

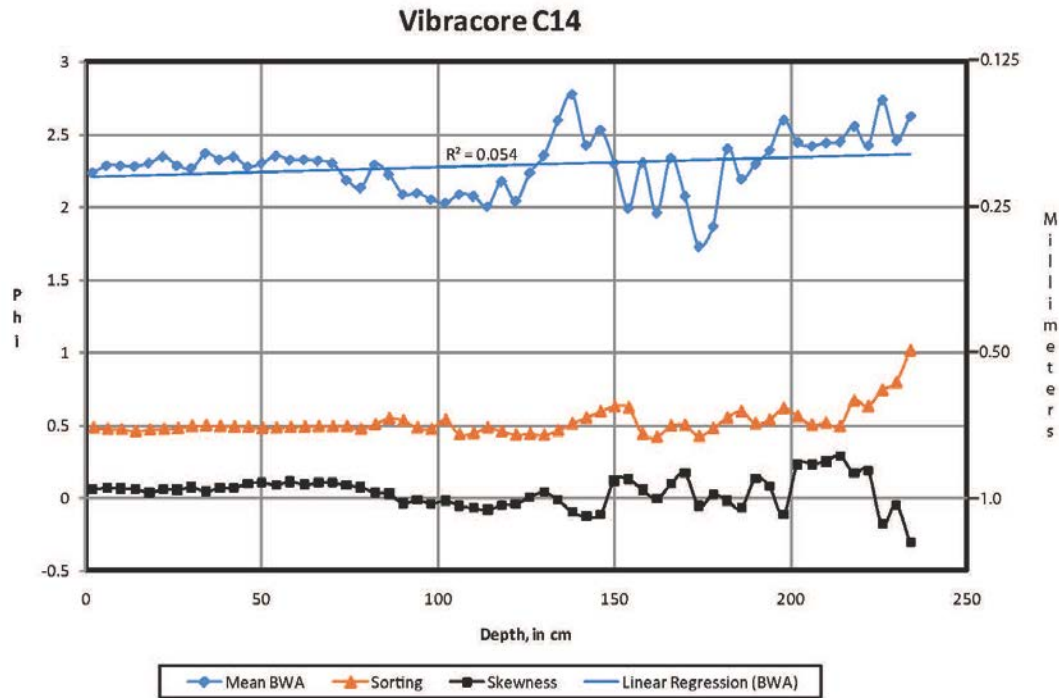


Figure 91: Grain-size graph for Vibracore C14 (BWA – beach-washover-aeolian). Skewness is dimensionless.

Figure 90 shows the depositional environment present in Vibracore C14. The beach-washover-aeolian deposits (Figure 91) coarsen upward, become better sorted upward, and trend from negative to positive skewness above the estuary deposits then become nearly symmetrical upward.

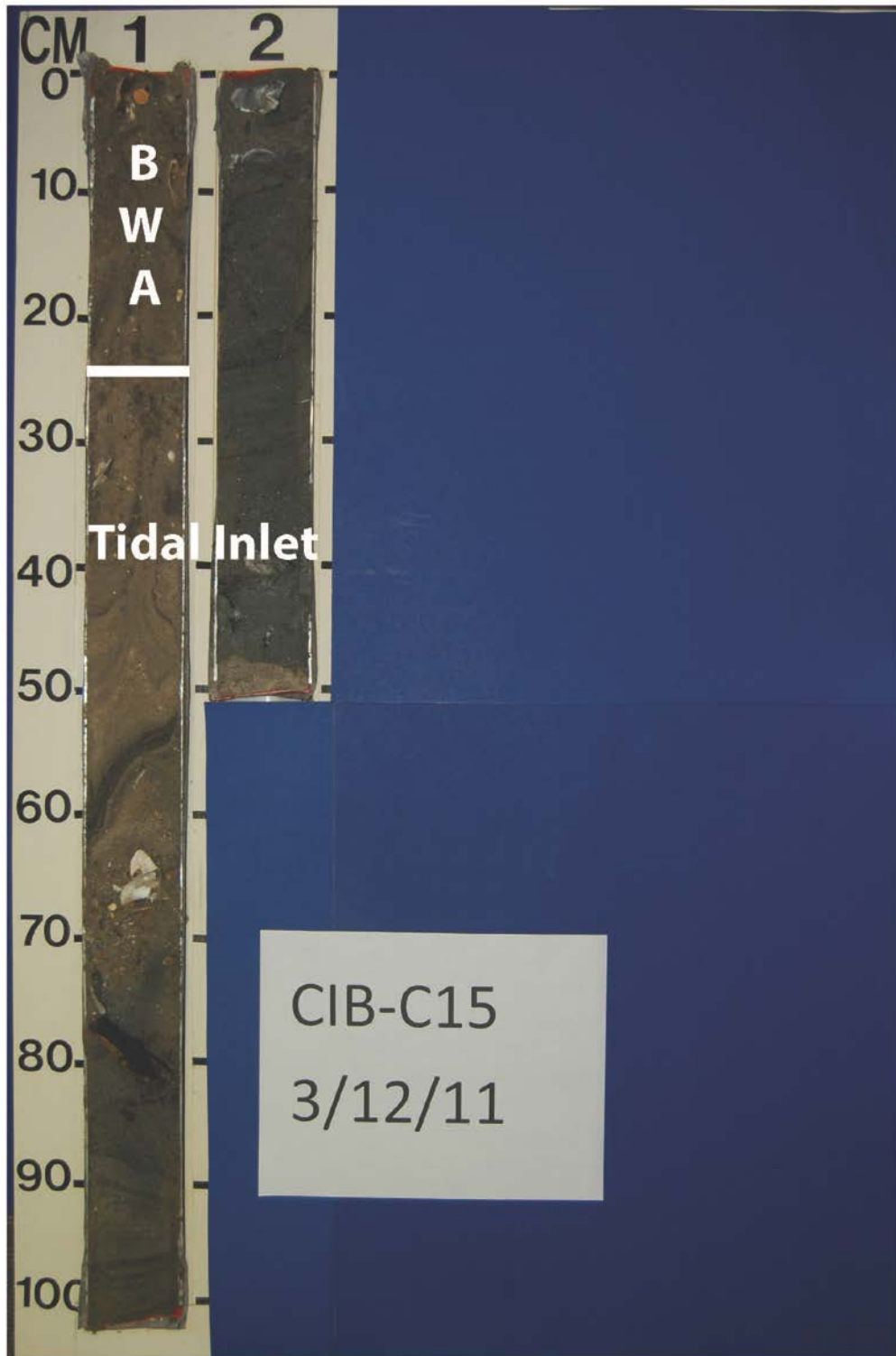


Figure 92: Photograph of Vibracore C15 with depositional environments delineated (BWA – beach-washover-aeolian).

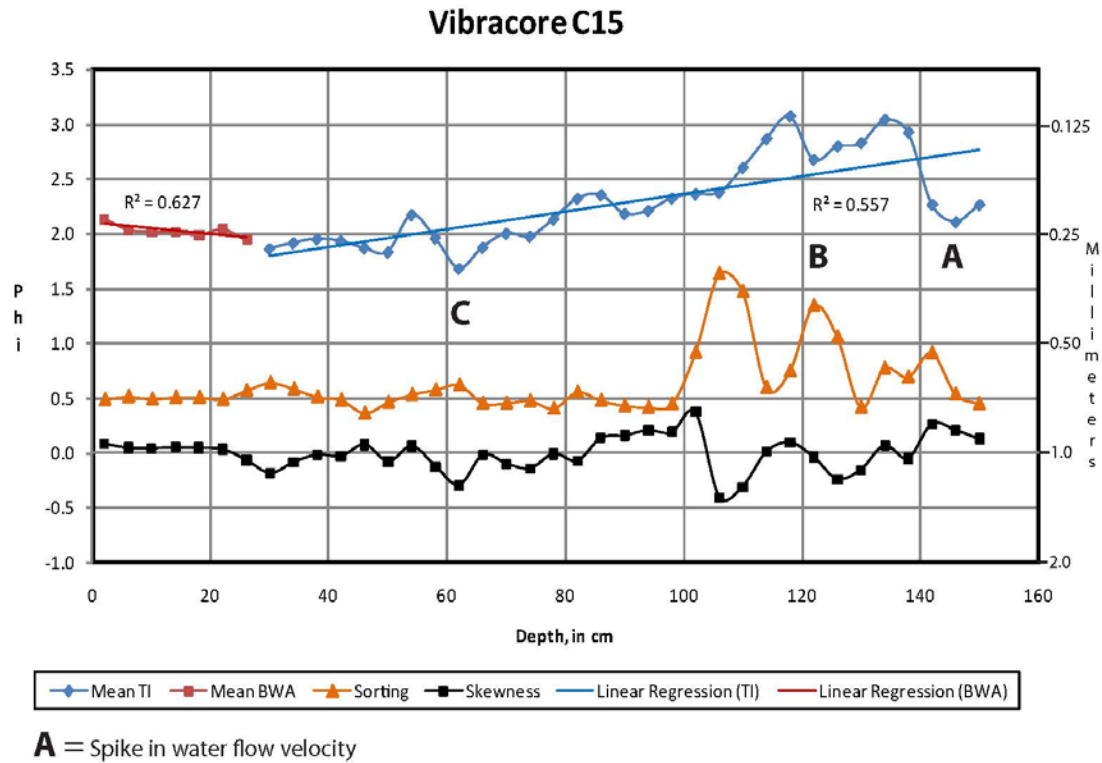


Figure 93: Grain-size graph for Vibracore C15 (BWA – beach-washover-aeolian, TI – tidal inlet). Skewness is dimensionless.

Figure 92 shows the depositional environments present in Vibracore C15. The grain-size data for C15 (Figure 93) show an overall trend of better sorting upward and skewness fluctuates at base and then becomes nearly symmetrical upward. The tidal-inlet deposits coarsen upward, trend to become better sorting upward, and a fluctuating trend regarding skewness upward. Three spikes exist that represent an increase in water-flow velocity in the tidal-inlet deposits, A, B and C (see Figure 93). Spike A, at a depth of 62 cm, coarsens upward, then fines upward with less sorting and negative to positive

skewness. Spike B, at a depth of 122 cm, and spike C, at a depth of 62 cm, coarsen upward then fine upward. Spike B becomes poorly sorted then better sorted. Spike C shows no attendant correlation with sorting and skewness. The beach-washover-aeolian deposits fine upward slightly, become slightly better sorted upward, and are nearly symmetrical (no trend).

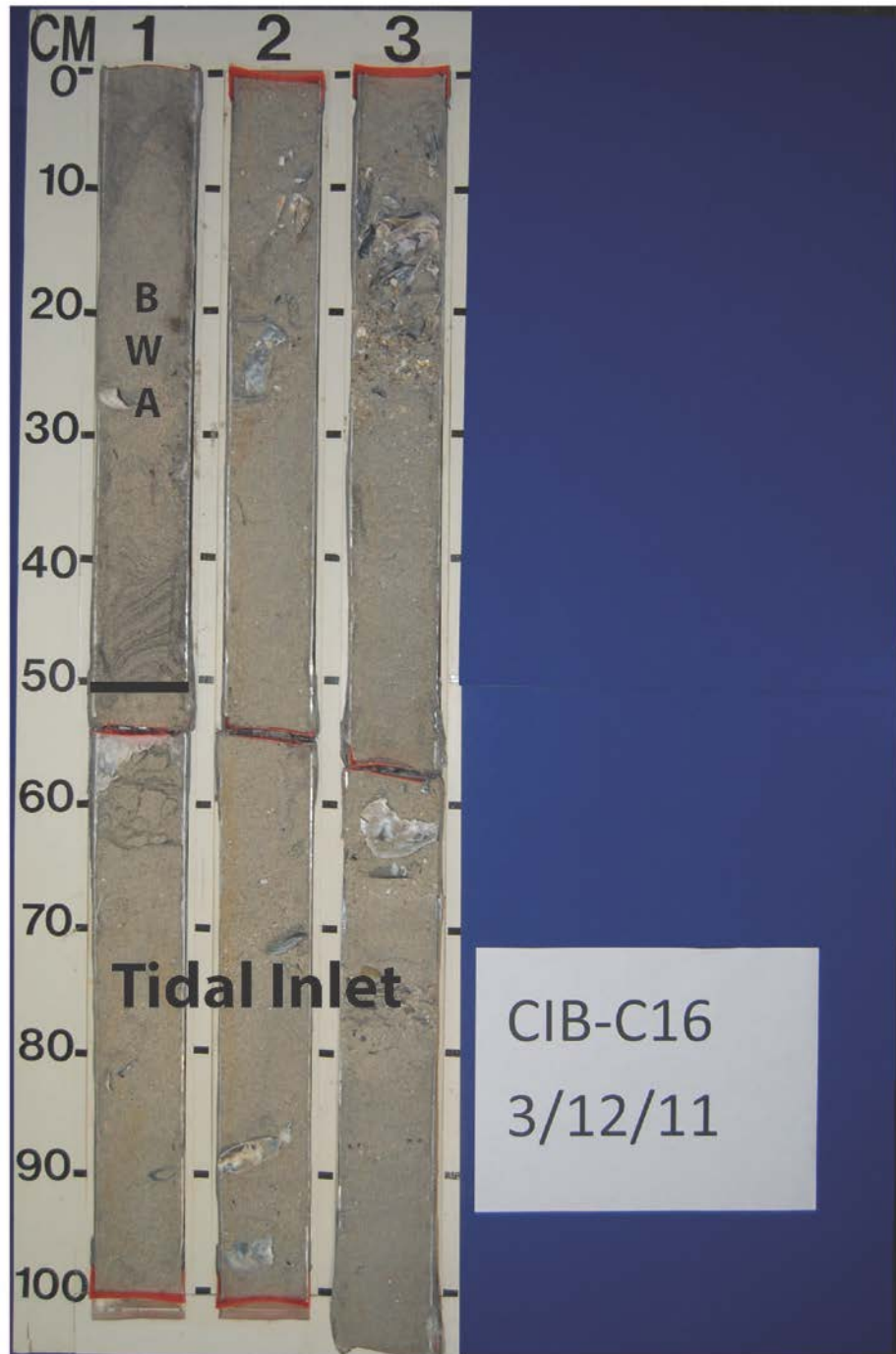
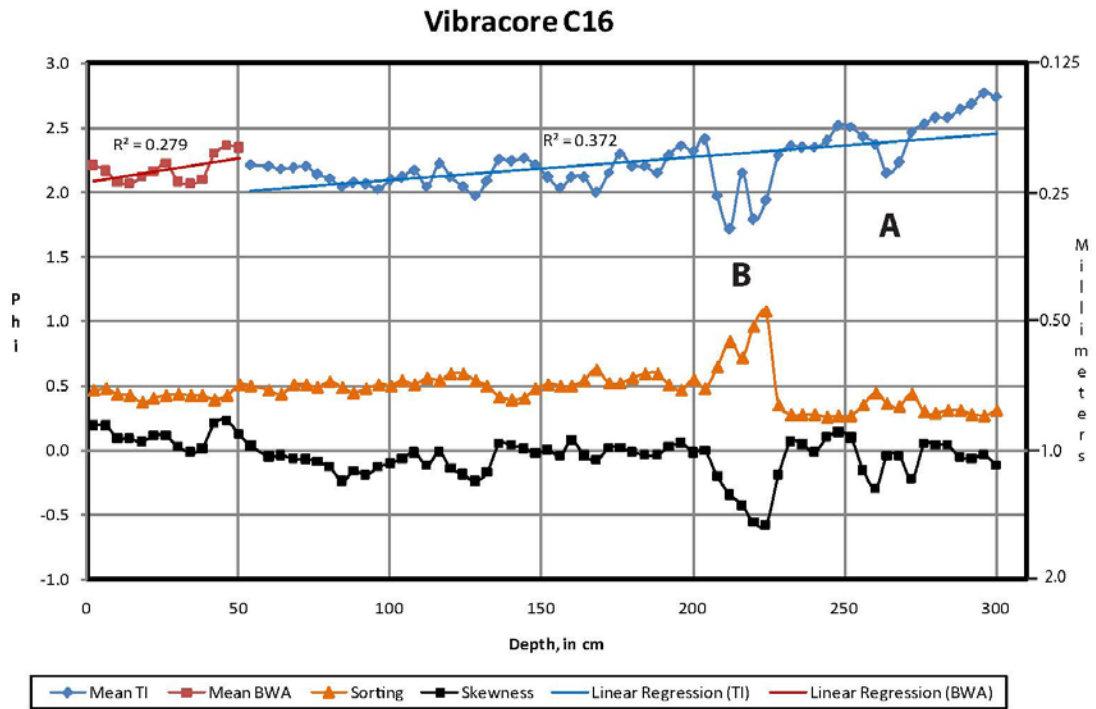


Figure 94: Photograph of Vibracore C16 with depositional environments delineated (BWA – beach-washover-aeolian).



A = Spike in water flow velocity

Figure 95: Grain-size graph for Vibracore C16 (BWA – beach-washover-aeolian, TI – tidal inlet). Skewness is dimensionless.

Figure 94 shows the depositional environments present in Vibracore C16. The grain-size data for C16 (Figure 95) show an overall trend of coarsening upward, become slightly less sorted upward, and trend from negative to positive skewness upward. The tidal-inlet deposits coarsen upward slightly, tend to be slightly less sorted upward, and trend towards negative skewness upward. Two spikes (see Figure 95) exist that represent an increase in water-flow velocity in the tidal-inlet deposit. Spike A, at a depth of 264 cm, coarsens upward, then fines upward. Spike B begins at a depth of 228 cm, coarsens upward, then fines upward at 220 cm, coarsens again at 212 cm, then fines upward again.

This corresponds to poor sorting followed by better sorting and a trend toward negative skewness followed by a return to near symmetry. The beach-washover-aeolian deposits coarsen upward slightly, become slightly less sorted upward, and trend to near symmetry upward.

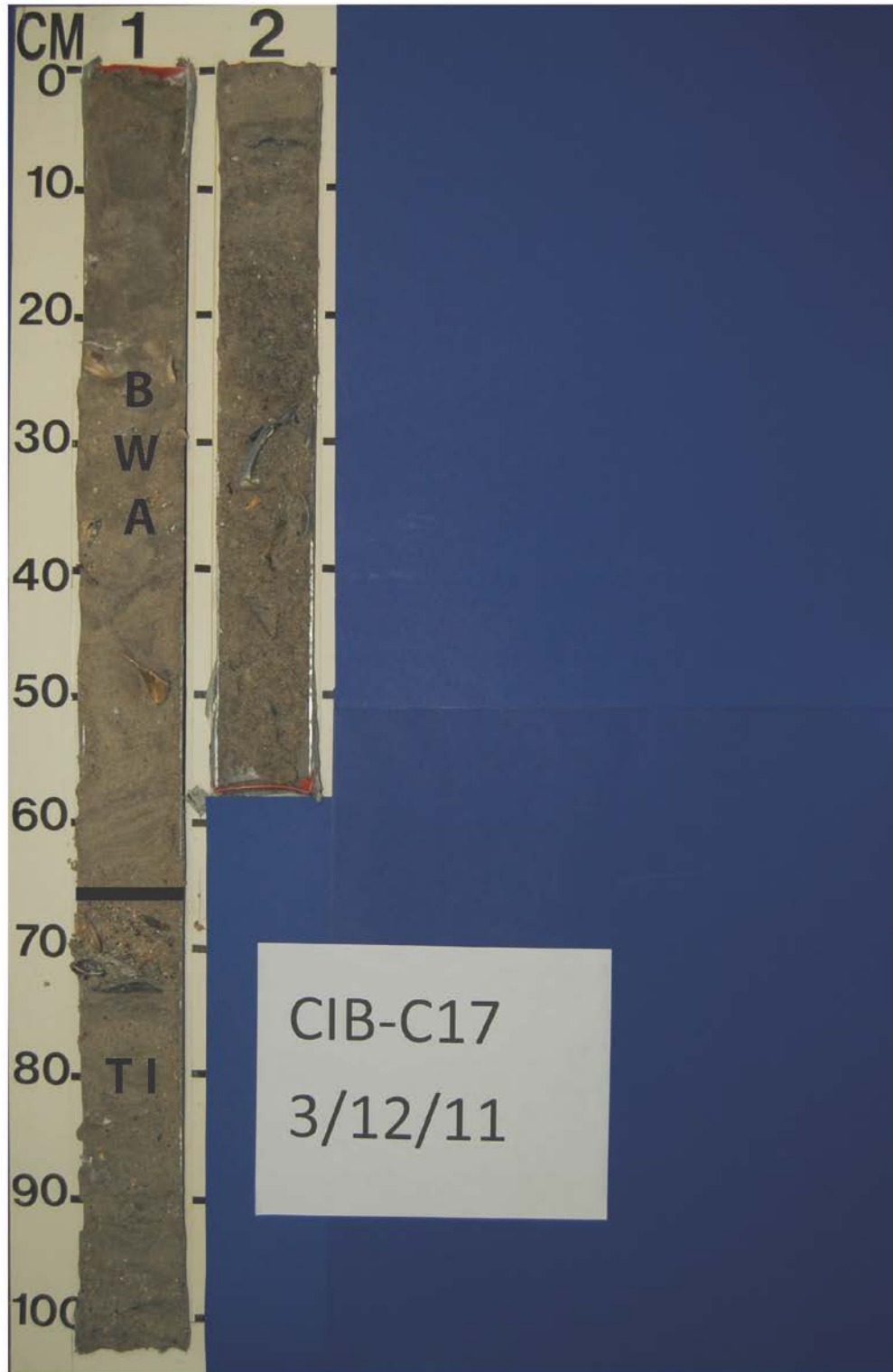
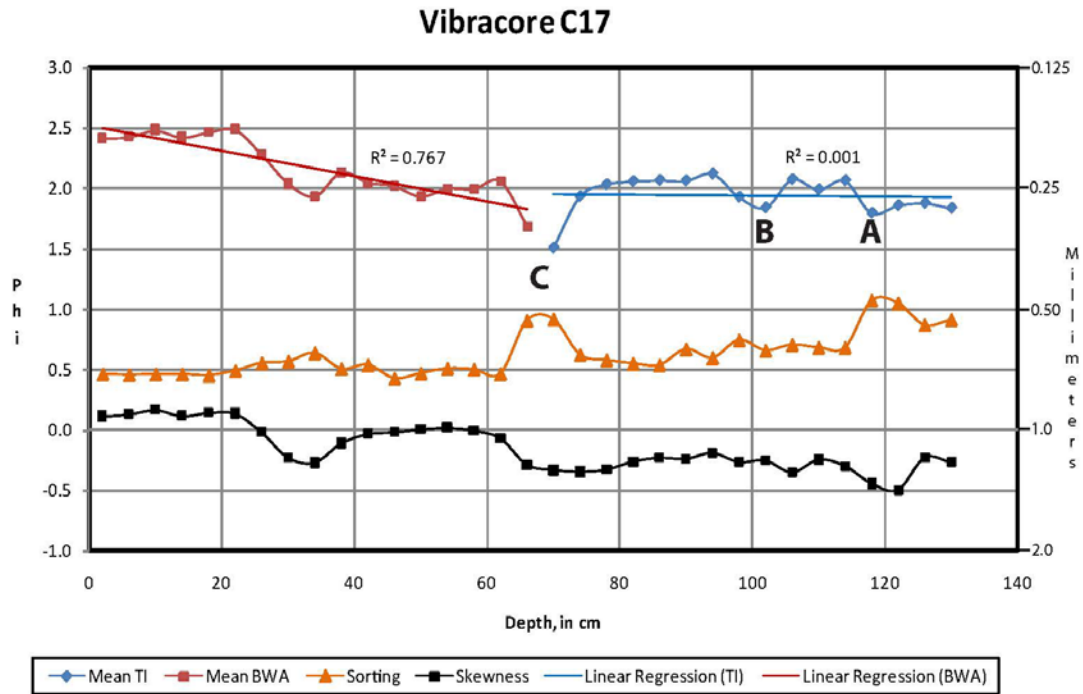


Figure 96: Photograph of Vibracore C17 with depositional environments delineated (BWA – beach-washover-aeolian, TI – tidal inlet).



A = Spike in water flow velocity

Figure 97: Grain-size graph for Vibracore C17 (BWA – beach-washover-aeolian, TI – tidal inlet). Skewness is dimensionless.

Figure 96 shows the depositional environments present in Vibracore C17. The grain-size data for C17 (Figure 97) show an overall trend that fines upward, becomes better sorted upward, and trends from negative to positive skewness upward. The tidal-inlet deposits are mostly fine-grained showing no upward trend, become better sorted upward, and show negative skewness. Three spikes exist (see Figure 97) that represent an increase in water-flow velocity in the tidal-inlet deposit. Spike A, at a depth of 118 cm, coarsens upward then fines upward with a trend to less sorting and negative skewness.

Spike B, at a depth of 102 cm, coarsens upward then fines upward. Spike C, at a depth of 70 cm, coarsens upward then fines upward, with less sorting. The beach-overwash-aeolian deposits fine upward, become better sorted upward, and trend from negative to positive skewness upward.

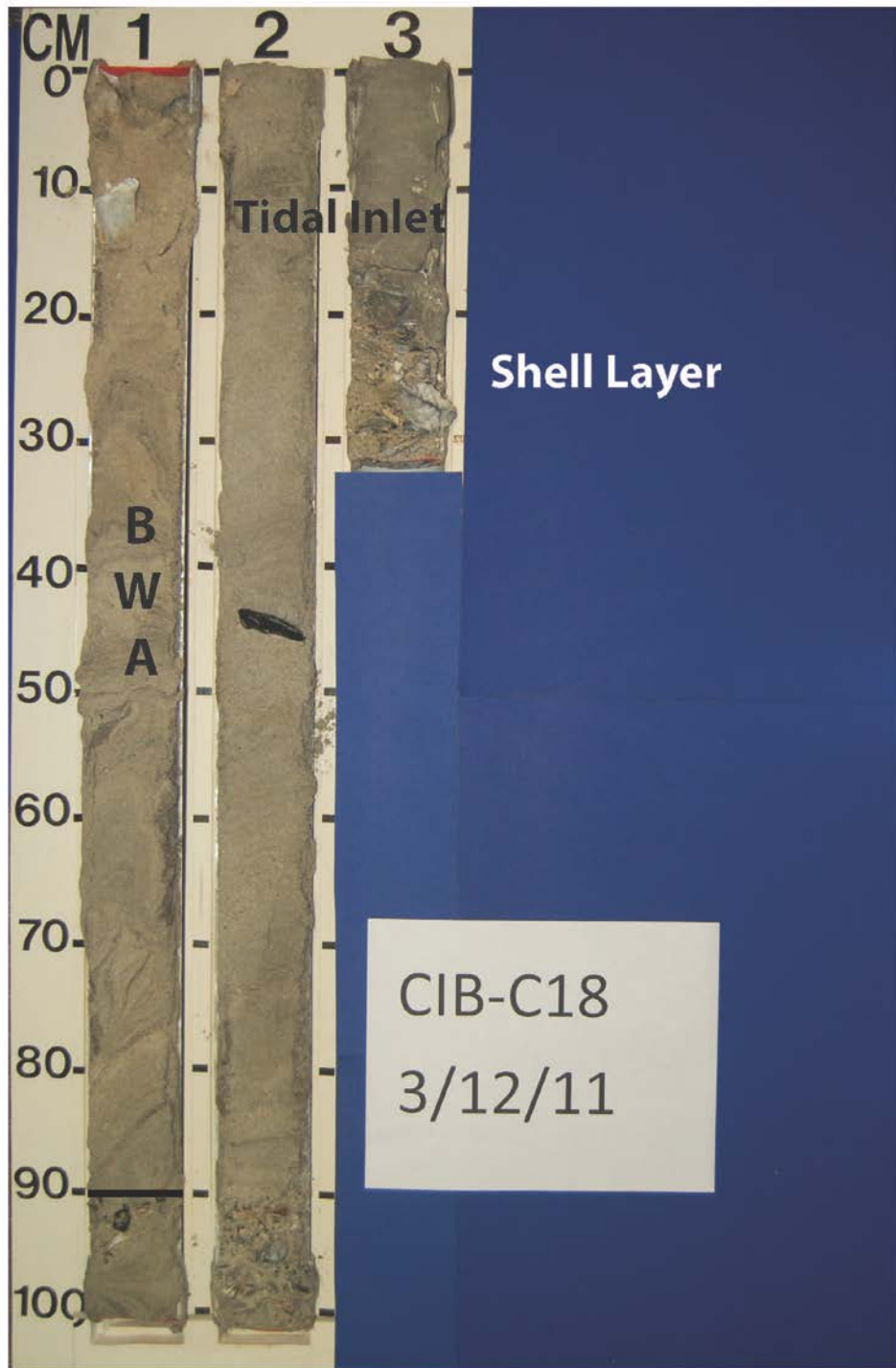
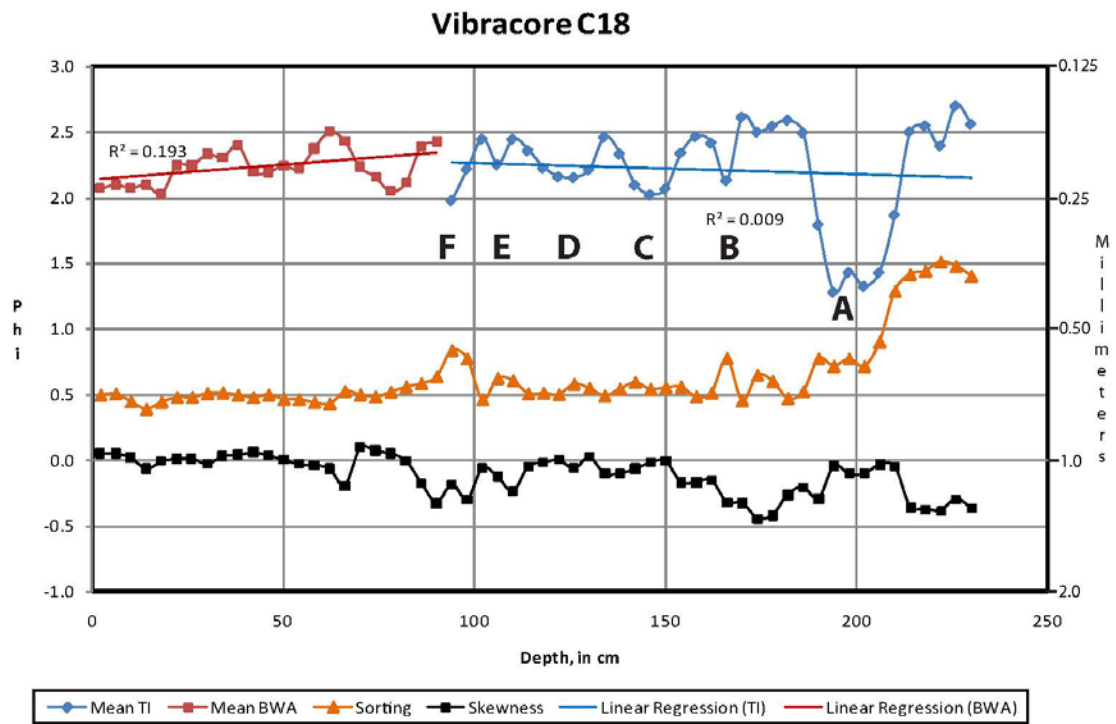


Figure 98: Photograph of Vibracore C18 with depositional environments delineated (BWA – beach-washover-aeolian).



A = Spike in water flow velocity

Figure 99: Grain-size graph for Vibracore C18 (BWA – beach-washover-aeolian, TI – tidal inlet). Skewness is dimensionless.

Figure 98 shows the depositional environments present in Vibracore C18. The grain-size data for C18 (Figure 99) show an overall trend becoming better sorted upward and trending from negative to positive skewness upward. The tidal-inlet deposits fine upward slightly, become better sorted upward, and trend from negative to positive skewness upward. Six spikes exist (see Figure 99) that represent an increase in water-flow velocity in the tidal-inlet deposits. All of these spikes coarsen upwards then fine upwards. Spike A, at a depth of 202 to 194 cm, has no attendant correlation with sorting

and skewness. Spike B, at a depth of 166 cm, is slightly more poorly sorted. Spikes C, D, and E, at depths of 146 cm, 124 cm, and 106 cm, respectively, have no attendant correlation with sorting and skewness. Spike F, at a depth of 94 cm, is more poorly sorted. The beach-washover-aeolian deposits coarsen upward, become slightly better sorted upward, and trend from negative to positive skewness upward.

The grain-size trends were plotted on location maps for each of the three depositional environments for which grain sizes were analyzed: beach-overwash-aeolian, tidal inlet, and flood-tidal delta. The beach-overwash-aeolian depositional environment has 20 cores that exhibit coarsening-upward trends, four cores with fining-upward trends, and three cores that show no trend (Fig. 100). Coarsening-upward sequences are characteristic of beach-washover-aeolian deposits (Leatherman & Williams, 1983). The cores with a coarsening-upward trend or no trend are located in the areas that are exposed to the processes that created these deposits. The three cores with a fining-upward trend are located on the northern edge of the ephemeral inlet's flood-tidal delta.

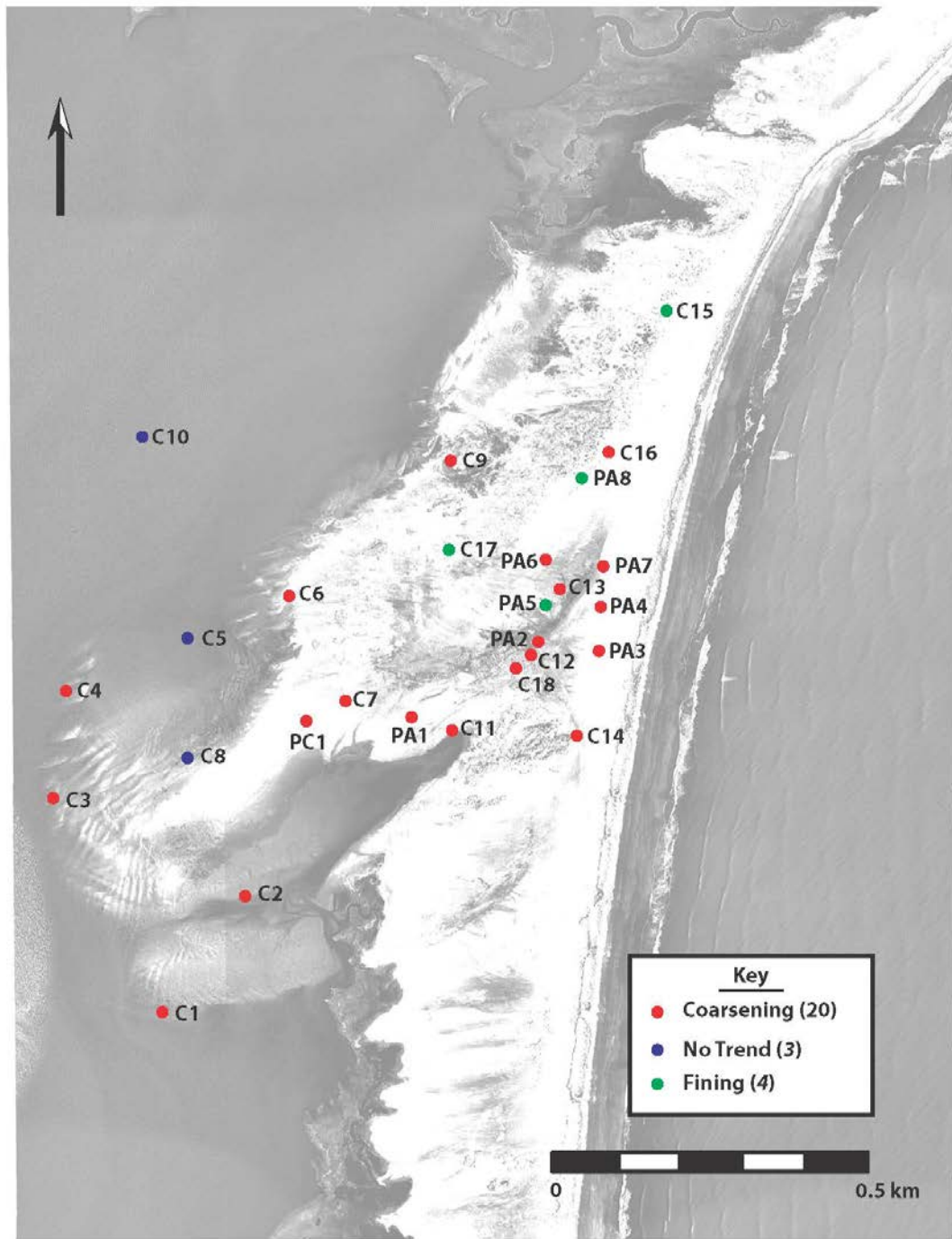


Figure 100: Location map of cores with beach-washover-aeolian depositional environment showing the upward trends of grain-sizes.

The vertical grain-size trends for the tidal-inlet depositional environment has 13 cores that exhibit coarsening-upward trends, five cores with fining-upward trends, and one that shows no trend (Fig. 101). A tidal-inlet channel fills in as it migrates and the waning energy of that channel leads to a fining-upward sedimentary succession (Kumar & Sanders, 1974; Moslow & Heron, 1978; Moslow & Tye, 1985). No published papers were found that document a coarsening upward sequence in tidal-inlet deposits. Fourteen cores with a coarsening-upward trend or no trend are found along the path of the ephemeral inlet as it migrated southward after opening. The three cores with fining-upward trends are in the last open position of the ephemeral inlet. Vibracore C11, which in the last open position of the ephemeral inlet, shows a coarsening upward sequence followed by a fining upward sequence.

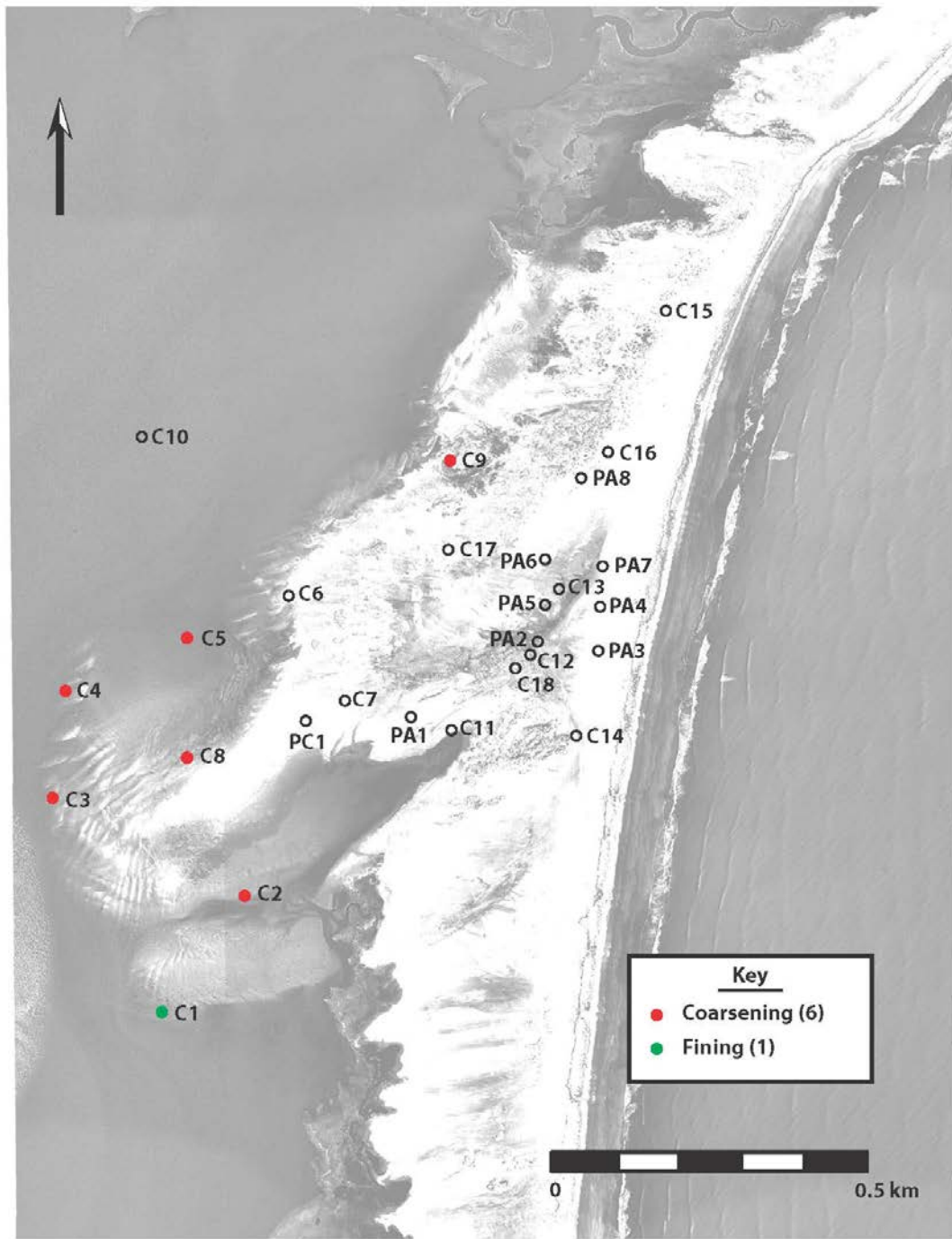


Figure 101: Location map of cores with tidal -inlet depositional environment showing the upward trends of grain-sizes.

The grain-size trends for the flood-tidal delta depositional environment have six cores that exhibit coarsening-upward trends and one core shows a fining-upward trend (Figure 102). The six with a coarsening-upward trend are located on the northern end of the ephemeral inlet's flood-tidal delta. Flood-tidal delta deposits generally coarsen-upward (Israel et al., 1987). The one with a fining-upward trend is located on the southern end of the ephemeral inlet's flood-tidal delta.

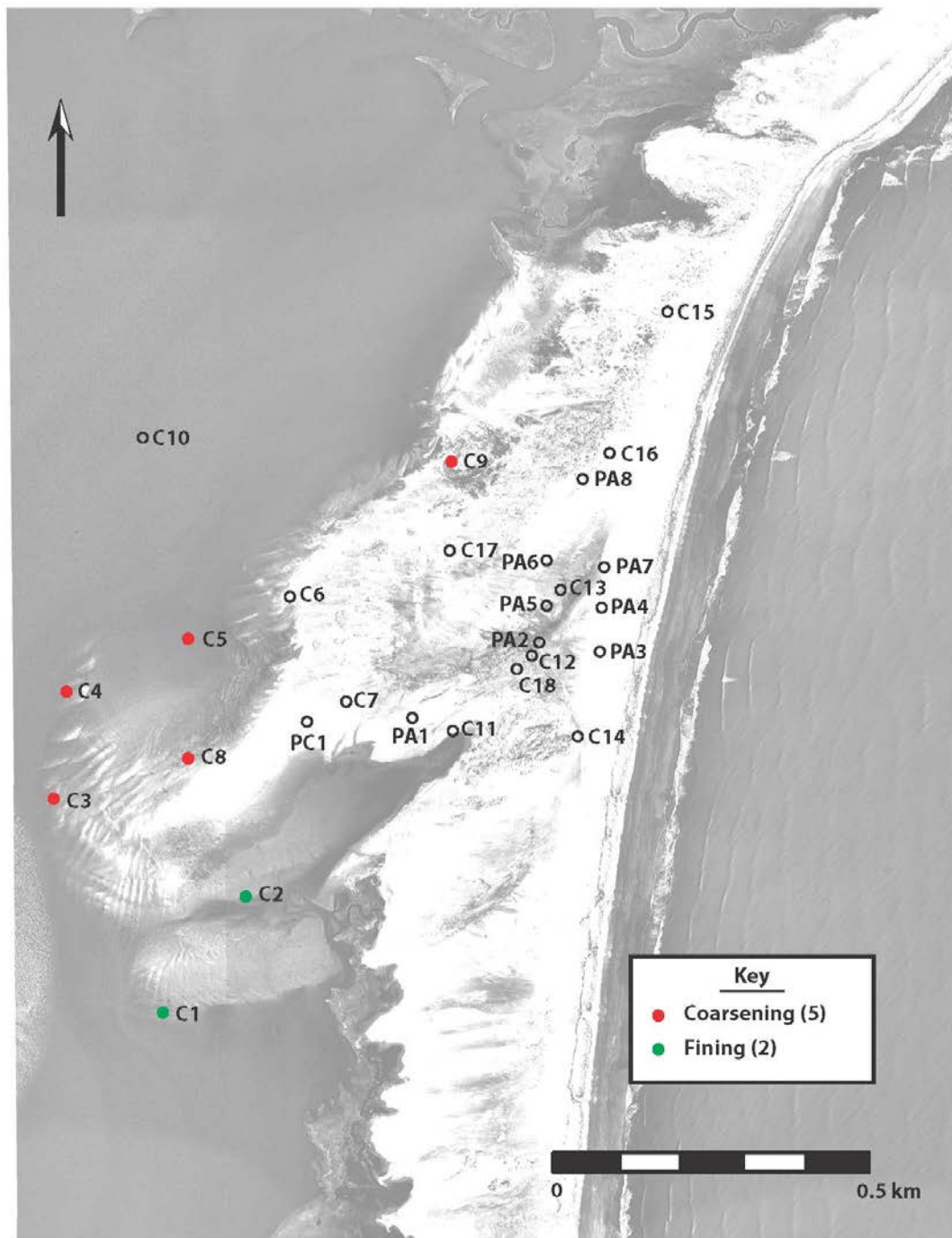
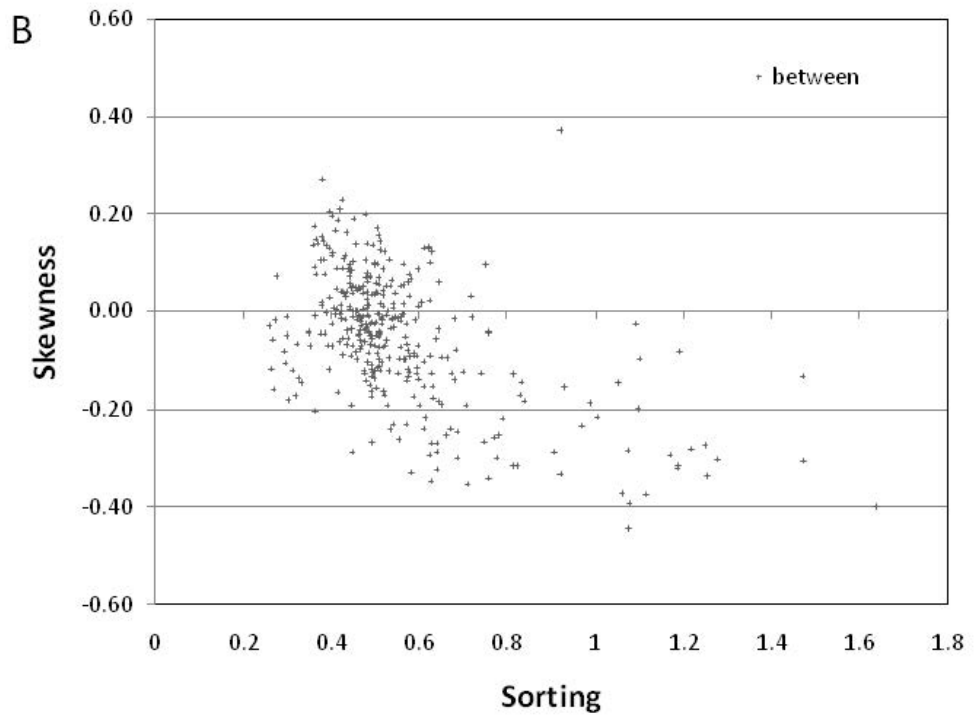
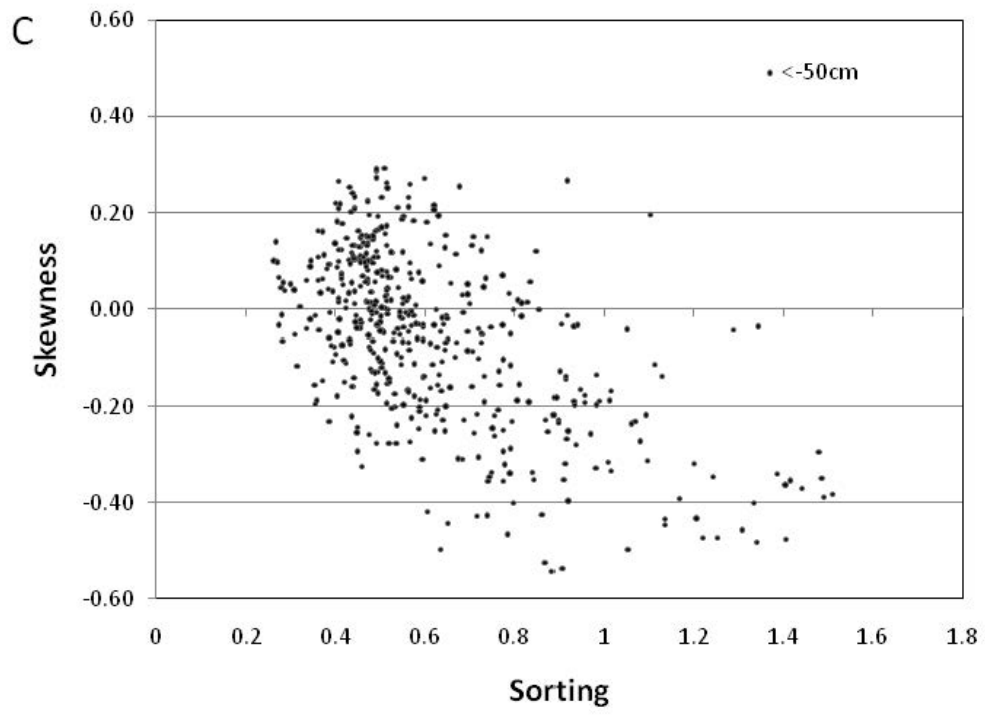


Figure 102: Location map of cores with flood-tidal delta depositional environment showing the upward trends of grain-sizes.

Sorting vs. skewness

Multiple techniques for analyzing the parameters of grain-size data have been used to interpret depositional environments (Boggs, 2006). Friedman (1967) plotted data for sorting (standard deviation) versus skewness of grain size to determine the depositional environments of the samples. In this study, the grain-size data for sorting versus skewness were analyzed in three elevation categories, relative to mean sea level (MSL): Above +50 cm in elevation, below -50 cm in elevation, and between +50 cm and -50 cm in elevation (Fig. 103). The samples above +50 cm (Fig. 103A) are moderately well to well sorted and tend to be positively skewed to nearly symmetrical. These deposits are from the upper intertidal or supratidal zone and are interpreted as being from a subaerial, aeolian environment. The samples collected between +50 cm and -50 cm (Fig. 103B) are mostly moderately well to well sorted, with a few being very well sorted, and range from positively to negatively skewness. The majority of these deposits are within the intertidal zone and represent a beach-foreshore-washover environment. The samples collected below -50 cm in elevation (Fig. 103C) are well sorted to poorly sorted and positively skewed to strongly negatively skewed. These samples are from the intertidal or subtidal zone and are interpreted as being from tidal-inlet and flood-tidal delta environments. Figure 103D plots the three depth ranges together. For tidal-inlet fill, Figure 103D shows that sorting improves upward and skewness tends to go from negative to positive upward.





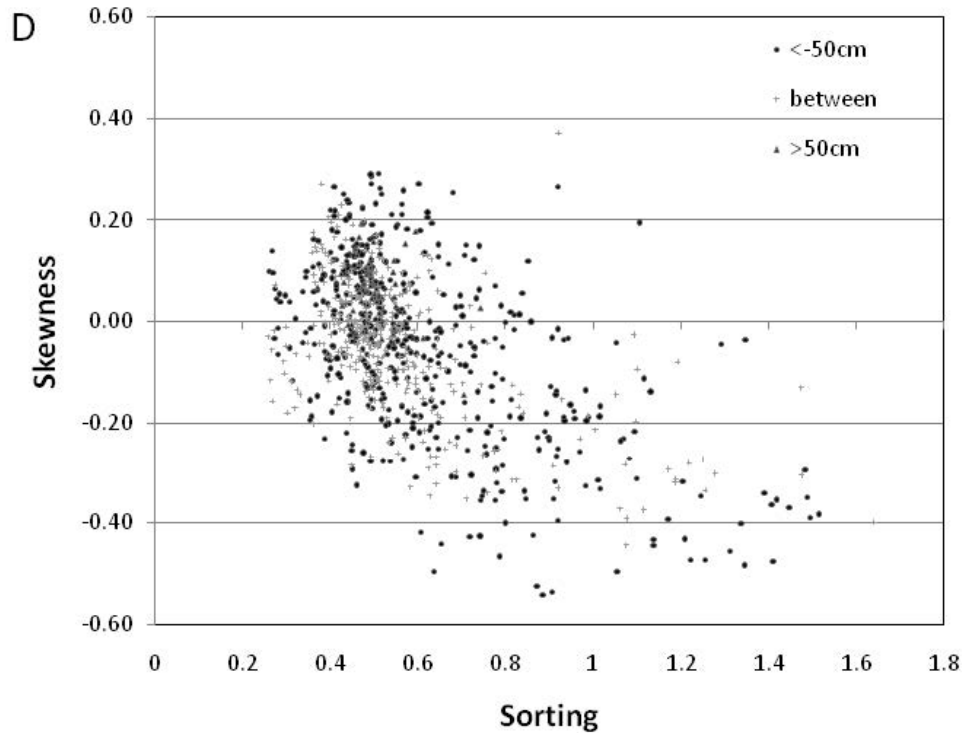


Figure 103: Sorting versus skewness. (A) Sediment samples from elevations above +50 cm (n = 69). (B) Sediment samples from elevations between +50 and -50 cm (n = 364). (C) Sediment samples from elevations below -50 cm (n = 471). (D) All sediment sample data combined (n = 904).

Cedar Island ephemeral inlet stratigraphy

Ten geologic cross sections were constructed to analyze the stratigraphic relationships of the four depositional environments in the study area. Figure 104 displays the location of all of these cross sections. Five cross sections (A-A', A-B', A-C', D-D', and E-D') are strike cross sections and were constructed to be approximately parallel to the shoreline. Five cross sections (H-H', C-D', F-F', G'G', and D'-G') are dip cross sections and were constructed to be approximately perpendicular to the shoreline and the strike cross sections. A separate location map for each cross section is included with the corresponding cross section.

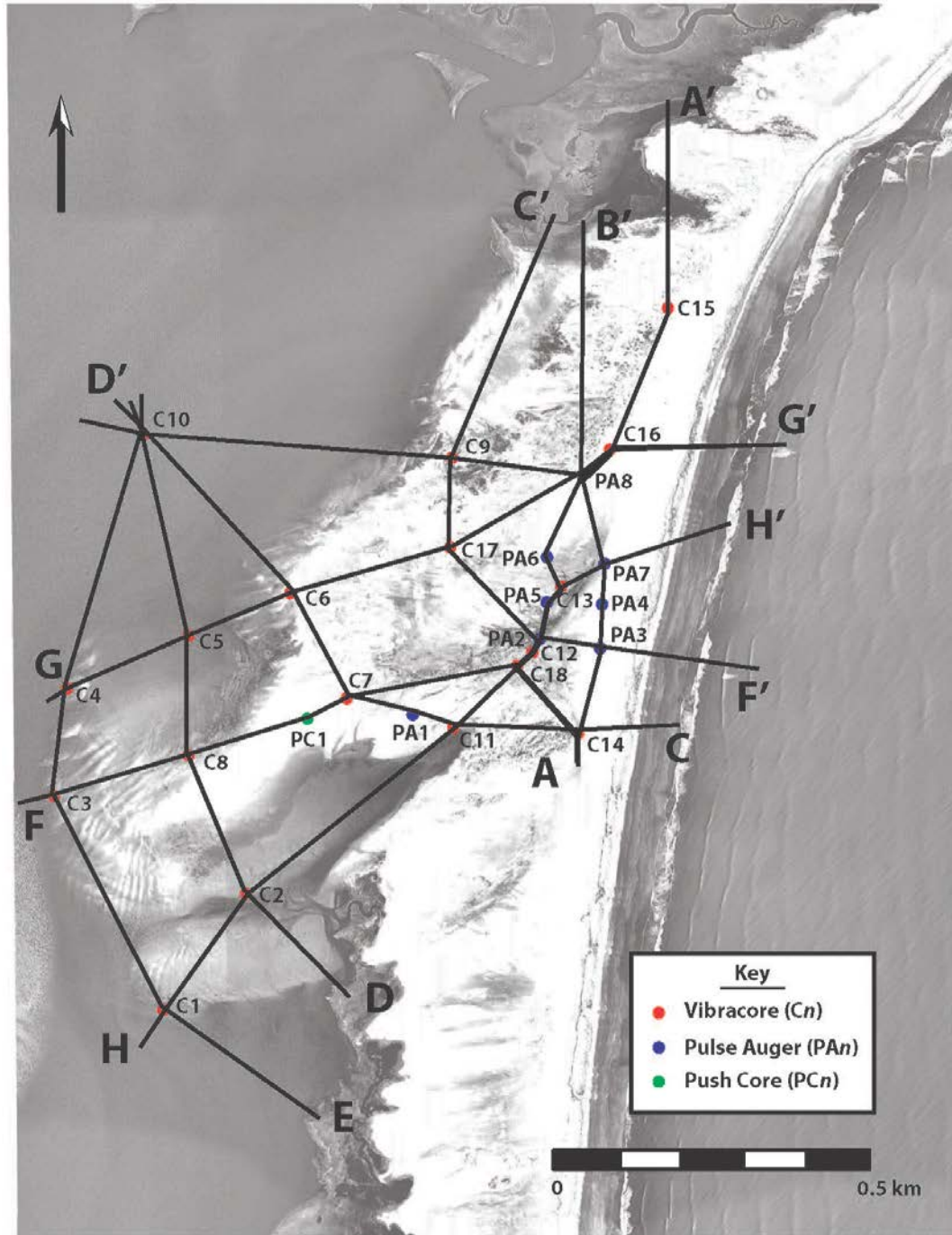


Figure 104: Location map of all ten cross sections.

Correlation of strike geologic cross sections

Figure 18 shows the locations of three strike geologic cross sections that show the sedimentary deposits along the migration path of the ephemeral tidal inlets on Cedar

Figure 105 shows the locations of three strike geologic cross sections that show the sedimentary deposits along the migration path of the ephemeral tidal inlets on Cedar Island. Figure 106 displays these geologic cross sections (A – A', A – B', and A – C').

These cross sections are dominated by tidal-inlet deposits laid down by the southward lateral migration of the most recent tidal inlet that was open from 1998 – 2007. Estuarine deposits underlie all of these cross sections. During the initial island-breaching process and subsequent lateral inlet migration to the south, tidal-inlet processes scoured into the estuarine deposits and laid down inlet-fill deposits. The tidal-inlet fill deposits are approximately 4 m thick or greater in cross section A – A' and less than 3 m on cross sections A – B'. On cross section A – C', the tidal-inlet fill deposits are up to 2.65 m thick in the south and they grade into flood-tidal delta deposits to the north. The entire top of these cross sections are capped by beach–washover–aeolian deposits that are thickest (~3 m) at the southern end at Core C14 in the dune area but are only a veneer over the salt marshes at their northern end.

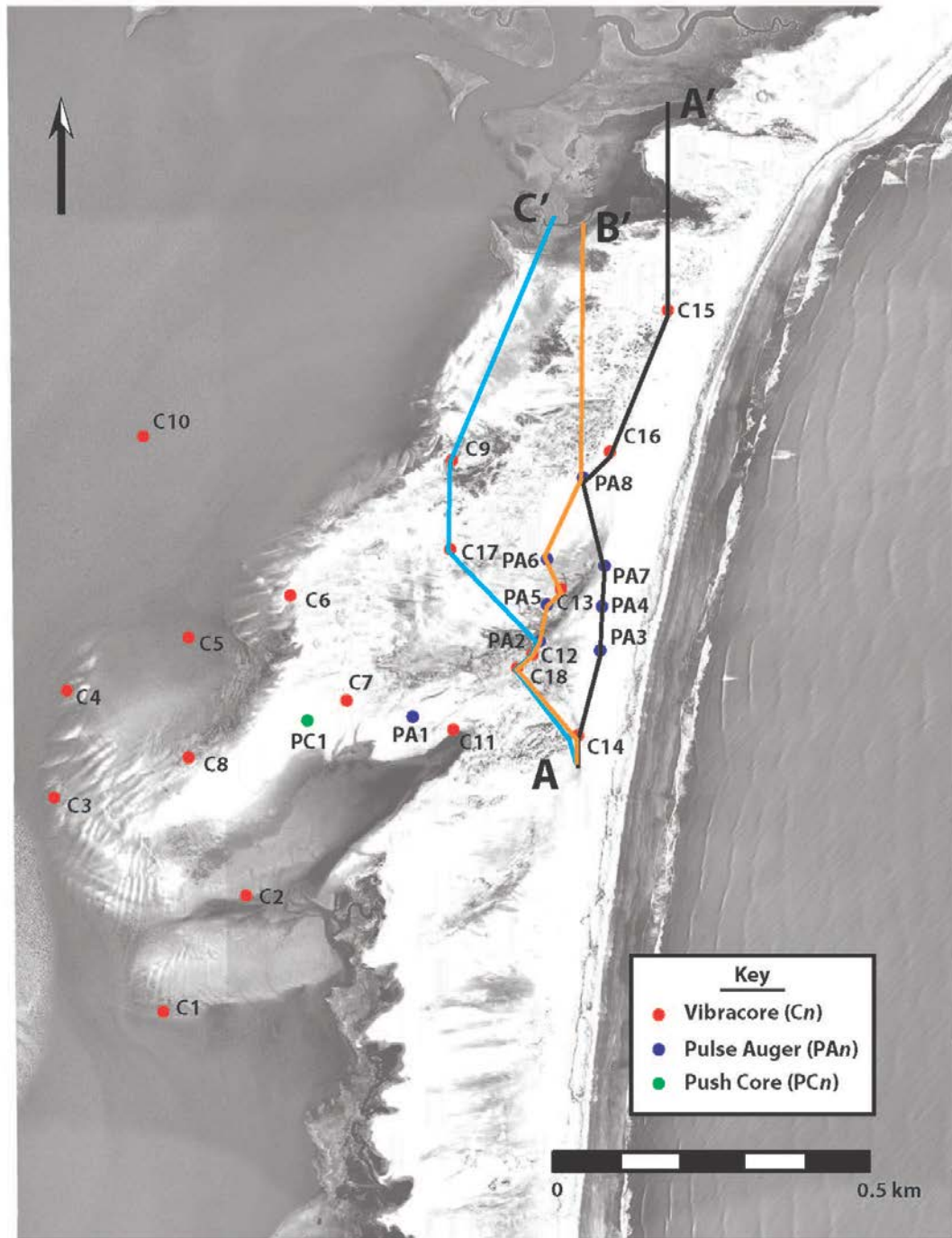
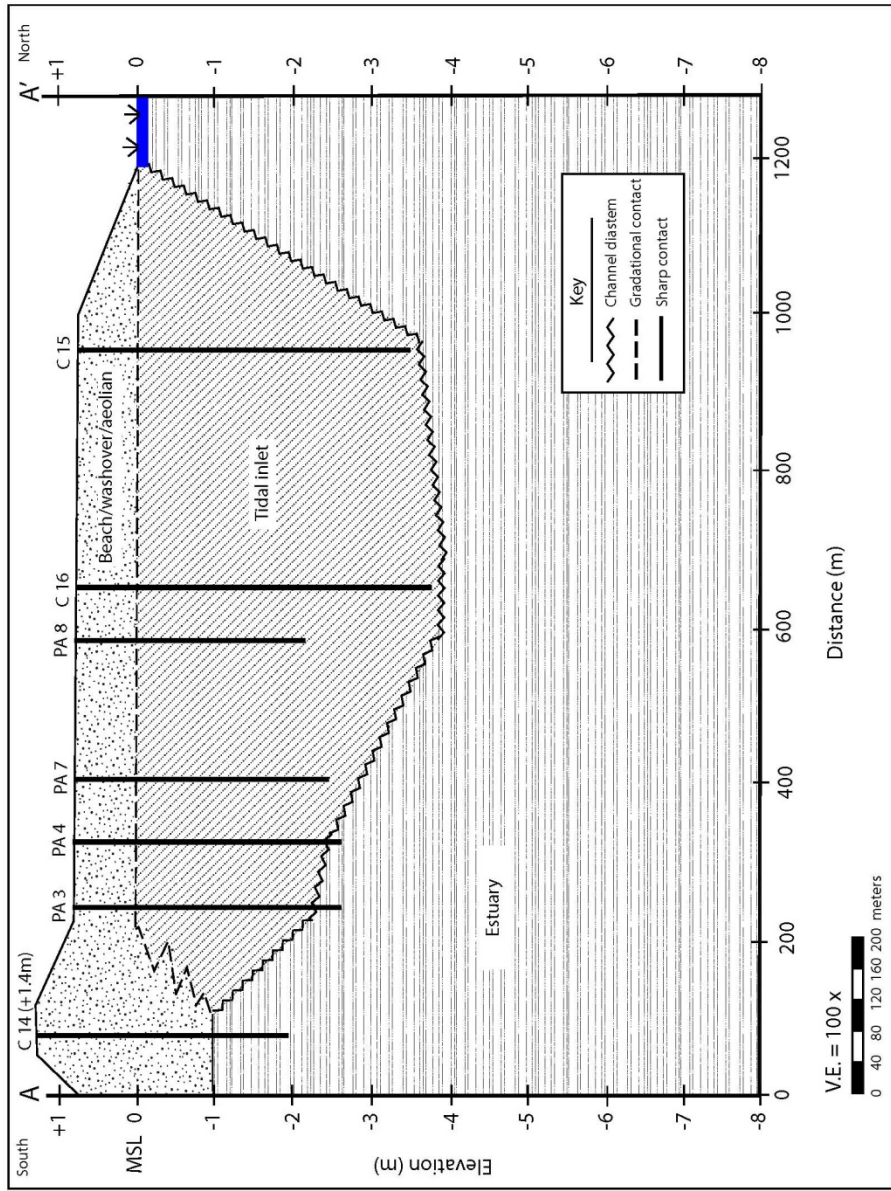
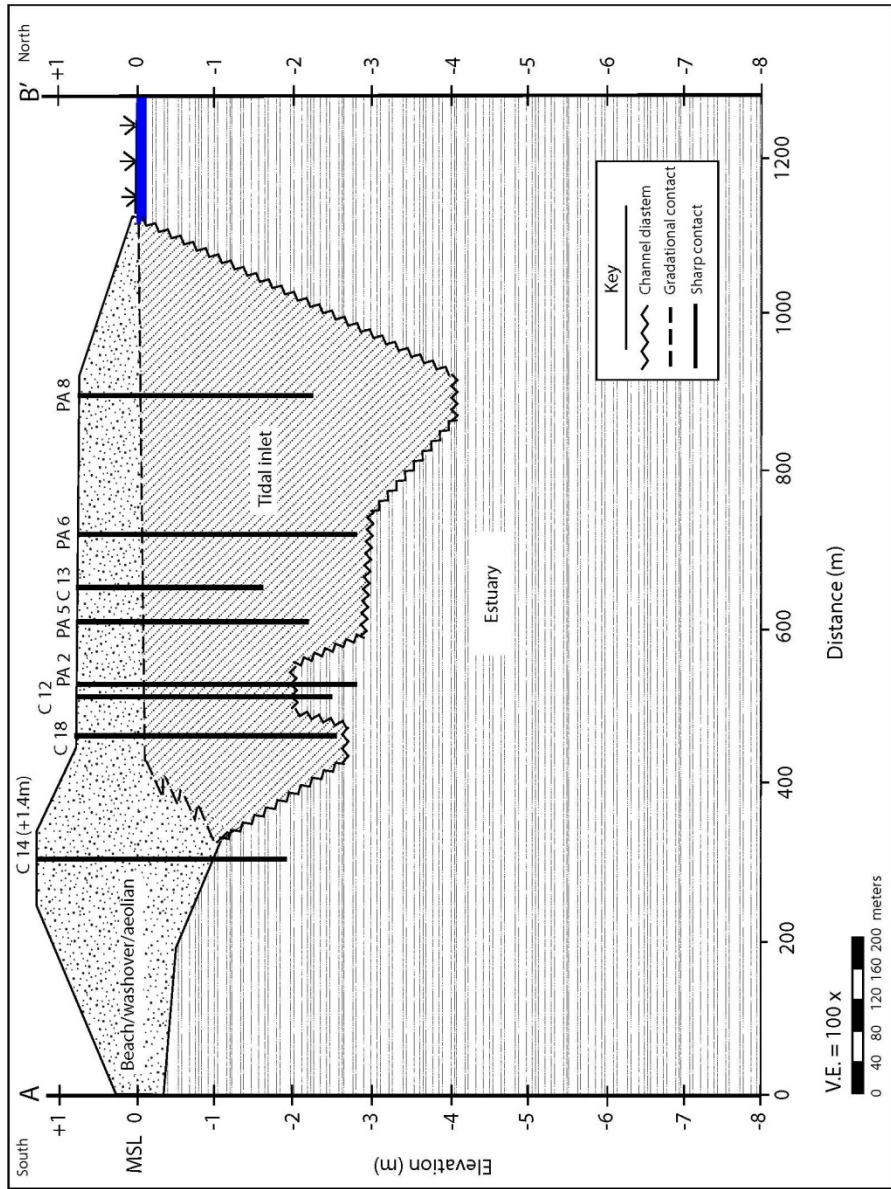


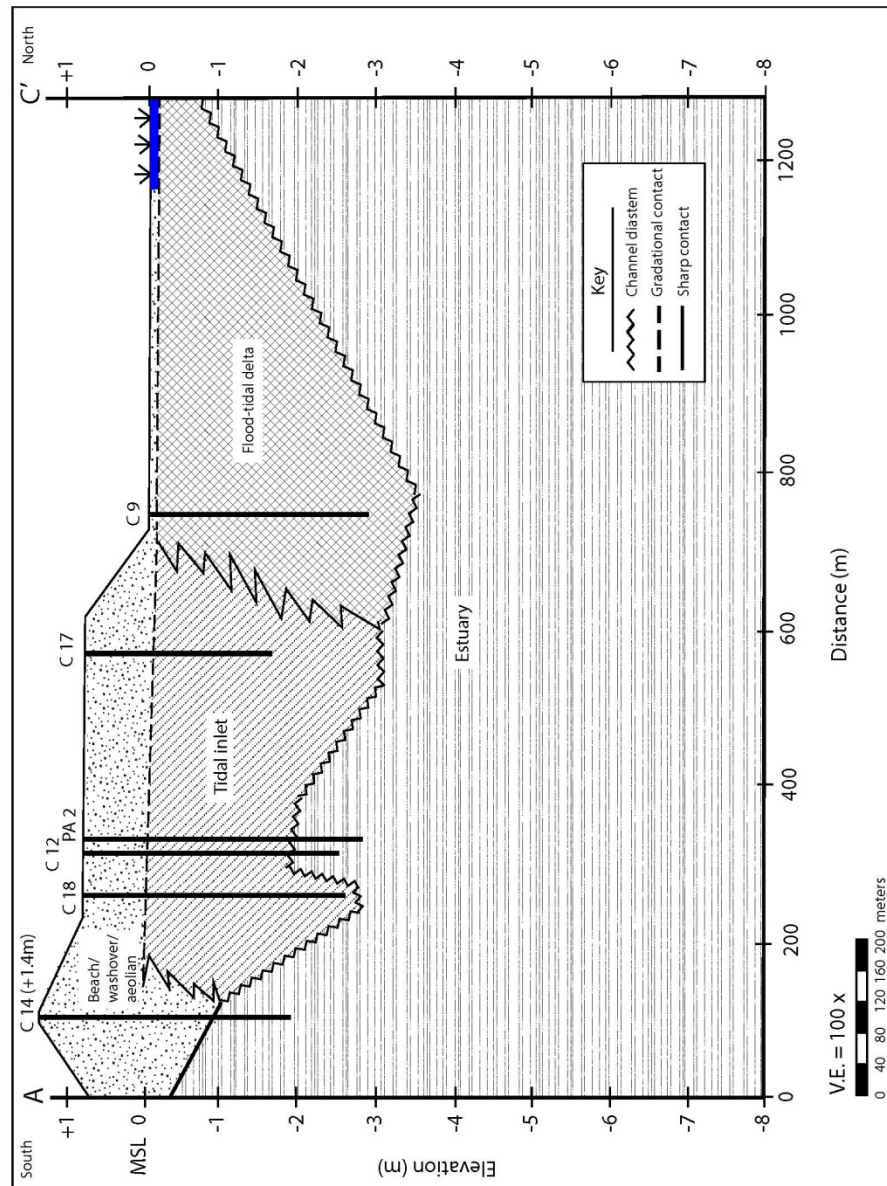
Figure 105: Location map for strike geologic cross sections A – A', A – B', and A – C'.



A



B



C

Figure 106: Strike geologic cross sections A – A' (A), A – B' (B), and A – C' (C).

Figure 107 shows the locations of two strike geologic cross sections that depict the sedimentary deposits across the flood-tidal delta located on the landward side of

Cedar Island. Figure 108 displays these geologic cross sections (D – D' and E – E'). These cross sections show all four of the primary depositional environments and are dominated by the southward lateral migration of the most recent ephemeral tidal inlet (1998 – 2007). Estuarine deposits form the foundation of these cross sections. At the northern end of both cross sections, Core C10 shows two estuarine deposits, one thick (~6 m) and one thin (~0.25 m). The thick deposit is part of the estuarine depositional environment that underlies the entire study area. The thin estuarine deposit directly overlies the flood-tidal delta unit. These thin estuarine deposits were laid down after the last tidal inlet, which was open from 1998 to 2007, had migrated southward away from this area. They are overlain by beach–washover–aeolian deposits with an average thickness of approximately 0.5 m. These deposits were interpreted to be washover deposits from the November 2009 storm Nor'Ida (maximum storm surge height of approximately 2.3 m), which occurred before the core was taken. Core C10 was collected from the shallow estuary, which coincides with a large area of washover deposits from Nor'Ida.

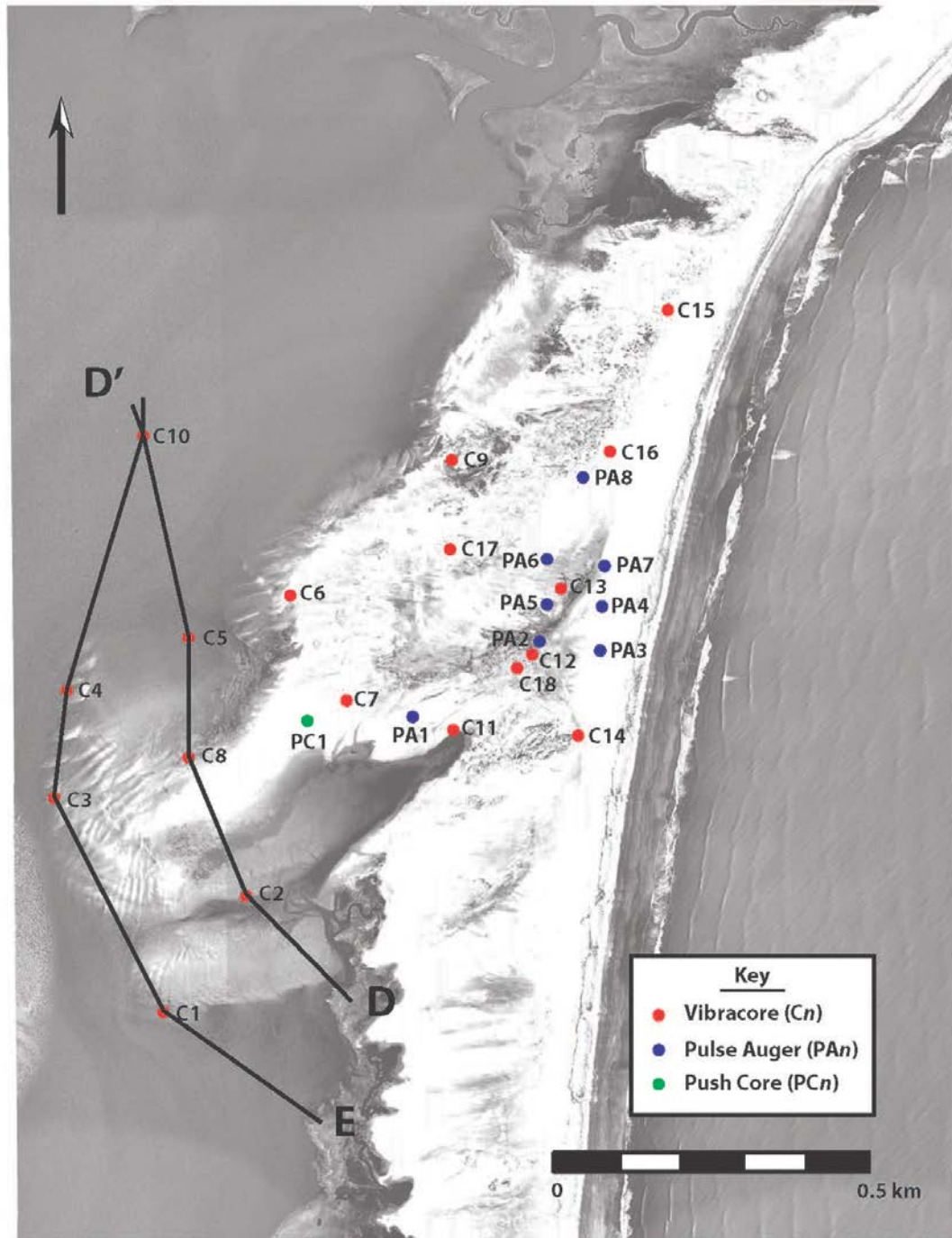
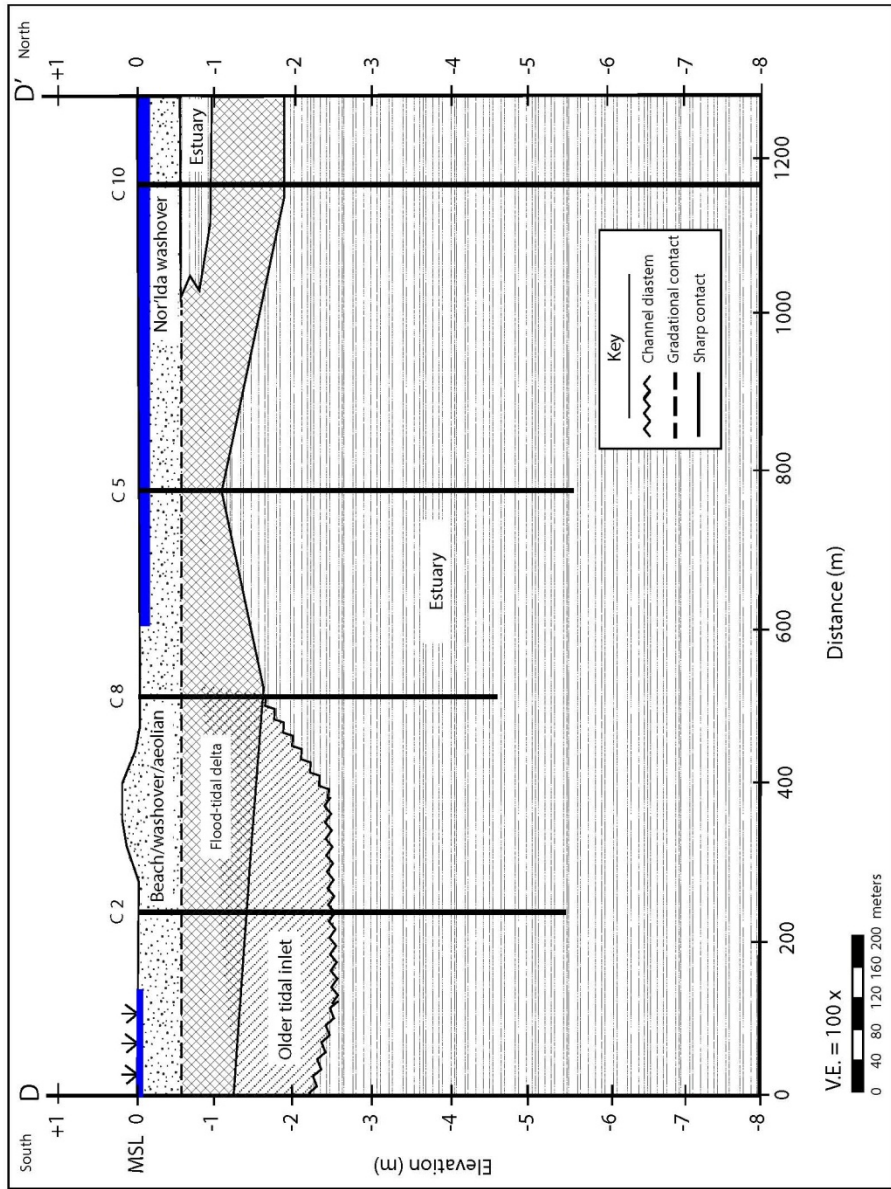
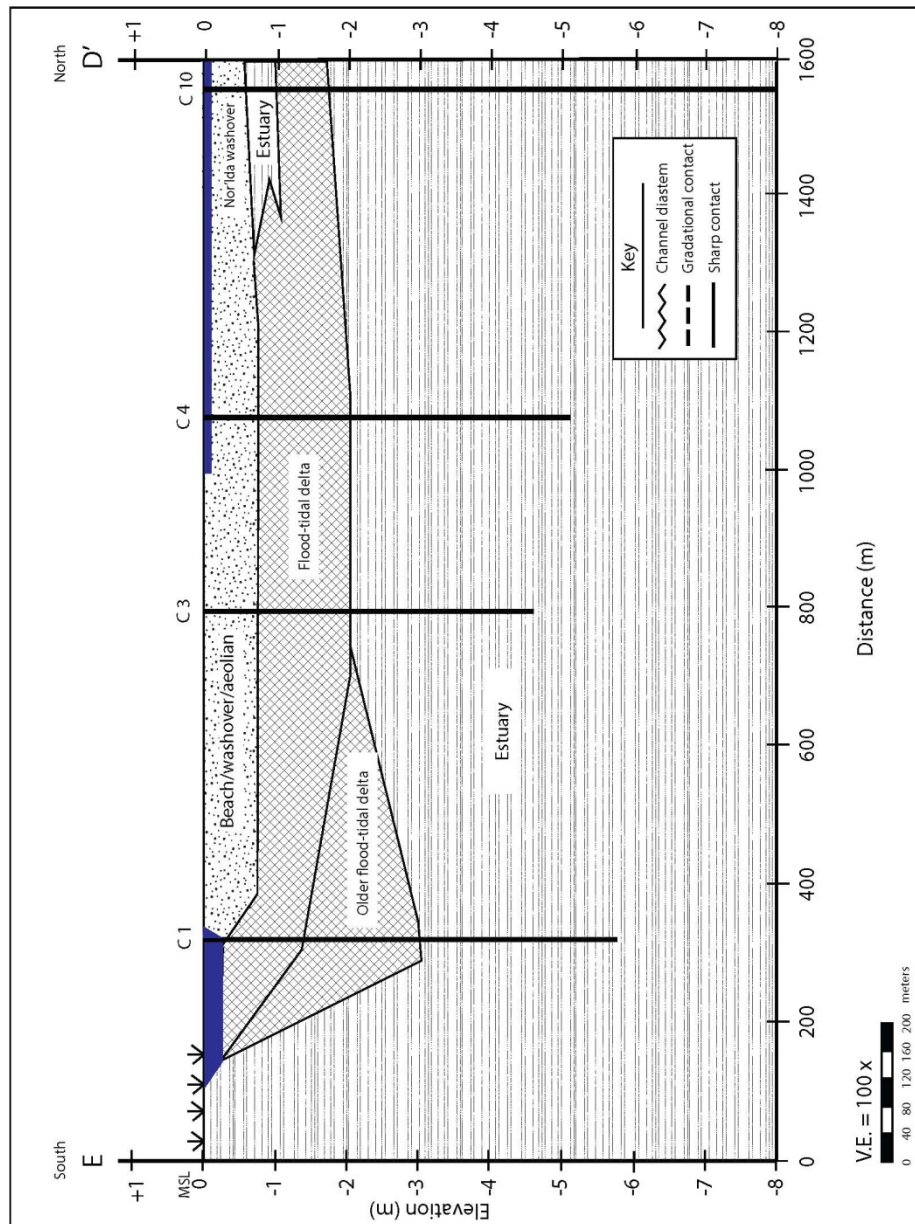


Figure 107: Location map for strike geologic cross sections D – D' and E – D'.



A



B

Figure 108: Strike geologic cross sections D - D' (A) and E - D' (B).

Cross section D – D' (Fig. 108A) shows tidal-inlet deposits that scoured into and overlie the estuarine deposits at the southern end of this cross section. These deposits are

interpreted as forming during a previous ephemeral tidal inlet (1956–1962 and/or 1993–1997) that are approximately 4 m thick. These deposits are overlain by younger tidal-inlet deposits of the most recent ephemeral tidal inlet (1998–2007) that are approximately 1 m thick. The tidal-inlet deposits grade into flood-tidal delta deposits to the north between Core C2 and Core C8. Beach–washover–aeolian deposits overlie the most recent ephemeral tidal-inlet deposits and have an average thickness of approximately 0.5 m.

Cross section E – D' (Fig. 108B), lying west of cross section D – D', shows flood-tidal delta deposits that overlie estuarine deposits. The flood-tidal delta deposits, from -1.3 m to -3 m, at the southern end of this cross section are interpreted to have been deposited during a previous ephemeral tidal inlet (1956–1962 and/or 1993–1997). These deposits are overlain by younger flood-tidal delta deposits from the most recent ephemeral tidal inlet (1998 – 2007). These deposits are approximately 1 m thick and extend to the north.

Correlation of dip geologic cross-sections

Figure 109 shows the locations of five dip geologic cross sections that depict the sedimentary deposits across Cedar Island. Figure 110 displays these dip geologic cross sections (H – H', F – F', G – G', D' – G', and D' - C). Cross section H – H' (Fig. 110 A) is a dip section from the estuary to the ocean along the axis of the former inlet throat, including the flood-tidal delta of the most recent ephemeral tidal inlet (1998–2007), which was the final channel position of the ephemeral tidal inlet before it closed. Estuarine deposits underlie this entire cross section. Tidal-inlet processes eroded the estuarine deposits and laid down tidal-inlet fill deposits that grade laterally to the

southwest (landward) into flood-tidal delta deposits above the estuarine deposits. The flood-tidal delta deposits in Core C1 from -3.0 m to approximately -1.25 m are interpreted to be from a previous ephemeral tidal inlet. These flood-tidal delta deposits grade into tidal-inlet deposits in Core C2 from approximately -5 m to -0.5 m and are interpreted as representing a previous tidal inlet or tidal inlets (1956–1962 and/or 1993–1997). Overlying these deposits are the flood-tidal delta deposits from the last ephemeral tidal inlet (1998–2007). These deposits grade northeast into tidal-inlet deposits from the last ephemeral tidal inlet. In Core C11 and cores collected seaward, these tidal-inlet deposits overlie estuarine deposits. The entire cross section is capped by a thin layer of beach–washover–aeolian deposits from approximately -0.5 m to the surface.

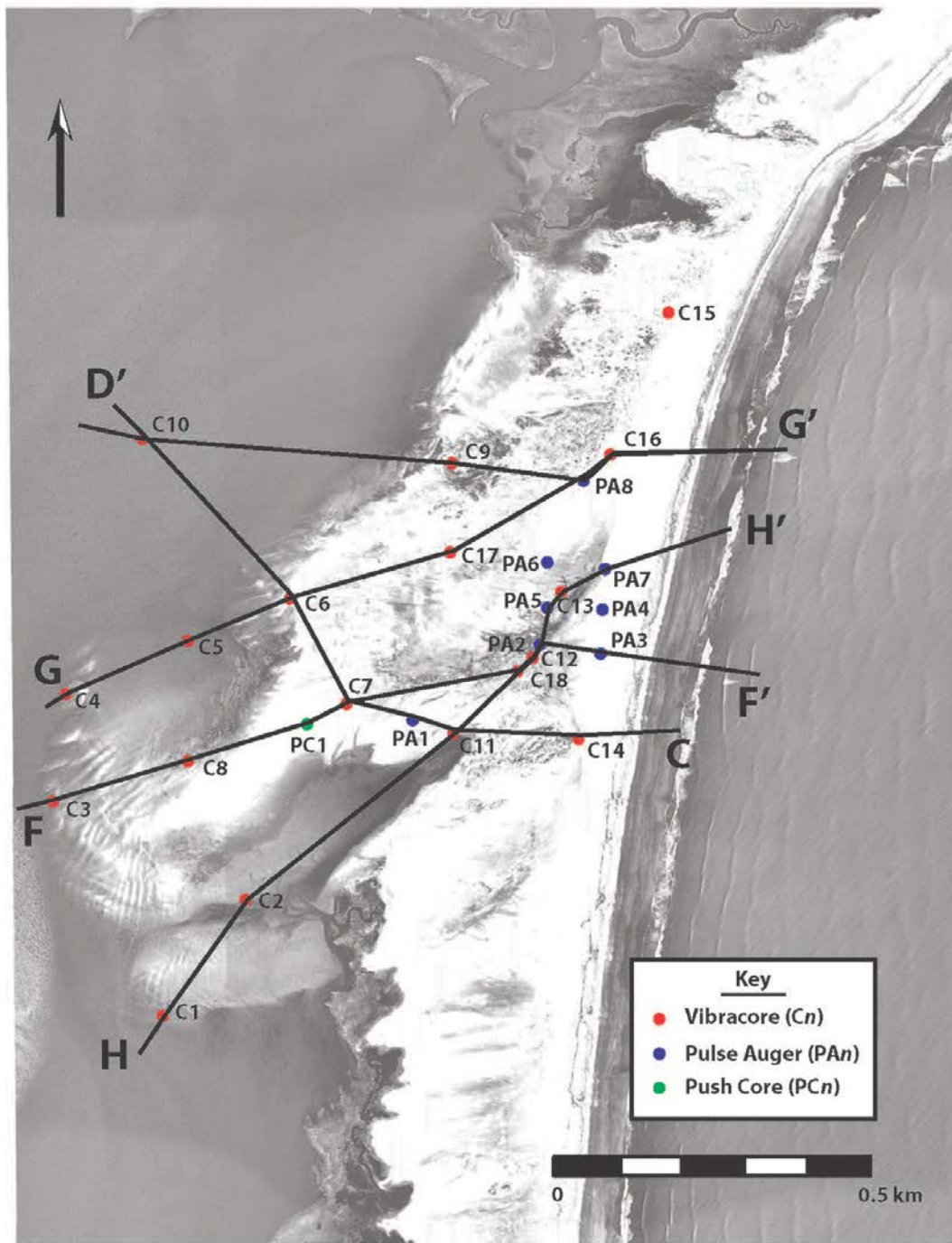
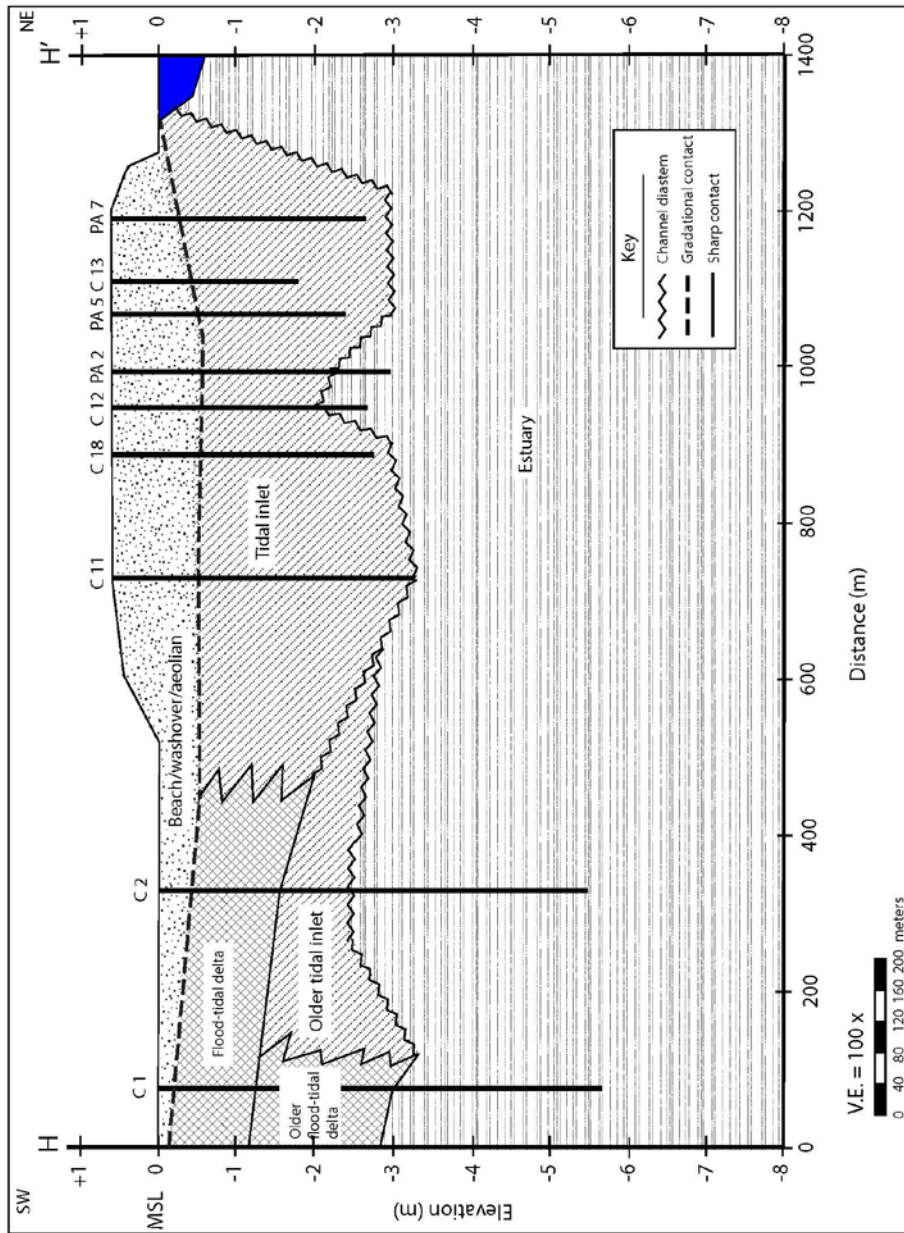
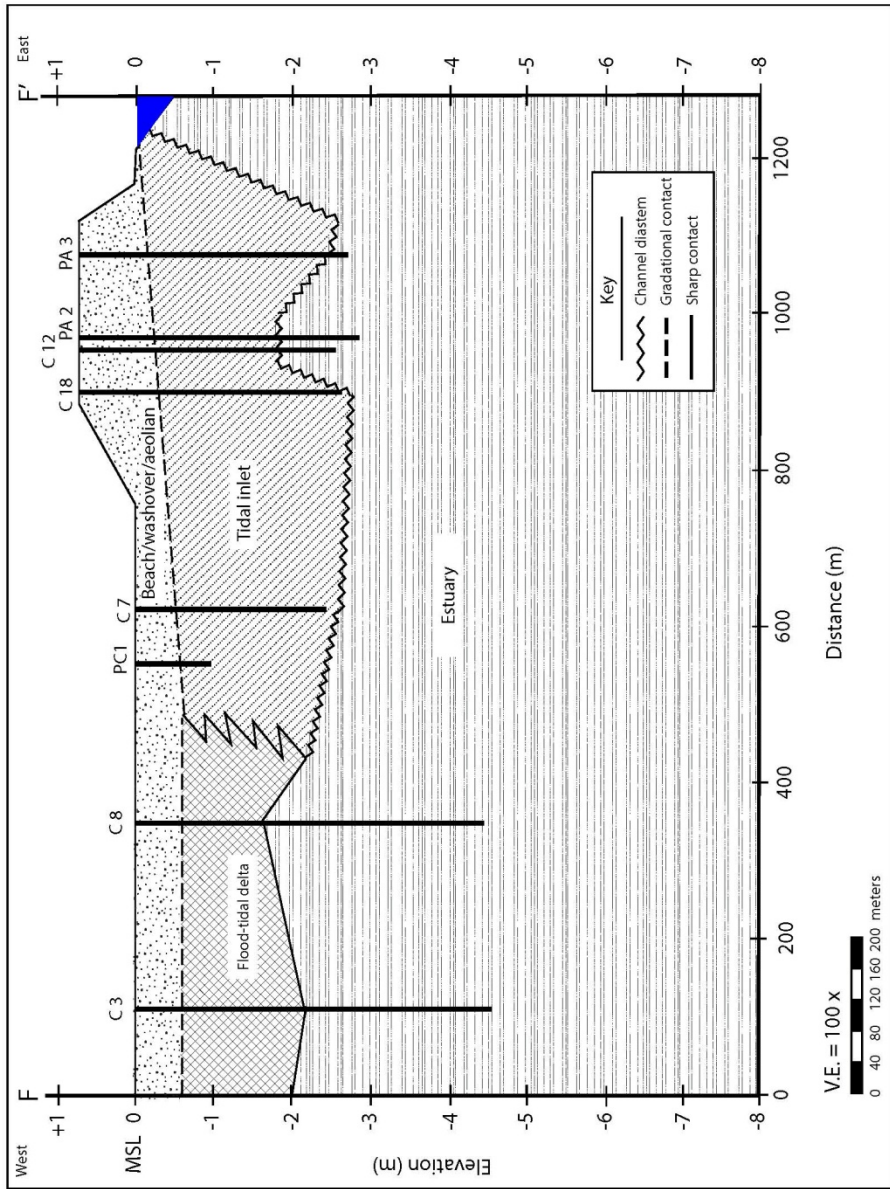


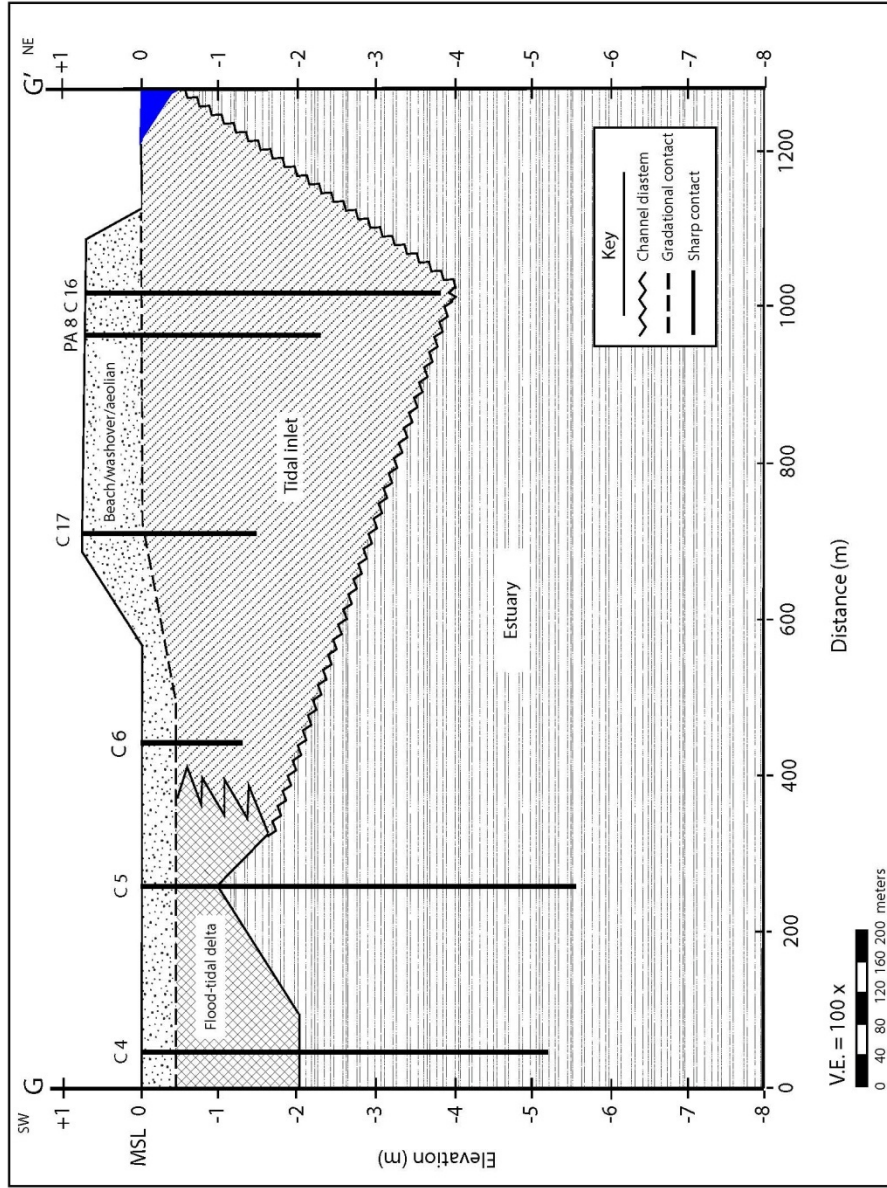
Figure 109: Location map for dip geologic cross sections H – H', F – F', G – G', D' – G', and D' - C.



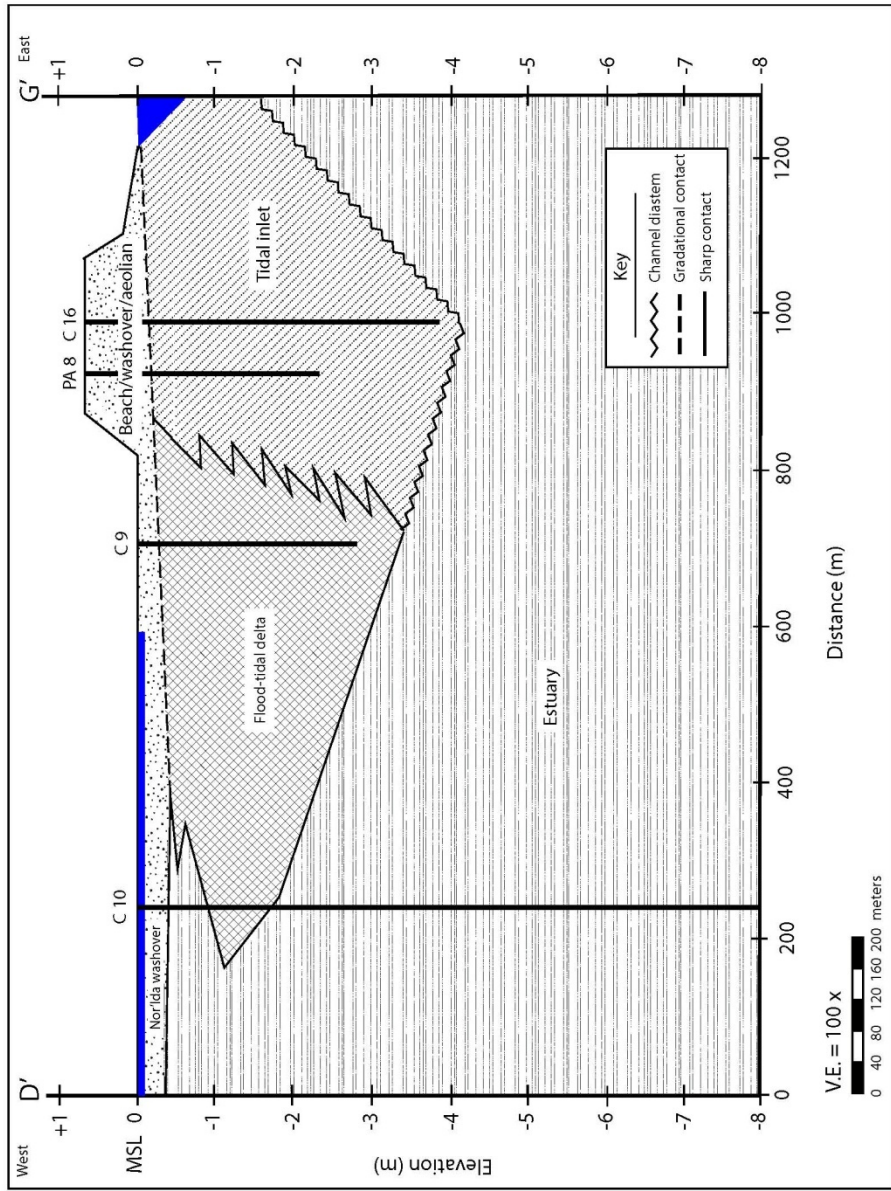
A



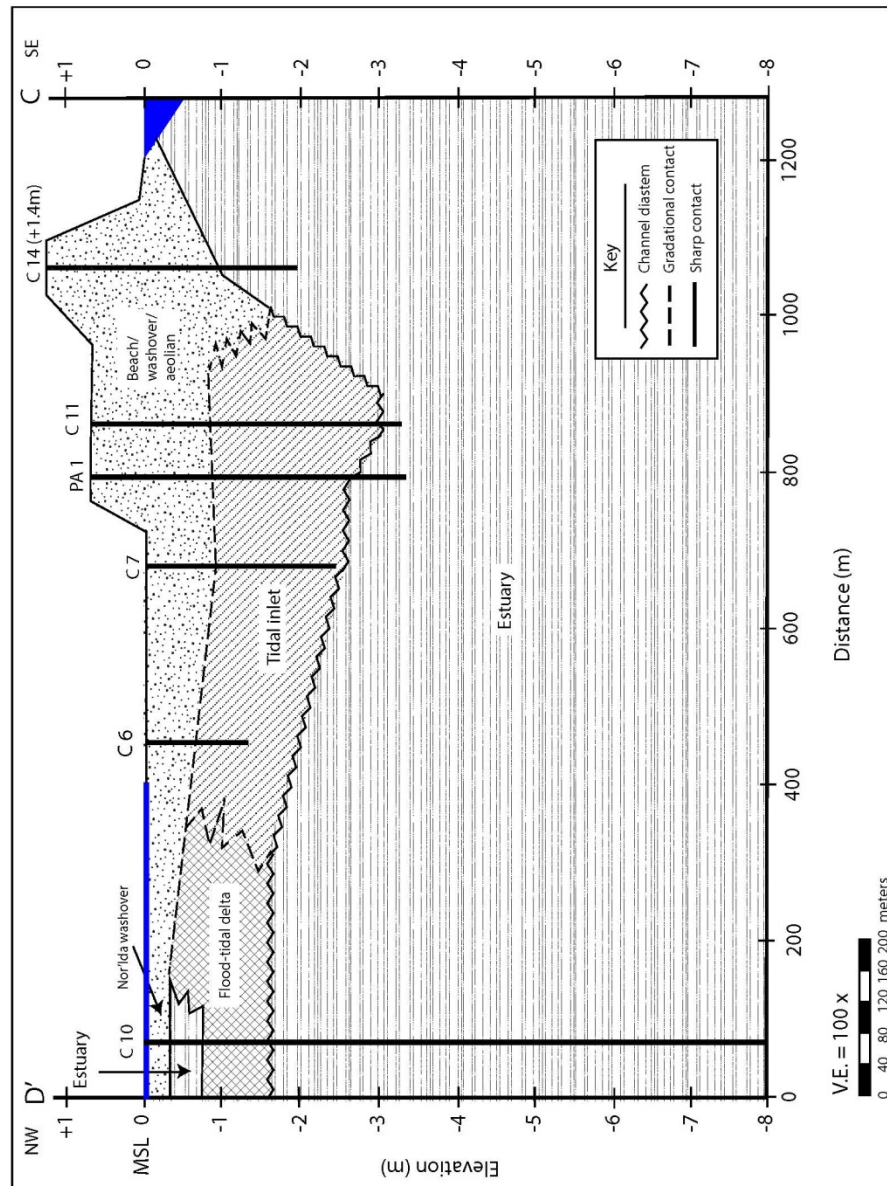
B



C



D



E

Figure 110: Dip geologic cross sections H – H’ (A), F – F’ (B), G – G’ (C), D’ – G’ (D) and D’ – C (E).

Cross sections F – F’, G – G’, and D’ – G’ (Fig. 110 B, C, and D, respectively) lie north of cross section H – H’. Cross section D’ – C (Fig. 110 E) extends from the back

bay, across H – H', and ends at the southernmost limit of the ephemeral tidal inlet. Estuarine deposits underlie all of these cross sections. They all show the tidal-inlet deposits on the ocean side of the barrier island and flood-tidal delta deposits going towards the back bay. Extending northwards from F – F' to D' – G', the flood-tidal delta deposits are thicker and closer to the backside of Cedar Island. All of these cross sections are capped with a thin layer of beach-washover-aeolian deposits from approximately -0.5 m to the surface and thin to sea-level at the ocean. Cross section D' – C extends to the southernmost limit of the ephemeral tidal inlet. Thus, the beach-washover-aeolian deposits thicken between C11 and C14 and extend from the surface to the estuarine deposits at -0.5 m below sea level.

Tidal Prism Calculations

The tidal prism for Cedar Island Inlet changed over time as the inlet migrated south and closed. The cross-sectional areas for the inlet locations that could be determined were calculated from the maximum inlet depth from the sediment cores and an estimate of the inlet throat width from Moyer (2007). The cross-sectional area of the inlet was estimated using the equation of the area under a parabola. The equation for the area under a parabola is $A = 2/3 (b * h)$, where b is the width of the inlet throat and h is the depth of the inlet. The core locations that were used are C15, C16, and PA3 from Cross section A – A' and C12 and C18 from Cross section A – B' (Figure 106). The Richardson-McBride-Seminack equation for the calculation of tidal prism based on cross-sectional area in metric units is from Richardson (2012):

$$P = (A/2.04 * 10^{-5})^{0.926}$$

Richardson (2012) calculated the tidal prism of Wachapreague Inlet to be $5.31 \times 10^7 \text{ m}^3$. This value was used to estimate the percentage of Wachapreague Inlet's tidal prism that each of the phases of the Cedar Island Inlet captured. The values and results for the various phases of Cedar Island inlet are found in Table 10. The tidal prism for Core C15 is after Cedar Island Inlet evolved from a breach to a tidal inlet and before it began to migrate. At this time, Cedar Island Inlet had captured about 12.4% of the tidal prism from Wachapreague Inlet. The tidal prism for Core 16 is the location of the deepest tidal-inlet deposits and represents the deepest that Cedar Island Inlet scoured into the southern spit. The inlet had captured 17.6% of Wachapreague Inlet's tidal prism.

Table 10: Tidal prism calculations for Cedar Island Inlet.

Core used	Inlet throat width, m	Inlet depth, m	Cross-section area, m^2	Tidal prism, $\times 10^6 \text{ m}^3$	Percent of Wachapreague Inlet tidal prism
C15	250	2.75	450	6.63	12.4%
C16	250	3.9	650	9.35	17.6%
PA3	54	2.25	81	1.34	2.5%
C18	54	2.8	100.8	1.64	3.1%
C12	54	2.0	72	1.20	2.3%
C2	60	5	200	3.11	5.8%

Cedar Island Inlet continued to migrate south, towards Wachapreague Inlet, and lost hydraulic efficiency to the larger and deeper Wachapreague Inlet. The three cores, C18, C12, and PA3 represent the location of Cedar Island Inlet's stalled migration where it finally lost all capacity to maintain any tidal prism and it closed. It became narrower and shallower. The tidal prism for Cedar Island Inlet became smaller relative to

Wachapreague Inlet's tidal prism capturing only 3.1% (C18), 2.5% (PA3), and 2.3% (C12) prior to closing completely.

In Cross-section D – D' (Figure 108), Core C2 has tidal inlet deposits below the flood-tidal delta deposits from the last Cedar Island Inlet and were interpreted to be from a previous ephemeral tidal inlet. The deposits extend down to 5 m below sea level and are on the south end of Cedar Island Inlet migration area. The inlet throat width was estimated to be 60 m, in accordance with the width measured by Moyer (2007). The tidal prism was larger than the latest Cedar Island Inlet's southern inlet-throat position and captured 5.8% of the Wachapreague Inlet's tidal prism.

DISCUSSION

The formation, migration, and infilling of barrier breaches influences the sediment budget and dynamic behavior of the barrier island system. Breaches are temporary features along barrier-island coastlines where overwash from storms often occurs. They allow water and sediment to be exchanged between the ocean and estuary. When a breach captures all or part of the tidal prism for a year or more, it becomes classified as a tidal inlet (see Seminack and McBride, 2015). When the tidal inlet opens and closes on an irregular basis in the same general location or zone and remains open for a year or more, it is classified as an ephemeral tidal inlet.

Southern Cedar Island has experienced breaches in the past and evidence exists that it continues to experience overwash and minor breaching. Three times over the past 60 years, a breach has opened through southern Cedar Island, captured part of the tidal prism from Wachapreague Inlet to the south and became a tidal inlet. Each time, the Cedar Island Inlet has migrated south, in the direction of net longshore sediment transport, eventually lost hydraulic efficiency and tidal prism to Wachapreague Inlet and subsequently closed, thus classified as an ephemeral tidal inlet.

During the investigation of Cedar Island Inlet, five depositional environments were established from facies descriptions and grain-size analysis. The estuary depositional environment underlies all of the study area. It is actively being exposed and

eroded on the shoreface as Cedar Island continues to migrate landward in response to sea-level rise and storm impacts. The estuarine deposits are characterized by light- to dark-gray mud that has horizontal laminations and shows bioturbation. Occasionally, estuarine bivalves are found with both shells together indicating that they died *in situ*. Overlying the estuarine depositional environment, except in the area of the ephemeral tidal inlet, is the beach-aeolian-overwash environment, which also overlies the two depositional environments of the tidal inlet. The sediments that make up this depositional environment are consist of tan to light-gray, very fine to medium sand with some large shell fragments and minor shell layers. Shells were found on the surface of southern Cedar Island where they are the result of overwash and wind deflation that concentrates them into shell layers. They are subsequently buried by overwash and aeolian processes, resulting in layers that may cause vibracore refusal, thus preventing deeper coring. Also found in the cores in this depositional environment are layers that are delineated by a concentration of heavy minerals grains.

The tidal-inlet depositional environment consists of sediments that were deposited within the tidal inlet as it opened, migrated, and closed. These sediments are mostly tan with some light- to medium-gray, fine to medium sand and have massive bedding with minor medium-gray laminations. They tend to be finely skewed and the mean grain-sizes either coarsen or fine upward. The tidal inlet succession is interspersed with shell layers and shell fragments with a shell lag at the base.

The flood tidal-delta depositional environment consists of sediments that were deposited in the estuary that is landward of Cedar Island Inlet. These sediments are light

to medium gray with some tan, fine to medium sand and silty sand with some small to medium shell fragments. Horizontal laminations with some bioturbation are present.

Compare and contrast ephemeral Cedar Island Inlet with other tidal inlets

Grain-size analyses were done for the sand samples and statistics (mean, sorting, skewness, and kurtosis) were calculated. After facies analysis was completed, the mean grain-size of each sample was classified as being in one of three depositional environments that contain sand: beach-washover-aeolian, tidal inlet, and flood tidal-delta. In previous studies, the trend of mean grain-size of tidal-inlet deposits tends to fine upwards, while the trend of the mean grain-size of beach-overwash-aeolian and flood tidal-delta deposits tends to coarsen upwards (Kumar & Sanders, 1974; Leatherman & Williams, 1983; Moslow & Tye, 1985; Hennessey & Zarillo, 1987; Nummedal & Swift, 1987; Seminack & Buynevich, 2013). As seen in Table 11, the trend with the largest percentage in each of the three depositional environments was coarsening upward. This is not consistent with the grain-size trends in tidal-inlet depositional environment (Kumar & Sanders, 1974; Moslow & Tye, 1985; Seminack & Buynevich, 2013).

Table 11: Upward trends in grain-size for depositional environments, Cedar Island Inlet.

Upward trend	Beach-washover-aeolian		Tidal inlet		Flood-tidal delta	
	Number	Percentage	Number	Percentage	Number	Percentage
Fining upward	3	16.7%	2	22.2%	3	33.3%
Coarsening upward	12	66.7%	5	55.6%	6	66.7%
No trend	3	16.7%	2	22.2%	0	0%

In the beach-washover-aeolian depositional environment, the fifteen vibracores with a coarsening-upward trend or no trend are located in the areas that are exposed to the processes that created these deposits. The three vibracores with a fining-upward trend are located on the northern fringe of the ephemeral inlet's flood-tidal delta.

In the tidal-inlet depositional environment, the seven vibracores with a coarsening-upward trend or no trend are found along the path of the ephemeral inlet as it migrated southward after opening. The two vibracores with fining-upward trends are in the last open position of the ephemeral inlet.

The grain-size trends for the flood-tidal delta depositional environment have six vibracores that exhibit coarsening-upward trends and one vibracore that shows a fining-upward trend. The six with a coarsening-upward trend are located on the northern end of the ephemeral inlet's flood-tidal delta. The one vibracore with a fining-upward trend is located on the southern, distal end of the ephemeral inlet's flood-tidal delta.

Additionally, Vibracore C2 shows a coarsening upward trend in all three of the depositional environments that were found in the core: beach-washover-aeolian, flood-tidal delta, and older tidal inlet. This indicates that is little or no difference in the grain-size trends between these depositional environments.

Therefore, some of the sediments deposited by Cedar Island Inlet, while it was open, would not be necessarily distinctive from beach-washover-aeolian deposits by using the mean grain-size analysis trends, though they are distinctive sedimentological facies. Therefore, the keys to distinguishing depositional environments in ephemeral

tidal-inlet deposits from beach-washover-aeolian deposits are the relative depth of the deposits and the facies descriptions.

The deposits from an ephemeral inlet will most likely not be preserved in the stratigraphic record; however, the lowermost unit of tidal inlet succession may be preserved if it lies below the shoreface ravinement surface (see Moslow and Tye, 1985). If sea level continues to rise, most of the ephemeral inlet's sediments will be eroded away like the uppermost part of the underlying estuarine unit is experiencing currently as Cedar Island continues to migrate landward. If sea level drops by more than a few meters, the deposits of the ephemeral inlet will be eroded away by overwash processes associated with hurricanes and northeasters that strike the area. These sediments will be dispersed and become part of deposits elsewhere.

Cedar Island Inlet was open three times from four to nine years in the past 60 years. Its opening is not a cyclic event but rather an episodic event that occurs when strong storms impact the area. The breach that Greenwood and Keay (1979) studied was open for six years. They observed that nine breaches occurred in the same barrier island system over the previous 45 years with an average period between them of five years. Although some of these breaches occur on the same barrier island, they did not state that any of them occurred in the same location as a previous breach. A wave-dominated tidal inlet rapidly migrates laterally over a limited shoreline length. Thus, it may erode previous inlet deposits and may be ephemeral in terms of both the time and stratigraphy.

Spikes in water-flow velocity

Seven vibracores are characterized by spikes in water-flow velocities (C7, C11, C12, C15, C16, C17, and C18) as reflected in the tidal-inlet deposits. These energy spikes, which show an initial trend of coarsening upward followed by a fining upward trend, are the consequence of higher water-flow velocities that result in the deposition of slightly coarser sediment. When the higher energy subsides, slightly finer sediment is deposited. It is hypothesized that these higher flow velocities are most likely associated with larger tidal prisms caused by storms, spring high tides, or perigean spring high tides.

Eight-stage depositional model of an ephemeral tidal inlet

This investigation led to the construction of an eight-stage model of an ephemeral, wave-dominated tidal inlet during which a breach opens, typically during a storm, becomes a tidal inlet, migrates in the direction of net longshore sediment transport, begins to lose hydraulic efficiency to another tidal inlet, and eventually closes. These eight stages are:

A storm opens a breach across the barrier island that is oriented normal or near normal to the shoreline (Figure 111). The storms that have opened Cedar Island Inlet have been northeasters and have occurred over a four to five day period (Moyer, 2007). The last breach (1998-2007) was opened by two northeasters that occurred within six days of each other with each lasting three to four days (Moyer, 2007). From 1852 to 2007, Richardson (2012) documented a long-term retreat rate in the breach area of -6.9 m/yr.

The breach captures enough tidal prism from the estuarine waters to become a tidal inlet (Figure 112). Since the last Cedar Island Inlet maintained an opening with a tidal prism as low as $1.2 \times 10^6 \text{ m}^3$, the breach must capture at least that amount to become a tidal inlet and remain open. The capture of tidal prism probably occurs over hours or days either during or shortly after the storm impact. Otherwise, the breach will close because it does not capture and maintain enough tidal prism from Wachapreague Inlet. Figure 113 is an aerial photograph of Cedar Island Inlet taken in 1994 after it reached Stage 2.

A flood-tidal delta forms within a few weeks to a month after opening (Figure 114). This stage shows an increase in captured tidal prism. Cedar Island Inlet has increased to a depth of over 2 m and has captured about 12% of Wachapreague Inlet's tidal prism. The flood-tidal delta increases in size as the inlet throat widens and the inlet channel deepens. The area of the flood tidal delta is approximately $150,000 \text{ m}^2$ with an average thickness of 1.5 m for an estimated sand volume of $225,000 \text{ m}^3$. Figure 115 shows Cedar Island Inlet after the formation of a flood-tidal delta (Stage 3).

The tidal inlet begins to migrate laterally at about 40 m/yr in the direction of net longshore sediment transport, which is southerly (Figure 116). Within a couple of months of the initial breach, Cedar Island Inlet started to shoal on the updrift side (Moyer, 2007). The inlet throat widens to 250 m and the inlet channel deepens to 3.9 m, which results in Cedar Island Inlet capturing almost 18% of Wachapreague Inlet's tidal prism.

The tidal-inlet channel begins to rotate counterclockwise with the landward end of the inlet channel moving more rapidly in the direction of net longshore sediment

transport than the seaward end of the inlet channel (Figure 117). The resulting channel orientation is shore-oblique with an angle of 47 degrees to the adjacent shoreline (southwest). Cedar Island Inlet began to rotate counterclockwise after the passage of hurricane Floyd in September 1999. This was confirmed by Moyer (2007), six months after Floyd's passage. Moyer (2007) found that the inlet channel had lengthened as well. The inlet starts out as a linear channel then evolves into a curvilinear channel as it shoals and begins to seal shut from longshore sediment transport. Figure 118 shows Cedar Island Inlet has rotated counterclockwise and is in Stage 6.

The tidal inlet continues to migrate laterally at 75 m/yr to the south and concurrently loses hydraulic efficiency because of the lengthening of the inlet channel (increased frictional drag), which results in a decrease in tidal prism and a sinuous channel (Figure 119). Figure 120 shows Cedar Island Inlet in Stage 6.

Since inlet closure in early 2007, the migration direction of the outer barrier-island shoreline along the breach zone reverses and advances (i.e., seaward) at an average rate of 0.7 m/yr but with some local advance rates as high as 30 m/yr (Richardson, 2012) as documented in Figure 121 and 122. These atypical short-term advance rates reflect shoreline recovery in response to inlet closure where net longshore sediment transport fills in the shoreline indentation.

In Stage 8, the barrier island returns to stasis until another storm opens a breach (Figure 123). Figure 124 shows Cedar Island Inlet

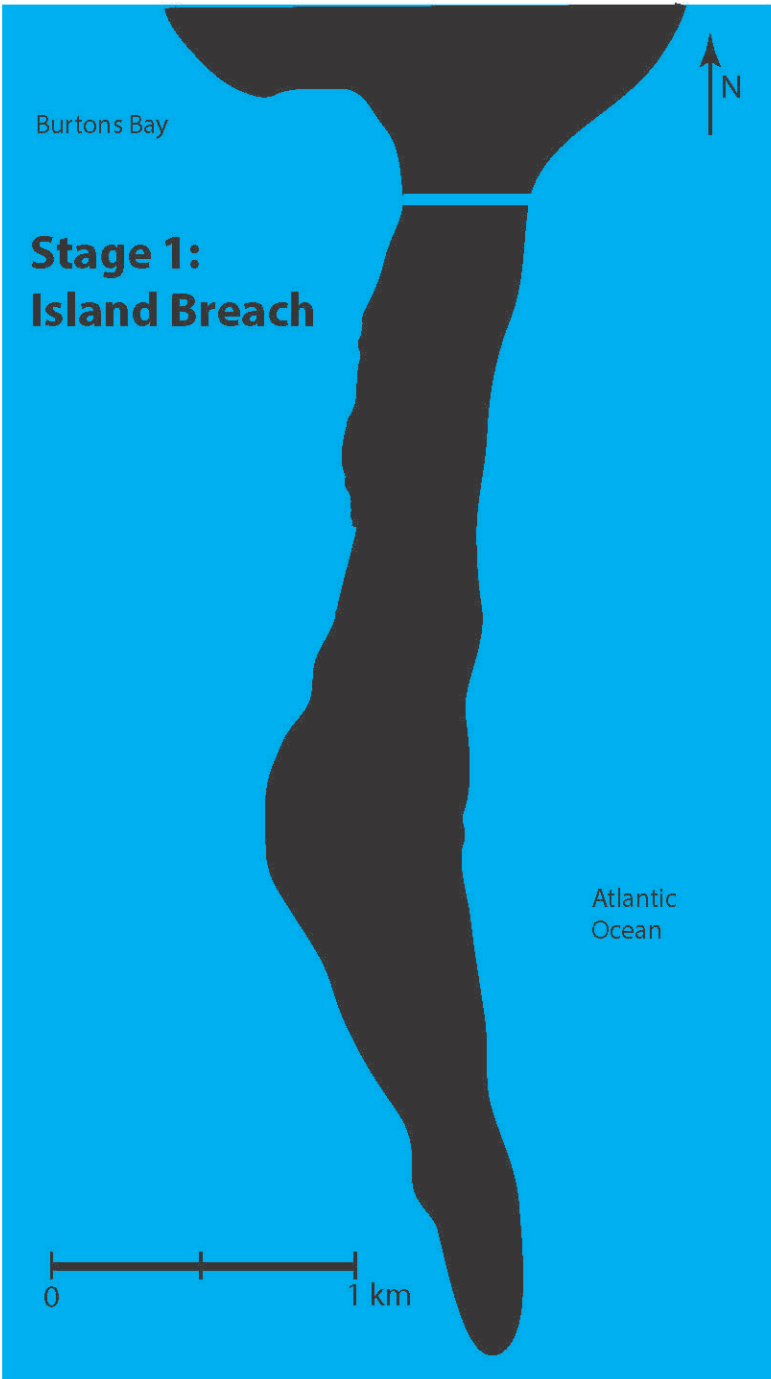


Figure 111: Stage 1 - Island Breach.

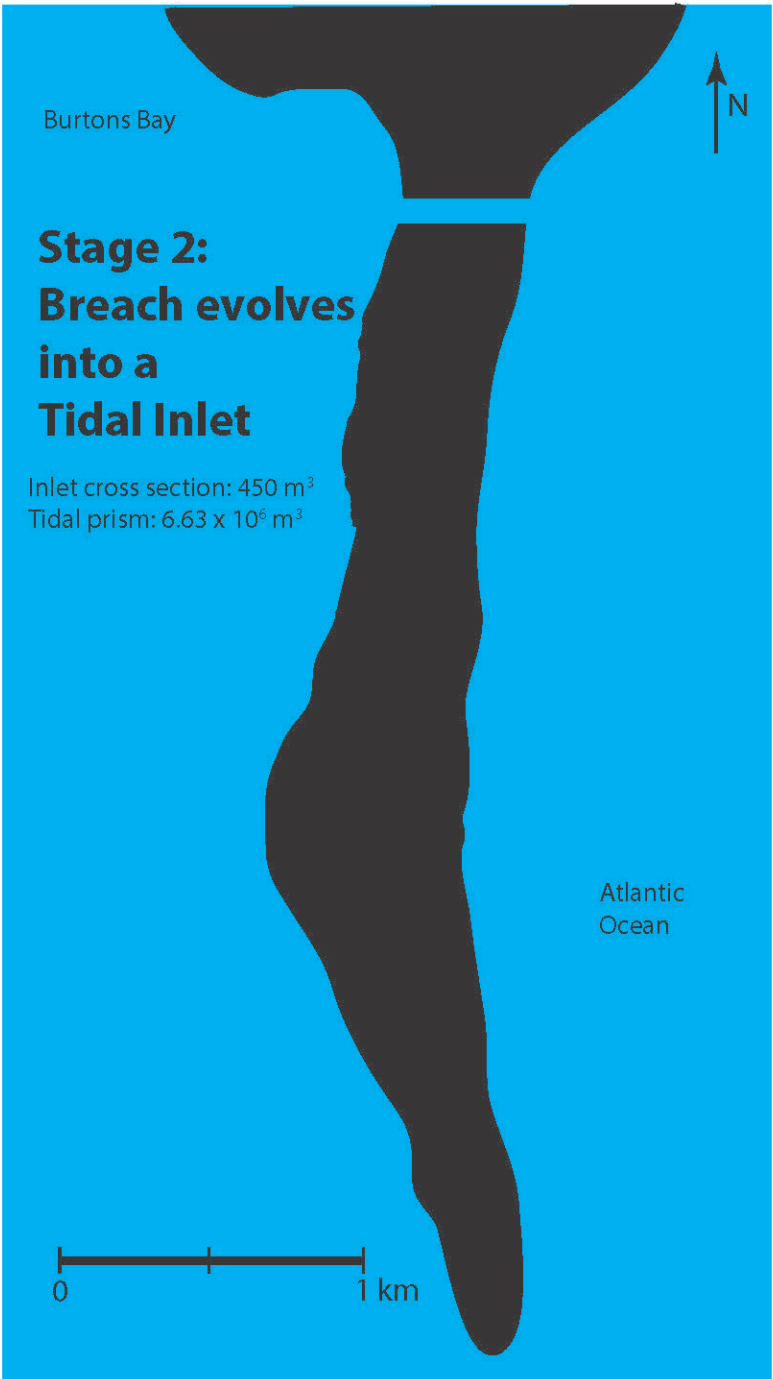


Figure 112: Stage 2 - Breach evolving to wave-dominated tidal inlet.



Figure 113: Aerial photograph of Cedar Island Inlet at Stage 2, taken March 19, 1994 (Google Earth, 2015b).

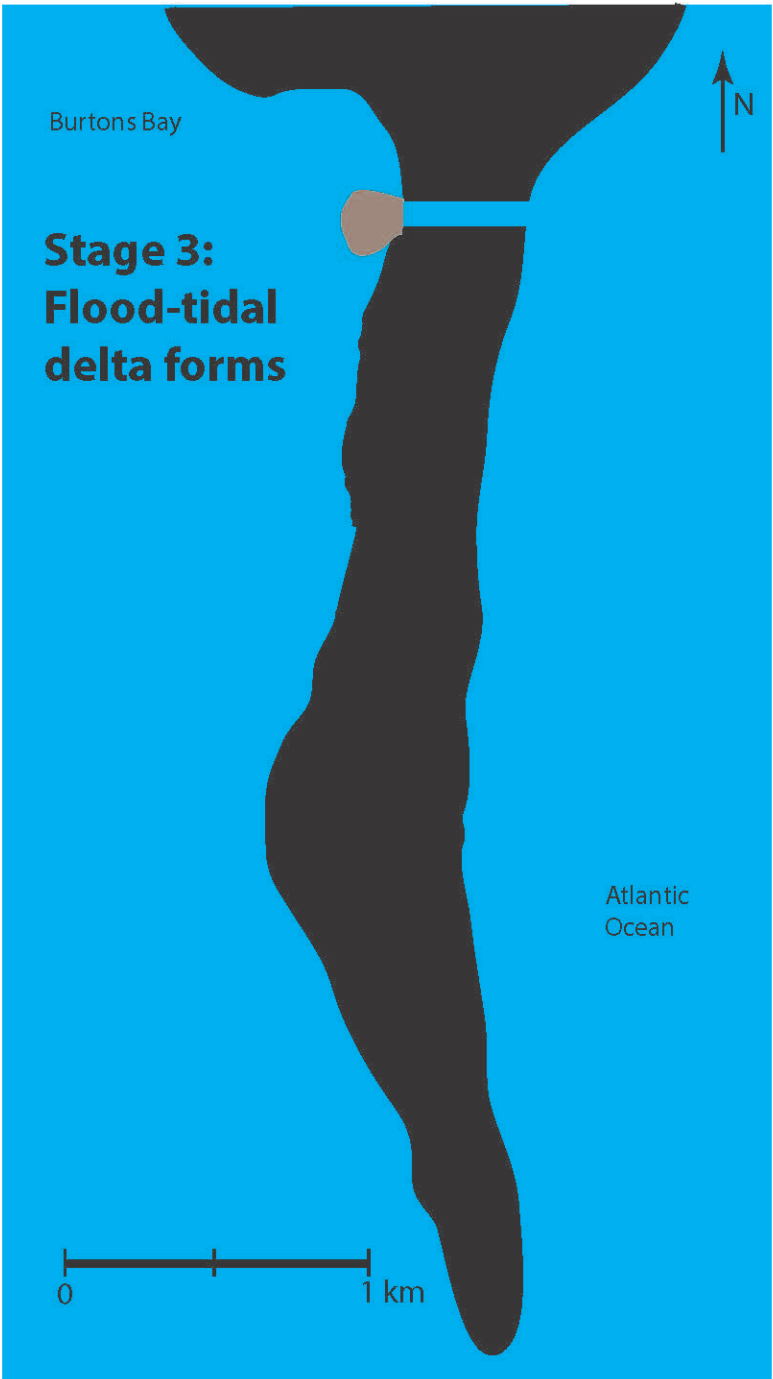


Figure 114: Stage 3 - Flood-tidal delta forms.

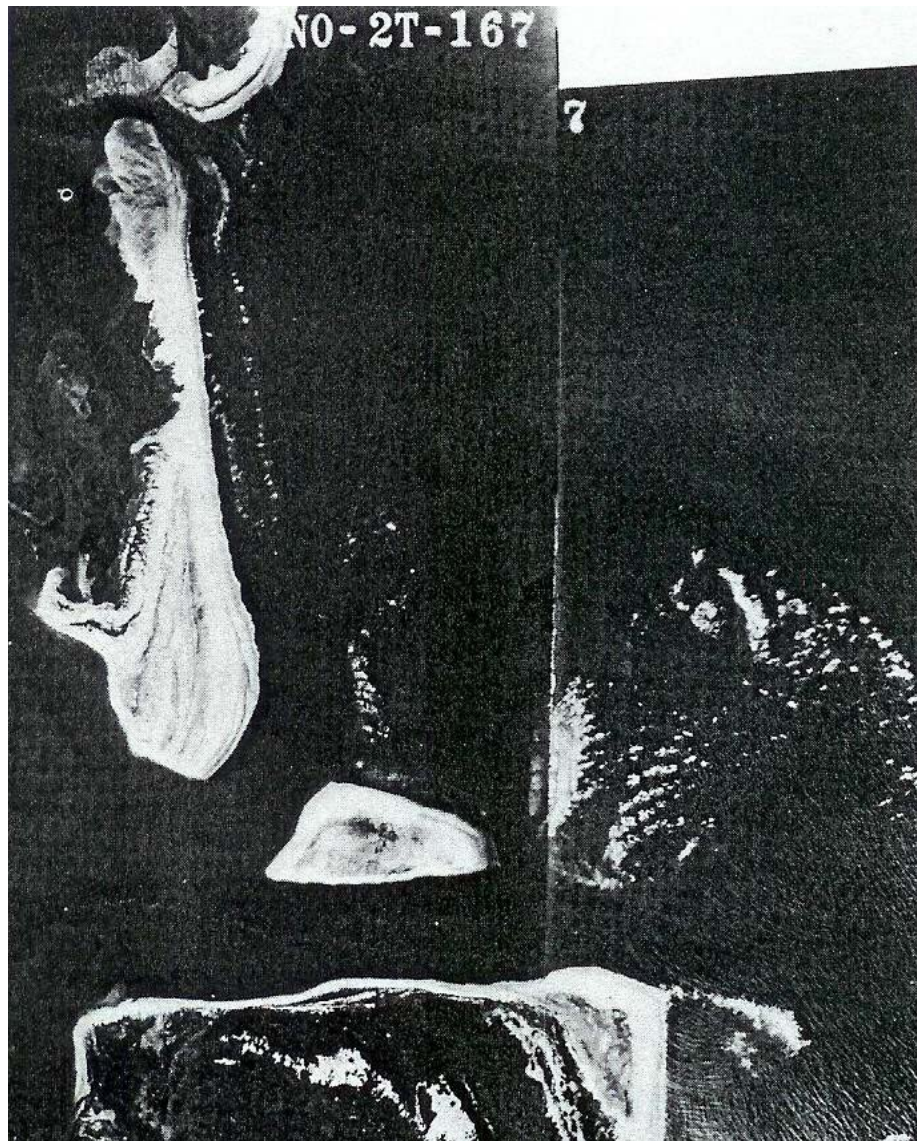


Figure 115: NASA photograph of Cedar Island Inlet in 1957 showing formation of a flood-tidal delta (Byrne et al. 1975).

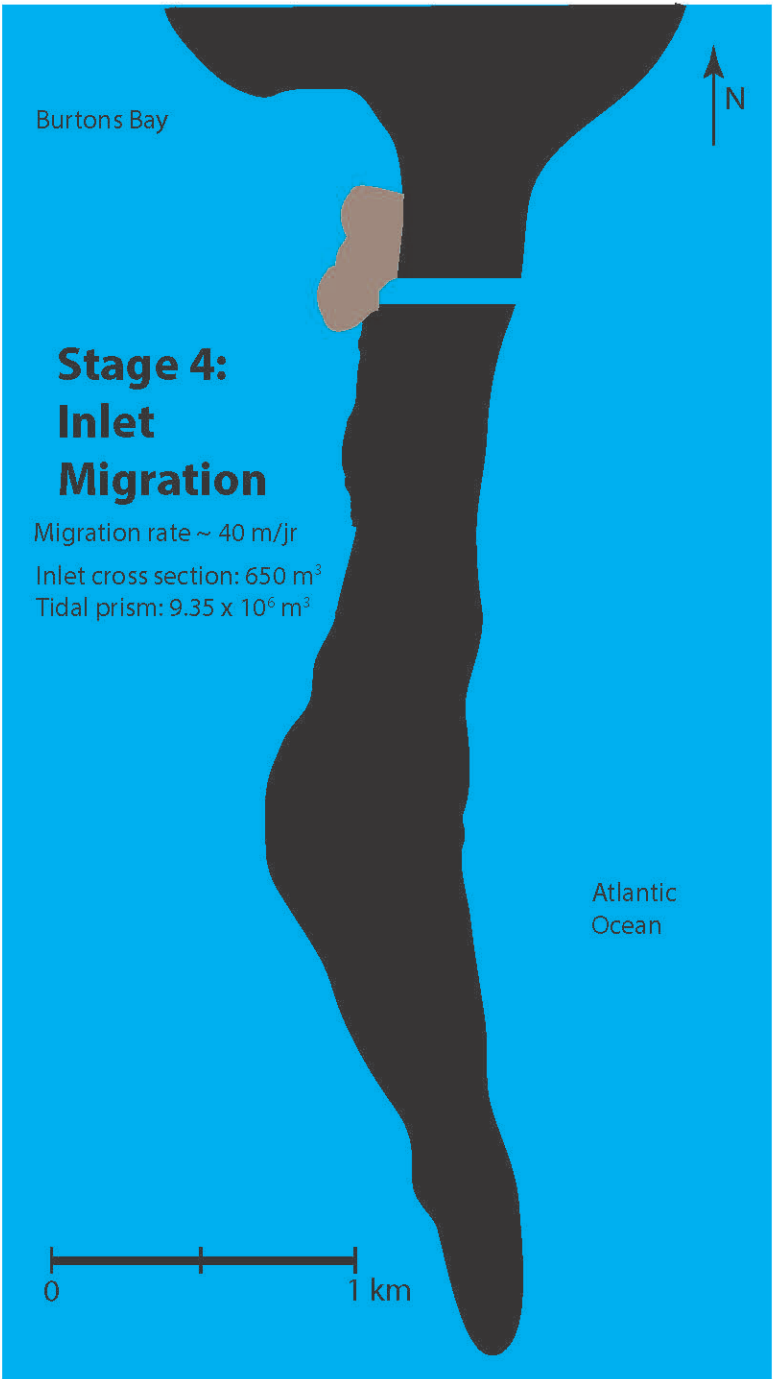


Figure 116: Stage 4 - Inlet migration.

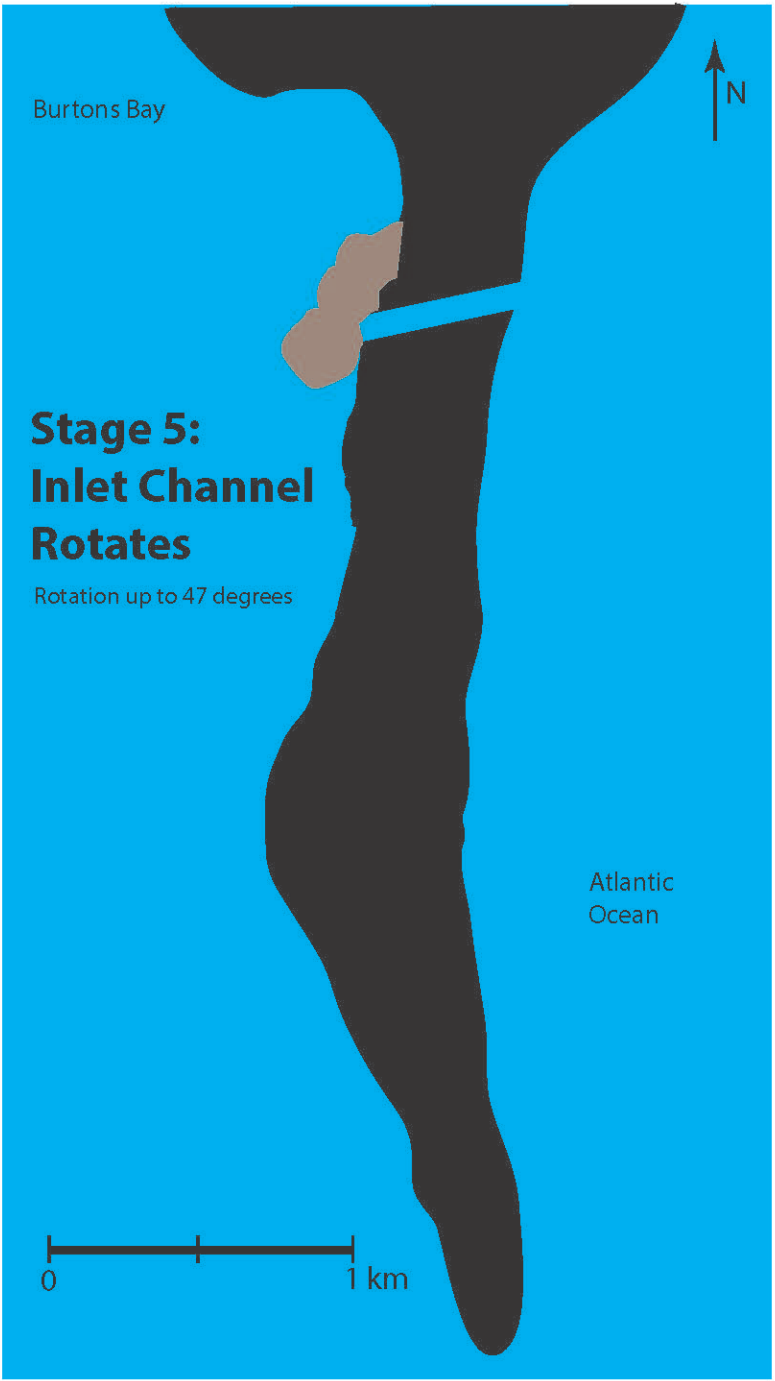


Figure 117: Stage 5 - Inlet channel rotates.

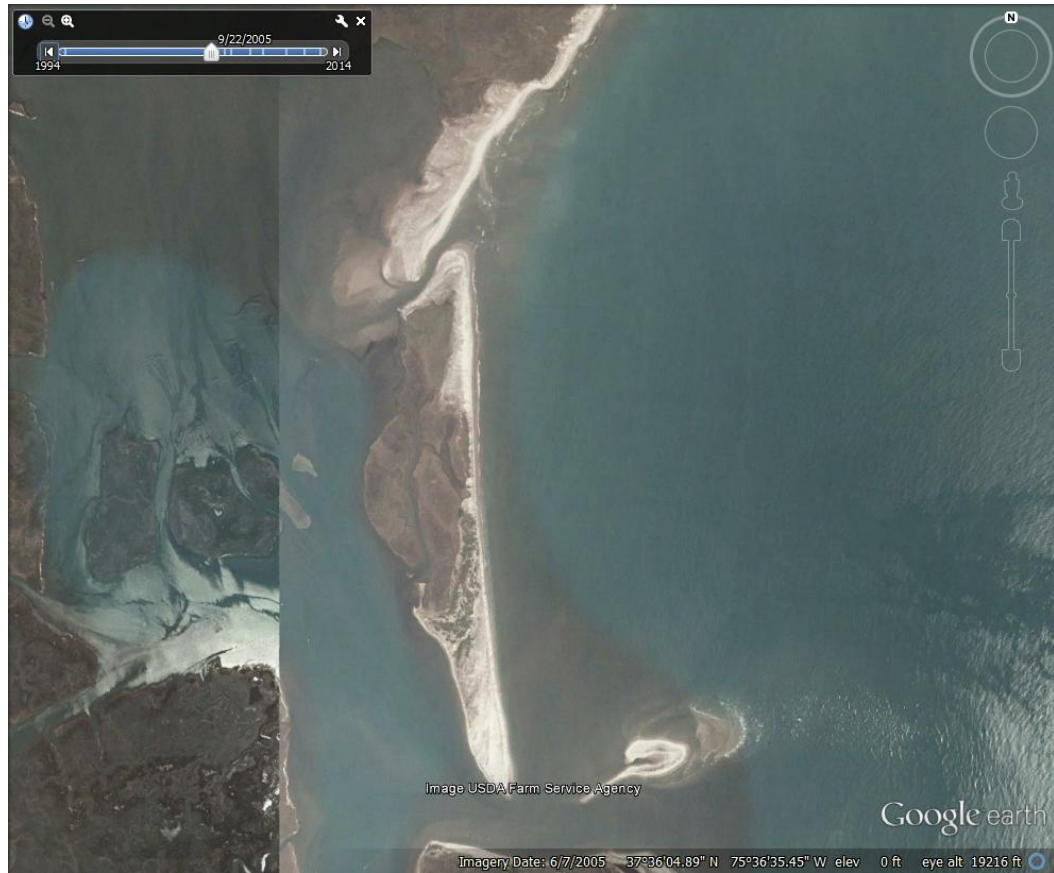


Figure 118: Aerial photograph of Cedar Island Inlet taken on September 22, 2005 showing the tidal-inlet channel counterclockwise rotation, Stage 5 (Google Earth, 2015b).

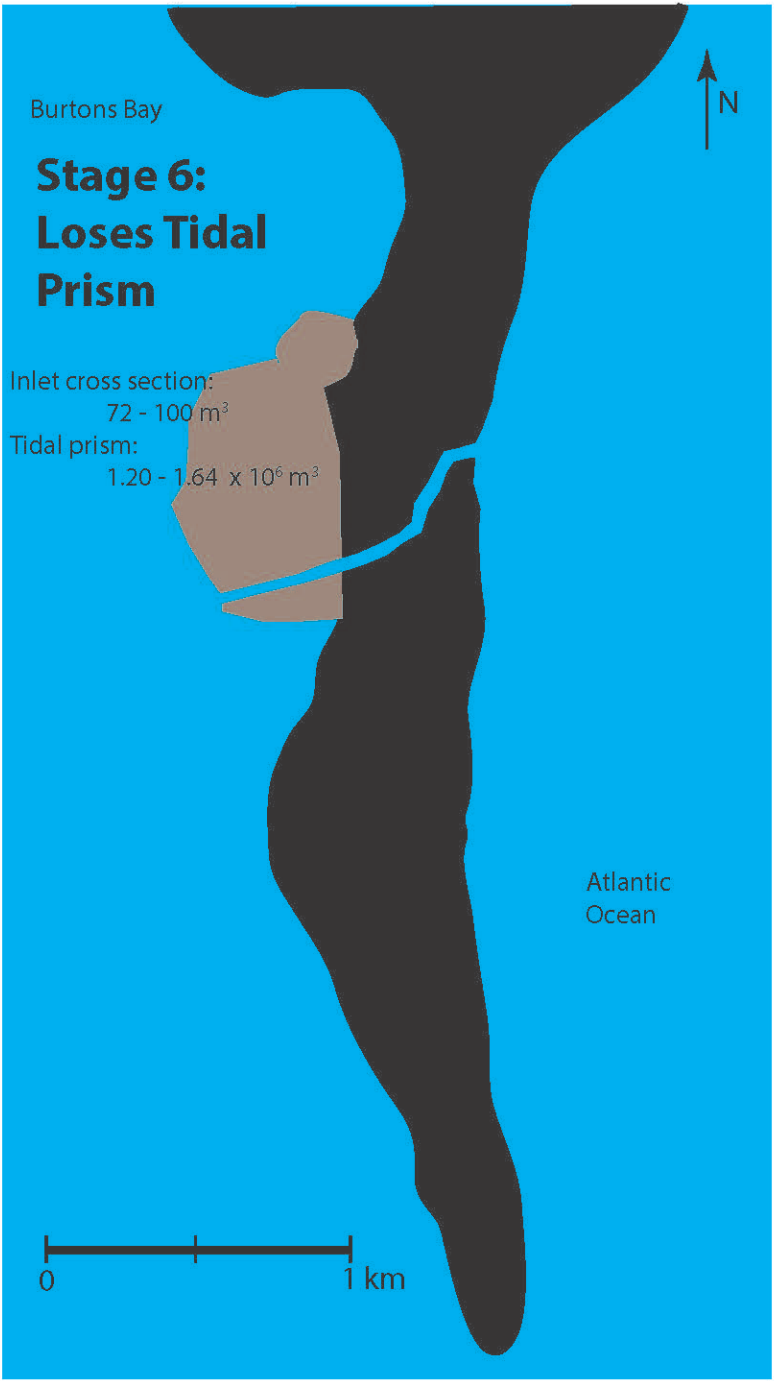


Figure 119: Stage 6 - Loses tidal prism.

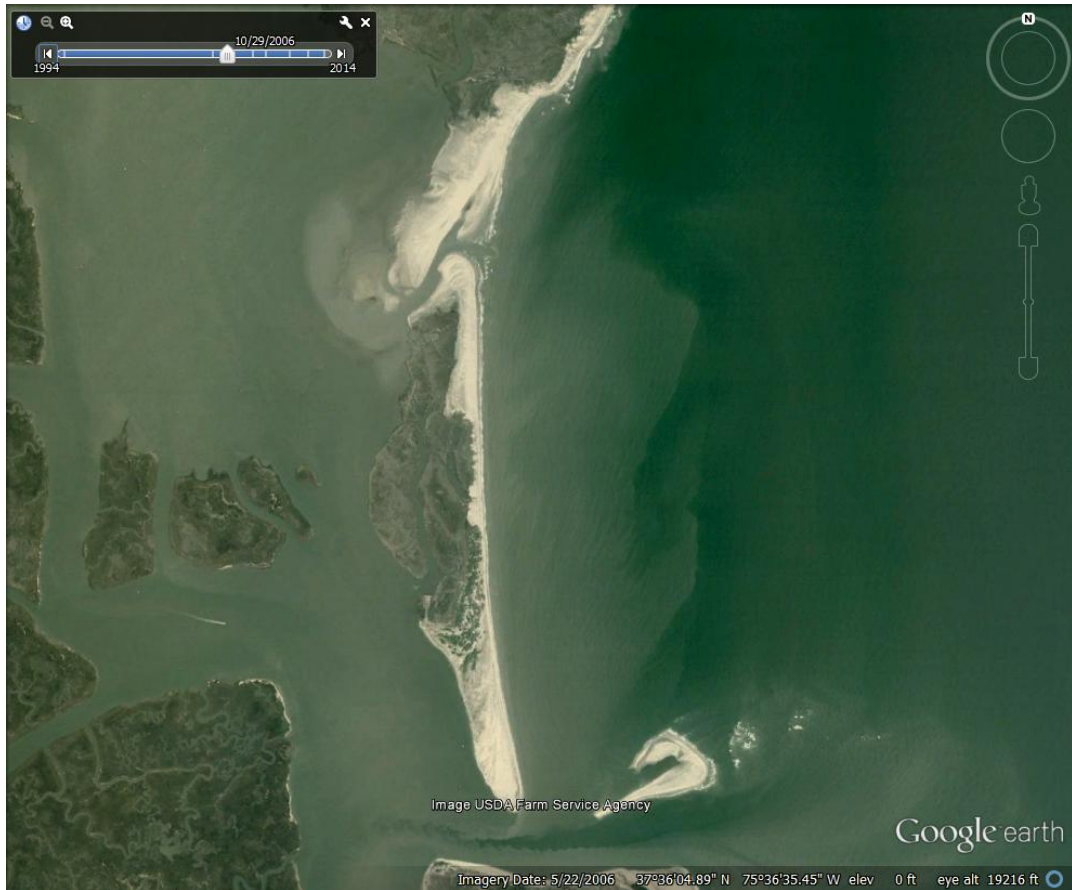


Figure 120: Aerial photograph of Cedar Island Inlet taken on October 26, 2006 in Stage 6 (Google Earth, 2015b).

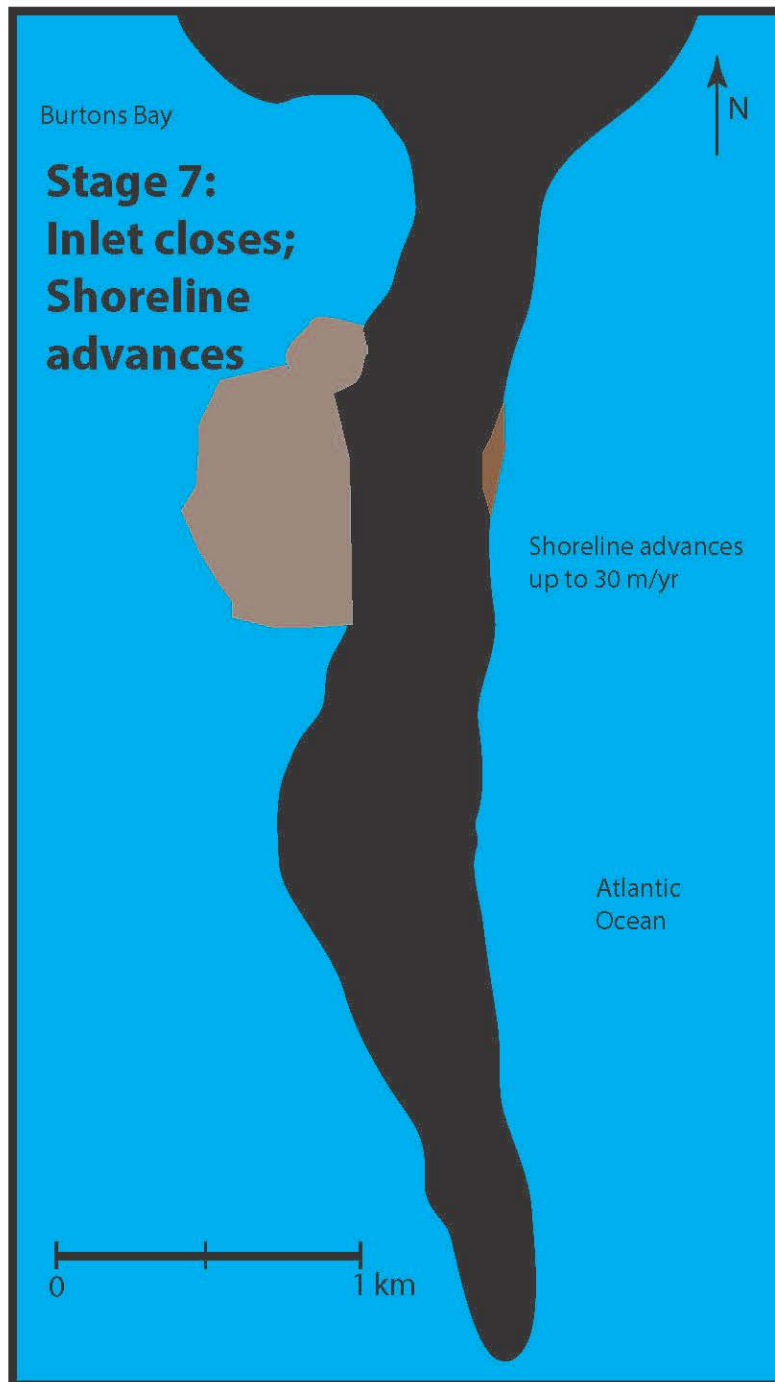


Figure 121: Stage 7 – After the inlet closes, shoreline advances along inlet breach zone.

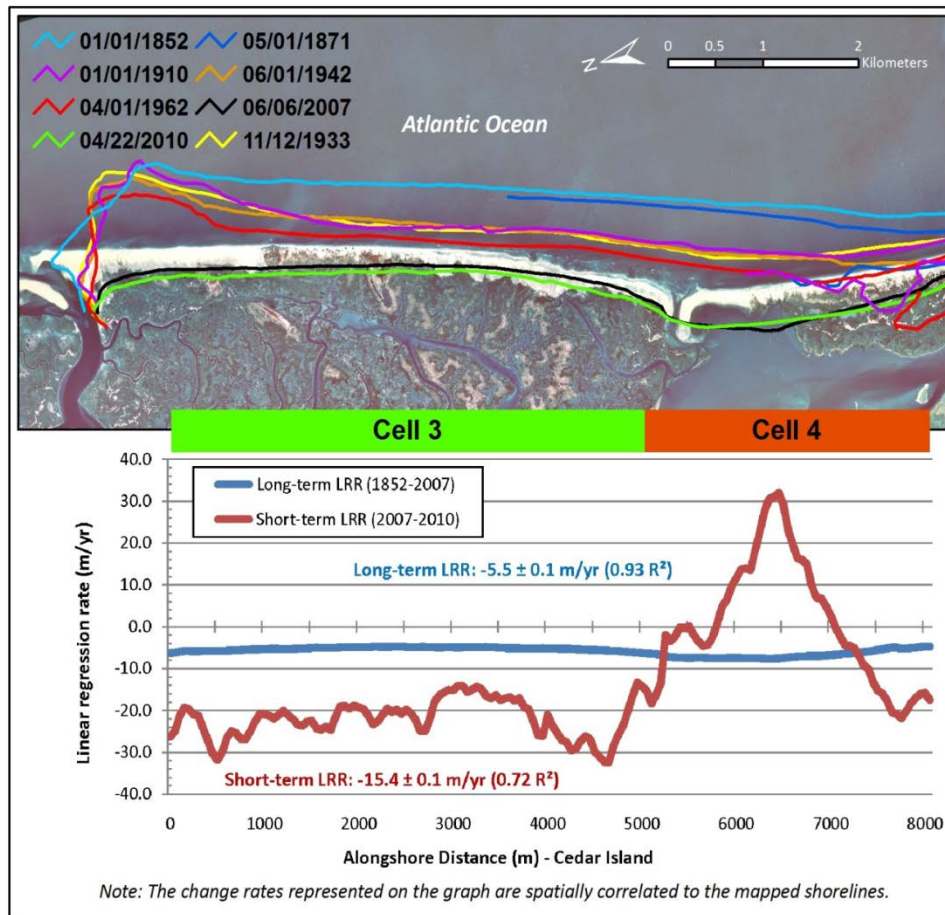


Figure 122: Long-term (1852 – 2007) and short-term (2007 – 2010) linear regression rates (LRR) of shoreline change of Cedar Island. Cell 4 is located in area of Cedar Island Inlet. The long-term rate is in blue and the short-term rate is in red (Richardson, 2012).

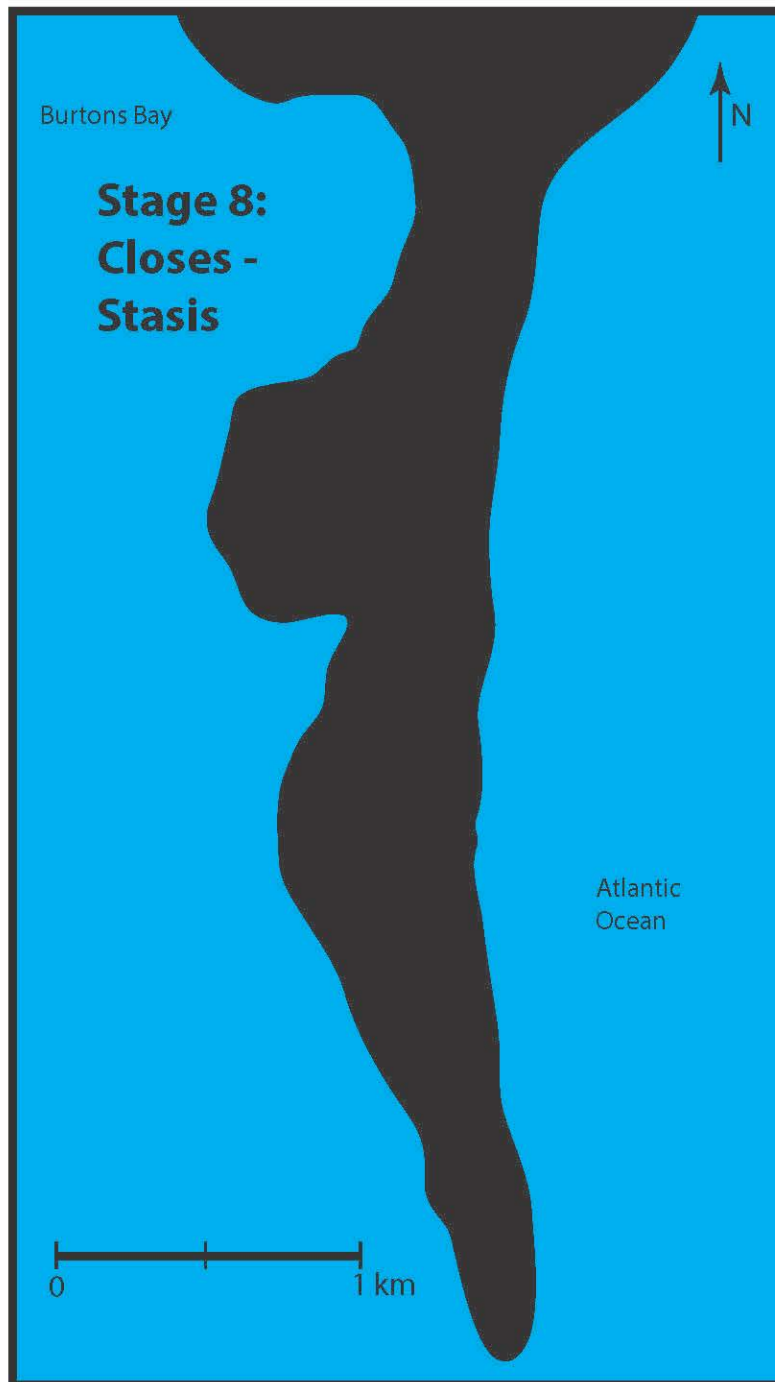


Figure 123: Stage 8 – Closes – Stasis.



Figure 124: Oblique aerial photograph showing the Cedar Island Inlet in Stage 8 (Randolph A. McBride, 2011).

CONCLUSIONS

This study of the stratigraphy and morphodynamics of the Cedar Island Inlet has 1) tested the hypothesis that Cedar Island Inlet has a similar or dissimilar stratigraphic signature to tidal inlets in recent or ancient tidal inlet deposits, 2) tested the hypothesis that the amount of the tidal prism captured remains the same or changes over the life of the ephemeral inlet, 3) documented the stratigraphic architecture of an ephemeral tidal inlet, and 4) formulated the stages of a model for the evolution of an ephemeral tidal inlet. Several additional conclusions were reached from this study and presented below.

Cedar Island Inlet stratigraphic signature. Although Cedar Island Inlet was a tidal inlet, the stratigraphy of some of its deposits is dissimilar to the stratigraphic signature of recent and ancient tidal-inlet deposits, which tend to fine upward. Grain-size analyses show that the tidal inlet, flood tidal-delta, and beach-overwash-aeolian environments can have mean grain-size trends that mostly coarsen upward and caution must be used to distinguish among these different depositional environments. However, they can be separated by visually logging the cores.

Tidal prism amounts over the life of Cedar Island Inlet. During the last opening of the Cedar Island Inlet, it captured a varying amount of Wachapreague Inlet's tidal prism, from 18% at maximum to a minimum of 3% just before closing. The amount of tidal prism that the ephemeral tidal inlet captured increased from its opening until the inlet

migrated southward when it reached the maximum amount that it captured (18%). As it continued to migrate south and rotated, it got closer to the larger Wachapreague Inlet and it began to lose tidal prism. As Cedar Island Inlet migrated to its southernmost location, it began to lose hydraulic efficiency and tidal prism as the inlet channel lengthened and it filled up with sediment from southerly net longshore sediment transport. Prior to Cedar Island Inlet closing, it was only able to maintain a small amount of the tidal prism (6% – 3%). Tidal prism then quickly decreased to zero as Cedar Island Inlet closed.

Stratigraphic architecture. The stratigraphic architecture of Cedar Island Inlet was documented. Fifteen different facies were identified, which included very fine to medium sand, shell layers, sand with silt and clay interlayers, and mud. These facies were grouped into four depositional environments: beach-overwash-aeolian, tidal inlet, flood tidal-delta, and estuary, which allowed construction of strike and dip geologic cross sections for interpretation of Cedar Island Inlet's migration and stratigraphic evolution.

Stages of evolution of an ephemeral tidal inlet. Three former, ephemeral, wave-dominated tidal inlets were investigated to determine the evolutionary stages of Cedar Island Inlet. From this, eight stages were identified that an ephemeral tidal inlet experiences from inlet opening to closing. The inlet begins as a breach which captures enough tidal prism to remain open and evolves into a tidal inlet. Then the inlet migrates in the direction of net longshore sediment transport. During the migration, the inlet begins to rotate. Finally, the inlet experiences hydraulic inefficiency because of the channel lengthening and its width reducing. As a result, tidal prism is lost to the larger

tidal inlet, Wachapreague Inlet, and ultimately the inlet closes. An eight-stage model is presented that synthesizes the morphodynamic evolution of Cedar Island Inlet.

Stratigraphic evidence of multiple tidal inlets. When the Cedar Island tidal-inlet channel first opens, it remains in place prior to migrating and scours the previous tidal-inlet deposits. In the latest opening, Cedar Island Inlet may have scoured to the estuary deposits below. As the inlet migrated to the south, it probably reworked most or possibly all of the deposits from the previous two inlet openings, thus removing any evidence of them. As Cedar Island Inlet migrated south, it began to slow its migration rate and lose tidal prism and hydraulic efficiency. This allowed for previous inlet(s) deposits to remain in place as evidenced by Vibracore C2 and the older flood-tidal delta deposits identified in Vibracore C1.

Sorting vs skewness. An indirect correlation exists between sorting and skewness, such that as the sediments become better sorted, they tend to become more nearly symmetrical in skewness, going from negative skewness. For the tidal-inlet fill, sorting improves upward and skewness tends to go from negative to positive upward.

Surface sediment distribution. The mean of the grain sizes for surface sediments is predominately fine sand (83%) and is found in the surface sediments in the inlet throat and flood-tidal delta. Coarser sediments are found along the beach and surf zone where winnowing and some deflation transport finer-grained sediments away from the beach. Sorting of surface sediments are either well sorted or moderately well sorted with a combined percentage of 91%. The skewness of these sediments are mostly nearly symmetrical (64%) while 20% exhibit positive skewness and 16% negative skewness.

Stratigraphic longevity of sediments. The sediments deposited by Cedar Island Inlet will most likely not be preserved in the stratigraphic record. If sea level continues to rise, most of Cedar Island Inlet's sediments will be eroded away.

Upward grain-size trends in cores. The majority of the vertical grain-size trends are coarsening upward. Therefore, most of the sediments from the tidal inlet and flood-tidal delta which were deposited by Cedar Island Inlet are not distinctive from those deposited in the beach-washover-aeolian deposits. The keys to distinguishing the depositional environments deposited by Cedar Island Inlet from those of the beach-overwash-aeolian environment are relative depth and facies description.

Stratigraphic correlation of water-flow spikes. No stratigraphic correlation exists between the energy spikes in the tidal-inlet deposits of the cores in this study. These spikes are the result of higher water flow velocities in the tidal inlet channel and are most likely produced by storms (northeasters or hurricanes), spring high tides, or perigean spring high tides.

Future research

Future research for the Cedar Island Inlet should include further observation of the breach area and monitoring for any island breach that remains open for longer than several weeks. In addition, more vibracoring should be pursued to further delineate the tidal-inlet area and better document the characteristics of the northern and southern boundaries of the area. Expansion of this research should include 1) locating other recent breaches along barrier-island systems that can be studied, 2) investigating new vibracore or coring technologies that can recover oriented cores to determine the direction of

laminations, and 3) investigate vibracore techniques that can penetrate the shell layers to get down to the estuary layers in order to recover the entire tidal-inlet fill deposit.

Additional statistical and stratigraphic analysis of the grain-size data will yield further results.

APPENDIX

Appendix A – Vibracore and pulse auger description sheets

VIBRACORE DESCRIPTION SHEET

CORE ID: CIB100917-C DATE COLLECTED: 9/17/10 DESCRIBED BY: HANLEY
 ELEVATION: ~ MSL COMPACTION: 0.08m DATE DESCRIBED: 6/26/12
 CORE LENGTH: 5.58m LAT/LONG: 37° 36' 21.462" N 75° 37' 21.285" W
 TOTAL DEPTH: 5.66m LOCATION: FLOOD TIDAL DELTA

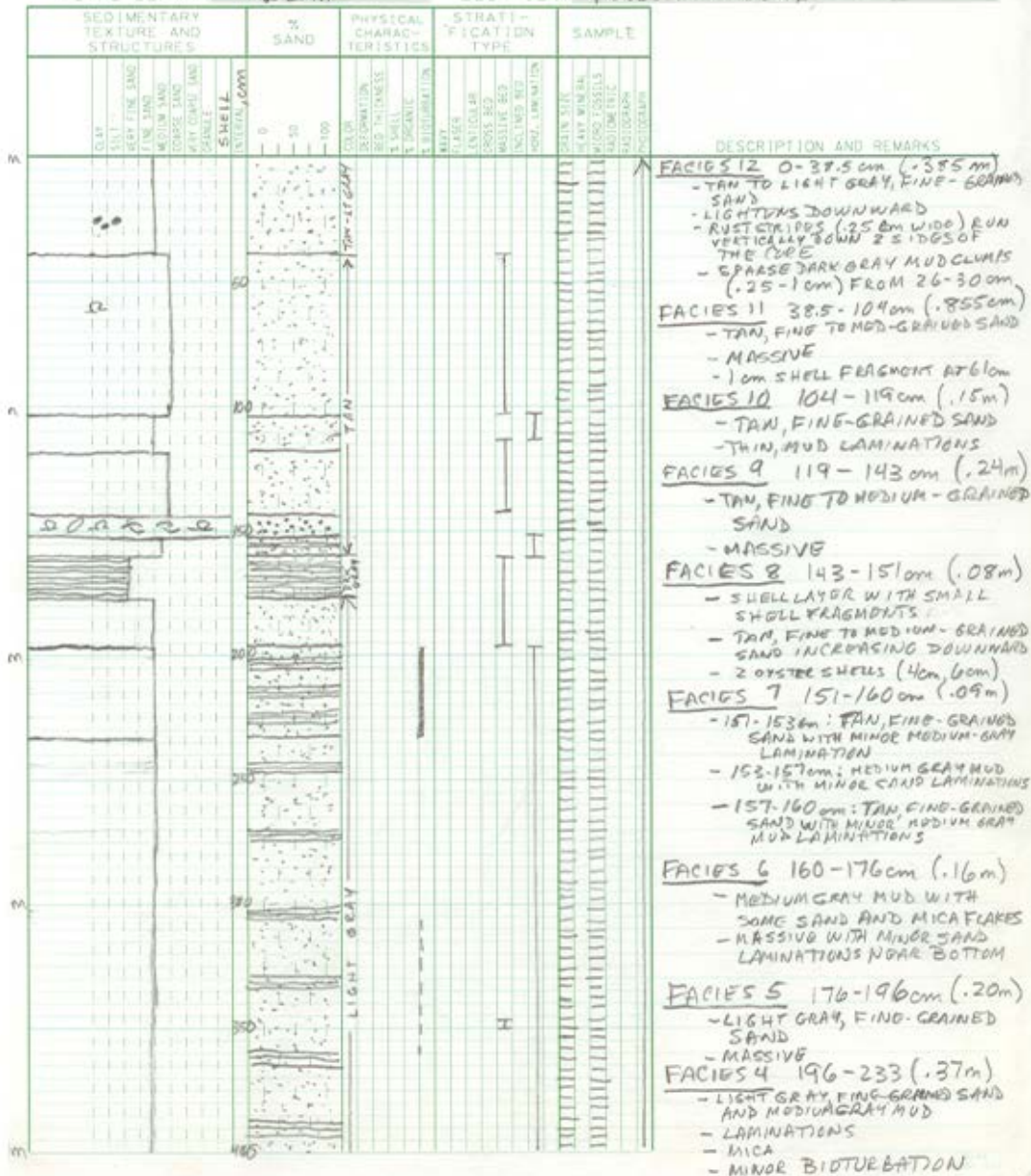
DEPTH (m)	SEDIMENTARY TEXTURE AND STRUCTURES					% SAND	PHYSICAL CHARACTERISTICS					STRATIFICATION TYPE	SAMPLE	DESCRIPTION AND REMARKS			
	CLAY	SILT	VERY FINE SAND	FINE SAND	MEDIUM SAND		COARSE SAND	VERY COARSE SAND	GRAVEL	COLOR	DEFORMATION				MOISTURE	SHRINKAGE	PLASTICITY
0																	
0.5																	
1.0																	
1.5																	
2.0																	
2.5																	
3.0																	
3.5																	
4.0																	
4.5																	
5.0																	
5.5																	
5.66																	

Vibracore C2

SHEET 1

VIBRACORE DESCRIPTION SHEET

CORE ID: CIB100917-C2 DATE COLLECTED: 9/17/10 DESCRIBED BY: HANLEY
 ELEVATION: ~MSL COMPACTION: 0.37m DATE DESCRIBED: 7/27/12
 CORE LENGTH: 5.5m LAT/LONG: 37°36'29.050"N 75°37'15.925"W
 TOTAL DEPTH: 5.52m LOCATION: FLOOD TIDAL DELTA



SHEET 2

VIBRACORE DESCRIPTION SHEET

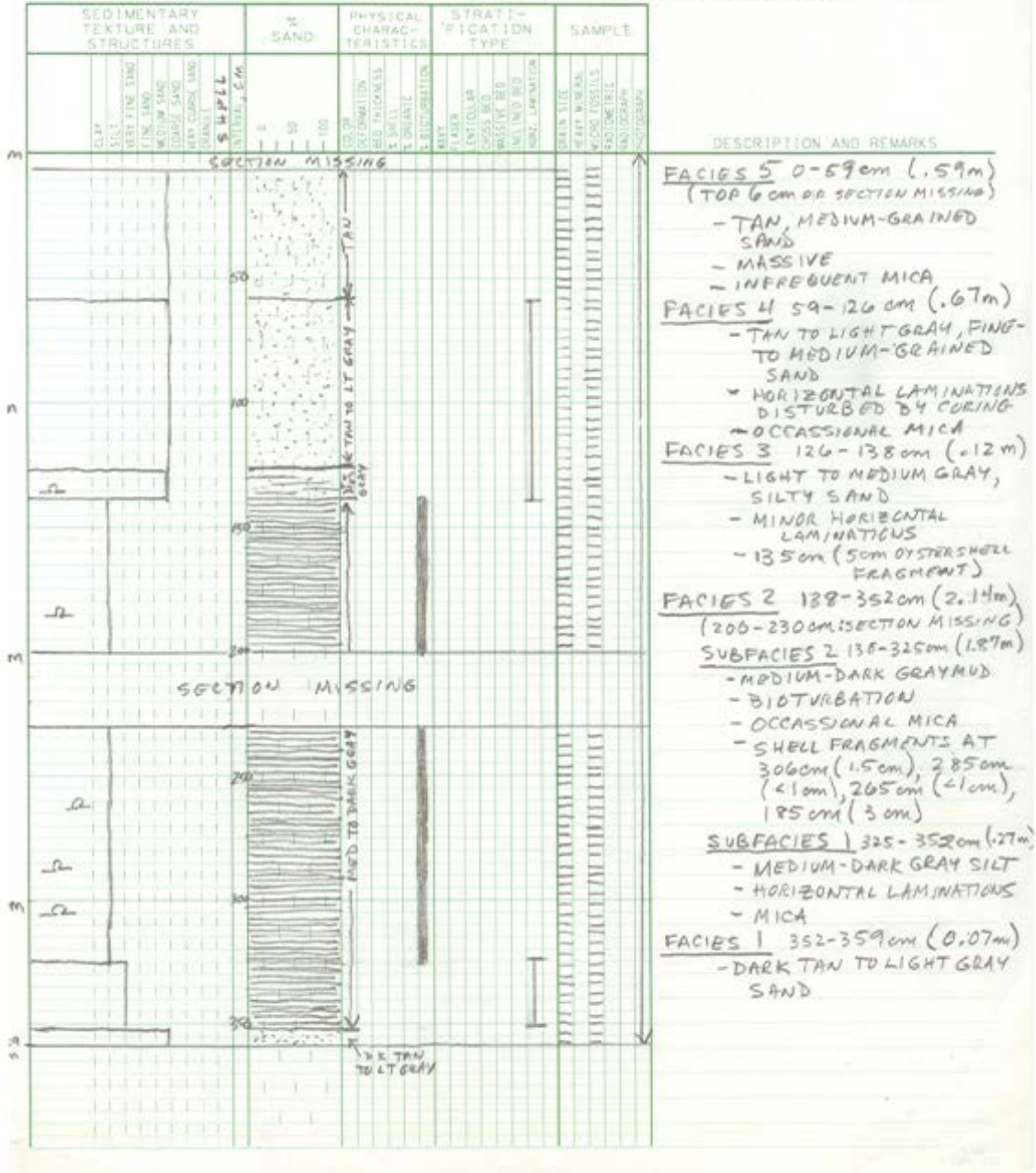
CORE ID: CIB100917-02 DATE COLLECTED: 9/17/10 DESCRIBED BY: HANLEY
 ELEVATION: ~MSL COMPACTION: 0.37m DATE DESCRIBED: 7/27/12
 CORE LENGTH: 5.15m LAT/LONG: 37°36'29.050"N 75°37'15.925"W
 TOTAL DEPTH: 5.52m LOCATION: FLOOD TIDAL DELTA

SEDIMENTARY TEXTURE AND STRUCTURES	% SAND	PHYSICAL CHARACTERISTICS	STRATIFICATION TYPE	SAMPLE	DESCRIPTION AND REMARKS																						
						CLAY	SILT	VERY FINE SAND	FINE SAND	MEDIUM SAND	COARSE SAND	VERY COARSE SAND	GRAVEL	INTERVAL, cm	COLOR	FORMATION	BED THICKNESS	% SHELL	% ORGANIC	% BIOTURBATION	TEXTURE	CLASER	LENTICULAR	CROSS BED	MASSIVE BED	WAGLING BED	ROOT LAMINATION
					<p>FACIES 3 233-420cm (1.87m)</p> <ul style="list-style-type: none"> - LIGHT GRAY, FINE-GRAINED SAND WITH MEDIUM GRAY MUD LAMINATIONS - MUD MASSIVE: 246-250cm - OCCASIONAL IRON STAINING 320-390cm - MICA - BIOTURBATION IN MIDDLE OF THE FACIES <p>FACIES 2 420-495cm (.75m)</p> <ul style="list-style-type: none"> - LIGHT GRAY, FINE-GRAINED SAND - MEDIUM GRAY MUD LAMINATIONS DECREASING DOWNWARD - MICA <p>FACIES 1 495-516cm (.21m)</p> <ul style="list-style-type: none"> - LIGHT GRAY MUD - MASSIVE - MICA 																						

Vibracore C4

VIBRACORE DESCRIPTION SHEET

CORE ID: C10100912-C4 DATE COLLECTED: 9/18/10 DESCRIBED BY: HANLEY
 ELEVATION: ~MSL COMPACTION: 1.60m DATE DESCRIBED: 9/21/11
 CORE LENGTH: 3.59m LAT/LONG: 37°36'42.214"N 75°37'27.446"W
 TOTAL DEPTH: 5.19m LOCATION: FLOOD TIDAL DELTA

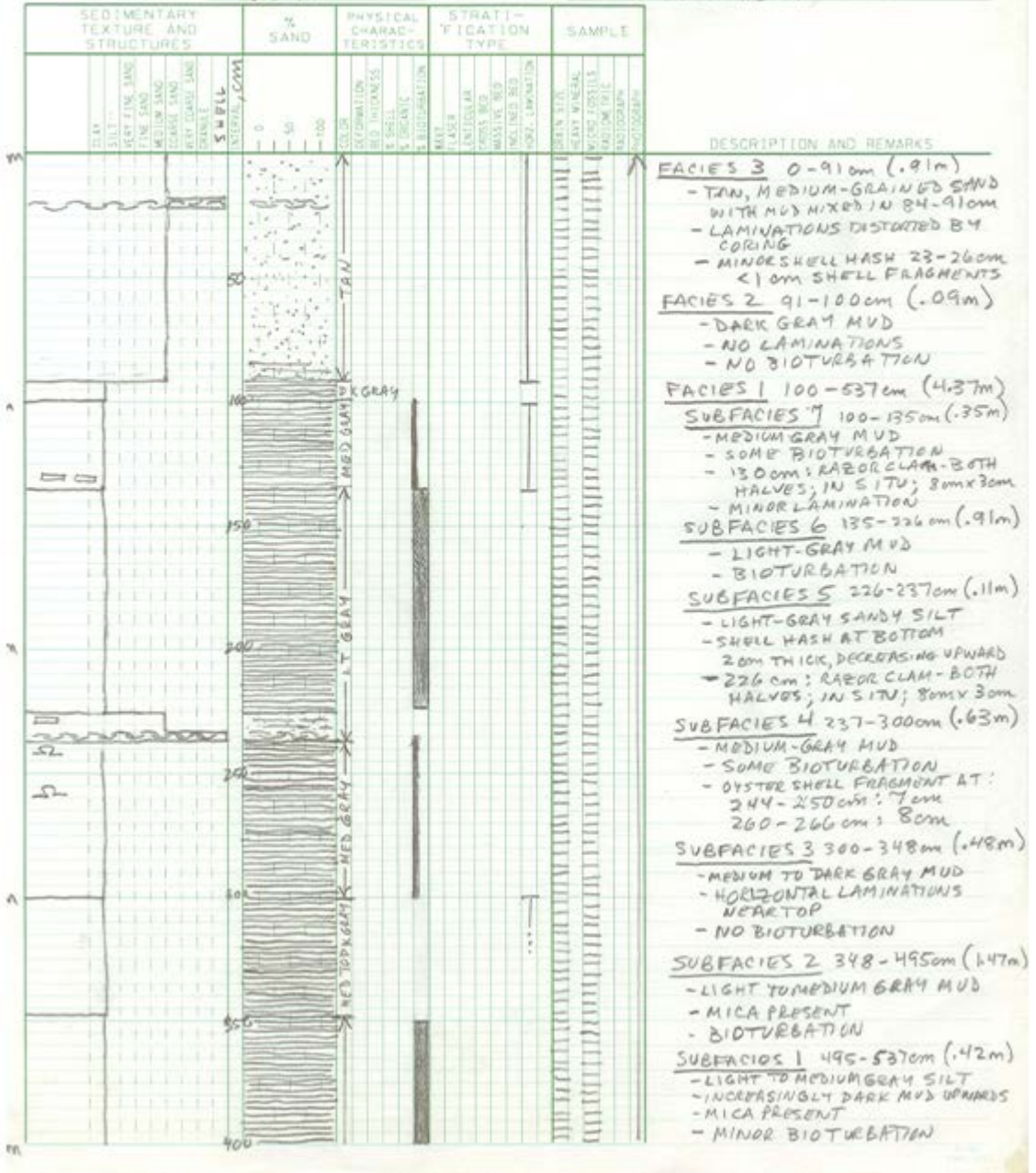


Vibracore C5

SHEET #1

VIBRACORE DESCRIPTION SHEET

CORE ID: C16100918-C5 DATE COLLECTED: 9/18/10 DESCRIBED BY: HANLEY
 ELEVATION: ~ MSL COMPACTION: 0.19m DATE DESCRIBED: 9/21/11
 CORE LENGTH: 5.37m LAT/LONG: 37°36'45.483"N 75°37'19.549"W
 TOTAL DEPTH: 5.56m LOCATION: FLOOD TIDAL DELTA



Vibracore C6

VIBRACORE DESCRIPTION SHEET

CORE ID: CIB100918-C6 DATE COLLECTED: 9/18/10 DESCRIBED BY: HANLEY
 ELEVATION: ~ MSL COMPACTION: 0.87m DATE DESCRIBED: 7/27/12
 CORE LENGTH: 0.30m LAT/LONG: 37°36'48.464"N 75°37'13.075"W
 TOTAL DEPTH: 1.17m LOCATION: FLOOD TIDAL DELTA

Interval, cm	SEDIMENTARY TEXTURE AND STRUCTURES						SAND	PHYSICAL CHARACTERISTICS				STRATIFICATION TYPE				SAMPLE				DESCRIPTION AND REMARKS							
	CLAY	SILT	VERY FINE SAND	FINE SAND	MEDIUM SAND	COURSE SAND		VERY COARSE SAND	GRAVEL	COLOR	COHESION	BED THICKNESS	% SHELL	% ORGANIC	BIOTURBATION	ROOT	FLASER	LANTILLA	CROSS BED		MASSIVE BED	UNCLINED BED	HOPEL STRATIFICATION	GRAIN SIZE	HEAVY MINERAL	WIND FOSSELS	FACTORIATIC
0-30																											FACIES! 0-30 cm (.3m) - TAN, FINE TO MEDIUM-GRAINED SAND - 1cm SHELL FRAGMENT AT 2cm - 8.5cm SHELL FRAGMENT AT 12cm - MASSIVE
30-100																											

Vibracore C7

VIBRACORE DESCRIPTION SHEET

CORE ID: CTB101008-C7 DATE COLLECTED: 10/8/10 DESCRIBED BY: HANLEY
 ELEVATION: ~ MSL COMPACTION: 609m DATE DESCRIBED: 10/24/11
 CORE LENGTH: 130cm LAT/LONG: 37°36'41.591"N 75°37'9.469"W
 TOTAL DEPTH: 2.39m LOCATION: INLET THROAT

SEDIMENTARY TEXTURE AND STRUCTURES	SHELLS / SHELL FRAGMENTS	% SAND	PHYSICAL CHARACTERISTICS	STRATIFICATION TYPE	SAMPLE	DESCRIPTION AND REMARKS																								
							CLAY	SILT	VERY FINE SAND	FINE SAND	MEDIUM SAND	COARSE SAND	VERY COARSE SAND	GRAVEL	COBBLES	SHALLS	SHALL FRAGMENTS	DEPTH, cm	COLOR	SEDIMENTATION	BED THICKNESS	% SHELLS	% ORGANIC	% BIOTURBATION	ROOT	FLAVER	LENTICULAR	CROSS BED	MASSIVE BED	INDICATED BED
						<p>FACIES 7 0-54 cm (.54m)</p> <ul style="list-style-type: none"> TAN, MED-GRAINED SAND MASSIVE MINOR BIOTURBATION AT TOP <p>FACIES 6 54-68 cm (.14m)</p> <ul style="list-style-type: none"> SHELLS AND TAN, MED-GRAINED SAND MATRIX LARGE BIVALVE SHELL FRAGMENTS (UPTO 10cm) SOME SMALL ROUNDED PEBBLES SOME SMALL ROUNDED SHELL FRAGMENTS <p>FACIES 5 68-93 cm (.25m)</p> <ul style="list-style-type: none"> TAN, MED-GRAINED SAND MASSIVE TWO LARGE BIVALVE SHELL FRAGMENTS AT ~ 78cm (4cm, 8cm) <p>FACIES 4 93-97 cm (.04m)</p> <ul style="list-style-type: none"> SHELLS AND TAN, MED-GRAINED SAND MATRIX LARGE BIVALVE SHELL FRAGMENTS (UPTO 6cm) SMALL ROUNDED SHELL FRAGMENTS <p>FACIES 3 97-105 cm (.08m)</p> <ul style="list-style-type: none"> TAN, MED-GRAINED SAND SMALL SHELL FRAGMENTS <p>FACIES 2 105-114 cm (.09cm)</p> <ul style="list-style-type: none"> SHELLS AND TAN, MED-GRAINED SAND MATRIX LARGE BIVALVE SHELL FRAGMENTS UPTO 8cm <p>FACIES 1 114-130 cm (.16m)</p> <ul style="list-style-type: none"> TAN, MED-GRAINED SAND SMALL SHELL FRAGMENTS WITH 2 LARGE BIVALVE SHELL FRAGMENTS (4cm, 5cm) 																								

Vibracore C9

VIBRACORE DESCRIPTION SHEET

CORE ID: CTB101002-C9 DATE COLLECTED: 10/8/10 DESCRIBED BY: HANLEY
 ELEVATION: +1 m MSL COMPACTION: 0.62 m DATE DESCRIBED: 8/30/12
 CORE LENGTH: 2.16 m LAT/LONG: 37°26'57.011"N 75°03'2.643"W
 TOTAL DEPTH: 2.78 m LOCATION: NORTH OF INLET THROAT

SEDIMENTARY TEXTURE AND STRUCTURES	% SAND	PHYSICAL CHARACTERISTICS	STRATIFICATION TYPE	SAMPLE	DESCRIPTION AND REMARKS																																																							
						INTERNAL, cm	COLOR	BIOTURBATION	GRAIN SIZE	GRAIN ORIENTATION	GRAIN CONTACT	GRAIN ARRANGEMENT	GRAIN SPACING	GRAIN SHAPE	GRAIN SURFACE	GRAIN COLOR	GRAIN LUSTER	GRAIN POLISH	GRAIN WEAR	GRAIN FRAGILITY	GRAIN PLASTICITY	GRAIN COMPRESSIBILITY	GRAIN PERMEABILITY	GRAIN COHESION	GRAIN ADHESION	GRAIN FRICTION	GRAIN DUCTILITY	GRAIN ELASTICITY	GRAIN STRENGTH	GRAIN STIFFNESS	GRAIN DENSITY	GRAIN SPECIFIC GRAVITY	GRAIN MOISTURE CONTENT	GRAIN ORGANIC CONTENT	GRAIN SULFUR CONTENT	GRAIN PHOSPHORUS CONTENT	GRAIN POTASSIUM CONTENT	GRAIN SODIUM CONTENT	GRAIN CALCIUM CONTENT	GRAIN MAGNESIUM CONTENT	GRAIN IRON CONTENT	GRAIN ZINC CONTENT	GRAIN COPPER CONTENT	GRAIN MANGANESE CONTENT	GRAIN NICKEL CONTENT	GRAIN CHROMIUM CONTENT	GRAIN BARIUM CONTENT	GRAIN STRONTIUM CONTENT	GRAIN RADIUM CONTENT	GRAIN POLYMERIZABLE ORGANIC CARBON	GRAIN TOTAL ORGANIC CARBON	GRAIN TOTAL NITROGEN	GRAIN TOTAL PHOSPHORUS	GRAIN TOTAL POTASSIUM	GRAIN TOTAL SODIUM	GRAIN TOTAL CALCIUM	GRAIN TOTAL MAGNESIUM	GRAIN TOTAL IRON	GRAIN TOTAL ZINC	GRAIN TOTAL COPPER
	<p>INTERNAL, cm</p> <p>0</p> <p>50</p> <p>100</p> <p>150</p> <p>200</p>	<p>COLOR</p> <p>BIOTURBATION</p> <p>GRAIN SIZE</p> <p>GRAIN ORIENTATION</p> <p>GRAIN CONTACT</p> <p>GRAIN ARRANGEMENT</p> <p>GRAIN SPACING</p> <p>GRAIN SHAPE</p> <p>GRAIN SURFACE</p> <p>GRAIN POLISH</p> <p>GRAIN WEAR</p> <p>GRAIN FRICTION</p> <p>GRAIN DUCTILITY</p> <p>GRAIN ELASTICITY</p> <p>GRAIN STRENGTH</p> <p>GRAIN STIFFNESS</p> <p>GRAIN DENSITY</p> <p>GRAIN SPECIFIC GRAVITY</p> <p>GRAIN MOISTURE CONTENT</p> <p>GRAIN ORGANIC CONTENT</p> <p>GRAIN SULFUR CONTENT</p> <p>GRAIN PHOSPHORUS CONTENT</p> <p>GRAIN POTASSIUM CONTENT</p> <p>GRAIN SODIUM CONTENT</p> <p>GRAIN CALCIUM CONTENT</p> <p>GRAIN MAGNESIUM CONTENT</p> <p>GRAIN IRON CONTENT</p> <p>GRAIN ZINC CONTENT</p> <p>GRAIN COPPER CONTENT</p> <p>GRAIN MANGANESE CONTENT</p> <p>GRAIN NICKEL CONTENT</p> <p>GRAIN CHROMIUM CONTENT</p> <p>GRAIN BARIUM CONTENT</p> <p>GRAIN STRONTIUM CONTENT</p> <p>GRAIN RADIUM CONTENT</p> <p>GRAIN POLYMERIZABLE ORGANIC CARBON</p> <p>GRAIN TOTAL ORGANIC CARBON</p> <p>GRAIN TOTAL NITROGEN</p> <p>GRAIN TOTAL PHOSPHORUS</p> <p>GRAIN TOTAL POTASSIUM</p> <p>GRAIN TOTAL SODIUM</p> <p>GRAIN TOTAL CALCIUM</p> <p>GRAIN TOTAL MAGNESIUM</p> <p>GRAIN TOTAL IRON</p> <p>GRAIN TOTAL ZINC</p> <p>GRAIN TOTAL COPPER</p> <p>GRAIN TOTAL MANGANESE</p> <p>GRAIN TOTAL NICKEL</p> <p>GRAIN TOTAL CHROMIUM</p> <p>GRAIN TOTAL BARIUM</p> <p>GRAIN TOTAL STRONTIUM</p> <p>GRAIN TOTAL RADIUM</p>	<p>STRATIFICATION TYPE</p> <p>GRAIN SIZE</p> <p>GRAIN ORIENTATION</p> <p>GRAIN CONTACT</p> <p>GRAIN ARRANGEMENT</p> <p>GRAIN SPACING</p> <p>GRAIN SHAPE</p> <p>GRAIN SURFACE</p> <p>GRAIN POLISH</p> <p>GRAIN WEAR</p> <p>GRAIN FRICTION</p> <p>GRAIN DUCTILITY</p> <p>GRAIN ELASTICITY</p> <p>GRAIN STRENGTH</p> <p>GRAIN STIFFNESS</p> <p>GRAIN DENSITY</p> <p>GRAIN SPECIFIC GRAVITY</p> <p>GRAIN MOISTURE CONTENT</p> <p>GRAIN ORGANIC CONTENT</p> <p>GRAIN SULFUR CONTENT</p> <p>GRAIN PHOSPHORUS CONTENT</p> <p>GRAIN POTASSIUM CONTENT</p> <p>GRAIN SODIUM CONTENT</p> <p>GRAIN CALCIUM CONTENT</p> <p>GRAIN MAGNESIUM CONTENT</p> <p>GRAIN IRON CONTENT</p> <p>GRAIN ZINC CONTENT</p> <p>GRAIN COPPER CONTENT</p> <p>GRAIN MANGANESE CONTENT</p> <p>GRAIN NICKEL CONTENT</p> <p>GRAIN CHROMIUM CONTENT</p> <p>GRAIN BARIUM CONTENT</p> <p>GRAIN STRONTIUM CONTENT</p> <p>GRAIN RADIUM CONTENT</p> <p>GRAIN POLYMERIZABLE ORGANIC CARBON</p> <p>GRAIN TOTAL ORGANIC CARBON</p> <p>GRAIN TOTAL NITROGEN</p> <p>GRAIN TOTAL PHOSPHORUS</p> <p>GRAIN TOTAL POTASSIUM</p> <p>GRAIN TOTAL SODIUM</p> <p>GRAIN TOTAL CALCIUM</p> <p>GRAIN TOTAL MAGNESIUM</p> <p>GRAIN TOTAL IRON</p> <p>GRAIN TOTAL ZINC</p> <p>GRAIN TOTAL COPPER</p> <p>GRAIN TOTAL MANGANESE</p> <p>GRAIN TOTAL NICKEL</p> <p>GRAIN TOTAL CHROMIUM</p> <p>GRAIN TOTAL BARIUM</p> <p>GRAIN TOTAL STRONTIUM</p> <p>GRAIN TOTAL RADIUM</p>	<p>SAMPLE</p> <p>GRAIN SIZE</p> <p>GRAIN ORIENTATION</p> <p>GRAIN CONTACT</p> <p>GRAIN ARRANGEMENT</p> <p>GRAIN SPACING</p> <p>GRAIN SHAPE</p> <p>GRAIN SURFACE</p> <p>GRAIN POLISH</p> <p>GRAIN WEAR</p> <p>GRAIN FRICTION</p> <p>GRAIN DUCTILITY</p> <p>GRAIN ELASTICITY</p> <p>GRAIN STRENGTH</p> <p>GRAIN STIFFNESS</p> <p>GRAIN DENSITY</p> <p>GRAIN SPECIFIC GRAVITY</p> <p>GRAIN MOISTURE CONTENT</p> <p>GRAIN ORGANIC CONTENT</p> <p>GRAIN SULFUR CONTENT</p> <p>GRAIN PHOSPHORUS CONTENT</p> <p>GRAIN POTASSIUM CONTENT</p> <p>GRAIN SODIUM CONTENT</p> <p>GRAIN CALCIUM CONTENT</p> <p>GRAIN MAGNESIUM CONTENT</p> <p>GRAIN IRON CONTENT</p> <p>GRAIN ZINC CONTENT</p> <p>GRAIN COPPER CONTENT</p> <p>GRAIN MANGANESE CONTENT</p> <p>GRAIN NICKEL CONTENT</p> <p>GRAIN CHROMIUM CONTENT</p> <p>GRAIN BARIUM CONTENT</p> <p>GRAIN STRONTIUM CONTENT</p> <p>GRAIN RADIUM CONTENT</p> <p>GRAIN POLYMERIZABLE ORGANIC CARBON</p> <p>GRAIN TOTAL ORGANIC CARBON</p> <p>GRAIN TOTAL NITROGEN</p> <p>GRAIN TOTAL PHOSPHORUS</p> <p>GRAIN TOTAL POTASSIUM</p> <p>GRAIN TOTAL SODIUM</p> <p>GRAIN TOTAL CALCIUM</p> <p>GRAIN TOTAL MAGNESIUM</p> <p>GRAIN TOTAL IRON</p> <p>GRAIN TOTAL ZINC</p> <p>GRAIN TOTAL COPPER</p> <p>GRAIN TOTAL MANGANESE</p> <p>GRAIN TOTAL NICKEL</p> <p>GRAIN TOTAL CHROMIUM</p> <p>GRAIN TOTAL BARIUM</p> <p>GRAIN TOTAL STRONTIUM</p> <p>GRAIN TOTAL RADIUM</p>	<p>DESCRIPTION AND REMARKS</p> <p>FACIES 9 0-25 cm (.25 m)</p> <ul style="list-style-type: none"> - TAN TO LIGHT GRAY, FINE-GRAINED SAND - MASSIVE - MICA <p>FACIES 8 25-33 cm (.08 m)</p> <ul style="list-style-type: none"> - LIGHT TO MEDIUM GRAY, FINE-GRAINED SAND, CLAYEY SILT - MINOR LAMINATIONS - MICA THROUGHOUT <p>FACIES 7 33-71 cm (.44 m)</p> <ul style="list-style-type: none"> - LIGHT GRAY, FINE-GRAINED SILTY SAND - LAMINATIONS DECREASES TOWARD TOP DISTURBED BY CORING - MICA THROUGHOUT <p>FACIES 6 77-120 cm (.43 m)</p> <ul style="list-style-type: none"> - LIGHT TO MEDIUM GRAY SANDY SILTY CLAY - BIOTURBATION DECREASING UPWARD - 5 cm VERTICAL TUBE (104.5-109.5) - SMALL SHELL FRAGMENTS AT 86-87 cm - RUSTY AREA AT 80 cm - MICA THROUGHOUT <p>FACIES 5 102-132 cm (.12 m)</p> <ul style="list-style-type: none"> - LIGHT GRAY, FINE-GRAINED SAND - MASSIVE - SMALL SHELL FRAGMENTS AT BOTTOM - MICA THROUGHOUT <p>FACIES 4 132-144 cm (.12 m)</p> <ul style="list-style-type: none"> - MEDIUM GRAY, SILTY CLAY - MINOR BIOTURBATION - MICA THROUGHOUT <p>FACIES 3 144-160 cm (.16 m)</p> <ul style="list-style-type: none"> - MEDIUM GRAY TO TAN FINE-GRAINED SILTY, CLAYEY SAND - LAMINATIONS DISTURBED BY CORING - MICA THROUGHOUT <p>FACIES 2 160-196 cm (.36 m)</p> <ul style="list-style-type: none"> - LIGHT CLAY TO TAN, FINE-GRAINED SAND - MODERATE LAMINATIONS DISTURBED BY CORING - MICA THROUGHOUT. LAYER OF INCREASED MICA AT 168-169 cm <p>FACIES 1 196-216 cm (.20 m)</p> <ul style="list-style-type: none"> - LIGHT GRAY, FINE-GRAINED SAND - MINOR LAMINATIONS DISTURBED BY CORING - MICA 																																																							

Vibracore C10

SHEET 1

VIBRACORE DESCRIPTION SHEET

CORE ID: C10101008-C10 DATE COLLECTED: 10/8/10 DESCRIBED BY: HANLEY
 ELEVATION: ~MSL COMPACTION: 0.37m DATE DESCRIBED: 2/10/12
 CORE LENGTH: 769m LAT/LONG: 37°36'58.533"N 75°37'22.585"W
 TOTAL DEPTH: 806m LOCATION: BACK BAY

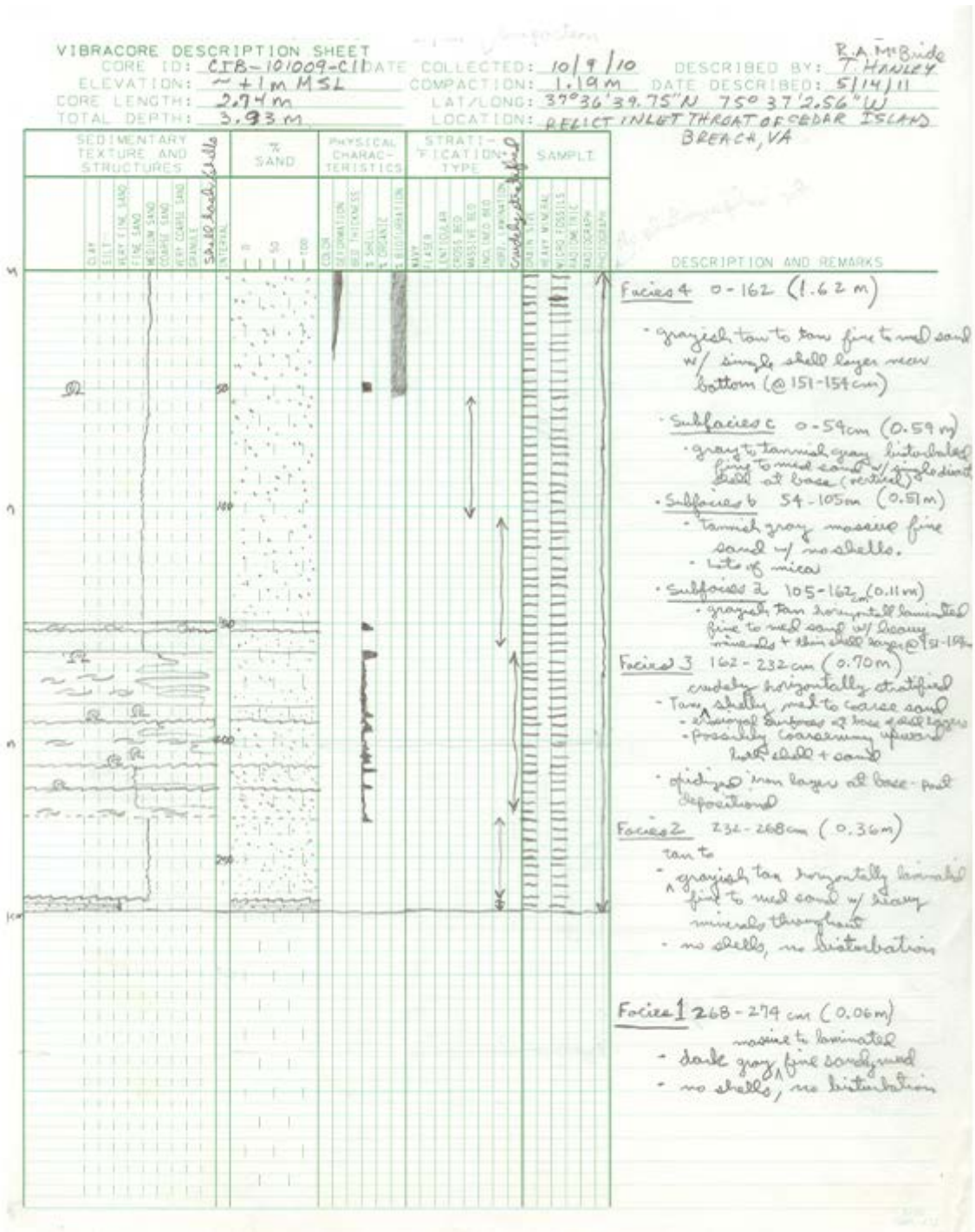
SEDIIMENTARY TEXTURE AND STRUCTURES	% SAND	PHYSICAL CHARACTERISTICS	STRATIFICATION TYPE	SAMPLE	DESCRIPTION AND REMARKS																				
						CLAY	SILT	FINE SAND	MEDIUM SAND	COARSE SAND	VERY COARSE SAND	GRAVEL	UTERILE, %	COLOR	SEDIMENTATION	SHELLS	ORGANIC	BIOTURBATION	ROOT	LAYER	ANTICLINAL	CROSS BED	MASSIVE BED	INCLINED BED	ORZ. LAMINATION
					<p>FACIES 9 0-16 cm (.16m)</p> <ul style="list-style-type: none"> - TAN TO LIGHT GRAY, FINE-GRAINED SAND - MASSIVE - MICA <p>FACIES 8 16-44 cm (.28m)</p> <ul style="list-style-type: none"> - TAN TO LIGHT GRAY, FINE-GRAINED SAND WITH MEDIUM-GRAY MUD INCLUSIONS - MASSIVE; NO MUD LAYERS - MICA <p>FACIES 7 44-76 cm (.32m)</p> <ul style="list-style-type: none"> - DARK GRAY MUD - MASSIVE - SOME MICA - NO BIOTURBATION - SMALL SHELL FRAGMENTS AT 49cm AND 62cm <p>FACIES 6 76-107 cm (.31m)</p> <ul style="list-style-type: none"> - LIGHT GRAY, FINE-GRAINED SAND WITH DARK-GRAY MUD LAMINATIONS - LAMINATIONS DECREASING DOWNWARD - SOME BIOTURBATION - MICA <p>FACIES 5 107-161 cm (.54m)</p> <ul style="list-style-type: none"> - LIGHT GRAY, FINE-GRAINED SAND - MASSIVE WITH DARK GRAY MUD INCLUSIONS - THIN, DARK GRAY MUD LAMINATIONS 114-120cm - MICA <p>FACIES 4 161-209 cm (.48m)</p> <ul style="list-style-type: none"> - MEDIUM TO DARK-GRAY MUD WITH SOME LIGHT GRAY, FINE-GRAINED SAND LAMINATIONS - SOME BIOTURBATION - MICA <p>FACIES 3 209-615 cm (4.06m)</p> <ul style="list-style-type: none"> - MEDIUM-TO-DARK GRAY MUD - MASSIVE - SOME BIOTURBATION - SHELL FRAGMENTS: 5cm LONG AT 542-547cm, 1cm LONG AT 517cm - MICA 																				

VIBRACORE DESCRIPTION SHEET

CORE ID: CIB101008-C10 DATE COLLECTED: 10/8/10 DESCRIBED BY: HANLEY
 ELEVATION: ~MSL COMPACTION: 0.37m DATE DESCRIBED: 8/10/12
 CORE LENGTH: 7.69m LAT/LONG: 37°36'58.533"N 75°37'22.585"W
 TOTAL DEPTH: 8.06m LOCATION: BACK BAY

DEPTH (m)	SEDIMENTARY TEXTURE AND STRUCTURES	% SAND	PHYSICAL CHARACTERISTICS	STRATIFICATION TYPE	SAMPLE	DESCRIPTION AND REMARKS																				
							CLAY	SILT	VERY FINE SAND	FINE SAND	MEDIUM SAND	COARSE SAND	VERY COARSE SAND	GRANULE	SHELLS INTERVAL, %	COLOR	SOIL OR BED TENDENCY	% SHELLS	% ORGANIC	% BIOTURBATION	TEXTURE	FACTOR	LENTICULAR	DESSIC BED	MASSIVE BED	INCLINED BED
4m						FACIES 2 615-628 cm (1.13m) - DARK GRAY MUD - SHELL HASH WITH UP TO 2cm SHELL FRAGMENTS																				
5m						FACIES 1 628-772 cm (1.44m) - DARK GRAY MUD - MASSIVE - SOME MICA - SOME BIOTURBATION - OCCASIONAL SMALL SHELL FRAGMENTS																				
6m																										
7m																										
8m																										

Vibracore C11



Vibracore C12

VIBRACORE DESCRIPTION SHEET

CORE ID: C12-101009-C12 DATE COLLECTED: 10/9/10 DESCRIBED BY: P.A. McBride/J. H. Kelly
 ELEVATION: +1 m MSL COMPACTION: .71 m DATE DESCRIBED: 12-23-10
 CORE LENGTH: 2.54 m LAT/LONG: 37° 36' 44.91" N 75° 36' 57.21" W
 TOTAL DEPTH: 3.25 m LOCATION: Relict inlet throat of Cedar Island beach, VA

SEDIMENTARY TEXTURE AND STRUCTURES	% SAND	PHYSICAL CHARACTERISTICS	STRATIFICATION TYPE	SAMPLE						DESCRIPTION AND REMARKS		
				GRAIN SIZE	HEAVY MINERAL	WEDGE ESSAYS	SOUNDNESS	SHrinkAGE	PHOTOGRAPHS			
CLAY SILT VERY FINE SAND FINE SAND MEDIUM SAND COARSE SAND VERY COARSE SAND GRAVEL SHELL OTHER	0 50 100	COLOR TEXTURE BED THICKNESS % SHELL % ORGANIC % SILT/CLAY MAY FLASK LENTICULAR CROSS BED WASSATE BED INGLINED BED ORNL LAMINATION										
												<p>Facies 4 0-68 cm (0.68 m) - tanish to light gray matrix to deformed fine to med sand - few shells (shell content greatly decreased from Facies 3)</p> <p>Facies 3 68-194 cm (1.26 m) - light gray to tan fine to med. quartz sand w/ low conc. of heavy minerals - thin shelly fine to med sand layers w/ erosion base + fine upward (shell frags + minor sand fragments at base) - planar laminations - subtly coarsens upward from fine to med sand (0-194 cm)</p> <p>Facies 2 194-194 cm (0.03 m) - fine sandy shell hash</p> <p>Facies 1 253-194 cm (0.59 m) - dark gray laminated silty clay w/ subtle disturbance throughout and some shells - shells - gastropods + molluscs</p>

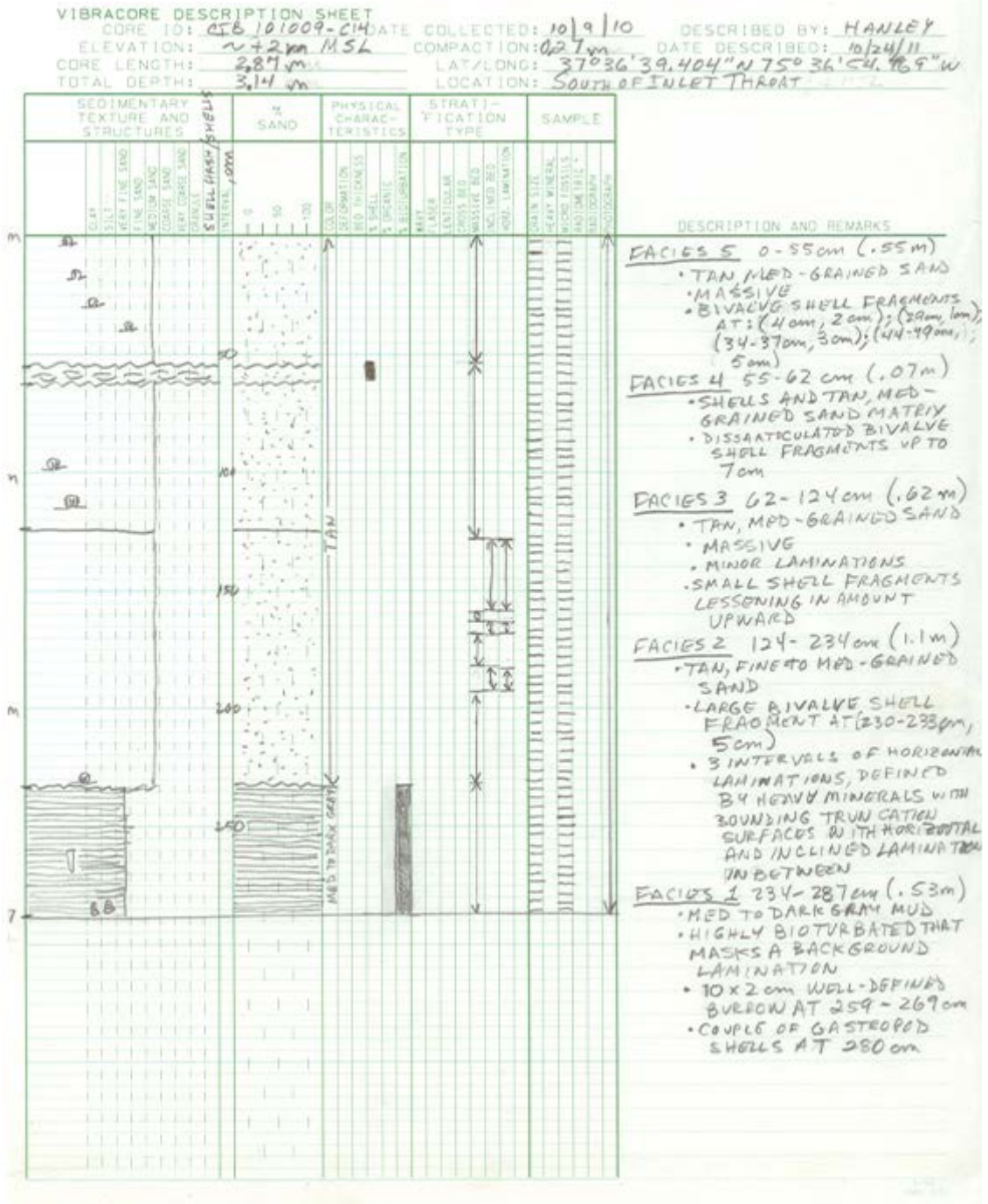
Vibracore C13

VIBRACORE DESCRIPTION SHEET

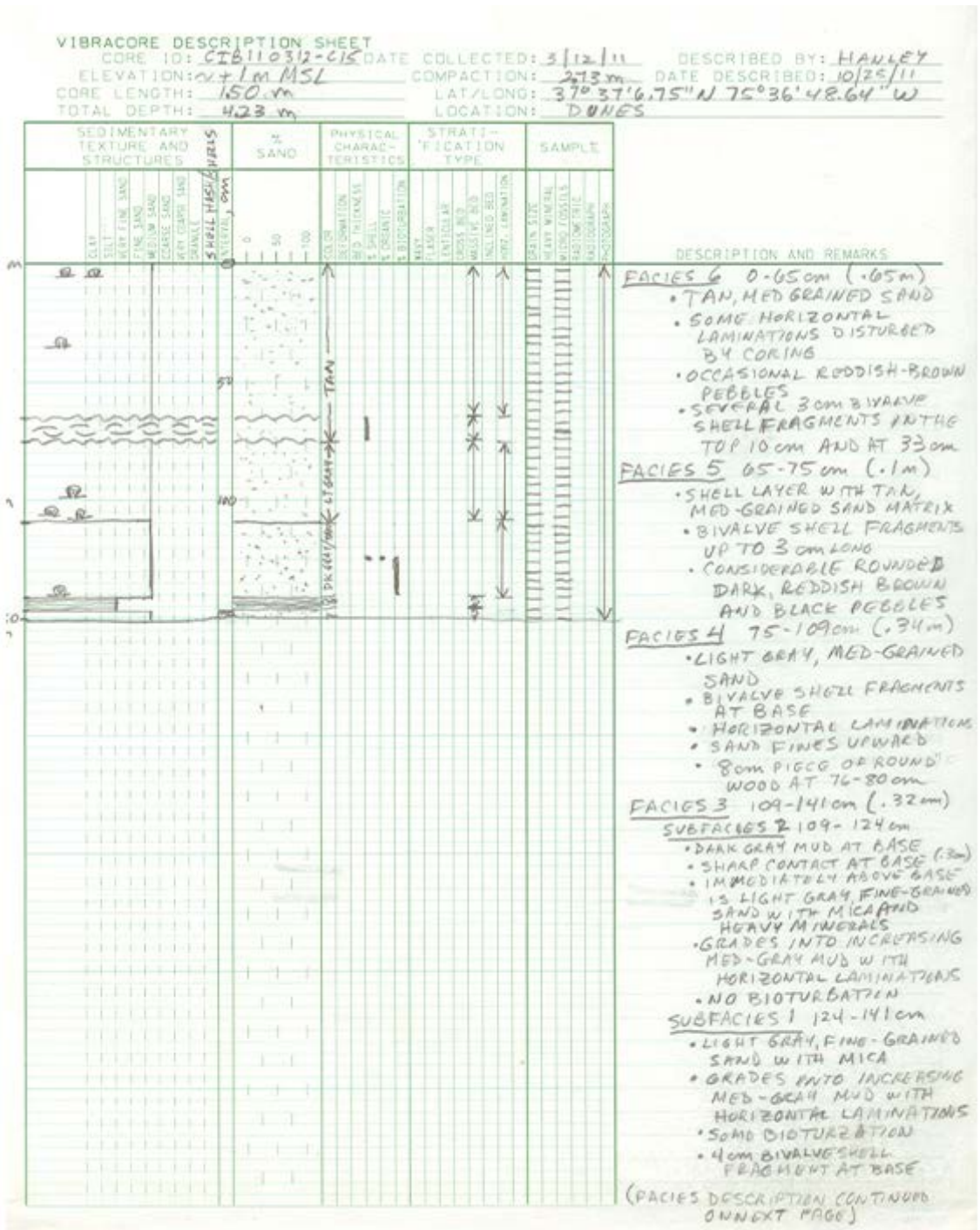
CORE ID: C13 DATE COLLECTED: 10-9-10 DESCRIBED BY: R.A.M. Bride
 ELEVATION: +1m COMPACTION: 63.5cm DATE DESCRIBED: 2/26/11
 CORE LENGTH: 173 LAT/LONG: 37°36'49.61"N 75°36'55.60"W
 TOTAL DEPTH: 236.5cm LOCATION: Rebet inlet throat of Cedar Island beach, VA

SEDIMENTARY TEXTURE AND STRUCTURES	% SAND	PHYSICAL CHARACTERISTICS	STRATIFICATION TYPE	SAMPLE	DESCRIPTION AND REMARKS																										
						CLAY	SILT	VERY FINE SAND	FINE SAND	MEDIUM SAND	COARSE SAND	VERY COARSE SAND	GRAVELL	WATER	0	50	100	COLOR	SEDIMENTATION	SED. THICKNESS	% SHELL	% ORGANIC	% BIOTURBATION	WET	FLASER	LANTICULAR	POOLS BED	MASSIVE BED	INCLINED BED	HORIZ. LAMINATION	DEFLECTED
<p>a. transported shell (not in situ)</p>					<p>Facies 2 0-93m (0.93m)</p> <ul style="list-style-type: none"> - light tan fine to med sand w/ some heavy minerals; laminations deformed - subfacies 1 0-58cm fine to med sand w/ shell top at base - subfacies 2 58-93cm fine to med sand w/ shell top at base <p>Facies 1 93-173m (0.8m)</p> <ul style="list-style-type: none"> - grayish-tan and tan horizontally laminated fine sand w/ heavy minerals, no shells - horizontal laminations well developed at base - can have distinct upward grading possibly into massive fine to med sand * coarsens upward from fine sand (2.5 phi) to med sand (2.0 phi) 																										

Vibracore C14



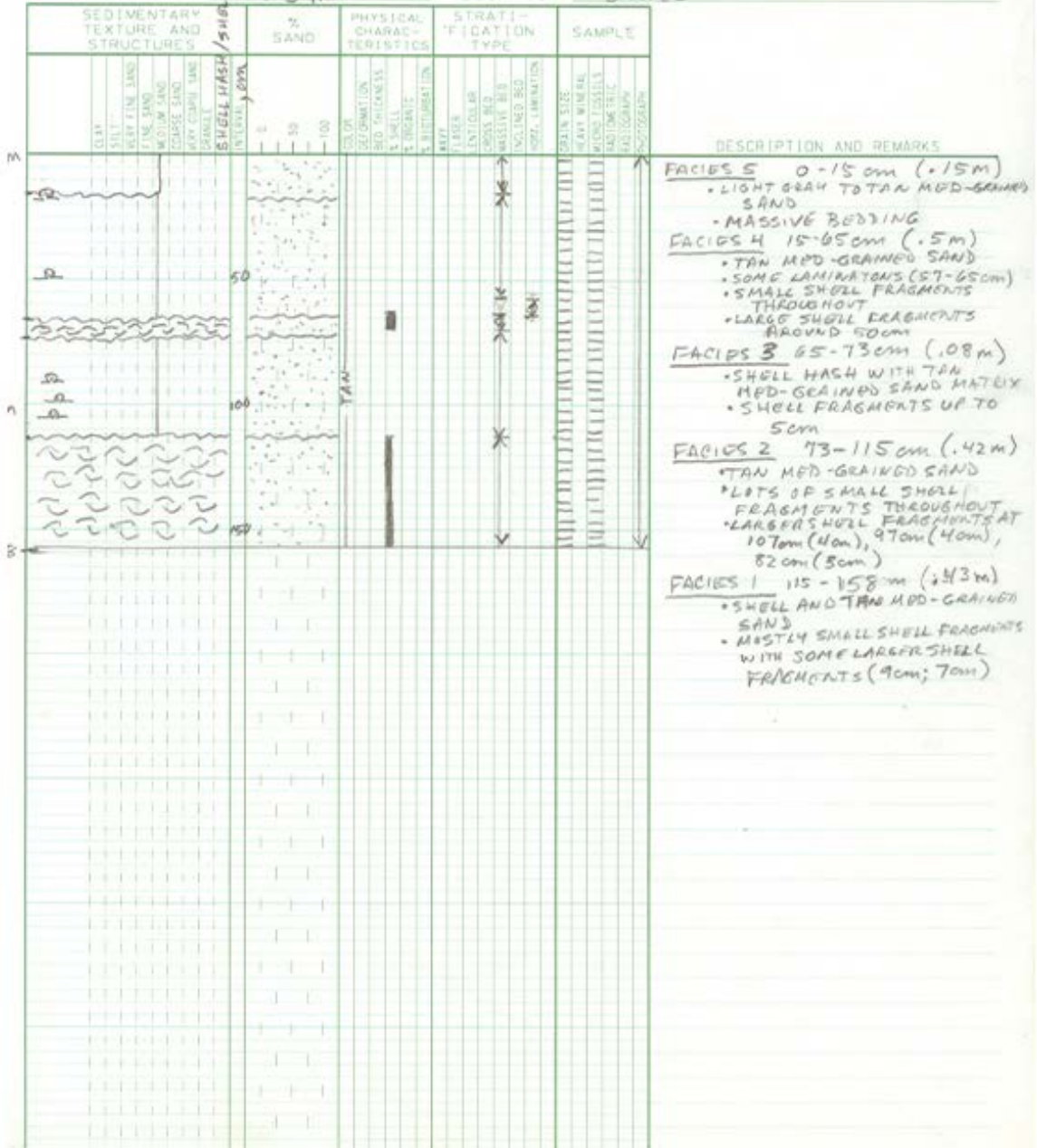
Vibracore C15



Vibracore C17

VIBRACORE DESCRIPTION SHEET

CORE ID: CT811032-C17 DATE COLLECTED: 3/12/11 DESCRIBED BY: HANLEY
 ELEVATION: +1m MSL COMPACTION: 0.65cm DATE DESCRIBED: 10/24/11
 CORE LENGTH: 158m LAT/LONG: 37°36'51.36"N 75°37'2.69"W
 TOTAL DEPTH: 223m LOCATION: DUNES



Vibracore C18

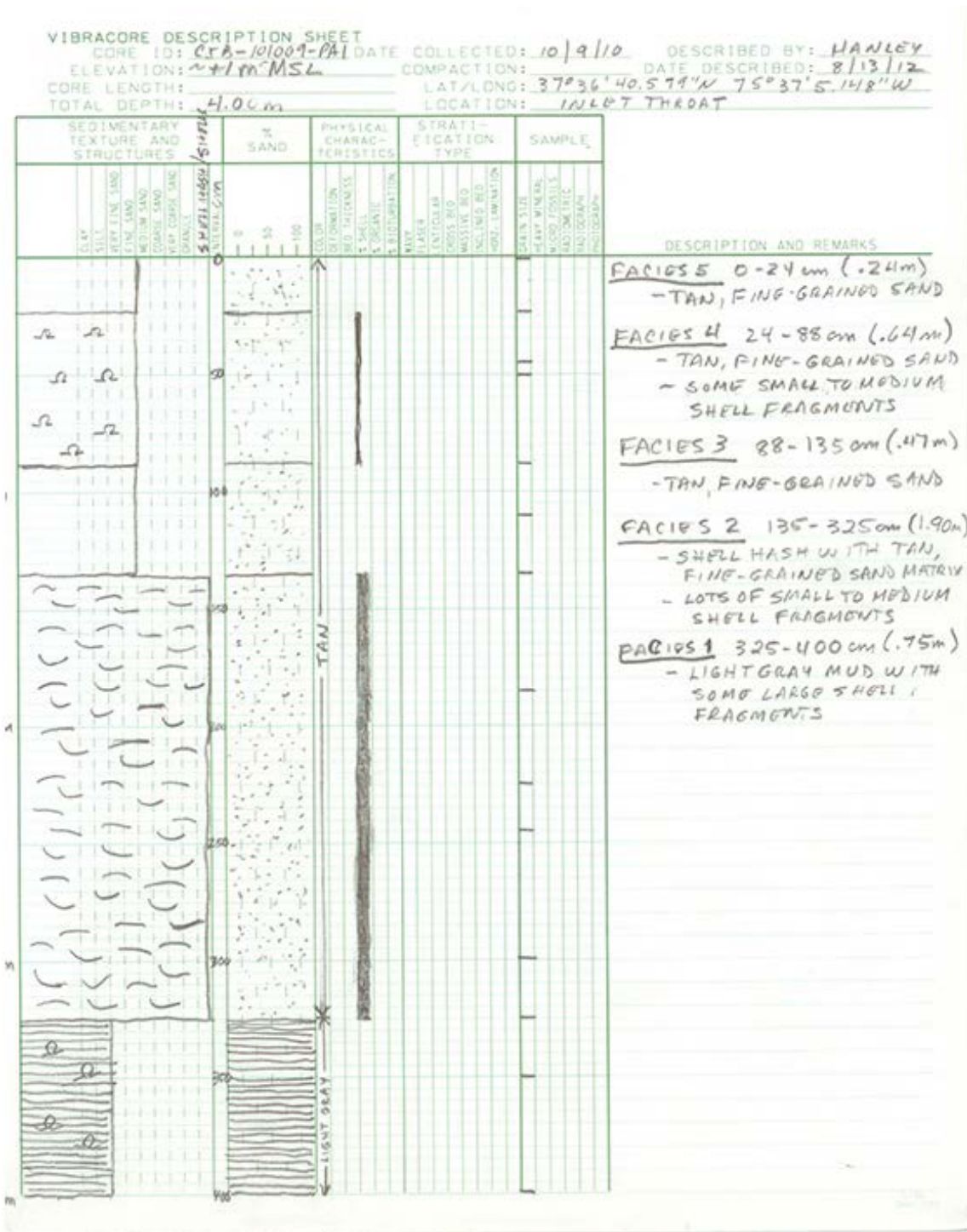
VIBRACORE DESCRIPTION SHEET

CORE ID: C18 110312-C18 DATE COLLECTED: 3/12/11 DESCRIBED BY: HANLEY
 ELEVATION: ~41m MSL COMPACTION: 107m DATE DESCRIBED: 10/24/11
 CORE LENGTH: 231m LAT/LONG: 37° 36' 43.68" N 75° 36' 58.29" W
 TOTAL DEPTH: 338m LOCATION: INLET THROAT

M	SEDIMENTARY TEXTURE AND STRUCTURES		% SAND	PHYSICAL CHARACTERISTICS		STRATIFICATION TYPE		SAMPLE	DESCRIPTION AND REMARKS				
	CLAY	SILT		DEFORMATION	BED THICKNESS	CLAY FLASHER	ENTRAPPED			MASSIVE BED	INCLINED BED	GRAIN SIZE	HEAVY MINERAL
0			0						FACIES 6 0-90cm (.9m)				
50			50						<ul style="list-style-type: none"> TAN, FINE TO MED-GRAINED SAND MINOR LAMINATIONS DISTURBED BY CORING SOME SMALL SHELL FRAGMENTS AT 11-18cm LARGE BIVALVE SHELL FRAGMENT AT 16cm 				
90									FACIES 5 90-96cm (.06m)				
100									<ul style="list-style-type: none"> SHELLS IN TAN MED-GRAINED SAND BIVALVE SHELL FRAGMENT UP TO 2cm 				
190									FACIES 4 96-190cm (.94m)				
200									<ul style="list-style-type: none"> TAN, MED-GRAINED SAND MASSIVE WITH OCCASIONAL LAMINATIONS AT 96-100cm, 109-112cm, 167-172cm DISTURBED 				
200									FACIES 3 190-200cm (.1m)				
210									<ul style="list-style-type: none"> SHELL LAYER WITH TAN, MED-GRAINED SAND MATRIX SHELL CONTENT INCREASES UPWARD MOSTLY BIVALVE SHELL FRAGMENTS UP TO 5cm GASTROPOD SHELL AT 198cm 				
216									FACIES 2 200-216cm (.16m)				
230									<ul style="list-style-type: none"> LIGHT GRAY TO TAN FINE-GRAINED SAND WITH MICA FLAKES MASSIVE 				
230									FACIES 1 216-230cm (.15m)				
230									<ul style="list-style-type: none"> SHELL LAYER WITH LIGHT GRAY TO TAN SAND MATRIX DISSARTICULATED BIVALVE SHELLS UP TO 7cm MATRIX CHANGES AT 222cm TO LIGHT GRAY FINE-GRAINED SAND AND MUD MIXED WITH SHELL FRAGMENTS 				

Pulse auger description sheets

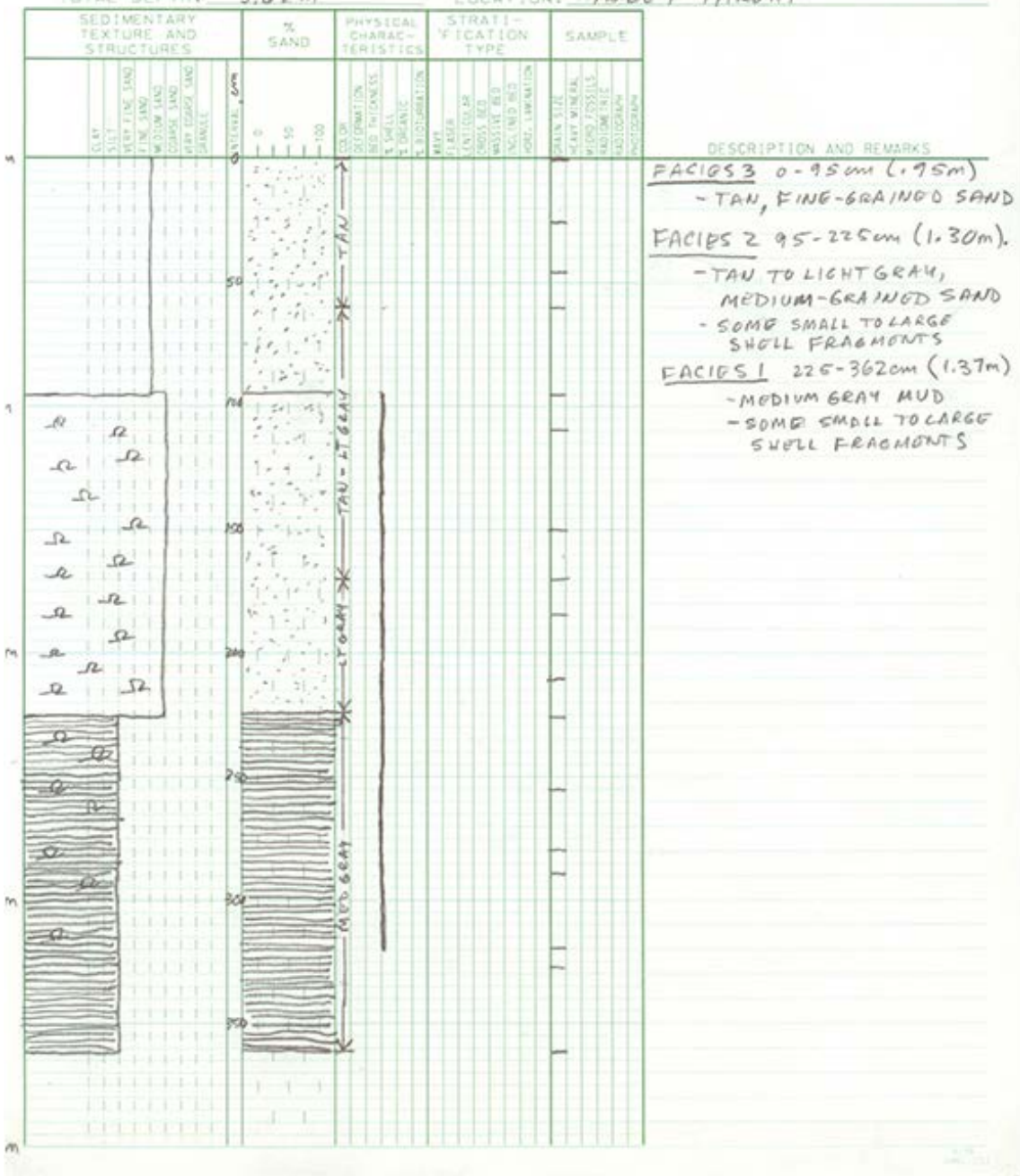
Pulse auger PA1



Pulse auger PA2

VIBRACORE DESCRIPTION SHEET

CORE ID: CIP-101009-PA2 DATE COLLECTED: 10/9/10 DESCRIBED BY: HANLEY
 ELEVATION: ~11m MSL COMPACTION: _____ DATE DESCRIBED: 8/13/12
 CORE LENGTH: _____ LAT/LONG: 37° 36' 45.218" N 75° 36' 57.149" W
 TOTAL DEPTH: 3.62m LOCATION: INLET THROAT



Pulse auger PA3

VIBRACORE DESCRIPTION SHEET

CORE ID: CIB-101009-PA3 DATE COLLECTED: 10/9/10 DESCRIBED BY: HANLEY
 ELEVATION: ~1 m MSL COMPACTION: _____ DATE DESCRIBED: 8/13/12
 CORE LENGTH: _____ LAT/LONG: 37°36'44.865"N 75°36'52.069"W
 TOTAL DEPTH: 3.45 m LOCATION: N SIDE OF INLET NEAR OCEAN

SEDIMENTARY TEXTURE AND STRUCTURES	% SAND	PHYSICAL CHARACTERISTICS	STRATIFICATION TYPE	SAMPLE	DESCRIPTION AND REMARKS															
						CLAY	SILT	VERY FINE SAND	FINE SAND	MEDIUM SAND	COARSE SAND	VERY COARSE SAND	GRAVEL	GRAVELLIER	FLASHER	CLASTIC	CONG. BED	MESSY BED	IND. BED	NO. OF BEDS
					<p>FACIES 4 0-20 cm (.20m) - TAN TO LT GRAY, FINE-GRAINED SAND - SOME SMALL SHELL FRAGMENTS</p> <p>FACIES 3 20-70 cm (.50m) - TAN TO LT GRAY, FINE-GRAINED SAND</p> <p>FACIES 2 70-310 cm (2.40m) - LIGHT GRAY, FINE-GRAINED SAND - MEDIUM TO LARGE SHELL FRAGMENTS</p> <p>FACIES 1 310-345 cm (.35m) - MEDIUM GRAY MUD</p>															

Pulse auger PA6

VIBRACORE DESCRIPTION SHEET

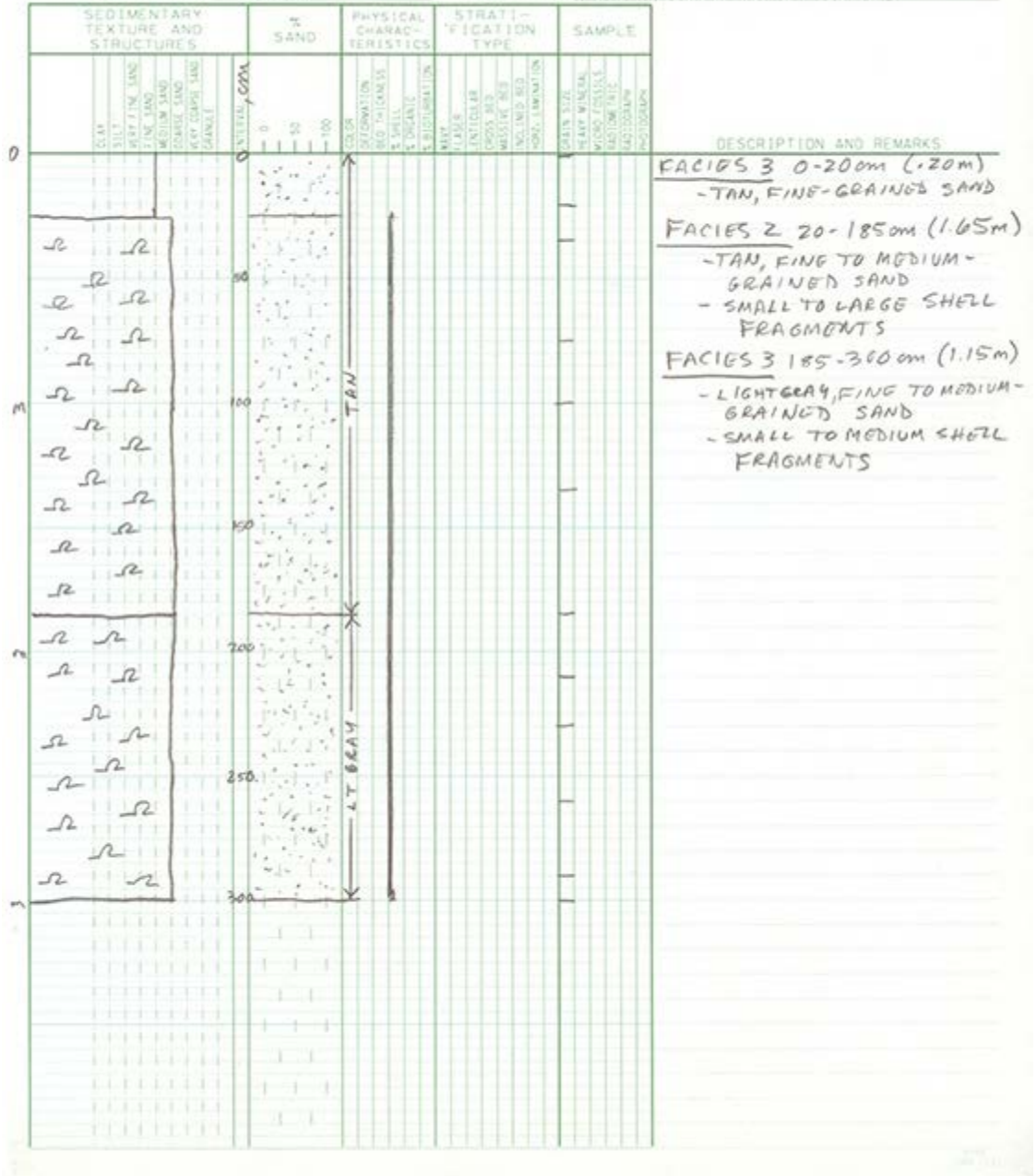
CORE ID: CIB-10100-PA6 DATE COLLECTED: 10/10/10 DESCRIBED BY: HANLEY
 ELEVATION: ~+1m MSL COMPACTION: DATE DESCRIBED: 8/13/12
 CORE LENGTH: LAT/LONG: 37°36'50.644"N 75°36'56.52"W
 TOTAL DEPTH: 3.60m LOCATION: N OF INLET NEAR DUNES

SEDIMENTARY TEXTURE AND STRUCTURES	% SAND	PHYSICAL CHARACTERISTICS	STRATIFICATION TYPE	SAMPLE	DESCRIPTION AND REMARKS																							
						CLAY	SILT	VERY FINE SAND	FINE SAND	MEDIUM SAND	COARSE SAND	VERY COARSE SAND	SHELLS	GRAVEL	WATER, cm	COLOR	SEDIMENTATION	BED THICKNESS	% SHELLS	% ORGANIC	% BIOTURBATION	RYBY	FLASER	LANTOULAR	PROSS BED	MASSIVE BED	WINDING BED	HOPE-LAMINATION
					FACIES 4 0-25cm (.25m) - TAN, MED-GRAINED SAND																							
					FACIES 3 25-80cm (.55m) - TAN, FINE TO MED-GRAINED SAND - SMALL TO MED. SHELL FRAGMENTS																							
					FACIES 2 80-165cm (.85m) - TAN TO LT GRAY, FINE-GRAINED SAND																							
					FACIES 1 165-360cm (1.95m) - LT TO MED GRAY, FINE-GRAINED SAND - SMALL TO LARGE SHELL FRAGMENTS																							

Pulse auger PA8

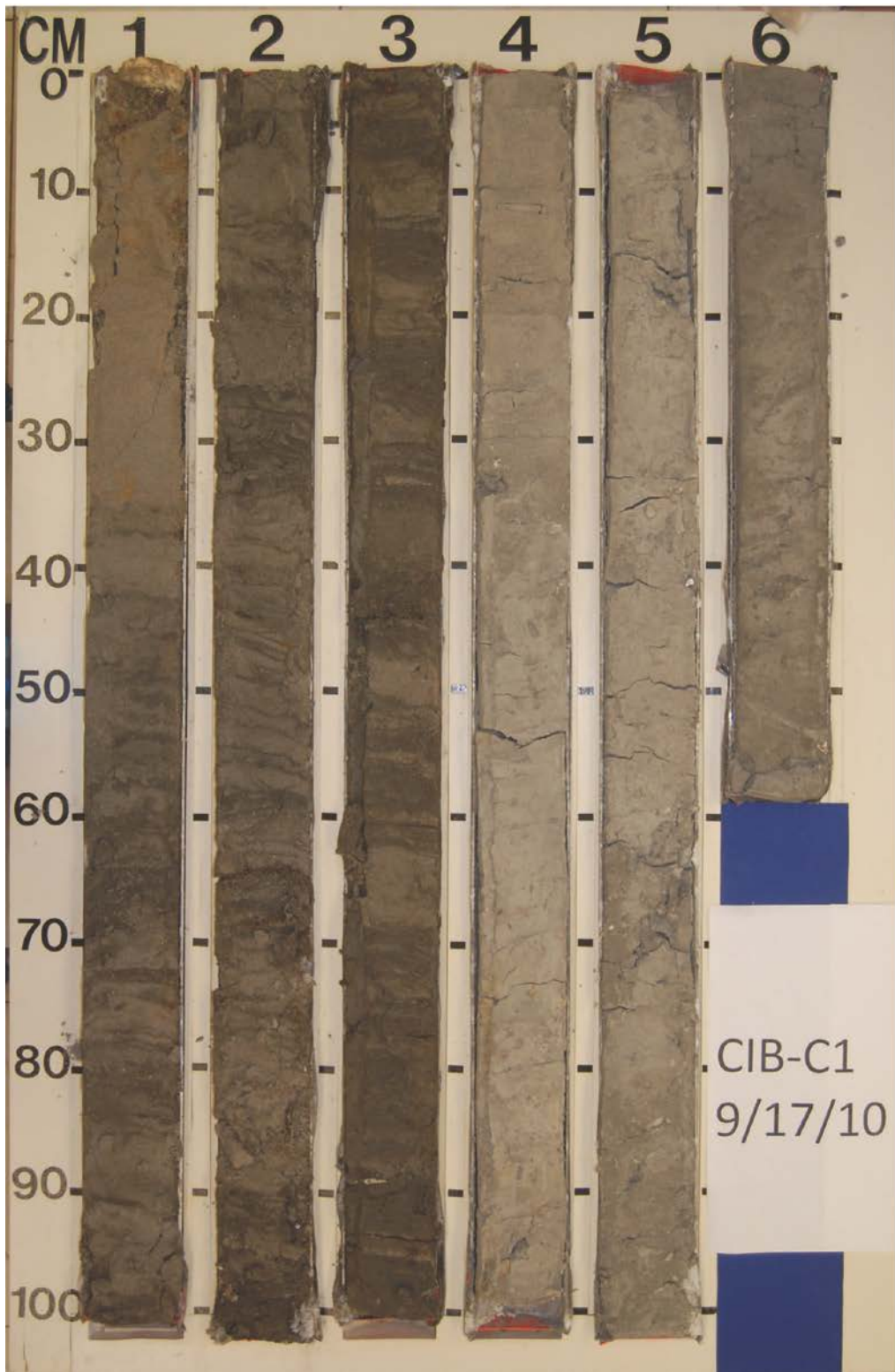
VIBRACORE DESCRIPTION SHEET

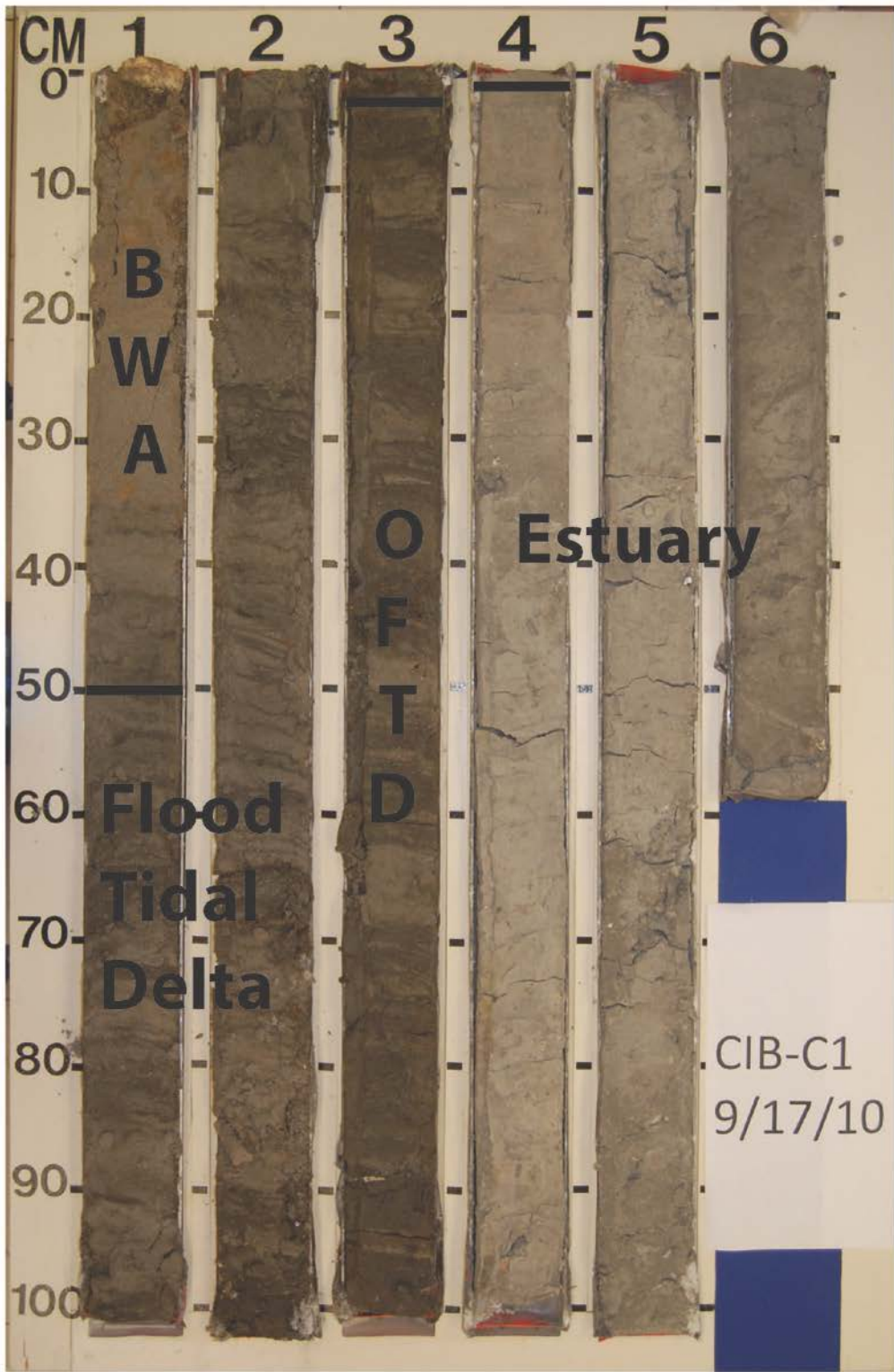
CORE ID: 026-101010-PA8 DATE COLLECTED: 10/10/10 DESCRIBED BY: HANLEY
 ELEVATION: ~1m MSL COMPACTION: _____ DATE DESCRIBED: 8/13/12
 CORE LENGTH: _____ LAT/LONG: 37°36'55.922"N 75°36'54.094"W
 TOTAL DEPTH: 3.00m LOCATION: N OF INLET NEAR DUNES



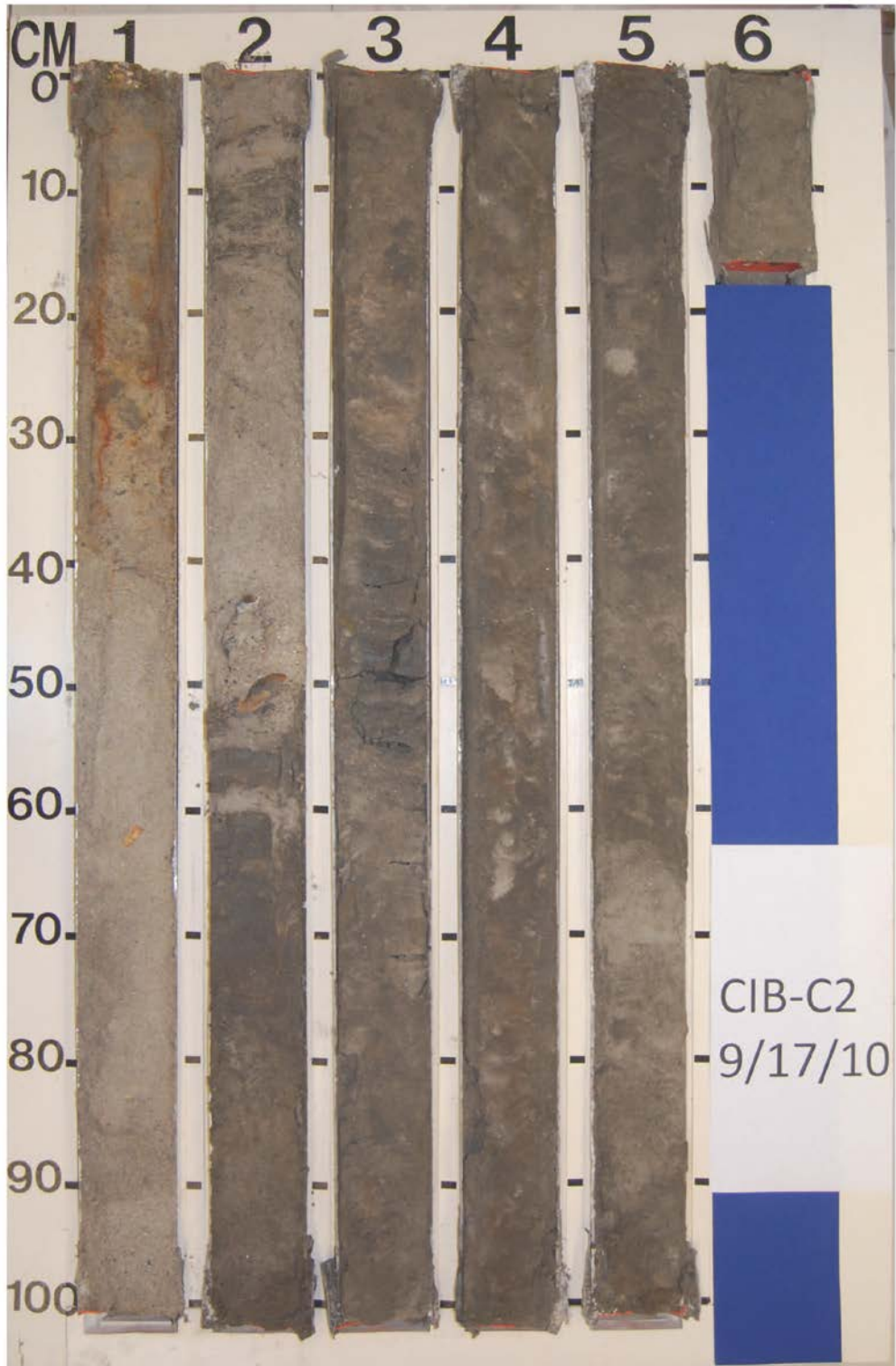
Appendix B – Vibracore photographs

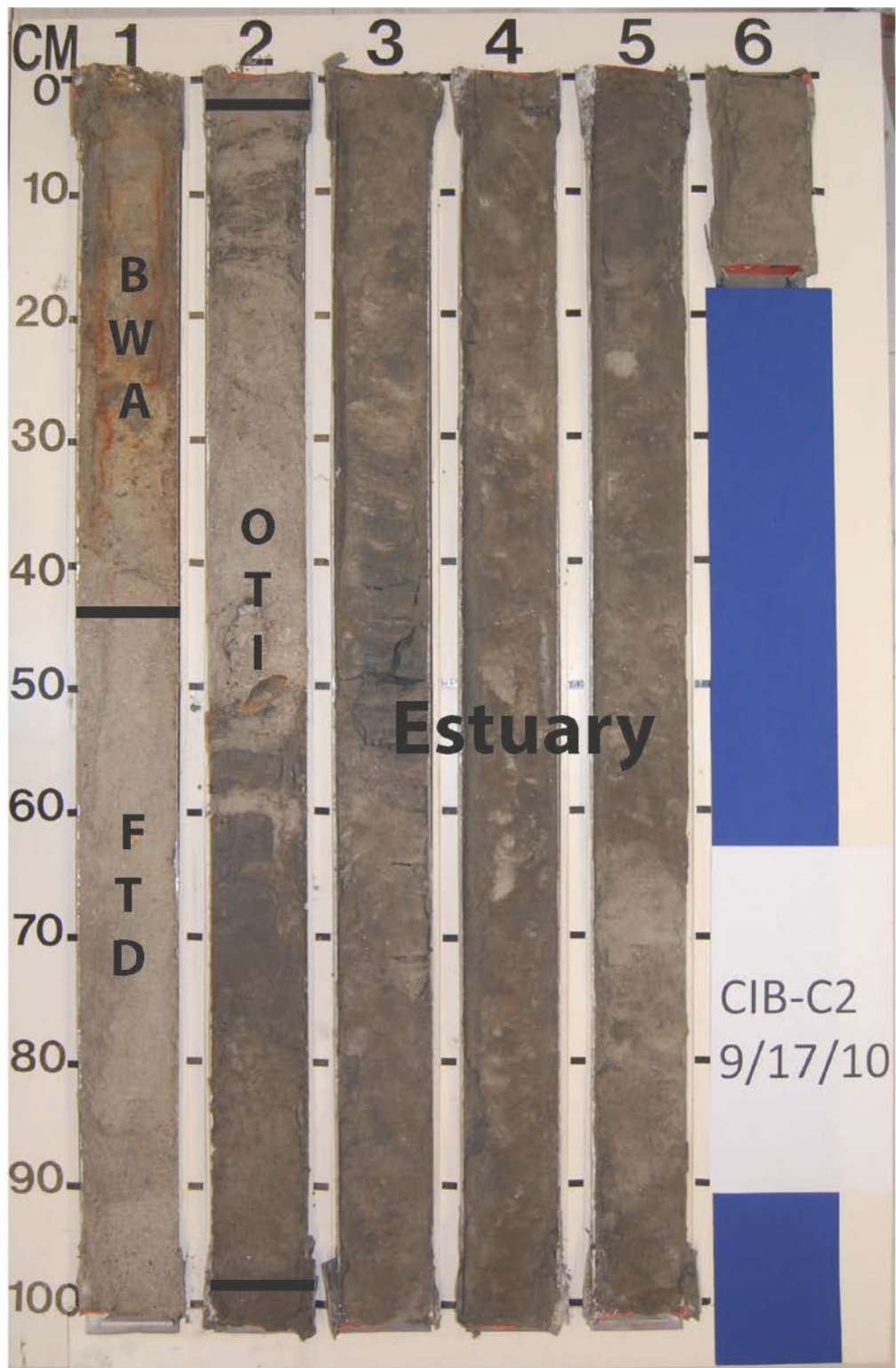
Vibracore C1



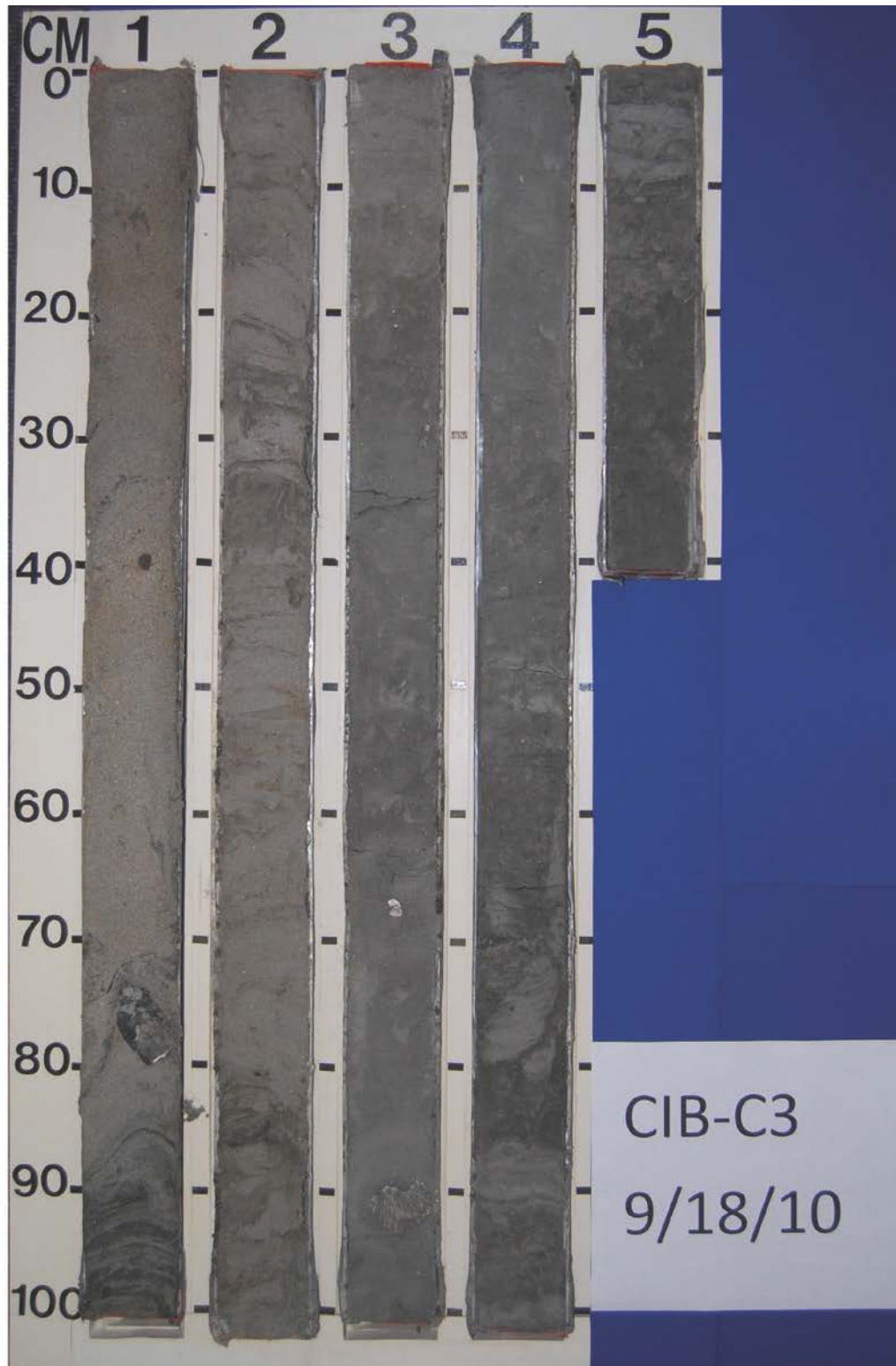


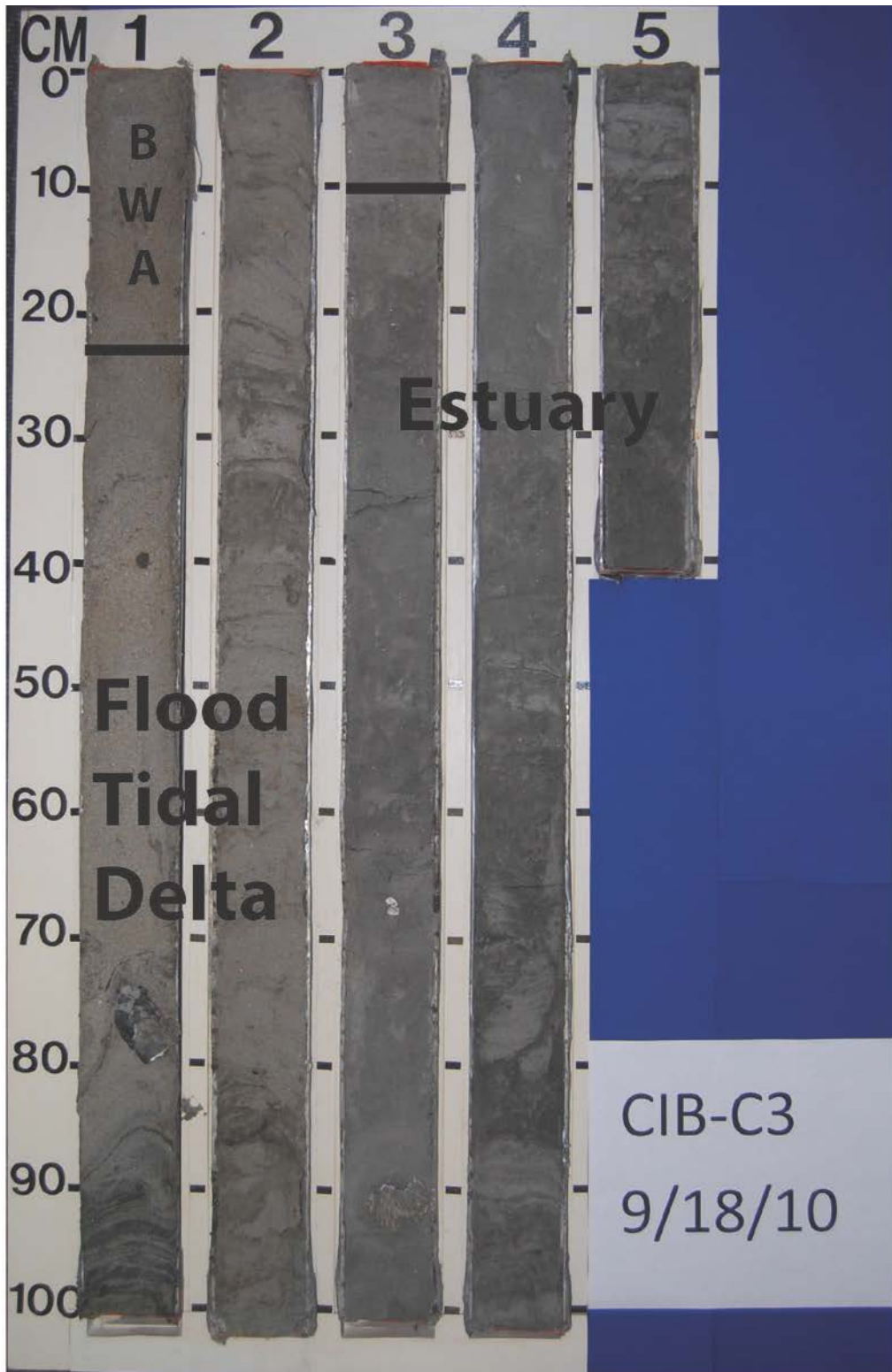
Vibracore C2



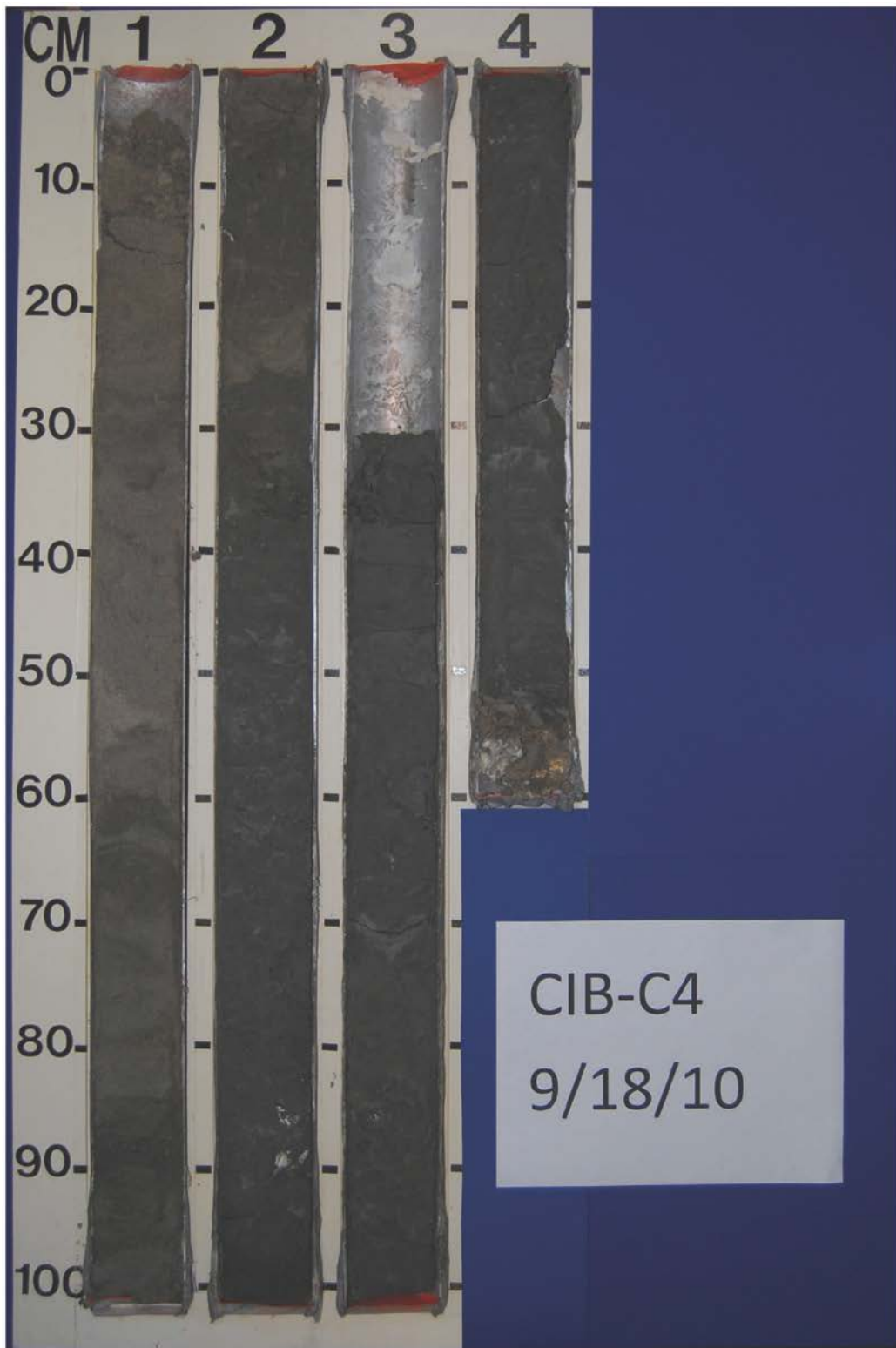


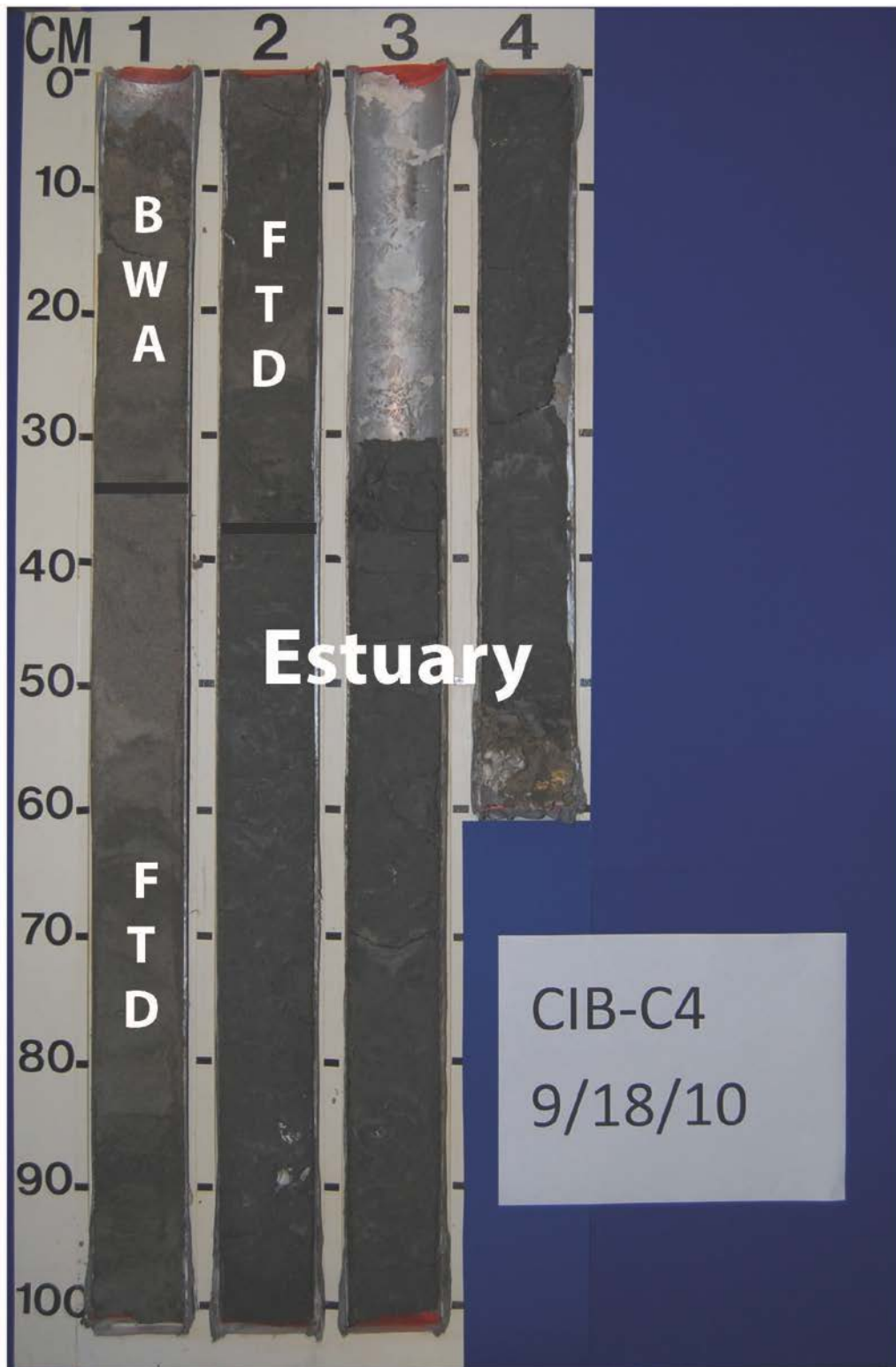
Vibracore C3



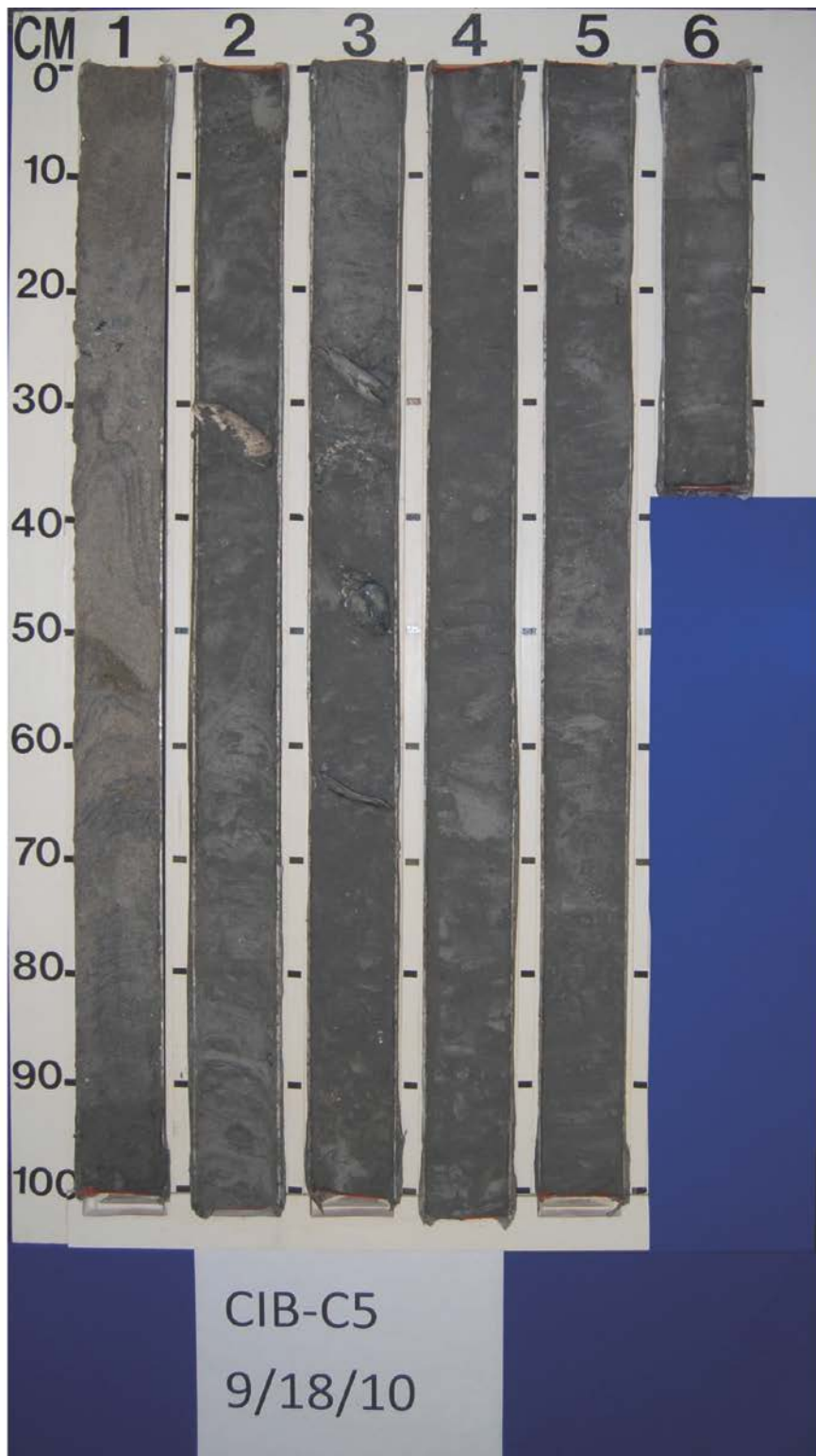


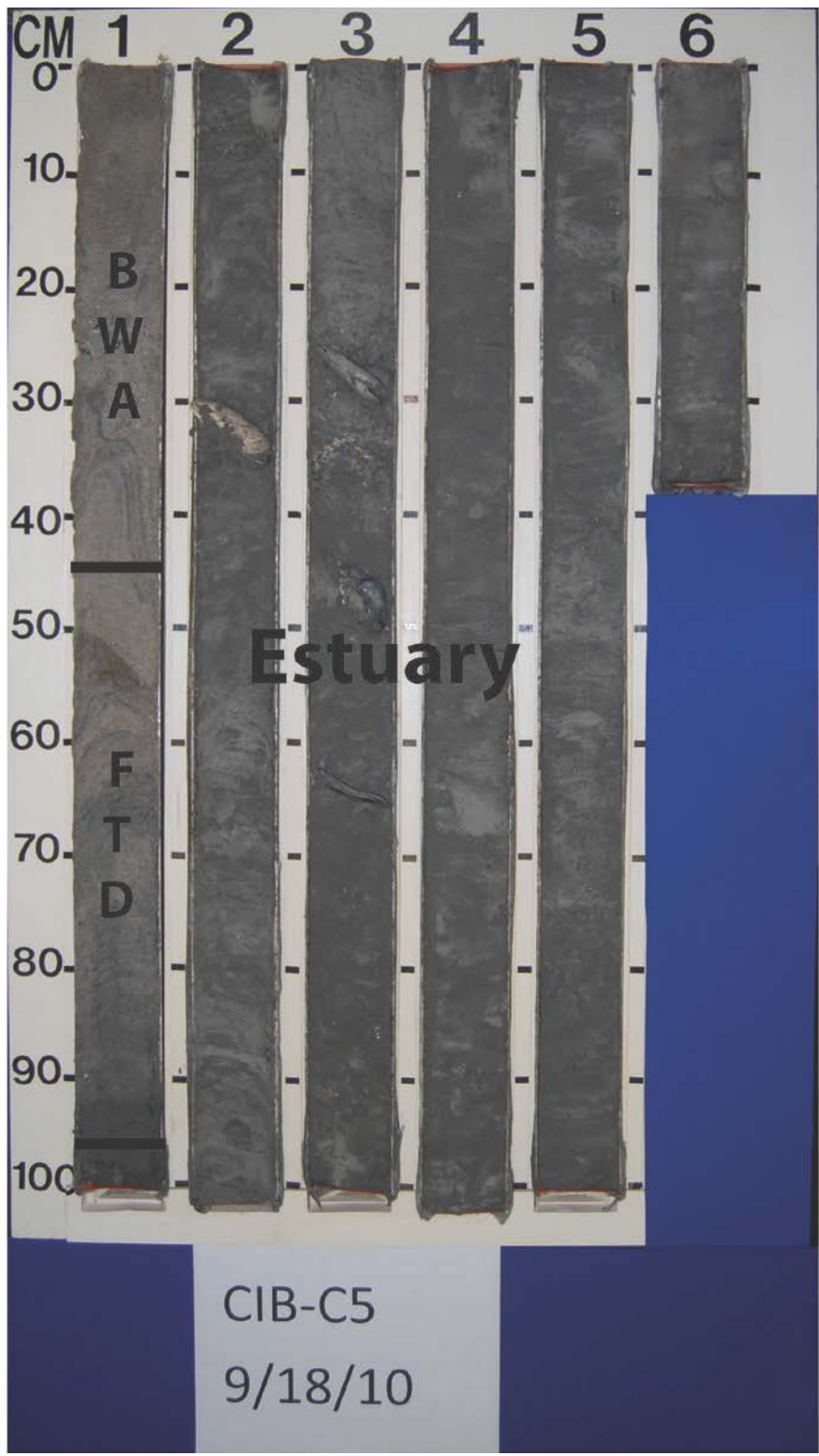
Vibracore C4



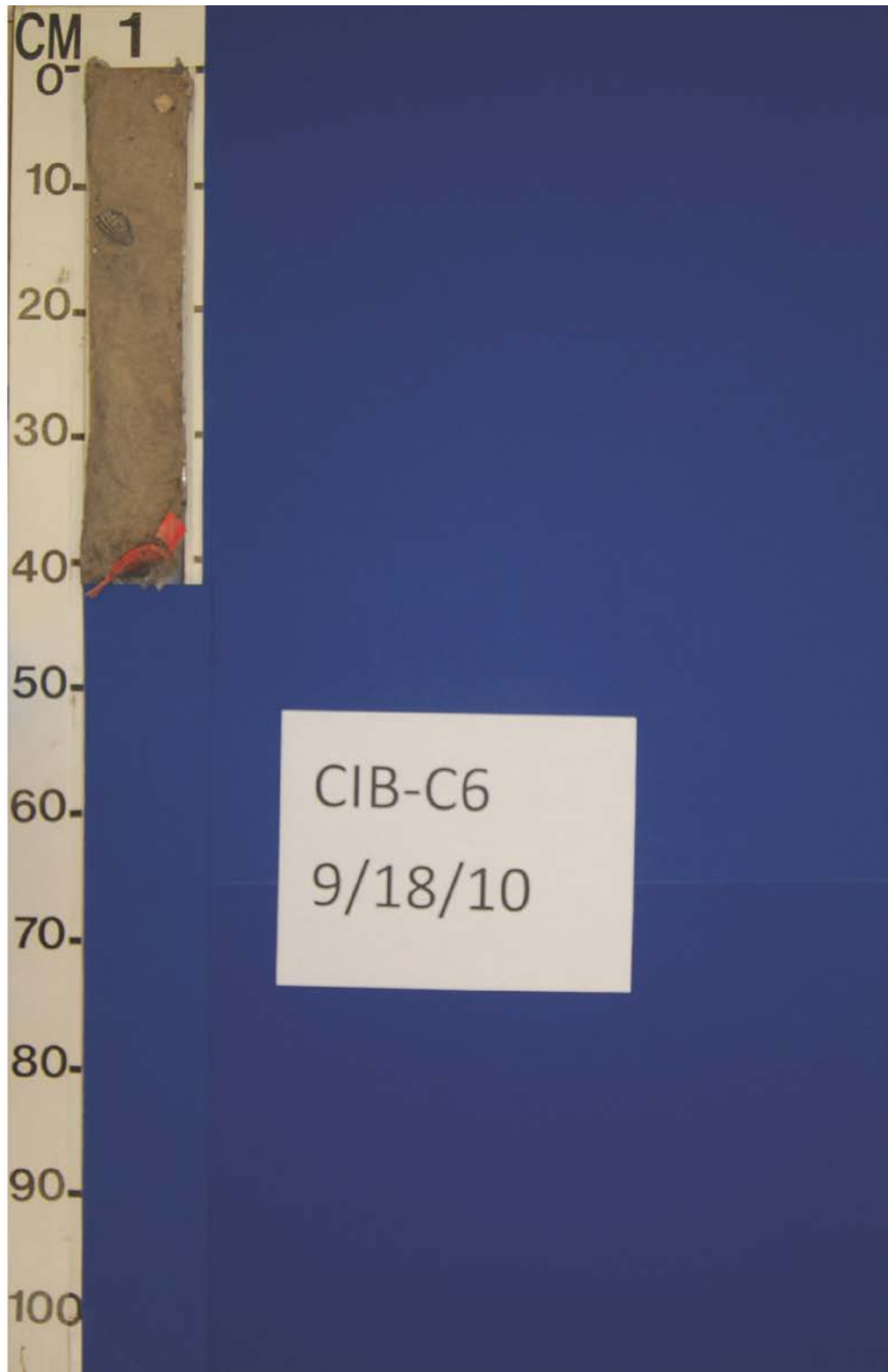


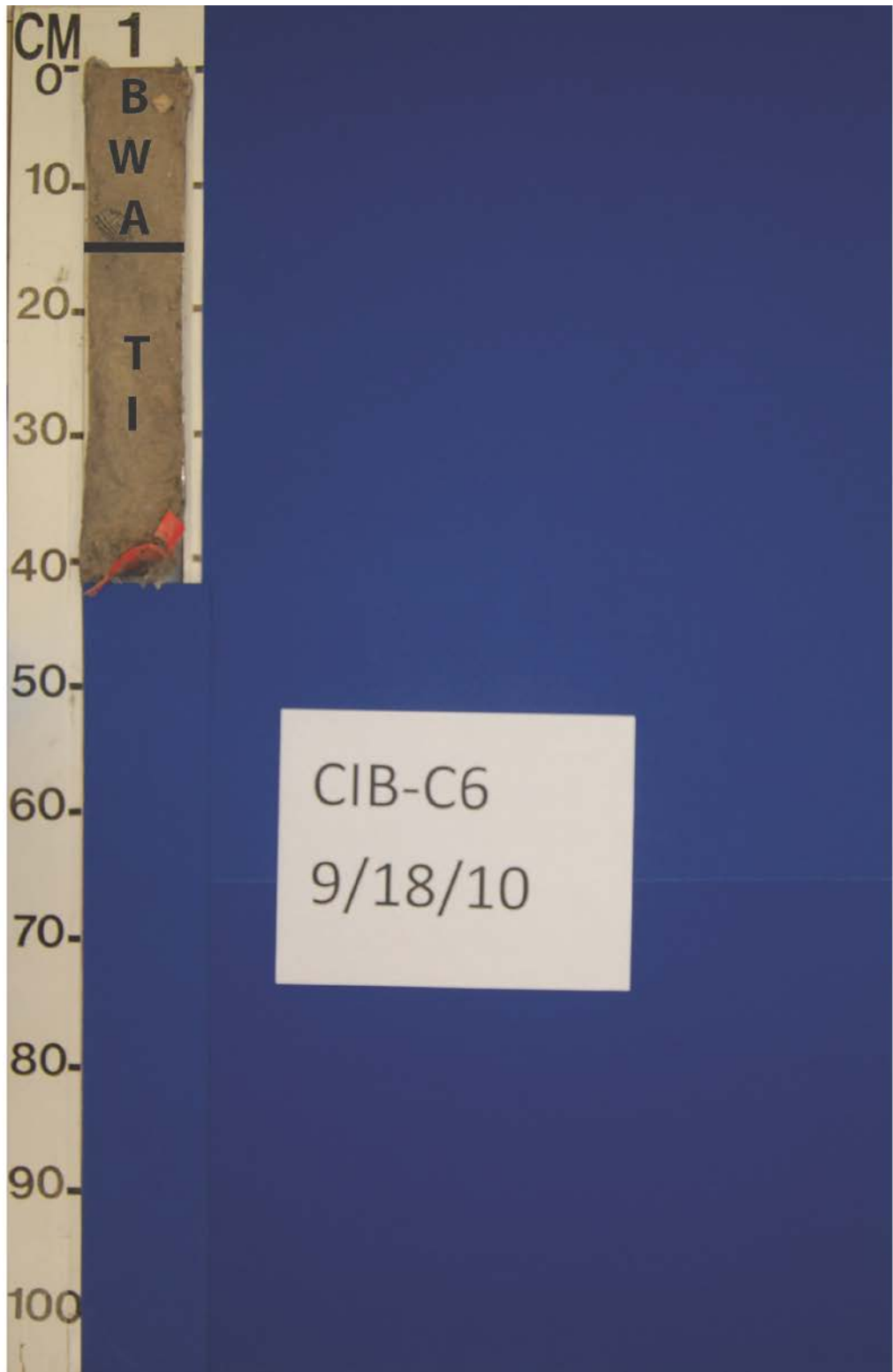
Vibracore C5



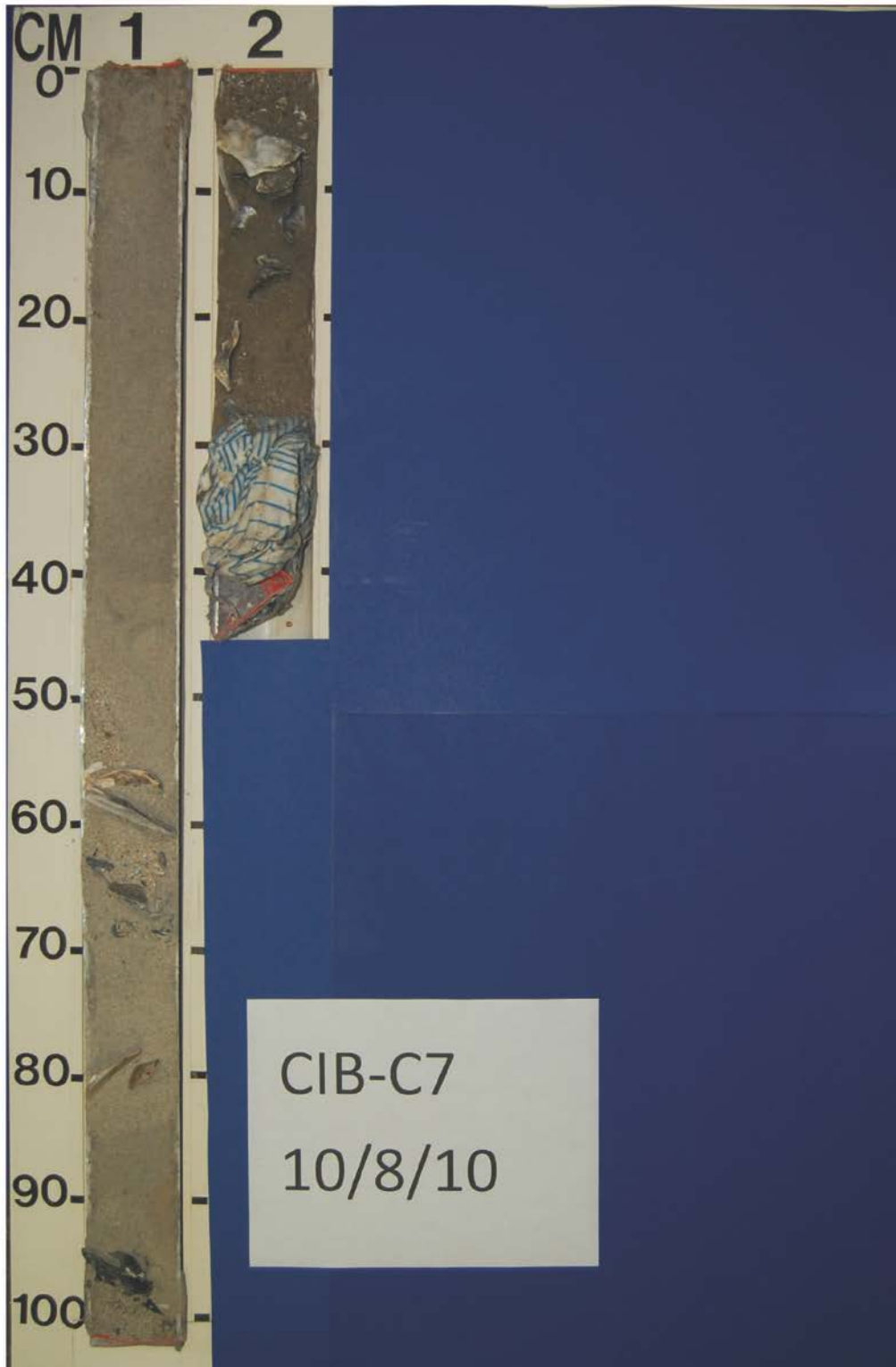


Vibracore C6



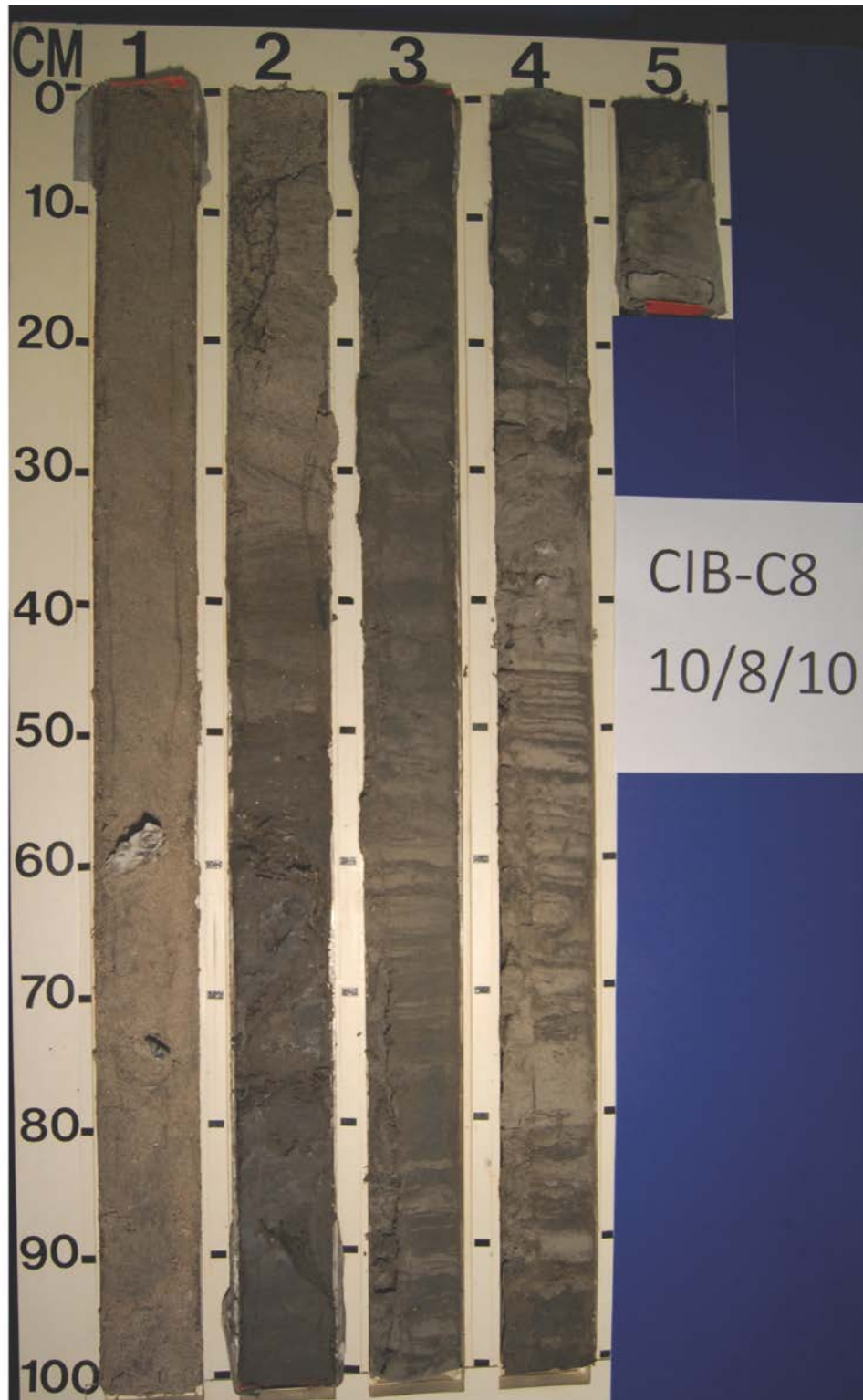


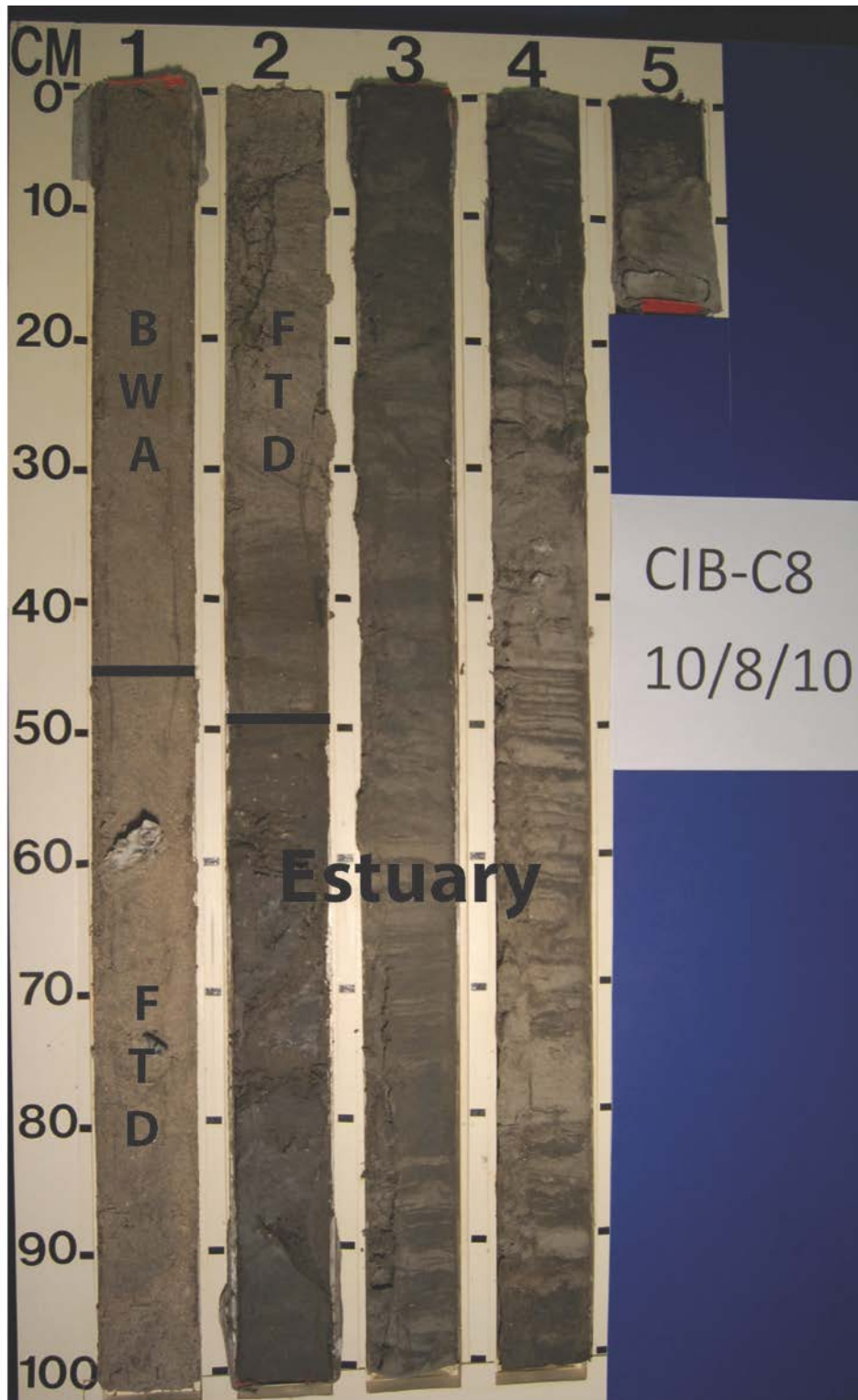
Vibracore C7



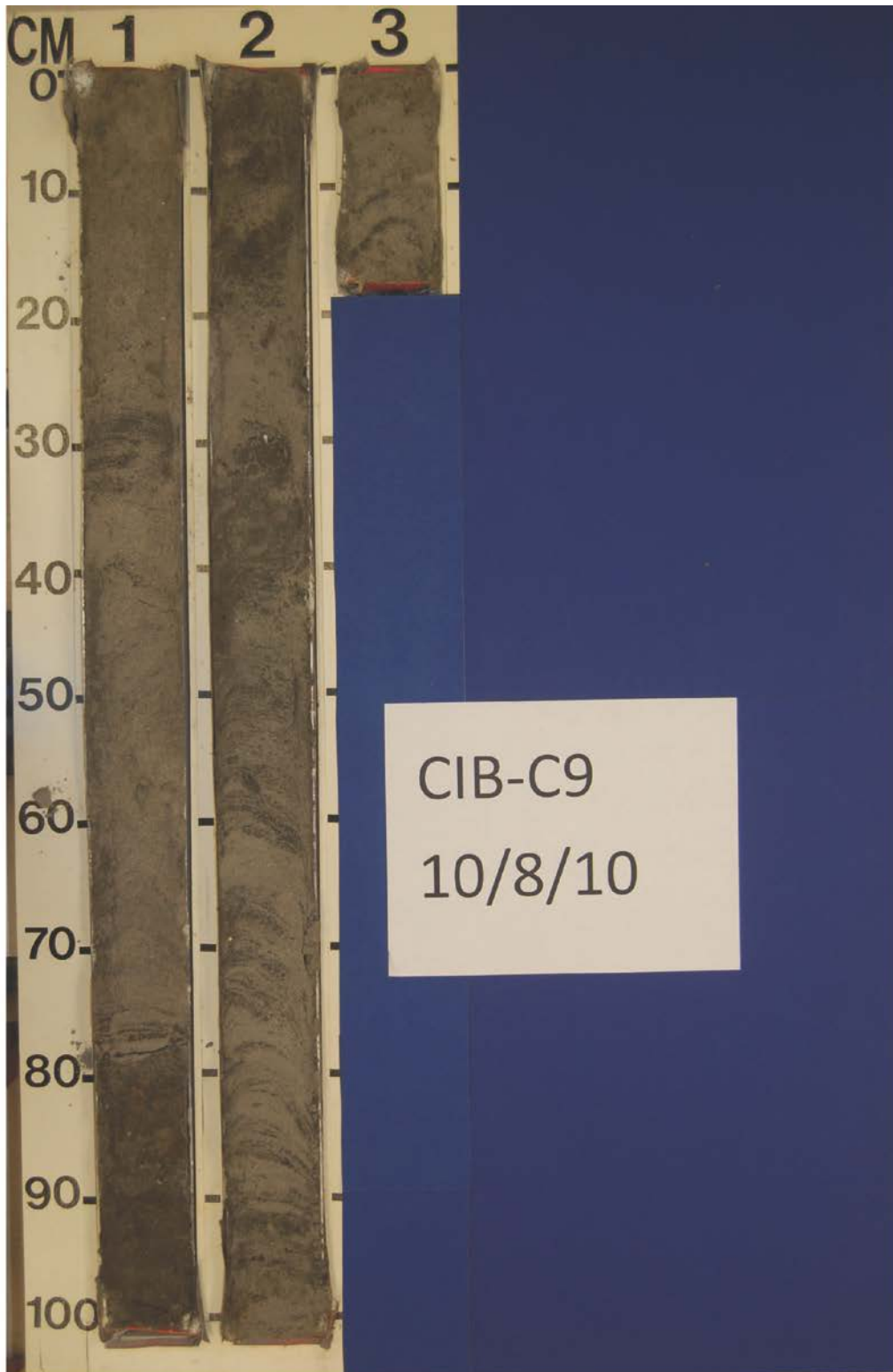


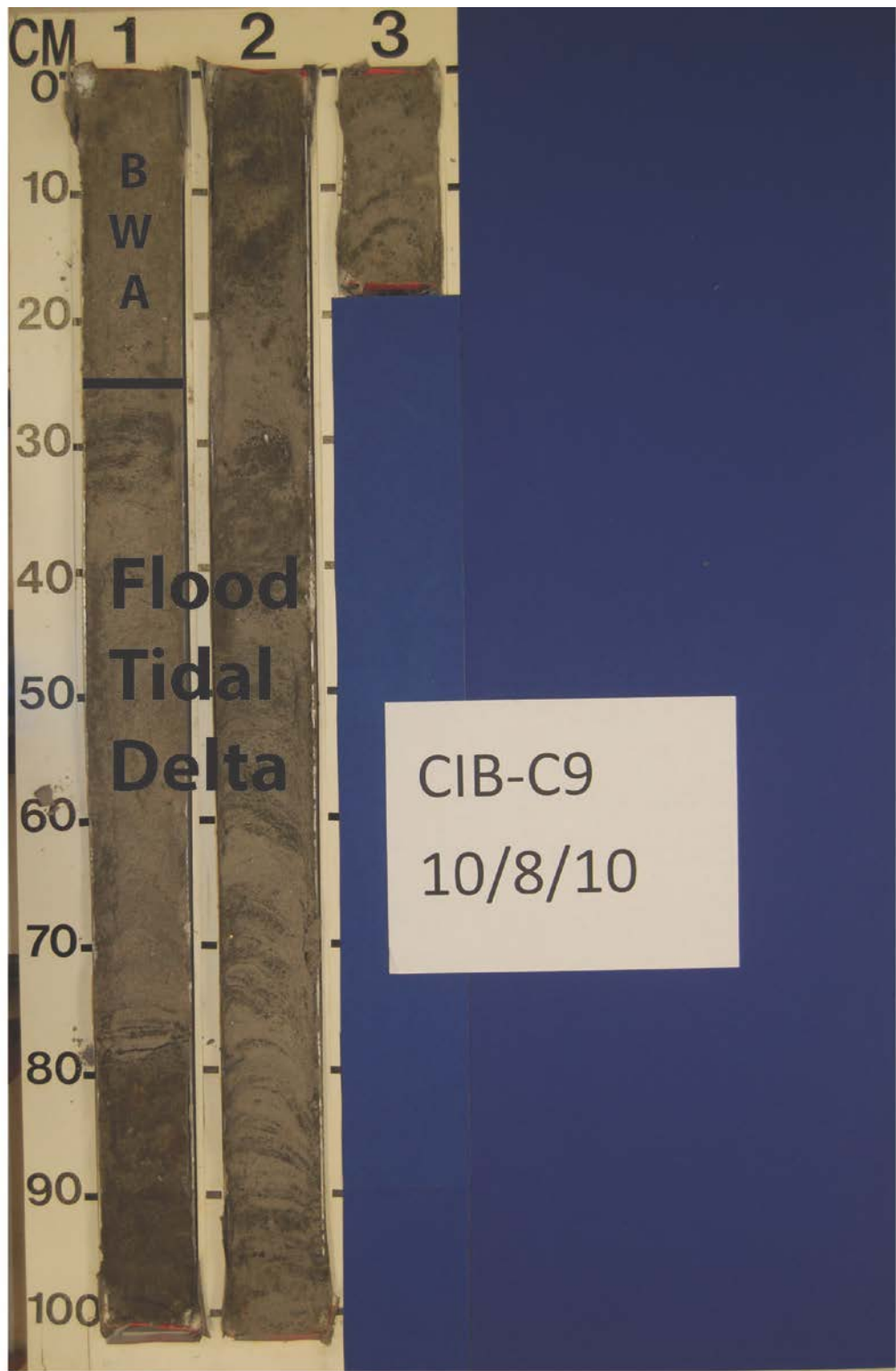
Vibracore C8



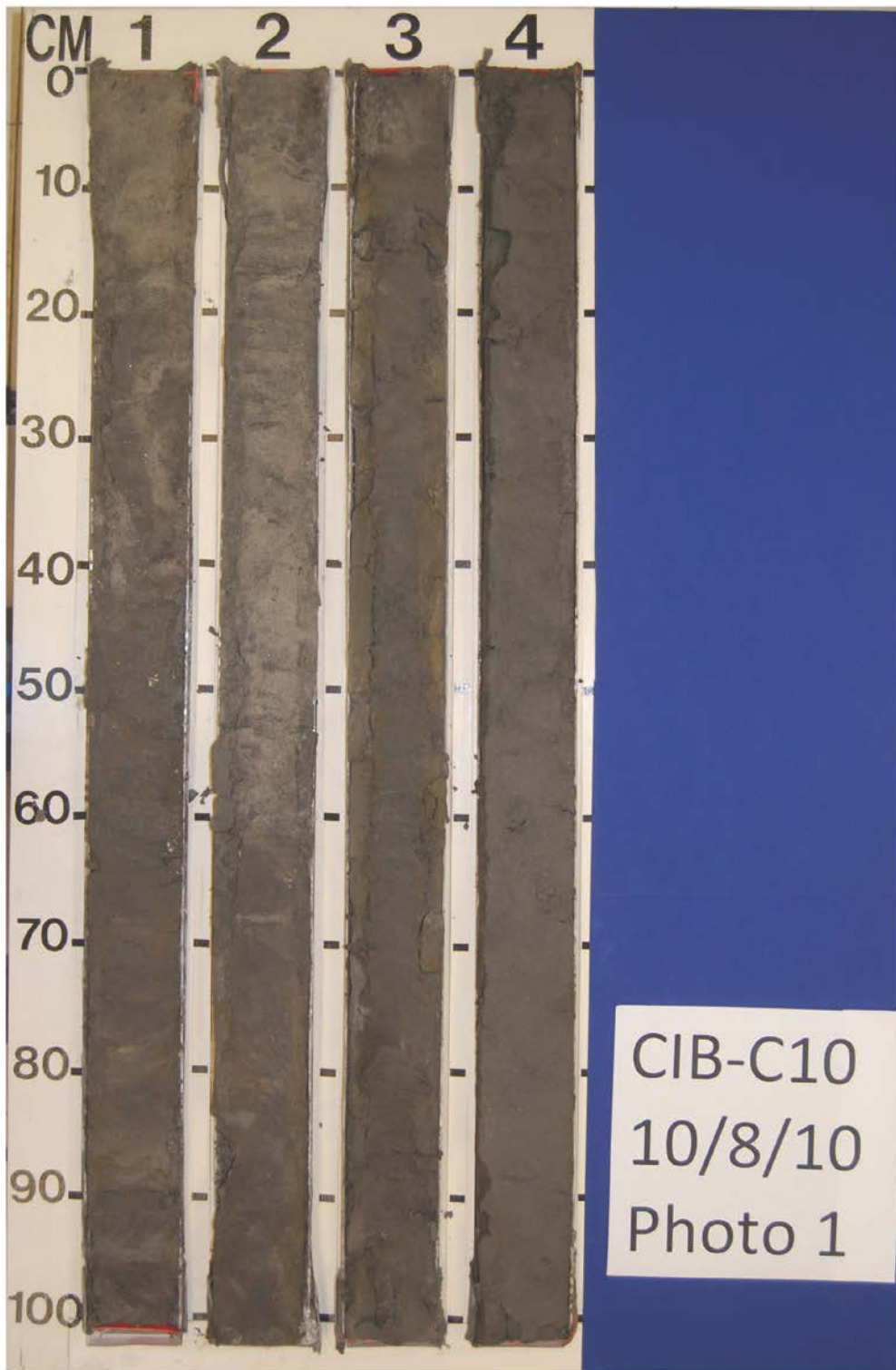


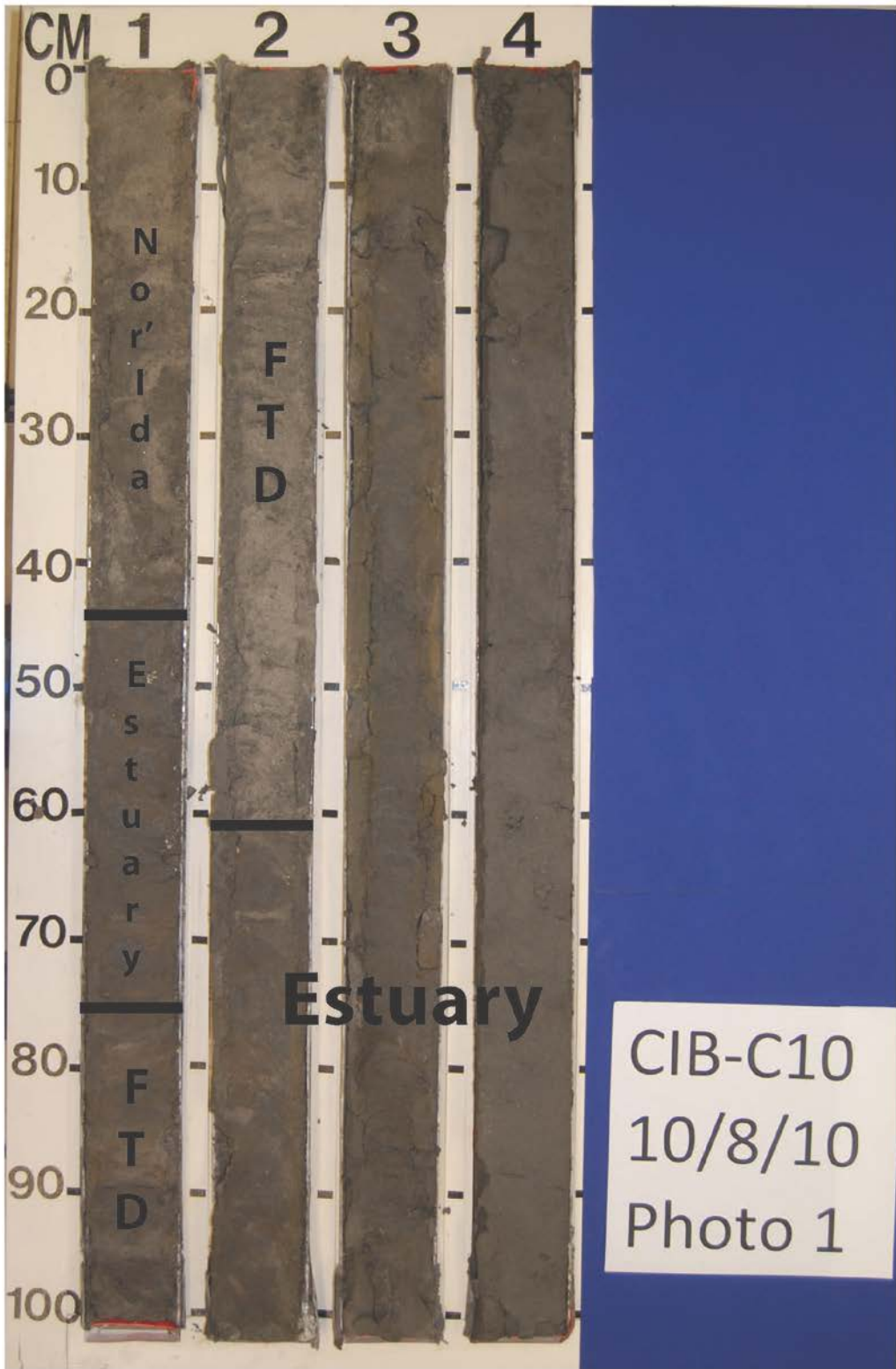
Vibracore C9

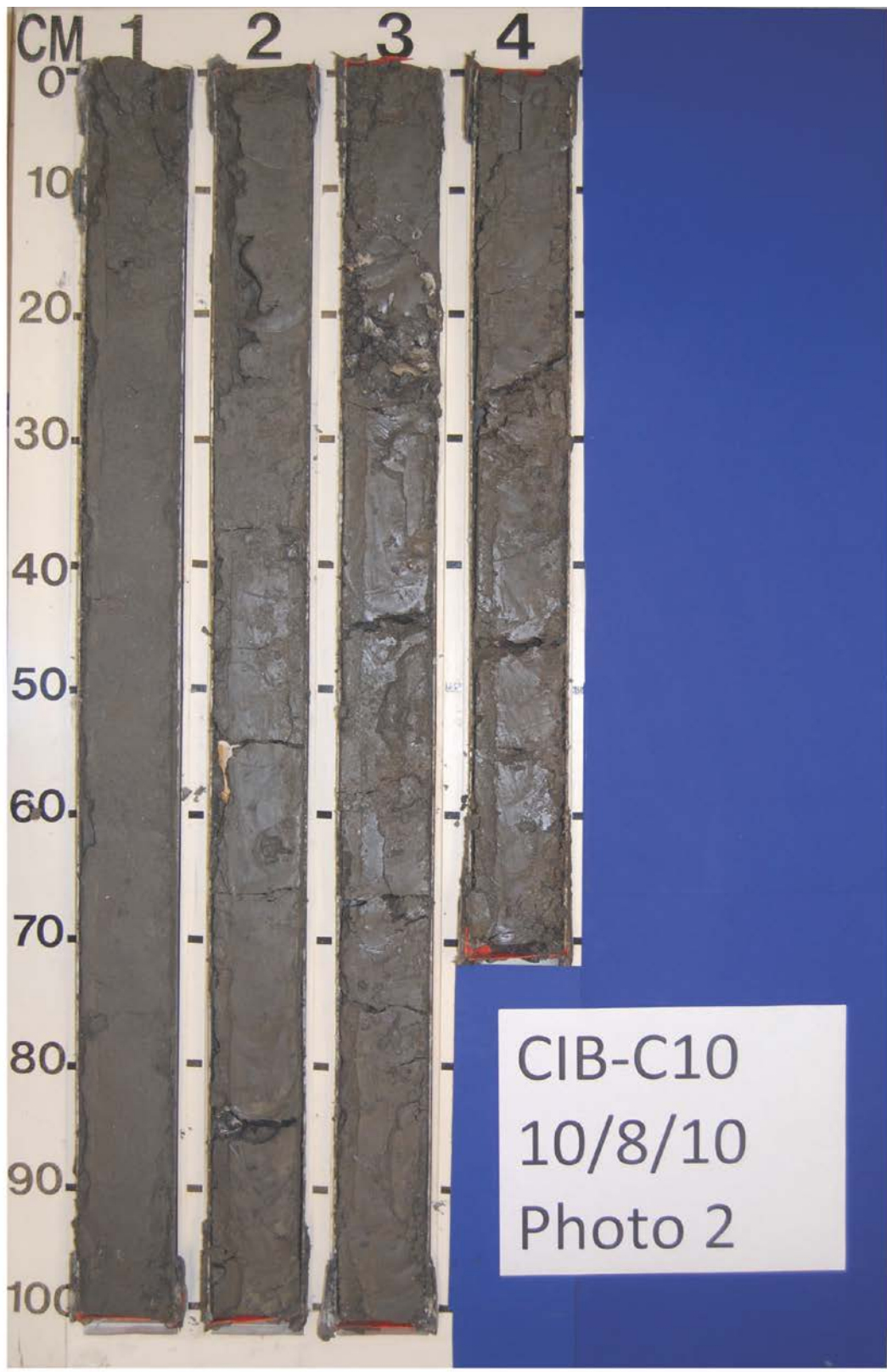


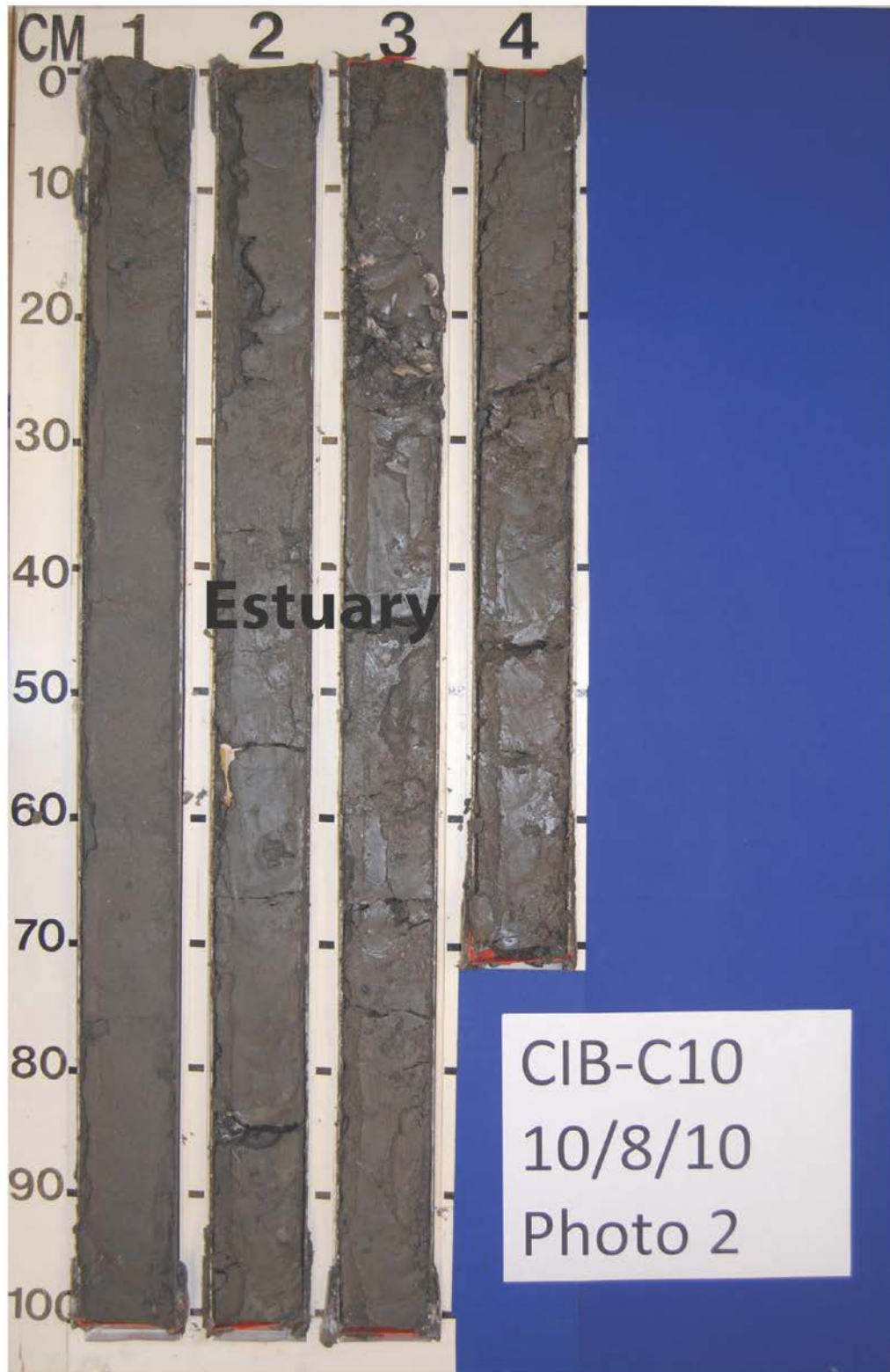


Vibracore C10

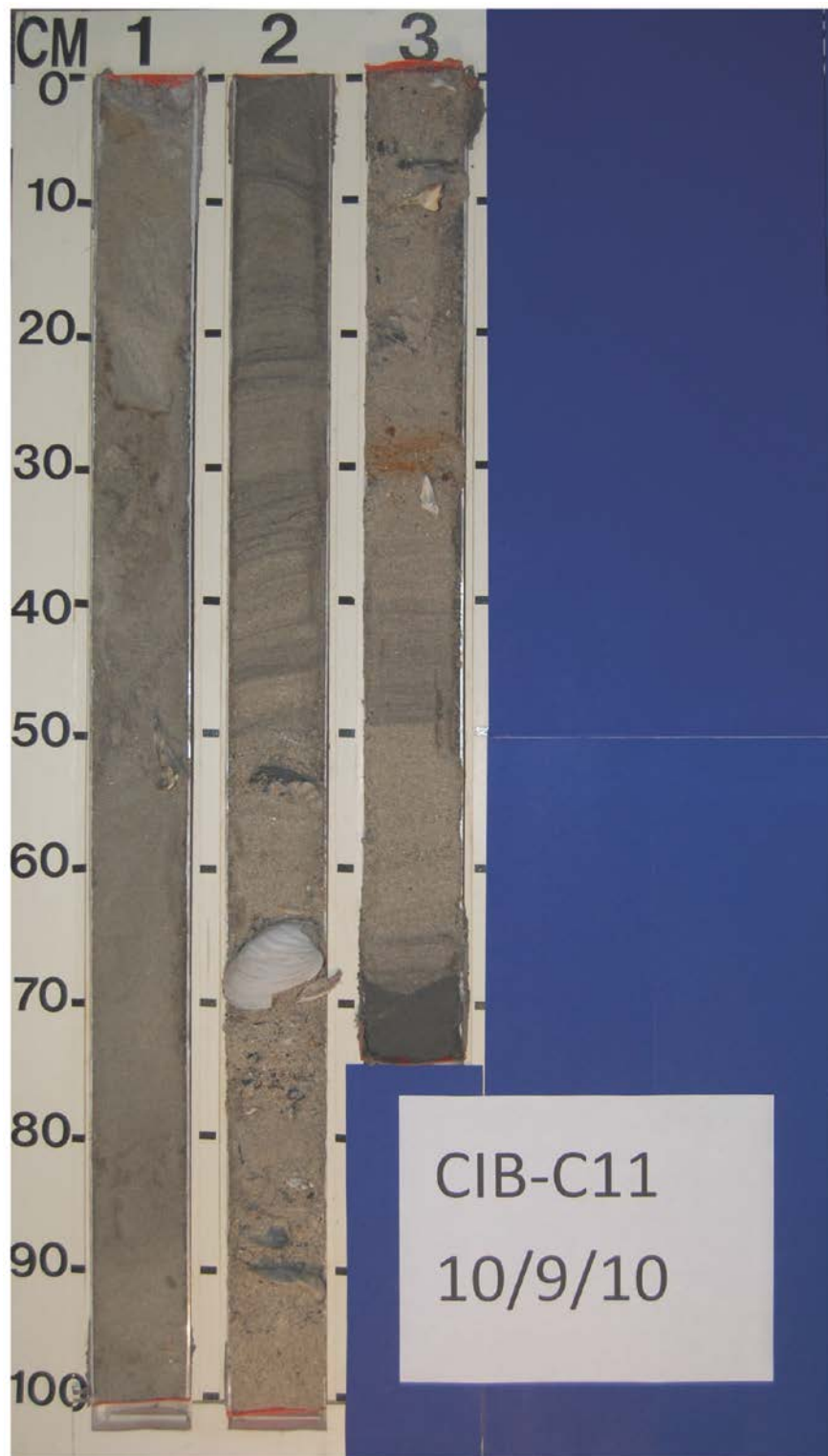


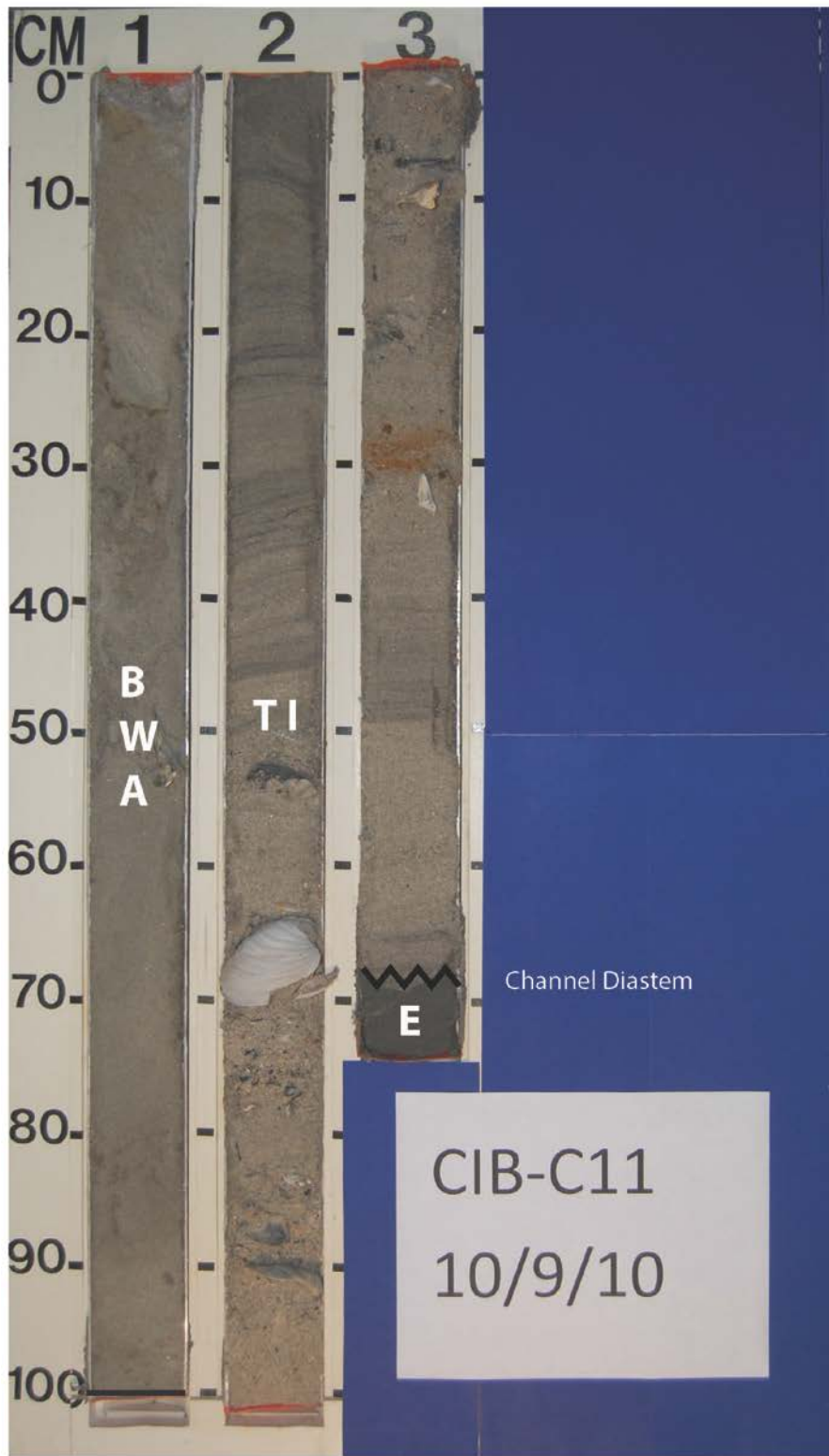






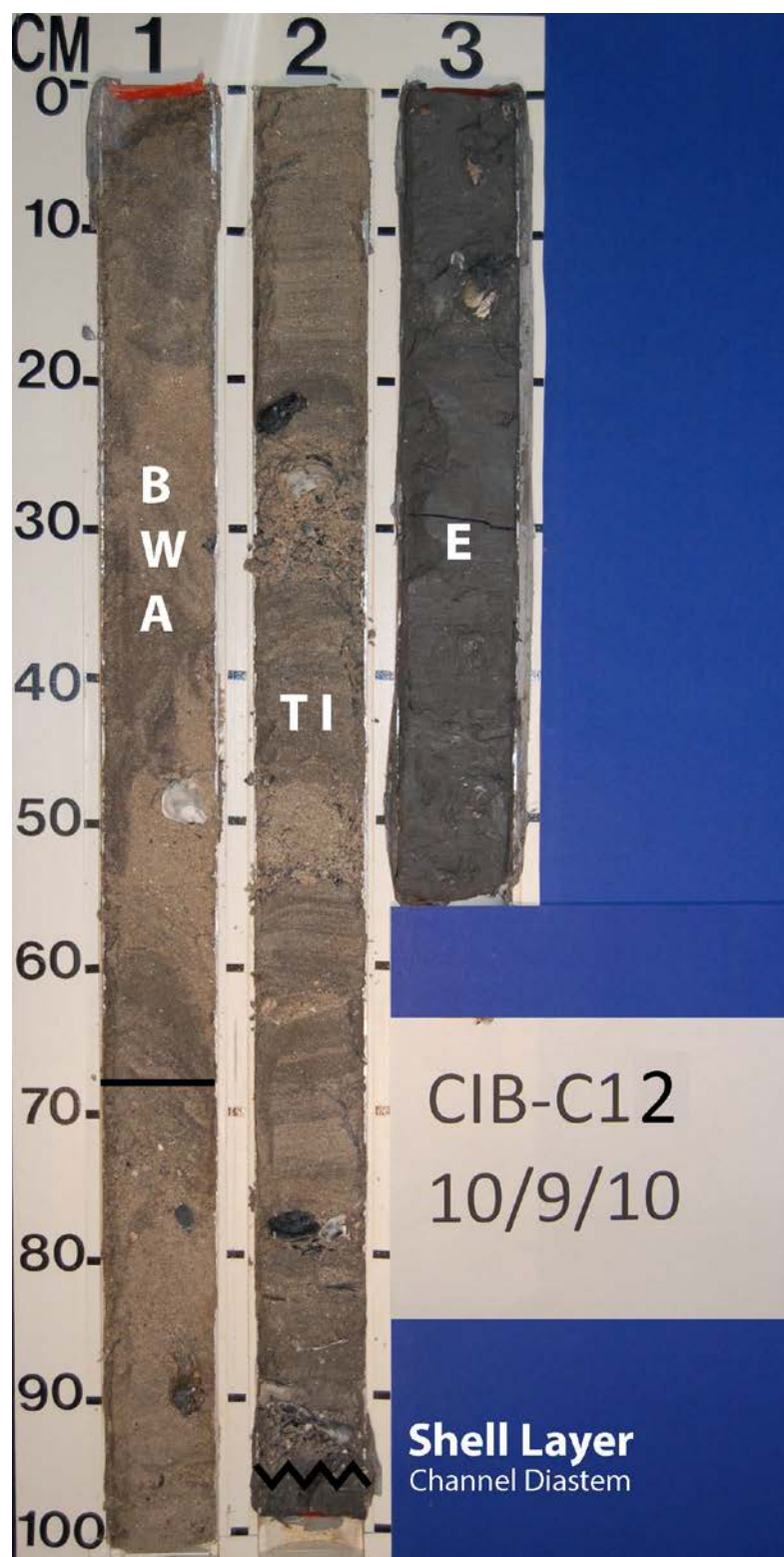
Vibracore C11



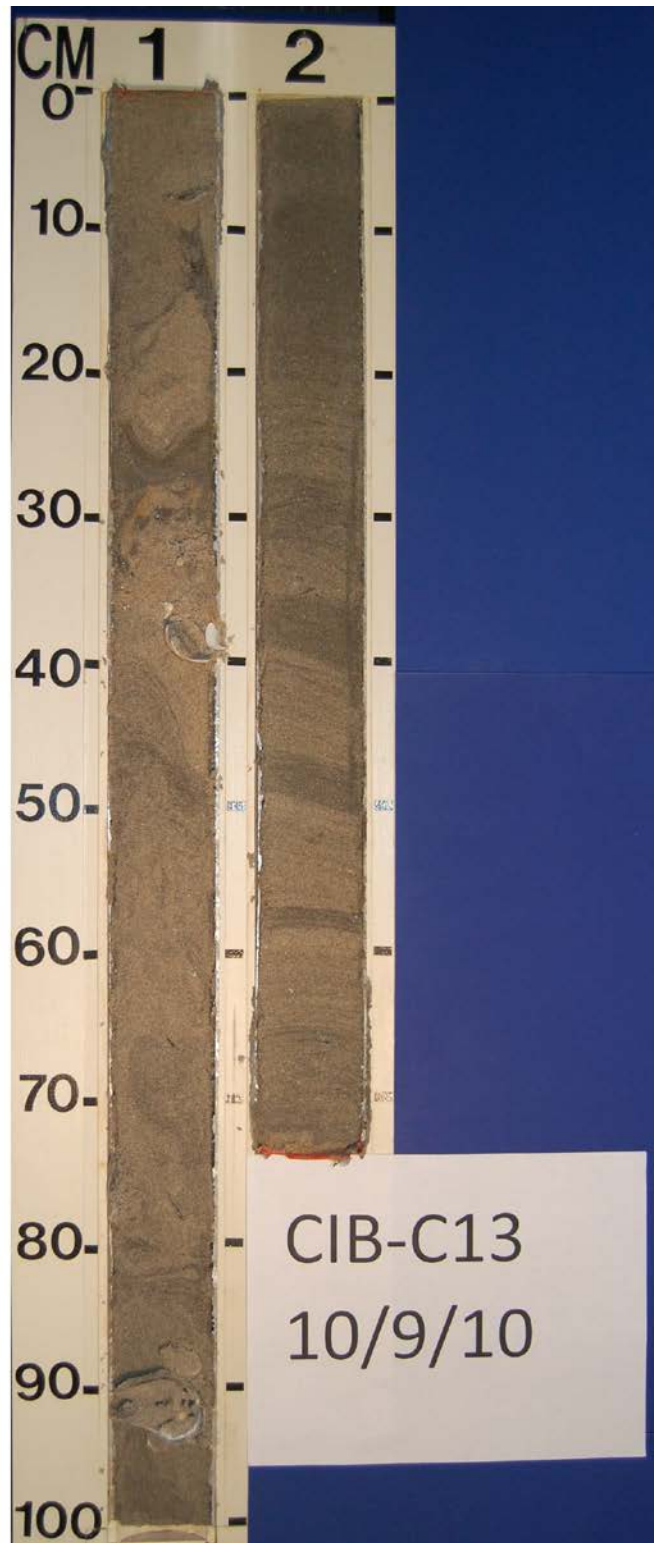


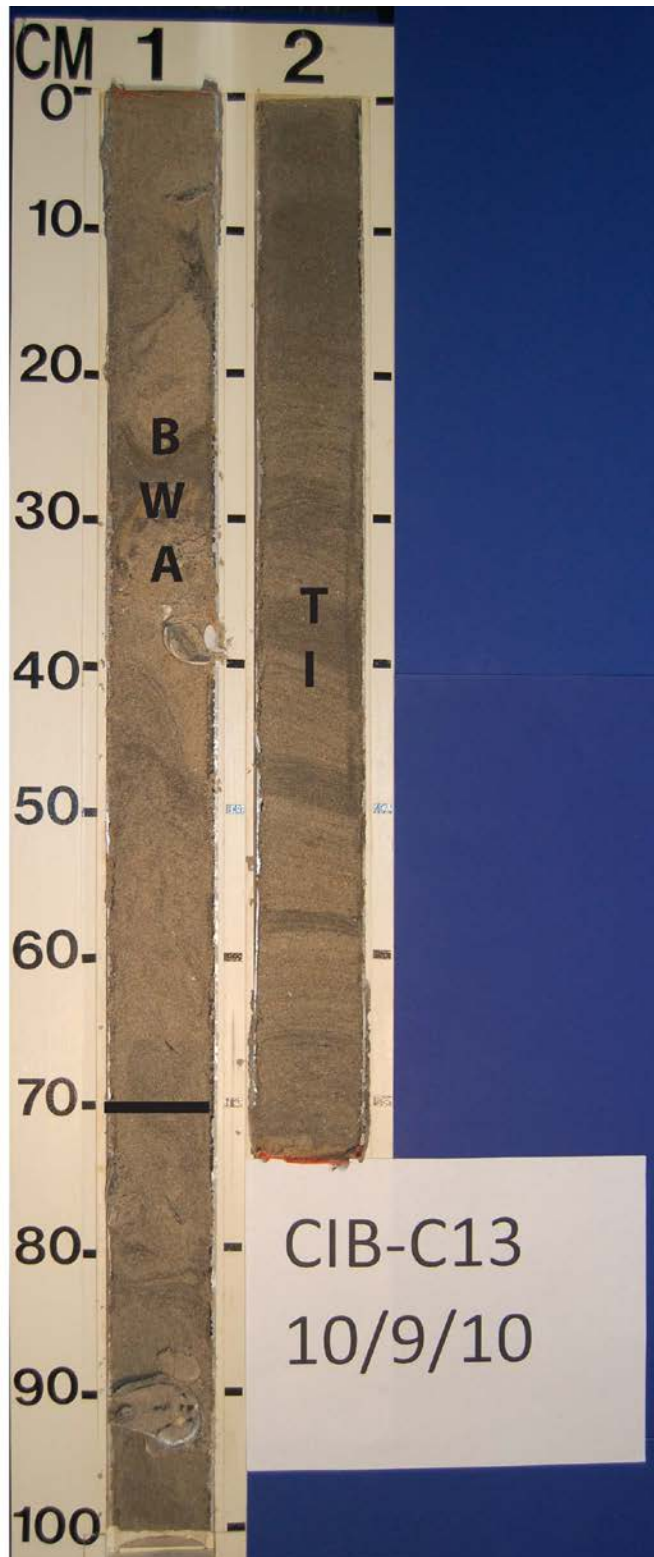
Vibracore C12



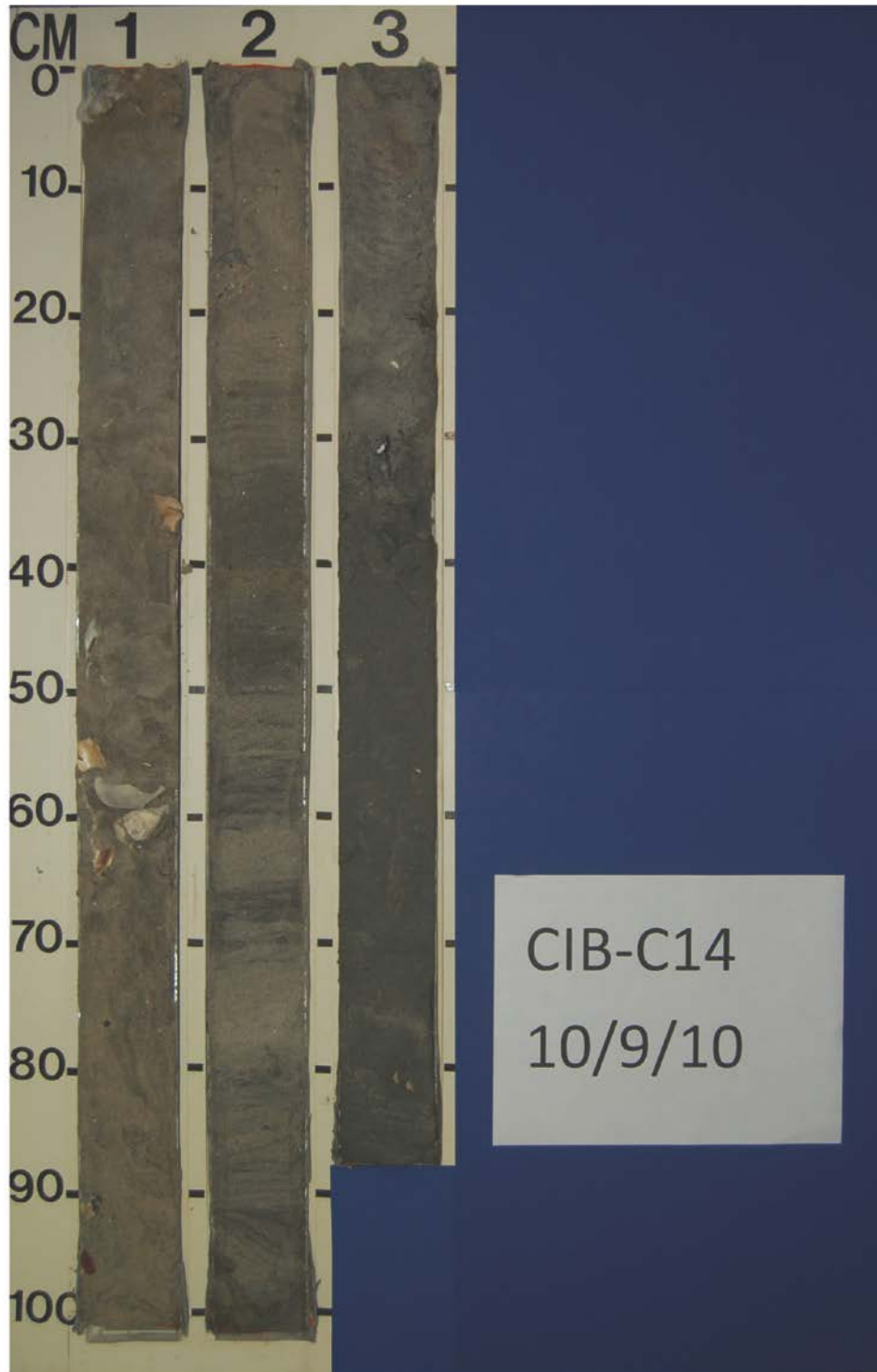


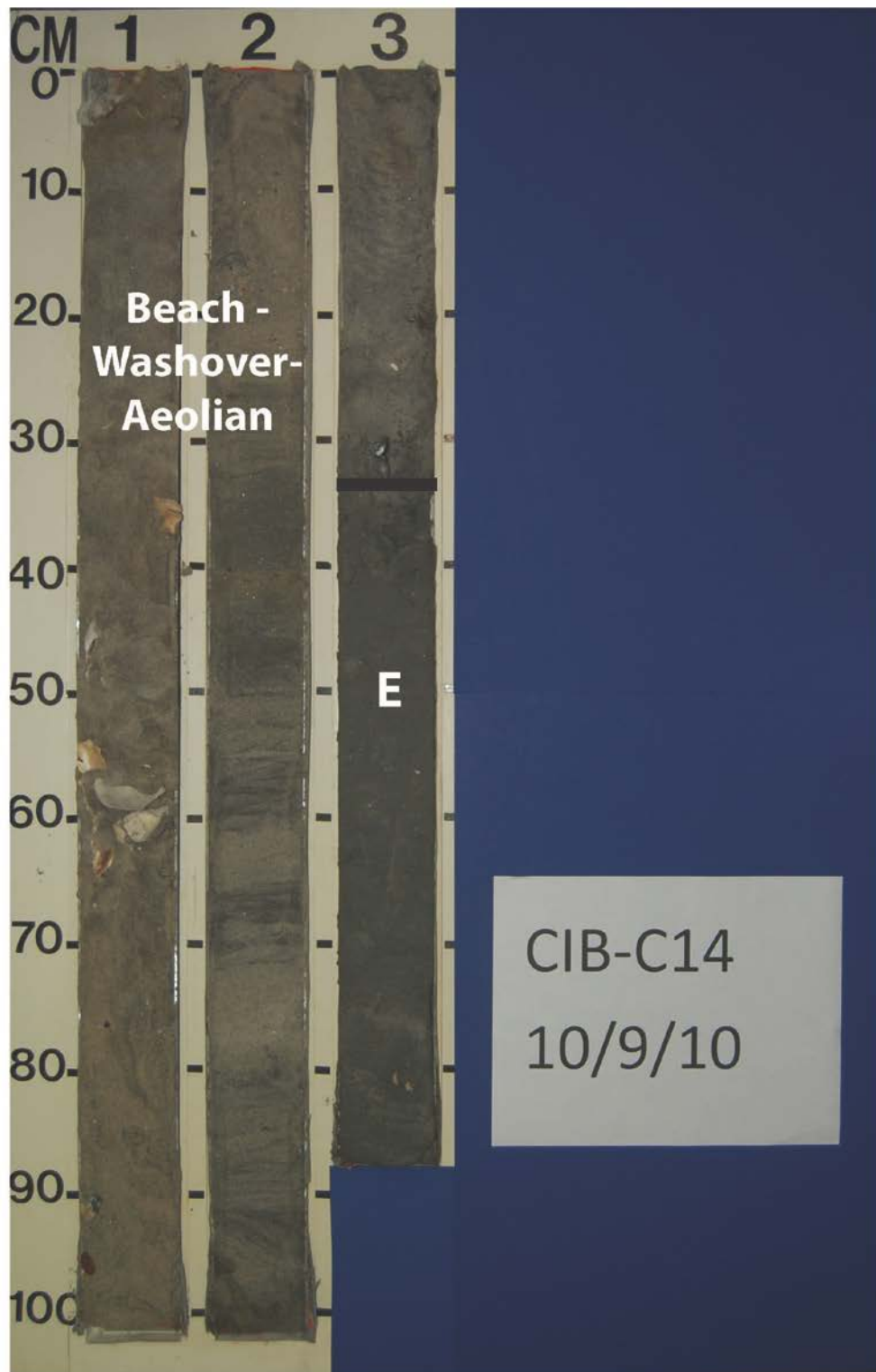
Vibracore C13



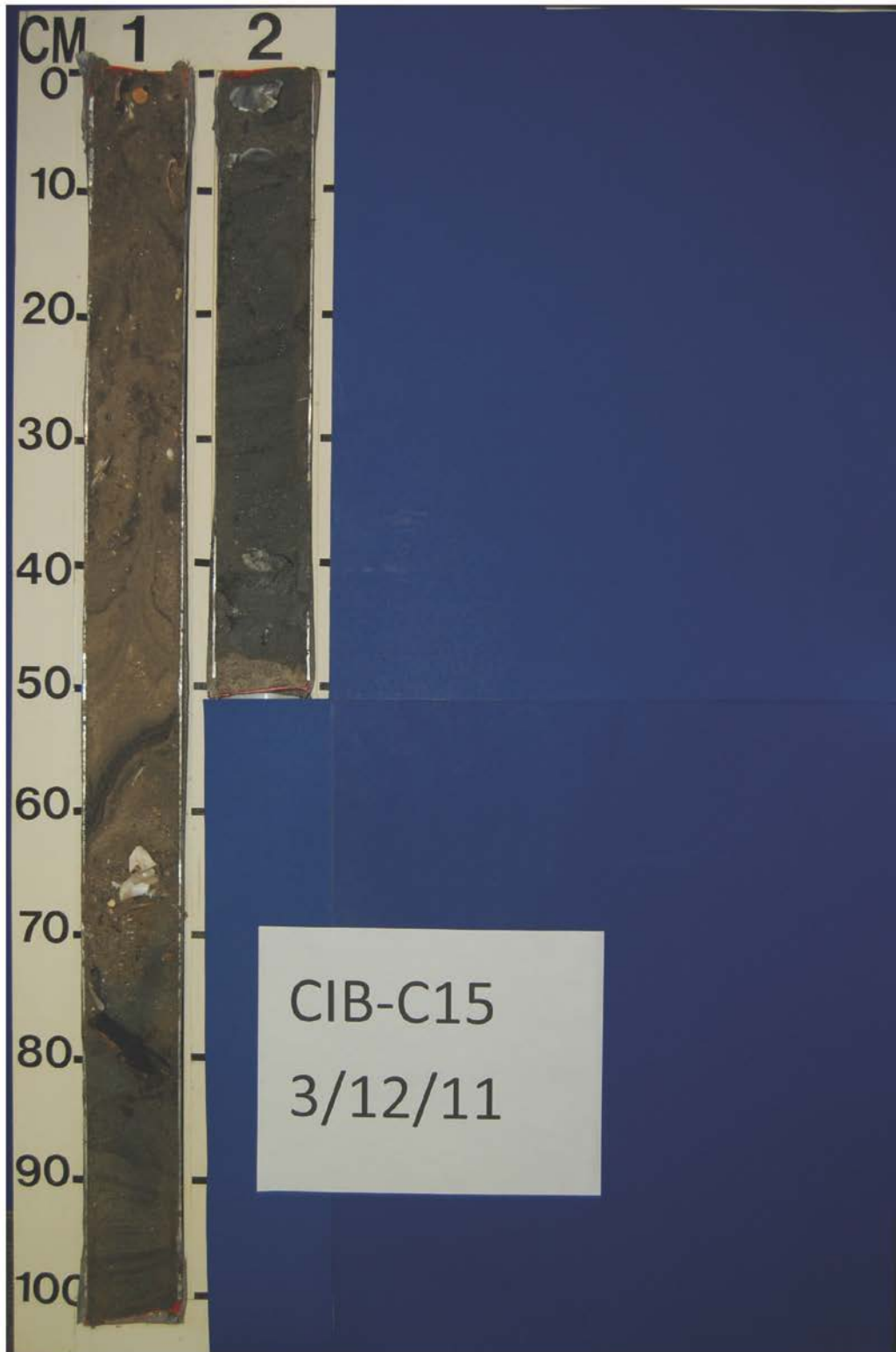


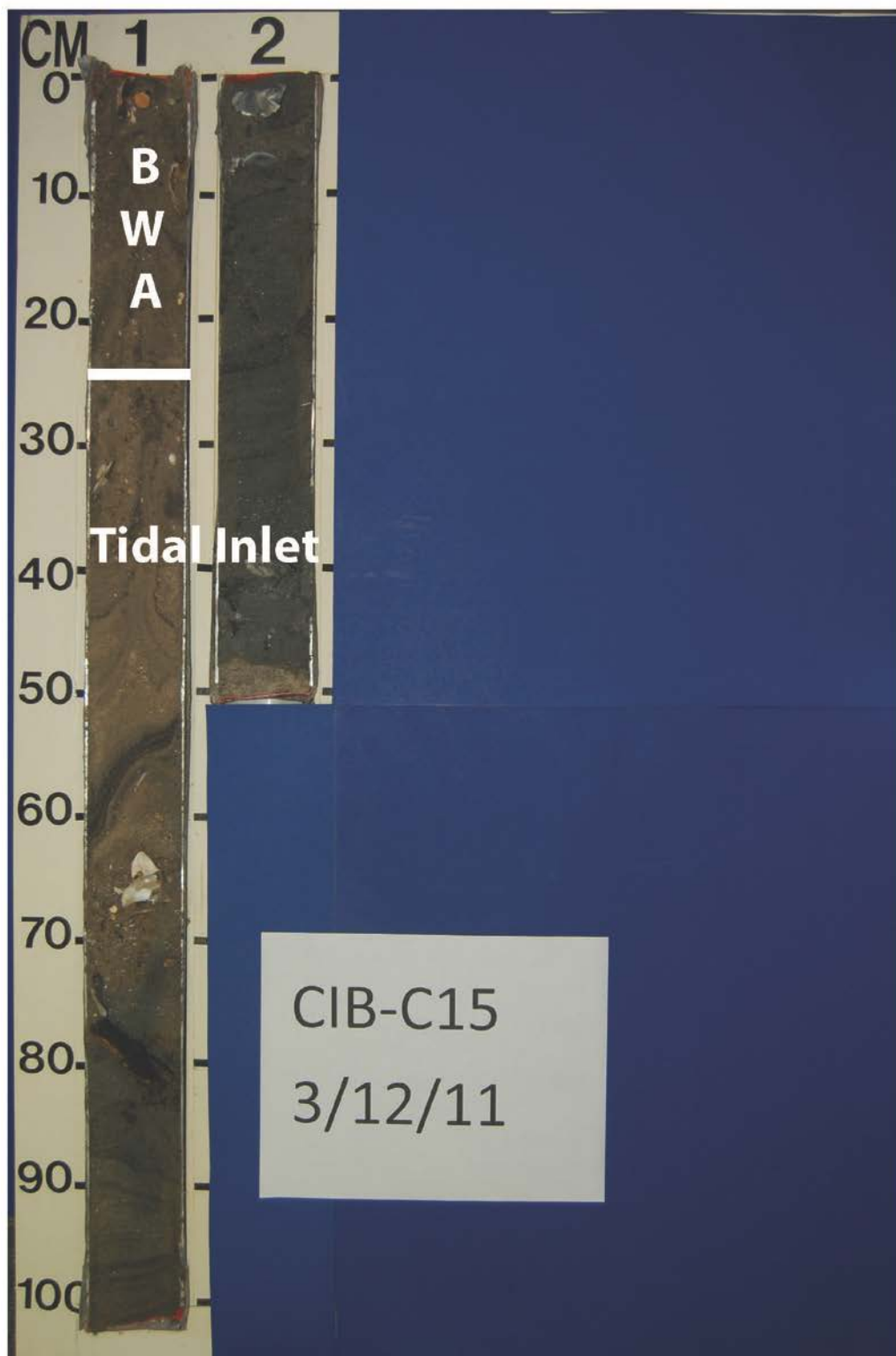
Vibracore C14



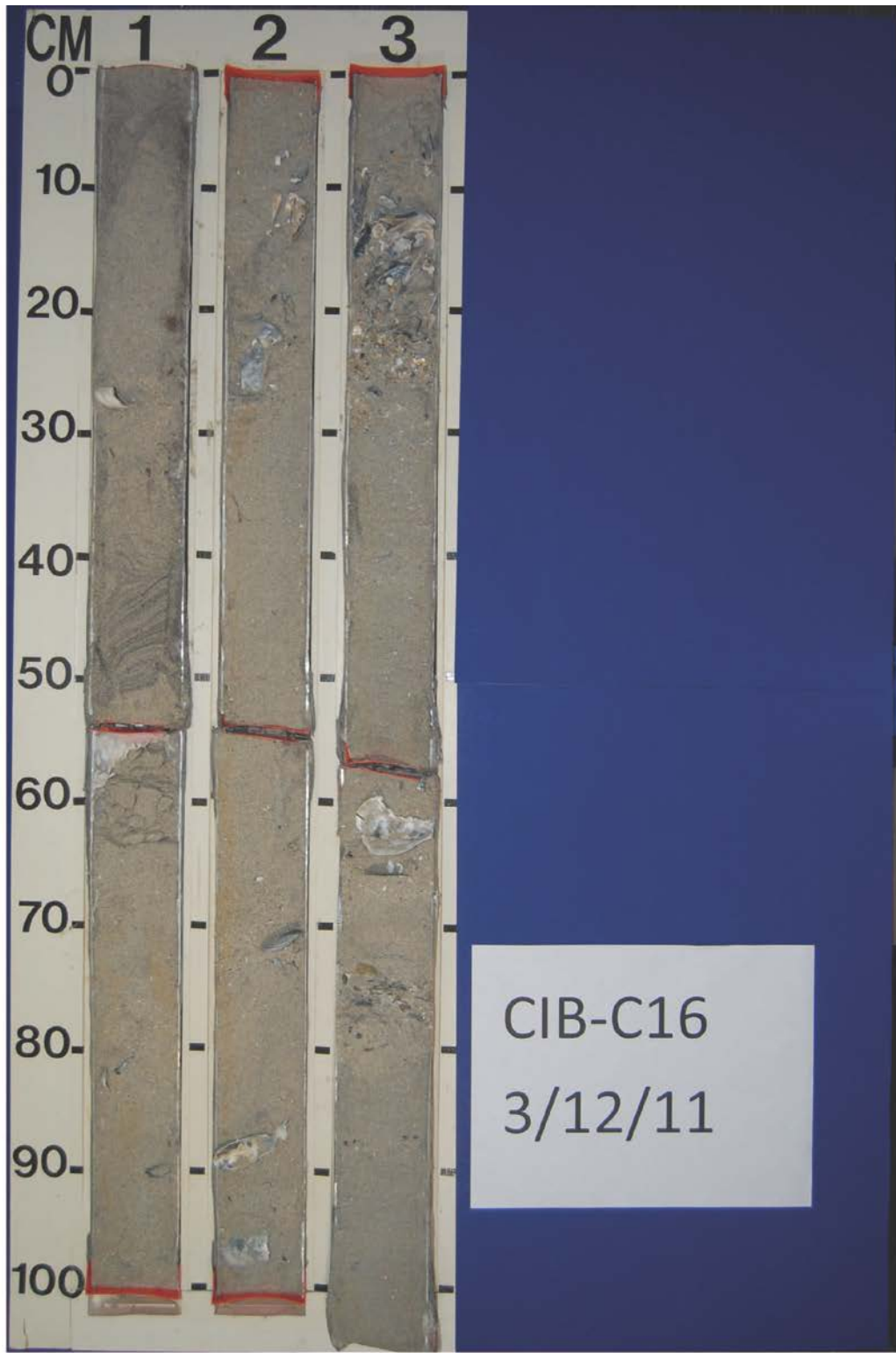


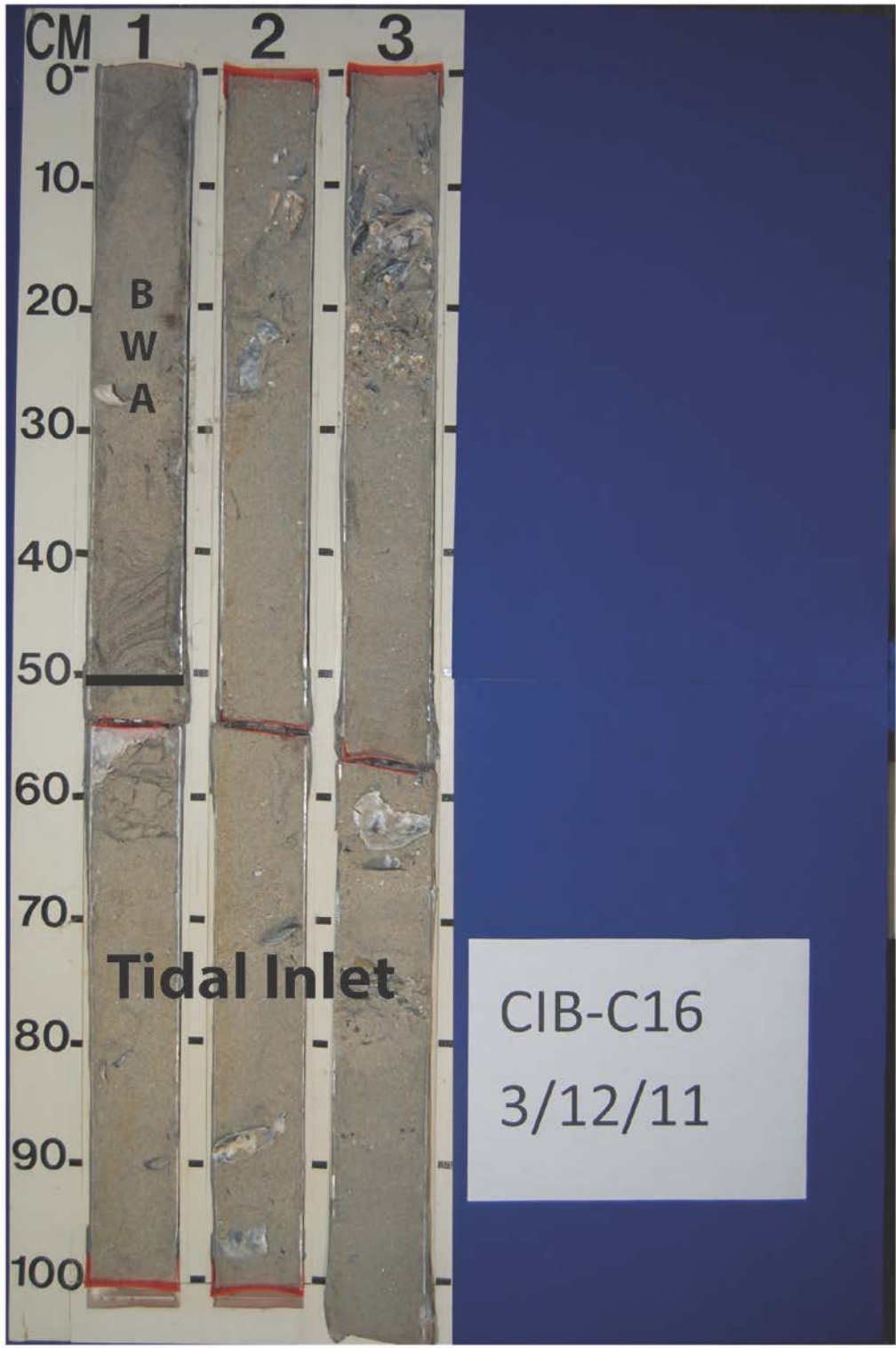
Vibracore C15



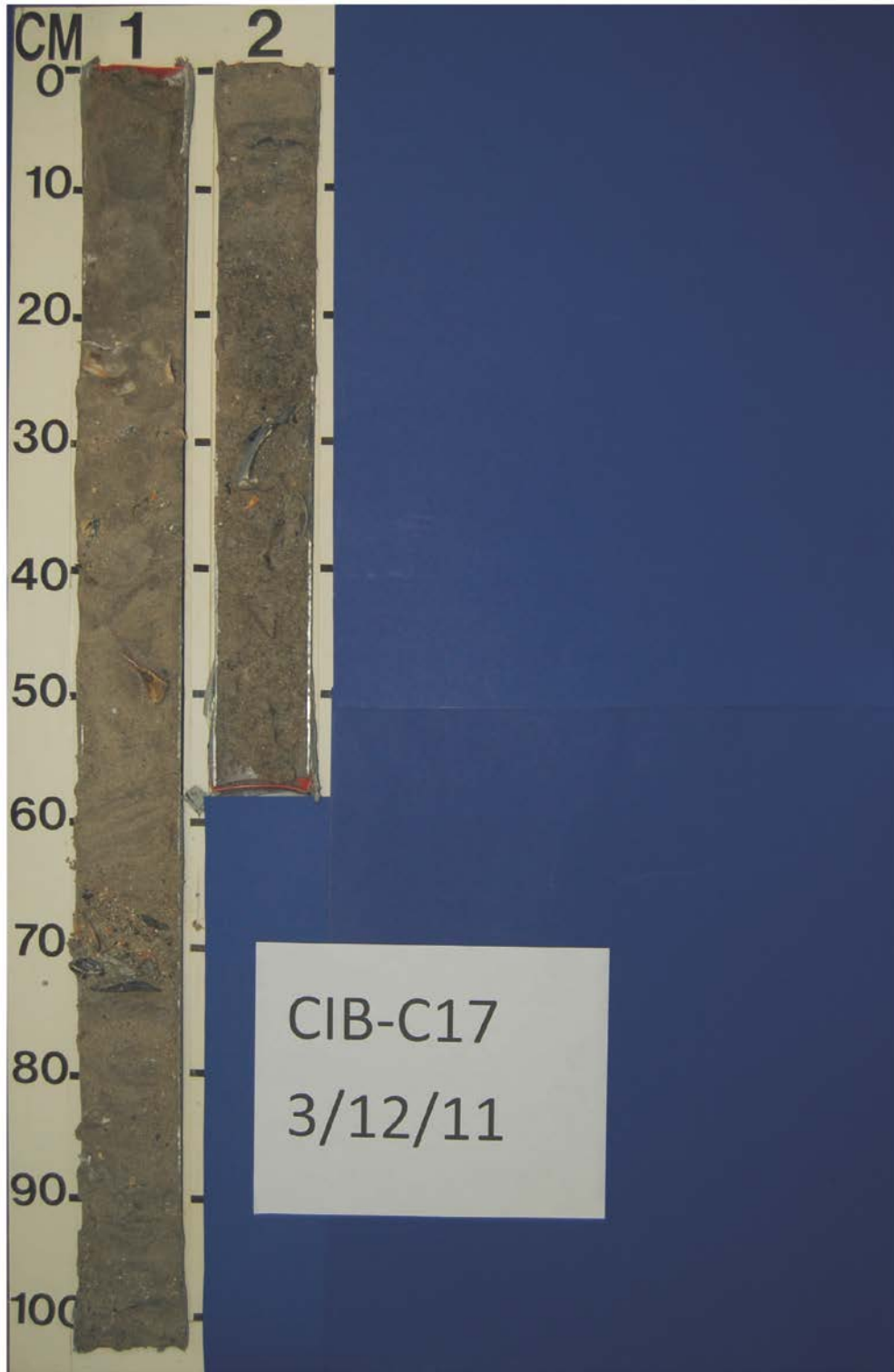


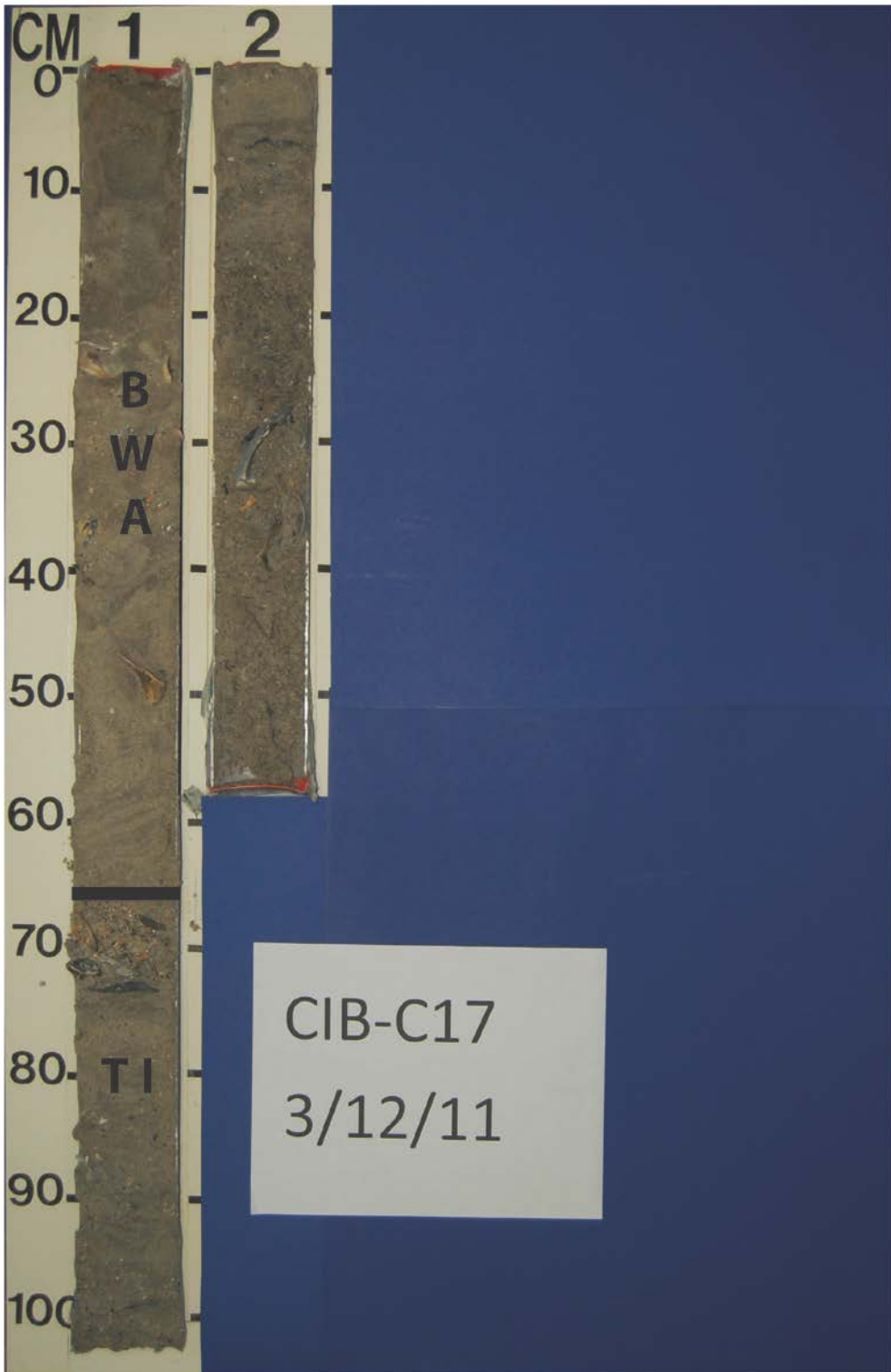
Vibracore C16



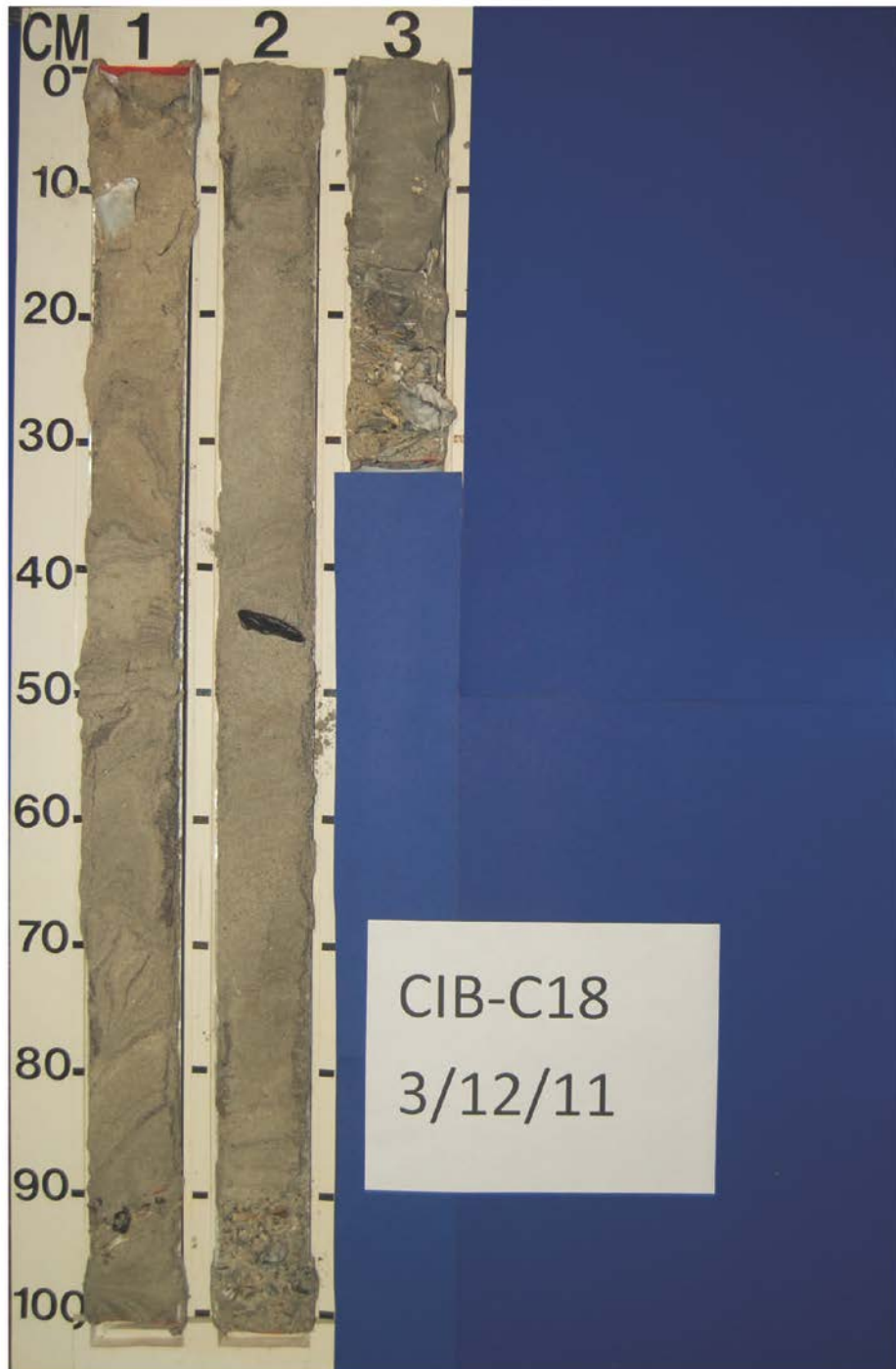


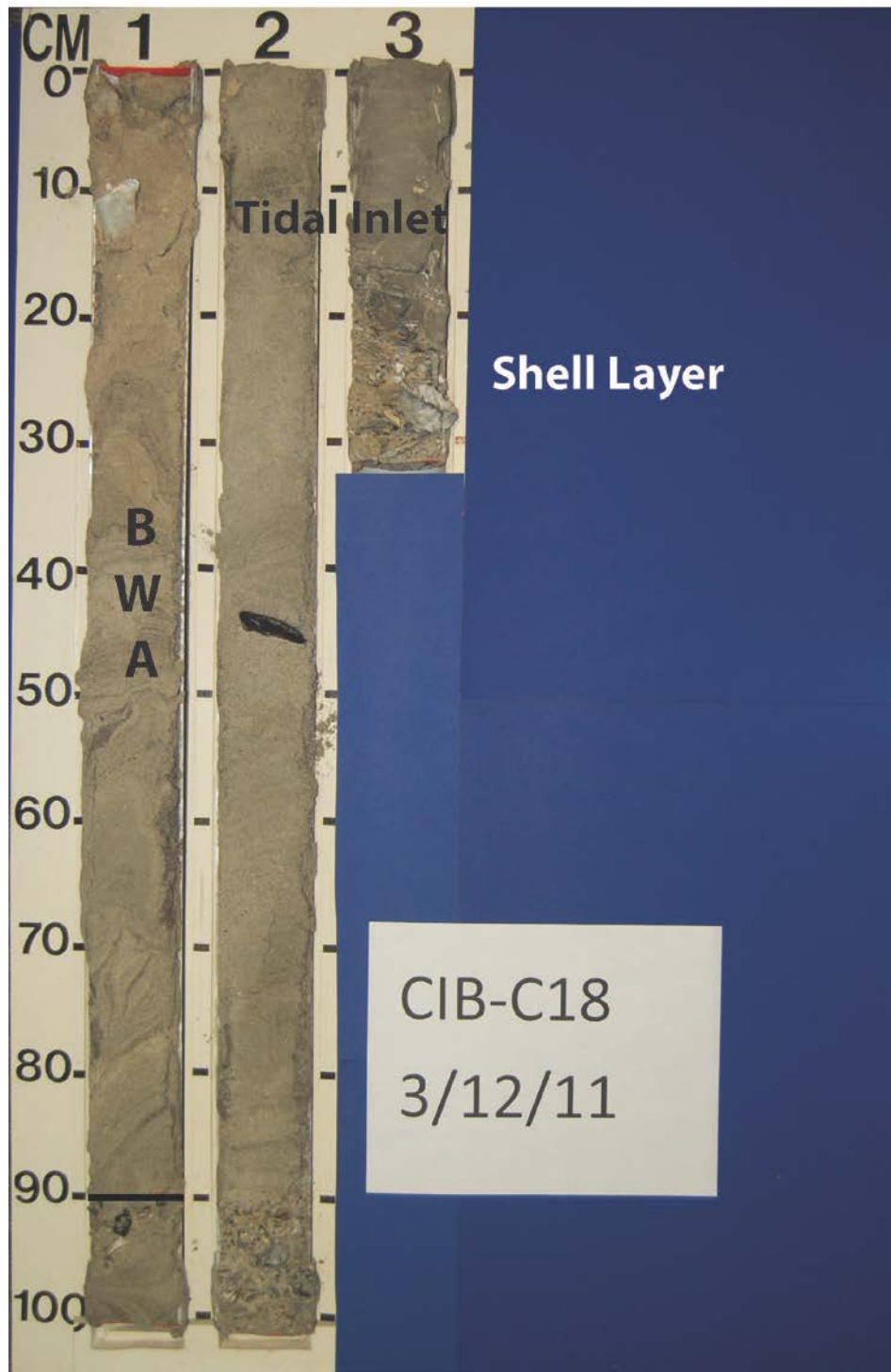
Vibracore C17





Vibracore C18



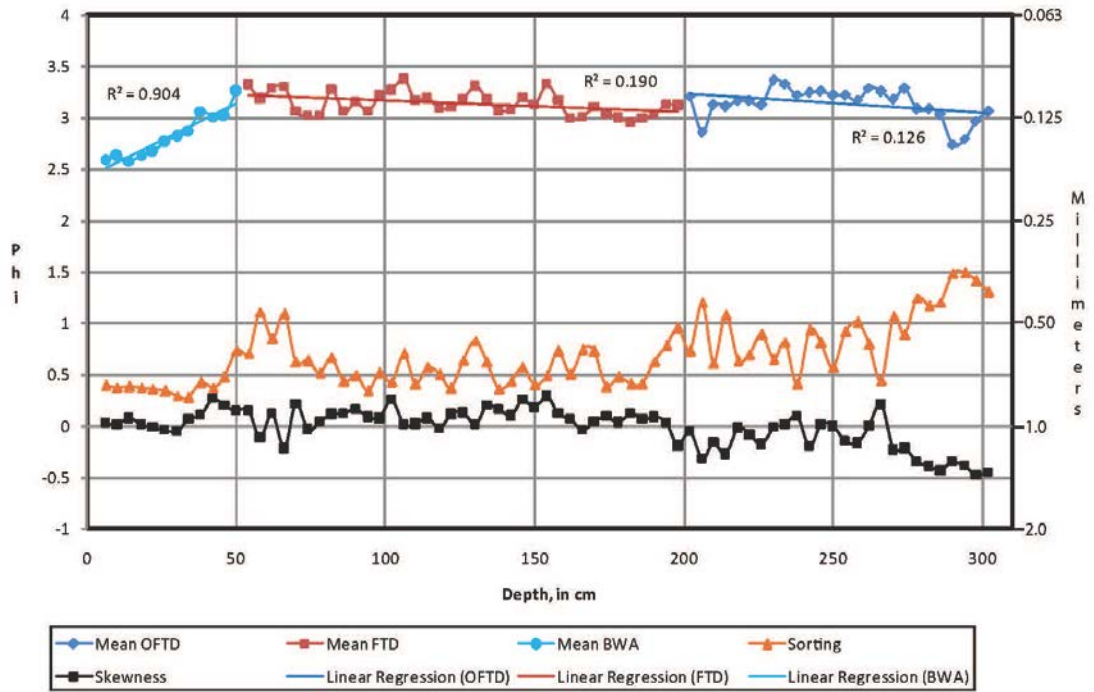


Appendix C – Plots of grain-size trends

Vibracore C1

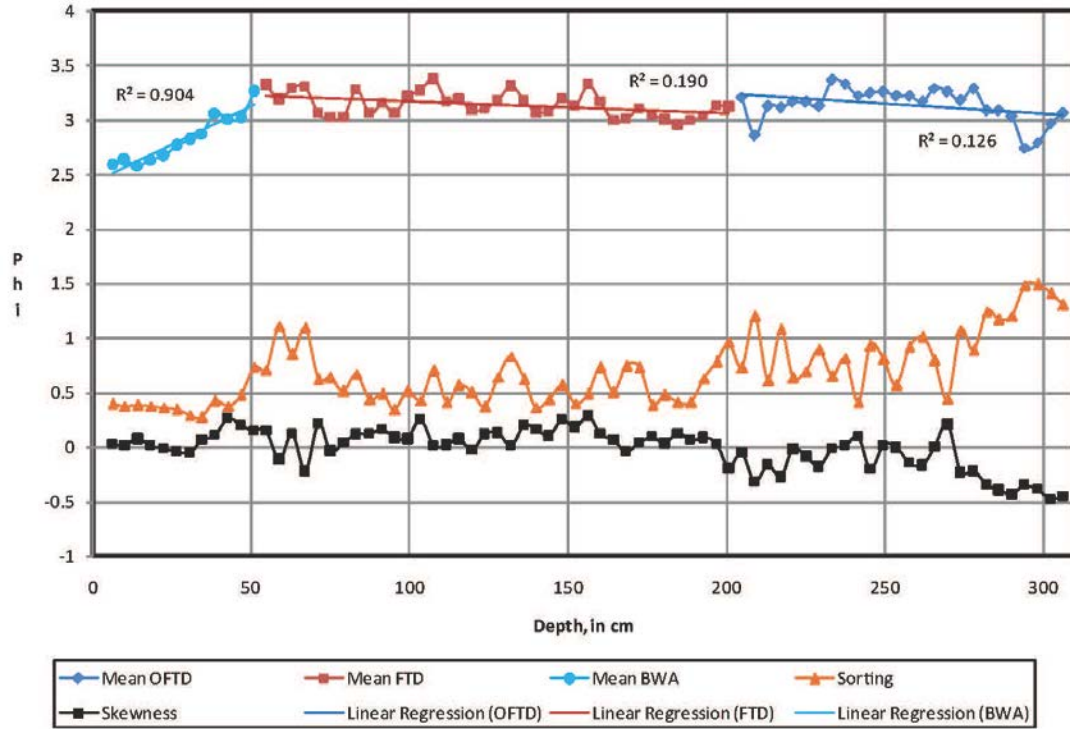
Compacted

Vibracore C1



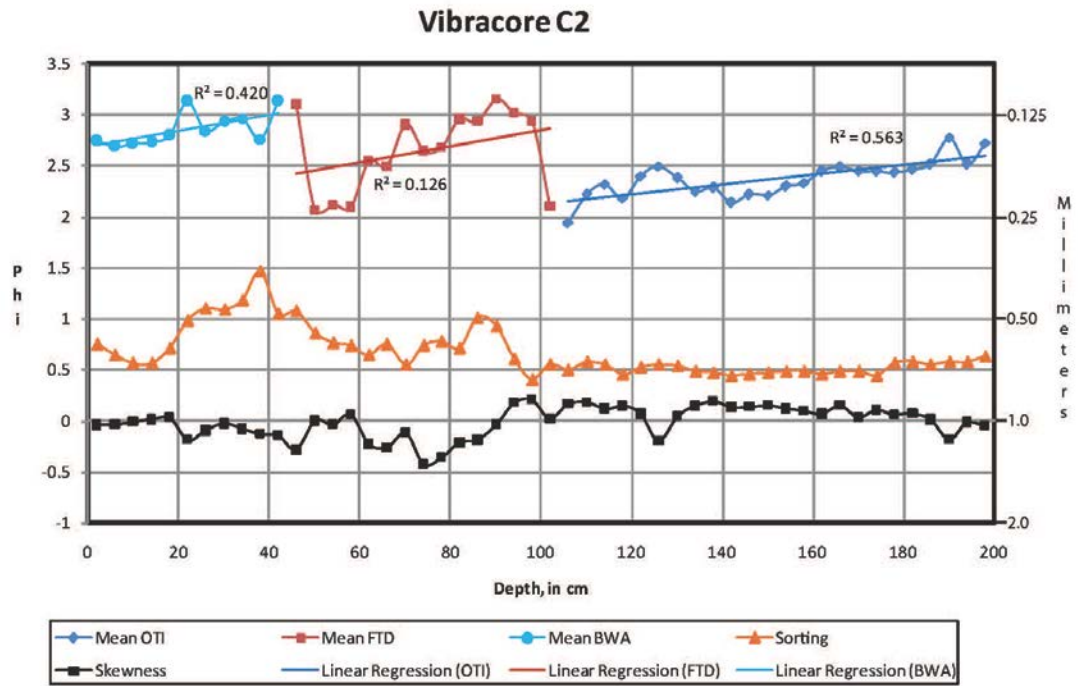
Uncompacted

Vibracore C1



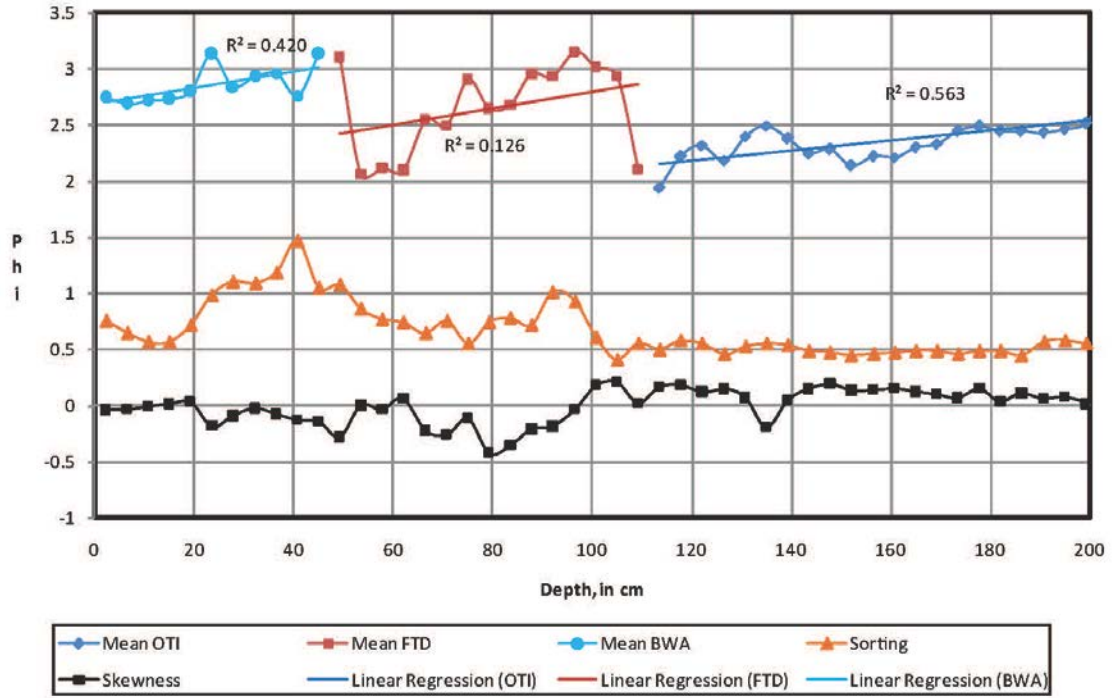
Vibracore C2

Compacted



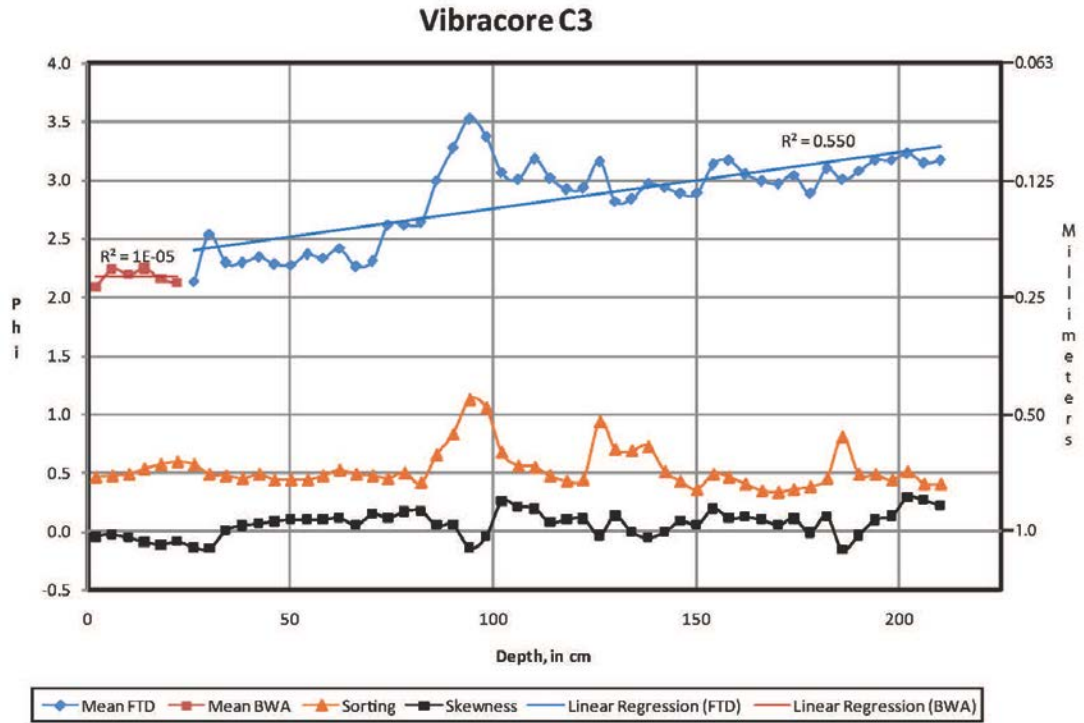
Uncompacted

Vibracore C2



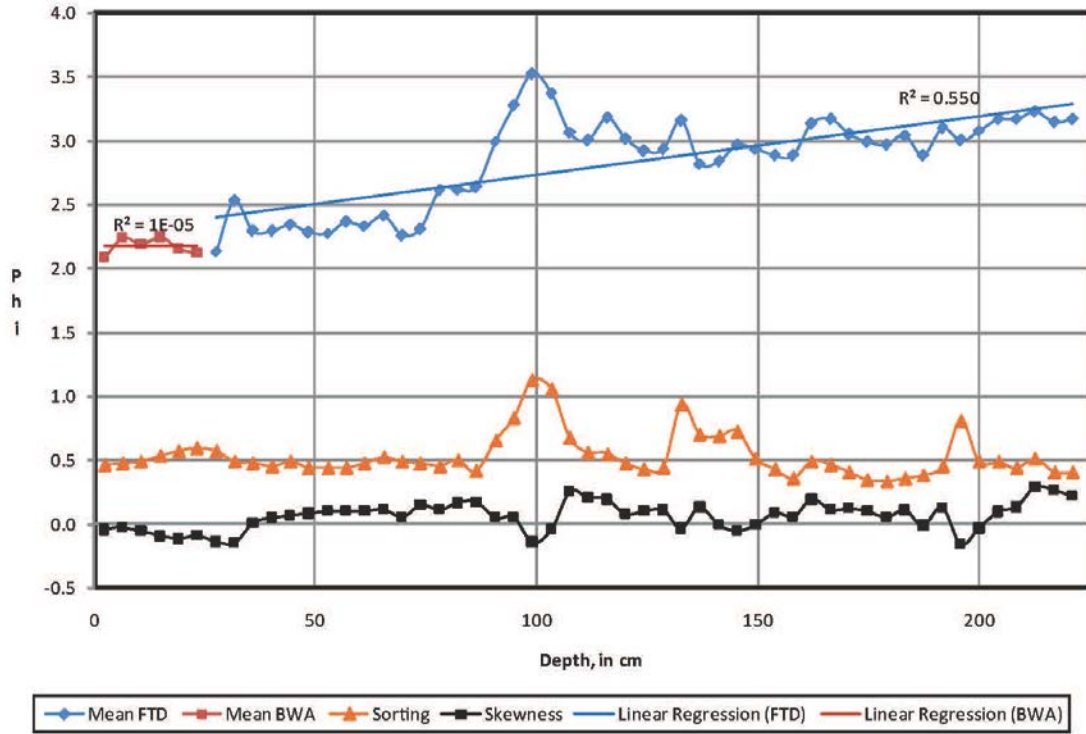
Vibracore C3

Compacted



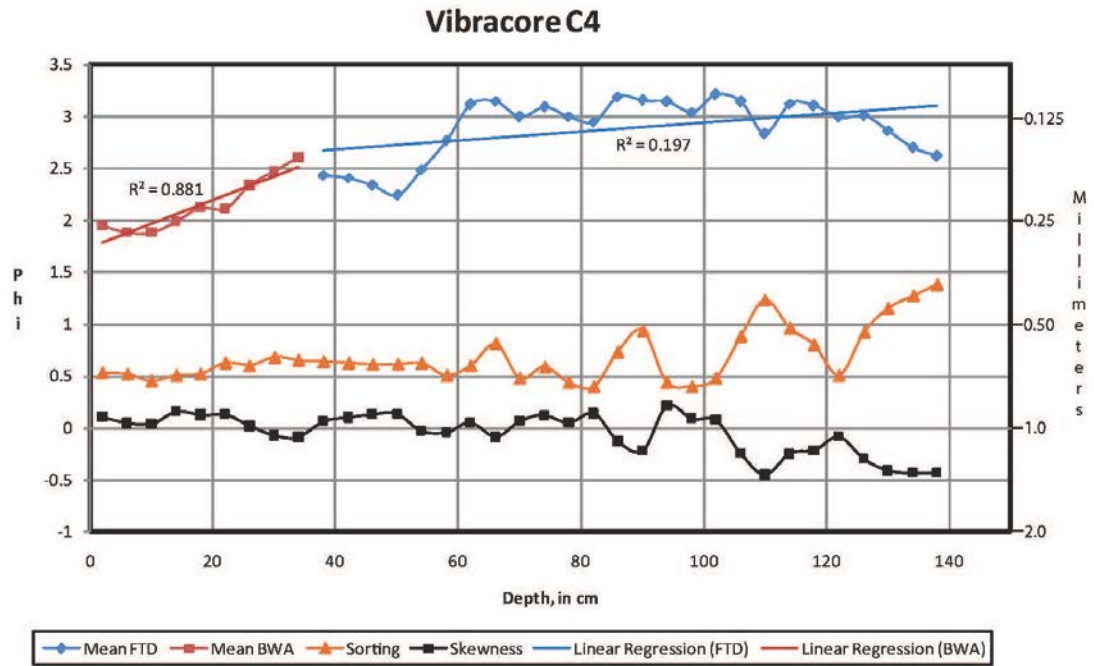
Uncompacted

Vibracore C3



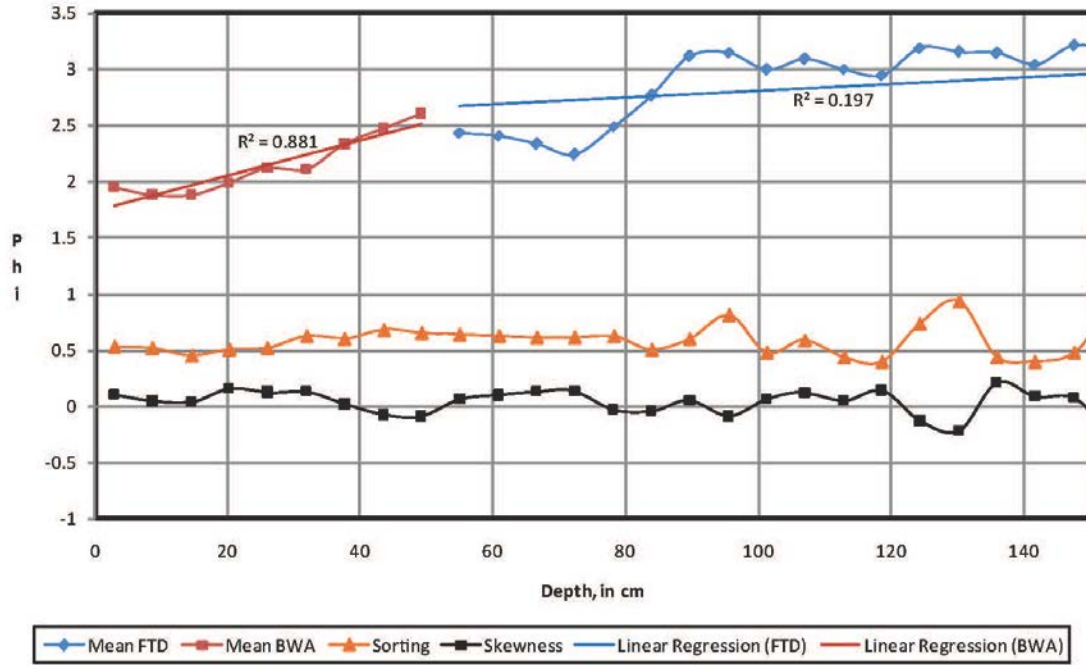
Vibracore C4

Compacted



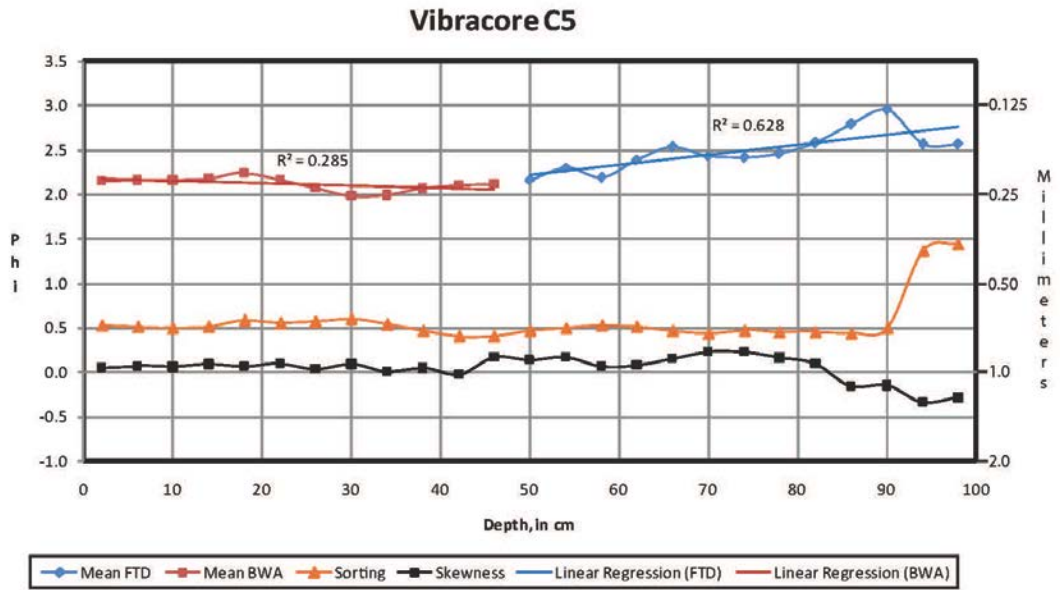
Uncompacted

Vibracore C4



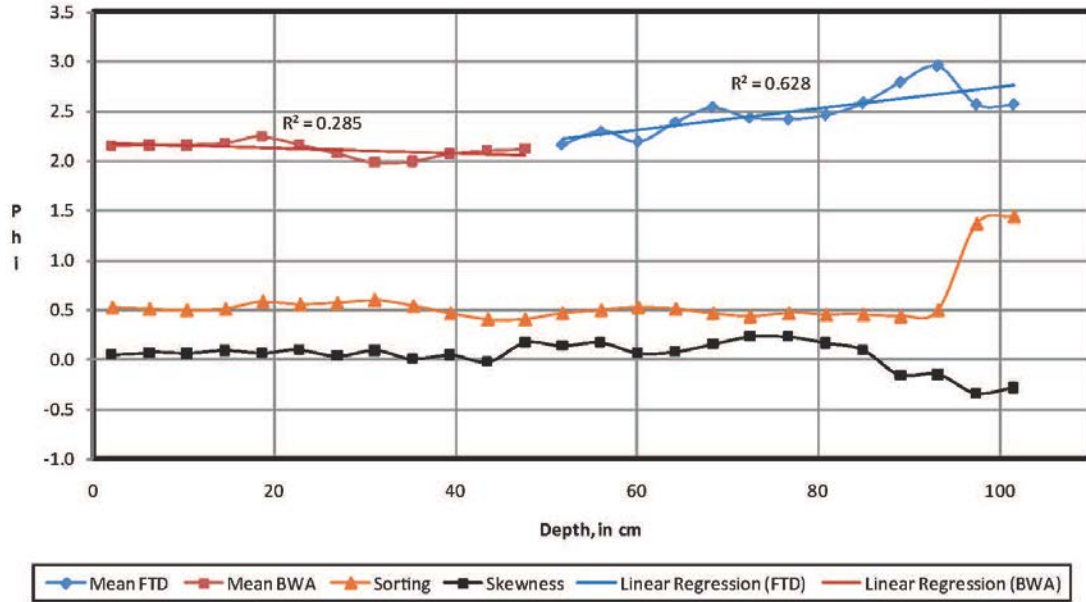
Vibracore C5

Compacted



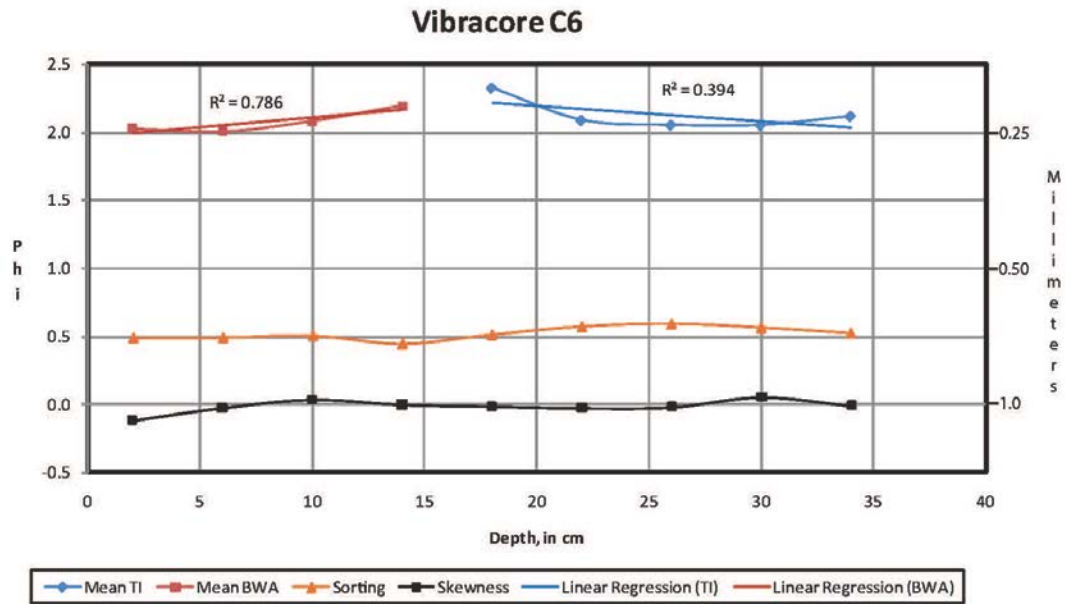
Uncompacted

Vibracore C5



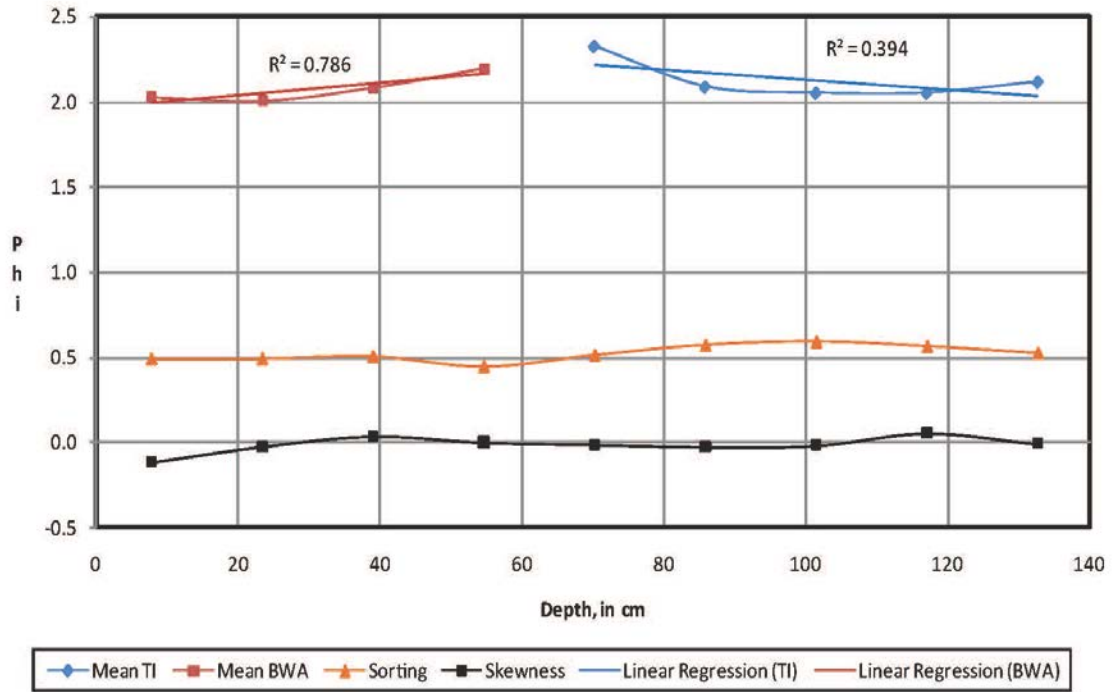
Vibracore C6

Compacted



Uncompacted

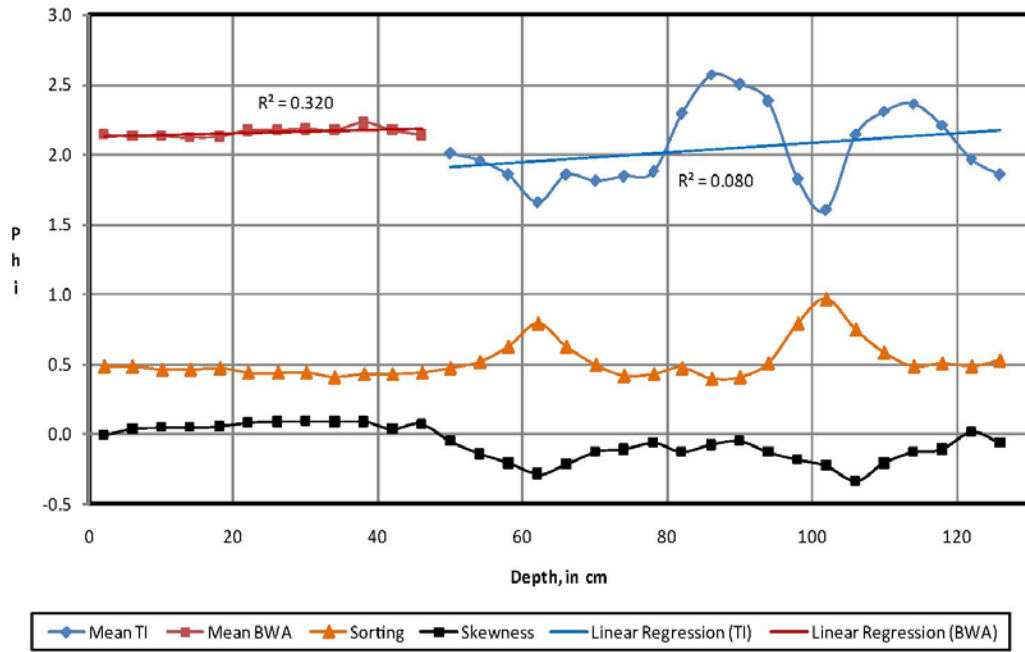
Vibracore C6



Vibracore C7

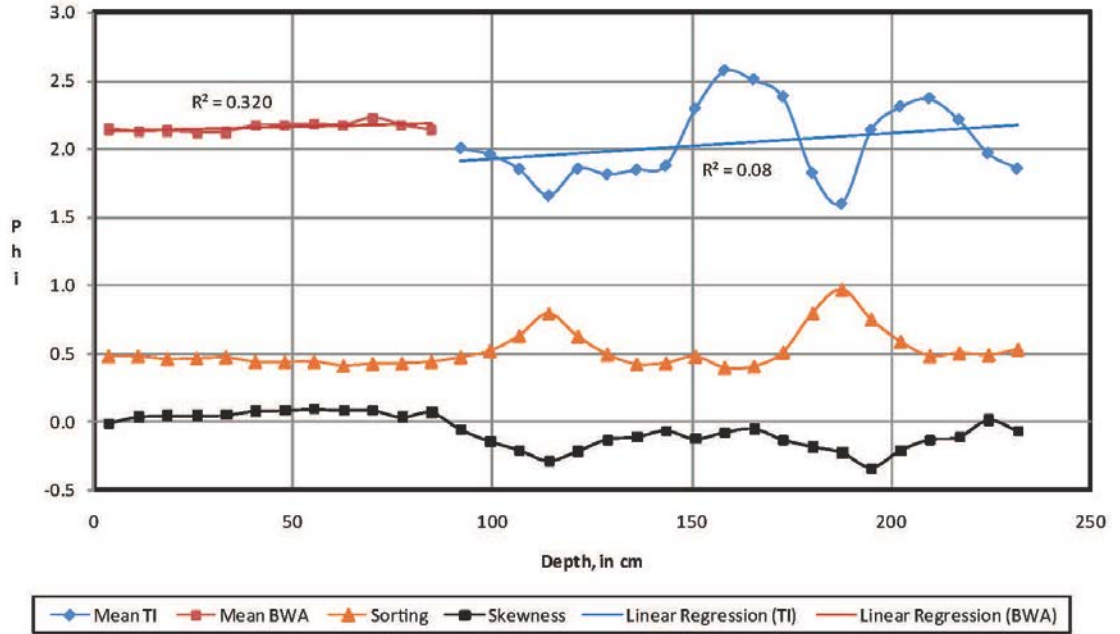
Compacted

Vibracore C7



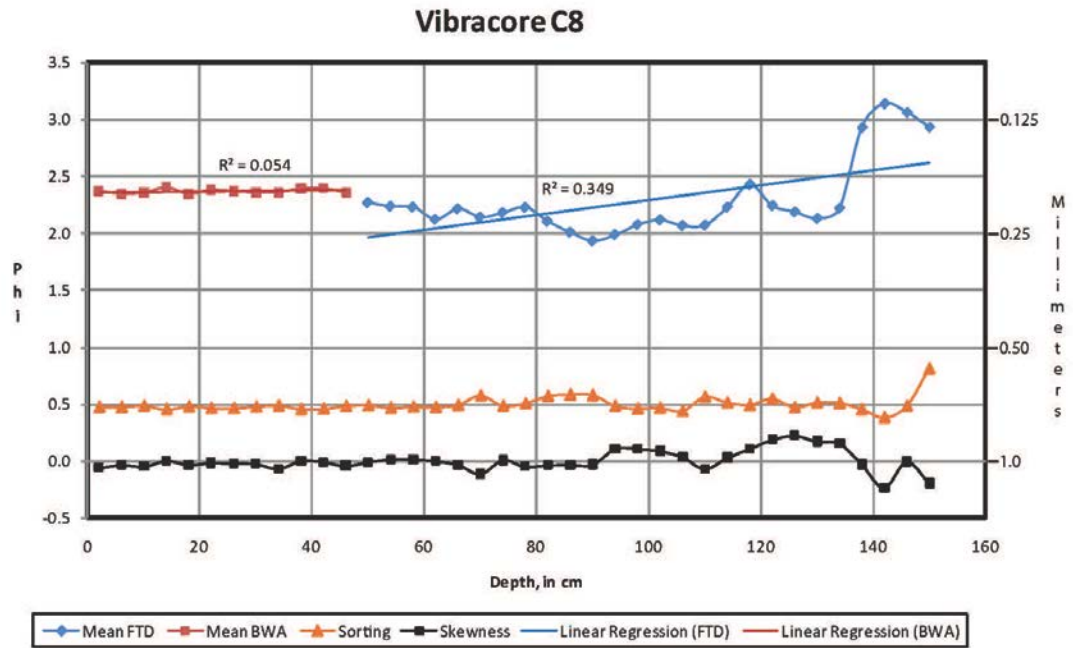
Uncompacted

Vibracore C7



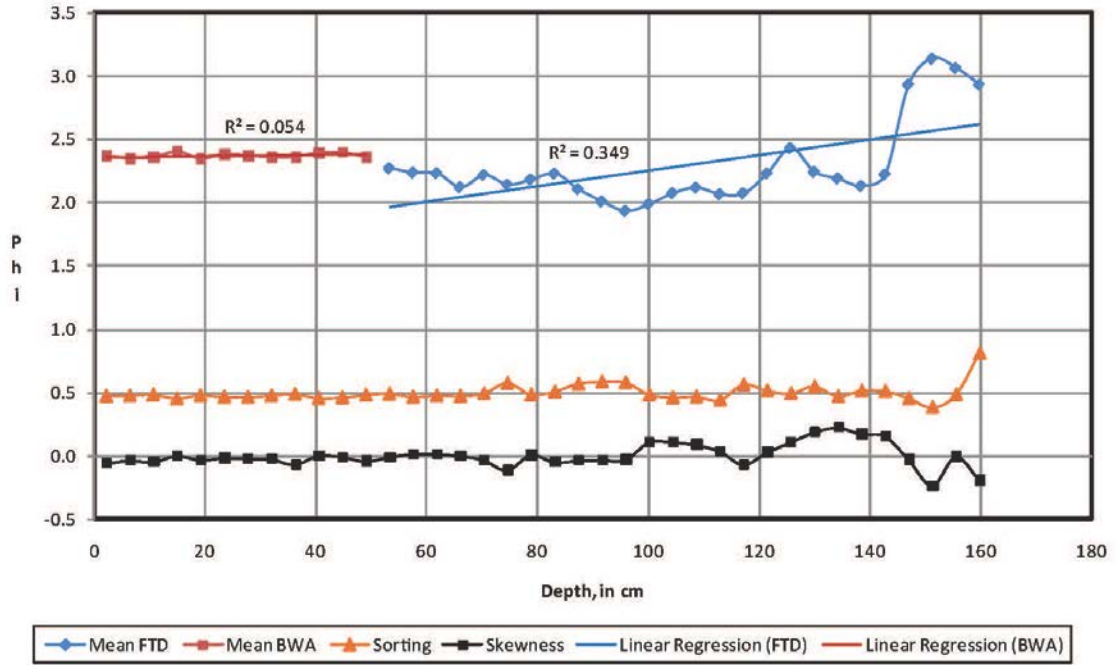
Vibracore C8

Compacted



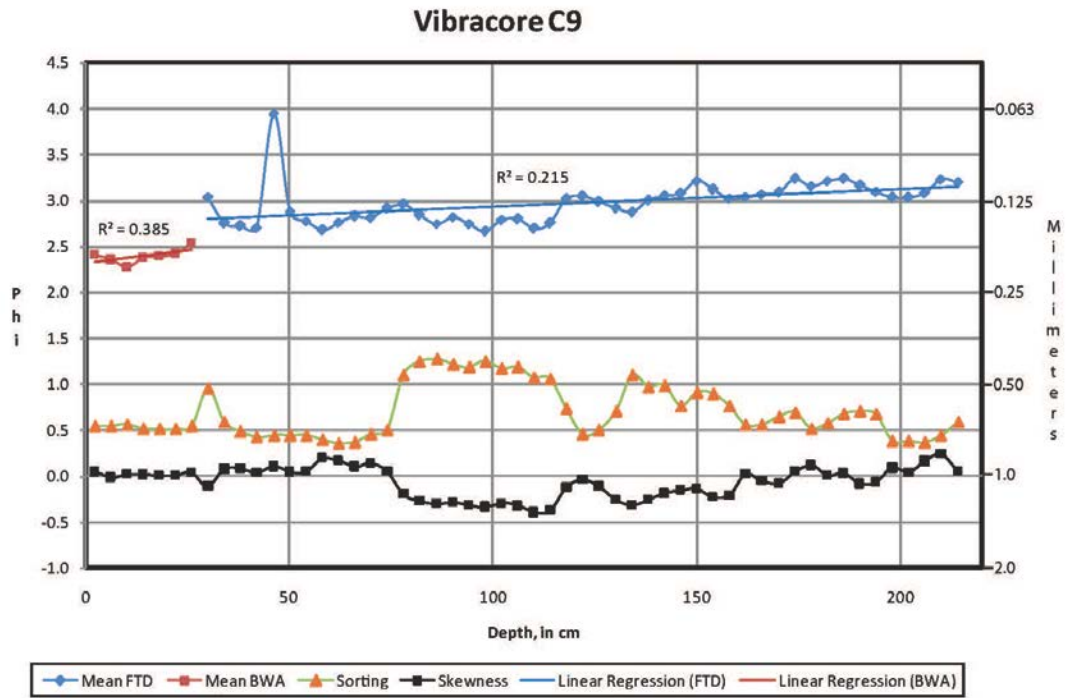
Uncompacted

Vibracore C8



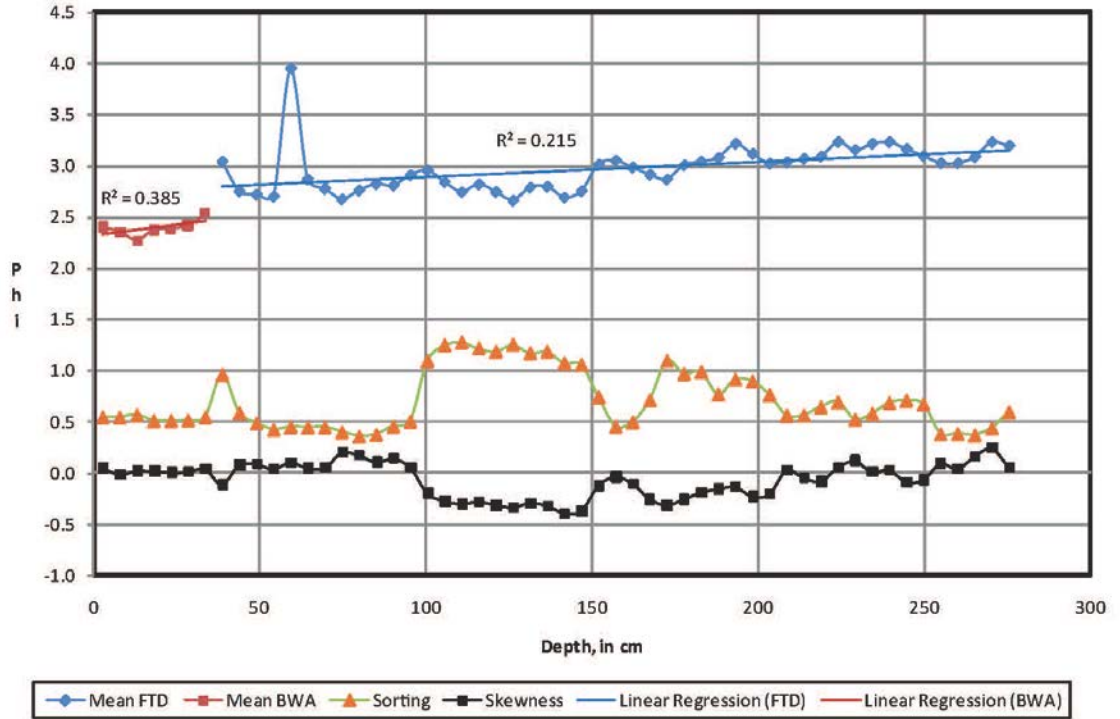
Vibracore C9

Compacted



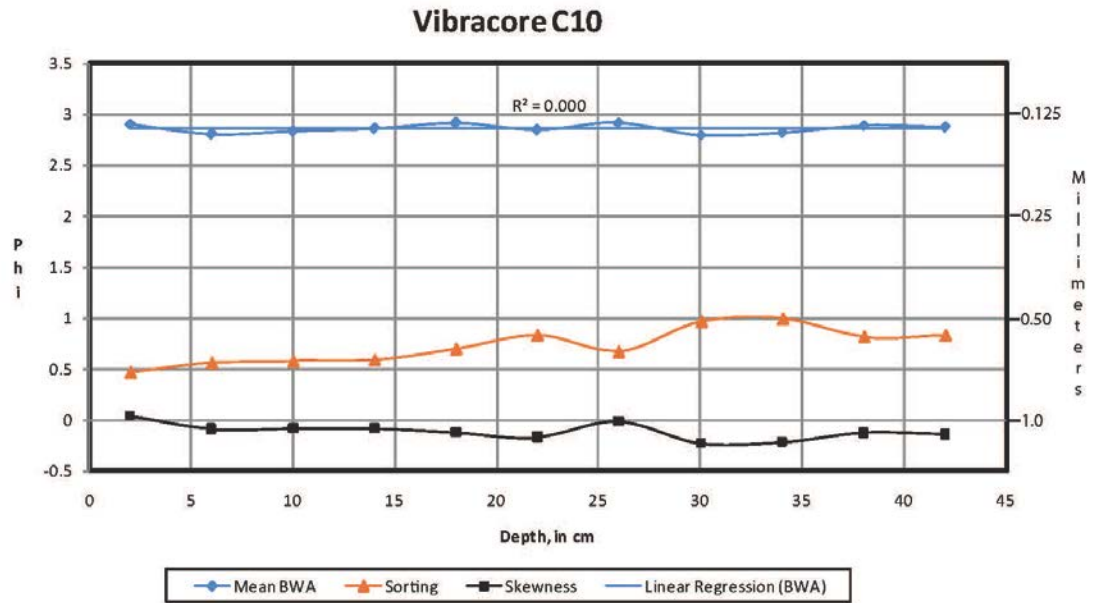
Uncompacted

Vibracore C9



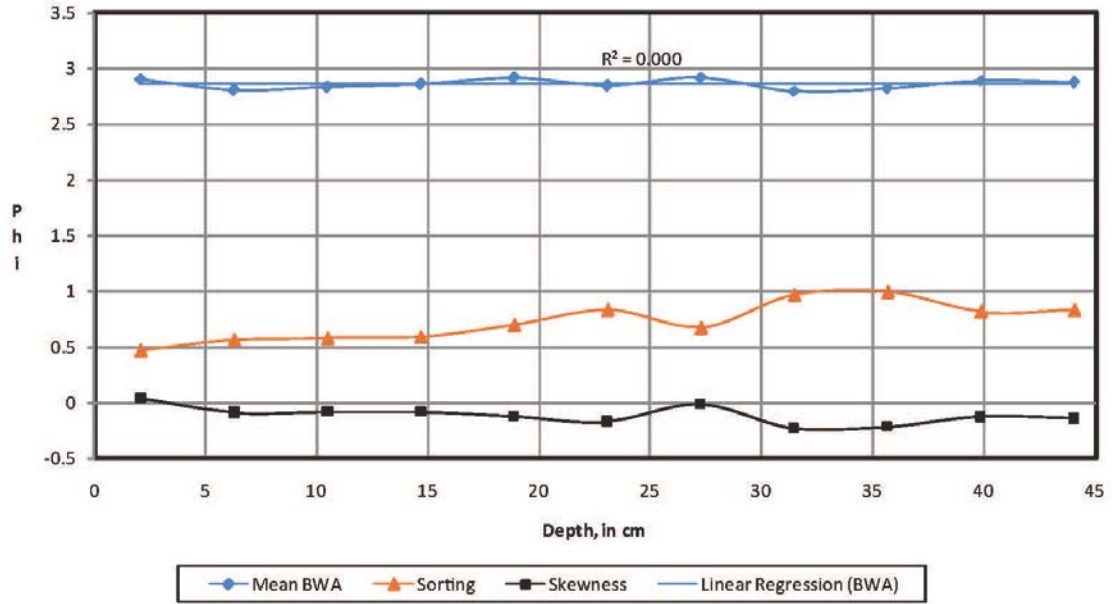
Vibracore C10

Compacted



Uncompacted

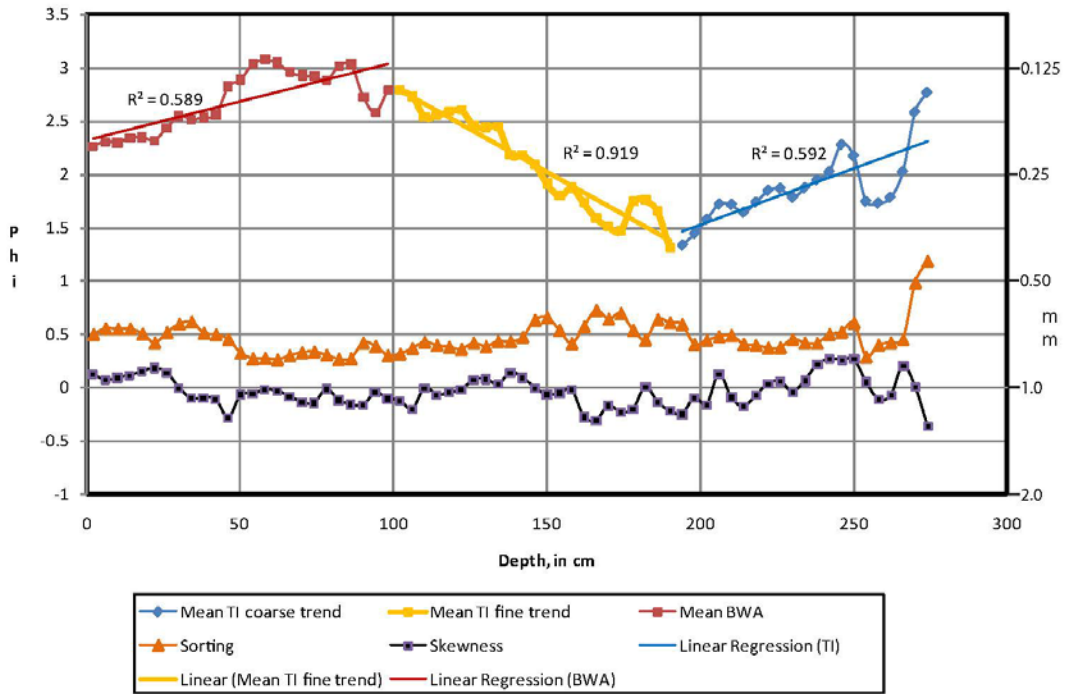
Vibracore C10



Vibracore C11

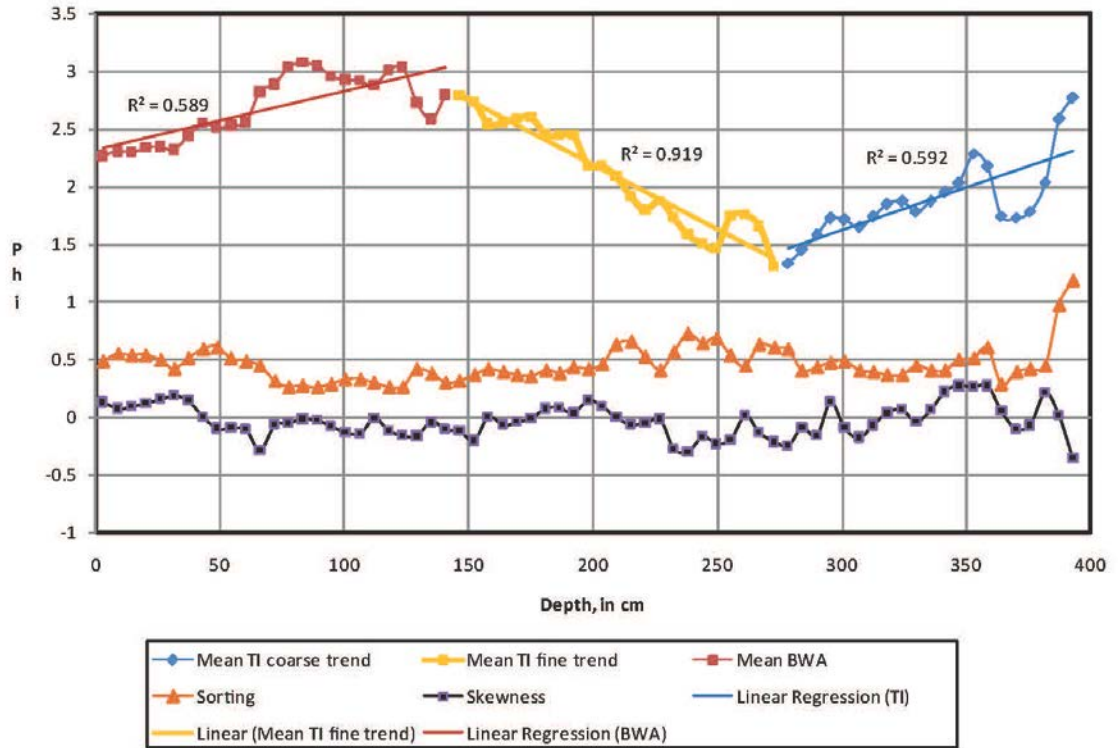
Compacted

Vibracore C11



Uncompacted

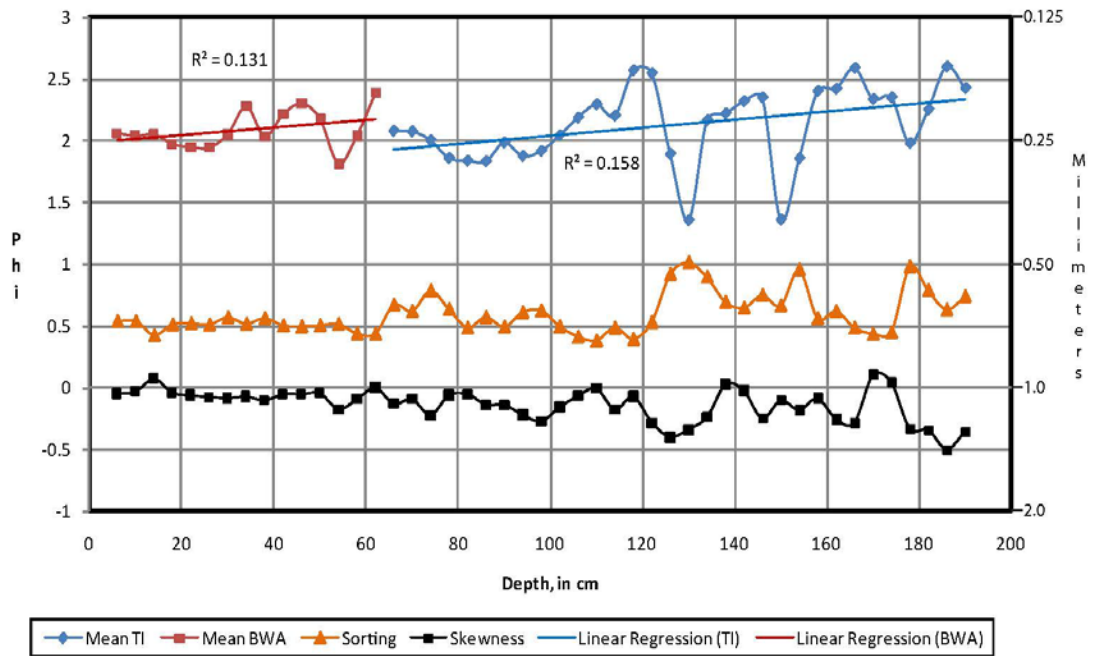
Vibracore C11



Vibracore C12

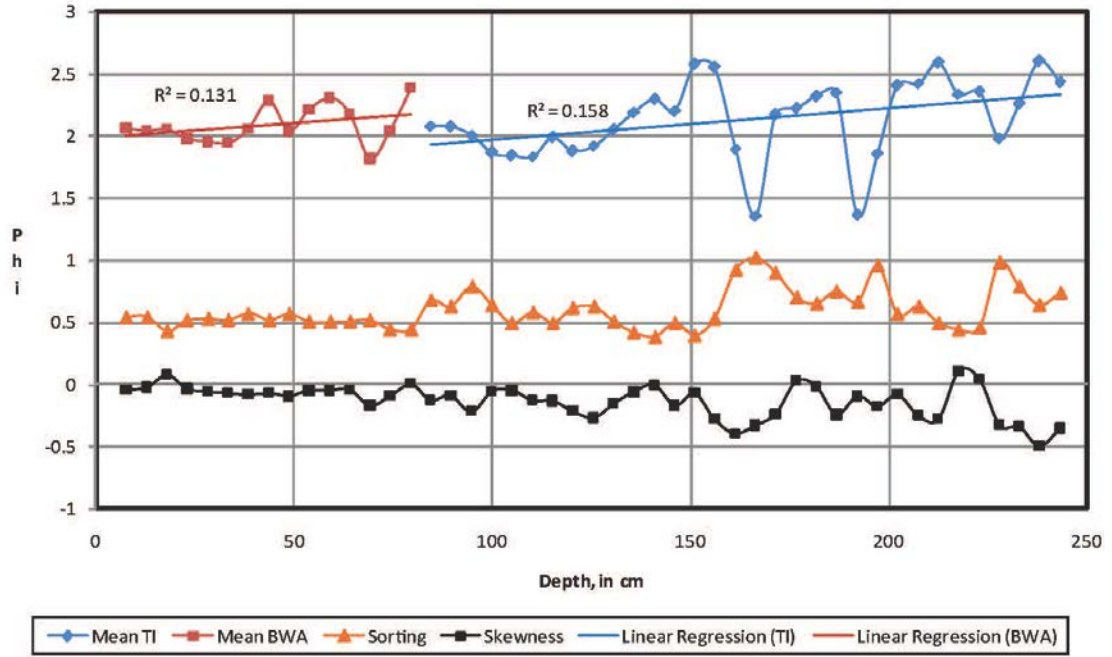
Compacted

Vibracore C12



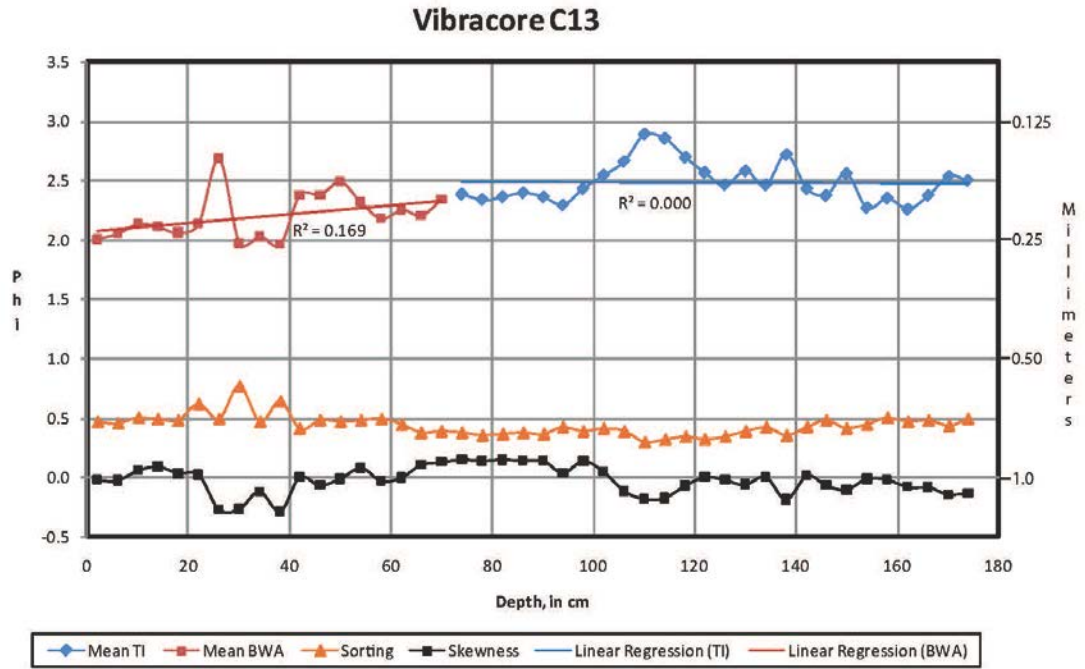
Uncompacted

Vibracore C12



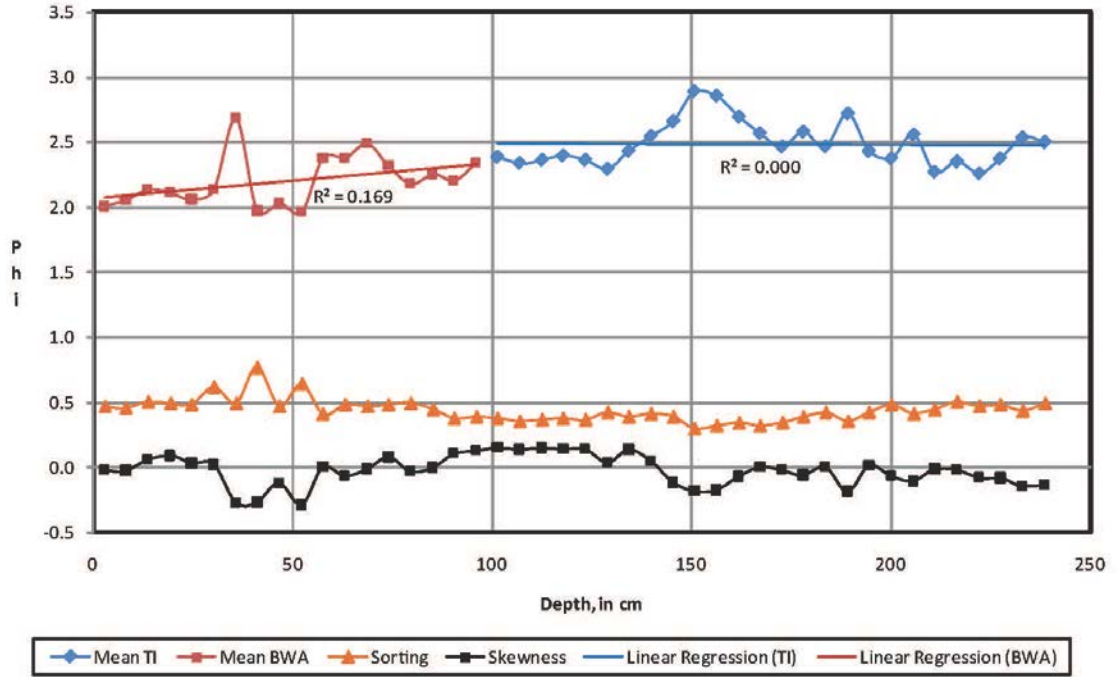
Vibracore C13

Compacted



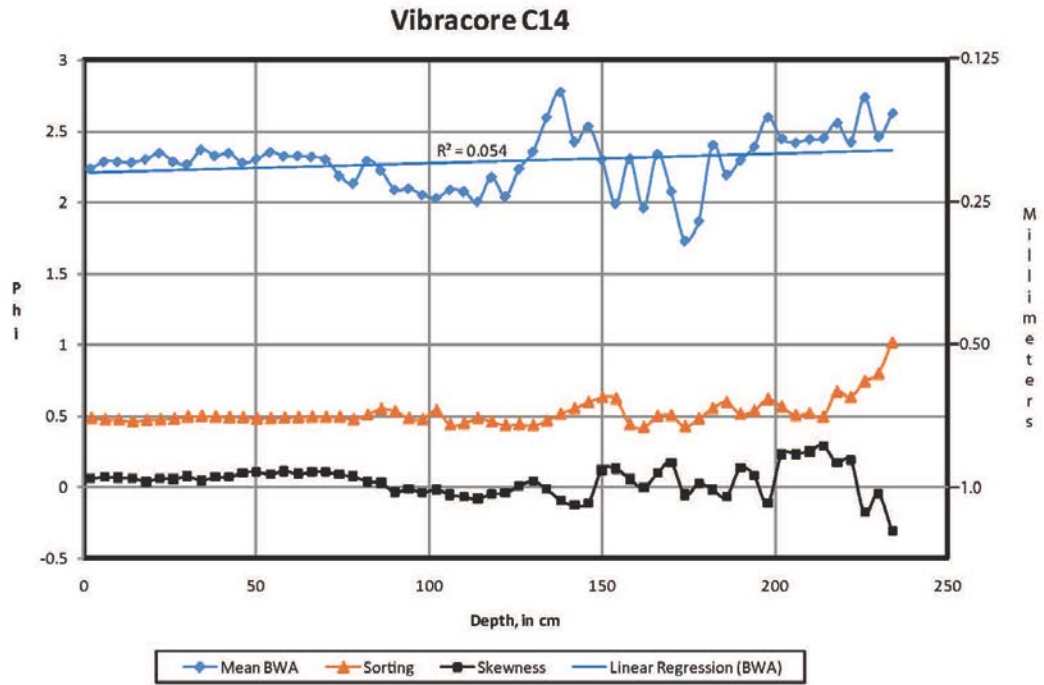
Uncompacted

Vibracore C13



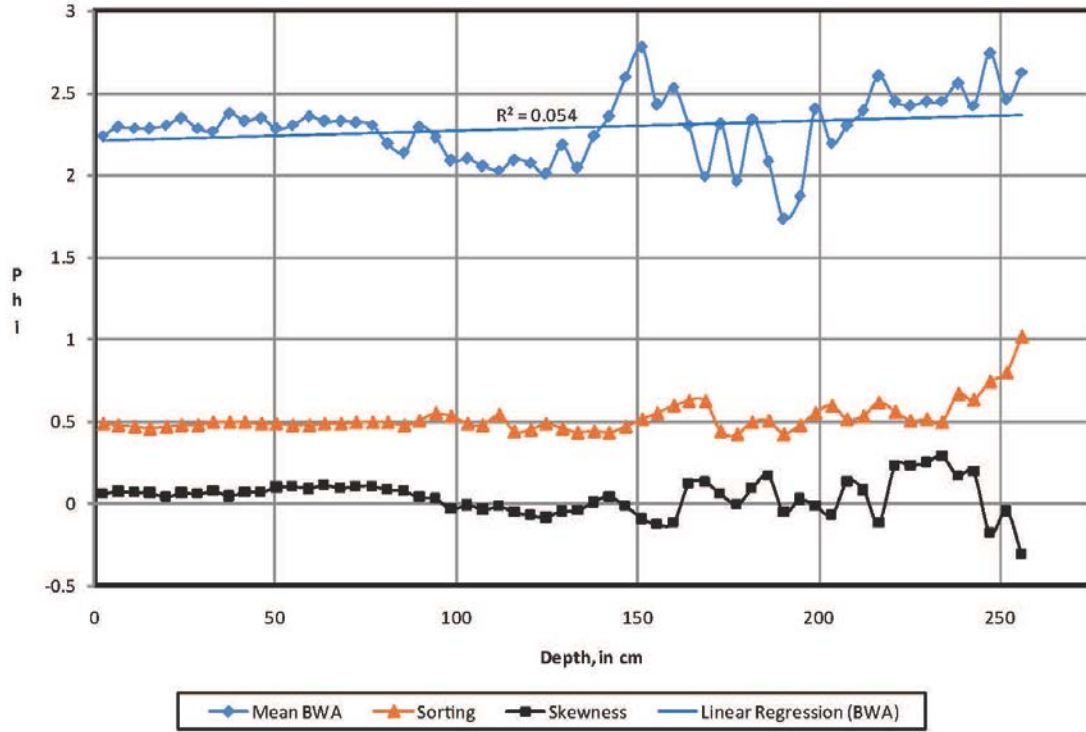
Vibracore C14

Compacted



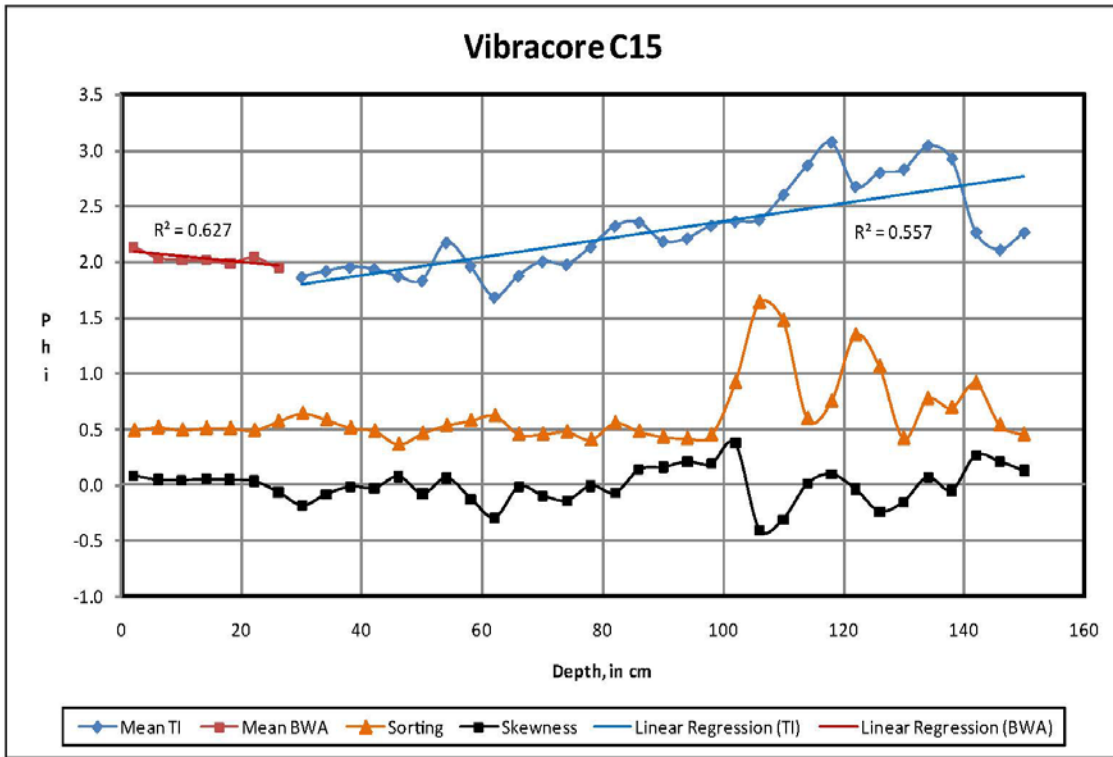
Uncompacted

Vibracore C14



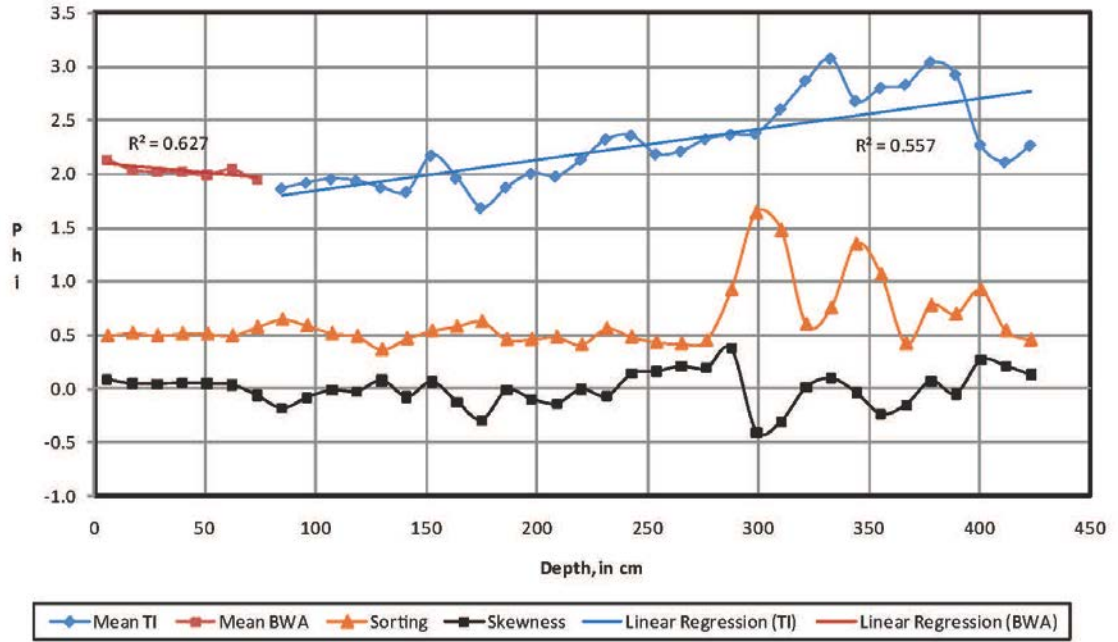
Vibracore C15

Compacted



Uncompacted

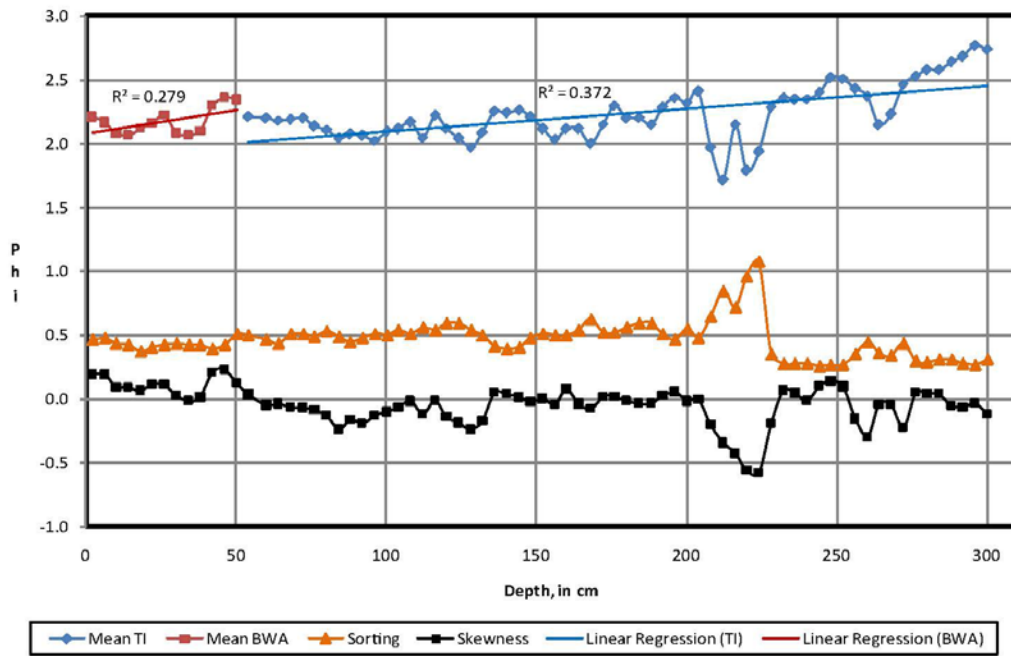
Vibracore C15



Vibracore C16

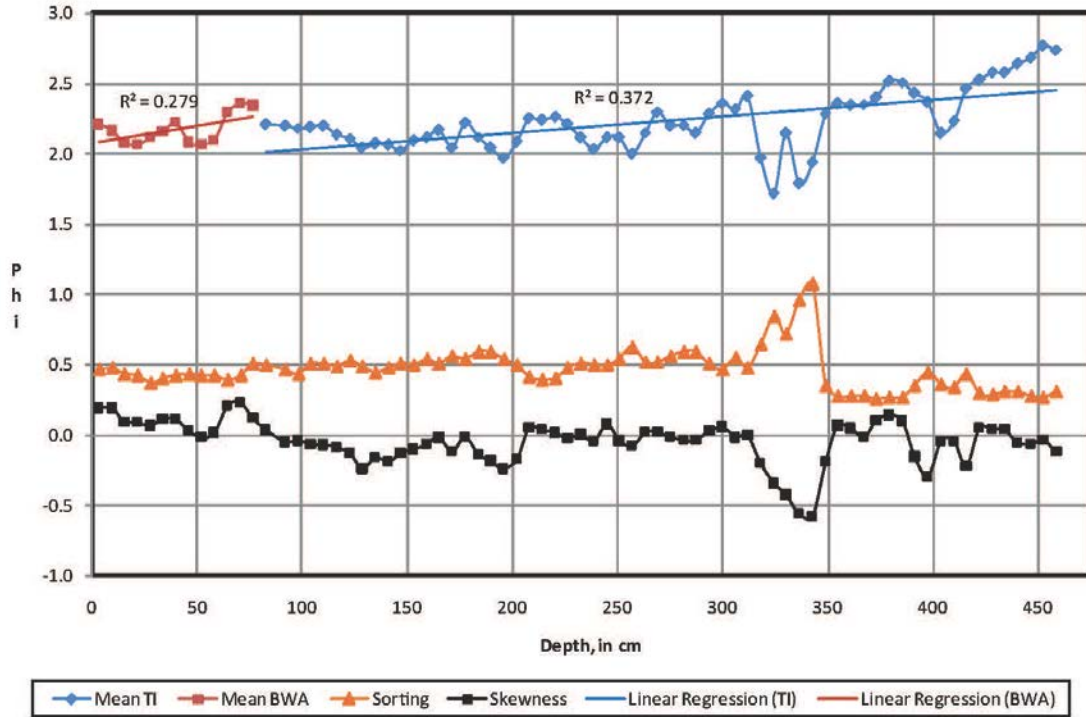
Compacted

Vibracore C16



Uncompacted

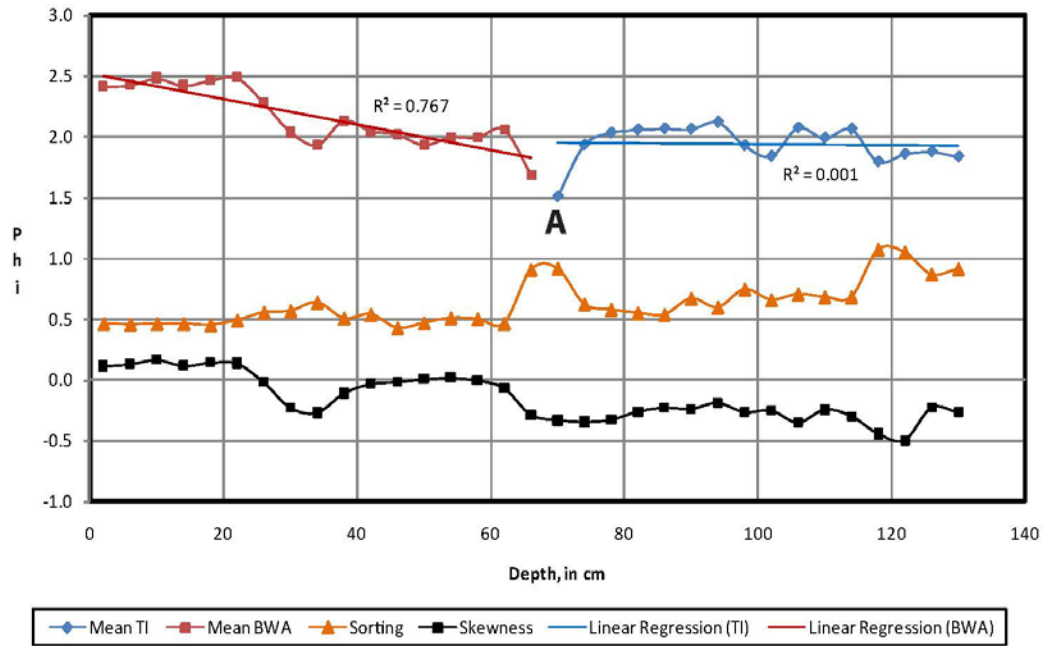
Vibracore C16



Vibracore C17

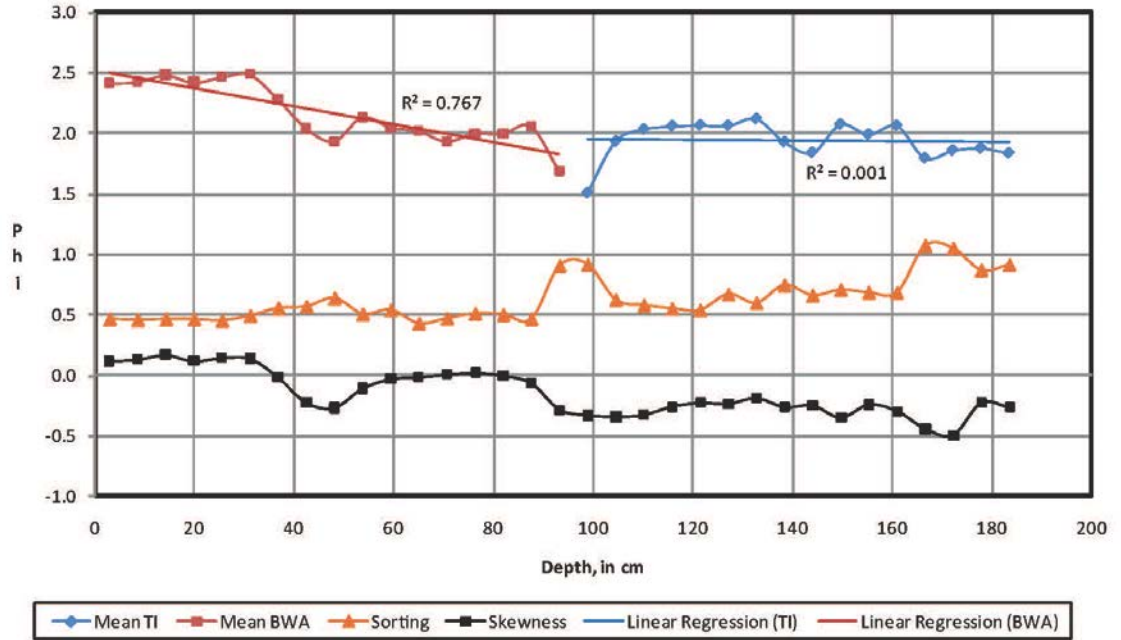
Compacted

Vibracore C17



Uncompacted

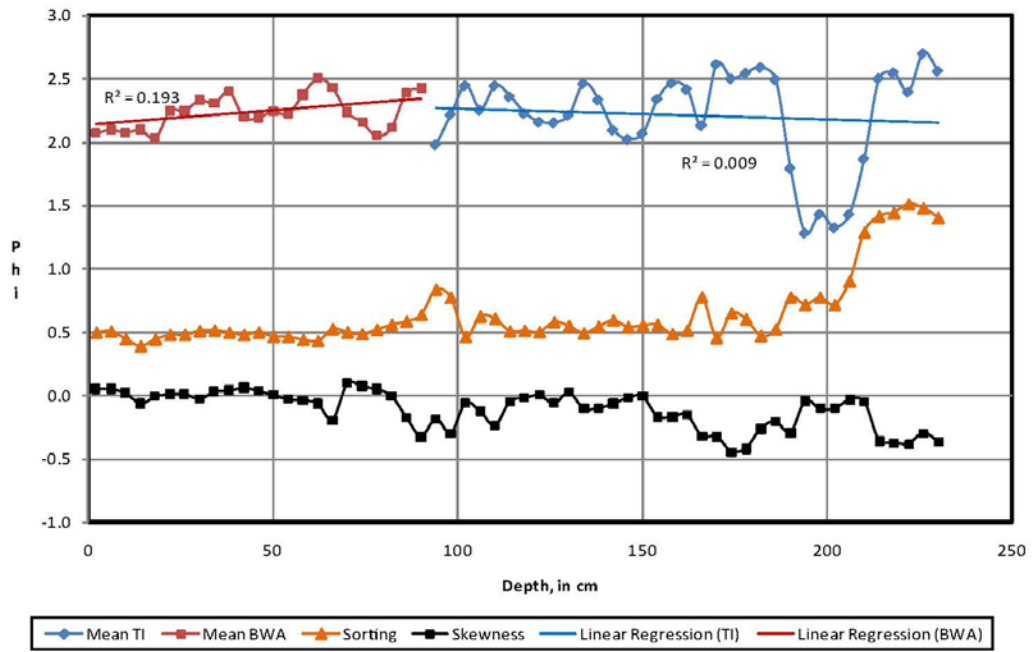
Vibracore C17



Vibracore C18

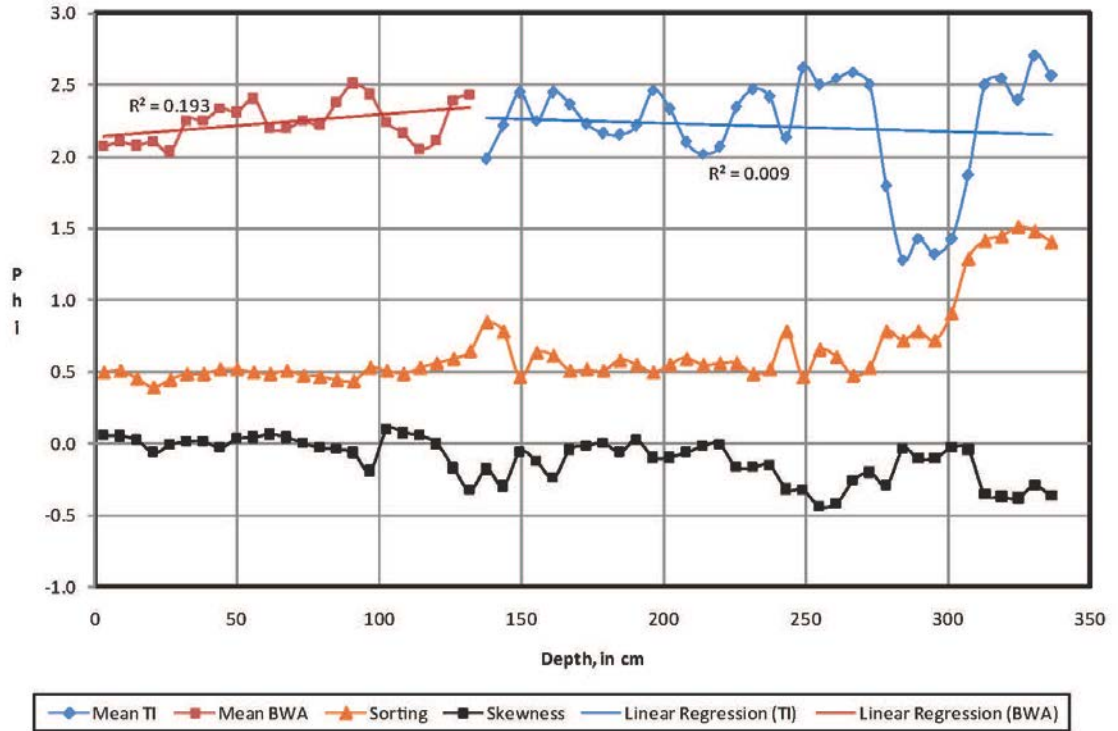
Compacted

Vibracore C18

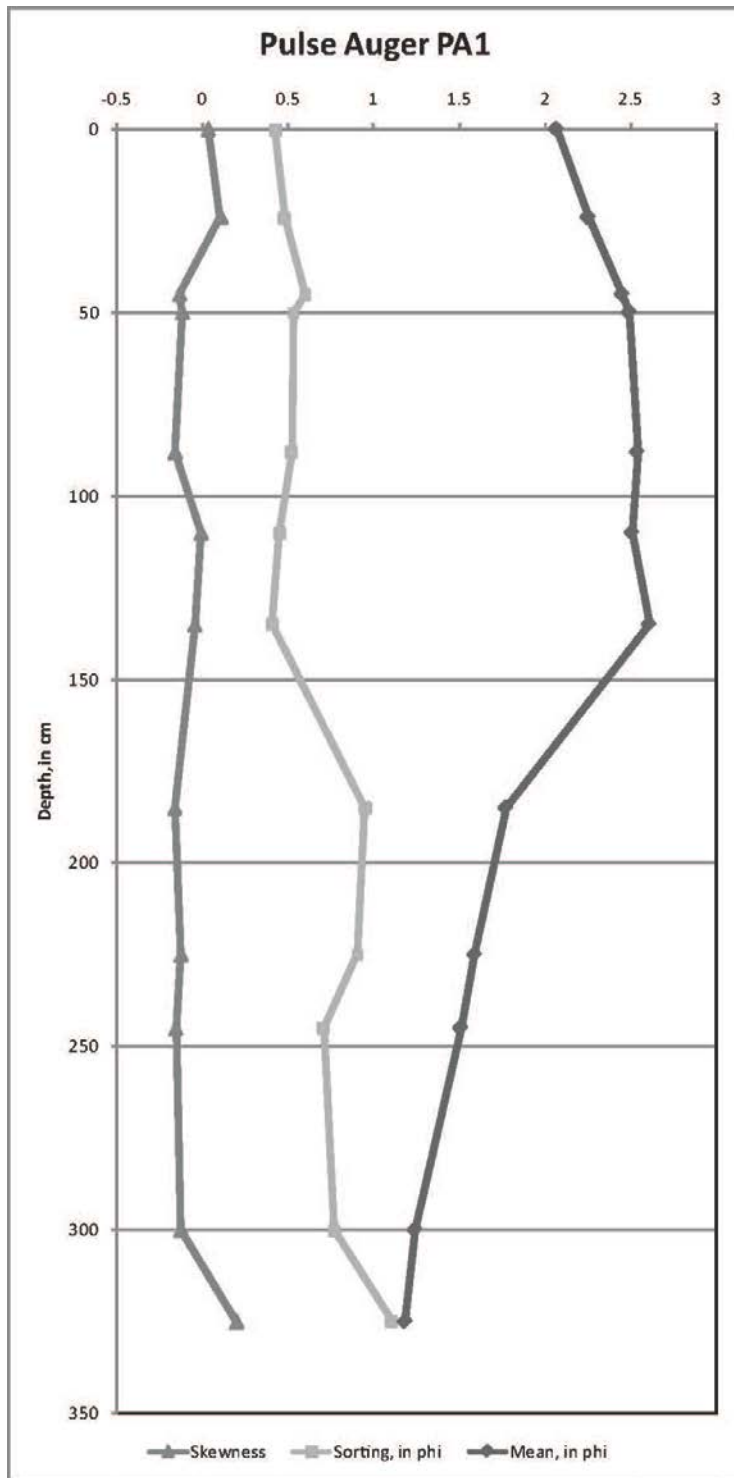


Uncompacted

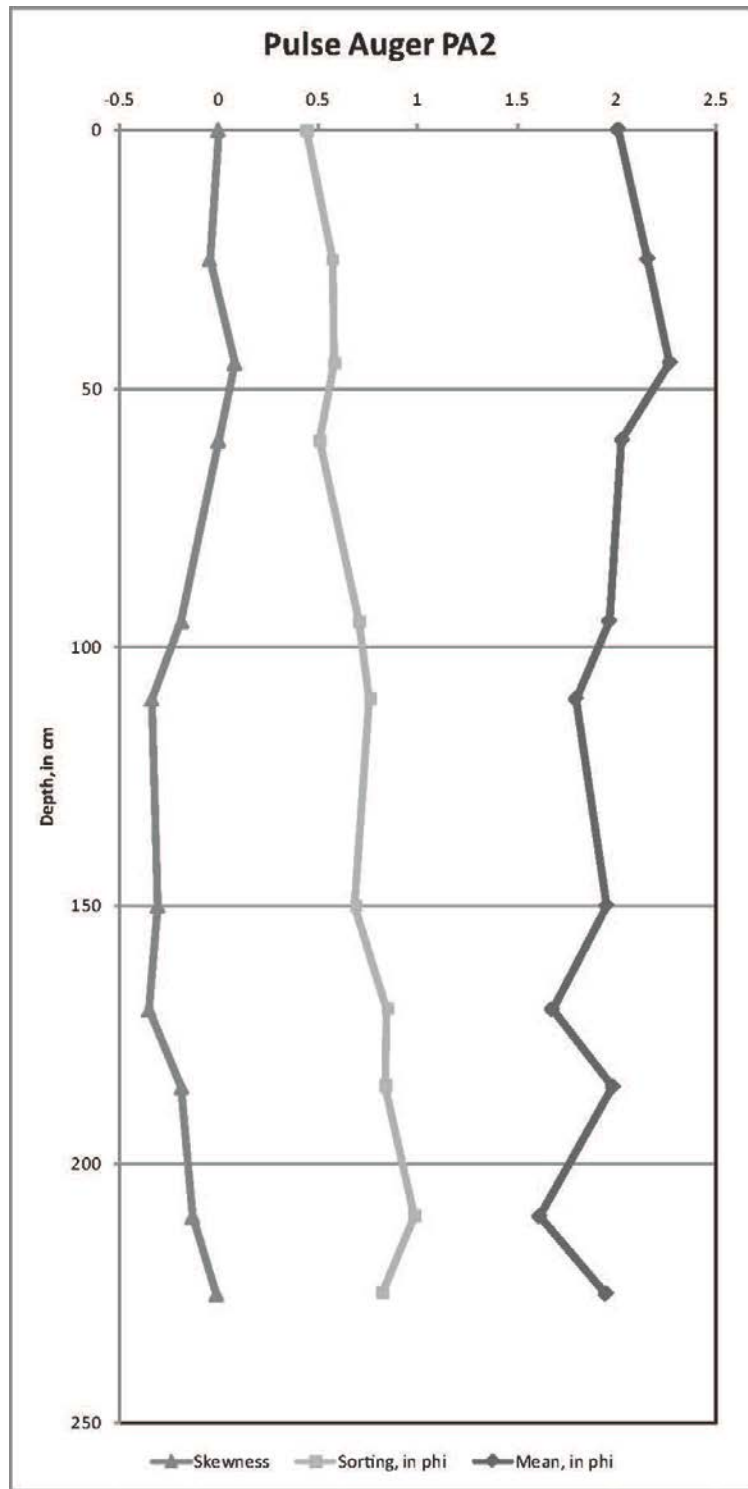
Vibracore C18



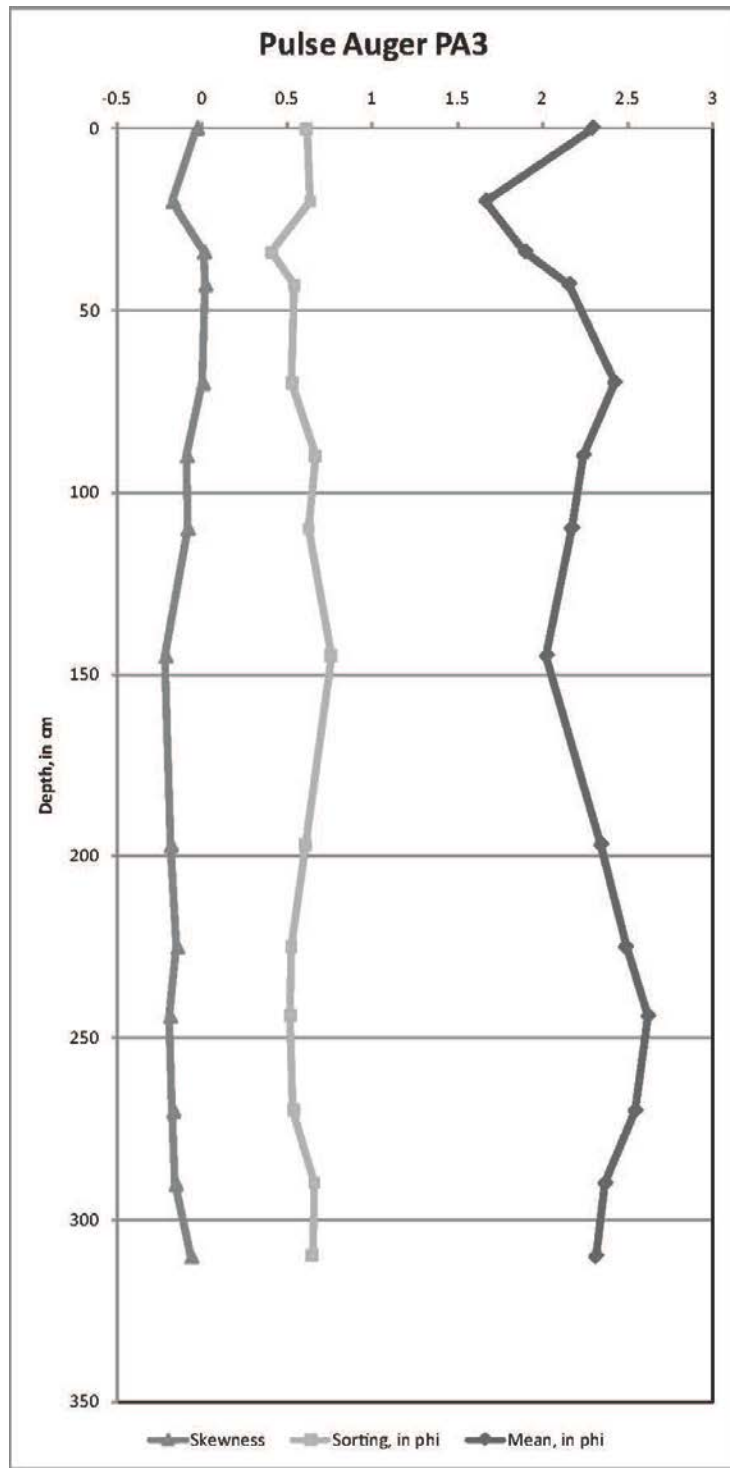
Pulse Auger PA1



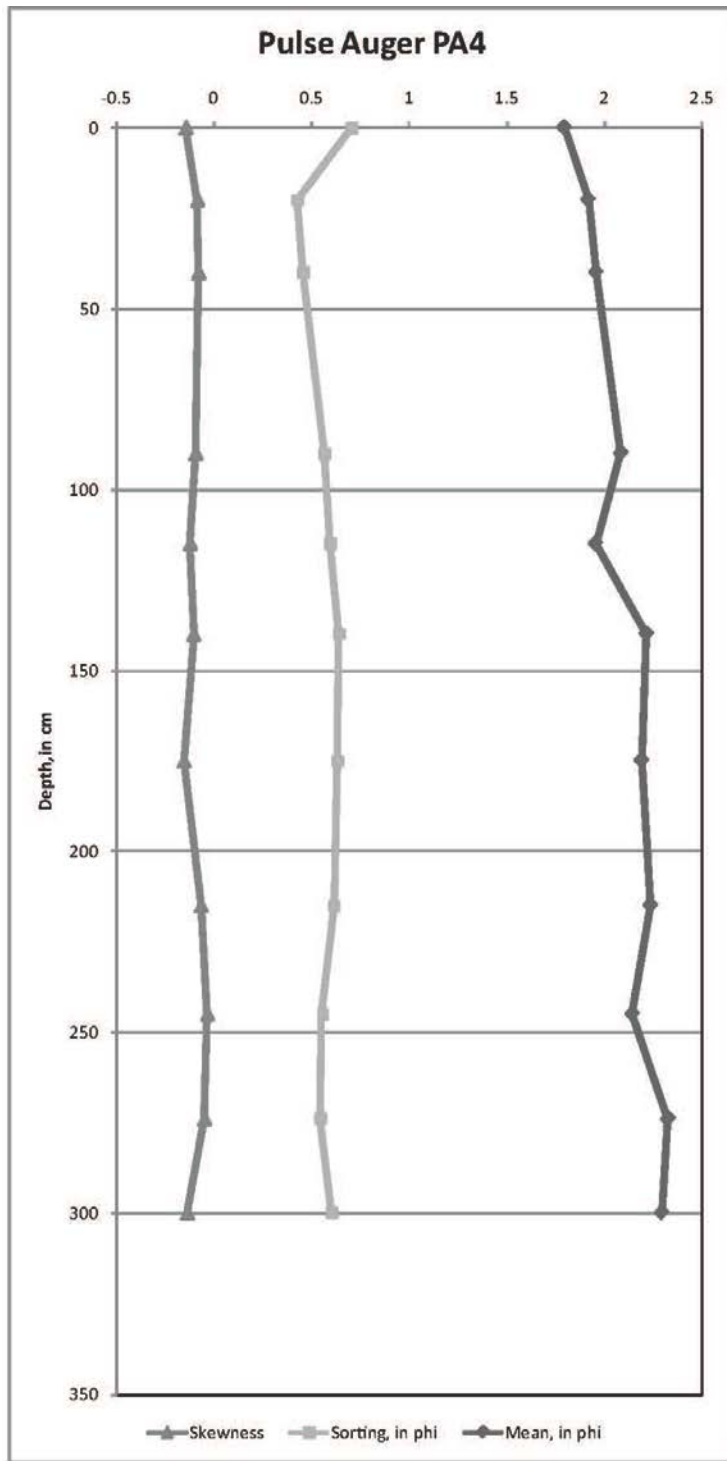
Pulse Auger PA2



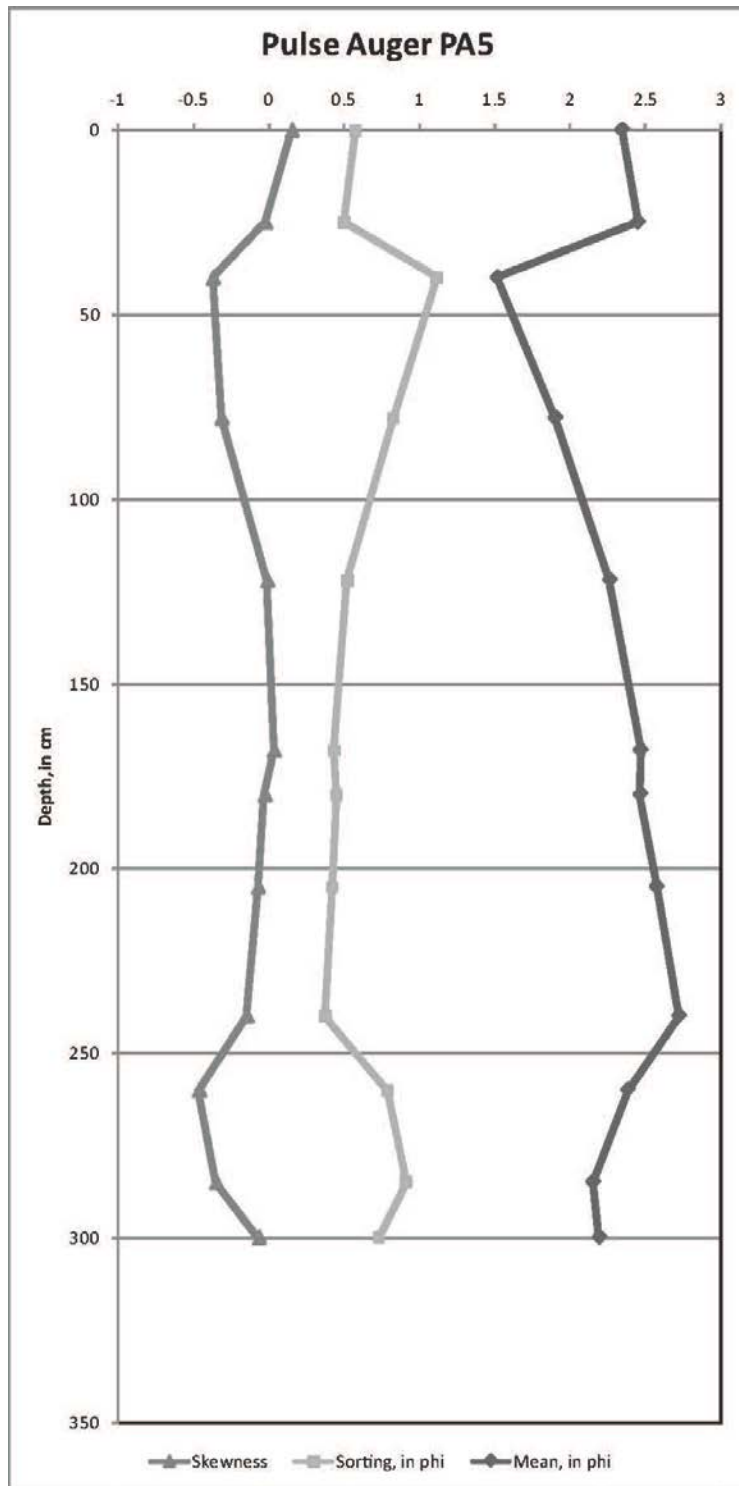
Pulse Auger PA3



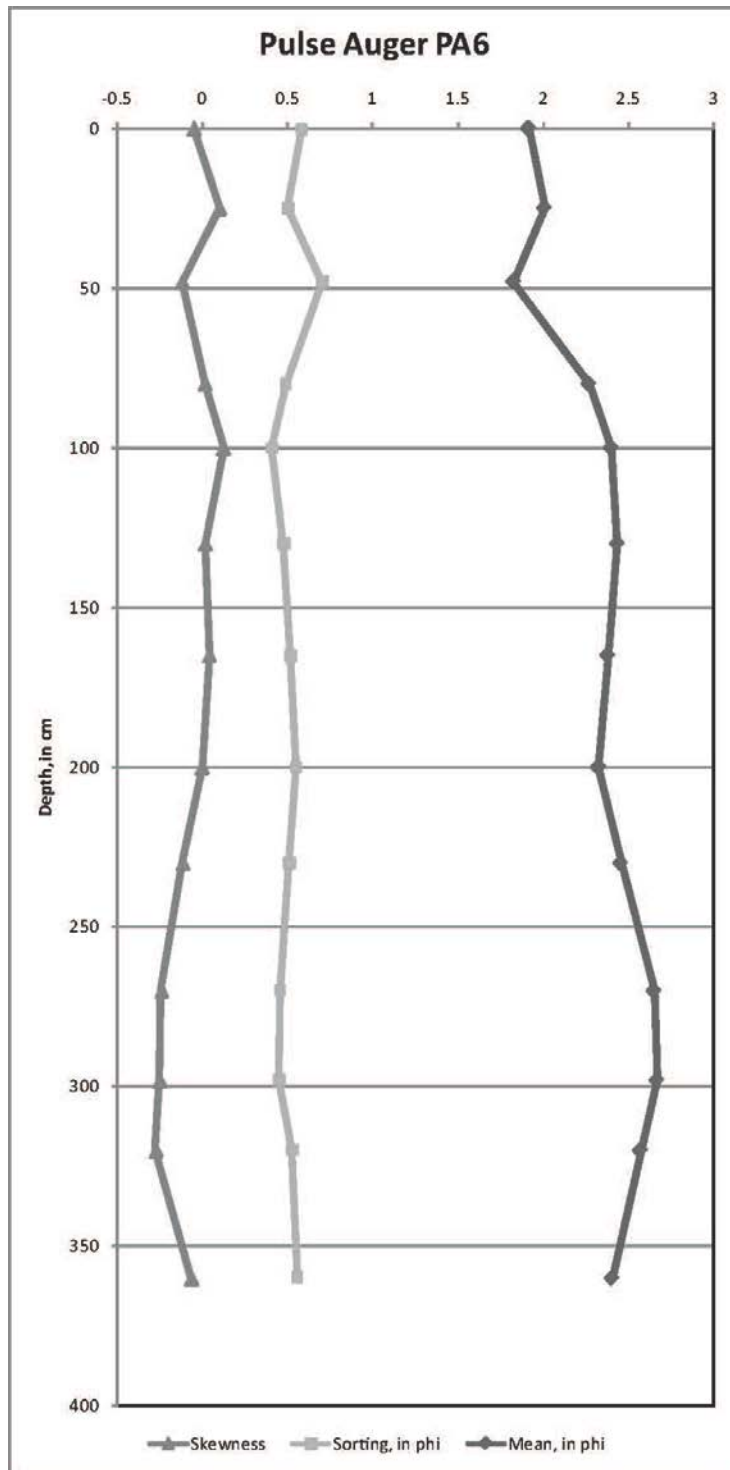
Pulse Auger PA4



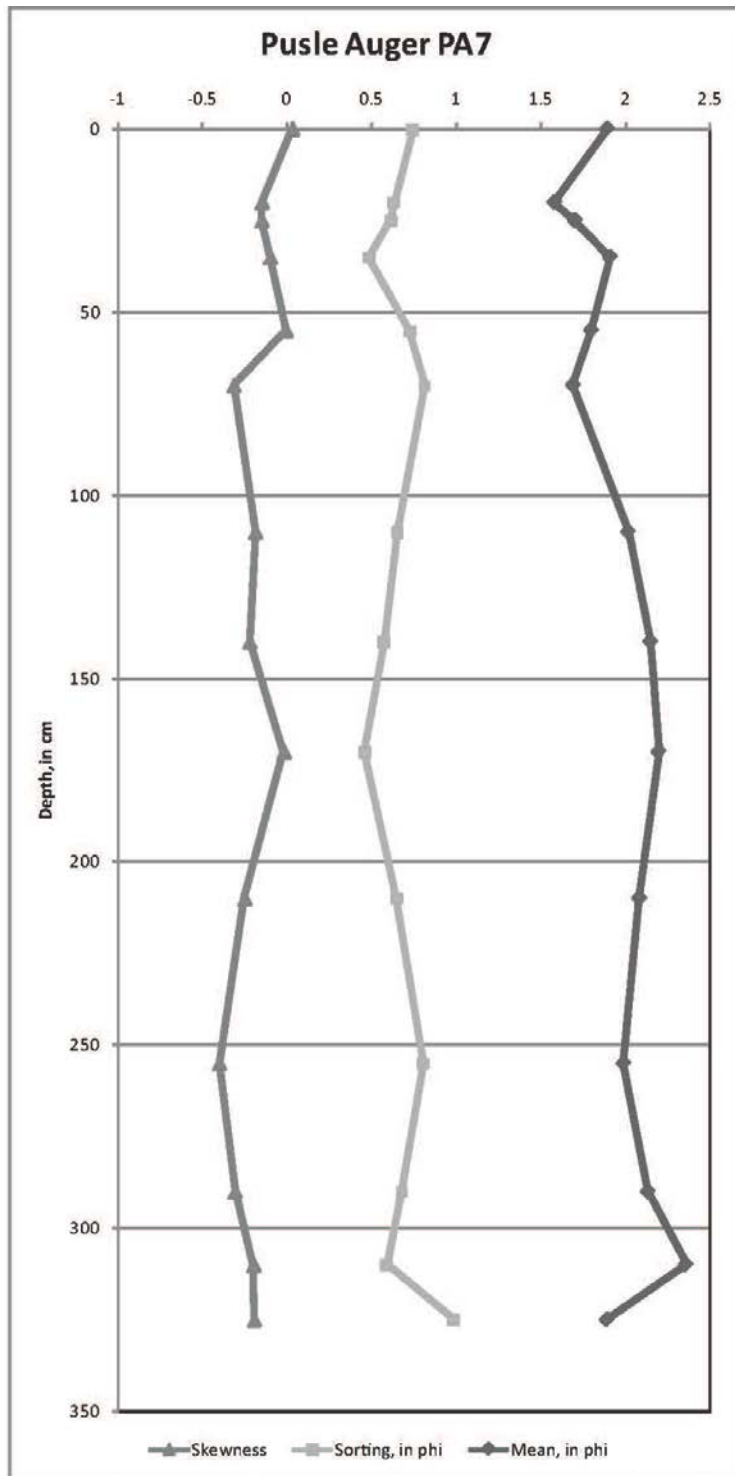
Pulse Auger PA5



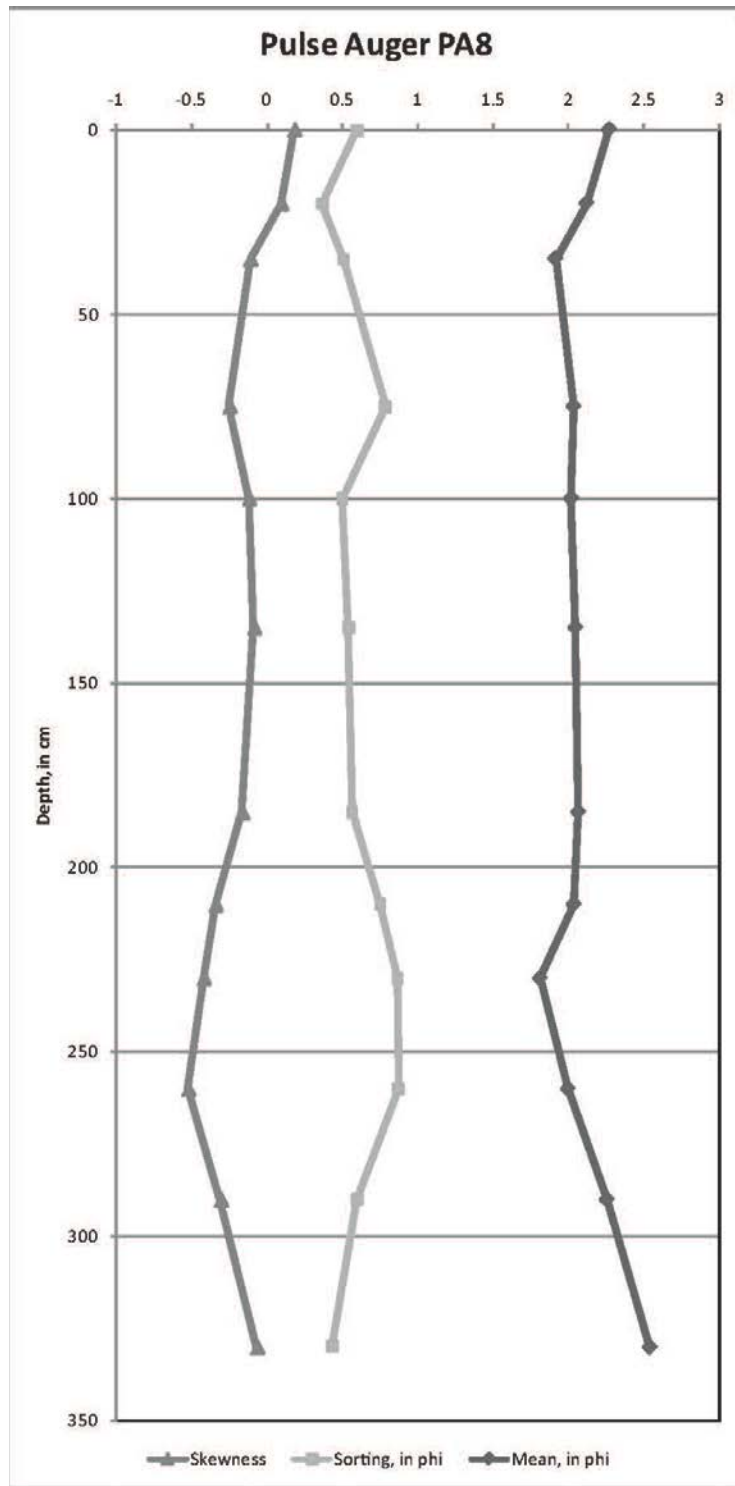
Pulse Auger PA6



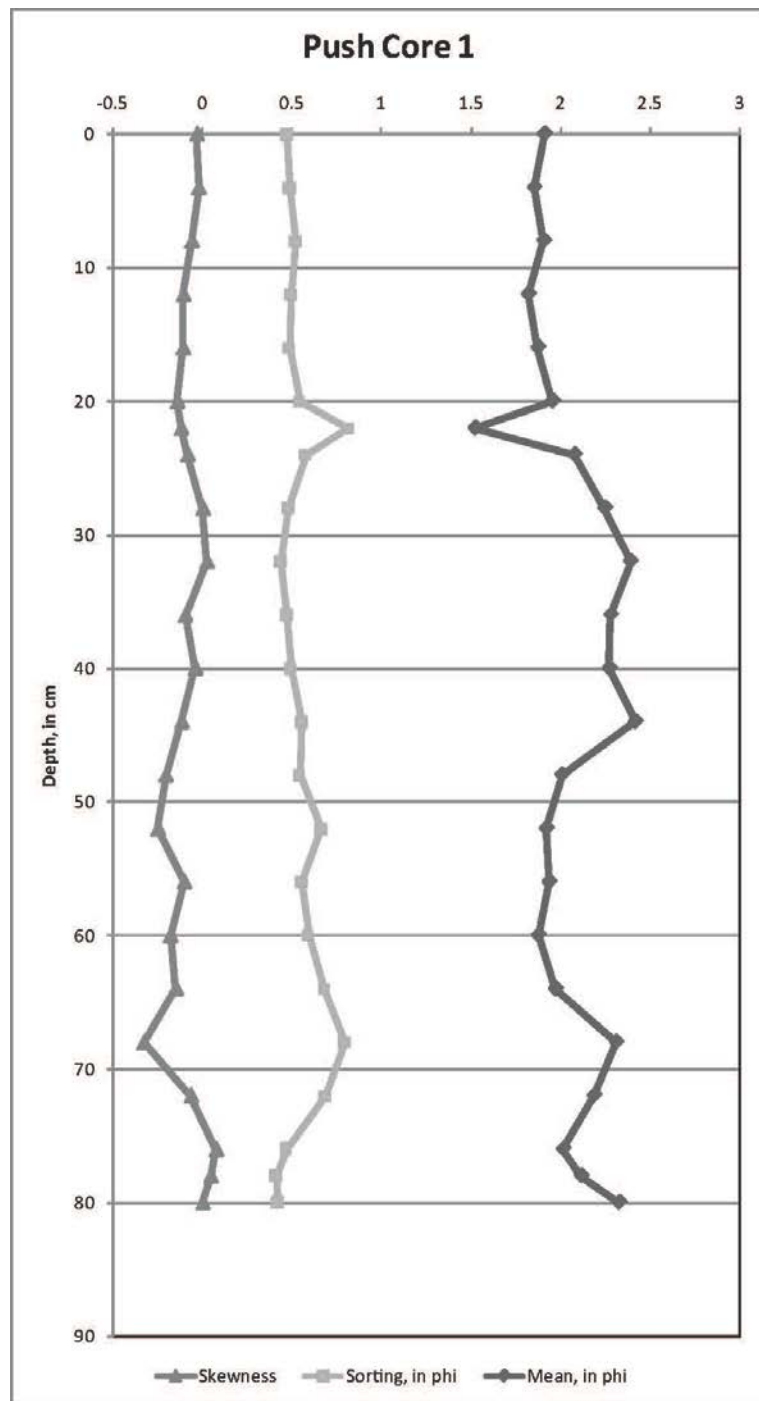
Pulse Auger PA7



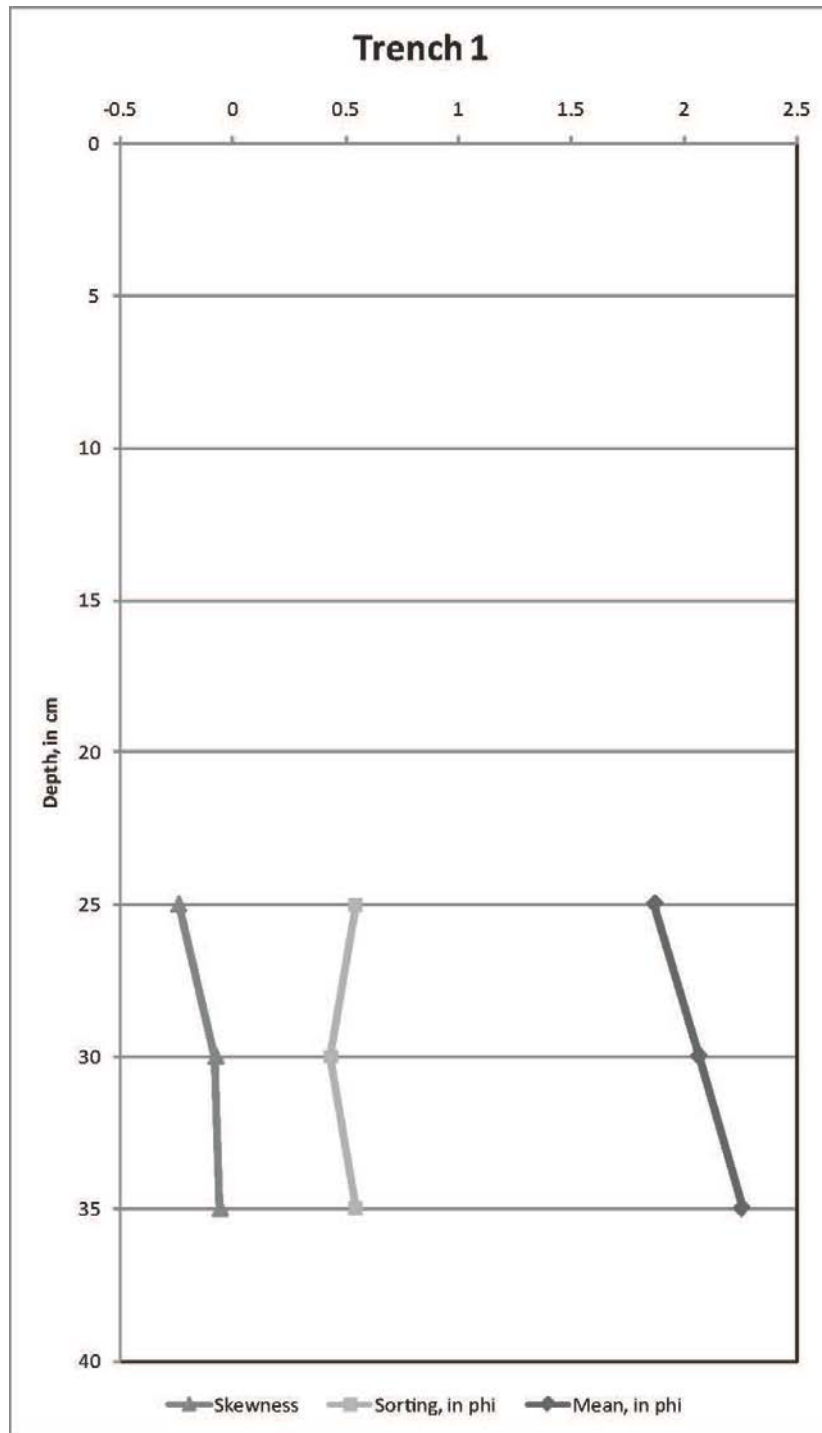
Pulse Auger PA8



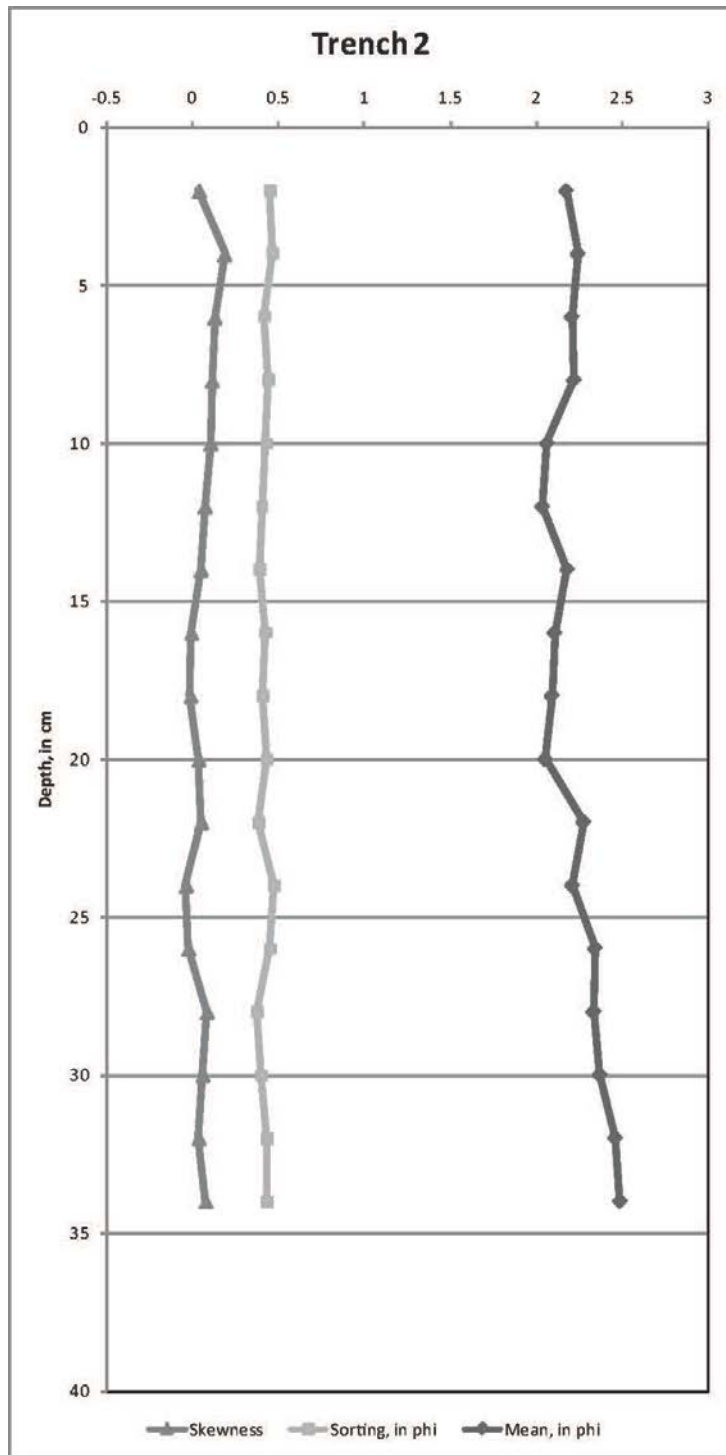
Push Core PC1



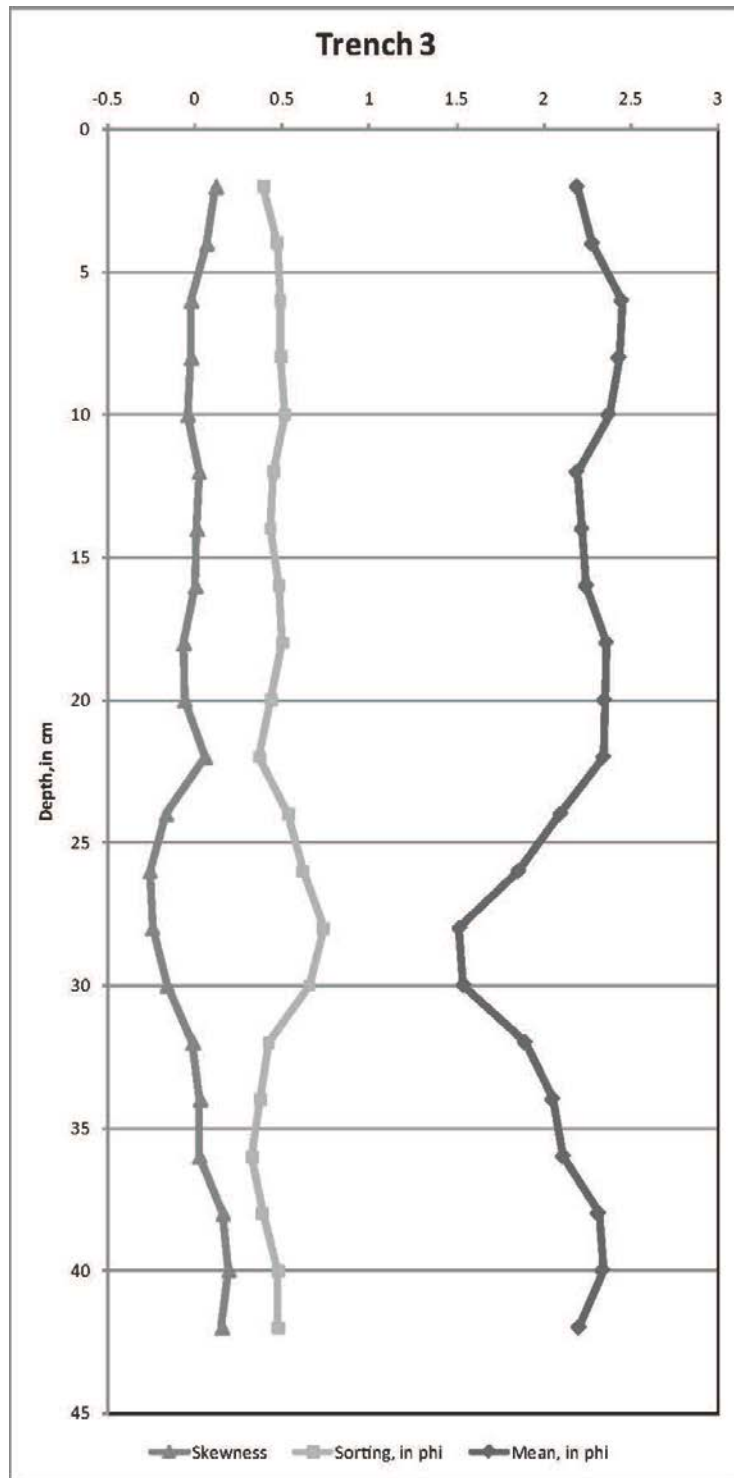
Trench T1



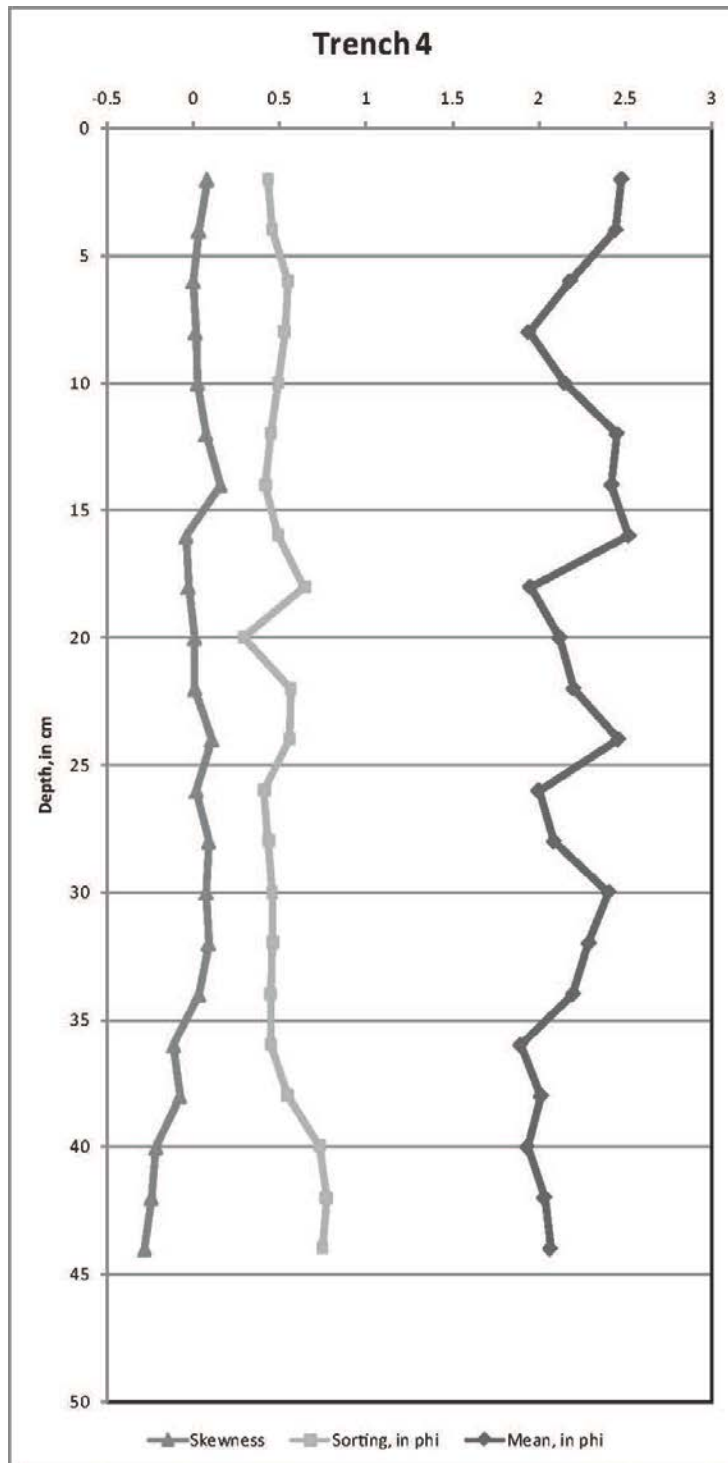
Trench T2



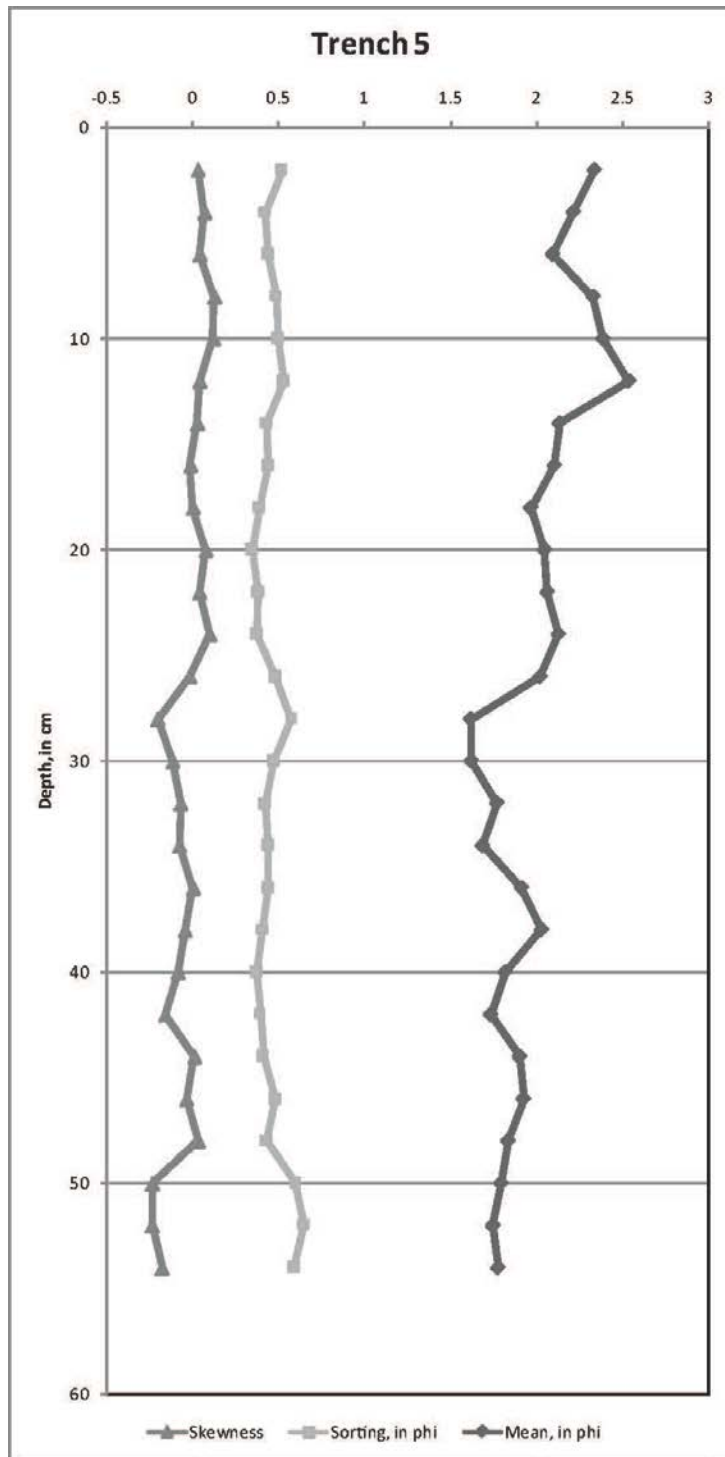
Trench T3



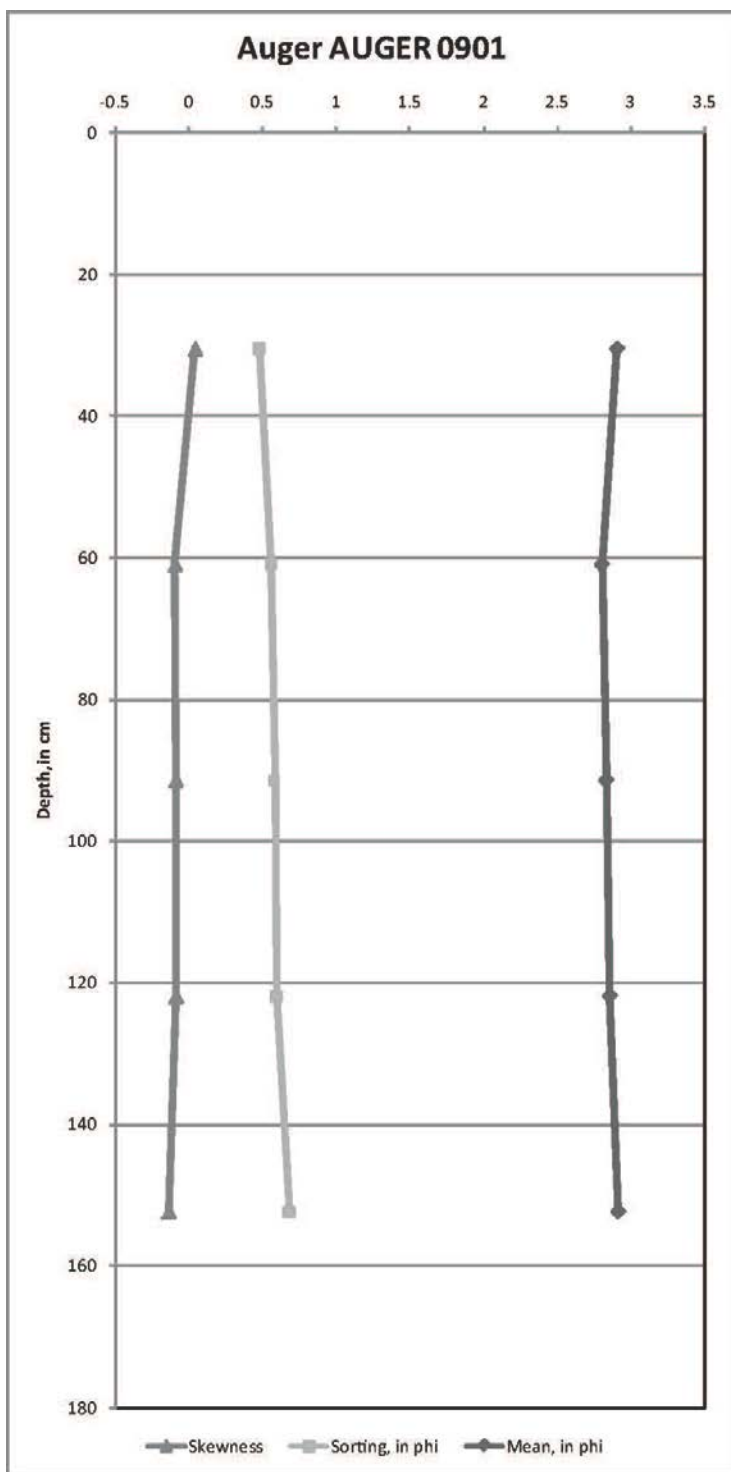
Trench T4



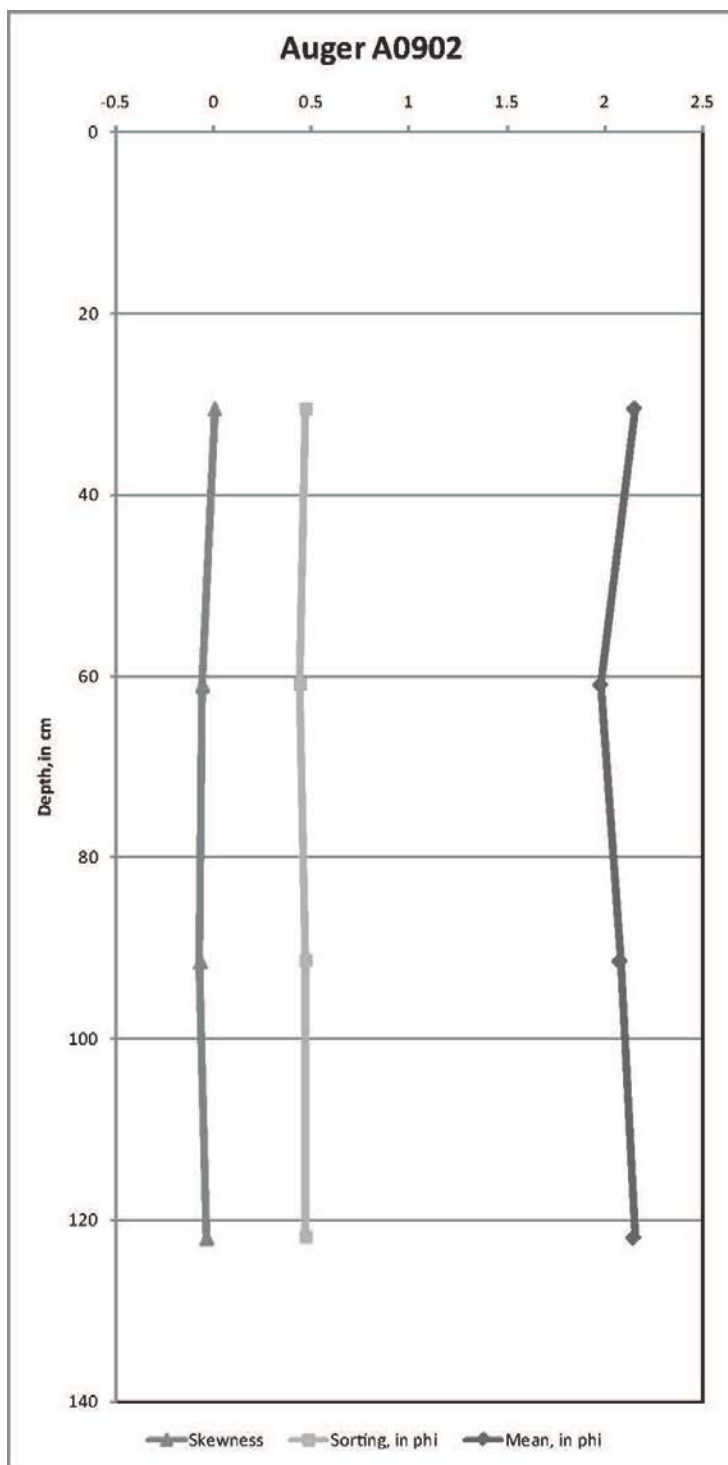
Trench T5



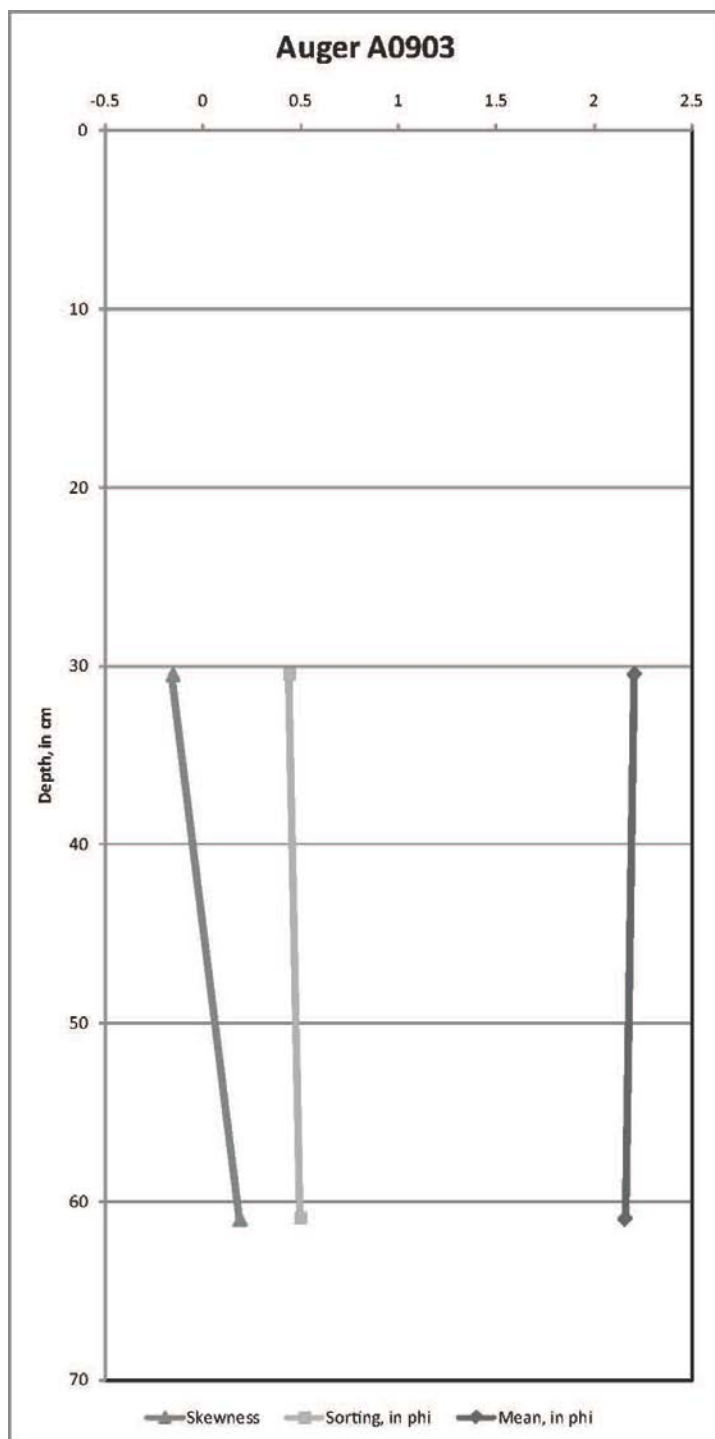
Auger AUGER 0901



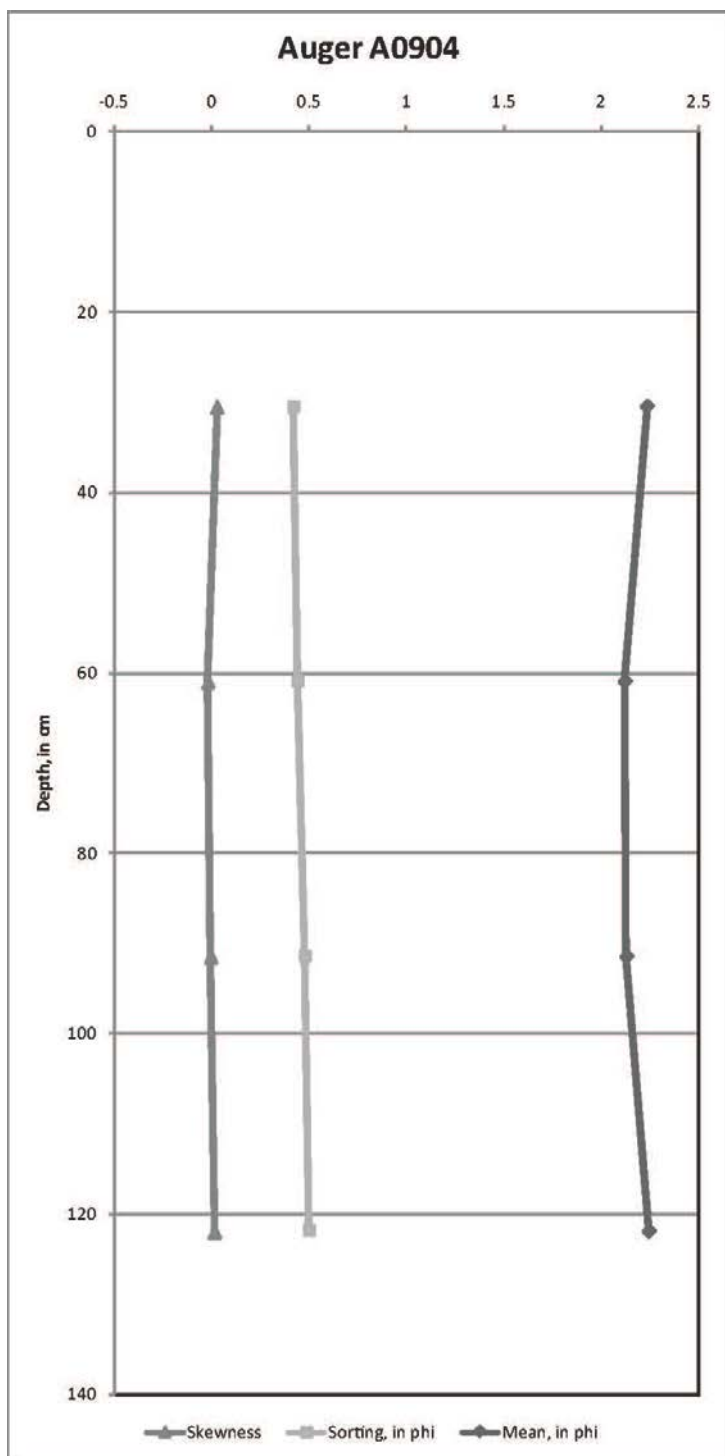
Auger A0902



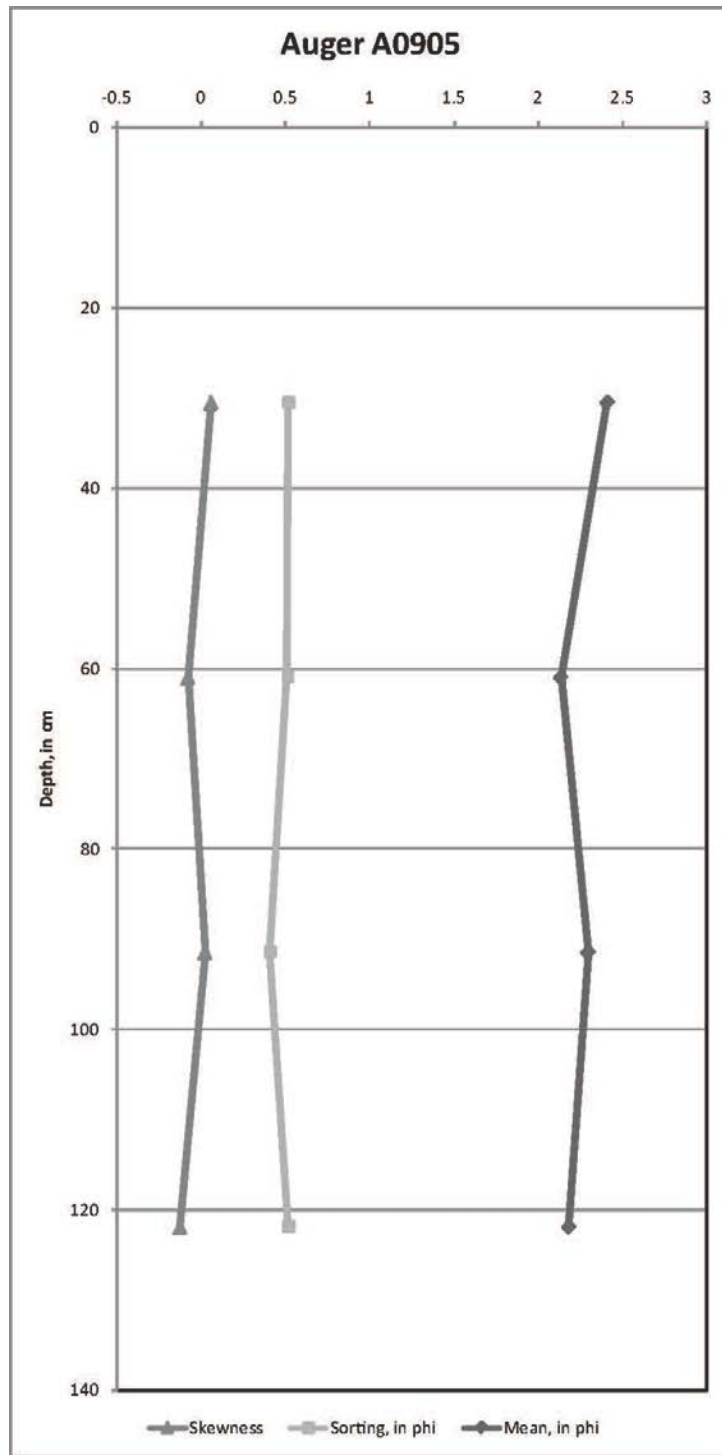
Auger A0903



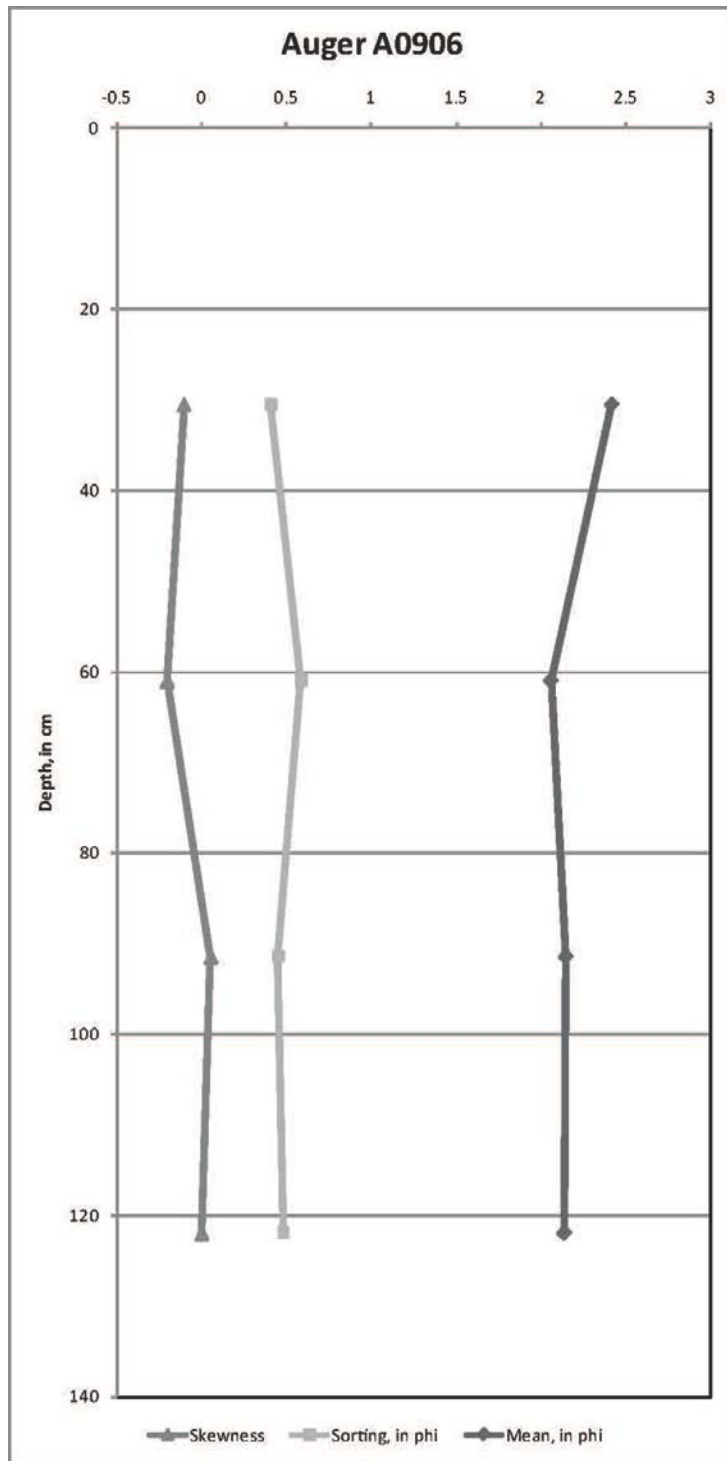
Auger A0904



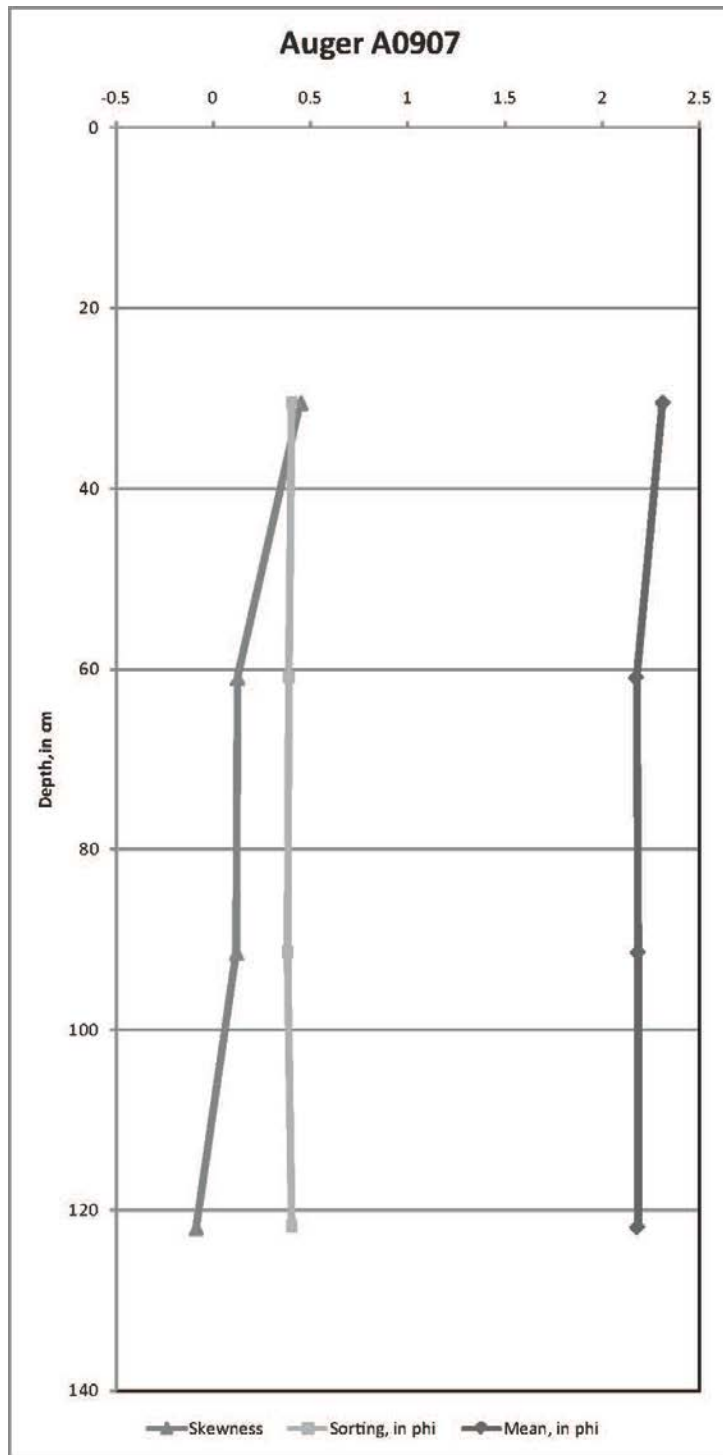
Auger A0905



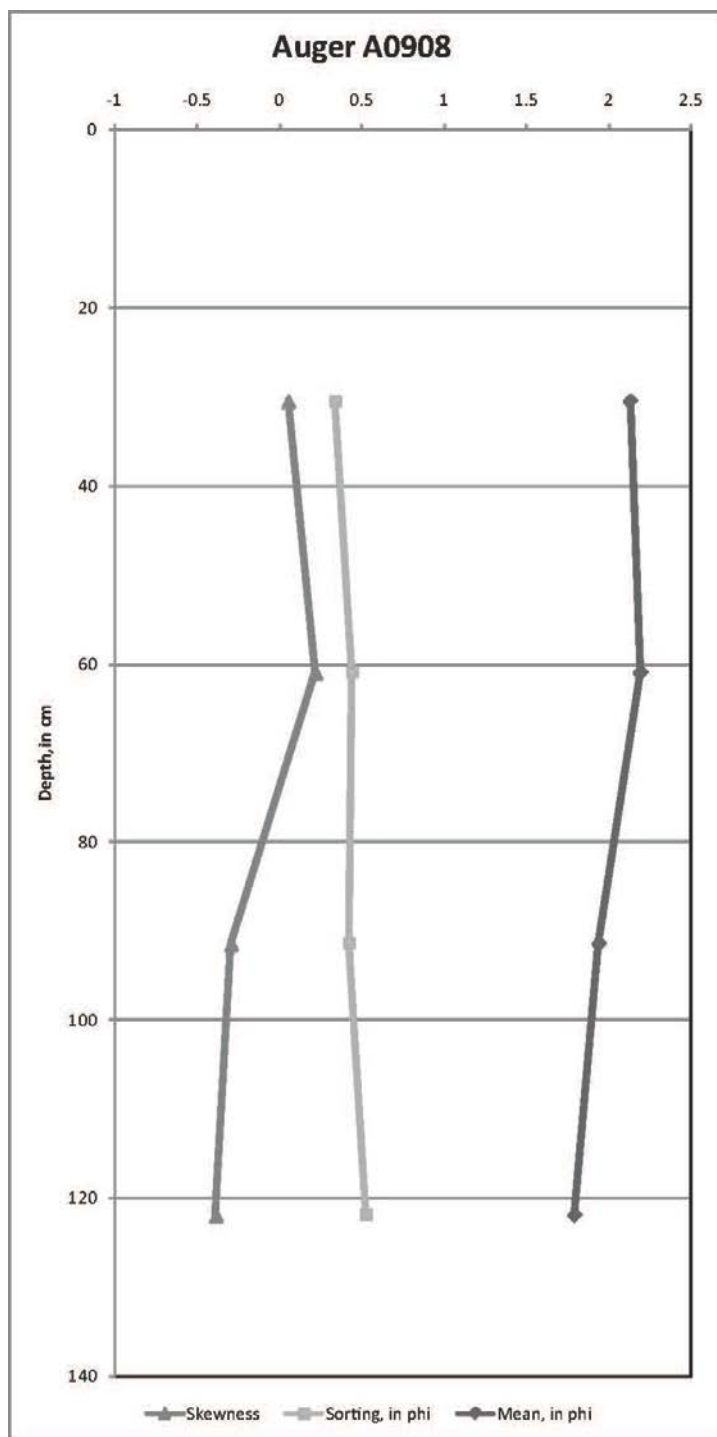
Auger A0906



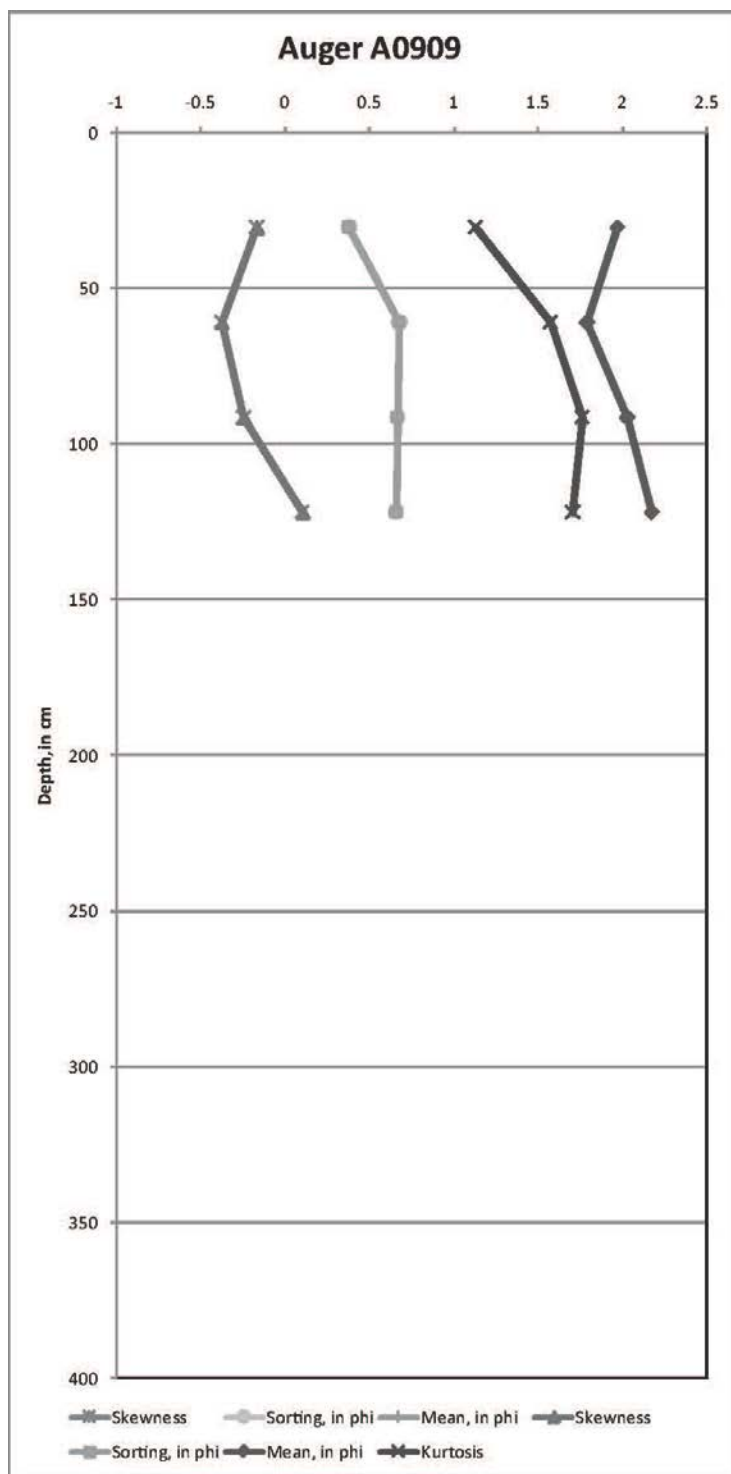
Auger A0907



Auger A0908



Auger A0909



REFERENCES

- Andrews, P.B., 1970. Facies and genesis of a hurricane-washover fan, St. Joseph Island, central Texas coast. Texas Bureau of Economic Geology Report No. 67.
- Barwis, J.H. & Makurath, J.H., 1978. Recognition of ancient tidal inlet sequences: an example from the Upper Silurian Keyser Limestone in Virginia. *Sedimentology*, 25, pp. 61 – 82.
- Belknap, D.F. & Kraft, J.C., 1985. Influence of antecedent geology on evolution of barrier systems. Barrier Island Special Issue, Oertel, G. and Leatherman, S.P. eds., *Marine Geology*, v. 63, p. 235-262.
- Blott, S.J. & Pye, K., 2001. GRADISTAT: a grain size distribution and statistics package for the analysis of unconsolidated sediments. *Earth Surface Processes and Landforms*, 26, pp. 1237 – 1248.
- Boggs, S., 2006. Principles of Sedimentology and Stratigraphy, Fourth Edition. Upper Saddle River, NJ, Pearson Education, 662 p.
- Boon, J.D. & Byrne, R.J., 1981. On basin hypsometry and the morphodynamic response of coastal inlet systems. *Marine Geology*, 41, pp. 27 – 48.
- Boothroyd, J.C., 1985. Tidal Inlets and Tidal Deltas. In Davis, R.A. ed., Coastal Sedimentary Environments. Springer-Verlag, New York, pp. 445 – 532.
- Boyles, L. M., Scott, A. J. & Rine, J. M., 1986. A logging form for graphic descriptions of core and outcrops. *Journal of Sedimentary Petrology*, 56, pp. 567-586.
- Byrne, R.J., DeAlteris, J.T. & Bullock, P.A., 1974. Channel stability in tidal inlets: a case study. Proceedings of the 14th coastal Engineering Conference. American Society of Civil Engineers, pp. 1585-1604.
- Byrnes, M.R. & Gingerich, K.J., 1987. Cross-island profile response to Hurricane Gloria. In Kraus, N.C., ed., Proceedings of a specialty conference on Advances in understanding of coastal sediment processes. American Society of Civil Engineers, pp. 1486 – 1502.

- Chase-Dunn, C., 2015. <http://www.irows.ucr.edu/cd/stories/boat/delmarva.htm>, Accessed Oct. 12, 2015.
- Davis, R.A., 1994. Barrier island systems – a geologic overview. In Davis, R.A., ed., *Geology of Holocene Barrier Island Systems*. Springer-Verlag, New York, pp. 1 – 46.
- Davis, R.A. & Fox, W.T., 1974. Coastal dynamics on Cedar Island, Virginia. *Technical report—Williams College*, 11, 66 p .
- Davis, R.E., Dolan, R. & Demme, G., 1993. Synoptic climatology of Atlantic Coast northeasters. *International Journal of Climatology*, 13, pp. 171–189.
- DeAlteris, J.T. & Byrne, R.J., 1975. The recent history of Wachapreague Inlet, Virginia. In L.E. Cronin, ed., *Estuarine Research*. New York: Academic Press. pp. 167–181.
- Demarest, J.M. & Leatherman, S.P., 1985. Mainland influence on coastal transgression: Delmarva Peninsula. *Marine Geology*, 63, pp. 19–33.
- Dickinson, K.A., Berryhill, Jr., H.L. & Holmes, C.W., 1972. Criteria for recognizing ancient barrier coastlines. In Rigby, J.K. & Hamblin, W.K., eds. *Recognition of ancient sedimentary environments*. SEPM Special Publication 16, Tulsa, OK, pp. 192 – 214.
- Donselaar, M.E. & Nio, S.D., 1982. An Eocene tidal washover type barrier island complex in the South Pyrenean Marginal Basin, Spain. *Geologie en Mijnbouw*, 61, pp. 343 – 353.
- Fenster, M. & Dolan, R., 1996. Assessing the impact on tidal inlets on adjacent barrier island shorelines. *Journal of Coastal Research*, 12, pp. 294 – 310.
- Fisher, J. J., 1967. Origin of barrier island chain shore lines: Middle Atlantic States. Abstracts with program, Geological Society of America, pp. 67 – 68.
- Fisher, J.J., 1982, Barrier islands. In Schwartz, M.L., ed., *The Encyclopedia of Beaches and Coastal Environments*, *Encyclopedia of Earth Sciences*: Stroudsburg, Pennsylvania, Hutchison Ross, v. 15, p. 124–133.
- Fitzgerald, D.M. & Fitzgerald, S.A., 1977. Factors influencing tidal inlet throat geometry. *Proceedings of Coastal Sediments '77*, ASCE, pp. 563 – 581.
- Folk, R. L., 1980, *Petrology of Sedimentary Rocks*. Hemphill Publishing Company, Austin, TX, 184 p.

- Folk, R.L. & Ward, W.C., 1957. Brazos River bar: a study in the significance of grain size parameters. *Journal of Sedimentary Petrology*, 27, pp. 3 – 27.
- Friedman, G.M., 1967. Dynamic processes and statistical parameters compared for size frequency distribution of beach and river sands. *Journal of Sedimentary Petrology*, 37, 2, p. 327–354.
- Gaunt, C.H., 1991. Recent evolution and potential causal mechanism of Cedar Island, Virginia, 1852 – 1986. Proceedings of Coastal Sediments '91, ASCE, pp. 2335 – 2349.
- Google Earth, 2015. <http://www.google.com/earth/index.html> (accessed on May 23, 2015).
- Google Earth, 2015b. <http://www.google.com/earth/index.html>(accessed on August 4, 2015).
- Goettle, M.S., 1981, Geological development of the southern portion of Assateague Island, Virginia. *Northeastern Geology*, 3, pp. 278 – 282.
- Greenwood, B. & Keay, P.A., 1979. Morphology and dynamics of a barrier breach: a study in stability. *Canadian Journal of Earth Sciences*, 16, pp. 1533–1546.
- Groot, J.J. & Jordan, R.R., 1999. The Pliocene and Quaternary deposits of Delaware: palynology, ages, and paleoenvironments. Report of Investigations No. 58, Delaware Geological Survey, 36 p.
- Hamberg, L., 1991. Tidal and seasonal cycles in a Lower Cambrian shallow marine sandstone (Hardeberga Fm.) Scania, Southern Sweden *in* Smith, D.G., Zaitlin, B.A., Reinson, B.E., and Rahmani, R.A. (eds.), *Clastic Tidal Sedimentology*. Canadian Society of Petroleum Geologists Memoir 16, Calgary, Alberta, pp. 255 – 274.
- Hapke, C.J., Himmelstoss, E.A., Kratzmann, M.G., List, J.H. & Thieler, E.R., 2010. National assessment of shoreline change: historical shoreline change along the New England and Mid-Atlantic coasts. US Geological Survey, Open-File Report 2010-1118, 57 p.
- Hayes, M.O., 1975. Morphology of sand accumulation in estuaries: An introduction to the symposium. In Cronin, L.E. ed., *Estuarine Research*, Volume 2. Academic Press, pp. 1 – 29.

- Hayes, M.O., 1980. General morphology and sediment patterns in tidal inlets. *Sedimentary Geology*, 26, pp. 135 – 156.
- Hayes, M.O., Goldsmith, V. & Hobbs, C.H., 1970. Offset coastal inlets. Proceedings of the 12th Coastal Engineering Conference. American society of Civil Engineering, pp. 1187–1200.
- Hennessey, J.T. & Zarillo, G.A., 1987. The interrelation and distinction between flood-tidal delta and washover deposits in a transgressive barrier island. *Marine Geology*, 78, pp. 35 – 56.
- Heward, A.P., 1981. A review of wave-dominated clastic shoreline deposits. *Earth-Sciences Reviews*, 17, pp. 223 – 276.
- Hobbs, C.H., 2004. Geological history of Chesapeake Bay, USA. *Quaternary Science Reviews*, 23, pp. 641–661.
- Hobday, D.K. & Horne, J.C., 1977. Tidally influenced barrier island and estuarine sedimentation in the Upper Carboniferous of southern West Virginia. *Sedimentary Geology*, 12, pp. 97 – 122.
- Hobday, D.K. & Tankard, A.J., 1978. Transgressive-barrier and shallow-shelf interpretation of the lower Paleozoic Peninsula Formation, South Africa. *Bulletin of the Geological Society of America*, 89, pp. 1733 – 1744.
- Hoyt, J.H. & Henry, Jr., V.J., 1965. Significance of inlet sedimentation in the recognition of ancient barrier islands. In DeVoto, R.H. & Bitter, R.K. eds., Sedimentation of Late Cretaceous and Tertiary outcrops, Rock Springs Uplift, 19th Field Conference. Wyoming Geological Association, Casper, WY, pp. 190 – 194.
- Israel, A.M., Ethridge, F.G., & Estes, E.L., 1987. A sedimentologic description of a microtidal, flood-tidal delta, San Luis Pass, Texas. *Journal of Sedimentary Petrology*, 57, pp. 288 – 300.
- Kanes, W., 1969. Tidal inlets, tidal deltas, and barrier islands versus alluvial deposits: A discussion of sedimentary criteria. In Donaldson, A.C. ed., Some Appalachian coals and carbonates: Models of ancient shallow-water deposition. West Virginia Geological and Economic Survey, Morgantown, WV, pp. 259 – 263.
- Kochel, R.C. & Dolan, R., 1986. The role of overwash on a mid-Atlantic coast barrier island. *Journal of Geology*, 94, pp. 902 – 906.

- Kraft, J.C., Chrzastowski, M.J., Toscano, M.A., Belknap, D.F. & Fletcher, C.H., 1987. The transgressive barrier-lagoon coast of Delaware: morphostratigraphy, sedimentary sequences and responses to relative rise in sea level. In Nummedal, D., Pilkey, O.H., and Howard, J.D., eds., *Sea Level Fluctuation and Coastal Evolution*. Soc. Econ. Paleontol. Mineral. Spec. Pub. 41, p. 129-143.
- Krantz, D. E., 2015. http://www.eescience.utoledo.edu/Faculty/Krantz/Va_Coast_figures/Virginia_Coast_figures.htm, Accessed on October 12, 2015.
- Kumar, N. & Sanders, J.E., 1974. Inlet sequence: a vertical succession of sedimentary structures and textures created by the lateral migration of tidal inlets. *Sedimentology*, 21, pp. 491 – 532.
- Krumbein, W.C., 1938. Size frequency distribution of sediments and the normal phi curve. *Journal of Sedimentary Petrology*, 8, pp. 84 – 90.
- Lanesky, D., Logan, B., Brown, R. & Hine, A., 1979. A new approach to portable vibracoring underwater and on land. *Journal of Sedimentary Petrology*, 49, pp. 654-657.
- Leatherman, S.P., 1976. Barrier island dynamics: overwash and aeolian transport. *Proceedings of the 15th Conference of Coastal Engineering (Honolulu)*, 2, pp. 1958 – 1974.
- Leatherman, S.P., Rice, T.E. & Goldsmith, V., 1982. Virginia barrier island configuration: A reappraisal. *Science*, 215 (4530), pp. 285 – 287.
- Leatherman, S.P. & Williams, A.T., 1983. Vertical sedimentation units in a barrier island washover fan. *Earth Surface Processes and Landforms*, 8, pp. 141 – 150.
- McBride, R.A., 1999. Spatial and temporal distribution of historical and active tidal inlets: Delmarva Peninsula and New Jersey, USA. *Proceedings of Coastal Sediments '99*, ASCE, pp. 1505–1521.
- McBride, R.A., Fenster, M.S., Seminack, C.T., Richardson, T.M., Sepanik, J.M., Hanley, J.T., Bundick, J.A. & Tedder, E., 2015. Holocene barrier-island geology and morphodynamics of the Maryland and Virginia open-ocean coasts: Fenwick, Assateague, Chincoteague, Wallops, Cedar, and Parramore Islands. In Brezinski, D.K., Halka, J.P. & Ort, R.A., Jr., eds., *Tripping from the Fall Line: Field Excursions for the GSA Annual Meeting, Baltimore, 2015*. Geological Society of America Field Guide 40, p. 1–115.

- Mixon, R.B., 1985. Stratigraphic and geomorphic framework of Uppermost Cenozoic Deposits in the Southern Delmarva Peninsula, Virginia and Maryland. US Geological Survey Professional Paper 1067-G.
- Morton, R.A. & Donaldson, A.C., 1973. Sediment distribution and evolution of tidal deltas along a tide-dominated shoreline, Wachapreague, Virginia. *Sedimentary Geology*, 10, pp. 285-299.
- Moslow, T.F. & Heron, Jr., S.D., 1978. Relict inlets: Preservation and occurrence in the Holocene stratigraphy of Southern Core Banks, North Carolina. *Journal of Sedimentary Petrology*, 48, p. 1275 – 1286.
- Moslow, T.F. & Tye, R.S., 1985, Recognition and characterization of Holocene tidal inlet sequences. *Marine Geology*, 63, pp. 129 – 151.
- Moyer, K.S., 2007. An assessment of an ephemeral breach along Cedar Island, Virginia. Master's Thesis. Environmental Science and Policy, George Mason University, 101 p.
- Nebel, S.H., Trembanis, A.C. & Barber, D.C., 2013. Tropical cyclone frequency and barrier island erosion rates, Cedar Island, Virginia. *Journal of Coastal Research*, 29, pp. 133 – 144.
- Newman, W.S. & Munsart, C.A., 1968. Holocene geology of the Wachapreague lagoon, Eastern Shore peninsula, Virginia. *Marine Geology*, 6, pp. 81-105.
- NOAA, 2006.
<http://www.tidesandcurrents.noaa.gov/waterlevels.html?id=8631044&units=metric&bdate=20060830&edate=20060904&timezone=GMT&datum=MLLW&interval=6&action=>, Accessed on June 19, 2014.
- NOAA, 2015a. http://www.stormsurge.noaa.gov/event_history.html, Accessed on March 7, 2015.
- NOAA, 2015b. <http://tidesandcurrents.noaa.gov/sltrends/sltrends.shtml>, Accessed on October 12, 2015.
- NOAA, 2015c. <http://www.tidesandcurrents.noaa.gov/stationhome.html?id=8631044>, Accessed on October 12, 2015.
- NOAA, 2015d. http://www.erh.noaa.gov/akq/adobe_pdf/Hurrhist.pdf, Accessed on October 12, 2015.

- Nummedal, D., 1983. Barrier Islands. In Komar, P.D. ed., CRC Handbook of Coastal Processes and Erosion. CRC Press, Boca Raton, FL, pp. 77 – 121.
- Nummedal, D. & Fischer, I.A., 1978. Process-response models for depositional shorelines: The German and the Georgia Bights. Proceedings of the 16th Coastal Engineering Conference, ASCE, pp. 1215 – 1231.
- Nummedal, D. & Swift, D.J.P., 1987. Transgressive stratigraphy at sequence-bounding unconformities: some principles derived from Holocene and Cretaceous examples. In Nummedal, D., Pilkey, O.H. & Howard, J.D., eds., Sea Level Fluctuation and Coastal Evolution. Society of Economic Paleontologists and Mineralogists Special Publication 41, pp. 241-260.
- Oertel, G.F., 1985. The barrier island system. In Oertel, G.F. & Leatherman, S.P. eds., Barrier Islands. *Marine Geology* 63, pp. 1 – 18.
- Oertel, G.F. & Kraft, J.C., 1994. New Jersey and Delmarva barrier islands. In Davis Jr., R.A., ed., Geology of Holocene Barrier Islands. Heidelberg, Germany: Springer-Verlag. pp. 207–232.
- Oertel, G.F., Allen, T.R. & Foyle, A.M., 2008. The influence of drainage hierarchy on pathways of barrier retreat: An example from Chincoteague Bight, Virginia, U.S.A. *Southeastern Geology*, 45, pp. 179-201.
- Oomkens, E., 1974. Lithofacies relations in the Late Quaternary Niger Delta complex. *Sedimentology*, 21, pp. 195 – 222.
- Owens, J.P. & Denny, C.S., 1979. Upper Cenozoic deposits of the Central Delmarva Peninsula, Maryland and Delaware. U.S. Geological Survey Professional Paper 1067-A.
- Pierce, J.W., 1970. Tidal inlets and washover fans. *Journal of Geology*, 78, pp. 230 – 234.
- Rice, T.E., Niedoroda, A.W. & Pratt, A.P., 1976. The coastal processes and geology: Virginia barrier islands. The Virginia Coast Reserve Study. The Nature Conservancy, Arlington, VA, pp. 109–382.
- Richardson, T.M., 2012, Morphodynamic changes of the Parramore-Cedar barrier island system and Wachapreague Inlet, Virginia from 1852 to 2011: A model of barrier island and tidal inlet evolution along the Southern Delmarva Peninsula, USA. PhD dissertation, Environmental Science and Policy, George Mason University, 281 p.

- Riggs, S.R., Cleary, W.J. & Snyder, S.W., 1995. Influence of inherited geologic framework on barrier island shoreface morphology and dynamics. *Marine Geology*, 126, pp. 213 – 234.
- Schwartz, R.K., 1975. Nature and Genesis of some Storm Washover Deposits. U.S. Corps of Engineers, Coastal Engineering Research Center Technical Memorandum No. 61.
- Scott, T.W., Swift, D.J.P., Whittecar, G.R. & Brook, G.A., 2010. Glacioisostatic influences on Virginia's late Pleistocene coastal plain deposits. *Geomorphology*, 116, pp. 175 – 188.
- Sedgwick, P.E. & Davis, Jr., R.A., 2003. Stratigraphy of washover deposits in Florida: implications for recognition in the stratigraphic record. *Marine Geology*, 200, pp. 31 – 48.
- Seminack, C.T., 2011. Reconstruction of a relict inlet system and historical storm signatures along southern Assateague Island, Maryland. Master's thesis, Temple University, 254 p.
- Seminack, C.T. & Buynevich, I.V., 2013. Sedimentological and geophysical signatures of a relict tidal-inlet complex along a wave-dominated barrier: Assateague Island, Maryland, U.S.A. *Journal of Sedimentary Research*, 83, pp. 132 – 144.
- Seminack, C.T. & McBride, R.A., 2015. Geomorphic history and diagnostic features of former tidal inlets along Assateague Island, Maryland-Virginia: A life-cycle model for inlets along wave-dominated barrier islands. *Shore & Beach*, 83, pp. 3 – 24.
- Smith, D.J., 1984. Vibracoring fluvial and deltaic sediments: tips on improving penetration and recovery. *Journal of Sedimentary Research*, pp. 660-663.
- Stone, C.R., 2006. Geology of a bayhead delta within a Potomac River tidal-freshwater estuary: Pohick Bay, Virginia. Master's thesis, George Mason University, 300 p.
- Swift, D.J.P., 1975. Barrier island genesis: Evidence from the central Atlantic shelf, eastern USA. *Sedimentary Geology*, 14, pp. 1 – 43.
- Tankard, A.J. & Barwis, J.H., 1982. Wave-dominated deltaic sedimentation in the Devonian Bokkeveld Basin of South Africa. *Journal of Sedimentary Petrology*, 52, pp. 959 – 974.
- Toscano, M.A. & York, L.L., 1992. Quaternary stratigraphy and sea-level history of the US middle Atlantic Coastal Plain. *Quaternary Science Reviews*, 11, pp. 301–328.

- Uhlir, D.M., Akers, A. & Vondra, C.F., 1988. Tidal inlet sequence, Sundance Formation (Upper Jurassic), north-central Wyoming. *Sedimentology*, 35, pp. 739 – 752.
- U.S. Air Force, 2015. <http://www.eglin.af.mil/news/story.asp?id=123205341>. Accessed on December 8, 2015.
- Weimer, R.J., Howard, J.D. & Lindsay, D.R., 1981. Tidal flats and associated tidal channels. In Scholle, P.A. & Spearing, D. eds., *Sandstone Depositional Environments*. AAPG, Tulsa, OK, pp. 191 – 245.
- Zhang, K., Douglas, B. & Leatherman, S., 2002. Do storms cause long-term beach erosion along the U.S. east barrier coast? *The Journal of Geology*, 110, pp. 493–502.

SUPPLEMENTAL MATERIAL A – GRAIN-SIZE DATA SHEETS

Supplemental Material A can be found in a separate pdf file.

SUPPLEMENTAL MATERIAL B – GRADISTAT OUTPUT SHEETS

Supplemental Material B can be found in a separate pdf file.

CURRICULAM VITAE

J. Thomas Hanley graduated from George C. Marshall High School, Falls Church, Virginia, in 1969. He received his Bachelor of Science in Geology from Virginia Polytechnic Institute and State University in 1973 and his Masters of Science in Geology from Syracuse University in 1975.